PICES Scientific Report No. 26
2004

PROCEEDINGS OF THE THIRD WORKSHOP ON THE OKHOTSK SEA AND ADJACENT AREAS

Edited by
Skip M^{c}Kinnell

September 2004
Secretariat / Publisher
North Pacific Marine Science Organization (PICES)
c/o Institute of Ocean Sciences, P.O. Box 6000, Sidney, B.C., Canada. V8L 4B2
E-mail: secretariat@pices.int Home Page: http://www.pices.int

TABLE OF CONTENTS

SESSION 3 POSTERS

SESSION 4

Foreword

"*The workshop brought together international scientists with an interest in the Okhotsk Sea and adjacent areas to review what is known, to learn of recent investigations and new knowledge, and to discuss the most important elements that should be included in the North Pacific Ecosystem Status Report*."

…**Dr. Lev Bocharov (June 4, 2003)**

This publication is the third in a series of PICES Scientific Reports on *The Okhotsk Sea and Adjacent Areas*. The themes covered by the third workshop were broadly based, for the purpose of integrating observations of physics, chemistry, and biology in the region. The first two sessions on climate variations, and physical and chemical processes were convened by Dr. Vyacheslav Lobanov (Pacific Oceanological Institute, Russia), Dr. Yutaka Nagata (Japan), Prof. Steven Riser (University of Washington, U.S.A.) and Prof. Sei-ichi Saitoh (Hokkaido University, Japan). The session on biological variability was convened by Dr. Elena Dulepova (TINRO-Center, Russia). Dr. Vladimir Radchenko (SakhNIRO, Russia), Dr. Keiichi Mito (Hokkaido National Fisheries Research Institute, Japan) and Dr. Tatyana Belan (FERHRI, Russia) chaired a session on anthropogenic effects and marine ecosystem response that included a variety of issues related to fisheries and to oil/gas exploration in East Sakhalin.

A novel element in the programme was an attempt to synthesize the major findings in a ½-day discussion session at the end of the presentations. The results of this workshop contributed significantly to the PICES North Pacific Ecosystem Status Report; a report that addresses questions such as: ·What is the current status of the Okhotsk Sea ecosystem and why?· How does it differ from historical observations?· How does this compare with other regions in the North Pacific?

The organizers of the workshop in Vladivostok, especially the hosts at TINRO-Center, offered the participants with a memorable scientific and social environment for collaboration.

Skip McKinnell, Ph.D.
Deputy Executive Secretary
North Pacific Marine Science Organization

SESSION 1
EVIDENCE AND CONSEQUENCES OF DECADAL-SCALE CLIMATE VARIATION IN THE OKHOTSK SEA AND NORTH-WESTERN PACIFIC OCEAN (Convenors: Steven Riser and Sei-Ichi Saitoh)

Interannual changes of air temperature over the Okhotsk Sea and adjacent areas as the results of wavelet analysis

Elena Ustinova[1] and George Shevchenko[2]

[1] Pacific Fisheries Research Centre (TINRO-Centre), 4 Shevchenko Alley, Vladivostok, 690950 Russia. e-mail: ustinova@tinro.ru

[2] Sakhalin Research Institute of Fisheries and Oceanography (SakhNIRO), 196 Komsomol'skaya Street, Yuzhno-Sakhalinsk, 693023 Russia. e-mail: shevchenko@sakhniro.ru

Introduction

A study of linear trends and cyclical variations of climate is very interesting because it gives some possibility to forecast changes of weather and marine environment. This problem is one of the most important in the fishery science, but it is rather difficult because of the complicated character of interannual temperature variations. Recent studies of air temperature over the Okhotsk Sea and adjacent areas were guided mainly by the detection of linear trends of centennial and semi-centennial series (Kim et al. 1997; Pestereva and Pushkina 1998; Ponomarev et al. 1999, 2000, 2001, 2002; Shevchenko and Kato 1999; Varlamov et al. 1997, 1998). The main features of long-lived tendencies have been described for this region, however in our opinion, oscillations with periods from 2 till 50 years have not been investigated sufficiently. Usage of the wavelet method of the analysis of temperature time series reveals new information about the contribution of various temporal scales to total variability and its temporal change. We suppose that the interannual variations of temperature could be regarded as modulation of seasonal fluctuations.

Data

Air temperature data are the longest time series of relatively homogeneous and regular information. For the analysis we used monthly mean air temperature data at coastal meteorological stations that were measured by Russian, Japanese and Korean hydro-meteorological agencies. The stations used for the analysis are located around the Okhotsk Sea (Fig. 1). Air temperature data were obtained from the NASA GISS web page (http://www.giss.nasa.gov/data/update/gistemp/station_data). The periods of observations differed among stations (Table 1) and unfortunately some of the Russian ones, including such interesting sites as Simushir and Icha, were abandonned in the late 1990s, which limited our analysis.

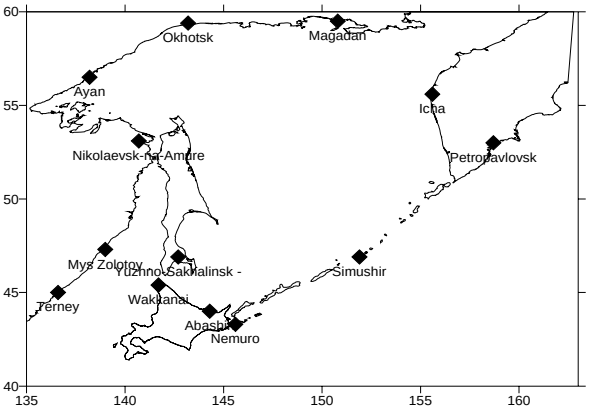

Fig. 1 Locations of selected meteorological stations on the Okhotsk/Japan seas. Some stations (St.Paul, Korf, Nikolskoe, Bering Sea; Izuhara and Akita, Japan Sea) are too far from the Okhotsk Sea so they were not shown.

Methods of analysis

Investigation of climate variation is a complex task because of strong modulations of seasonal

Table 1 The names of meteorological stations, period of observations, their latitude and longitude and parameters of linear trends (°C y^{-1}) for summer and winter.

Station	Period of observation	Latitude	Longitude	Summer trend	Winter trend
Magadan	1932 – 1990	59.5 N	150.8 E	-0.0023	0.0226
Okhotsk	1912 – 2002	59.4 N	143.2 E	0.017	0.0259
Ayan	1932 – 2002	56.5 N	138.2 E	0.0188	0.0182
Nikolaevsk-na-Amure	1925 – 2002	53.1 N	140.7 E	0.0064	0.0223
Yuzhno-Sakhalinsk	1942 – 2002	46.9 N	142.7 E	-0.0061	0.0233
Terney	1940 – 1994	45.0 N	136.6 E	0.0274	0.0334
Wakkanai	1938 – 2002	45.4 N	141.7 E	-0.007	0.0266
Abashiri	1890 – 2002	44.0 N	144.3 E	0.0037	0.0105
Nemuro	1880 – 2002	43.3 N	145.6 E	0.00004	0.0082
Akita	1886 – 2002	39.7 N	140.1 E	0.0097	0.0176
Izuhara	1887 – 2002	34.3 N	129.2 E	0.0049	0.0113
Simushir	1949 – 1997	46.9 N	151.9 E	0.0046	0.027
Icha	1935 – 1999	55.6 N	155.6 E	0.0078	-0.0016
Petropavlovsk-Kamchatskiy	1981 – 2002	53.0 N	158.7 E	0.0241	0.0433
Nikol'skoe	1922 – 2002	55.2 N	166.0 E	-0.0002	0.0039
Korf	1936 – 2002	60.4 N	166.0 E	0.007	-0.0418
St. Paul	1916 – 2002	57.1 N	170.2 W	0.0109	0.0042

oscillations. The seasonal signal is strongly manifested in air temperature in the area of the Okhotsk Sea (Fig. 2), so its modulations cause some difficultness for spectral analysis of observational data. For example, calculations of annual mean values are incorrect for future spectral analysis because of aliasing that can produce incorrect peaks. Probably this effect is one of the causes of inadequate results in a number of investigations of the climate problem.

To solve this problem, we analyzed summer mean (June-July-August) and winter mean (December-January-February) values separately as highest and lowest envelope of initial monthly mean data (Fig. 2). Additionally, we estimated the amplitudes of the annual harmonics that were calculated using least square method for each year. This parameter describes the modulation of seasonal oscillations most exactly.

Another cause of difficulties may be the unstable character of climate variations. So usually we obtain the wide, illegible peaks in the spectra of air and water temperature. It means that estimations of cycles are not sufficiently exact for weather forecasting.

The usual spectral methods give incorrect results for periods of more than 25 years with typical duration of observations 50-80 years. To solve this problem, we used the method of spectral-time analysis (Dzievonski et al. 1969) that is used to study changes in time of spectral amplitudes for different frequencies. This method is very close to the wavelet analysis.

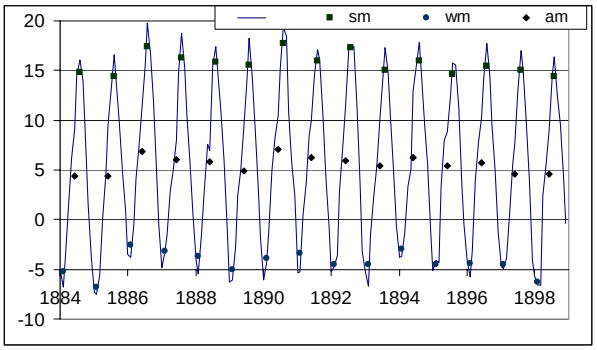

Fig. 2 Monthly mean air temperature and annual mean (rhombs), summer mean (squares) and winter mean values (circles) which were obtained from meteorological station Nemuro (northeastern Hokkaido Island).

The method reveals the temporal variability of spectral characteristics of a signal and achieves the most precise resolution in the low frequency bands. Briefly, the idea of this method is as follows. We choose a time series of air temperature (or another parameter) and the highest (ω_1) and the lowest (ω_N) frequencies corresponding to our interest and duration of observations. Also we choose a number (N) of frequencies from ω_1 to ω_N using a logarithmic scale. Fourier transformation was applied to each frequency; smoothing with the use of Gaussian filter is carried out in the frequency area. Inverse Fourier transformation is carried out for each frequency too, in this way we are obtaining the changing in the time of spectral amplitudes for different frequencies, the results are represented in spectral-time diagrams that look similar to wavelet diagrams.

All air temperature series were analyzed in the same way. At first, linear trends for annual mean, summer mean and winter mean values for each station were calculated using standard procedure of Microsoft Excel. Amplitudes of annual harmonics for each year were estimated and spectral-time diagrams for all parameters were constructed.

For easy comparison, the group of diagrams of the same type were normalized to the same spectral maximum that usually equals 1˚C for summer and annual amplitude and 2˚C for winter because of more intensive oscillations in this season. The color palette was scaled on a logarithmic scale from maximum (red color) with step 1 decibel. The blue color corresponds to the very weak oscillations; red, orange and yellow colors correspond to significant oscillations.

Results and discussion

Time series of annual mean, summer mean, winter mean temperatures, and linear trends for two of stations (Nemuro and Okhotsk) have a positive tendency in all cases. However, it is less expressed in the southern part of the Okhotsk Sea, relatively weak warming in winter about 1°C per 125 years and almost no trend in summer. In the northern part we observed significant winter warming (1°C per 40 years) and weaker in summer time (about 1°C per 60 years). We found the similar picture in the "continental" stations (Ayan, Nikolaevsk-na-Amure, Magadan, Petropavlovsk-Kamchatsky) and the "marine" stations (Abasiri, Akita, Izuhara, Simushir, Nikolskoe, St.Paul). Probably this difference is caused by different influences of Pacific Ocean and Asia continent where warming processes are well-expressed, especially in a winter time. "Winter cooling" was observed at the Korf station that is located somewhat north of the other stations. Probably, there are other atmospheric processes in this area.

Spectral-time diagrams for Okhotsk meteorological station are shown in Figure 3. In winter, high-frequency oscillations with 2-3 year periods are strongly manifested in the air temperature. These oscillations are not stable, resembling stochastic processes and therefore they have a negative effect for weather forecasting. We can see a very interesting effect of frequency deviation in the 6-10 year period band. In the first 25-year interval relatively low-frequency oscillations with periods 8-10 years were observed; in the next 25-year interval these periods changed to 5-7 years.

Relatively stable, well-expressed oscillations with period about 18-19 years can be seen in Figure 3. In contrast to high-frequency fluctuations, these oscillations may be a good base for the climate forecasting in winter.

In summer we can see the same picture of unstable high-frequency oscillations in the 2-10 year period band. There are also clear stable peaks at about 22-25 and 50 year periods. The great difference between low-frequency fluctuations in winter and summer is a very surprising result. It means that the changes of air temperature in warm and cold seasons have been influenced by different processes in atmosphere.

On the spectral-time diagram for Nemuro air temperatures in summer (Fig. 4), high spectral powers are evident at periods of about 55 and 25 years, which is similar to the Okhotsk station. Oscillations with 15-17 year periods are evident in the beginning and at the end of the time series, and 10-12 year periods appear in the middle of the series. The oscillations with periods of about 5-6 and 2-3 years are the most intensive and unstable.

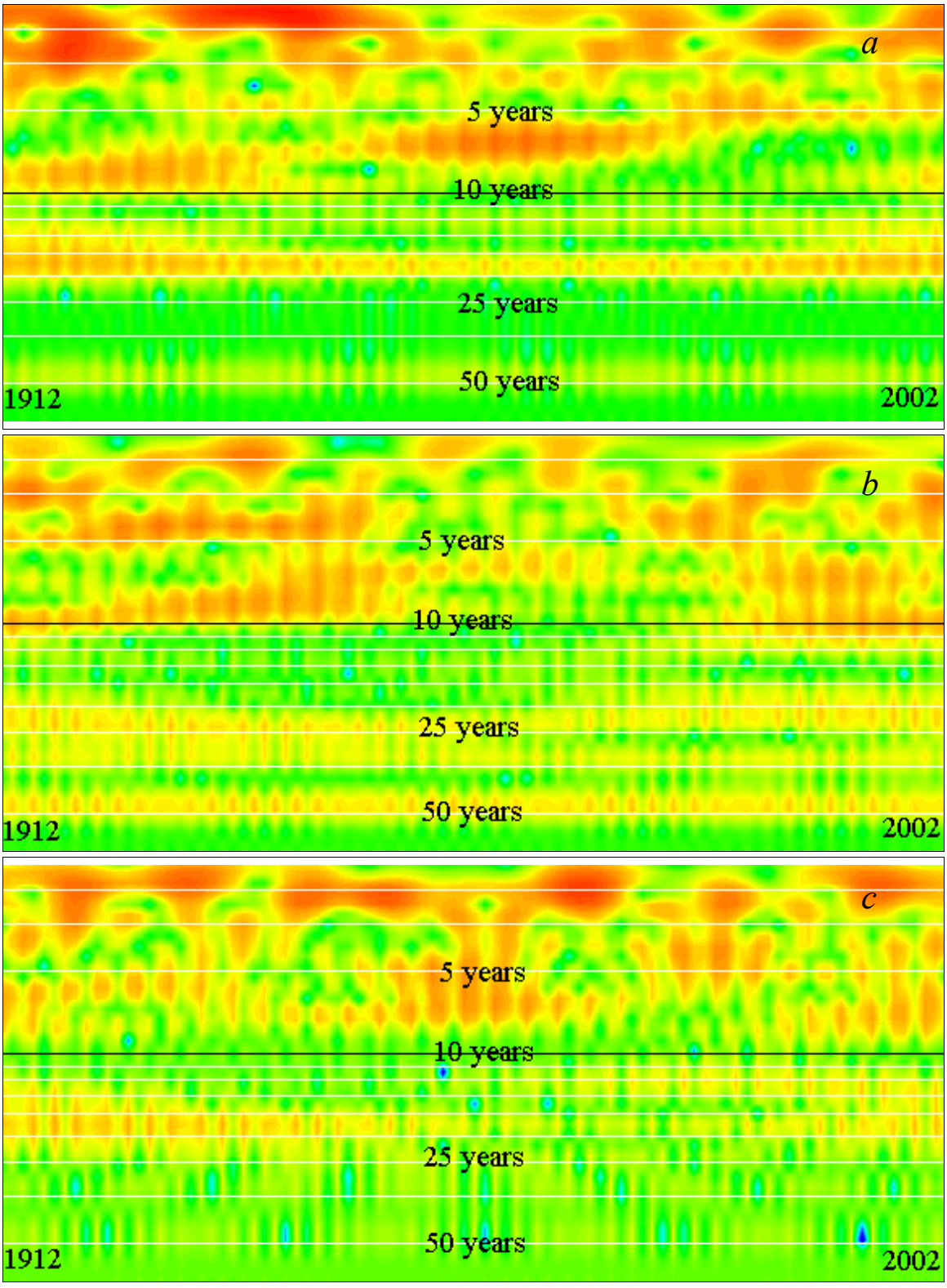

Fig. 3 Spectral-time diagrams of (a) winter mean air temperature, (b) summer mean air temperature and (c) amplitude of annual harmonics for the Okhotsk station. Horizontal axis is years and vertical axis is frequency on a logarithmic scale. Main periods are marked. Logarithmic palette is used with the step of 1 decibel from maximal spectral amplitude (red color) which is 2˚C (panel *a*) and 1˚C (panels *b*, *c*).

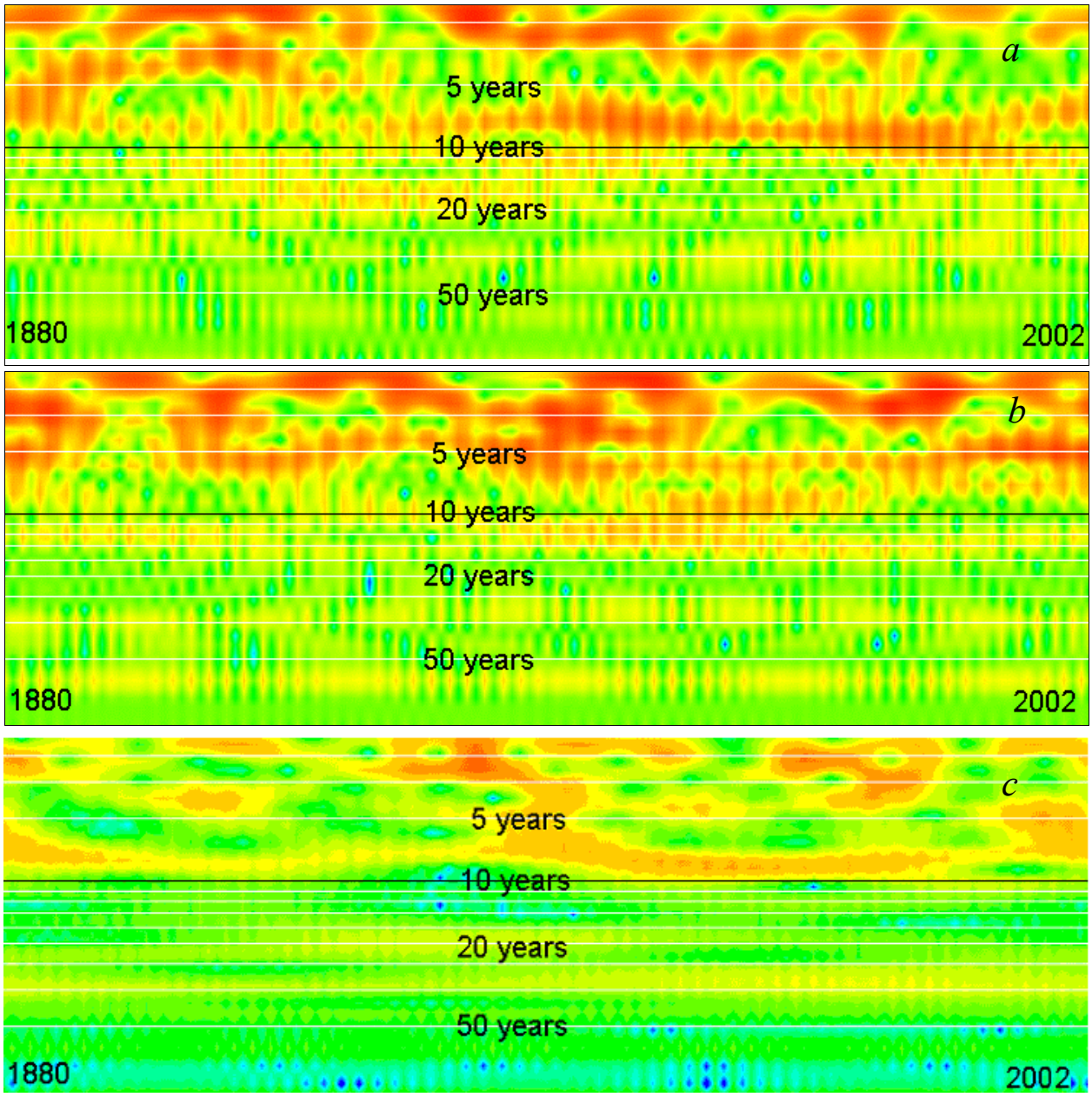

Fig. 4 Spectral-time diagrams of (a) winter mean air temperature, (b) summer mean air temperature, and (c) amplitude of annual harmonics at Nemuro, Hokkaido. Horizontal axis is years and vertical axes are frequency on a logarithmic scale. Main periods are marked. Logarithmic palette is used with the step of 1 decibel from maximal spectral amplitude (red color) which is 2˚C (panel *a*) and 1˚C (panels *b*, *c*).

In winter, the spectral-time diagram lacks variations with 25 and 50 year periods, and oscillations with 6-8 and 2-3 year periods dominate. Oscillations with 12-15 year periods appear midway through the time series. Station Abashiri (near Nemuro) has a major likeness with Nemuro, but it is not identical. Station Icha had a similar pattern with 5-7- year oscillations.

Now we shall consider stations that are located some distance from the Okhotsk Sea. At St. Paul (Bering Sea), interannual variability of air temperature has a very different character. There are 11-year oscillations, and at high frequencies, the spectrum decreases slowly with peaks poorly separated. In the 5-11 year frequency band, the structure of variations of frequency of cruption

outbursts is similar to the majority of stations in the Okhotsk Sea. In winter air temperature oscillations are stronger than in summer.

In the Korea Strait area (station Izuhara), the character of oscillations also differs strongly from those in the Okhotsk Sea. The low-frequency oscillations with periods more than 10 years are negligible in winter and summer. High-frequency fluctuations with 2-5 year periods dominate in this area. So, the spectral-time diagrams are characterized by non-stationary dynamic modes. The modes have a rather ranked character. They appear through the whole length of a series. As a rule, it is low-frequency oscillations. The 18-20 year rhythm prevails in them and 50 year oscillations are observed on the western coast of the Okhotsk Sea. It is noteworthy, that they also contribute to the formation Okhotsk Sea ice cover.

Conclusions

On the spectral-time diagram for temperature in summer, the bands of high spectral power are strongly expressed at periods of about 50 and 25 years, which testifies to the permanent presence of these oscillations. The oscillations with a 15-17 year period are marked in the beginning and in the end of the time series, and 10-12 year periods in the middle of the series. The oscillations with periods about 5-6 and 2-3 years are the most intensive.

The spectral-time diagram is different for winter. Low-frequency variations with 25 and 50 year periods are absent, and the oscillations with 6-8 and 2-3 year periods dominate. Oscillations with 12-15 year periods appear in the middle of the time series.

Thus the variations of climate in the northwestern Pacific in winter and summer seasons are formed by essentially different factors. As a result, different cyclic components were revealed by wavelet analysis.

References

Dzievonski, A., Bloch, S. and Landisman, M. 1969. The method of spectral-time analysis of seismological information. Bull. Seism. Soc. Am. 59: 427-444.

Kim, Y.S., Han, Y.H., Cheong, H.B., Dashko N.A., Pestereva, N.M. and Varlamov, S.M. 1997. Characteristics of weather and climate over the Okhotsk Sea. Journal of the Korean Fisheries Society 30: 974-983.

Pestereva, N.M. and Pushkina, H.G. 1998. Recent Climate Changes in the Okhotsk Sea Region. Climatic and interannual variability in the atmosphere-land-sea system in the American-Asian sector of Arctic. Proc. Arctic Regional Center. Vladivostok. Vol. 1: 11- 30 [in Russian].

Ponomarev, V.I., Trusenkova, O.O., Ustinova, E.I. and Kaplunenko, D.D. 1999. Interannual variations of oceanographic and meteorological characteristics in the Sea of Okhotsk. PICES Scientific Report No. 12: 31-40.

Ponomarev, V.I., Kaplunenko, D.D. and Ishida, H. 2000. The 20th century climate change in the Asian–Pacific region. Proc. of CREAMS 2000 Int. Symp., Vladivostok, May 15-16, 2000, pp. 129-136.

Ponomarev, V., Kaplunenko, D. and Ishida, H. 2001. Centennial and semi-centennial climatic tendencies in the Asian continental and Pacific marginal areas. Bulletin of Japan Sea Research Institution, Kanazawa University, Japan, Vol. 32: 77-90.

Ponomarev, V.I., Kaplunenko, D.D. and Ustinova, E.I. 2002. Climate change in the Northwest Pacific Margin and mid-latitude Asia. Reports of the International Workshop on Global Change Studies in the Far East. 7-9 Sept., 1999, Vladivostok, Russia, Vladivostok: Dalnauka, Vol.2. pp. 6-33.

Shevchenko, G.V. and Kato, A. 1999. Seasonal and interannual changes of atmospheric pressure, air and water temperatures in the area of the Kuril Ridge. PICES Scientific Report 12: 41-47.

Varlamov, S.M., Dashko, N.A. and Kim, Y.S. 1997. Climate change in the Far East and Japan Sea area for the last 50 years. Proc. CREAMS'97 Intern. Symp., Fukuoka, Japan. pp. 163-166.

Varlamov, S.M., Kim, Y.S. and Han, E.Kh. 1998. Recent variations of temperature in the East Siberia and in the Russian Far East. Meteorologiya i Hidrologiya. Vol. 1, pp. 19-28 (in Russian).

The influence of atmospheric processes on the water circulation off the west Kamchatka coast

Eugeniy Samko, S.Y. Glebova and V.M. Petruk
Pacific Fisheries Research Centre (TINRO-Centre), 4 Shevchenko Alley, Vladivostok, 690600 Russia. e-mail: petruk@tinro.ru

The basic elements of the water circulation off the west coast of Kamchatka are (Fig. 1b):

- West Kamchatka Current is a northward stream that is initiated by the penetration of Pacific waters through the northern Kuril straits;
- The Compensatory Current is a southward current that reaches from the Khayryuzovo shoals along the Kamchatka coast up to Bolsheretsk;
- Mesoscale features of various nature.

These characteristics were derived from the usual representations (Luchin 1982, Luchin 1987, Figurkin 1997, Chernhyavskij, 1981).

Considering the position and orientation of the West Kamchatka and Compensatory currents, it is possible to assume the presence of connection between these streams. However, analysis of their volume transports in springs of 1983-1995 (Figurkin 1997) has shown that intensive development of the Compensatory Current was observed both in years with small and large volume transports in the West Kamchatka Current. Hence, a direct connection between these two streams is absent. It is necessary to note that the location of the calculated sections varied such that, to some degree, subjectivity may have affected the results.

In the present work, the authors have considered the interrannual variability of characteristics of West Kamchatka and Compensatory currents and have tried to connect it with the variability of synoptic atmospheric processes above the Okhotsk Sea.

Table 1 Data sources.

Year	Data	Vessel	Number of stations	Depth of observation (m)
1984	06.05	Mys Yunony	5	200
1985	18-19.04	Mlechniy Put	10	200
1986	19-20.04	Darvin	7	200
1987	14-15.05	Lensk	5	200
1988	16-18.04	Mys Dalniy	8	500
1989	18-19.04	Pr. Kaganovskiy	10	200
1990	30.04	Mys Tihiy	6	200
1991	12-17.04	Shantar	7	200
1992	22-23.04	Shantar	6	200
1993	11-12.04	Novokotovsk	8	500
1995	18-19.04	Borodino	4	500
1996	16-17.04	Lesozavodsk	6	500
1997	17-18.04	TINRO	7	500
1998	15-16.04	TINRO	6	500
1999	15-16.04	TINRO	8	500
2000	19-20.04	TINRO	7	500
2001	23-24.04	TINRO	7	500
2002	21.04	Pr. Kaganovskiy	7	500

The oceanographic information was obtained from 18 TINRO-TURNIF complex surveys off the West Kamchatka coast in the spring period of 1983-2002 (Table 1). The analysis of maps of the dynamic topography constructed from the results of all surveys has shown that, in most cases, the West Kamchatka and Compensatory currents are observed on 53-56°N. Therefore, for comparison among years, an east/west section along 55°N was selected.

Geostrophic currents speeds relative to 500 dbar and the water transport in a layer of 0-500 m were calculated. As measurements of temperature and salinity were often executed up to 200 m, current speeds and volume transport were also calculated to a 200 dbar surface. Characteristics of the atmospheric circulation above the Okhotsk Sea basin were estimated by methods developed by one of authors especially for Okhotsk Sea (Glebova 1999, Glebova 2002). The identification of synoptic types was made using ten-day average maps of surface pressure for the period 1980-2002. The main criterion used to identify types was the position of the main pressure formations (cyclones and anticyclones) relative to the Okhotsk Sea. In total, seven types of atmospheric processes were identified.

From the same 10-day synoptic maps, values of the Kats index (Kats 1960) were calculated for the area 40-60°N, 130-160°E, which provided an estimate of the interannual variability of intensity and orientation of meridional movement of air masses above the Okhotsk Sea basin. The anomalies of the Kats index relative to their average for the period of 1980-2002 were used for the analysis.

The analysis of the location of currents along the 55°N section indicates that during all periods of observation the midstream of the West Kamchatka Current was situated between 153°30' – 154°30'E (Fig. 1c), while the Compensatory Current was situated to the east of 154°30'E (Fig. 1). Both streams can be traced to the bottom.

The ocean depth in the area of the West Kamchatka Current is about 500 m, and about 200 m or less in the area of the Compensatory Current. So 500 and 200 m depths are logical choices as reference levels for calculating dynamical characteristics. However, as was shown earlier (Table 1), surveys with observations up to 500 m were carried out, basically, in second half of the period (56 percent of cases).

The volume transports of the West Kamchatka Current relative to 200 and 500 dbar reference levels are given in Table 2. From this, it is possible to conclude that the basic volume transports of the West Kamchatka Current occur in the top 200-meter layer (the ratio between Q200 and Q500 varies from 0.71 up to 0.82). An exception occurred in 2002 when this ratio was 0.39.

Comparison of the volume transports of the West Kamchatka Current relative to 200 and to 500 dbar indicates a close correlation (r= 0.97 at significant factor of correlation 0.87 with confidence level 99.9%). Hence, the tendencies of interannual variability of volume transports of the West-Kamchatka Current for a 500-meter thickness can be inferred from calculations of volume transports relative to a 200 dbar level. Using this approach almost doubles the number of observations.

Table 2 The volume transport of the West Kamchatka Current on the section along 55°N.

Parameter	**Year**									
	1988	**1993**	**1995**	**1996**	**1997**	**1998**	**1999**	**2000**	**2001**	**2002**
Q_{200}, Sv	0.77	0.56	1.24	1.04	0.93	0.32	0.58	0.62	0.4	0.24
Q_{500}, Sv	0.99	0.74	1.62	1.46	1.28	0.39	0.79	0.79	0.56	0.61
Q_{200}/Q_{500}	*0.78*	*0.76*	*0.76*	*0.71*	*0.73*	*0.82*	*0.73*	*0.78*	*0.71*	*0.39*

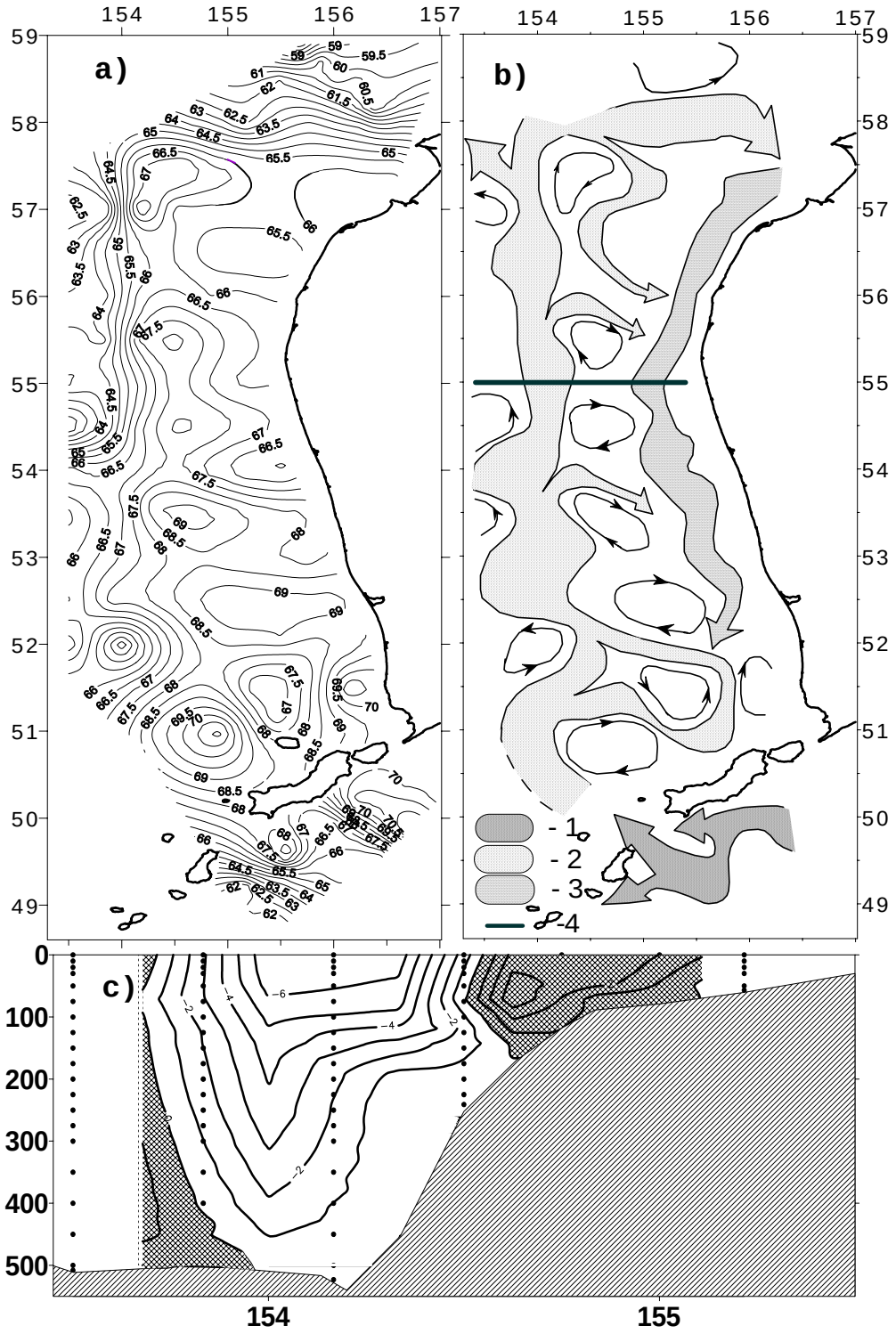

Fig. 1 Circulation off the west coast of Kamchatka in spring of 2001. (a) The dynamic topography relative to 500 dbar (dyn. Dm); (b) Geostrophic currents off West Kamchatka where: 1 – Kuril Current, 2 – West Kamchatka Current, 3 – Compensatory Current, and 4 – section along 55°N; (c) The distribution of current speed values on the 55°N section; cross-hatched area is southerly flow.

Table 3 Volume transports 0-200 dbar of the main currents off the West Kamchatka coast on the section along 55°N.

Current	Year								
	1984	**1985**	**1986**	**1987**	**1988**	**1989**	**1990**	**1991**	**1992**
West Kamchatka	0.24	0.39	0.40	0.24	0.77	0.37	0.28	0.23	0.24
Compensatory	0.02	0.07	0.08	0	0.09	0	0	0.02	0
	1993	**1995**	**1996**	**1997**	**1998**	**1999**	**2000**	**2001**	**2002**
West Kamchatka	0.56	1.24	1.04	0.93	0.32	0.58	0.62	0.40	0.24
Compensatory	0.04	0	0	0	0.02	0.03	0.06	0.08	0

In Table 3, the variability of volume transports of the West Kamchatka and Compensatory currents relative to 200 dbar along 55°N is presented. Note that the volume transport of the West Kamchatka Current has varied from 1.24 Sv in 1995 down to 0.23 Sv in 1991. The maximal volume transport of the Compensatory Current was 0.09 Sv and this occurred in 1988. This current was not observed along 55°N in 1989, 1990, 1992, 1995-1997 and 2002.

Several periods of direct or contrary dependencies between the volume transports of these currents were observed (Fig. 2). Thus it may be to eliminate the periods of 1984-1990, 1993, 1999-2000, when the increase or reduction of West-Kamchatka current volume transport resulted the similar changing of the Compensatory Current volume transport. In 1991-1992, 1995-1998, 2001 there was recorded the contrary picture.

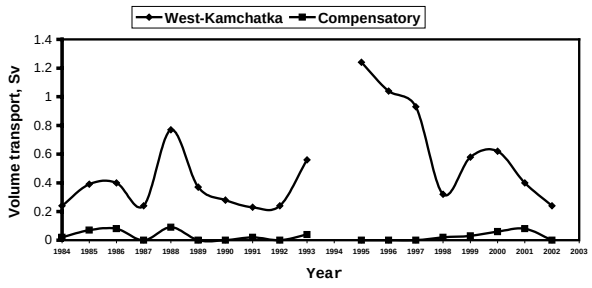

Fig. 2 Interannual variability of volume transports in the West Kamchatka and Compensatory currents along 55°N.

As a working hypothesis, it was proposed that the interdependence of these currents were conditioned by the prevalence of certain types of synoptic atmospheric processes in the region.

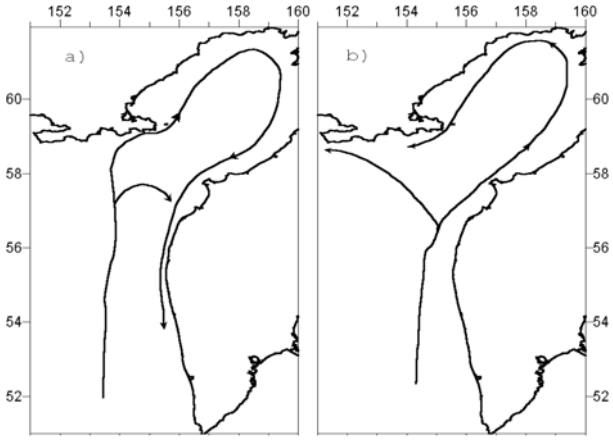

Fig. 3 Direct (a) and reverse (b) dependencies between volume transport of the West Kamchatka and Compensatory currents.

During periods of small pressure gradients or when westward and northwestward forcing occurred, the West-Kamchatka Current flows along the Kamchatka coast, enters Shelikhov Bay and forms part of the clockwise circulation in the bay, leading to the formation of the Compensatory Current (Fig. 3a). When eastward and northeastward predominate, transport in the main part of the West Kamchatka Current deviates to the west, taking part in the circulation along the northern Okhotsk Sea shelf. Under these conditions, it does not penetrate into Shelihov Bay and does not influence the Compensatory Current. In years of increased intensity of the West Kamchatka Current, part of this current flows northward along the west coast of Kamchatka (in

the region where the Compensatory Current normally forms) causing cyclonic circulation in Shelikov Bay and preventing the formation of the Compensatory Current (Fig. 3b).

To test the hypothesis, we constructed diagrams of interannual variability of the frequency of synoptic atmospheric patterns (Fig. 4). As the character of currents mostly likely depends on the influence of wind driven transports during the long previous period, the data on total recurrence of identifiable typical synoptic situations during the entire previous year were used.

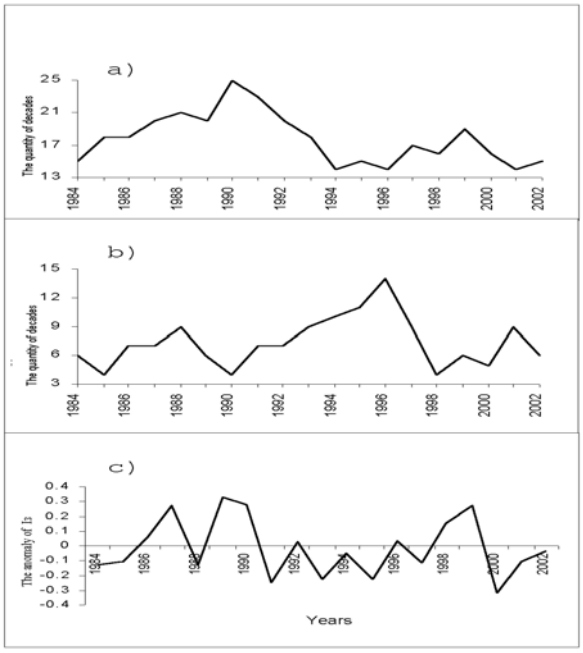

Fig. 4 Interannual variability of frequency of types of the atmosphere synoptic patterns above the Okhotsk Sea: (a) I+IV types (westward and weakened transfer); (b) VI+VII types (mainly eastward transfer in the northern part of the Okhotsk Sea; (c) annual average anomaly of zonal index – Iз.

Synoptic patterns were summarized according to:

a. The recurrence of the small gradient I type (with weak and unstable transport) and type IV causing the distribution above mostly water area of northwest and western winds.
b. Wind transports of primarily eastward orientation which are connected mainly to types VI and VII. Under type VI eastward transport dominates over the entire Okhotsk Sea basin, while under type VII, transport is influenced by cyclonic circulation, winds from the south above the West Kamchatka shelf and eastward over northern part of Sea of Okhotsk.

As was noticed earlier, up to approximately 1992, the development of the West Kamchatka and Compensatory currents was uniform, their strengthening and weakening occurring simultaneously. The analysis of diagrams indicates, that over this period, there was a gradual increase of the total amount of types I and IV (average frequency of these two types was about equal during 20 ten-day periods in the year). The frequency of synoptic types VI and VII was low (6 times in a year). Thus the frequency of atmosphere processes with westward and/or weakened transports exceeded the frequency of eastward direction of air mass transfer by more than three times. The diagram of zonal Kats index anomalies (Fig. 4c) illustrates the trend and intensity of this atmosphere circulation quantitatively. It is obvious that positive anomalies of the zonal Kats index predominated up to 1992. This is related with a noticeable strengthening of westward transports in those years.

After 1992 the atmospheric regime changed and the frequency of types I and IV decreased to an average of ≤16 10-day periods in a year. The mean level of recurrence of types VI and VII increased up to eight 10-day periods (maximum of 13 in 1996). Thus, the change in proportions of synoptic processes was reflected in the formation of resulting transports. The predominance of negative zonal Kats index anomalies during this period may indicate a weakening of westward circulation and even to possible changes in eastward transports.

Therefore, it is quite logical to consider that those changes which are evident in the character of the correlation of the West Kamchatka and Compensatory currents, namely the existence of periods of synchronous and asynchronous changes in volume transports are closely connected to reorganizations in the atmosphere, especially with changes in the character of atmospheric circulation above the Okhotsk Sea.

It may also be possible to interpret why a positive correlation between both currents appeared in 1999 and 2000 given the tendency for a negative correlation after 1993. In those years, a change in the behavior of atmosphere processes (Fig. 4) occurred again. The frequency of types I and IV increased, and the frequency of types VI and VII decreased sharply. That change in the atmosphere regime was influence at once on the character of atmosphere circulation; the zonal Kats index anomalies were positive and achieved levels observed during the 1980s. The strengthening of the westward transfers above the Okhotsk Sea did not persist, but it affected the character of water circulation in subsequent years. In 1999 and 2000 the volume transport trends for the West Kamchatka and Compensatory currents were synchronous.

References

Glebova, S.Yu. 1999. Types of synoptic situations and the weather phenomena connected to them above Sea of Okhotsk. Izv. TINRO 126: 572-586.

Glebova, S.Yu. 2002. Classification of processes above the Far East seas. Meteorology and Hydrology 7: 5-15.

Kats, A.L. 1960. Seasonal changes of the general circulation of an atmosphere and long-term forecasts. Hydrometeoizdat, 270 p.

Leonov, A.K. 1960. Regional oceanography. Hydrometeoizdat, 766 p.

Luchin, V.A. 1982. Diagnostic calculation of circulation of waters of Sea of Okhotsk in the summer period. Trudy DVNII 96: 69-77.

Luchin, V.A. 1987. Circulation of waters of Sea of Okhotsk and features of its inner year variability by results of diagnostic calculations. Trudy DVNII 36: 3-11.

Moroshkin K.V. 1964. The new scheme of surface currents of Sea of Okhotsk. Oceanology 4: 641-643.

1998. Sea of Okhotsk / Hydrometeorology and hydrochemistry of the seas. The project "Sea". V. 9, N 1. Hydrometeorological conditions: Hydrometeoizdat. 342 p.

Teylor D. 1985. Introduction in the theory of mistakes. World, 272 p.

Figurkin A.L. 1997. Circulation of West Kamchatka shelf waters in the spring of 1983-1995. Complex investigations of the Okhotsk Sea ecosystem. VNIRO: 25-29.

Chernhyavskij V.I. 1981. Circulating systems of Okhotsk Sea. Izv. TINRO 105: 13-19.

EOF and wavelet analysis of satellite SST data in the northern Pacific

George Shevchenko, Zhanna Tshay and Constantine Puzankov
Sakhalin Research Institute of Fisheries and Oceanography (SakhNIRO), 196 Komsomol'skaya Street, Yuzhno-Sakhalinsk, 693023 Russia. e-mail: shevchenko@sakhniro.ru

Introduction

Climate variability is a very important problem for people, hydrobiology and fishery, that is why so many researchers from different countries are studying it. This problem is priority for SakhNIRO too. Biologists of our institute usually need a forecast of abiotic conditions in the Sea of Okhotsk and adjacent of waters for two-three years. The main question they are interested in is what will happen, for example in 2005; will it be "cold" or "warm". To answer this question, we need to study the cyclical fluctuations of climate because such fluctuations with trends of temperature are the basis for any climatic forecast. Also, we should understand the mechanisms of the formation of these cycles in order to be sure of our results. Therefore determination of low-frequency SST cycles and their spatial extent in the North Pacific was a main goal of our work.

Interannual changes of air and water temperature are very difficult subjects to analyze because interannual variability is manifested as a modulation of seasonal variations. The seasonal signal is very strong with a well-expressed peak in the spectra of SST oscillation in the Okhotsk and Japan seas, so its modulation is a cause of some problems for SST data analysis. The example of GDAAC SST data in the spots which are located in these basins are shown in Figure 1.

To solve this problem, we analyzed the summer mean (July – August – September) and winter mean (January – February – March) SST series separately, although for the Okhotsk Sea, the winter SST data is not adequate because of ice cover, therefore we did not consider these results in the present work. Also we analyzed the changes of amplitude of the annual harmonics that were calculated for each year separately using least square method for each spot in the North Pacific. The annual harmonic is the main constituent of the seasonal signal, so year-to-year changes of the annual amplitude describe its low-frequency modulation most exactly. That is why we considered this parameter most carefully in the present work.

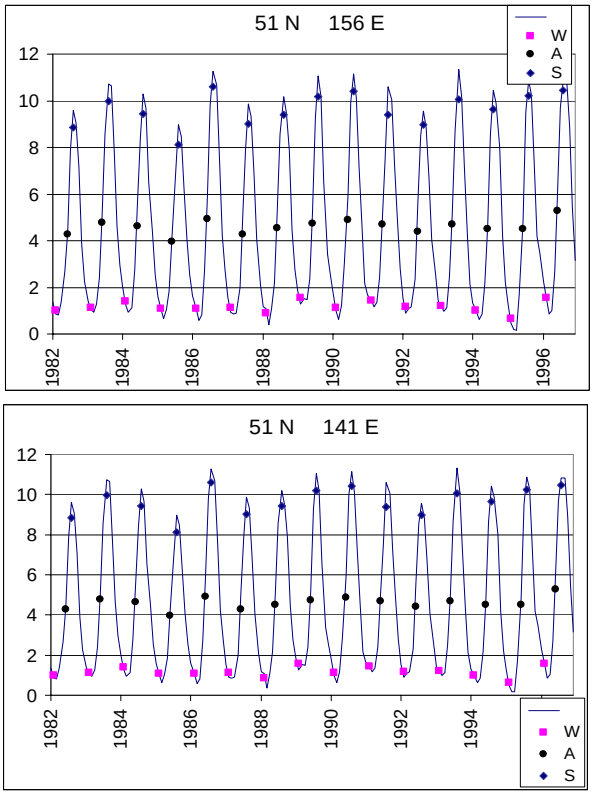

Fig. 1 Monthly mean SST at coordinates 51˚N 141˚E (Tartar Strait, Sea of Japan) and 51˚N 156˚E (Sea of Okhotsk) and annual mean (circles), winter mean (red squares) and summer mean values (rhombs).

Data and method

We used the 15-year (1982-1996) series of GDAAC monthly mean SST data in the northern part of Pacific that were averaged by 1° squares. We see two methods of analyzing these data sets. The first is to calculate spectra at each spot and to make maps of the spectral amplitudes for the periods represented by the main spectral peaks.

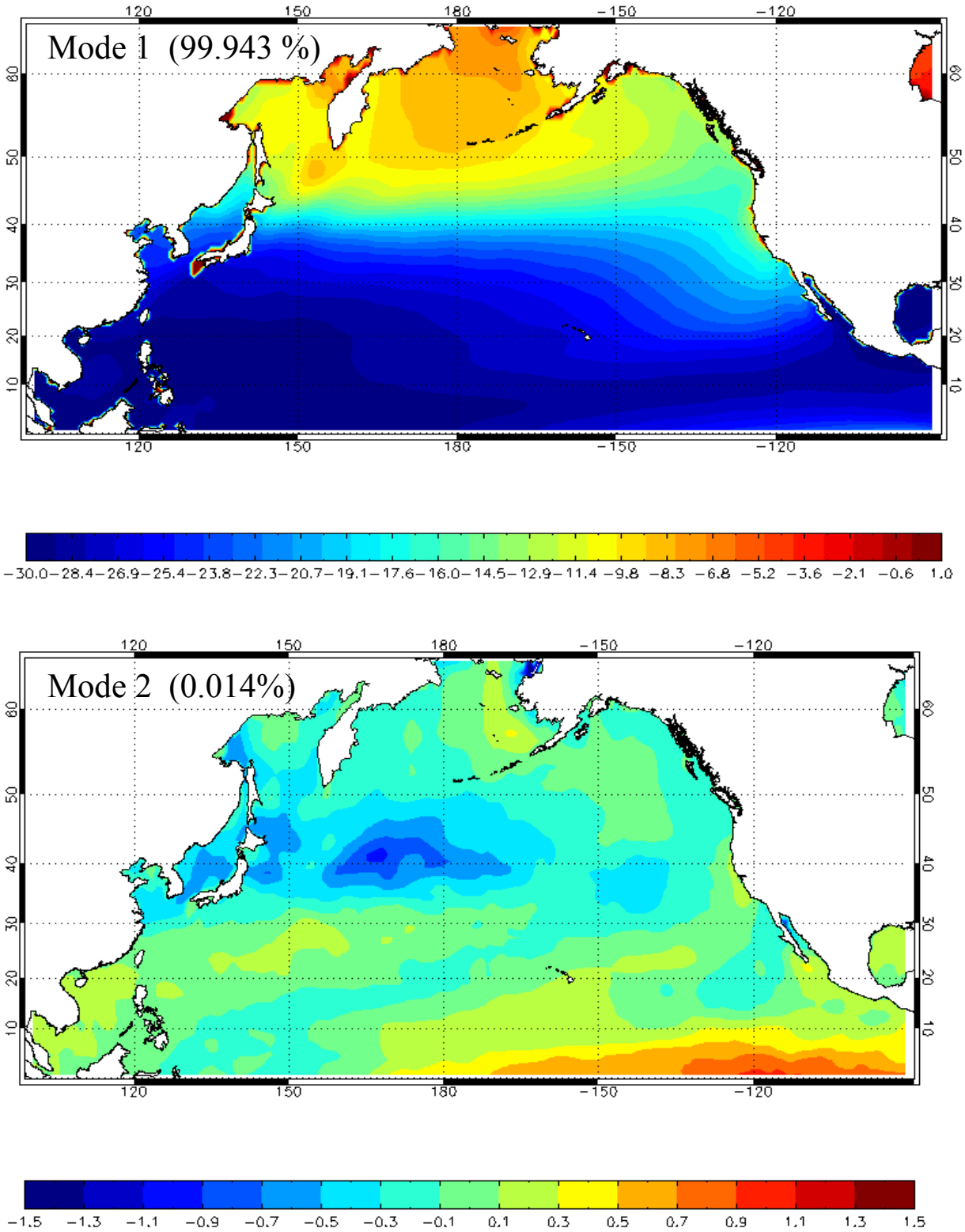

Fig. 2 Summer average SST (July-August-September) from GDAAC data 1982-1996, spatial distribution of first (upper picture) and second (lower) EOF modes.

However we have not yet prepared the necessary software for such a large database. Another way is use to EOF method to analyze the spatial structure of summer and winter mean SSTs and to use spectral-time analysis (one kind of wavelet method) to estimate main peaks in amplitudes of several EOF modes.

Results and discussion

The first modes of both winter and summer SSTs (Fig. 2) describe water temperature changes with latitude. Some interesting properties of SST (relatively cold water off California and warmer water near Alaska) can be recognized. The amplitude of this mode is almost exactly -1˚ (Fig. 3) and its change with time is negligible.

The distribution of the second mode (Fig. 2) is more interesting. We see the opposite character of SST changes in equatorial zone (values are about 1

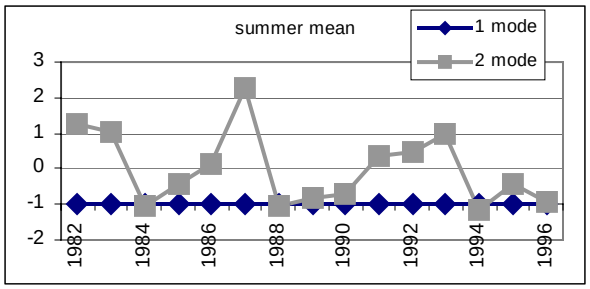

Fig. 3 Amplitudes of 2 first EOF modes of summer mean SST.

~ 1.3) and in the area of the Kuroshio and Tsushima Warm Currents, and also in the western part of the Okhotsk Sea (-1.75 ~ -1.3). The amplitude of this mode had changed from -1 up to 2.5, and oscillations with period about 5 years area apparent in the spectral-time diagram (Fig. 4). It is interesting that we did not obtain a decadal cycle from our analysis of summer SST data.

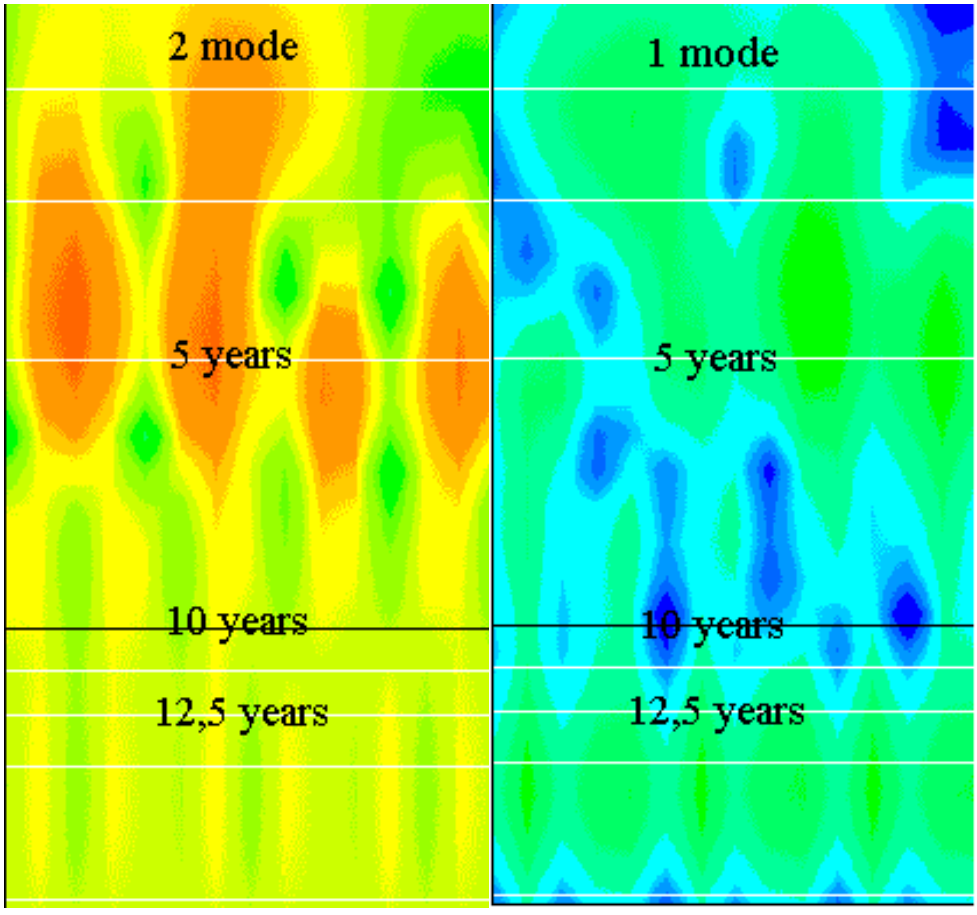

Fig. 4 Spectral-time diagrams of amplitudes of two first EOF modes of summer mean SST (horizontal axis is time in years, and the vertical axis is frequency, with the main periods marked). Spectral maximum (red color) equals 0.1˚C for first and 2˚C for second mode, logarithmic scale palette with step 1 decibel.

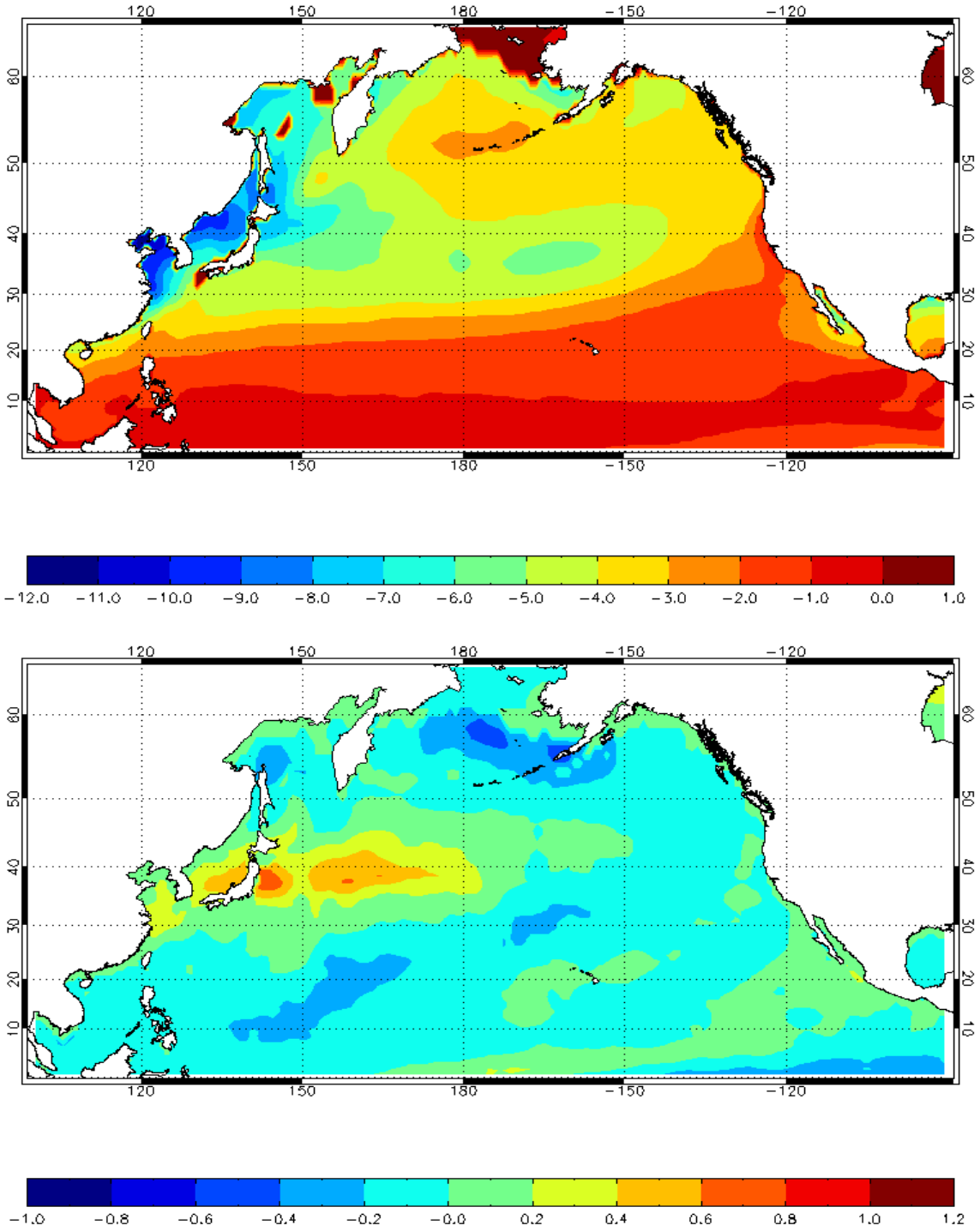

Fig. 5 Amplitude of annual harmonic calculated from monthly mean SSTs from GDAAC data 1982-1996, spatial distribution of first mode (98.88%, upper panel) and second mode (0.24%, lower panel).

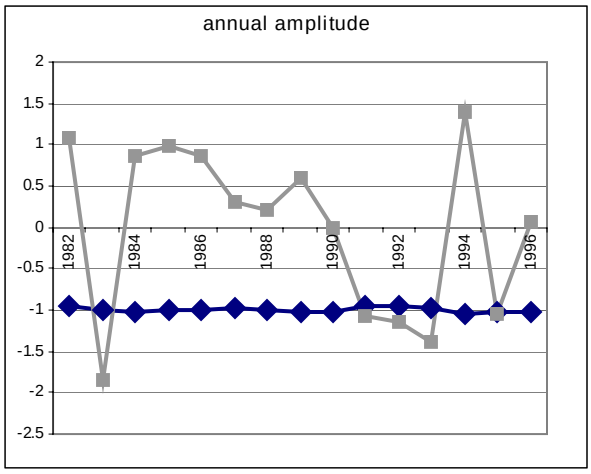

Fig. 6 Amplitudes of first (■) and second (◆) EOF modes of amplitude of annual harmonics.

However, the most interesting results were obtained for amplitude of annual harmonic. The spatial structures of two first modes are shown in Figure 5 and their amplitudes are shown in the Figure 6. The values of the first mode are negative for almost all points in the northern part of the North Pacific. The amplitude of this mode is about –1, indicating that equatorial and tropical areas have relatively weak seasonal changes. The opposite is evident in the Yellow and Japan seas. In the area of the Kuroshio and North Pacific currents, where the seasonal signal is very strong, the amplitude of the annual harmonic reaches 10-12˚C (total changes are about 20-24˚C).

We obtained a complex structure in the Sea of Okhotsk. There are strong seasonal oscillations in the southwestern and northwestern parts of the sea, and weak ones near Kashevarov Bank, and in the central and northern parts of the Kuril Ridge.

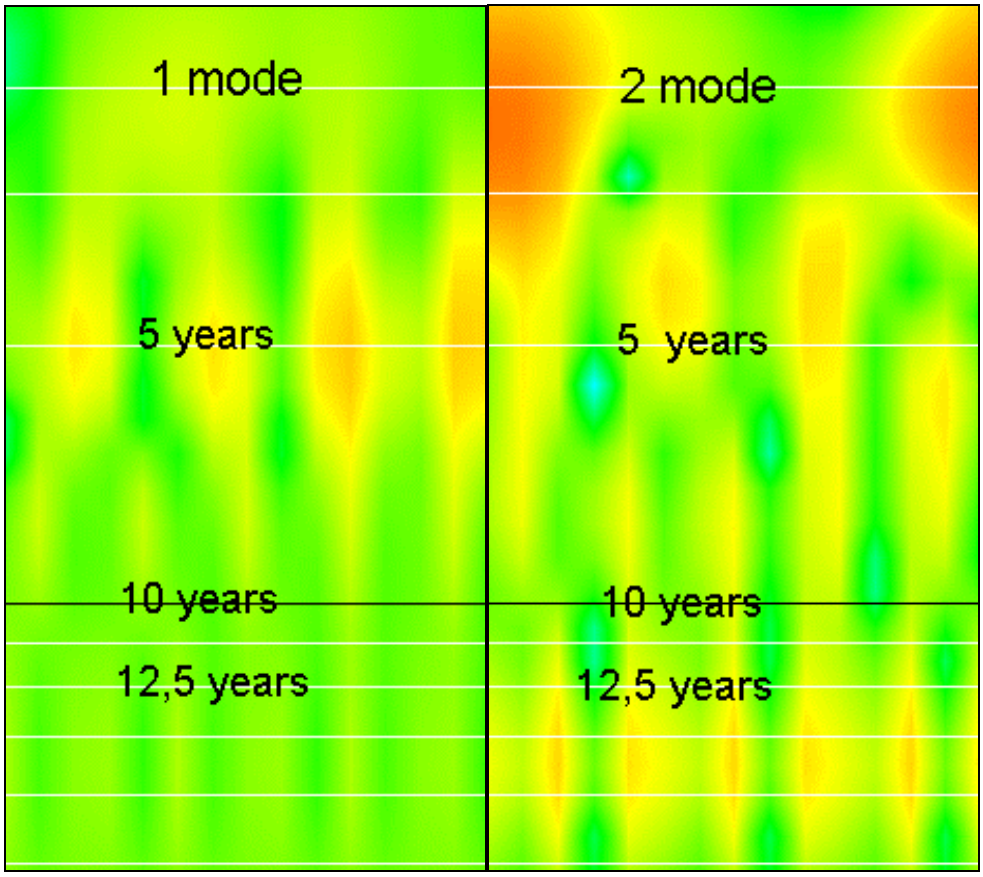

Fig. 7 Spectral-time diagrams of the amplitudes of the two first EOF modes of annual harmonic amplitude. Horizontal axis is years, vertical axis is frequency, main periods are marked. Spectral maximum (red color) equals 0.1˚C for first and 2˚C for second mode, logarithmic scale color palette with step 1 decibel.

Areas of the Kuroshio and Tsushima Warm currents are strongly manifested in the structure of the second EOF mode (positive values). Areas with negative values can be seen in the eastern part of the Bering Sea and in the Sea of Okhotsk, northeastward from Sakhalin Island.

We used wavelet analysis to determine the interannual variability of first and second mode amplitudes. Spectral-time diagrams are shown in Figure 7. Only one peak with a period of about 5 years is seen in the spectra of the first mode. The amplitude of this five year cycle is relatively small (about 0.1°C), however for the southwestern part of the Okhotsk Sea it reaches 1°C, for Yellow Sea and western part of Japan Sea it reaches 1.2°C.

A low frequency peak with a period of 13-14 years and some unstable high-frequency oscillations with periods of 2-4 years were determined in the spectra of second mode. Probably, the period of observation is too short to determine low frequency oscillations exactly so our results are very limited, and we will develop our study using more complete SST data.

Conclusion

Modulation of SST seasonal oscillations in the northern Pacific was studied using EOF and wavelet analysis. Well-expressed 5-year cycles were found in the summer SSTs and in the amplitude of the annual harmonic in the area of the Kuroshio and Tsushima Warm currents as well as in the western part of Okhotsk Sea.

The 5-year cyclical fluctuation may be useful and effective for the forecast of abiotic conditions in the Okhotsk and Japan seas and adjacent waters of Pacific Ocean. The more low frequency oscillations and their spatial scales were estimated inexactly because of the short period of observations. More reliable results may be obtained by analysis of more complete data.

References

Miller, A. 2002. Decadal variability in the Pacific and its effect in marine ecosystems. PICES Eleventh Annual Meeting, Program & Abstracts (October 18-26, 2002, Qingdao, People's Republic of China). 185p.

Minobe, S. 2002. A review of decadal variability over the North Pacific and some ideas for future studies// PICES Eleventh Annual Meeting, Program & Abstracts (October 18-26, 2002, Qingdao, People's Republic of China). 185p.

Minobe, S. 2002. Interannual to interdecadal changes in the Bering Sea and concurrent 1998/99 changes over the North Pacific. Progress in Oceanography.55: 65-76.

Minobe, S. and Mantua, N. 1999. Interdecadall modulation of interannual atmospheric and ocean variability. Progress in Oceanography 43: 163-192.

Does the fresh water supply from the Amur River flowing into the Sea of Okhotsk affect the decadal variation of the sea ice?

Yoshihiro Tachibana[1], M. Ogi[2], M.A. Danchenkov[3]

[1] IARC, Frontier Research System for Global Change, Tokyo, 105-6791 Japan. / Research Institute of Civilization, Tokai University, Hiratsuka, 259-1242 Japan. e-mail: tachi@rh.u-tokai.ac.jp

[2] Institute of Low Temperature Science, Hokkaido University, Sapporo, 060-0819 Japan.

[3] Far Eastern Regional Hydrometeorological Research Institute, 24 Fontannaya Street, Vladivostok, 690600 Russia.

The impacts of ground hydrology on the high-latitude oceans, such as melting glaciers and discharge from rivers in the oceans, can affect global climate by mediating the flow of low-density, fresh water inflow that strengthens the ocean's stratification. This suppresses the thermohaline circulation and also promotes sea-ice formation. Our time series analysis based on sea-ice and river-discharge data indicates that the effect of this fresh water on the sea-ice in the Okhotsk Sea, into which the second largest Siberian River, the Amur, discharges, is relatively unimportant. Interannual variations in the ice extent are negatively correlated with the amount of discharge. We find circumstantial evidence that the inflow of warmer river water tends to raise the sea surface temperature, and that it suppresses ice formation in the following winter. This potential explanation for the negative correlation implies that sensible heat transported by large rivers in high latitudes should be reconsidered in studying global climate change.

Anemobaric effect on the water area of the La Perouse Strait

Andrew A. Bobkov[1] and Valery Yu. Tsepelev[2]
[1] Saint-Petersburg State University, St. Petersburg, 199178 Russia. e-mail: abbk@AB2480.spb.edu
[2] Information Centre of Weather, 48 Prof. Popova Street, St. Petersburg, 197022 Russia.
e-mail: v0010200@rol.ru

Introduction

The Kantakov and Shevchenko (2001) article "The analysis of residual currents in the La Peruse Strait associated with the level variation and wind effect" has attracted our attention because of an interpretation of a unique long-term experiment to measure currents in La Perouse Strait in 1999 using mooring stations located just in the middle of the strait. One interesting result, and an emphasis in the paper, was the observation of a change in the flow vectors that occurred twice, on March 6-7 and 21, which the authors explained as variability of the Soya Current that normally enters the Okhotsk Sea at the mooring station location. One reason for what might have caused such turns was described by Kantakov and Shevchenko as the result of a storm and its accompanying east wind. In the present work, we have decided to continue research in this direction in order to support or deny their viewpoint.

Data sources

1. Illustrations borrowed from Kantakov and Shevchenko (2001), a refereed paper;
2. Daily northern hemisphere sea level pressure mean field from NCAR taken from the 5° latitude by 5° longitude data set;
3. Daily northern hemisphere surface U and V wind components from NCEP/NCAR re-analysis taken from the 2.5° latitude by 2.5° longitude data set at a point 45°N, 142.5°E;
4. Merged altimetric TOPEX/POSEIDON data set obtained from the NASA Physical Oceanography Distributed Active Archive Center at the Jet Propulsion Laboratory/ California Institute of Technology.

All the materials were picked up for a period from November till March 1999-2002, however with purposes of expanding the research period, the additional data for March for the period 1980-2003 were used. In total, 712 daily synoptic situations were studied.

Results and discussion

According to common viewpoints, the Soya Current in La Perouse Strait is generally deemed to have an east- and southeastward flow that is more expressed in the warm period of the year. Maximum of the flow velocity occurs in August-September when its speed reaches 2-3 knots. The velocity minimum occurs from December – February. It is assumed that the Soya Current is driven be the sea level difference between the Japan and Okhotsk seas.

Aiming to study anemobaric situations over La Perouse Strait area in those months when the Soya Current is poorly developed, we first chose all daily synoptic maps for a period from November to March during which current vector observations were available. Figure 1 shows an example of current vector reversals in February-March 1999. These cases correspond to only two types of synoptic situations (Fig. 2):

- sea level center of a deep cyclone settles down over Hokkaido Island and a high pressure area is located above the Okhotsk Sea. In this case the significant meridional sea level pressure gradient zone stretches over the La Perouse Strait. This zone causes strengthens east direction winds;
- sea level center of deep cyclone is located southeastward of La Perouse Strait and the high pressure area is found toward the northwest. Winds of a northeast direction predominate over the area under discussion.

Storm winds of east and northeast directions that are maintained for 1 to 3 days tend to favor the occurrence of barogradient currents which should prevail above the permanent ones from the Japan Sea. Their consequence should be a storm surge observed at coastal stations in rows of sea level and sea surface temperature as well as in short-term turn of vectors of the surface flow from general southeast direction to west and northwest, that will cause movement of water from the Okhotsk Sea. However, wind forcing cannot be considered as the only cause of the turn of water flow. As it is shown in Figure 3, changes of wind at the nearest grid point to La Perouse Strait do not fully confirm the current changes except on March 15-17 and 18-22; the direct correlation being absent on March 6-8. That is why we suppose that not only storm winds from the east, but sea level pressure distributions affect the sea surface through baric gradients causing differences in level and as result, the reversal of the Soya Current.

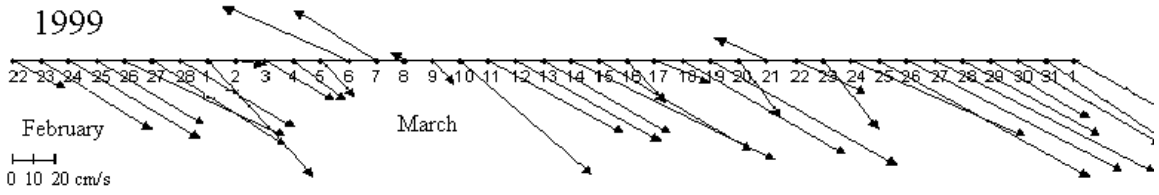

Fig. 1 Vectors of currents in the La Perouse Strait drawn by Kantakov and Shevchenko.

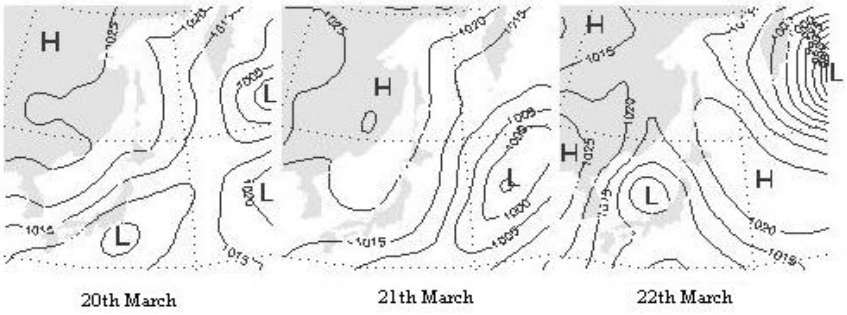

Fig. 2 Anemobaric situations contributed to the Soya Current reversal in March 1999.

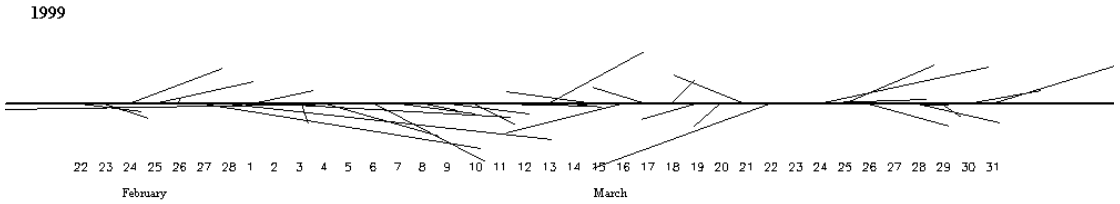

Fig. 3 Re-analysed vectors of winds at point 45°N, 142.5°E.

In Table 1, the dates of current reversals observed in Figure 1 are aligned with occurrences of strong easterly wind and baric center locations. Of 16 cases when the current changed, 14 cases (87%) correspond to east or northeast winds and in 12 cases (75%), the centers of cyclones were located directly above Hokkaido Island. It should be noted that the influence of the anemobaric effect is evident down to a depth of 45 m (second horizon of measurements) after a lag of about two days.

Analysis shows that synoptic situations above La Perouse Strait area, when storm winds of east direction develop, are observed rather frequently. In all Marchs from 1980 to 2003, 74 cases were revealed, in which there could be a potential opportunity for Soya Current reversal due to the influence of eastern storm winds.

Table 1. Correlation between dates of turn of current in the La Perouse Strait and east winds.

	Anemobaric situations Azn/Zn	Dates of turn of current	Predominant dates with east storm wind
1	+	02.03.1999	27-28.02.1999
2	+	06-08.03.1999	05.03.1999
3	+	21.03.1999	20-22.03.1999
4	-	02.12.2000	n.a.
5	+	07-10.12.2000	05-10.12.2000
6	-	14-15.12.2000	n.a.
7	+	16.12.2000	16.12.2000
8	+	24-25.12.2000	23.12.2000
9	+	27-28.12.2000	26.12.2000
10	+	31.12.2000	30-31.12.2000
11	+	04-06.01.2001	02-04.01.2001
12	-	14.01.2001	11-13.01.2001
13	-	16-18.01.2001	17-18.01.2001
14	+	21.01.2001	21.01.2001
15	+	26-27.01.2001	25-27.01.2001
16	+	07.03.2001	04-07.03.2001

In March, for last 23 years, it is possible to identify three periods of increased probability of storm winds of easterly direction. These are dates from March 3 to 8, 14-18 and 20-24. In 31% of cases, the anemobaric situations that can cause strengthening of wind surges and promote Soya Current reversals are revealed on March 15-18 and 24.

Concluding remarks

Joint analysis of synoptic and oceanographic situations confirms Kantakov and Shevchenko hypothesis that winds cause a reversal of the current vectors. Hence, such situations in the La Perouse Strait area in winter can arise sporadically. In the summer-fall period when the Soya Current is fully developed, its flow does not react to the anemobaric effect and reversed flow does not occur. It should be noted that the influence of cyclones was observed at up to 45 m depth after a one to two day lag.

Processes affecting the Soya Current extension in the La Perouse Strait area have a very complex character, with tidal influences and other disturbances like eddy formation. Moreover, it is suggested that the reversed flow occurs during the winter period because the sea level difference between the Japan and Okhotsk seas is minimal. That is why it is not correct to assume that winds are the only cause of flow reversals. The barometric pressure field only favors barogradient currents stretching into the Japan Sea during periods when the the permanent flow is weekly developed in winter.

References

Kantakov, G.A. and Shevchenko, G.V. 2001. Dynamic processes on the shelf of Sakhalin and the Kuril Islands. Edition of Institute of Marine Geology and Geophysics, Sakhalin Science Center FEB RAS. Yuzhno-Sakhalinsk, 2001. pp.62-74 (in Russian).

Dynamics of temperature and solar shine of cold period at the coast of the Far East

N.V. Grichkovskaja and V.A. Platonova
Far Eastern State University, 8 Sukhanova Street, Vladivostok, 690600 Russia.
e-mail: platonova@meteo.dvgu.ru

This work was carried out within the framework of research of climatic changes along the Russian Far East coast. The purpose of this work, in particular, is to understand the change of various meteorological parameters at the coast of the Far East, especially changes of the last decade. The choice of points of observations was defined by the duration of observations in areas that are useful for studying changes and fluctuations of climate, and secondly, by the continuity of record, and thirdly, by the availability of the information on the Internet. Five Far Eastern locations, located mainly in the coastal zone, were selected. These included Magadan, Nikolaevsk-na-Amure, Poronaisk, the Sovetskaja Gavan, Rudnaja Pristan and Vladivostok. The period of observations ranged from 1917 to 2002.

To define dates of steady transitions of air temperature, downturns and increases with step-type behavior 10°C from 0 up to -30°C were used the daily data inside the cold period. Also the mode of duration of solar light and short-wave solar radiation was considered.

For the cold period, the basic statistical characteristics of the monthly sums of duration of solar shine, total and direct solar radiation have been designed for horizontal and normal surfaces to a beam. Also these characteristics paid off for dates and durations of the periods with a various level of temperatures. Inertia of processes was investigated on the basis of various communications.

From the analysis of average values and factors of variation of the specified characteristics it is possible to note the following. The monthly sums of light exposure are minimal in December. For all considered zones, the small share of a nucleus of winter in all the cold period is characteristic. Inertia of winter processes is well shown on all considered stations. In particular the beginning of the cold period everywhere predetermines its duration and duration of the period with temperatures lower than 0°C and more -10°C. Duration of the period with the lowest temperatures is connected to the date of its beginning. The greatest variability characterizes dates of transition of temperature increases.

Dynamics of researched meteorological values in a long-term section have been appreciated with use of a linear trend, averaging of Afanasieva, and also with the help of the autocorrelation and spectral analysis.

As any statistical size, factors of autocorrelation are subject to casual fluctuations. Therefore tests of their significance were conducted. Confidence intervals inside which the researched characteristic with probability of 95% did not differ from zero.

It has been determined, that practically all researched parameters it is possible to count process of change casual, that is these lines statistically are homogeneous. However on 95% a significance value some factors of correlation overstep the bounds of confidence area, but at more rigid confidence level (99%) all factors of autocorrelation do not differ from zero.

Average of meteorological process received by method Афанасьева, reveal in researched lines middle-period (cycles of 1 rank) and long-period (cycles 2 ranks) fluctuations.

Cycles of the first rank at all stations are comparable on duration. The period of them changes from 9 till 20 years. As in researched lines long fluctuations (cycles 2 ranks) with the periods of 50-100 years for dates of transition through 0° in the autumn and about 50 years for

dates of transition through 0° are revealed in the spring.

For calculation of functions of spectral density lines have been transformed into lines of sliding five years' average in volume of 80 values. The maximal shift has been designed proceeding from 10% of accuracy of its calculation, and has made 40 years. The basic functions of spectral density have allocated the periods of fluctuations bringing the greatest contribution to variability of researched sizes.

Thus, for the majority of stations the most significant are middle-period fluctuations of researched meteorological value. During the winter period the coast of the Far East possesses significant enough stocks of a solar energy. For last decade duration of the cold period decreases.

Variability of the West-Kamchatka Current during 1995-2002

Gennady V. Khen and N.S. Vanin
Pacific Fisheries Research Centre (TINRO-Centre), 4 Shevchenko Alley, Vladivostok, 690950 Russia.
e-mail: khen@tinro.ru

In the mid-1990's TINRO-Center began to sample a hydrographic section from Sakhalin Island to Kamchatka Peninsula (49°30' - 52°19'N). The basic purpose is to estimate the inter-annual variability of temperature, salinity and water transport of the West Kamchatka Current (WKC). As a rule, the section is being conducted during March-April when the western half of the sea is covered with an ice fields and the eastern part (to the east of 149°E) of the section is accessible only for research. Nevertheless the WKC front, located between 150-154°E, is encompassed completely by investigations.

Cooling of the Okhotsk Sea started in late 1990s, occurring non-uniformly. In the active layer (0-200 m) it began in 1998-1999 and has lasted till 2001. In intermediate and deep waters a sharp downturn of temperature occurred in 2000. In the early part of the next decade, a general increase of temperature in the whole water column developed but values remained below those observed during the mid-1990's. During the 1995-1997 warm period positive SSTs prevailed. In intermediate layers an uplift of deeper waters along the continental slope was noted. The core of deep Pacific waters, identified by the 2.5°C isotherm rose to 600 m, and its width attained 150-200 km. During the 1999 till 2001 cold period, negative SSTs dominated, and an uplift of the deep waters was not observed. The core of deep water was located beneath 700 m and its width did not exceed 150 km.

The salinity in the 0-200 m layer conformed to that of temperature. In deep layers an appreciable salinity rise was observed in 1999 and 2001. That related to a strengthening of the WKC, the intensity of which depends on water exchange with the Pacific. Along with weakening of the WKC in the beginning of current decade the salinity decreased to the level of mid 1990s.

Sea surface temperature in the Sea of Okhotsk has a high correlation ($r = -0.95$ with 95% level significance) with an ice cover extent that, in turn, depends on intensity of cooling. The temperature of intermediate and deep waters is well correlated with each other ($r = 0.96$) and with current velocities in the layer 500-1000 m (-0.82 and –0.81 m s^{-1} respectively) that reflects the intensity of inflow of Pacific water.

Thus thermohaline changes in the upper and deep layers are influenced by different causes. Respectively, the correlation between the sea surface and deep water temperature is weak ($r = 0.5$), indicating that inter-annual changes in different layers of the Okhotsk Sea do not occur in an identical mode and processes there should be investigated individually.

The interannual variability of the water temperature of the Okhotsk Sea

Vladimir A. Luchin[1], I.A. Zhigalov[2] and V.V. Plotnikov[3]

[1] Far Eastern Regional Hydrometeorological Research Institute, 24 Fontannaya Street, Vladivostok, 690600 Russia. e-mail: vluchin@hydromet.com

[2] Pacific Research Fisheries Centre (TINRO-Centre), 4 Shevchenko Alley, Vladivostok, 690600 Russia. e-mail: zhigalov@tinro.ru

[3] V.I. Il'ichev Pacific Oceanological Institute, Far-Eastern Branch of Russian Academy of Sciences, 43 Baltiyskaya Street, Vladivostok, 690041Russia. e-mail: vlad_plot@poi.dvo.ru

The interannual variability of thermal conditions in the Okhotsk Sea has been described in papers by Vinokurova T.T. (1965, 1972), Kitani (1973), Davydov I.V. (1975), Chernyavsky V.I. (1973, 1992), Pavlychev V.P. et al. (1989), Luchin V.A. and Lavrentiev V.M. (1997), Figurkin A.L. (1997), Moroz V.V. (1999), Zhigalov I.A. (2000, 2001), Zhigalov I.A. and Luchin V.A. (2002), and Khen G.V. (2002). These authors used different criteria to identify long-term water temperature fluctuations. Data was analyzed for several parts of the sea only, some data sets being limited in time. In addition, there are gaps in observational series that, on the whole, made it difficult to define warm and cold periods in the Okhotsk Sea thermal regime.

We examined the long-term variability of the oceanographic regime of the Okhotsk Sea in the second half of the twentieth century using data at about 94,000 oceanographic stations that were collected by different organizations in Russia, Japan, and the U.S.A. To assess interannual variability, the Okhotsk Sea was divided into relatively homogeneous regions of 2° latitude by 3° longitude.

Water temperature anomalies arising from the influence of thermodynamic factors are evident for a long time within a year and cover extended areas because large-scale characteristics of water temperature distribution at the depth of 50 m that form in winter are preserved till September and because seasonal warming of the top quasi-homogeneous layer in spring and summer does not, as a rule, exceed 30 m depth.

The spatial and temporal structure of the water temperature fields were analyzed and the missing data restored using the method of initial fields decomposition by the empirical orthogonal functions (EOF). To exclude the seasonal trend, water temperature data were preliminarily centered, i.e. every calculated point was represented as a deviation from the average multi-year monthly values at 50 m depth. The fields reconstructed from the yearly anomalies of water temperature registered from March to July served as the initial data for calculations.

The first four components of the EOF decomposition (Fig. 1) describe the main features of the large-scale thermal variability. Components of a higher order are formed under the influence of multiple small-scale factors that are difficult to interpret. Besides, the variability of higher-order components is of a magnitude that is comparable with the error level of the observations and calculation process. Thus, their exclusion may be interpreted as additional data smoothing that minimizes generality of the system analyzed.

The first EOF is related to synchronous interannual fluctuations over much of the Okhotsk Sea (Fig. 1), except the very southern part. The second EOF shows lower-scale processes, maximum variability being observed in the very southern part of the sea. This component also reflects the antiphase character of water temperature fluctuations in the northern and southern areas. The third EOF shows the antiphase character occurring in the central part of the sea and peripheral areas. As is seen from the spatial pattern of the fourth component, thermal processes in the central and southern part of the sea are in antiphase position with the northern part of the sea and the area adjacent to the Kuril Islands (Fig. 1).

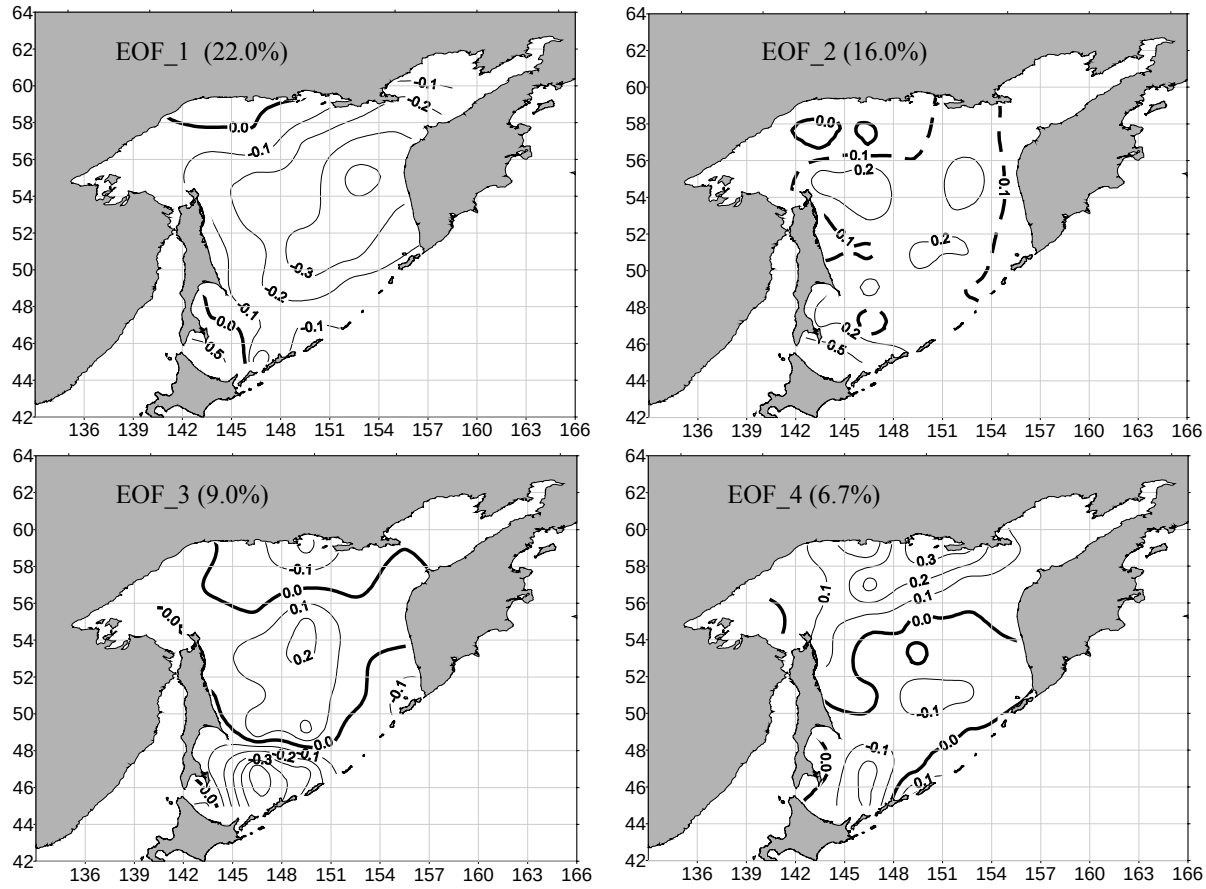

Fig. 1 Distribution of the first four EOFs of water temperature at 50 m depth in the Okhotsk Sea.

As was noted above, the first component describes the largest scale processes and accounts for the synchronous fluctuations in water temperature within the Okhotsk Sea. Other components show the redistribution of the thermal potential between separate parts of the Okhotsk Sea and reflect local influences. Thus, they should be taken into account when assessing the thermal regime of separate parts of the Okhotsk Sea. This is especially critical for the waters that are subject to the influence of EOF component extremes. This is confirmed by a correlation matrix that shows the comparative significance of the first EOF component and the sum of the first four components for those areas where component extremes are found (Fig. 2).

Table 1 Correlation matrix of contribution of the first EOF component only with the sum of the first four components for the different "squares" of the Okhotsk Sea.

	(v1) a	**Sum.(a)**	**Sum.(b)**	**Sum.(c)**	**Sum.(d)**	**Sum.(e)**	**Sum.(f)**
v1(a)	1	0.89	-0.72	0.83	0.26	0.18	0.71
Sum.(a)	0.89	1	-0.35	0.96	0.29	0.14	0.63
Sum.(b)	-0.72	-0.35	1	-0.34	0.02	0.04	-0.50
Sum.(c)	0.83	0.96	-0.34	1	0.00	0.02	0.44
Sum.(d)	0.26	0.29	0.02	0.00	1	0.28	0.73
Sum.(e)	0.18	0.14	0.04	0.02	0.28	1	-0.13
Sum.(f)	0.71	0.63	-0.50	0.44	0.73	-0.13	1

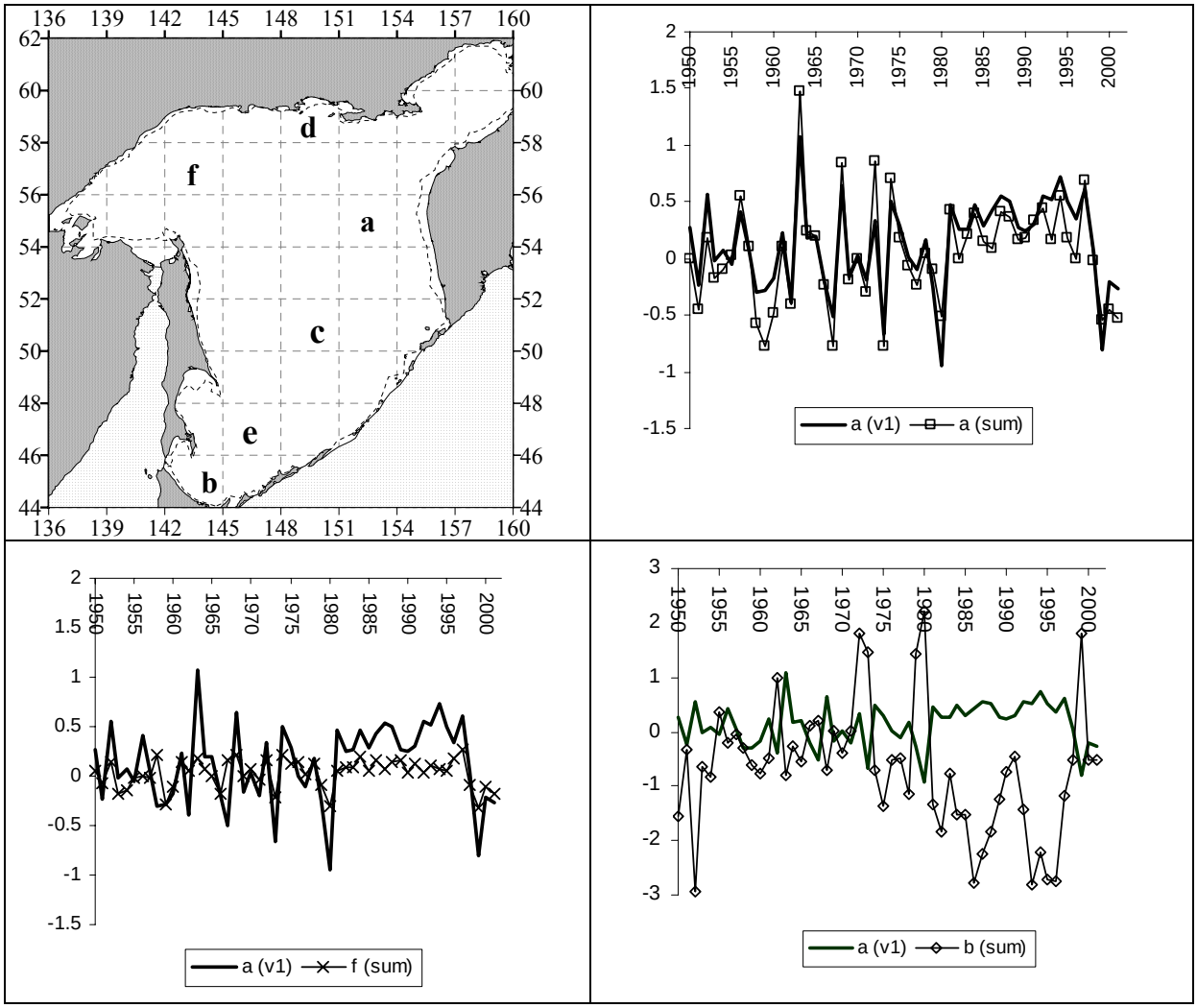

Fig. 2 Interannual variability of contribution of the first EOF component only (bold) and the sum of the first four components (light) at the horizon of 50 m (ºC) for the different squares of the Okhotsk Sea.

The temporal variability of the first EOF and that of the sum of the first four components is also assessed (Fig. 2). Analysis of the diagrams indicates that 2-4-year fluctuations make the main contribution of water temperature variability. The following climatic tendencies are traced in the thermal regime of the Okhotsk Sea (Fig. 2). They indicate a warming period from the 1970s to middle 1990s and a cooling period from mid-1990s to the present.

Acknowledgements

This work was supported in part by the Russian Foundation for Basic Research (grant No. 01-05-64098a).

Typification of thermal structures in the Japan Sea by satellite information

Aleksander A. Nikitin and A.M. Kharchenko
Pacific Fisheries Research Centre (TINRO-Centre), 4 Shevchenko Alley, Vladivostok, 690600 Russia.
e-mail: root@tinro.marine.su

Composite images of the distribution and variability of fronts, eddies, and currents make it difficult for researchers to understand variability of oceanographic conditions of the Japan Sea and to allocate annual patterns to one type or another. The results of processing and analysis of satellite information for the last 20 years now make it possible to classify annual conditions in the Japan Sea which greatly simplifies the analysis of interannual variability. In a basis the rule of the Subarctic "Polar" front in western part of the Japan Sea was offered to this typification, as its general rule in central and in east part remains rather stationary. Three are allocated such as a rule of the Subarctic front in western part of the sea: southern, northern and intermediate (Fig. 1). Conditionally it is possible to consider, that at the first type (C) in area of a northwest part of the sea, at southern Primorye there are conditions for a type of "cold" years, at second (W) - "warm" years, and at third (Int.). - intermediate. We speak "conditionally", as the allocated types testify only to prevalence of subtropical waters to north, or subarctic to the south. The absolute meanings of temperatures at the surface of the sea thus can be above or below average, and at a "warm" type on our classification in a northwest part of the sea the negative anomalies of temperature or, on the contrary can be marked, at a "cold" type - positive. In addition, to the basic three types, two subtypes were added: (Ca) – a cold subtype when strong southward advection of cold coastal currents along coast of Korea and southern Primorye, and (Wa) – occurs when there is significant development of the East Korean Current and, as the result, significant northward advection of heat along the coast of Korea with only a narrow, rather cold zone.

The classification scheme was applied to all seasons. On the basis of this scheme, almost all 1980s appeared cold, and based on the development of a branch of the Tsushima Current in the 1990s, are similar to years with significant development of the East-Korean current (warm

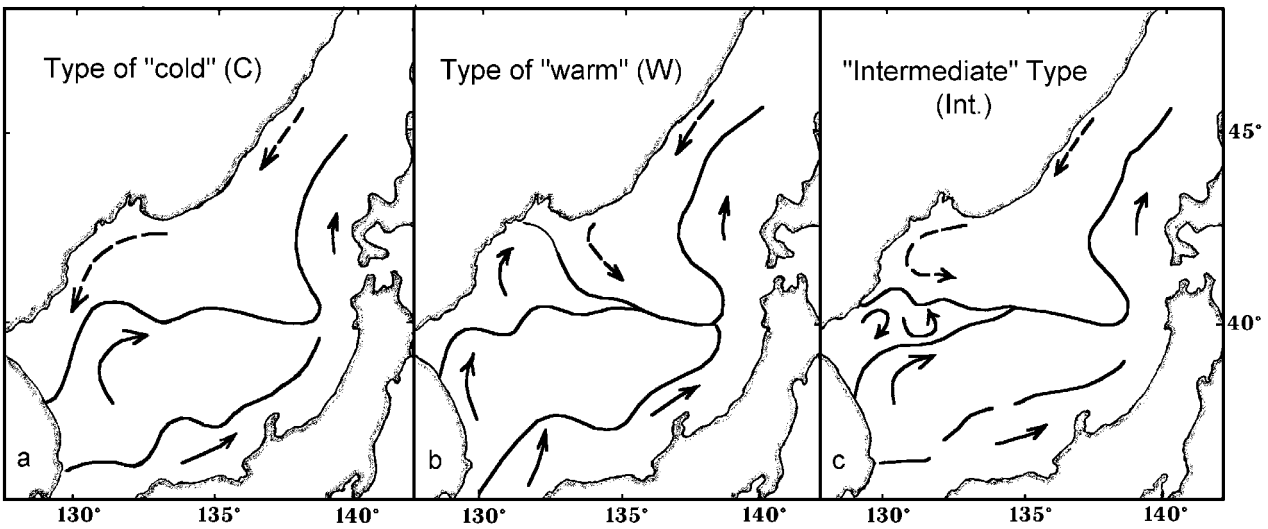

Fig. 1 Characteristic spatial patterns of major currents and the Subarctic "Polar" front in the Japan Sea during "cold" years (C), warm years (W), and intermediate years (Int.).

type). The same type can persist in all seasons (e.g.: 1982 and 1995) and there are years (e.g.: 1981, 1983, 1984) when different types appear within a single year. This is due to the direct influence of solar radiation and the atmosphere, especially during summer seasons.

It is natural that pure types of each classification are not observed in nature. The general picture is complicated by vertical structure of branches of currents, meandering, and also seasonal and interannual variability of conditions. It is influenced by the monsoon climate. The large influence changes the character of exchange of water through the three straits (Korean, Tsugaru, La Perouse). Therefore, hydrological structures in the Japan Sea can differ substantially from the offered pattern. It is also brings an interesting perspective that the mechanism of advection of waters to Peter the Great Bay, as it can be connected to the direction and volume of flows and deep-sea of fishes living in the winter in the southern part of the Japan Sea.

The main thermal patterns (fronts, eddies and meanders) are reported in Table 1.

Table 1 Typification of thermal patterns (fronts, eddies and meanders) in the Japan Sea by the satellite information.

N	Season	Type of Season	Year
1	Winter	C* Ca**** W** Wa*****	1981, 1983, 1984, 1986, 1988 1982, 1987 1985, 1990, 1992, 1993, 1995, 1996, 1997, 1998, 1999 1979, 1980, 1989, 1994, 2000, 2001 1991
2	Spring	C* Ca W Wa Int.***	1977, 1981, 1983, 1985, 1987, 1988 1982 1990, 1995, 1996, 1997, 1998, 1999 1979, 1980, 1984, 1986, 1989, 1992, 1993, 1994, 2000 1978, 1991
3	Summer	C Ca W Wa Int.	1986, 1985, 1987 1982, 1983 1980, 1988 1981, 1984, 1989, 1992, 1993, 1994, 1995, 1996, 1997, 1998, 1999, 2000 1990, 1991
4	Autumn	C Ca W Wa	1985 1982, 1983, 1984, 1987, 2000 1988, 1989, 1990, 1994, 1995, 1996, 1997, 1998, 1999 1979, 1991, 1993 1980, 1981, 1986, 1992

*- Type of Cold; ** - Type of Warm; *** - Intermediate; ****- Type of Cold (cold of subtype (Ca)); ******- Type of Warm (warm of subtype (Wa)).

Last isolation of Kuril Island as a result of post-glacial transgression

Sergey P. Pletnev
V.I. Il'ichev Pacific Oceanological Institute, Vladivostok, Russian Academy of Science, 43 Baltiyskaya Street, Vladivostok, 690041 Russia. e-mail: annin@poi.dvo.ru

The main morphological features and shape of the modern coastal line of the Sea of Okhotsk were formed by the Pleistocene (about 1.8 million years ago). The further evolution of the basin was basically limited by global climate changes, reflected in the alternation of interglacial and glacial epochs. Growth and melting of polar ice caps resulted in fluctuations of sea level from minus 110-130 m to plus 10 m (Markov and Syetova 1965). Modern ecosystems in the Kuril archipelago were formed over the course of the large-scale Late Wurm regression and following transgression.

At the last climatic minimum (15-18,000 y.b.p.) the sea level was lower by 130 m and most of the modern shelf was land. We constructed a map of Sea of Okhotsk of that time (Beszvernyi et al., 2002) where the islands of Sakhalin, Hokkaido, Kunashir, and probably Iturup formed a single block connected with Prymorye. The islands of Paramushir and Shumshu were connected with Kamchatka. The islands of Urup and Black Brothers were combined as separate territorial blocks, and also Ekarma, Shiashcotan, Harimcotan and Onecotan, apparently. At this time, various species of biota were available to penetrate from the south and the north. However, severe climatic conditions interfered with the penetration of thermophilic elements from the south, and migrations from the north were interfered by Krusenstern's, Byssol, and Frieze deep-water passages.

Global warming started about 15-13,000 y.b.p. and the postglacial transgression began. The rate of sea level rise was maximal (8 mm y^{-1}) before 7000 years, which was reduced thereafter to 1.4 mm y^{-1}. The transition from cold conditions was very sharp, so in eastern China for example, the average annual air temperature rose by 7°C over a period of 800 years (13,200-14,000 ybp) (Yang Yuai-jen, 1983). The recent isolation of the southern and northern Kuril islands began (Table 1), and it had a significant influence on the modern biota of the Kuril islands.

Table 1

Strait	Islands	Average depth (m)	Time of isolation (ka)
First Kuril	Kamchatca-Shumshu	50	10.0
Second Kuril	Shumshu-Paramushir	28	8.5
Kreniscan	Onecotan-Harimcotan	54	10.5
Severgina	Harimcotan-Shiashcotan	98	12.5
Urup	Black Brothers-Urup	180	15.0-14.0(?)
Katerina	Iturup-Kunashir	230	15.0-14.0(?)
Izmena	Kunashir-Hokkaido	25	7.5
Nevelscoy	Sakhalin-Primorie	15-20	7.0
Laperusa	Hokkaido-Sakhalin	60-70	12.0-11.0

SESSION 2
PHYSICAL AND CHEMICAL PROCESSES IN THE OKHOTSK SEA AND NORTHWESTERN PACIFIC OCEAN (Convenors: Yutaka Nagata and Vyacheslav Lobanov)

Definition of spatial variability of tide characteristics in Sea of Okhotsk from satellite altimetry data

George Shevchenko[1], Alexander Romanov[2] and Alexey Bobkov[3]

[1] Sakhalin Research Institute of Fisheries and Oceanography (SakhNIRO), 196 Komsomol'skaya Street, Yuzhno-Sakhalinsk, 693023 Russia. e-mail: shevchenko@sakhniro.ru

[2] All-Russia Research and Design Institute for Economics, Information and Automated Management Systems of Fisheries (VNIERKH) – Moscow, Russia. e-mail: romulas@vnierkh.ru

[3] Environmental Company of Sakhalin, 426 Mira Avenue, Yuzhno-Sakhalinsk, 693004 Russia. e-mail: bobkov@ecs.sakhalin.ru

Introduction

Changes in the level of the World Ocean obtained with the aid of altimetry sensors established on satellite within the framework of project TOPEX-Poseidon (TP), have received recently a wide expansion at research of the broad audience of dynamic processes - seasonal fluctuations of a level and circulation in various areas, allocation of vortical structures and some others, having the important scientific and applied value for scientific tasks. Identification of vortical formations with simultaneous measurement of SST and chlorophyll *a* concentrations are used intensively in hydro-biological research, including fisheries management. Many studies (Crawford and Batten 2002, Romanov et al. 1997, Shatohin 1981) are devoted to these questions.

However, in coastal areas of the ocean and in particular in the marginal seas, altimetry data has some essential difficulties due to the inability of the global tidal models to account for ocean tides (Anderson et al. 1995, Choi et al. 1999, and Ray 1999). Various corrections have been developed for each specific region based upon more exact regional numerical models that assimilate the available data on the characteristics of tide, received from coastal sea level gauges or independent buoy stations. Recently, some attempts have been undertaken for the Sea of Japan, though the amplitude of tide in this region is rather insignificant (Hirose et al. 1999, Morimoto et al. 2000).

There is a much more important question of having a reliable model of tides in the Sea of Okhotsk because tidal amplitudes are so much greater. The range of tidal level fluctuations in northwest and especially in the northeast parts of Sea of Okhotsk reaches several meters in amplitude. At the same time, according to coastal observations, the amplitude of the annual harmonic, giving the basic contribution to seasonal variations, does not exceed 10 cm (Poezzhalova and Shevchenko 1997) and the deviations of sea level due to eddies and other interesting phenomena have approximately the same amplitude. Therefore, analysis of the satellite altimetry data, particularly to identify eddy activity and research of other dynamic processes in this area, to provide a reliable accounting for tides is extremely important. Their deforming influence can cause significant errors for data processing and interpretation of results.

The spatial structure of tides in the Sea of Okhotsk has a rather complex character. Tidal waves penetrate from the Pacific Ocean through the straits of the Kuril ridge, reflect off the coastal borders and form the complex interference pattern

that is observed; for semidiurnal tidal waves, some areas of amphidromy are formed and etc.

Significant seasonal variability of amplitudes and phases of tidal waves is observed. Ice cover formation and even complete freezing (to the bottom) in some shallow areas occur, as does the formation of ice-free zones in areas with strong tides and squeezing winds and nonlinear effects (Sgibneva 1981, Shevchenko 1996). Thus tidal modeling in the Sea of Okhotsk is rather difficult, so the results of calculations within the framework of regional models (Kowalik and Polyakov 1998, Romanekov 1996, Suzuki and Kanari 1986) as well as global (Choi et al. 1999), do not provide enough accuracy to process the satellite data on fluctuations of sea level.

One of the most effective methods of solving this problem is an approach suggested by Canadian scientists (Cherniawsky et al. 2001), based on the analysis of characteristics of tidal fluctuations directly at a point in the sea from obtained in it satellite altimetry dataset, direct calculation of harmonic constants and subtraction of the predicted tide.

At the present time, datasets are sufficiently long that reliable results, free of the tidal influence, are possible. Data on acyclic fluctuations of sea level and the defining features of the spatial structure of tidal waves in the Sea of Okhotsk are other important problems to be tackled. These tasks, in addition to developing a reliable method of tidal filtration from TP altimetry data, are the basic purpose of the present research.

The initial data

Radar altimeter (RA) is usually a nadir-oriented active microwave sensor, radiating in the range from 13-14 GHz. The downward-oriented electromagnetic impulse interacts with the terrestrial or sea surface and reflects back to the altimeter antenna. The full propagation cycle time from the RA to the surface and back is measured with high accuracy, and then by multiplication to speed of distribution of electromagnetic radiation, the height of the reception antenna of the satellite above a reflecting surface is calculated.

The atmosphere and ionosphere slow the speed of radio impulses, proportional to the full weight of the atmosphere, to water vapor weight in the atmosphere, and to the number of free electrons in the ionosphere. The impulse is not reflected from an average sea level, but from levels determined by wave height and wind speed. As a consequence of these effects, mistakes in determining sea surface height cannot be ignored.

TOPEX/Poseidon altimetry data were used as initial altimetry data. These data were obtained from the NASA Physical Oceanography Distributed Active Archive Center at the Jet Propulsion Laboratory, California Institute of Technology.

For sea level calculations relative to a reference ellipsoid (the first-order definition of the non-spherical shape of the Earth as a revolving ellipsoid with an equatorial radius of 6378.1363 km and a flattening coefficient of 1/298.257) from satellite altimeter data, the following equations were applied:

$$H_Y = H_C - (H_A + C_{WT} + C_{DT} + C_I + C_{EMB}) - H_{IB}$$

Where H_Y - a sea level, Hc - height of an orbit of the satellite, H_A - altimetry range, C_{WT} - wet troposphere correction, C_{DT} - dry troposphere correction, C_I - ionosphere correction, C_{EMB} - electromagnetic bias correction, H_{IB} - inverse barometer correction.

To obtain all necessary corrections to the altimetry signal, standard techniques from a TOPEX/Poseidon MGDR-B dataset were considered according to recommendations in (Benada 2002).

The dry troposphere correction adjusts for the influence of “dry” gases on the distribution of the electromagnetic signal in the troposphere. These gases contribute to troposphere refraction, depending on their density and temperature. Further, if the conditions of ideal gases are satisfied, and if the hydrostatic equation is used, we note that the vertical distribution of the signal delay depends only on surface pressure P, hence:

$$C_{DT} = -2.227P(1 + 0.0026\cos(2\varphi)).$$

where φ – is the latitude of a point of supervision. So it is possible to calculate the correction in a range of 2.2-2.3 meters, to within millimeter accuracy. We note that this correction is practically constant and determined to within several millimeters. The error of the correction on dry troposphere is approximately 0.7 cm.

The wet troposphere correction cannot be calculated as precisely as the dry troposphere correction because it depends on amounts of water vapor. Direct simultaneous measurement is applied, using active or passive microwave radiometer soundings on two or more frequencies. TOPEX microwave radiometer (TMR) uses signals on frequencies 18, 21 and 37 GHz: the water vapor signal is measured by 21 GHz channel, while 18 GHz channel deletes surface issue (influence of a wind speed), and 37 GHz channel removes other atmospheric contributions (influence of a covering, clouds etc.). Measurements are incorporated to estimate errors in distance due to water vapor. An error of similar measurements is approximately 1.2 cm.

As with the wet troposphere correction, an ionosphere correction range is strongly changeable so it is better to estimate this by direct measurement, using double frequencies of the microwave sensor. Until now, except for TOPEX/Poseidon, all other satellites have been equipped with devices with a unique frequency. The two-band radar (Ku and C ranges) of the TOPEX/Poseidon satellite provides reliable TEC (total electron content in the ionosphere) estimation and, hence, the reliable correction of optical length of a path. The following equation is used:

$$C_I = \frac{-403 * TEC}{f^2}$$

in this case C_I in mm.

Because of sea waves, troughs create more reflecting elements than crests. There is an additional error leads at averaging to displacement aside of hollows, underestimating a real level. Such, so-called, electromagnetic bias (EMB) grows with increase in significant wave height (SWH) and is usually corrected by an empirical function using altimeter-measured SWH. The theoretical understanding of electromagnetic bias remains limited and continues to be a topic of ongoing research. The current, most exact estimations are based on Gaspar results:

$$EMB = - SWH\,[a + b*SWH + c*U + d*U2],$$

where EMB - electromagnetic displacement (m), SWH - significant wave height (m), and U - wind speed (m s^{-1}).

TOPEX	Poseidon
a = + 0.0203	a = + 0.03360
b = -0.00265	b = + 0.0082
c = + 0.00369	c = -0.00144
d = -0.000149	d = + 0.000052

Sea surface height tends to decrease or increase in reaction to variation in atmosphere pressure. In general, an increase of 1 mb in atmospheric pressure lowers sea surface height by approximately 1 cm. Hence, the effect of an inverse barometer is just the deepening of sea surface level under the weight of a column of air pressing on this surface. Pressure is calculated as follows:

$$P = C_{DT} / (-2.277 \times (1 + (0.0026 * \cos(2\times10^{-6} \times f \times \pi/180.0))))$$

where C_{DT} - the correction on dry troposphere, f - frequency in GHz. The inverse barometer correction is

$$H_{IB} = -0.09948\,(P-1013.3)$$

The correction is added to an altimeter range or subtracted from a sea surface height. The multiplier 9.948 is based on theoretical value of a static inverse barometer in mid-latitudes. Also, 1013.3 is a rating value of atmospheric pressure in the mid-latitudes.

Further, the processed altimetry data were assembled in a regular grid as follows. The area in the vicinity of a grid node are taken with radius in 2.5° where the altimetry sea level data were chosen. Then, if there is more than one altimetry data value in the chosen area, there was an

averaging procedure for existing sea level values with respect to the number of satellite passes. Thus, only the same satellite pass and time-close altimetry level points were used in the spatial and temporal averaging procedure for a particular pass and so on for all values chosen in the area of altimetry measurements. On Figure 1, the regular grid node arrangement with a 1° × 1° step is represented, chosen for a region with real TOPEX/Poseidon passes. In the area in the vicinity of several units of a regular grid, especially in the southern part of an area, there were no altimeter data, due to the increasing distance between satellite tracks. In this case, the unit simply did not participate in the further research.

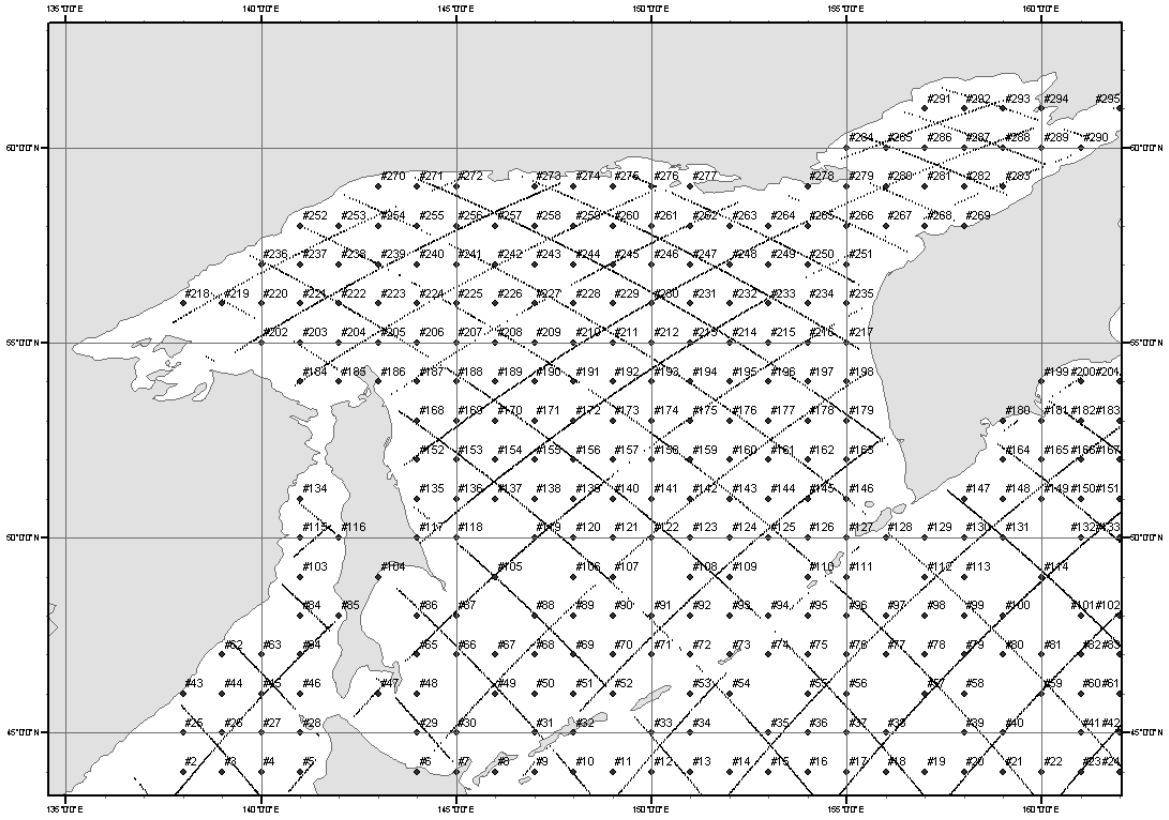

Fig. 1 Scheme of TP tracks in the Okhotsk Sea and adjacent areas and 1° × 1° grid in which satellite altimetry sea level data were analysed.

Design procedure of harmonic constants of tide

The tidal level in some point of the sea at time moment t can be presented as a combination of a set of *L* harmonics (tidal waves) (Duvanin 1960; Godin 1972):

$$X(t) = S + \Sigma f_j(t)\, H_j \cos(\omega_j t - U_j(t) - g_j)$$

where S is an average level, $f_j(t)$ is an amplitude multiplier, $U_j(t)$ is the phase correction, both parameters for each wave depend on time, but are known (could be determined by astronomical conditions at the moment of measurement), ω_j is the wave frequency, H_j g_j are harmonic constants, amplitudes and phases. Namely, a definition from supervisions is the primary goal of the tidal analysis.

Some well-known modifications of the least squares method (Godin 1972) for a case when the data are registered irregularly or when measurements cover too large an interval over which it is impossible to count astronomical parameter constants for the period of measurements are represented.

For each countdown t_k it is possible to predefine $f_j(t_k)$ and $U_j(t_k)$ and, using the cosine

decomposition by the difference of corners formula:

$$X(t) = S + \Sigma f_j(t)\, H_j \cos(\omega_j t - U_j(t) - g_j) = \Sigma f_j(t)\, H_j \{\cos(\omega_j t - U_j(t)) \cos g_j + \sin(\omega_j t - U_j(t)) \sin g_j\},$$

Introduce:

$$A_j(k) = f_j(t_k) \cos(\omega_j t - U_j(t_k))$$
$$B_j(k) = f_j(t_k) \sin(\omega_j t - U_j(t_k))$$

and the new variables subject to definition $Y_j = H_j \cos g_j$, $Z_j = H_j \sin g_j$, concerning to them we receive a system of linear equations

$$X(t_k) = S + \Sigma A_j(k)\, Y_j + B_j(k)\, Z_j ,$$

which allows an application of the least squares method under the standard scheme. Here S - one more variable is subject to definition. Such approach has been chosen according to (Puzankov and Shevchenko 2001) where by applying harmonic analysis to SST seasonal fluctuations in the Sea of Okhotsk, a problem of "average value bias" appeared because of asymmetry in the number of available data during winter and summer period that resulted in mistakes in the estimated amplitudes of the annual and semi-annual harmonics. In this case this precaution appeared excessive - distinction between average values on a set and by results of calculations for the majority of points was in the third decimal place, and only in separate cases reached 1 mm.

Thus, we have the standard method of the least squares normal system of the linear equations

$$\mathbf{Ax = b},$$

Where **A** is a square matrix $m \times m$ (see Table 1) where $m = 2L+1$, the maximal number of considered harmonics $L = 67$, including annual and semi-annual waves Sa and Ssa, the length of measurements sequence is not limited.

We used decomposition of an initial matrix as **A = UDR** where matrix **U** consists of m mutually orthogonal nonzero rows, **R** - the top triangular matrix with $m \times m$ size, and $\mathbf{D} = (\mathbf{U}^T\mathbf{U})^{-1}$. Such decomposition exists, if the rows of matrix **A** are linearly independent. Condition $\mathbf{U}^T\mathbf{(b-Ax)} = 0$ defines nonsingular triangular system of equations $\mathbf{Rx} = \mathbf{U}^T\mathbf{b}$ which can be solved by a method of back-substitution. We shall notice, that matrix $\mathbf{R} = \mathbf{U}^T\mathbf{A}$ and vector $\mathbf{U}^T\mathbf{b}$ are received with the aid of the same transformation U^T applied to matrix A and vector **b** accordingly.

Reducing to the form $\mathbf{Rx} = \mathbf{U}^T\mathbf{b}$ is carried out for m the steps as a matter of fact representing procedure of Gauss exception with simultaneous rows orthogonalization of matrix **A**. As matrix U is orthonormalized, then **R** represents the top triangular matrix in Holetsky decomposition for $\mathbf{A}^T\mathbf{A}$, that enables to use iterative specification of the decision.

In each iteration, the residual vector $\mathbf{r}^{(s)} = \mathbf{b} - (\mathbf{RR}^T)\mathbf{x}^{(s)}$, ($s$ – iteration number) and a correction $(\mathbf{RR}^T)\mathbf{d}^{(s)} = \mathbf{r}^{(s)}$, $\mathbf{x}^{(s+1)} = \mathbf{x}^{(s)} + \mathbf{d}^{(s)}$ are computed. It is considered, that iterative process misses, if residual norm are obtained at the next iteration exceeds a quarter of a vector norm of the decision $\left\|r^{(s+1)}\right\| \le \frac{\left\|x^{(s)}\right\|}{4}$. Iterations end if one of the following conditions become true: (1) the corrections become too small $\left\|r^{(s+1)}\right\| \le \left\|x^{(s)}\right\| * \varepsilon^2$ i.e. where ε is the smallest number for which $1 + \varepsilon > 1$ with machine accuracy[1] or (2) the norm of the next correction is less than previous after 100 or more times). If the program finds out, that the rows of matrix **A** are linearly dependent (within machine accuracy), or the iterations fail, a message on impossibility of a solution is displayed.

Usually a similar problem arrives for tidal waves with close frequencies. There is Rayleigh criterion (Godin 1972) for definition of division opportunity for such waves in case of the usual sets received by the standard tide gauge device, which are the values with the fixed step-type behavior. However for TP data, taking into account the interruptions in the Okhotsk Sea because of ice cover on most of the sea, it is not possible to formulate similar criterion. We did not go beyond the above-mentioned formal definition of the system decision stability of the harmonics set formation in this case.

[1] For a Pentium processor, it is $2.2*10^{-16}$

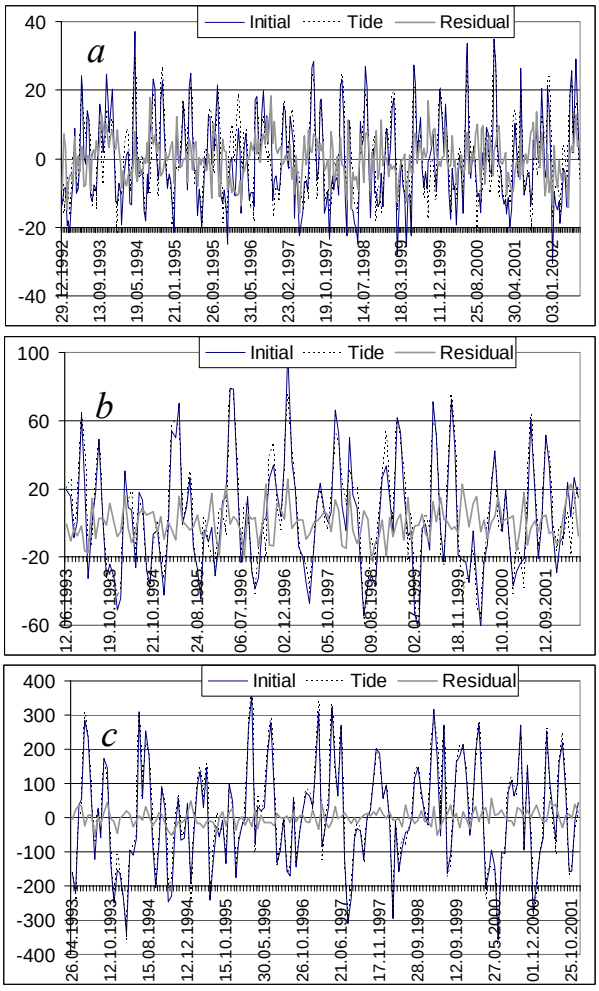

Fig. 2 Initial, predicted tidal and residual altimetry sea level data in the spots 64 (a, Japan Sea, weak tides and well-expressed seasonal oscillations), 185 (b, Sakhalinsky Bay, the shortest data set because of ice cover) and 294 (c, Penjinskaya Guba, very strong tides).

It is necessary to note that the absence of altimetry data in winter results in instabilities for calculating annual (Sa) and semi-annual (Ssa) components such as were applied in the northeastern Pacific Ocean (Cherniawsky et al. 2001). For conditions of the Sea of Okhotsk it was necessary to exclude them. A similar problem has arisen for seasonal level fluctuations in the Bering Strait region (Cherniawsky et al. 2001).

Where, as a result of interpolation from two tracks the number of sea level values exceeded 500, 60 harmonics were reliably determined. Where the length number of sea level values was within 280-320, more than 40 harmonics were calculated, athough on further calculations, following (Cherniawsky et al. 2001), we were limited to estimating the parameters of 18 tidal waves with the dominant role in determining tides in the Sea of Okhotsk. The calculation of these waves is stable within the bounds of the study area, including the Gulf of Sakhalin where the ice cover is steadiest and where the shortest TP dataset for 10 years is obtained - 144 values (Fig. 2a).

Probably, the absence of harmonic pairs for which in the mentioned above work the aliasing phenomenon was observed, is caused by increase in the analyzed period of observation (with 6 to 10 years in the present work), and also usage of steadier algorithm for the linear systems solving.

The high correspondence between initial sea level values and the residual tide values, as well as between the measured values of amplitudes and phases in the next points, and also the size of the residual fluctuations including seasonal variations and the response of sea surface under the influence of surface atmospheric pressure and wind speed variations (having an amplitude rms about 10 cm) indicates to a reliable estimation of harmonic constant tidal waves. This value is close to an average size estimation of the residual variations calculated for Sakhalin coastal tide gauges (Shevchenko 1997).

A little bit large, but close enough range of residual fluctuations has been received and in a northeast part of the sea, on approaches to Gulf Penjinskaya Guba where tides reach the greatest value - apparently from Figure 2c, their range at a given point is about 8 m. Here again it was not possible to identify seasonal variations in residual fluctuations. It is caused by influence of an ice cover also.

This type of sea level fluctuation is well determined in the southwestern part of the Sea of Okhotsk, where the amplitudes of the annual harmonic having, according to satellite altimetry data about 7-8 cm, and accorded with the results of calculations for stations Korsakov, Starodubskoe and Poronaysk (Poezzhalova and Shevchenko 1997). There are no problems to calculate the annual and semi-annual harmonics in the analyzed

part of the Sea of Japan (Fig. 2a), nor at the Kuril region of the Pacific Ocean where the influence of ice is insignificant.

The given examples show, that a tidal component according to satellite altimetry data is quite stably determined and might be predicted and removed from initial dataset with high accuracy. More than 90% of the chosen points have got the amplitude rms of residual fluctuations about 8-10 cm, and 12-16 cm for the others that allows to approach to the circulation in the Sea of Okhotsk research problems solving, to determining of various type vortical structures and the some other important problems settling at completely different level of accuracy.

Spatial distribution of amplitudes and phases of the basic waves

Let us now consider the results of the harmonic analysis of the satellite altimetry data from the point of view of features of spatial structure of the basic tidal waves. On Figure 3b, the amplitude isolines and phase for the main daily wave, K1, are constructed from calculated grid points by means of Surfer software. This harmonic has its smallest amplitudes in the southwestern part of the research area where its range is about 7-10 cm, and the quantity grows in a northwest direction. The greatest values of K1 amplitude exceed 2 m in Shelikhov Bay, on approaches to Gulf Penjinskaya Guba. These results corresponding well with the coastal measurement analysis (Anon. 1960). Let us note that numerical modeling of tides in Sea of Okhotsk for the given area have great difficulties, and the estaimted heights of the daily tide are essentially below the real values (Choi et al. 1999; Kowalik and Plolyakov 1998; Suzuki and Kanari 1986). More exact results for the given area have been obtained (Romanenkov 1996) but the calculations were carried out to estimate the efficiency of a planned tidal power station in the Penjinskaya Guba region. Also from the numerical modeling, the area of greatest amplitude extended from the entrance of Shelikhova Bay to the open sea, approximately along of the shelf edge, was not allocated in such obvious kind. The area of lower than observed amplitudes, daily tides at southeast coast of Sakhalin, is caused most likely by the large distance from the coast to our chosen grid points.

The spatial structure of K1 phase distribution has a simple character and corresponds quite well to results of numerical modeling. It specifies a zonal, west-oriented wave direction in adjoining area of Pacific Ocean and the basic inflow to the Sea of Okhotsk through straits in the northern part of the Kuril ridge. Inside the sea, the primary distribution of daily tide from the northern Kuriles travels in a northwest direction, reaching the coasts of Sakhalin and Magadan at approximately the same time, and achieves Shantarskie islands in some hours.

The spatial distribution of the amplitudes and phases of another important daily wave, O1, has a structure similar to K1 (Fig. 3). Let us note that the combination of these waves creates the characteristic fortnight variability of tides in the Sea of Okhotsk, shown both in sea level fluctuations and in tidal currents (Putov and Shevchenko 1998; Odamaki 1994; Shevchenko and Kantakov 2001). It is quite possible, that an unsatisfactory removal of tides from the satellite altimetry data, namely this modulation, creates false anomalies of "pure tidal origin" that are perceived as quickly displaced vortical structures.

A more complex and interesting picture is evident for the basic semidiurnal wave M2 (Fig. 4a, b). The distribution of amplitudes has sharp increases in the northern part of Tatar Strait, along the continental coast in northern part of the Okhotsk Sea (>1 m), at the Kamchatka coast of Shelikhova Bay, and on approaches to Gulf of Penjinskaya Guba. These also correspond well to the analysis of coastal tide gauges.

The semidiurnal tide amphidromes, areas with very small amplitudes of M2, are found in the southern part of Tatar Strait, along the east coast of Sakhalin and at its northern extremity, and also at the western coast of Shelikhova Bay. The presence of these amphidromic regions was first demonstrated by (Ogura 1933) from analysis of the coastal measurements, and but also received as a result of numerical modeling (Suzuki and Kanari 1986; Kowalik and Polyakov 1998; Choi et al. 1999; Romanenkov 1996). The exception was the area along the east coast of Sakhalin that was not identified by results of calculations at all (Suzuki and Kanari 1986; Choi et al. 1999).

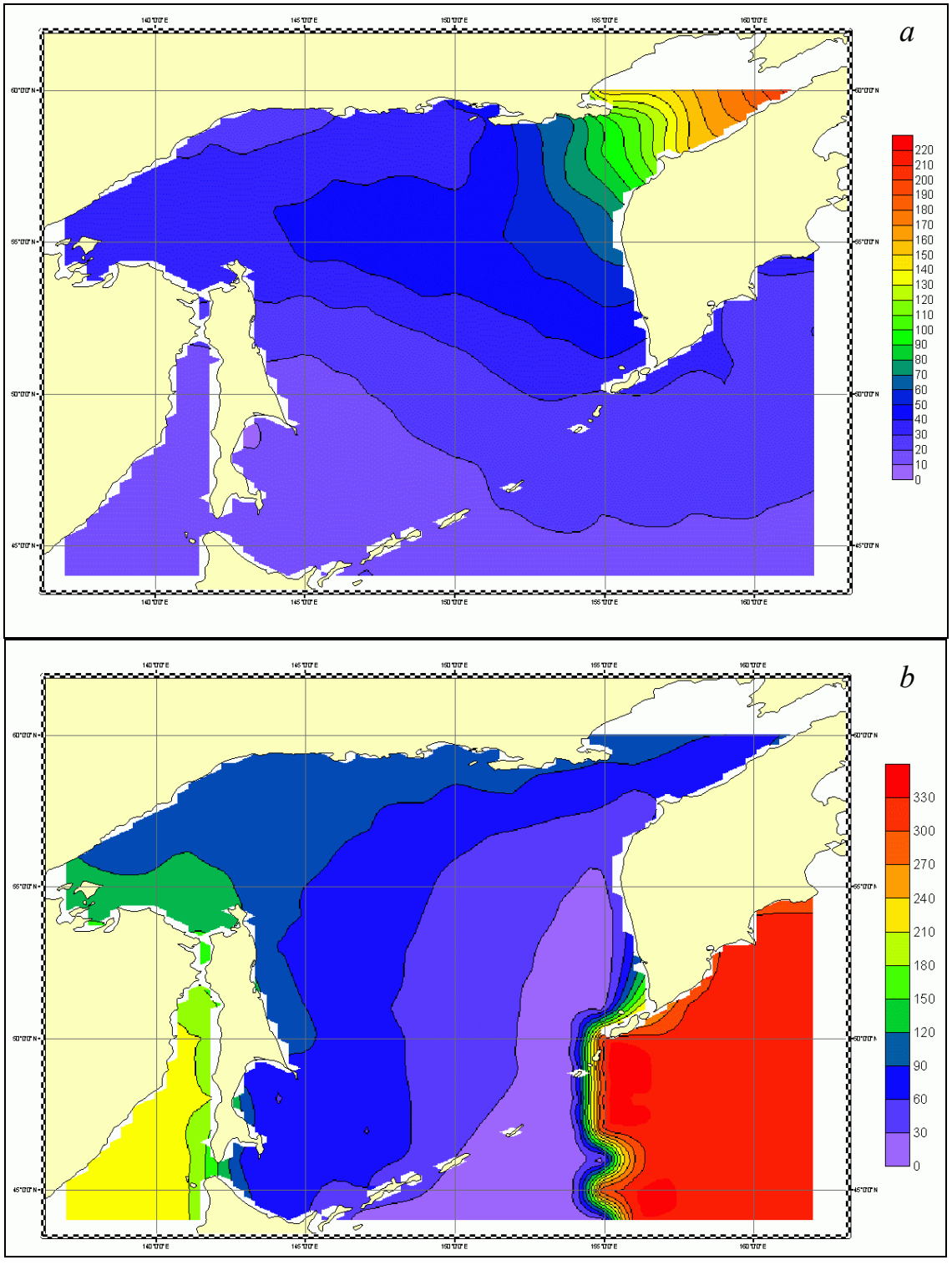

Fig. 3 Spatial distribution of amplitude (a, cm) and phase (b, deg) of main diurnal harmonic K1 in the Okhotsk Sea and adjacent areas.

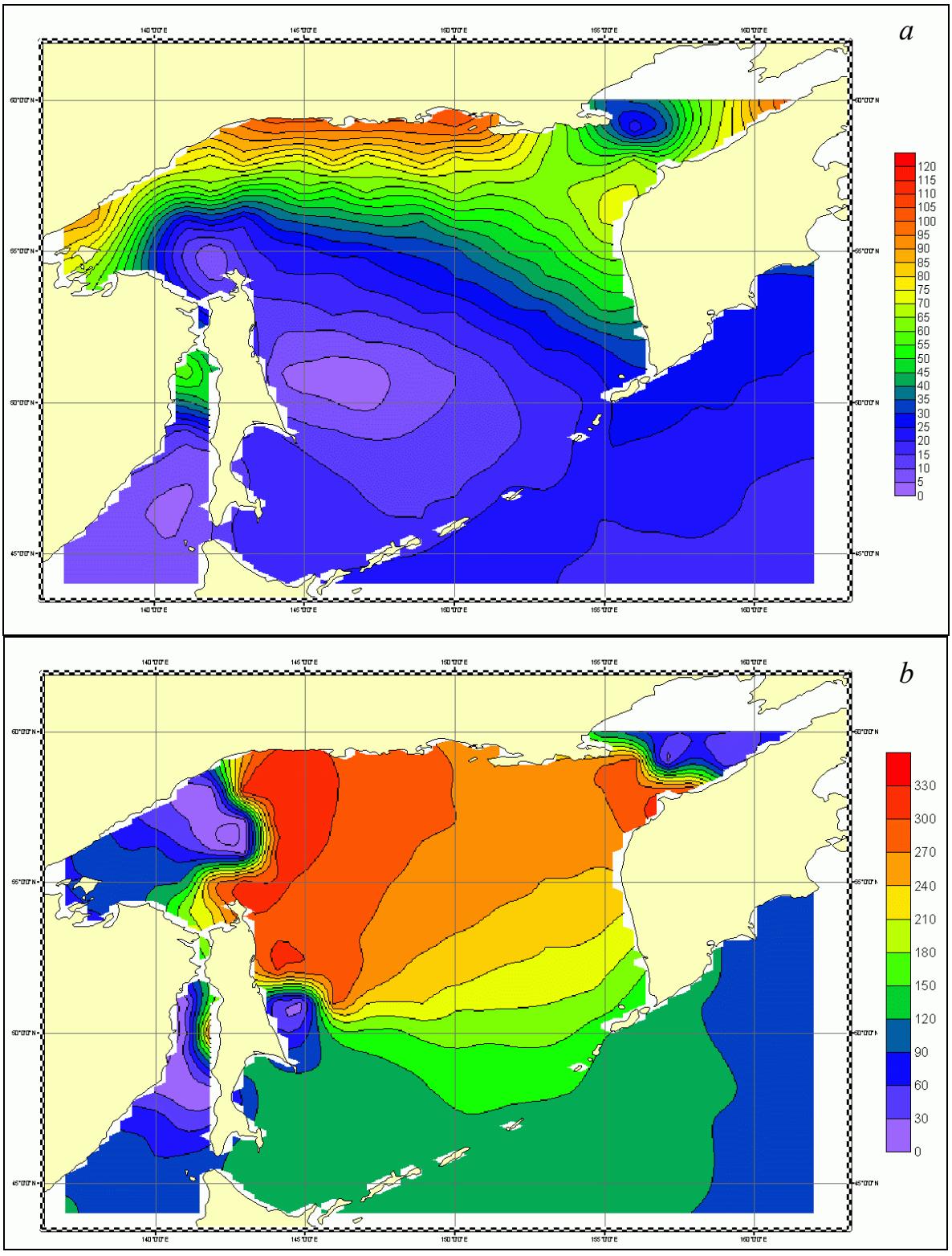

Fig. 4 Spatial distribution of amplitude (a, cm) and phase (b, deg) of main semidiurnal harmonic M2 in the Okhotsk Sea and adjacent areas.

Both the position and the range of the amphidromes at the northern end of Sakhalin Island and in Shelikhova Bay are well matched to the results of numerical modeling. At the same time, areas of small amplitudes of M2 in the southern part of Tatar Strait and in particular in the central part of the Sea of Okhotsk (Fig. 3b) look a little more extensive than it could be considered. Obviously, it is caused by the complex character of the bottom relief and coastline of the Sea of Okhotsk. Probably, this circumstance was the main reason for the difficulties in modeling the semidiurnal tides in this area.

The mentioned above M2 amphidromy area in Tatar Strait, according to satellite altimetry data, not only appears more extensive, but is located a little bit to the south than it should be considered.

The spatial distribution of another important semidiurnal wave, S2, has a character that is very close to M2, only with an appreciable reduction of amplitude. In the East Sakhalin region, the amphidromy area is displaced from the coast to the open sea direction, and small amplitudes are closer to continental coast in Tatar Strait. Amphidromy is not expressed in the latter case, the reduction of amplitude is observed, and circular movement of phases is absent.

The results have provided a detailed picture of harmonic constant tidal waves distribution in such a complex pool as the Sea of Okhotsk. They also can be used for calculation of tidal current speeds and tidal energy dissipation estimation in the entire sea and its separate parts, including calculation of position of theoretical zero of depths and other important applied problems.

Conclusions

1. An effective way of eliminating tidal components from the satellite altimetry data is offered, allowing a residual tide with rms amplitude of about 10 cm at the range of the measured fluctuations from 2 to 8 m.
2. Spatial distributions of amplitudes and phases of the basic tidal waves in the Sea of Okhotsk and adjoining areas are made. More than 2 m of daily waves amplitude values on approaches to the Gulf of Penjinskaya Guba, and also areas of high intensity of fluctuations in the open sea in region, adjoining to Shelikhova Bay that has not been found in known regional numerical models are received.
3. For main semidiurnal waves, M2 and S2, all known amphidromies were identified. It is shown that the area of small amplitudes of M2 has a more southern location and occupies a larger area than was considered in Tatar Strait and has a significant extension to the open sea region on the east coast of Sakhalin as well.
4. The estimated values of the harmonic constants of tides in the Sea of Okhotsk can be used to calculate tidal current speeds, tidal energy dissipation estimation and the settling of some other problems that demand an exact knowledge of a tidal mode.

References

Andersen, O.B., Woodwort, P.L. and Flather, R.A. 1995. Intercomparison of recent of ocean tide models. J. Geophys. Res. 100(C12): 25261-25282.

Benada, R., PO.DAAC Merged GDR (TOPEX/POSEIDON)-B Users Handbook, Rep. JPL D-11007, Jet Propulsion Laboratory, Pasadena, CA, 2002.

Anonymous. 1960. Tables of the tides. Waters of Asian part of USSR and adjacent foreign areas. L.: Hydrometeoizdat (in Russian).

Cherniawsky, J.Y., Foreman, M.G.G., Crawford, W.R. and Henry, R.F. 2001. Ocean tides from the TOPEX/POSEIDON sea level data. J. of Atmospheric and Oceanic Technology 18 (4): 649-664.

Choi, B.H., Kim, D.H. and Fang, Y. 1999. Tides in the East Asian seas from a fine-resolution global ocean tide model. MTS journal 33(1): 36-44.

Crawford, W.R. and Cherniawsky, J.Y. 2002. Observations of sea level anomalies in Bering Strait and surrounding seas using satellite altimetry observations. PICES: Eleventh Annual Meeting, Program & Abstracts (October 18-26, 2002, Qingdao, People's Republic of China). pp.140.

Crawford, W.R. and Batten, S.D. 2002. The influence of coastal origin eddies on ocean plankton distribution in the eastern Gulf of Alaska. PICES: Eleventh Annual Meeting, Program & Abstracts (October 18-26, 2002,

Qingdao, People's Republic of China). pp.117.
Duvanin, A.I. 1960. Tides in the sea. Leningrad: Hydrometeoizdat. (in Russian)
Godin, G. 1972. The analysis of tides. Toronto Press.
Hirose, N., Fukomori, I. and Yoon, J.H. 1999. Assimilation of Topex/Poseidon altimeter data with a reduced gravity model of the Japan Sea. Journal of Oceanography 55: 53-64.
Kowalik, Z. and Polyakov, I. 1998. Tides in the Sea of Okhotsk. J. Phys. Oceanogr 28(7): 1389-1409.
Morimoto, A., Yanagi, T., and Kaneko, A. 2000. Tidal corrections of altimetric data in the Sea of Japan. Journal of Oceanography 36: 31-41.
Odamaki, M. 1994. Tides and tidal currents along the Okhotsk Coast of Hokkaido. Journal of Oceanography 50: 265-279.
Ogura S. 1933. The tides in the seas adjacent to Japan. Bull. Hydrographic Department. Imp. Japan Navy Vol. 7- Tokyo.
Poezzhalova, O.S. and Shevchenko, G.V. 1997. The Okhotsk Sea mean level variations. Tsunami and accompanying phenomena. IMGG RAS, Yuzhno-Sakhalinsk.pp.131-144 (in Russian).
Putov, V.F. and Shevchenko, G.V. 1998. Peculiarities of tidal regime on the northeastern shelf of Sakhalin Island. FERHRI special issue. Vladivostok, Dalnauka, pp. 61-82. (in Russian)
Puzankov, K.L. and Shevchenko, G.V. 2001. Seasonal changes of sea surface temperature in the Sea of Okhotsk on the base of satellite data 1987-1988. *In* Dynamic processes on the shelf of Sakhalin and Kuril Islands. Institute of Marine Geology & Geophysics RAS. Yuzhno-Sakhalinsk, 2001, pp. 94-100.
Romanov, A.A., Rodin, A.V., and Mishkin, V.M. 1997. Conception of the service of satellite industrial monitoring of the Global Ocean fishing areas. Remote sensing methods of fishing areas monitoring in the Global Ocean for industrial tasks of information support of scientific researches. M.: VNIRO, pp.7-32. (in Russian)
Romanenkov, D.A. 1996. Prognostic modeling of tides in the Okhotsk Sea. Ph.D. thesis. St. Petersburg, 16 p. (in Russian)
Ray, R.D. 1999. A global ocean tide model from Topex/Poseidon altimetry: GOT99.2. – NASA Tech. Memo. 209478.
Sgibneva L.I. 1981. Variability of harmonic regular tide as consequence of nonlinear effects. Trudy GOIN 156: 33-40. (in Russian).
Shatohin, B.M. 2002. The methodical basis and practice of the task solution of the short-term fishing forecasting using satellite altimetry information. XII International Conference on Fisheries and Oceanology. Thesis of reports. - Kaliningrad: AtlantNIRO, pp. 266-267. (in Russian)
Shevchenko, G.V. 1996. A quasi-periodic seasonal variability of harmonic regular tides in the northwestern Sea of Okhotsk. Meteorology and hydrology 8: 90-99.
Shevchenko, G.V. 1997. Statistical characteristics of storm surges in the southern Sakhalin Island. Izv.RGO 129(3): 94-107. (in Russian)
Shevchenko, G.V. and Kantakov, G.A. 2001. Results of direct measurements of the currents in the La Perouse (Soya) Strait. The 16th International Symposium on Okhotsk Sea Ice, 4-8 February 2001, Mombetsu, Hokkaido, Japan: Abstracts.- Mombetsu. pp. 323-333.
Suzuki, K. and Kanari, S. 1986. Tides in the Okhotsk Sea. Marine Sci. 18(7): 445-463.

Water masses and circulation pathways in the Okhotsk Sea observed using profiling floats

Stephen C. Riser[1], K. Ohshima[2], and Y. Volkov[3]

[1] School of Oceanography, University of Washington, Seattle, Washington, 98195 USA e-mail: riser@ocean.washington.edu

[2] Institute of Low Temperature Science, Hokkaido University, N19W8, Sapporo, 060-0819 Japan.

[3] Far Eastern Regional Hydrometeorological Research Institute, 24 Fontannaya Street, Vladivostok, 690600 Russia.

We examine the circulation and water properties in the western and southern Okhotsk Sea during the years 2000-2003 using data from an array of profiling floats deployed from Russian and Japanese research vessels. The subsurface drift data from these instruments, from depths of 400-1600 m, show unmistakable evidence of the East Sakhalin Current and the southward transport of dense shelf water at densities in the range of sq of 26.2-27.0 at speeds of 5-15 cm s^{-1}. In the southwestern Okhotsk Sea, near Soya (LePerouse) Strait, there is evidence of a closed, cyclonic circulation at mid-depths. A number of the floats have exited the Okhotsk Sea through Bussol Strait and other, shallower straits farther south. The temperature and salinity profiles measured by these floats show evidence that Okhotsk Sea water can maintain its integrity far into the North Pacific, as these floats spread to the south along the Hokkaido coast and to the northeast to the Aleutian Islands.

Relationships between nitrate and phosphate concentrations as a tracer of the northern Okhotsk Sea waters

Nikolay S. Vanin[1], Alexander P. Nedashkovskiy[2] and Gennady V. Khen[1]

[1] Pacific Fisheries Research Centre (TINRO-Centre), 4 Shevchenko Alley, Vladivostok, 690600 Russia. e-mail: vanin@tinro.ru

[2] V.I. Il'ichev Pacific Oceanological Institute, Far-Eastern Branch of Russian Academy of Sciences, 43 Baltiyskaya Street, Vladivostok, 690041 Russia. e-mail: alned@poi.dvo.ru

Within the framework of TINRO research of biological resources in the Okhotsk Sea during the period from August 2001 until July 2002, 926 hydrological stations were occupied, of which 539 had a complete set of hydrochemical measurements (dissolved oxygen, nitrate, nitrite, phosphate and silicate concentration).

Observations completely covered the shelf and most of the abyssal region, including the Kuril Basin, the central part of the Okhotsk Sea and adjacent areas of the Pacific Ocean. The hydrological measurements were carried out using a Mark-III CTD. Samples for hydrochemical analysis were taken selectively taking into account the thermal structure of the water column. The quantity of samples obtained at each station varied from three to 12 depending on the depth and complexity of features in the water column. The correctness of bottle samples was determined by comparing the salinity of the bottle sample, determined using a salinometer, with the data obtained from the CTD.

In the abyssal region, a well-determined linear connection between nitrate and phosphate concentrations was observed during the late winter season. For stations located to the west of the Kuril Islands the equation of connection (m = 418, $R^2 = 0.99$, $1s^2_y = 0.64$) looks like:

$$[NO_3] = 14.89*[PO_4] - 5.54 \qquad (1)$$

For stations located on the Pacific side of the Kuril Islands, the relationship is expressed by:

$$[NO_3] = 15.78*[PO_4] - 6.80 \qquad (2)$$

where (m = 89, $R^2 = 0.99$, $1s^2_y = 0.66$ (dimensionality in μmol/kg).

For both equations the regression coefficients are close to Redfield's ratio between nitrate and phosphate variability.

At the same time in boreal part of the sea, including the shelf, the continental slope region and TINRO Basin, regular residuals from the linear model obtained for the abyssal stations are observed. These deflections are expressed in lower nitrate concentration in relation to a given phosphate concentration. The size of these deflections named in the further nitrate deficit (dNO_3), can be expressed quantitatively as:

$$dNO_3 = [NO_3]regress - [NO_3]observ$$

where: $[NO_3]$regress is the concentration of nitrate in equation (1) and $[NO_3]$observ is the observed nitrate concentration.

The greatest nitrate deficits appear in the bottom layer of the northwestern part of the shelf and in the deep waters of the TINRO Basin. Without examining the hydrochemical mode of the TINRO Basin in detail, we note that at depths from 500 m to the bottom (980 m), lower concentrations of nutrients correspond with increasing concentrations of oxygen and declining temperature. These features allow us to assume that the region of formation of deep waters of the TINRO Basin is, apparently, on boreal shelf of the Okhotsk Sea.

The region of maximum nitrate deficit on the northwestern shelf matches the extent of dense bottom water (depth 125-150 m) in the area that is occupied by polynyas during the winter season; the low concentrations of nutrients and elevated oxygen content confirm this idea. The increased nitrate deficit on the continental slope in the

northwestern part of the Derugin Basin, showing the submergence of dense shelf waters is also marked. Along the southwestern slope of Lebed' Rise, there is an obvious transformation of Pacific waters, mixing with shelf bottom waters, as a large nitrate deficit here is observed at high nutrient concentrations.

On zonal sections, the nitrate deficit is clearly observed in the western part of the abyssal pool near the East Sakhalin shelf. In the area of 49°N it can be traced down to depths of 600 m. It is also linked, in our opinion, to the sinking of bottom shelf waters along the continental slope. The nucleus of these waters is confined to a 26.8 σ_θ density surface (depth about 300 m). Along the southern periphery of the counterclockwise circulation, these waters extend to the east reaching the Kuril straits. On the eastern side of the Okhotsk Sea, off the West-Kamchatka shelf, high values of nitrate deficit are also revealed in summer. The core of these residuals is located mainly at depths of 40-60 m (26.2-26.3 σ_θ). This nitrate deficit is possibly caused by decomposition of organic matter accumulated at the pycnocline.

The potential physical causes of the nitrate deficit include: denitrification (regeneration of nitrate to N_2 or N_2O), reduced rate of nitrate regeneration during organic matter decomposition (in comparison with speed of phosphate regeneration), various proportions of nitrate and phosphate assimilation by coastal and abyssal plankton, etc. Irrespective of the causes of formation of the nitrate deficit, the latter in our opinion, can be used as a tracer of water formed on the northern shelf of the Okhotsk Sea. It seems that the distinction of coefficients of proportionality between variability of phosphate and nitrate for the Pacific waters and waters of an abyssal part of the Okhotsk Sea is explained by participation in formation of the latter the shelf waters of boreal part of the sea.

Chemical parameter distributions in the Kuril Basin of the Okhotsk Sea in winter 2003: Role of the anticyclonic eddies

Andrey Andreev[1], V. Chastikov[2], S. Gladyshev[3], G. Kantakov[2] and G. Shevchenko[2]

[1] V.I. Il'ichev Pacific Oceanological Institute, Far-Eastern Branch of Russian Academy of Sciences, 43 Baltiyskaya Street, Vladivostok, 690041 Russia. e-mail: andreev@poi.dvo.ru

[2] Sakhalin Research Institute of Fisheries and Oceanography (SakhNIRO), 196 Komsomol'skaya Street, Yuzhno-Sakhalinsk, 693023 Russia.

[3] P.P. Shirshov Institute of Oceanology, Russian Academy of Sciences, Nakhimovsky Prospekt 36, Moscow, 117997 Russia.

A survey of the Kuril Basin region in the Okhotsk Sea was conducted in February–March 2003 using the *R/V Dmitry Peskov* (Sakhalin Research Institute of Fisheries and Oceanography). The goal was to observe aspects of winter circulation in the ice-free zone of the Okhotsk Sea based on observations of CTD, dissolved oxygen, nutrient and carbonate parameters.

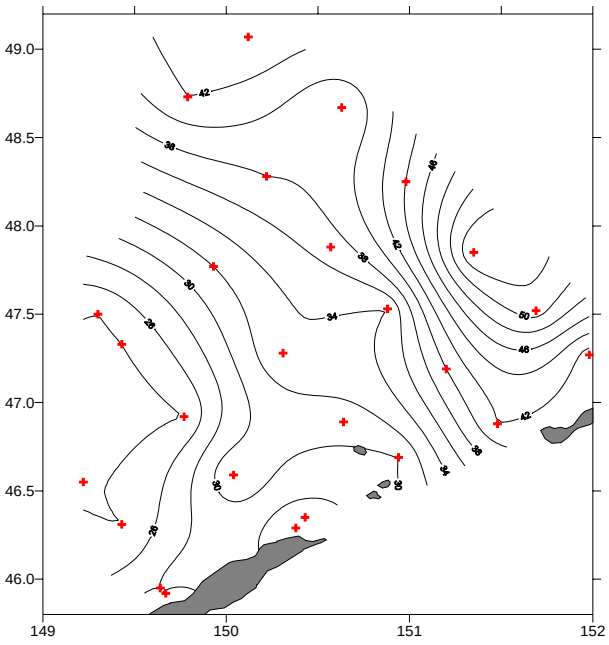

Fig. 1 Horizontal distributions of surface silicate (μmol/l) for the Kuril Basin area in February 2003.

The distribution of chemical parameters in the Kuril Basin in the winter of 2003 were affected by two anticyclonic eddies: located southwestward of the Bussol Strait (E1 eddy) and northward of the Bussol Strait (E2 eddy). The eddy cores were formed by warm, saline, low oxygen, high silicate Pacific waters.

The surface layer of E1 eddy was composed of cold, fresh Okhotsk Sea water. A strong vertical salinity gradient prevents the deepening of the surface layer by winter cooling and thus the surface waters of E1 eddy were characterized by low silicate (Fig. 1) with a partial pressure of CO_2 of ~30–40 ppm below saturation (Fig. 2).

The surface layer of E2 eddy was composed of weakly stratified saline waters, probably formed by intensive vertical mixing in the Kuril straits. These waters had high concentrations of silicate (Fig. 1) and were supersaturated with CO_2 due to vertical mixing (Fig. 2). The highest density water, highest concentration of silicate and pCO_2 in the surface layer were associated with the E2 eddy core, mainly due to deep winter convection.

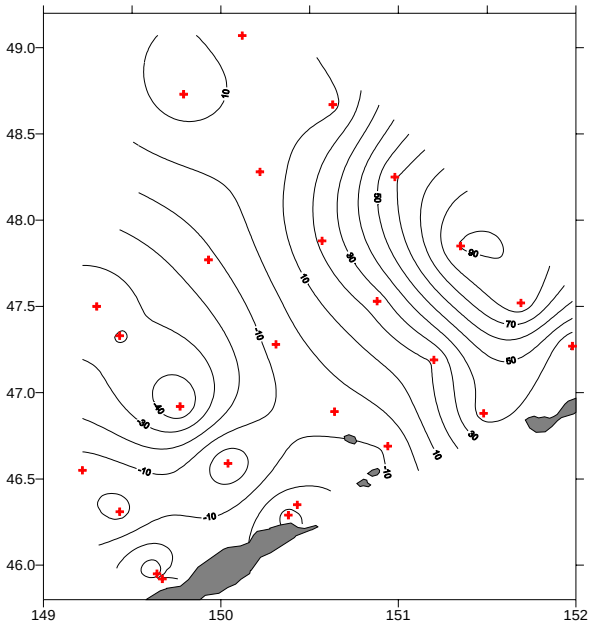

Fig. 2 Distributions of sea-air pCO_2 difference (ppm) for the Kuril Basin area in February 2003.

Deep water formation in the Derugin Basin of the Sea of Okhotsk

Anatoly Salyuk[1], G. Winckler[2] and G. Y. Pavlova[1]

[1] V.I. Il'ichev Pacific Oceanological Institute, Far-Eastern Branch of Russian Academy of Sciences, 43 Baltiyskaya Street, Vladivostok, 690041Russia. e-mail: san@poi.dvo.ru

[2] Lamont-Doherty Earth Observatory, PO Box 1000, 61 Route 9W, Palisades, NY, 10964 USA

The Derugin Basin is the second big "appendix" in the Sea of Okhotsk after the Kuril Basin. It has a maximum depth of about 1760 m and is connected to the Kuril Basin by 2 channels with sill depth of about 1300 m each. Due to strong stratification in the Derugin Basin reinforced by influxes of Pacific waters in the deep layers, is not renewed directly from the surface. The formation and renewal of deep waters in the Derugin Basin is discussed using new hydrochemical and isotopic data obtained during a joint Russian-German project KOMEX (Kurile Okhotsk Marine Experiment) from 1998-2002. Deep waters in the Derugin Basin show some features of stagnant waters such as very low dissolved oxygen (≤14 μM/kg) and high silica (≤267 μM/kg). The hypothesis of long renewal time of deep waters is not consistent with the tritium data. The relatively thin deep bottom layer observed on vertical profiles of potential temperature and salinity and the relatively high spatial variability of some water properties such as oxygen suggest relatively rapid exchange with the Pacific Ocean. Low dissolved oxygen in the Derugin Basin deep water not only indicates poor ventilation, but also that waters overflowing to the Derugin Basin belong to the strong intermediate oxygen minimum layer (about 35 μM/kg) in the Sea of Okhotsk.

Interannual variability of the ventilated water masses in the Okhotsk Sea

Sergey Gladyshev[1], Gennady V. Khen[2] and Gennady A. Kantakov[3]

[1] P.P. Shirshov Institute of Oceanology, Russian Academy of Sciences, Nakhimovsky Prospekt 36, Moscow, 117997 Russia. e-mail: gladyshev@sio.rssi.ru

[2] Pacific Fisheries Research Centre (TINRO-Centre), 4 Shevchenko Alley, Vladivostok, 690950 Russia.

[3] Sakhalin Research Institute of Fisheries and Oceanography (SakhNIRO), 196 Komsomol'skaya Street, Yuzhno-Sakhalinsk, 693023 Russia.

Winter CTD surveys taken in January – March of 1999-2003 in the ice-free areas of the Okhotsk Sea were used to study winter convection. These measurements indicate that convection usually penetrates to a depth of 100-150 m and forms a mixed layer with a density greater than 26.6 σ_θ within the North Pacific inflow. These modified North Pacific waters however do not reach the freezing point. Winter convection does not penetrate deeper than 100 m and forms a mixed layer with a density lower than 26.5 σ_θ in the Okhotsk Sea waters due to their low surface salinity. Interannual variability of winter convection is also discussed.

In addition, for the central Okhotsk Sea between 47-52°N, five CTD surveys taken in September-November 1998-2002 were used to perform volumetric T/S analysis in terms of Modified Dense Shelf Waters (MDSW) and Modified North Pacific Waters (MNPW) in the density range 26.7-27.0 σ_θ. Our calculations show that the MDSW volume has extremely large interannual variability, contributing between 1% to 27% of the total volume of the chosen area. Moreover, we observed MDSW in the 26.9-27.0 density range only in 1999 and 2001. The MNPW volume shows much less variability contributing 23-36% to the total volume. The five-year average mixing ratio between MDSW and MNPW is 1:10 and the five-year average residence time of the upper Okhotsk Intermediate Water (OIW) is 2.4 years. The large interannual variability of the main components of the OIW causes the large interannual variations of the isopycnal T/S properties.

Physical processes in the bottom waters and instability over trenches in the subarctic North Pacific

Leonid Muratov[1] and O. Muratova[2]

[1] V.I. Il'ichev Pacific Oceanological Institute, Far-Eastern Branch of Russian Academy of Sciences, 43 Baltiyskaya Street, Vladivostok, 690041Russia. e-mail: lemur321@mail.ru

[2] Vladivostok State University of Service and Economics, Ecology, 41 Gogolya Street, Vladivostok, 690600 Russia. e-mail: copsmile@mail.ru

The Pacific Ocean is ringed by deep trenches around much of its margin. Today, long-term deep current measurements over trenches at the western and northern edges of the Pacific Ocean Central basin are available through Internet. Some of the readily available long-term deep current measurements over trenches are found at the Home Page of Division of Physical Oceanography, Ocean Research Institute, University of Tokyo.

Since the purpose of the North Pacific Marine Science Organization is to promote and co-ordinate marine scientific research in the temperate and subarctic region of the North Pacific, we will analyze, in this report, the circulation over the northern part of the Izu-Ogasawara Trench, Japan Trench, Kuril Kamchatka Trench and Aleutian Trench. We will follow Johnson (1998) in the first part of report using the illustrations of this work.

No bottom water is formed in the North Pacific Ocean. It enters the Pacific Ocean central basins via a deep western boundary current from the south. Data obtained from a current meter array at the northern end of the Izu-Ogasawara Trench provide evidence of a cyclonic circulation there. Statistics for these current meter records are available on the home page of the Division of Physical Oceanography in the Ocean Research Institute at the University of Tokyo. Some of data were analyzed (Johnson 1998). In this paper, attention was focused on 30 current meter records, nominally located along 34°N, with deployments starting as early as November 1987 and as late as May 1995. The record lengths range from 266 to 536 days, with an average of 401 days. Their longitudes range from 141.17°E to 142.55°E and their depths range from 3830 to 8961 m. The moorings are roughly clustered at six locations, and the deep velocities are similar for most depths and deployments at each location.

Data from moorings along 34°N (available on the home page for the Division of Physical Oceanography, Ocean Research Institute, University of Tokyo) near the north end of the Izu-Ogasawara Trench are records exceeding 100 days. All are below 3800 m depth. Data near 36°N (Hallock and Teague 1996) are between 2000 and 4200 m at the southern end of the Japan Trench. Vectors are averaged at each location (record length weighted) from instruments within these depth intervals.

The mean directions are very closely aligned with the isobaths, and there is a sense of cyclonic circulation around the trench axis. On the western side of the trench, the flow is nominally equatorward with magnitudes of 3.6, 4.6, and 2.4 cm s^{-1}, roughly over the 4500, 6000, and 9000-m isobaths, respectively. At the center of the trench the velocity has a minimum at 0.8 cm s^{-1}, nominally equatorward. On the eastern side of the trench the magnitude is 3.0 and 12.8 cm s^{-1}, but nominally poleward, roughly over the 9000 and 6000 m isobaths, respectively.

Deep current meter data have been discussed over the Kuril-Kamchatka Trench (Johnson 1998), which come from a recent deployment of nine moorings ranging in position along a line from 36.40°N, 146.11°E to 42.30°N to 150.23°E. The current meter records are consistent with a deep cyclonic circulation over the trench, with westward flow on its poleward side and eastward flow on its equatorial side.

Current meters were deployed at nominal depths of 2000, 3000, and 4000 m for a length of 744 to

758 days, with one exception of a 379 day record. The northwestern mooring is located roughly over the 4000 m isobath on the poleward side of the trench axis. The magnitude of the mean velocity at 2000 and 3000 m is only 0.2 and 0.5 cm s^{-1}, respectively, but there is a 4.3 cm s^{-1} flow toward 259°, nominally westward and roughly parallel to the isobaths at 4000 m.

The next mooring to the southeast is located between the 7000 and 6500 m isobaths just on the equatorward side of the trench axis. The flow directions and magnitudes at this mooring are similar at all depths and the record-length average is 8.1 cm s^{-1} toward 59°, nominally eastward, again roughly parallel to the trench axis.

Another current meter array was occupied over the Aleutian Trench along 175°W (Warren and Owens 1985; 1988). Since only two moorings are located over the trench, a cyclonic sense of circulation around the trench is only suggested by these data. This circulation may be shifted poleward of the trench axis because there is eastward flow over the axis. Five moorings were deployed over a fourteen-month period from 45.972 to 50.990°N, with current meters located at nominal depths of 2000, 3000, and 4500 m. Vertical profiles of the mean velocity show a moderate (>3 cm s^{-1}) negative, nominally westward, flow along isobaths on the poleward side of the trench, banked against the Aleutian Island arc.

Interest in the problem of water-column stability in the deep sea basins was stimulated by discussion of possibility of burying radioactive wastes there. Real hydrological conditions in trenches make it possible to apply the disturbance method for theoretical research. Firstly, super-adiabatic gradients of density and temperature are small enough to solve the problem linearly. The conditions are stationary since the main factor, geothermal heat flux, does not seem to noticeably rotate within the time scales under study. Secondly, negative stratification layers have a significant vertical extent, usually some hundred meters. Due to a large vertical scale of motion, the rotation of the earth and the Coriolis acceleration play a decisive role in establishing critical convection parameters. The thickness of the convective layer and horizontal dimensions of cells are of the same order of magnitude. Hence, it becomes necessary to take both horizontal and vertical components of the Coriolis force into account. For meridionally aligned trenches, a weak thermal shear flow is possible under the impact of meridional temperature gradient (Muratov 1991). Together with a stabilizing effect of the earth's rotation, this flow can destabilize and change the convection threshold in oceanic trenches.

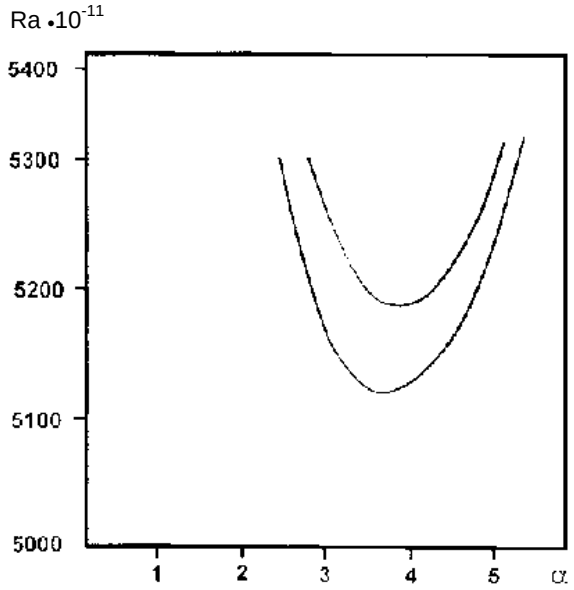

Fig. 1 Calculated neutral curves for Kuril-Kamchatka Trench (above) and Japan Trench (below).

The mathematical approach was developed (Muratov 1991) where salinity variations were neglected and purely thermal convection was considered. The neutral curves for the Kuril-Kamchatka and Japan trenches were obtained by solving a system of eigenvalues. Figure 1 indicates that with less horizontal temperature gradient, the threshold of vertical convection increases. The critical Rayleigh number for the Kuril-Kamchatka Trench was 5.19×10^{13}, and 5.12×10^{13} for the Japan Trench. The minimum of the neutral curve for the former is slightly shifted relative to the minimum of the latter; 3.8 and 3.6 respectively so we can conclude that destabilization is produced by the advective current in the presence of a meridional temperature gradient of a convective regime in bottom layer of trenches.

Another factor that can lead to instability in the bottom layers is the interaction of tidal flows with a layer of "convection with velocity shift". We used the equations for horizontal velocity components (Muratov 1991). To describe friction tension we involved Prandtl's hypothesis of mixing (Fang and Ichiye 1983).

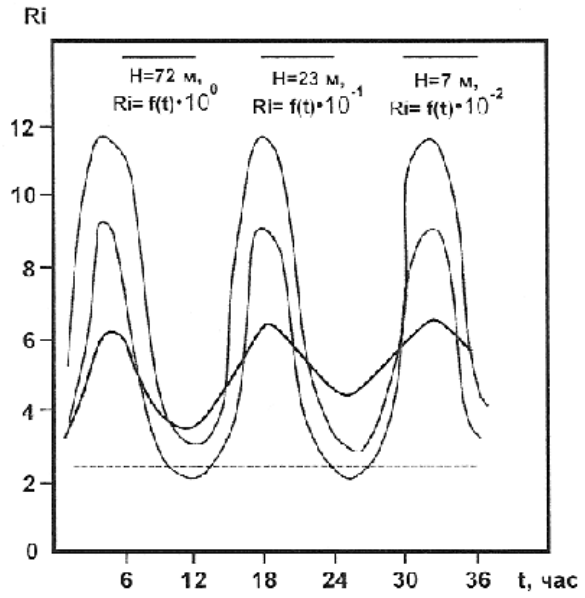

Fig. 2 Time variability of Richardson's number for harmonic O1 for Kuril Kamchatka Trench.

Figure 2 shows the results of calculations of dynamic instability. At first, dynamic stability for parameters typical of South Kuril-Kamchatka Trench was studied. Figure 2 presents the time variability of Richardson's number on some horizons for harmonic O1 when the Hesselberg-Sverdrup parameter is equal to 1. On the whole, dynamic stability decreased with depth. In the case of the central Japan Trench, the velocity of the flux induced by the meridional temperature gradient amounts to 2.2 cm s^{-1} outside the friction layer and turns out to be comparable with tidal velocities. We also calculated Richardson's number alteration in time on some horizons for the M2 tidal wave and values of the tidal flux components were 4.3 cm s^{-1} and 3.6 cm s^{-1} (not shown). Transition to instable dynamic regime occurs between the horizons of 0.5 and 1 m. The period of its fluctuation amounts to 9 hours; the same periodicity here should be expected in intensity of the fine structure generation as well. The change of fluctuation frequency of the dynamic stability parameter occurs, in this case, due to the interaction of an advective shift current induced by meridional temperature gradient with tidal flux.

References

Johnson, G.C. 1998. Deep water properties, velocities, and dynamics over ocean trenches. J. Mar. Res. 56: 329-347.

Hallock, Z.R. and Teague, W.J. 1996. Evidence for a North Pacific deep western boundary current. J. Geophys. Res. 101: 6617-6624.

Muratov, L.F. 1991. Convective and Dynamic Instability in Meridional Trenches. GeoJournal 23: 207-214.

Fang, G. and Ichiye, T. 1983. On the vertical structure of tidal currents in a homogeneous sea. Geophys. J. R. Astr. Soc. 73: 65-82.

Warren, B. A. and Owens, W. B. 1985. Some preliminary results concerning deep northern-boundary currents in the North Pacific. Prog. Oceanogr. 14: 537-551.

Warren, B. A. and Owens, W.B. 1988. Deep currents in the central subarctic Pacific Ocean. J. Phys. Oceanogr. 18: 529-551.

The ρ-, T- , S- of fine structure on the P1W WOCE Section in the Okhotsk Sea in summer

Vladimir N. Vologdin[1], Vladimir B. Darnitskiy[1] and Gennady I. Yurasov[2]

[1] Pacific Fisheries Research Centre (TINRO-Centre), 4 Shevchenko Alley, Vladivostok, 690050 Russia. e-mail: laitik@mail.primorye.ru

[2] V.I. Il'ichev Pacific Oceanological Institute, Far-Eastern Branch of Russian Academy of Sciences, 43 Baltiyskaya Street, Vladivostok, 690041 Russia. e-mail: yugi@poi.dvo.ru

In the fall of 1993 an opportunity arose to conduct a CTD and hydrographic survey along a line of stations through the Okhotsk Sea. This line of observations was conducted to WOCE (World Ocean Circulation Experiment) specifications for accuracy of sampling and nominal spacing (30 nautical miles) of stations. The observations were acquired as a joint project involving scientists from Canada and Russia to execute the westernmost leg of the WOCE line P1, hereinafter referred of to as P1W, from the research vessel *Academik Nesmeyanov* operated by the Pacific Oceanological Institute in Vladivostok, Russia (Freeland, Yurasov et al. 1996).

Thirty-five stations were occupied, and vertical profiles extended to the bottom or 3,500 metres, whichever was shallower. The cruise began on August 30th and was completed on September 21st, 1993 (Freeland et al. 1996). Hydrographic conditions along the P1W (WOCE program) section were considered in the papers (Dyakov et al. 1996; Freeland et al. 1996).

The elements of fine structure (FS) in the Okhotsk Sea, up to depths of 3500 m, had not previously been considered. Information on the FS of North Pacific Intermediate Water in region 155°E (near the beginning of the P1W section) is presented in (Maximenko and Tscherbina 1996).

The influence of various scales of variability of physical fields, especially microstructures, on the behaviour of marine organisms, has been investigated extremely poorly. The necessity of such research is obvious for better understanding of plankton and fish larvae dynamics (Nabatov 1993). For example, the alternated character of turbulence and it existence as separate cellulars is one from the reasons of cellulary distribution of plankton, that essentially influences on trophic relations in a food chains.

The P1W section (first six stations) crosses a region of Pacific water adjacent to the Kuril Ridge that is characterized by strong eddy activity. These mesoscale features are well known from oceanographic observations and from satellite images (Solomon 1979; Bulatov and Lobanov 1983; Darnitskiy and Bulatov 1997). The periodic amplifications of FS interactions on spatial scales from 26.9 up to 100.1 m in the range of the first tens of meters, and from 103.1 – 429.1 m in the range of the first hundreds of meters are established from spectral analysis of vertical structures of seawater density in these stations. The spectral density, or density function of variances on spatial frequencies of a continuous spectrum (Ventsel 1969) for these intrusions were changed within the limits of 0.0012 – 0.0084 for thin-layer stratification and 0.1257 – 0.0260 for large vertical scales. Intensification of the thin structure in the deep water strata was fixed on scales 850.5, 1502.0 and 1701.0 m. The appropriate significance of spectral density was changed within the limits of 0.0317; 0.0326 and 0.0659 accordingly.

The FS stratification on an amount of maximum of ρ-, T-, S- of FS increased twofold, on average, from oceanic stations to the Kuril Ridge, making about 12 centers of ρ-, T-, S- of FS in the upper 400 m stratum near the Kuril Ridge. At the depth of the bottom (Station 6, 2320 m), it has decreased more than twofold in comparison with the seaside deep-water stations (5000-6760 m). The reason for magnification of the intensity of FS stratification of waters near to Kuril Ridge can be explained by amplified exchange of Pacific and Okhotsk Sea waters through the Kuril Straits.

The maximum vertical scale in the Okhotsk Sea is specified only near Academia Nauk Rise (Station 10) and has made 1049.0 m. Maximum scales of thin structure above Derugin Basin were observed at 630, 640 and 649 m (Stations 16, 17, 11).

The amplification of FS stratification of waters was observed on a direction from deep-water stations to a slope (Stations 22, 23), where the amount of fine structure formations was again increased by 2 times compared with the deep-water regions. At that, the decrease in the vertical scale of the strata up to 116-214 m (Stations 24, 22) happened, and to the north of Station 25 (depth = 330 m) fine structure stratification had the scales: meters - first tens meters, minimizing to shallow stations (to Station 30) up to meters. The reason of that is an amplification of factors of vertical exchange at 3-15 times and a horizontal turbulence scales have the magnitude 50-370 m in slope regions (Ozmidov 1985).

The initial stratification of intrusion waters in the region of interaction of Kuril Island arc system happens under the influence of topography, intensive tidal fluctuations of interacting water masses in boundary layers (Darnitskiy and Bulatov 1997) and intensification of internal disturbance (Miropolskiy 1980; Navrotskiy 1990).

More deep-water fine structure features are probably conditioned by inertial-gravitational oscillations of waters and up to 5000 m and more are observed (Orlanski and Bryan 1969; Pochapsky and Malone 1972; Feodorov 1976, 1978). In our case excitation of the seized of Poincare's waves on external (Pacific) part of Kuril Ridge are conditioned by overfall depths in some thousands of meters. The obtained evaluations probably correspond to resonance characteristic of reflected ocean waves, determinate by the form and sizes of Kuril shelf (Fine, 1984).

The differentiation of density, temperature and salinity of FS on depth will be considered in the report.

Specific features of seasonal and interannual variability of water structure and circulation in Aniva Bay during 2001-2003

Valentina D. Budaeva[1], George V. Shevchenko[2], Vyacheslav G. Makarov[3], Gennady A. Kantakov[2] and V.N. Chastikov[2]

[1] Far Eastern Regional Hydrometeorological Research Institute, 24 Fontannaya Street, Vladivostok, 690600 Russia. e-mail: vbudaeva@hydromet.com

[2] Sakhalin Research Institute of Fisheries and Oceanography (SakhNIRO), 196 Komsomol'skaya Street, Yuzhno-Sakhalinsk, 693023 Russia.

[3] Interdisciplinary Center of Marine Sciences of National Polytechnic Institute, La Paz, 23096 Mexico.

Introduction

In 2001-2003 SakhNIRO carried out complex observations of Aniva Bay shelf waters aboard *R/V Dmitry Peskov*. Observations included CTD-sounding of the water column from the sea surface to the bottom at the fixed coordinates on four standard sections in the bay and at three additional sections in La Perouse Strait, with detailed water sampling. The number of stations amounted to 131 in 2001 (April, June, August, October, and November), 161 in 2001 (January, April, June, August and October), and 58 in 2003 (April and June) (Fig. 1). On average every survey took about 2 days. Hydrological observations in the bay were aimed at diagnosing oceanological fields, determining the nature of density and wind induced water circulation, and identifying specific features of seasonal and interannual water and heat exchange between Aniva Bay and surrounding shelf waters.

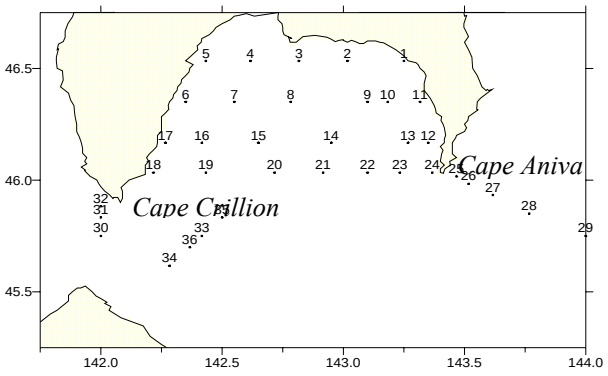

Fig. 1 Location of CTD stations.

Besides the tidal effects and significantly variable seasonal atmospheric conditions, hydrophysical structure of the La Perouse Strait and Aniva Bay waters is mainly dependent on interaction of waters of different origin (Biryulin 1954; Shelegova 1958; Leonov 1960; Watanabe 1963; Moroshkin 1964, 1966; Aota 1970, 1975, 1984; Akagawa 1977; Takizava 1982; Aota et al. 1988; Watanabe 1995; Budaeva and Makarov 1996, 1999; Itoh and Ohshima 2000). Aniva Bay waters are close to subarctic waters and have a similar stratification. The vertical thermal structure of Aniva Bay water is characterized by a cold intermediate layer (CIL) with a negative water temperature (-1.5 to -1.6°C). Low water temperature in the CIL core is a first indicator of its renewal.

Data and methods

Sea currents in the relatively shallow Aniva Bay were estimated from an updated 3D numerical baroclinic Ekman-type model with constant coefficients of vertical turbulent exchange (Budaeva and Makarov 1999). This sigma-coordinate model takes into account the real bottom relief and coastline, nonuniform distribution of density and surface wind, and water flows through the open boundaries. A horizontally regular 5′ × 5′ grid was used. Sea currents at 8 specified horizons were determined by one-dimensional interpolation of vertical profiles of the 3D velocity vector components calculated at every horizontal point. Coastline and sea depth in the grid were taken from a bathymetric map of Aniva Bay and La Perouse Strait (1:250000 scale along 52° parallel, 1992). Boundary conditions at the open boundaries were specified according to (Kantakov et al. 2002).

Calculated sea currents were verified over precomputed characteristics of the density water

Table 1 The general characteristics of Aniva Bay density structure from 2001-2003.

Year	Month	Density, σ_t, 0 m	Density, σ_t, near bottom	Horizontal density gradient, σ_t/km	Vertical density gradient, σ_t/m	Pycnocline depth, m
2001	*April*	25.42-25.97	25.78-26.62	0.032	0.02-0.05	5-45
	June	24.05-25.07	25.21-26.55	0.045	0.05-0.21	4-34
	August	22.43-23.35	25.27-26.60	0.01-0.06	0.20-0.50	5-20, 4-36
	October	23.92-24.60	24.54-26.57	0.060	0.10-0.50	15-60
	November	24.42-24.82	24.60-26.43	0.016	0.01-0.12	15-70
2002	*January*	25.18-25.28	25.28-26.21	0.009	0.04	15-80
	April	25.21-25.81	25.58-26.54	0.034	0.09	10-55
	June	24.42-24.93	24.57-26.58	0.028 (0.03)	0.14	6-34
	August	21.82-23.89	23.40-26.40	0.075	0.35 (0.44)	15-45 (50)
	October	23.70-24.62	24.25-26.49	0.060	0.24	15-60
2003	*April*	25.69-26.01	25.91-26.55	0.017	0.015-0.045	10-55
	June	24.34-25.12	25.83-26.54	0.045	0.05-0.23	5-23

structure, such as pycnocline depth and intensity and horizontal density gradients. These parameters were used to identify location of eddy cores, coastal frontal sections and vergence zones, and anomalous water dynamics in Aniva Bay.

Density distribution

Annual variability of the density structure in 2001-2003 (Table 1) was characterized by two extreme features: increased nonuniformity of hydrophysical fields with high absolute values of horizontal (up to 0.045-0.075 σ_t km^{-1}) and vertical (up to 0.35-0.50 σ_t m^{-1}) density gradients in summer, and more homogeneous distributions in winter with low magnitudes of density gradients (up to 0.009 σ_t km^{-1} and 0.04 σ_t m^{-1}, respectively).

Annual variability of the surface density in the bay is mainly explained by the seasonal change of temperature. These processes are in antiphase. In April-August background surface density was falling steadily (from 25.75-26.00 to 22.40-23.6 σ_t), whereas it started growing everywhere in autumn-winter, from September to March approximately. On the contrary, mean values of near-bottom density were falling in autumn-winter (mainly due to low water salinity) and growing in spring-summer (Table 1). Location of the 26.5 σ_t isopycnal might be an indirect tracer of the near-bottom density variability within a year. In November 2001 and October 2002, an area of near-bottom waters within this isopycnal was much smaller than in spring and summer of the same years. In January 2002, such waters were not registered in the southern deep-water part of Aniva Bay. Hence, the annual cycle of the near-bottom density variability finished with the end of the calendar year (2001-2002, 2002-2003). There is a good reason to assume that such a completion repeats every year.

Interannual variability of density was characterized by significant freshening of all the bay waters during a warm season of 2002. As a result, mean values of surface and near-bottom density during this year were lower than density registered in 2001 and 2003 (Table 1). The presence of closed isolines in the field of pycnocline depths might be interpreted as the local dynamic structures (see Fig. 2).

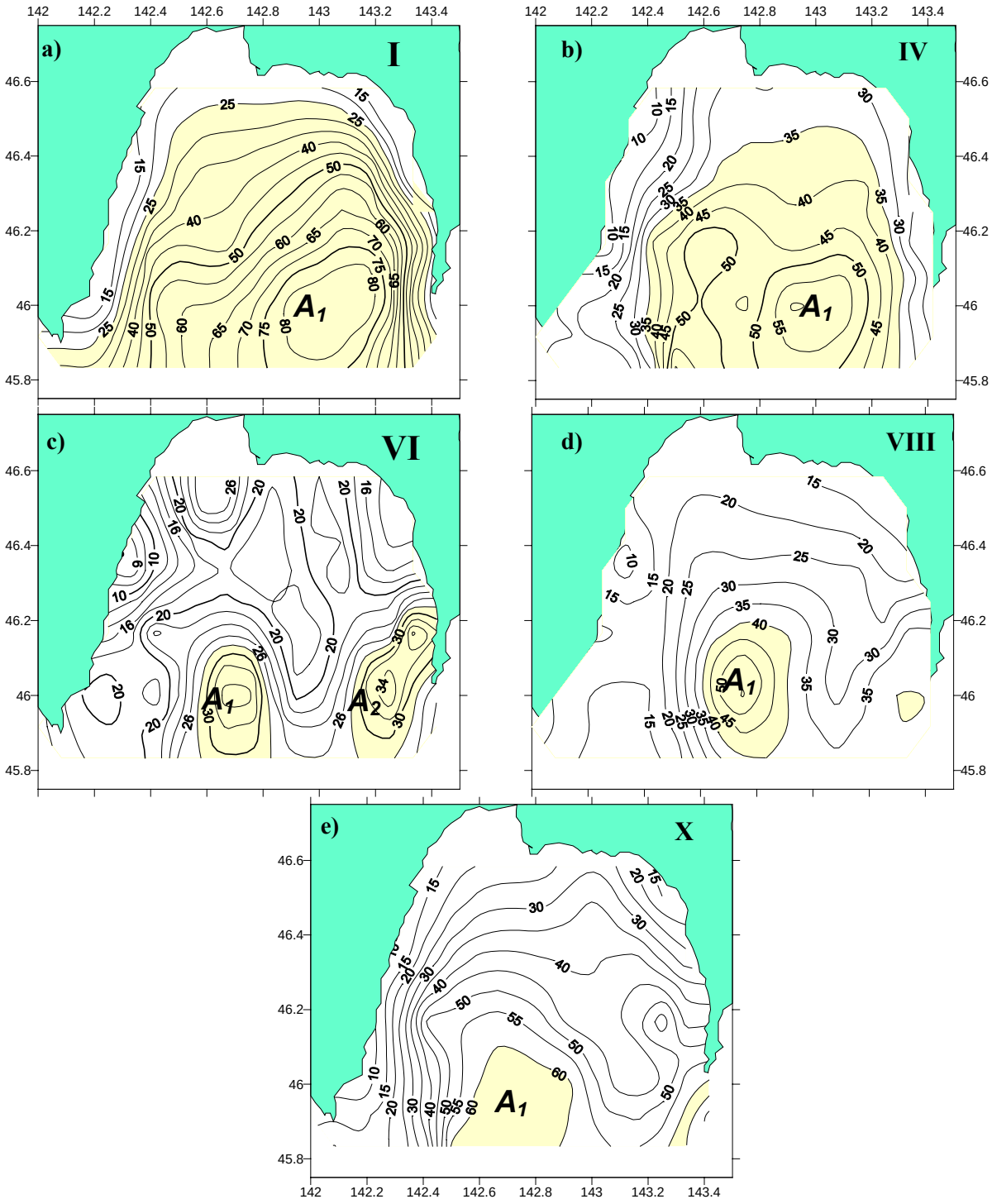

Fig. 2 Depth of the maximum vertical density gradient, m: (a) January, (b) April, (c) June, (d) August, (e) October, 2002.

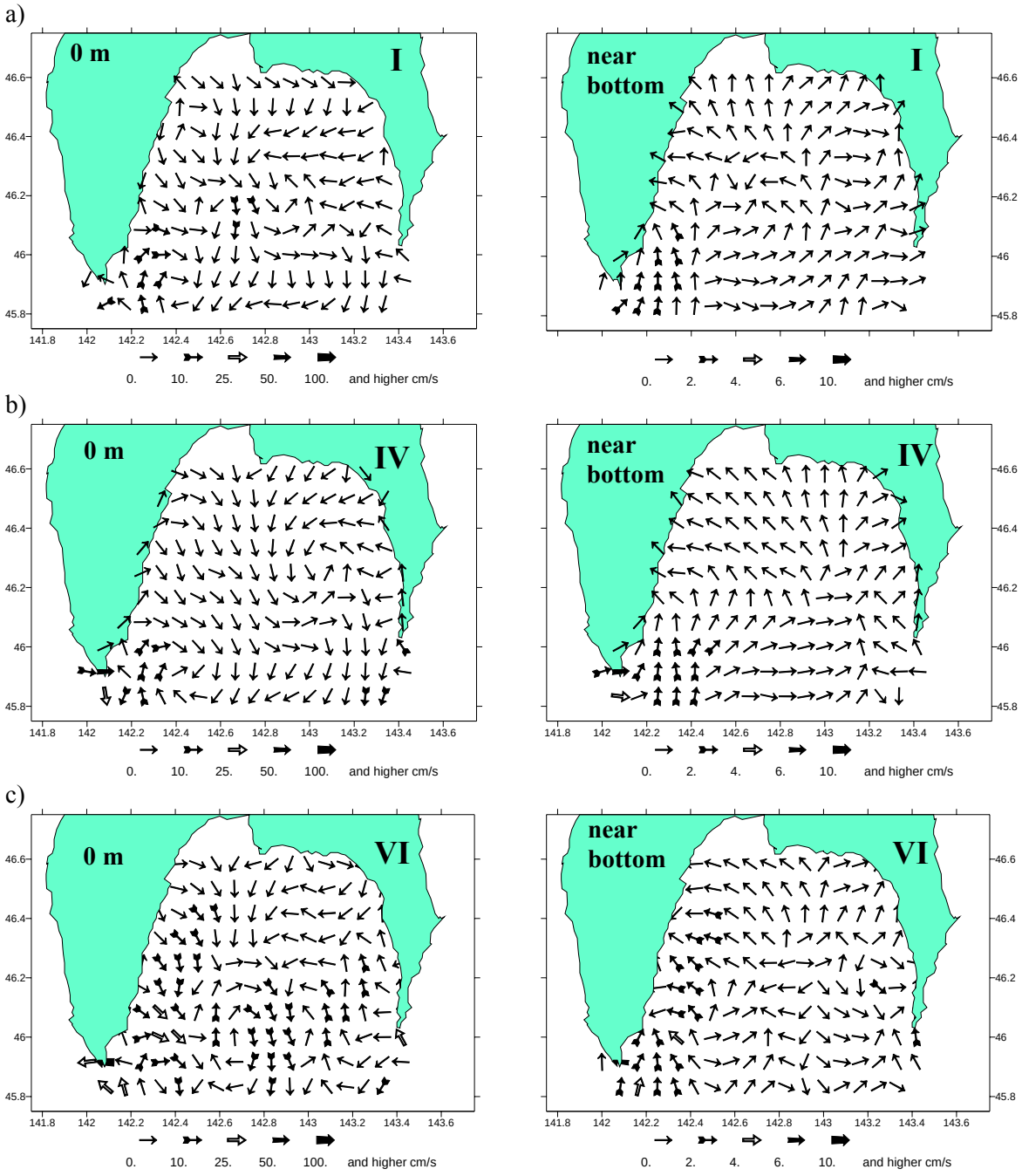

Fig. 3 Sea currents in Aniva Bay, 2002.

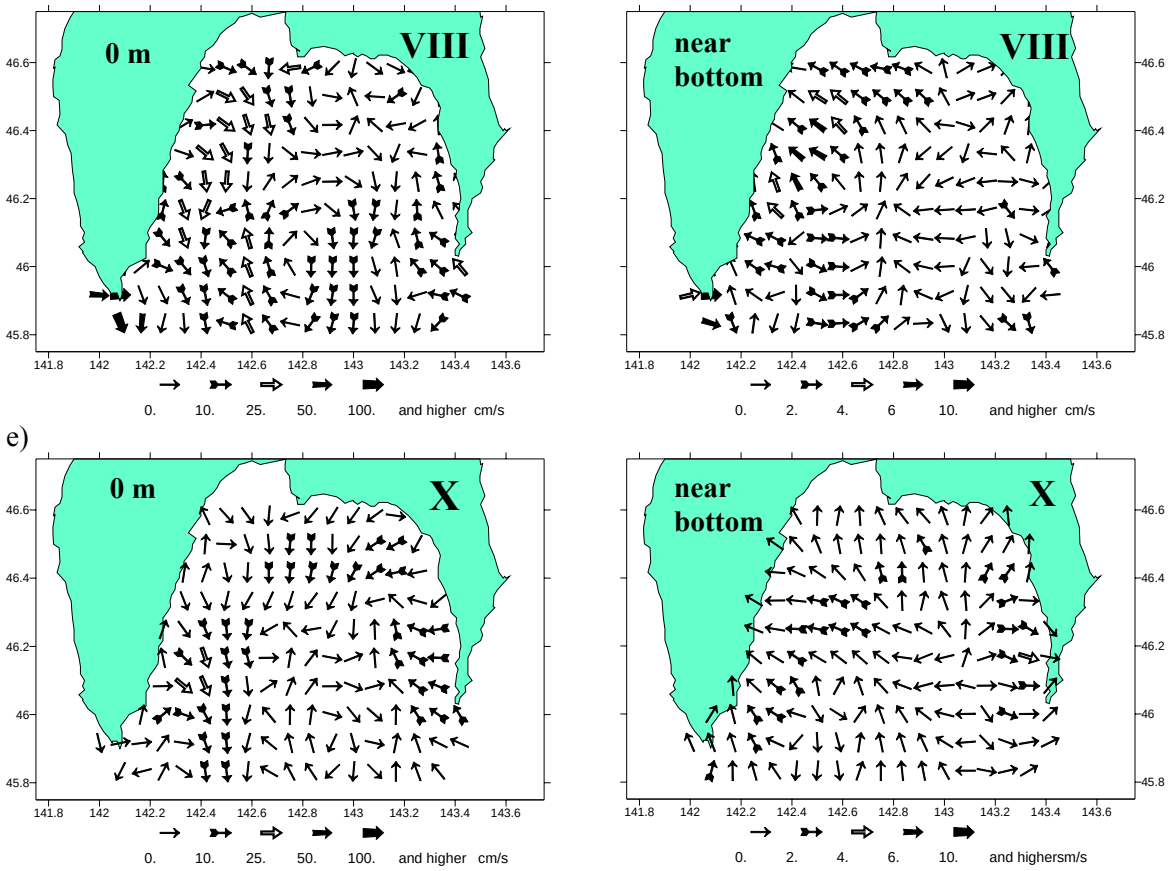

Fig. 3 (continued) Sea currents in Aniva Bay, 2002.

The character of pycnocline deepening indicates that the currents have an anticyclonic vorticity during all seasons of the year, but with differing extents. A quasi-stationary anticyclonic eddy A_1 is the main structural element here. Due to convergence, this eddy can be the permanent accumulator of heat (cold) and polluted coastal waters.

The deepest pycnocline location (up to 70-80 m) in Aniva Bay during winter is connected with the downward density convection, the intensity and depth of which are dependent on the extent of the cooling of surface waters. The area of eddy A_1 and its intensity with depth are considerably larger in winter than in summer. At the end of the calendar year, the whole water mass of Aniva Bay is included in this eddy, except for a thin near-bottom layer. However, despite its larger size in winter compared with summer, its dynamics are significantly lower, probably due to the relatively homogeneous distribution of both horizontal and vertical density gradients and their low magnitudes.

Circulation and water exchange in Aniva Bay

Surface currents in winter are generated by dominating northwesterly and northerly winds (winter monsoon) that usually push the water level away from Aniva Bay. In autumn, the winter monsoon leads to the development of intensive southward currents. Outflow of the surface waters from the northern shallow part of the bay initiates compensatory reverse flows near the bottom and elevation of the sea level at the coast. At the same time, wind-induced flow near the bottom increases against the background of the permanent thermohaline currents. On the whole, the winter monsoon facilitates development and homogenization of anticyclonic circulation in the bay. Longitudinal and transversal diameters of eddy A_1 and its intensity increases with depth. In winter, when the spatial and vertical heterogeneity of the density field is low (~0.0005-0.0015 σ_t km^{-1} and

0.01-0.03 σ_t m^{-1}, respectively), water circulation in Aniva Bay is weakly dynamic (January 2002), except for the bottom layers in western part of the bay with intrusions of the Japan Sea waters (Fig. 4a, b). There were nearly no thermohaline currents registered in the shallow waters of the northern coast (section at 46.32°N); some stations had almost uniform vertical density distribution.

Intensified water circulation in Aniva Bay in spring-summer coincides with intensification of the Soya Current and increasing contribution of haline factors into the formation of the current field. Precipitation and river discharge intensifies stratification in the thermocline and formation of coastal fronts. Vertical exchange weakens and horizontal circulation strengthens. As a result, the character and intensity of water exchange between the bay and surrounding shelf change as well. Coastal jet currents evolve, as a rule, at the surface at the periphery of A_1. Increasing heterogeneity of water stratification in summer and typical southeasterly winds transform A_1; its area diminishes and it splits into several smaller eddies (Figs. 2-3, summer 2002).

The other remarkable feature of water dynamics in Aniva Bay is that the water exchange is driven mainly by meridional flows. As is seen from the vertical sections of a meridional component (V) of the velocity across eddy A_1 at the latitude of 46°N (Fig. 4a, c), it is highly variable in both the magnitude (maximum values amount to 20-25 cm sec^{-1}), and direction.

Interannual variability

It is not possible to evaluate the scale of interannual variations of winter circulation in the bay, because the only one detailed hydrophysical survey (CTD-observations with 1 meter resolution) in Aniva Bay was carried out during winter (January 2002). At that time waters in the narrow belt along the bay perimeter were the coldest ones (up to -1.0 – -1.3°C) as compared to the surrounding waters (up to -0.5 – -0.9°C). A new CIL (see Fig. 4b) was registered within this zone where the density convection reaches the bottom. Coastal waters are evident as the main local source of the CIL in Aniva Bay. However, there were no traces of the previous year's CIL found in deep waters of the bay during the second 10-day period of January 2002 as well. Hence, it might be concluded that complete renewal of the previous year's CIL was completed at the end of 2001.

Using January 2002 data, water salinity maps of the surface and near-bottom waters demonstrate only the general features of winter haline conditions in Aniva Bay (Fig. 4e). Waters of the prevalent East Sakhalin Current (ESC) initiated intensive freshening of the whole water mass (up to 31.35-31.40 psu at the surface and 31.40-32.50 psu – near the bottom) from autumn to winter. Winter conditions are distinguished by the absence of the 32.5 psu isoline within the bay basin. Such a significant freshening of the whole water mass of the bay apparently indicates annual complete renewal of local waters, rather than their local transformation. Even winter water convection and increasing salinity due to formation of ice are not able to withstand this tendency.

The range of interannual variations of water dynamics in Aniva Bay in early spring (April) is much lower than in summer. In spite of significant differences in thermal conditions in April 2001, 2002, and 2003, the estimated spatial structure of the surface currents was almost the same: the lightest and freshest waters were slowly (less than 5-10 cm s^{-1}) flowing out from the top of the bay (Fig. 3). In April 2001, the permanent current with a northward component was observed in the upper 0-50 m layer along 46°N. This current was related to the second (eastern) core of eddy A_1 that was also distinctly traced in the pycnocline layer and surface salinity near Cape Aniva. Near the bottom there were traces of external shelf waters that entered the coastal zone. The presence of such waters was indirectly confirmed by the formation of near-bottom fronts with high gradients. For example, there were inflows (especially active in April 2002) of the Japan Sea waters to the western part of Aniva Bay (Fig. 3).

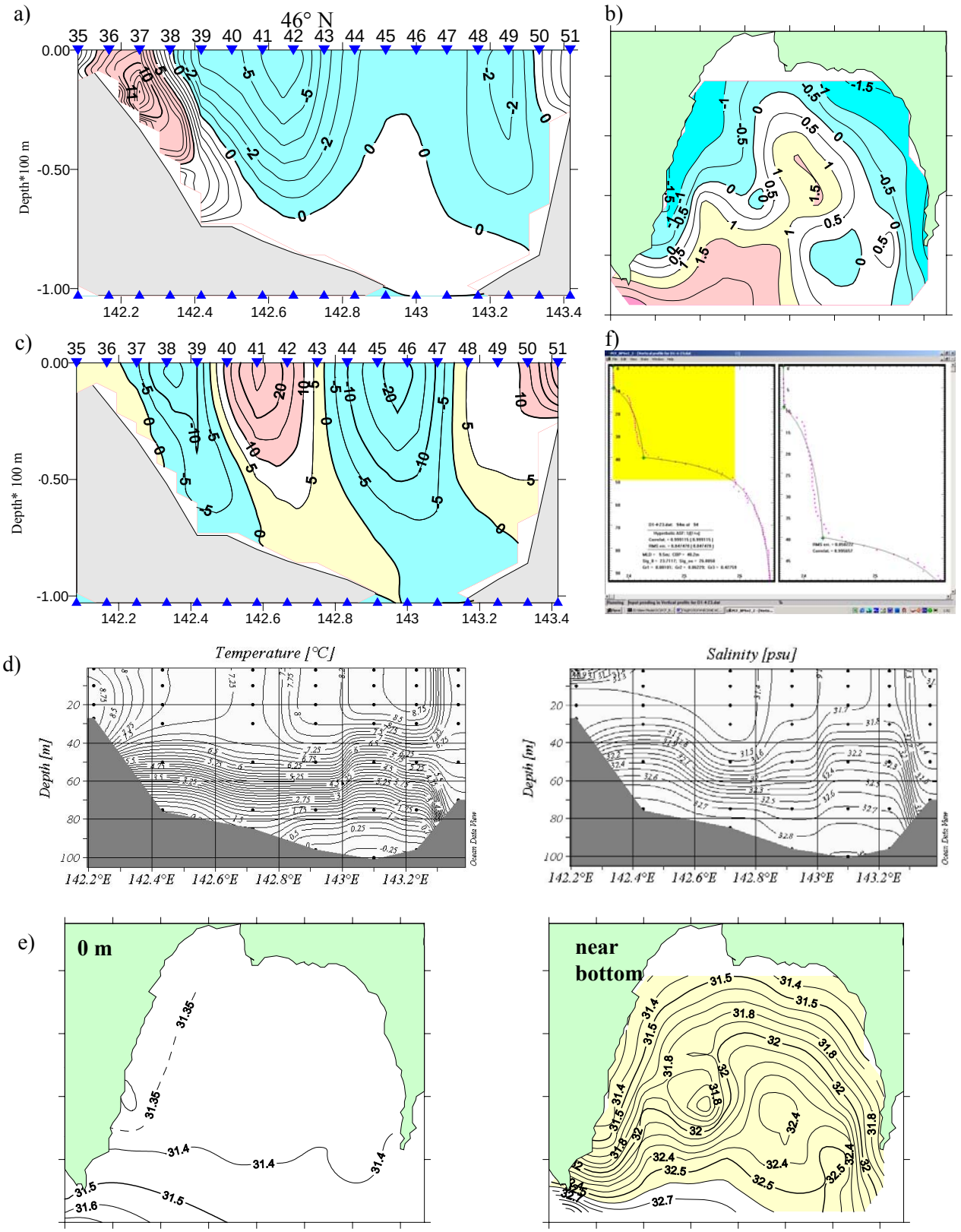

Fig. 4 Vertical section of current velocity (V component) A_1, 46°N – a) January; c) August; b) near-bottom temperature (°C); d) temperature and the salinity in October; e) salinity in January; f) profile of density (from an analytical model) in August, 2002.

While thermohaline factors (river discharge, precipitation, etc.) were becoming more important during the warm period of 2001 and 2002, water exchange between the bay and the surrounding shelf was intensifying with the enhancement of the Soya Current and with increase of the sea level gradient between the Japan and Okhotsk Seas. Summer of 2002 was characterized by active water mass exchanges in the surface (20-30 m) layer in western Aniva Bay. Here, the lightest and freshest waters were observed to move from the coast (Lososi Bay) to the open part of the bay. The other area of the summer accumulation of the bay waters is the eastern periphery of anticyclonic eddy A_1. As was mentioned before, the high water dynamics are caused by extreme freshening of the surface waters. Figure 3 (Summer 2002) shows the resultant coastal fronts associated with the intensive southward currents (up to 20-30 cm s^{-1}). In summer of 2001 and 2002 water masses near the bottom were transported mainly northward, that is deep into the bay. However, the spatial structure of bottom currents in summer of 2001 was rather smooth, while in summer of 2002 it was characterized by generation of local eddies and increase of current speed (up to 6-10 cm/s vs. 2 cm s^{-1}). The above differences are due to specific weather conditions during the surveys (moderate NW-NE winds, 5-10 cm s^{-1}) and active interaction between the genetically different water masses. Wind effects and mixing of heterogeneous water masses caused uneven distribution of hydrophysical characteristics (in particular, the second additional water density jump- Fig. 4f) with associated patchiness of currents in Aniva Bay in summer of 2002.

In the beginning of autumn, hydrological conditions in the bay were influenced mainly by the ESC. In November 2001 and October 2002, the ESC waters entered the bay and spread mainly along the eastern periphery of anticyclonic eddy A_1 as a narrow northward stream. Due to Amur River discharge, ESC waters were less saline as compared to external shelf waters and highly homogeneous as compared to the local waters. The most evident intrusion of ESC waters was observed at a longitudinal section along 46°N and confirmed indirectly by distribution of water salinity, water temperature and meridional component of current velocity (V) in November 2001 and October 2002. According to the sections shown in Figure 4d, in October 2002 the ESC occupied the whole water column near Cape Aniva, and its western edge coincided with 31.7 psu isohaline. At the same time, the thermocline near the shelf edge (near Cape Aniva) thickened and split, accompanied by the upper isotherms/isohalines coming to the surface and lower isotherms/isohalines deepening. As a result, near-bottom fronts formed. In autumn 2002, horizontal water circulation was represented by alongshore currents conditioned on the southward discharge current (25 cm s^{-1}) in the western part of the bay and on northward compensatory flow formed by the ESC that enters the bay off Cape Aniva (10-25 cm s^{-1}). Maximum speeds were registered near the 50 m isobath. An anticyclonic eddy A_1 (5-10 cm s^{-1}) was also observed in the open part of the bay, westward of 143°E. The outflow of relatively warm surface waters from the bay during the autumns of 2001 and 2002 was marked in the western part of the bay mainly, near the local frontal section. Compensatory flows, mainly N, NW and NE, were registered near the bottom, their speed amounting to 2-3 cm s^{-1}.

However, due to model restrictions, the current fields shown in Figure 3 capture only the general description of seasonal and interannual variability of water circulation in the bay. At the same time the model calculations are quite adequate in reproducing intensification of currents in summer and autumn and their weakening in winter, as well as the prevalence of meridional flows in the water exchange between the bay and external shelf, and agree well with observations (Shevchenko et al, 2004).

Conclusions

Data from 12 CTD surveys were used to study the features of seasonal and interannual variability of water structure in Aniva Bay. Coastal and near-bottom fronts were found. As a rule, water circulation in the bay has two layers: surface discharge of relatively fresh currents with rather high speeds (up to 20-30 cm s^{-1}) and slower compensatory currents of Okhotsk Sea origin with bottom intrusions of Japan Sea waters that spread from the west under an anticyclonic eddy A_1.

The morphometric characteristics of eddy A_1 and the thermal parameters of the CIL change considerably within a year, indicating its complete annual renewal. The CIL in Aniva Bay is mainly of local origin, caused mainly by convective cooling of waters at the northern periphery of A_1.

Water salinity is greatly determined by river discharge, precipitation and intensification of ESC. In late fall (October-December), this current causes significant salinity changes in the whole water mass of the bay.

References

Akagawa, M. 1977. Characteristics of oceanographic conditions in the Okhotsk Sea and meteorological conditions over the Far East in November. Oceanogr. Mag. 28: 33-45.

Aota, M. 1970. Study of the variation of oceanographic condition North-East of Hokkaido in the Sea of Okhotsk. II Low Temperature Seine. 28: 261-279.

Aota, M. 1975. Studies on the Soya Warm Current. Low Temp. Phys. Sci. 33: 152-172.

Aota, M. 1984. Oceanographic structure of the Soya Warm Current. Bull. Coast Oceanogr. 22: 30-39 (in Japanese).

Aota, M., Ishikawa, M., Yamada, T. 1988. Dynamic of flow in the Soya Strait. Low Temp. Phys. Sci. 47: 147-160.

Biryulin, G.M. 1954. Hydrometeorological description of fishery areas in the Southern Sakhalin. Proceedings of Kuril-Sakhalin marine expedition of ZIN-TINRO, 1947-1949. -M. Publishing House of USSR Academy of Science 1: 167-303 (in Russian).

Budaeva, V.D. and Makarov, V.G. 1996. Modeling of the typical water circulation in the La Perouse Strait and Aniva Gulf region. PICES Sci. Report. Sidney. Canada No. 6: 17-20.

Budaeva, V.D. and Makarov, V.G. 1999. A peculiar water regime of currents in the area of the Eastern Sakhalin shelf. Proceeding of the Second PICES Workshop on the Okhotsk Sea and adjacent Areas, Sidney, Canada.pp. 131-138.

Itoh, M. and Ohshima, K. 2000. Seasonal variations of water masses and sea level in the southwestern part of the Okhotsk Sea. J. Oceanogr. 56: 643-654.

Kantakov, G.A., Chastikov, V.N. and Shevchenko, G.V. 2002. Present-day sea current observations in fishery areas of the Sakhalin-Kuril region. Biology, stock and living conditions of hydrobionts in the Sakhalin-Kuril region and adjacent waters. SakhNIRO Proceedings. 4: 3-21.

Leonov, A.K. 1960. Regional oceanography. L.: Hydrometeoizdat 765p. (in Russian).

Moroshkin, K.V. 1966. The Okhotsk Sea water masses – M., Nauka. 66p. (in Russian).

Moroshkin, K.V. 1964. A new pattern of surface currents in the Okhotsk Sea. Oceanology 4: 641-643. (in Russian).

Shelegova, E.K. 1958. The influence of the Japan Sea waters on the thermal regime and fishery near Sakhalin southeastern coast. Bulletin of Technical and Economic Data. Yuzhno-Sakhalinsk: SNH, pp. 7-9 (in Russian).

Shevchenko, G.V, Kantakov, G.A., Chastikov, V.N. 2004. Direct current measurements in the Aniva Bay during fall 2002. Proceedings of the 19th international symposium on Okhotsk Sea & Sea Ice. 22-28 February 2004. Mombetsu, Hokkaido, Japan. pp. 287-293.

Takizava T. 1982. Characteristics of the Soya Warm Current in the Okhotsk Sea. J. Oceanogr. Soc. Japan 38: 281-292.

Sea surface eddy detection on IR- satellite images under cloudy conditions

Anatoly I. Alexanin and M.G. Alexanina
Institute of Automation and Control Processes, Far-Eastern Branch of Russian Academy of Sciences, Radio Street 5, Vladivostok, 690041 Russia. e-mail: aleks@satellite.dvo.ru

Thermal structures of sea surface can be determined from the dominant orientations of thermal contrasts (DOTC) on IR satellite images. Essentially DOTC are the statistically significant tangents to the isotherms in the vicinity of a point. High correlation of dominant orientations with directions of sea surface current velocities and their stability during some days makes it possible to detect meso-scale eddies from the composition of DOTC fields. In the work presented, a question of creating composition of DOTC fields under the cloudy conditions of Okhotsk Sea was considered. The Kuril region was chosen as the most cloudy and dynamic for this purpose. High coincidence between the dominant orientations of thermal contrasts and sea surface current directions allowed construction of an algorithm for automatically detecting eddies and their parameter estimation based on an analytic eddy model. The model is characterised parameters that include the eddy center location, size, eddy boundaries and location of maximum velocity zone. The work was supported by the RFBR grant № 03-01-00812.

Methane flux in the Seas of Okhotsk and Japan

Galina Mishukova, Vasiliy Mishukov and Anatoliy Obzhirov
V.I. Il'ichev Pacific Oceanological Institute, Far-Eastern Branch of Russian Academy of Sciences, 43 Baltiyskaya Street, Vladivostok, 690041 Russia. e-mail: pacific@online.marine.su

Introduction
Different scientists remark that the formation of ozone holes and greenhouse effects can be explained by large variations of methane in the atmosphere, which is connected with natural sources of methane. Various authors have determined that the Sakhalin shelf and the Okinawa trough can produce significant intrusions of methane during periods of strong seismic activity in these regions. These investigations emphasize the importance of methane flux research, particularly in seismically active zones.

Experimental research
Methane distribution in Primorsky region has been studied for the last decade. Averaged data for some parts of Primorsky region are demonstrated in Table 1. Averages from various sources include: a) surface fresh waters such as spring waters, brooks, sand-pits, lakes and rivers; these are practical sources of methane input in atmosphere from land; b) underground water such as draw-wells, bore-wells and well-pits that characterise the potential of methane input from land; c) marine coastal surface waters. The investigation of methane distribution was done in cross-section from Vladivostok to Niigata at November 1995 in the Sea of Japan and in different regions and seasons for the Sea of Okhotsk from 1999-2001.

Discussion
Table 1 demonstrates the existence of powerful sources of methane at Luchegorsk and Chernigovka regions but does not demonstrate much influence of the Baranovskiy volcano. One can see strong methane supersaturation of fresh waters in the Primorsky region.

We observed underwater maximums of methane concentration at 50-150 m and 300-600 m depth which were formed in Japan Sea areas. Fall-winter convection destroyed this maximum at stations near Vladivostok. Methane concentrations in surface marine waters were under-saturated with atmospheric methane concentrations.

Table 1 Methane concentration (nl/l) in various waters in Primorsky region.

Part of Primorsky region (town name)	Surface fresh water	Underground water	Marine coastal water	Year
Luchegorsk	14670	24640		1997
Novopokrovka	905	60654	—	1997
Gornye Kluche	252	14277	—	
volcano Baranovskiy	43	1228	—	1997
Chernigovka	10740	—	—	1996
Gornovodnoe	3	1107	—	
Anisimovka	645	88	—	1996
Artem	271	1308	—	1996
Khasanskiy region	50 1760 25	280906 130259 —	— — 66	1995 1996 1997
Ussuriyskiy Bay	813	357	525	1997
Popov Island	6	268	61	1997

Mathematical model for computation of methane flux between the Sea of Japan and atmosphere was proposed which permitted to take into account the influence of bursting bubbles on gas exchange. For the Sea of Okhotsk we observed many underwater sources of gas bubble plumes on the sea bottom. These plumes give very changeable picture of distribution of methane in seawater for different regions and seasons. Surface waters are supersaturated and methane fluxes to the atmosphere were from 7 - 90 mol/km^2*day in summer and from 14 to 175 mol/km^2*day in autumn.

"Car-jam" effect and concentration anomalies in rising bubble plumes

Alexey O. Maksimov
V.I. Il'ichev Pacific Oceanological Institute, Laboratory of Nonlinear Dynamical Systems, Far-Eastern Branch of Russian Academy of Sciences, 43 Baltiyskaya Street, Vladivostok, 690041 Russia. e-mail: maksimov@poi.dvo.ru

Natural hydrocarbon seeps are found in varying intensity along most continental shelves. These seeps emit gas, oil, or a mixture of both from seafloor vents. Free bubbles rise from the sea bed into the water column and form a flare. Bubble flares are registered by standard shipboard sonar as acoustic anomalies in backscattering and are seen as dark curtains on sonar paper chart records (Anon. 1988; Leifer and Patro 2002). Bubble-mediated transport for a natural hydrocarbon seep is a complex process dependent upon many parameters. Some seeps are little more than gentle emanation of bubbles from a few vents, while others bubble vigorously from dense vent clusters. This research seeks to provide the necessary theoretical background to allow modeling of gas bubble streams and to solve inverse problem of evaluation of parameters of gas vents using echo-sounding data.

A comprehensive review of theory and the basic equations governing of bubble mediated gas transfer is presented in (Leifer and Patro 2002). Unfortunately, the native publications (Ezerskii et al. 1989; Goncharov and Klement'eva 1996; Maksimov 1998) are absent in this review. Seep bubbles are often observed escaping from the seabed as a stream of nearly pure CH_4 bubbles. Bubble CH_4 is highly supersaturated with respect to the bulk ocean and rapidly outflows from the bubble, causing bubble dissolution. The mass flow for any gas (CH_4, N_2 and O_2) is described by (Ezerskii et al. 1989; Leifer and Patro 2002)

$$dN_i / dt = 4\pi R^2 k_{Bi}(R, \nu_i, D_i)(c_i - P_{Bi} / H_i) \qquad (1)$$

where N_i is the number of moles in the bubble, R is the bubble radius, c_i is the aqueous concentration, P_{Bi} is the partial pressure in the bubble, H_i is Henry's Law constant. The gas transfer rate k_{Bi} is strongly dependent on R, the ratio of molecular diffusivity D to advective transport and effect of surfactants. The internal bubble pressure $P_B = \sum P_{Bi}$ is primary a function of hydrostatic pressure $P_B = P_0 + \rho_w g z = P_0(1 + z/h)$, where ρ_w is the water density, g is the gravitational constant, z is the water depth (positive with increasing depth) and h is the characteristic depth where hydrostatic pressure is doubled ($h \approx 10$ m); the Laplace pressure is negligible for bubbles larger than 7 μm.

As a bubble rises, its radius changes due to mass flux and decreasing hydrostatic pressure. The equation describing variation in bubble radius can be derived from the ideal gas law, and if isothermal, in differential form as

$$\frac{4\pi}{3} R^3 \frac{dP_{Bi}}{dt} + 4\pi P_{Bi} R^2 \frac{dR}{dt} = \mathrm{i} T \frac{dN_i}{dt}, \text{ or}$$

$$\frac{dR}{dt} = \sum_i k_{Bi} \frac{\mathrm{i} T}{P_0} \frac{[c_i - (P_{Bi} / H_i)]}{1 + (z/h)} - \frac{R}{3} \frac{d(z/h)/dt}{1 + (z/h)} \qquad (2)$$

While the CH_4 outflows from the bubble, dissolved air inflows, slowing the rate of bubble dissolution. For the case when air inflow has a negligible effect on R Eq. (2) can be rearranged to yield

$$\frac{dR}{dt} = k_B \frac{\mathrm{i} T}{P_0} \frac{\left[(c - c_0)/c_0 - (z/h)\right]}{1 + (z/h)} - \frac{R}{3} \frac{d(z/h)/dt}{1 + (z/h)} \qquad (3)$$

here c_0 is the equilibrium concentration for CH_4 under atmospheric pressure and we omitted index. Newly formed bubbles rapidly accelerate to their terminal rise velocity $v_B(R)$, as determined by the balance between the buoyancy and drag forces. Thus the final differential equation needed to describe bubble evolution has the following form

$$\frac{dz}{dt} = -v_B = -\left(\frac{2}{9}\right) g \frac{R^2}{\nu} \qquad (4)$$

The explicit expression for the velocity corresponds to dirty bubbles and small *Re,* here ν is the viscosity. For the same case Eq. (3) takes the form

$$\frac{dR}{dt} = -\frac{2}{\pi}\left(\frac{2}{9}\right)^{1/3}\left(\frac{D^2 g}{\nu}\right)^{1/3}\frac{c_0}{\rho_g}\frac{(z/h)}{1+(z/h)} - \frac{R}{3}\frac{d(z/h)/dt}{1+(z/h)} \quad (5)$$

where we neglect difference between aqueous and equilibrium concentrations.

Equations (3) and (4) with appropriate choice of k_B and v_B now together define the vertical motion of the bubble, and its change in radius and composition with time. Using these equations the occurrence of anomalies in concentrations of gas inclusions can be predicted. The inhomogeneity of bubble rise velocity with depth results in that the growth of bubble concentration occurs at the horizon with minimal velocity. One can draw a close analogy to the effect, arising in the theory of transport flows, when at braking "car-jam" occurs and, on the contrary, at acceleration decreasing of concentration takes place.

The bubble distribution, as a function of position **r**, time t and radius R — $f(\mathbf{r},R,t)$, satisfies a kinetic-type transport equation

$$\frac{\partial f}{\partial t} + \frac{\partial}{\partial z}\left(\frac{dz}{dt}f\right) + \frac{\partial}{\partial R}\left(\frac{dR}{dt}f\right) = 0 \quad (6)$$

Remind that the normalization of the distribution function — number of bubbles in unit volume with radii in interval $[R,\ R+\Delta R]$ is $\mathrm{m^{-3}\mu m^{-1}}$. We transform governing equations (4-6) into non-dimension form by introducing $t' = t/\tau^*$, $\tau^* = (3\pi/2)(3/4\pi)^{1/9}(c_0/\rho_g)^{-2/3}(\nu^5 h^3/D^4) \approx 137s$;
$R^* = (162/\pi^3)^{1/9}(c_0/\rho_g)^{1/3}(D^2\nu^2 h^3/g^2) \approx 1.9\cdot 10^{-4}\mathrm{m}$,
$R' = R/R^*$ $z' = z/h$. A steady state solution of kinetic equation (6) satisfies to

$$\frac{\partial}{\partial z'}(R'^2 f) + \frac{\partial}{\partial R'}\left[\left(\frac{z'}{1+z'} - \frac{1}{3}\frac{R'^3}{1+z'}\right)f\right] = 0\,. \quad (7)$$

It may be shown [5] that Eqs. (4, 5) have an integral

$$\frac{R'^3}{3}(1+z') - \frac{z'^2}{2} = Const\,, \quad (8)$$

so that on substituting (8) in (4, 5) exact solutions can be obtained. The characteristics of kinetic equation (7) are simply the bubble dynamic equations. Bubbles trajectories in the space of depths $z' = z/h$ and sizes $R' = R/R^*$ are shown in Figure 1.

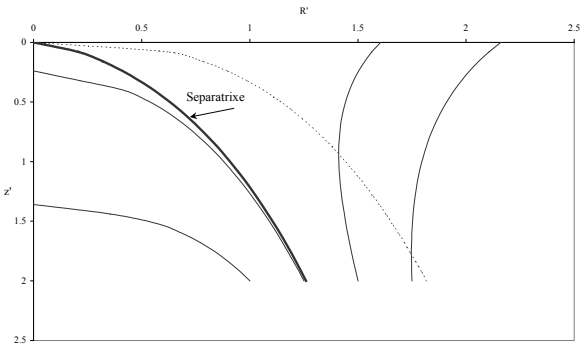

Fig. 1 Bubble rise trajectories in the space of depths z' and sizes R'. Separatrixe is shown by the heavy line. The dashed line corresponds to the states where dissolution rate is equal to zero ($\partial N/\partial t = 0$).

The formal solution of kinetic equation can be expressed as a linear integral along characteristic curves. Integrating yields

$$f(z', R'(z')) = \frac{(1+z')}{(1+z_0')} f(z_0', R_0') \quad (9a)$$

$$\frac{R'(z')^3}{3}(1+z') - \frac{z'^2}{2} = \frac{R_0'^3}{3}(1+z_0') - \frac{z_0'^2}{2} \quad (9b)$$

If at the seabed $z' = z_0'$, the bubble size distribution emitted by vents is $f(z_0', R_0')$, then the size distribution at depth z' $f(z', R')$ will be defined by expression (9a), where $R'(z')$ and R_0' are coupled by trajectory equation (9b).

Let us suppose that emitted size distribution is a sharp function located near an average radius $\bar{R}_0'$. We than can approximate it by δ-function: $f(z_0', R_0') = n\delta(R_0' - \bar{R}_0')$, and obtain at the depth z' the following number of bubbles

$$f\left(z', \left[R_0'^3 \frac{(1+z_0')}{(1+z')} - \frac{3}{2}\frac{z_0'^2 - z'^2}{(1+z')}\right]^{1/3}\right) = \frac{(1+z')}{(1+z_0')} n\delta(R_0' - \bar{R}_0') \quad (10)$$

or, if we return to the natural variable R'

$$f(z', R') = \frac{(1+z')}{(1+z_0')} n\delta\left(\left[R'^3 \frac{(1+z')}{(1+z_0')} - \frac{3}{2}\frac{z'^2 - z_0'^2}{(1+z_0')}\right]^{1/3} - \bar{R}_0'\right) = n\frac{\bar{R}_0'^2}{\bar{R}'(z')^2}\delta(R' - \bar{R}'(z')) \quad (11)$$

where $(\bar{R}'(z')^3/3)(1+z') - z'^2/2 = (\bar{R}_0'^3/3)(1+z_0') - z_0'^2/2$.

Since the bubble radius, and as a consequence of Eq. (4), the terminal rise velocity depend on the depth, it appears that bubble concentration is quite inhomogeneous with depth. The form of solution (Eq. 11) can be obtained directly from the kinetic equation (Eq. 7). Integrating the both terms of Eq. (7) over R' within the limits, where the sharp distribution function is negligibly small, we obtain zero from the second term and the condition of constancy of the vertical flow from the first term. Since the rise velocity is proportional to R'^2 we find that solution may be written in the form (Eq. 11).

Let us now analyze the degree of space inhomogeneity for bubble distribution. Consider the characteristic size

$$R'_{cr} = R'_{cr}(z_0') = (3/2)^{1/3}[z_0'^2/(1++z_0')]^{1/3}$$

coinciding with the bubble radius at the seabed for the separatrixe trajectory. This trajectory is defined by Eq. (8) when *Const* = 0 (see Fig. 1) and separates the domain of bubble states (trajectories) rising along which bubble will inevitably dissolve and will not reach the surface and those providing bubble-mediated CH_4 transport to the surface. For $z_0' >> 1$ ($z_0 >> 10$ m) we have

$$f(z', R') = \frac{\bar{R}_0'^2 (2/3)^{2/3} (z'/z_0')^{2/3}}{z_0'^{1/3}\left[(z'^2/z_0'^2) + \bar{R}_0'^3/R_{cr}^3(z_0') - 1\right]^{2/3}} n\delta(R' - \bar{R}'(z')) \quad (12)$$

From equations (9b) and (12) we see that rising bubbles with $\bar{R}_0' < R'_{cr}$ diminish in size monotonically till the horizon of dissolution $z_s' = z_0'\left[1 - \bar{R}_0'^3/R_{cr}^3(z_0')\right]^{1/2}$, and correspondingly the rise velocity decreases monotonically. As a result, bubble concentration will increase, as bubbles approach the stopping horizon in accordance with classical "car-jam" effect. Power singularity in Eq. (12) will not be realized in reality as the solution is to remain finite. Really, as the rise velocity decreases to a value comparable with random (turbulent) pulsation, one should account additional (diffusion-like) terms (Maksimov and Sosedko 2001) in the kinetic equation (6), which will lead to smoothing this singularity.

Bubbles with radii $\bar{R}_0' > R'_{cr}$ will always attain the surface. Those with initial radii $1 < (\bar{R}_0'/R_{cr}')^3 < 2(1+1/z_0')$ will decrease their sizes at the initial stage till rising at depth $z_m' = \sqrt{1 + z_0'^2[\bar{R}_0'^3/R_{cr}^3(z_0') - 1]} - 1$, where their radius $R_{\min}' = R'(z_m') = (3z_m')^{1/3}$ and rise velocity are minimum and, correspondingly, concentration is at greatest. During further rising, bubble radius grows as well as the velocity, but concentration decreases.

Finally, bubbles with radii $(\bar{R}_0'/R_{cr}')^3 > 2(1+1/z_0')$ growth monotonically as they ascend to the surface, the rise velocity increases and concentration decreases.

Current methods of interpreting echo-sounding records of clouds of bubbles are based on the assumption of a dominant contribution of the resonant bubbles in the back-scattering cross section. Measurements have been made by calibrated transducers for generating and receiving sound appear to provide evaluation of the resonant bubble population at different depths (at the sonar frequency, a bubble of the given size

$R_r(z') = R_r(0)\sqrt{1+z'}$ is in resonance with the exciting sound wave at depth z', where $R_r(0)$ is the resonant radius at atmospheric pressure). The existence of different gas flare types, in particular those registered by acoustic techniques only at definite depths and do not spread to the sea bottom (see for example [1]), makes it difficult to evaluate the parameters of gas vents on the basis of data from acoustical echo-sounding. As it follows from this study, an attempt to maintain direct relations between the measured bubble population and one emitted by a vent can lead to significant mistakes. If the radii of registered bubbles at the moment of their birth at seabed are smaller than $R*R'_{cr}$, this attempt will lead to overestimation of methane seep rate, and on the contrary, if the corresponding radii are greater than $R*R'_{cr}$, this can result in underestimation of seep rate.

Acknowledgments

This study was supported by the Russian Foundation for Basic Research, project No. 01-05-96901.

References

Anonymous. 1988. Report of *R/V M. Keldysh* Cruise 11 A. Gas hydrate accumulation in Okhotsk Sea. Leningrad. IO AS: 125-174.

Leifer, I. and Patro, R.K. 2002. The bubble mechanism for methane transport from the shallow sea bed to the surface: A review and sensitivity study. Continental Shelf Research 22: 2309-2428.

Ezerskii, A.B., Sandler, B.M. and Selivanovskii, D.A. 1989. Echo-sounding observations of gas bubbles near the sea surface. Akust. zhurnal 35(5): 829-833.

Goncharov, V.K. and Klement'eva, N.Yu. 1996. Modeling the dynamic and conditions of sound scattering by gas bubbles floating up from deep-water oil and gas deposits. Akust. Zhurnal 42(3): 371-377.

Maksimov, A.O. 1998. Time variation of back scattering from the ascending bubble plume. In Marine Technologies. Vladivostok. IPMT FEBRAS 2: 167-175.

Maksimov, A.O. and Sosedko, E.V. 2001. Dynamic of dissolution of ascending gas bubbles in random flows. In Marine Technologies. Vladivostok. IPMT FEBRAS 4: 193-202.

Aerosol research of the Okhotsk and Japan Seas area of Russia

Vasiliy Mishukov
V.I. Il'ichev Pacific Oceanological Institute, Far-Eastern Branch of Russian Academy of Sciences, 43 Baltiyskaya Street, Vladivostok, 690041 Russia. e-mail: pacific@online.marine.su

Introduction

The atmosphere is an intensive and constant source of various substances for the ocean. In the northwestern part of the Pacific Ocean, westerly winds play a large role in carrying atmospheric aerosol particles over large distances. In Primorsky Krai (Vladivostok City), yellow dust is observed not only with arrival of a spring, but also in the winter as strong westerly winds bring particles of a dust from Asia. The materials deposited include both natural and polluting substances.

Aerosols define not only the chemical structure, but also the optical properties of the atmosphere and consequently, the thermal and radiating modes of the surface of the Earth and World Ocean. The atmospheric inputs can influence primary production in the ocean (Prospero 1996; Saydam 1996). Certain interrelations between the flows of substances in the ocean and aerosol contents in atmosphere have been reported (Honjo 1996).

In the present study, some results of analyzing the aerosol contents in the Far-East regions of Russia are given and some interrelations between atmospheric and marine processes are considered.

Experimental research

The sampling of atmospheric aerosols is carried out uniformly at Japanese installations using techniques adopted by the international program SEAREX (Uematsu et al. 1983). Besides, rain and snow (after melting), river and waste waters were sampled in polyethylene bath and then particulate and dissolved forms of matter were separated by filtration through nuclei filters with pore diameter nearly 40 microns. Element concentrations in aerosol, rain, snow, river and waste waters were determined by neutron-activation and atomic-activation methods.

Aerosol sampling stations were located in Vladivostok, Okha on the Sakhalin (north part), Paratunka on the Kamchatka peninsula (central part) and on research vessels in different regions of the Russian Far East.

Discussion of results

We observed that increasing dust concentrations usually coincide with increases in elemental concentrations. Elements were separated into five groups:

1. Macroelements – Na, Al, Ca, Fe;
2. Anthropogenic elements – Pb and Zn;
3. Trace natural elements – Ni and Cu;
4. Trace pollution elements – Cd and Co;
5. Very changing pollution element – As.

Increases of the macroelements (e.g. K, Ba, Fe, Al, Ca, Na and others) in the atmosphere of Vladivostok in the winter-spring period is marked. On average, concentrations of microelements in atmosphere of Vladivostok are higher than in atmosphere of Sapporo (Michoukov et al. 1997).

Table 1 demonstrates the correlation coefficients between concentrations of elements in aerosols for Vladivostok. Only Fe is closely correlated with dust concentration. We observed the correlation between concentrations of Ca, Mg, Cu, Fe, Mn, Co, Ni, and Zn. For samples from Okha (Table 2) all elements are negatively correlated with dust concentration but closely correlated with each other. This result demonstrates that aerosols are influenced by other sources than in Vladivostok.

For aerosols from the Paratunka we observed correlations between Mn, Zn, Fe, Co, Pb (Table 3). This analysis demonstrates that different sources influence on chemical composition of aerosols in the Russian Far East.

Table 1 Correlation coefficients between concentrations of elements in aerosols for Vladivostok.

	Dust conc.	**Ca**	**Mg**	**Cu**	**Fe**	**Mn**	**Co**	**Ni**	**Pb**	**Cd**	**Cr**	**Zn**
Dust concent.	1											
Ca	0.471	1										
Mg	0.375	**0.986**	1									
Cu	-0.089	**0.765**	**0.830**	1								
Fe	**0.834**	**0.834**	**0.795**	0.467	1							
Mn	0.265	**0.962**	**0.986**	**0.876**	**0.720**	1						
Co	0.467	**0.952**	**0.945**	**0.745**	**0.820**	**0.954**	1					
Ni	-0.051	**0.585**	**0.607**	**0.816**	0.374	**0.699**	**0.678**	1				
Pb	-0.322	**0.551**	**0.637**	**0.934**	0.229	**0.679**	0.470	**0.691**	1			
Cd	-0.324	0.032	0.127	0.519	0.005	0.234	0.197	**0.725**	0.522	1		
Cr	-0.271	-0.252	-0.284	-0.250	-0.395	-0.187	-0.132	0.208	-0.291	0.168	1	
Zn	0.323	**0.722**	**0.774**	**0.785**	**0.734**	**0.797**	**0.811**	**0.776**	**0.606**	**0.649**	-0.188	1

Table 2 Correlation coefficients between concentrations of elements in aerosols for Okha.

	Dust conc.	**Ca**	**Mg**	**Cu**	**Fe**	**Mn**	**Co**	**Ni**	**Pb**	**Cd**	**Zn**
Dust concent.	1										
Ca	-0.401	1									
Mg	-0.396	**0.890**	1								
Cu	-0.418	**0.802**	**0.921**	1							
Fe	-0.383	**0.734**	**0.814**	**0.900**	1						
Mn	-0.420	**0.725**	**0.745**	**0.733**	**0.858**	1					
Co	-0.400	**0.878**	**0.959**	**0.936**	**0.868**	**0.805**	1				
Ni	-0.320	**0.815**	**0.970**	**0.864**	**0.721**	**0.593**	**0.894**	1			
Pb	-0.471	**0.787**	**0.846**	**0.925**	**0.939**	**0.814**	**0.904**	**0.753**	1		
Cd	-0.354	**0.599**	**0.817**	**0.800**	**0.775**	**0.784**	**0.856**	**0.742**	**0.764**	1	
Zn	-0.445	**0.768**	**0.873**	**0.972**	**0.960**	**0.799**	**0.906**	**0.793**	**0.962**	**0.789**	1

Table 3 Correlation coefficients between concentrations of elements in aerosols for Paratunka.

	Mn	**Zn**	**Cu**	**Fe**	**Ni**	**Co**	**Cd**	**Pb**
Mn	1							
Zn	**0.791**	1						
Cu	0.313	0.510	1					
Fe	**0.803**	**0.570**	0.414	1				
Ni	**0.535**	**0.668**	0.422	0.462	1			
Co	**0.655**	**0.526**	0.317	**0.732**	0.488	1		
Cd	0.301	0.423	0.486	0.422	0.442	**0.503**	1	
Pb	**0.519**	**0.636**	0.298	**0.599**	0.453	**0.526**	**0.542**	1

In Table 4, the aerosol element concentrations from various regions of Russian Far East are reported. These data demonstrate that in sea regions Sr and Ba have redundant values under known data.

Table 4 Aerosol element concentration in sea atmosphere in spring-summer.

Region	Dust concen. mg/m^3	Element concentration, ng/m^3												
		Na	Sc	Cr	Fe	Co	Zn	Se	Pb	Sr	Ba	Hf	Hg	Th
Tatar Strait	0.032	450	0.06	–	600	1.6	58.0	–	–	13.0	130	–	–	0.3
	0.038	530	0.10	2.6	570	–	190.0	–	1.0	14.0	–	0.3	–	–
Japan Sea	0.011	960	0.50	2.1	660	–	–	–	0.4	5.4	200	0.6	–	0.2
Nakhodka Bay	0.047	–	0.60	5.6	2500	–	14.0	–	–	47.0	–	2.6	–	0.7
	0.016	510	0.04	1.3	530	–	21.0	–	0.5	1.0	–	0.4	0.3	0.2
Okhotsk Sea	0.013	950	0.07	2.0	200	–	8.6	1.3	0.5	6.1	–	0.2	1.8	0.2
	0.010	820	0.04	2.0	250	–	19.0	1.6	0.3	8.6	42	–	0.9	0.0
	0.013	–	–	–	200	0.4	29.0	2.0	0.5	–	96	0.5	–	0.1
	0.011	950	0.20	1.7	200	0.5	–	1.3	0.5	14.0	57	0.07	–	0.2
Bering Sea	0.007	570	0.03	–	–	–	11.0	–	0.9	4.9	–	0.2	–	0.1

Conclusions

The results indicate the formation of atmospheric aerosols in the Russian Far East the large influence renders global atmospheric carry, which was observed in winter-spring period. In these periods occur inputs of an atmospheric dust from regions of an Asian continent.

References

Prospero, J.M. 1996. The atmospheric transport of particles to the ocean. *In* V. Ittekkot, P. Schafer, S. Honjo and P.J.Depetris (Eds.) Particle Flux in the Ocean. John Wiley and Sons Ltd., pp. 18-52.

Saydam, A.C. 1996. Can we predict harmful algae blooms. Harmful Algae News 15: pp.5-6.

Honjo S. 1996. Fluxes of particles to the interior of the open oceans. *In* V. Ittekkot, P. Schafer, S. Honjo and P.J.Depetris (Eds.) Particle Flux in the Ocean. John Wiley and Sons Ltd., pp. 18-52.

Uematsu, M., Duce, R.A., Prospero, J.M., Chen, L., Merrill, J.T. and McDonald, R.L. 1983. Transport of mineral aerosol from Asia over the North Pacific Ocean. Journal of Geophysical Research 88: 5343-5352.

Michoukov V., Uematsu, M. and Medvedev, A.A 1997. Some Results of Aerosol Study in Russian East Regions. *In* Proceedings of International Marine Science Symposium on Biogeochemical Processes in the North Pacific, Mutsu, Japan, November 12-14, 1996. Japan Marine Science Foundation, Tokyo, pp. 392-413.

Wind wave fields and swell in the Subarctic Front Zone

Antonina M. Polyakova and S.S. Sugak
V.I.Il'ichev Pacific Oceanological Institute, Far Eastern Branch of Russian Academy of Sciences, 43 Baltiyskaya Street, Vladivostok, 690041 Russia. e-mail: polyak@poi.dvo.ru, sugak@poi.dvo.ru

The location of the Subarctic Front Zone (SFZ) (Anon. 1972) predetermines the distribution of the wind-induced wave and swell fields to a considerable extent, as the SFZ is situated along the route of most of the mid-latitude cyclones and parts of typhoons (Polyakova 1999; Terasova 1971) possessing a turning point (Figs. 1, 2). The largest wind-induced waves and swell develop in the southwestern quarter of cyclones. Cyclone trajectories in the northern Pacific are categorized according to six types of atmosphere circulation (Polyakova 1999). The main part of cyclones of all six types cross the Subarctic Front Zone at various angles or travel parallel to it (Fig. 1).

Under the North Western type (NW) of atmospheric processes, the cyclones pass along the northern boundary of the SFZ generating waves over all of its water area, with its southern half being the most violent. The Okhotsk-Aleutian type (OA) of synoptic process, during all period of its effect via the Okhotsk Depression, generates waves in the Subarctic Front Zone. The Latitudinal Aleutian type (LA) occupies the SFZ with the ultimate southern periphery of the cyclone/storm field, where the largest wind-induced waves and swell are observed. The southern latitudinal type (SL) is distinctive in that the main part of these cyclones pass over the whole SFZ. The Okhotsk-Hawaiian type (OH), with its Okhotsk Depression, induces a direct influence on the wave formation in the whole water area of the SFZ throughout the duration of its effect. The "cyclones over the ocean" type (CO) is distinguished by the presence of mainly cyclonic vortices, including those over the water area of the SFZ, so they make a considerable input into the process of the development of the wind waves and swell in all its water area.

The wave formation processes change considerable during a year, as the intensity of the atmosphere circulation effect varies in significant bounds with regard to a season. Especially violent atmospheric processes occur in winter: December –February. During this period, the cyclones reach an unusual development, both in depth (to 970-950 mb), and radius of action (up to 1000 km and more). In this connection, the wind velocity in large water areas may reach 15-20 m s^{-1} and more, and the wave height, including those in the SFZ reach dangerous (>6 m) and elemental (>8 m) values. In winter, under the intensive development of cyclones, the wind wave height can reach 10-12 m and more; the average period here is 11-12 s, and the mean length increases to 200-250 m. The swell waves decline after the storm in due course, but their period and length are increasing. As a result, they continue to mix the sea to a depth equal to half a wavelength for not less than a day after the wind weakens. When a deep cyclone is passing, wave mixing occurs to a depth of 100-125 m and lasts for not less than two days. The wind waves and swell here develop fully as their fetch is not limited in the open ocean. The wave heights of 5% probability (5 waves out of 100 ones are equal to or exceed the given value) can reach the exclusive development, up to 9 m and more. The swell waves remain for a long time after the passage of an intensive storm; in a day they change their height to 6 m and more, in two days – 3 m and more (Polyakova 1975). In autumn, from September to November, the intensity of atmospheric circulation is the same large scale and just somewhat yields to a winter one. Deep cyclones are passing, with pressures in the range of 990-960 mb, and storm radii up to 1000 km and more, with wind velocities of 12-18 m s^{-1} and more. Wind waves and swells of the dangerous

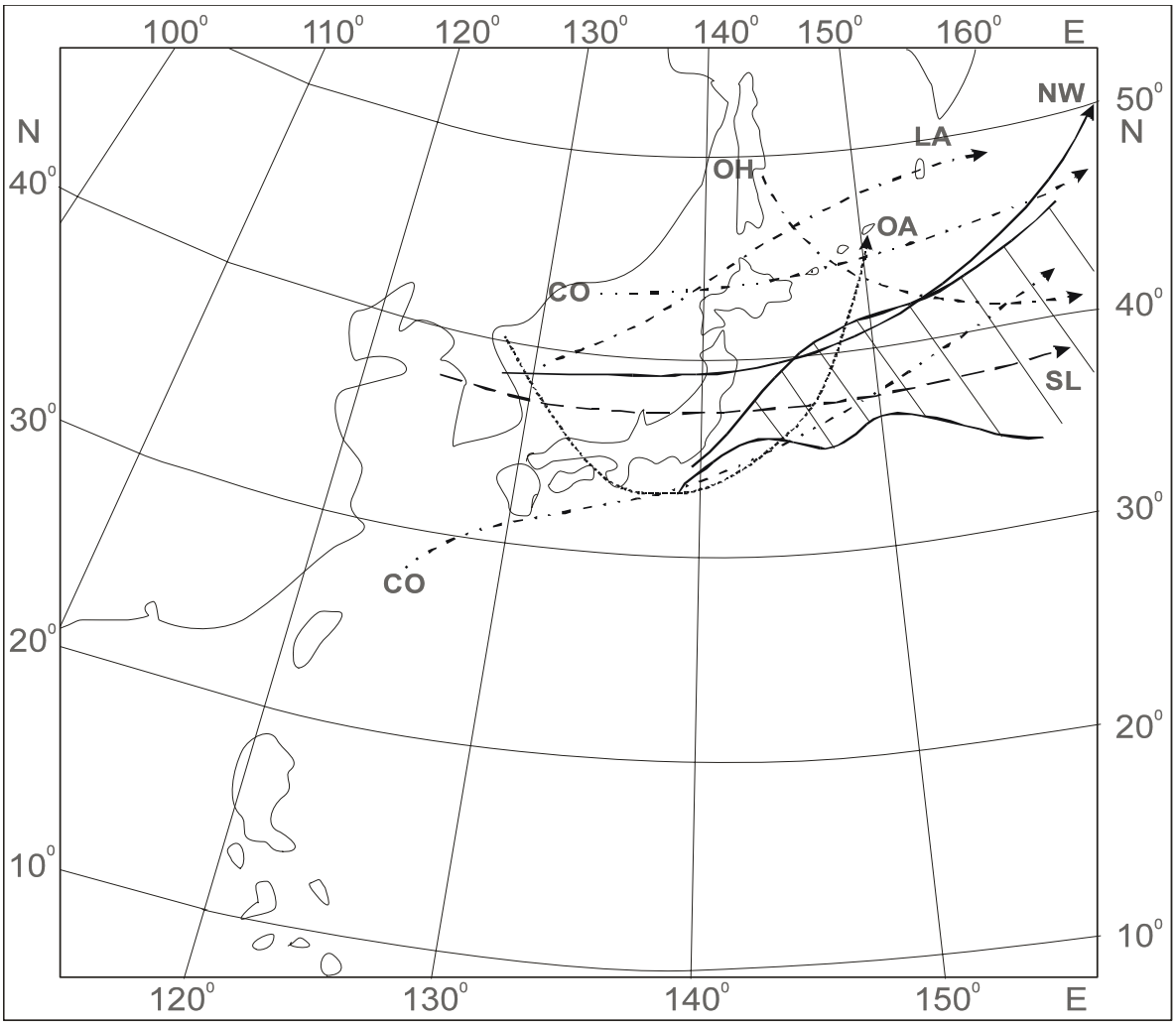

- the Subarctic Front location
- cyclone trajectories of North Western type (NW),
- cyclone trajectories of Okhotsk-Aleutian type (OA),
- cyclone trajectories of Latitudinal Aleutian type (LA),
- cyclone trajectories of Southern latitudinal type (SL),
- cyclone trajectories of Okhotsk-Hawaiian type (OH),
- cyclone trajectories of the type “cyclones over the ocean” (CO).

Fig. 1 Main paths of cyclones and the Subarctic Front location.

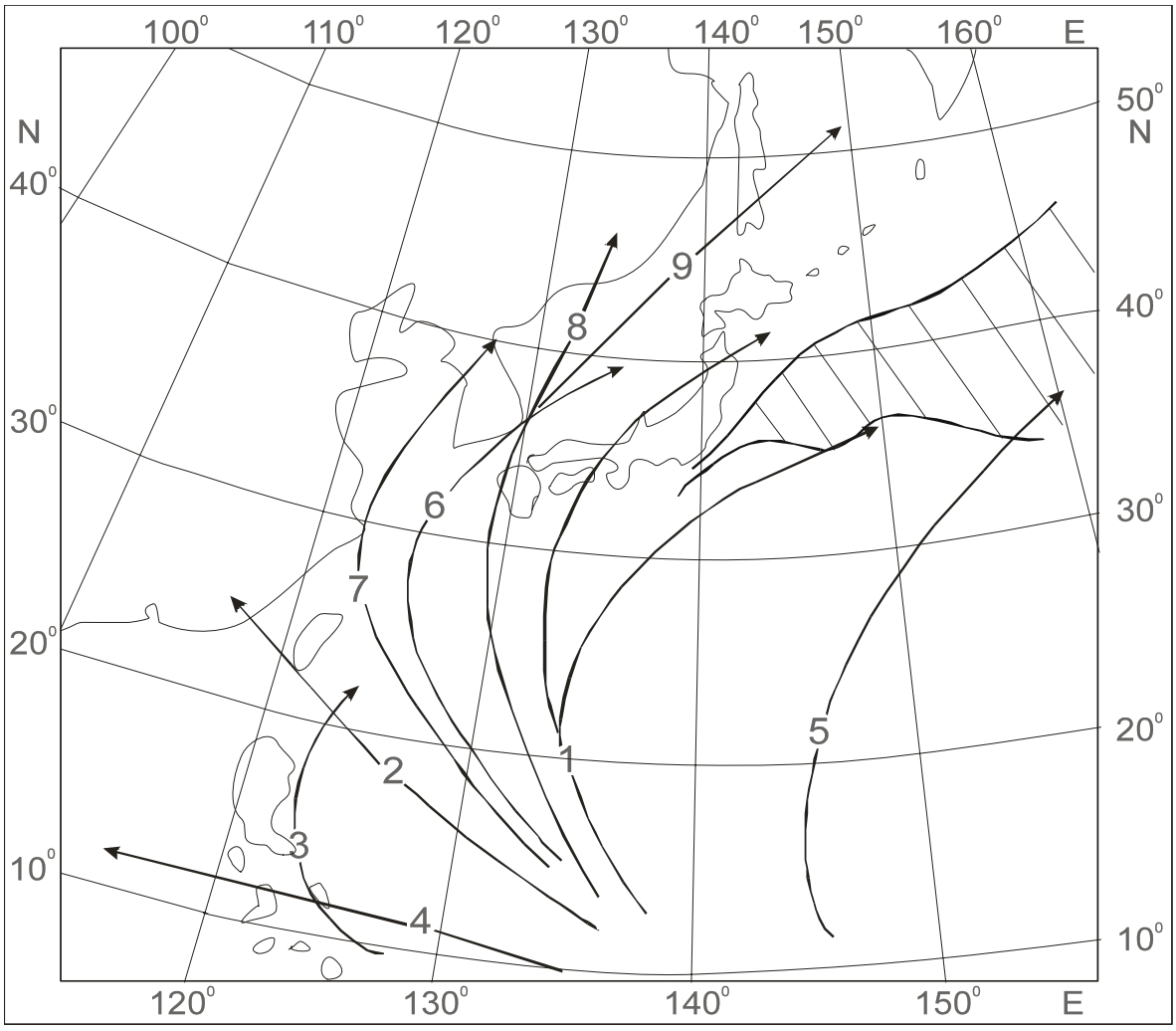

Fig. 2 Main trajectories of typhoons and the location of the Subarctic Front (after Tarasova 1971).

and elemental heights, with corresponding wave periods and lengths similar to winter ones and, consequently, the depth of the wave mixing in the SFZ is not significantly less than in winter. In spring, especially in April – May, the intensity of the atmospheric processes sharply decreases, compared to autumn. The depth of cyclones most often does not exceed 1000-980 mb, the cyclone radius is decreasing, respectively, the storm winds are more rare, moderate and even weak ones are more often observed. The field development of the wave winds and swell is considerably weakening. Most often, moderate and weak waves occur with heights ranging from 1.5 to 3.5 m, an average period of 3-6 s, and a mean length of 15-30 m. In spring, sometimes there are more intensive cyclones, most often in March. In this case, the wave heights can reach the dangerous and elemental values, and the depth of mixing reaches 100 m and more. In summer, all atmospheric processes are inert. Cyclone depth is mostly about 1000 mb, most often it is contoured with one, rarely two isobars. Breezes are gentle and moderate, the waves mostly up to 1.5 m. Wind mixing is observed in the surface layer. Intensive development of the atmospheric processes in summer is most often related to the passage of typhoons which generate dangerous and elemental wave heights. After the passage of a typhoon in the ocean, in particular in the SFZ, the waters are mixed to a depth of 100 m and more.

Table 1 Percentages by type of the atmospheric circulation, annual maximums by type are in bold.

	Type of atmospheric circulation					
Month	**NW**	**OA**	**LA**	**SL**	**OH**	**CO**
I	30.4	13.0	6.9	**9.0**	5.0	34.8
II	42.6	11.3	6.0	7.8	5.3	27.0
III	42.6	21.3	8.7	4.2	**9.7**	4.8
IV	42.3	29.7	14.0	0.0	3.3	10.7
V	34.5	**35.0**	13.5	3.2	0.0	13.5
VI	46.0	27.3	7.6	3.7	1.7	13.3
VII	**48.7**	26.5	17.4	0.2	0.0	5.8
VIII	45.0	23.5	**24.5**	1.0	0.6	5.6
IX	32.2	32.6	21.0	3.6	0.0	10.6
X	26.4	28.7	21.0	0.0	2.3	21.6
XI	31.0	19.7	20.0	0.0	2.0	27.8
XII	27.0	17.7	13.2	3.2	2.6	**36.1**

Each of 6 types of the atmospheric situations has a definite frequency and seasonal motion, so it brings its input into the formation of the wind wave and swell fields and, consequently, the depth of the water mixing in the SFZ (Table 1).

The average monthly frequency of the NW type in the cold half of the year varies from 27% to 43%. Consequently, not less than 1/3 of each month has the North Western type of circulation generating wave fields in the Subarctic Front Zone. After storms pass, the swell waves having rested after it, also influence the SFZ for not less than two days, i.e. they enlarge the continuation of the North Western type effect on the SFZ.

The Okhotsk-Aleutian type of atmospheric process, as compared to the NW, in late autumn and in winter has significantly less frequency (11.3-19.7%), so its influence in the SFZ is considerably less than that of the NW type.

The Latitudinal-Aleutian type of atmospheric circulation, in the period of the intensive development has a frequency of 6-21% as a whole; even less than the OA type so consequently, its total influence on the mixing in the SFZ is less than the two previous types. Nevertheless, they have their effect on the formation of the intensive wave throughout the whole zone of the Subarctic Front, where to it comes the loop of the wind waves and swell produced by the cyclones passing far to the north.

The Southern Latitudinal type of the atmospheric circulation has a non-significant frequency in the period of the intensive development of the atmospheric processes (0-9%), so the total input of the given type into the water mixing processes in the SFZ is the least essential, as compared to the previous types.

The Okhotsk-Hawaiian type of atmospheric processes, as with the Southern Latitudinal type, has a non-significant frequency (2-3%) at the period of the intensive development of the atmospheric processes, and induces a non-significant influence on the depth of the water mixing in the SFZ.

The “cyclones over the ocean” type during the period of the intensive development of the atmospheric circulation has the frequency from 27 to 36.1%. Note that the intensity of this type can often be exclusive, especially in winter and autumn. The wave height in the vast water areas in the SFZ can reach 10 m and more. Throughout the whole zone of the Subarctic Front, under the action of the “cyclones over the ocean” type, it is possible the elaboration of the intensively developed fields of the wind waves. After the storm, during 2-3 days, the swell waves are

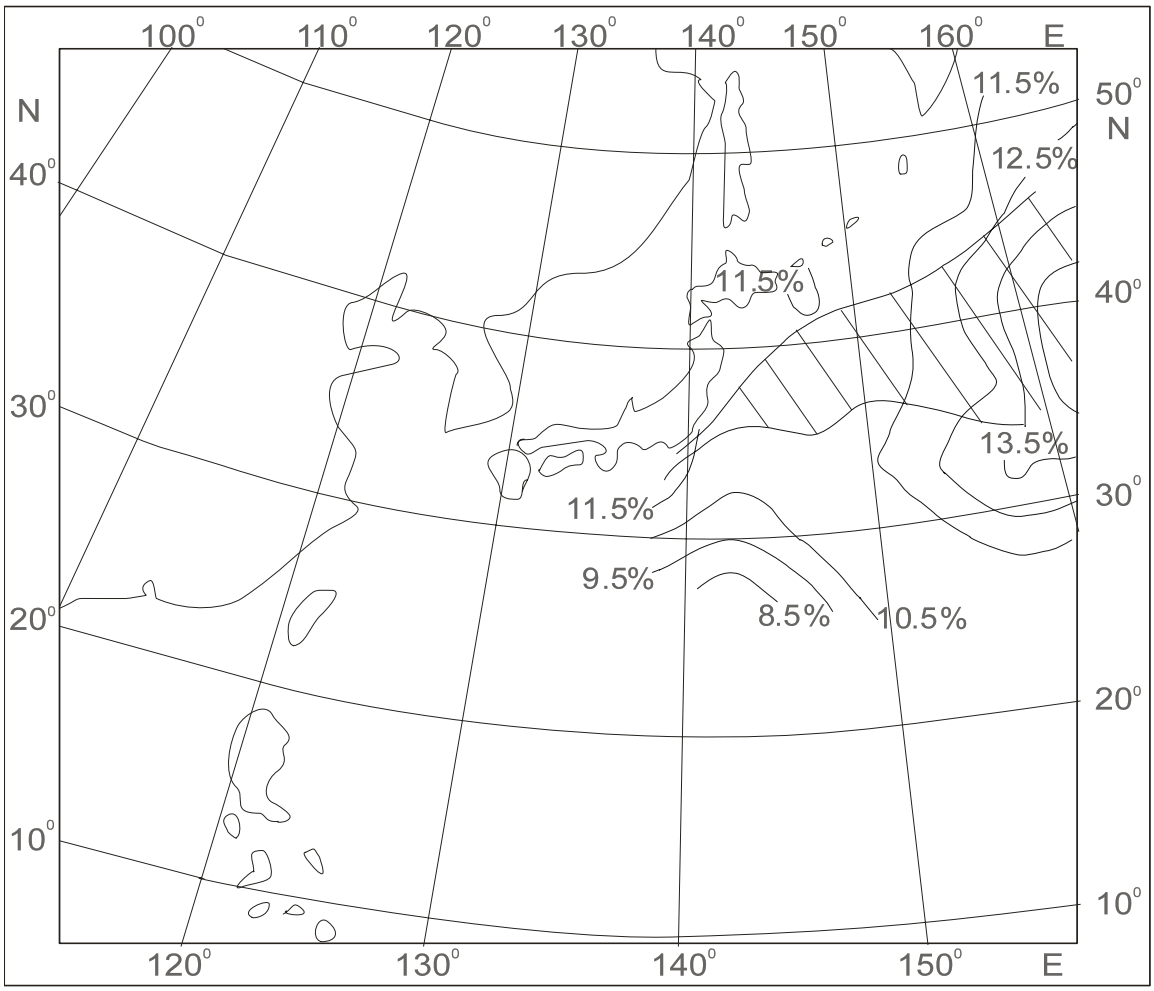

Fig. 3 Area of intensive sea in the Subarctic Frontal Zone.

maintained, gradually decreasing to 6 m on the first day, 4 m on the second day, and to 2 m on the third. Taking into account the considerable frequency, especially in the cold period, often the exclusive intensity of the development, we may consider that the CO type has a significant influence on the formation of the wind wave fields in the Subarctic Front Zone.

Thus, to the formation of the wind waves fields in the SFZ the largest input is done by the typical atmospheric processes of the NW and "cyclones over the ocean", substantially less – by the OA and LA ones, insignificantly – SL and OH. Nevertheless, all typical situations influence the formation of the wind wave fields in the SFZ.

The largest part of the Subarctic Front is located in a zone of the intensive wave, which is located in the Western Pacific (Fig. 3) (Polyakova and Sugak 2003), and the proper zone of the intensive rough sea is created by the convergence of trajectories of cyclones and typhoons to the east of Japan.

Conclusions

The Subarctic Front Zone in the NW Pacific is located in the area of the intensive sea; consequently, the depth of the wave mixing here is larger than in the ambient waters of the ocean.

The presence of the intensive sea zone is predetermined by the effect of convergence of the major trajectories of cyclones and typhoons to the east of Japan.

References

Polyakova, A.M. 1975. Wind waves and swell under various types of synoptic processes. The northern half of the Pacific Ocean: Inform. Bull. 425. MMF, DVMP, DVNIGMI. Vladivostok, 71 p.

Polyakova, A.M. 1999. Calendar of types of atmospheric circulation considering non-stationarity over the Northern Pacific and their brief characteristics. Vladivostok. DVGU, 116p.

Polyakova, A.M. and Sugak, S.S. 2003. Wave height in the Northern Pacific. Vladivostok, 60p. Deposited in VINITI 16.06.03 N 1156-B2003.

Anomymous. 1972. Subarctic Front of the NW Pacific. POI FEB RAS, Vladivostok, 133 p.

Tarasova G.M. 1971. Typhoons coming on to the territory of the Far East. Trudy GMCs SSSR. Leningrad: Gidrometeoizdat, Issue 87. pp.39-52.

Regional satellite monitoring of far east seas: Modern state and perspectives of development

Anatoly I. Alexanin, M.G. Alexanina, D.A. Bolovin, F.E. Herbeck, A.V. Gromov, I.I. Gorin, Y.V. Naumkin, E.V. Fomin and Y.S. Epstain

Institute of Automation and Control Processes, Far-Eastern Branch of Russian Academy of Sciences, 5 Radio Street, Vladivostok, 690041 Russia. e-mail: aleks@satellite.dvo.ru

The Center for Satellite Monitoring of environment was created on the base of Satellite Monitoring Laboratory of IACP FEB RUS at 1999. The purpose of the Center is to receive, process, deliver and acquire of satellite data regularly. The Center and its data sets have been registered in Global Change Master Directory (NASA subdivision) last year. At the present time the Center carries out receiving and processing two types of high resolution satellite data: data of the polar satellites (NOAA) for sea surface observation and the data of geo-stationary meteorological satellites (GMS-5 and FY-2B) for atmosphere monitoring. New equipment received allows to increase the Center opportunities and to organize work with such satellites as FY-1C, FY-1D and MTSAT. Joint processing of various satellite data allows get more complete information in time and space about sea surface and atmosphere phenomena. The Okhotsk Sea weather conditions are hard cloudy usually. Therefore the different special methods are developed for detection, tracing and evaluation of thermodynamic parameters of the sea surface. The base output products are the calibrated images in Mercator projection (IMP) (at 1.1 km/pixel resolution). In addition output products involve such charts as different spectral channels combination, the sea surface temperature in isotherms and in 24 and 48 pseudo-thermal colors (SSTC), sea surface current velocity vectors (SSCV), calculated with manual feature tracing method, thermal structures on the base of dominant orientations of thermal contrasts (DOTC), overlap of SSTC with DOTC and etc. All output products have been tested during the real operational work. This work has been supported by the RFBR grant № 03-01-00812.

Diagnostic current calculation for the Sea Of Okhotsk

Pavel A. Fayman
Far Eastern Regional Hydrometeorological Research Institute, 24 Fontannaya Street, Vladivostok, 690600 Russia. e-mail: pfayman@hydromet.com

Introduction

Much attention has been drawn to the seasonal variability of the Okhotsk Sea currents for the last 40 years. The seasonal variability of the currents structure all over the Okhotsk Sea is described in Darnitskiy and Luchin (1997), Anonymous (1998) Luchin (1982, 1987) and Vasiliev and Khrapchenkov 1996). In Darnitsky and Luchin (1997), Anonymous (1998) Luchin (1982, 1987), the current field is calculated from Sarkisyan's model D1. Calculations of Luchin (e.g. Darnitsky and Luchin 1997; Luchin 1982, 1987) are based on the monthly average instrumental water temperature and salinity. In Vailiev and Khrapchenko (1996), the modelled water density serves the initial data. The seasonal variability of currents in different parts of the Okhotsk Sea is described in Budaeva and Makarov (1996a); Budaeva and Makarov (1996b) (the Aniva Bay), Figurkin (2002) (the western shelf of Kamchatka), Figurkin and Zhigalov (1999); Khen et al. (2002) (the northern part of the Okhotsk Sea) and Budaeva and Makarov (1999); Gruzevich et al. (1996) (the Sakhalin shelf). In most of the cited papers the sea currents are calculated over a dynamic model. In Darnitsky and Luchin (1997) and PICES (1995) all the general data accumulated by 1995 on the seasonal variability of the Okhotsk Sea are given. The present study concentrates on the diagnostic calculation of the 3D current field for June, August, and October using the most complete data set.

Data and methods

The diagnostic baroclinic linear model of Sarkisyan D1 (Marchuk and Shaydurov 1979; Sarkisyan 1977) is used to currents. The smoothed bottom relief, real density field and atmospheric pressure field serve the initial data. As the Richardson's extrapolation is applied (Marchuk 1989; Marchuk and Sarkisyan 1979), the model equations are determined by the method of finite differences with the numeric scheme of the second order of accuracy. Bathymetric data were from the 5-minute ETOPO5 grid. Density fields averaged by month were reconstructed using data from RODC FERHRI, ODC RIHMI-WDC and other Russian oceanographic organizations, and data published in the Levitus Atlas (on CD-R) (see Rykov 1999). Atmospheric pressure data were taken from monthly average data (1962-1990) obtained by re-analysis.

Results

General current scheme

A branch of the Kuril-Kamchatka Current flows through the Fourth Kuril Strait, enters the Okhotsk Sea and forms the West Kamchatka Current that can be traced to Shelikhov Bay. A branch, the Middle Current, deviates from the West Kamchatka Current at 52°N and flows to the northwest. Another branch of West Kamchatka Current, the Penzhinskoe Current in Shelikhov Bay – deviates at 58°N and causes cyclonic circulation in the bay. The West Kamchatka Current then flows to the west along the northern coast of the Okhotsk Sea past Kekurniy, Babushkin and Zabiyaka bays and transforms into Yamskoe Current. The current structure near the northwestern coast of the Okhotsk Sea is represented by North Okhotsk Current that can be traced from Taunskaya Guba to Shantary Islands. Near the islands, a branch of the North Okhotsk Current flows to the east and forms the North Okhotsk reverse flow and East Sakhalin Current (Figs. 1-3).

The East Sakhalin Current flows along the eastern Sakhalin coast. Near the southeast of Cape Terpeniya, the current divides into two flows; one of the branches flows to the north and forms East Sakhalin reverse flow and another branch flows to the northeast and forms the Northeastern Current. The latter flows toward the central Kuril islands, turns to the south and joins with Kuril-Kamchatka Current. The East Sakhalin Current rounds Cape Terpeniya, flows along the southeastern Sakhalin coast to the south of Aniva Bay. Here, the East

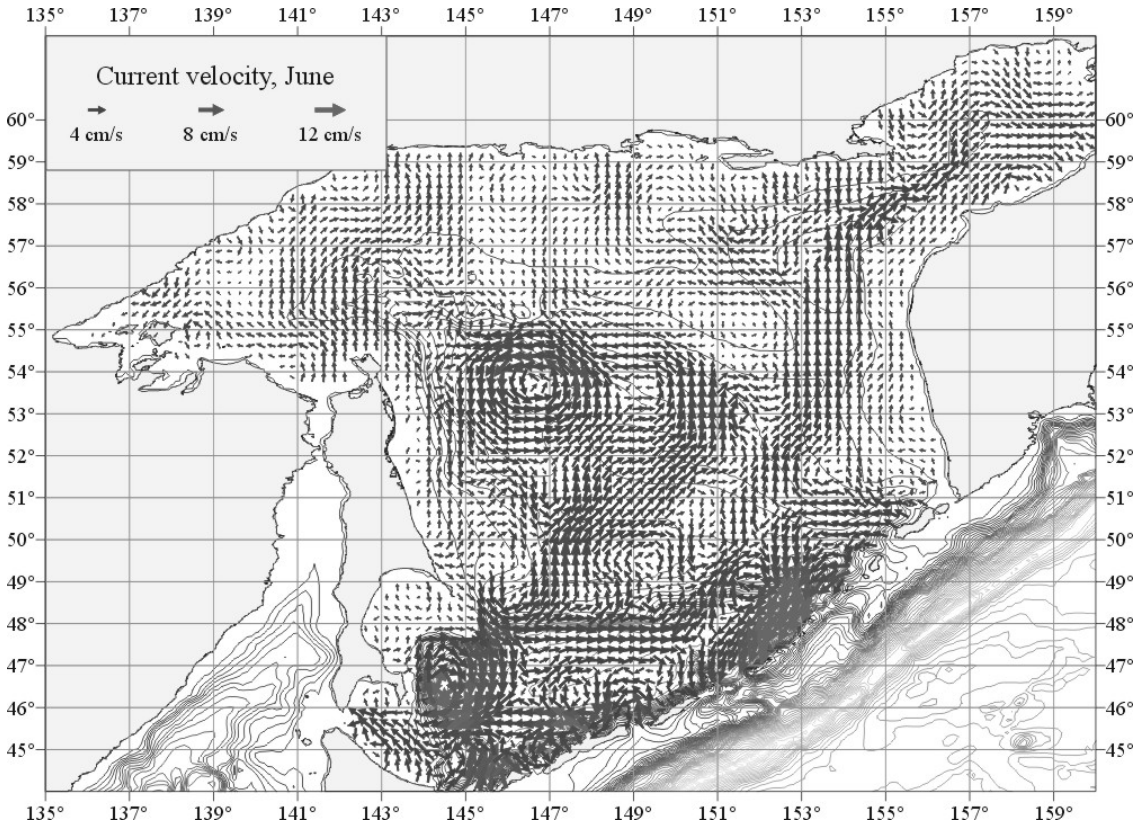

Fig. 1 Currents at 10 m depth in June.

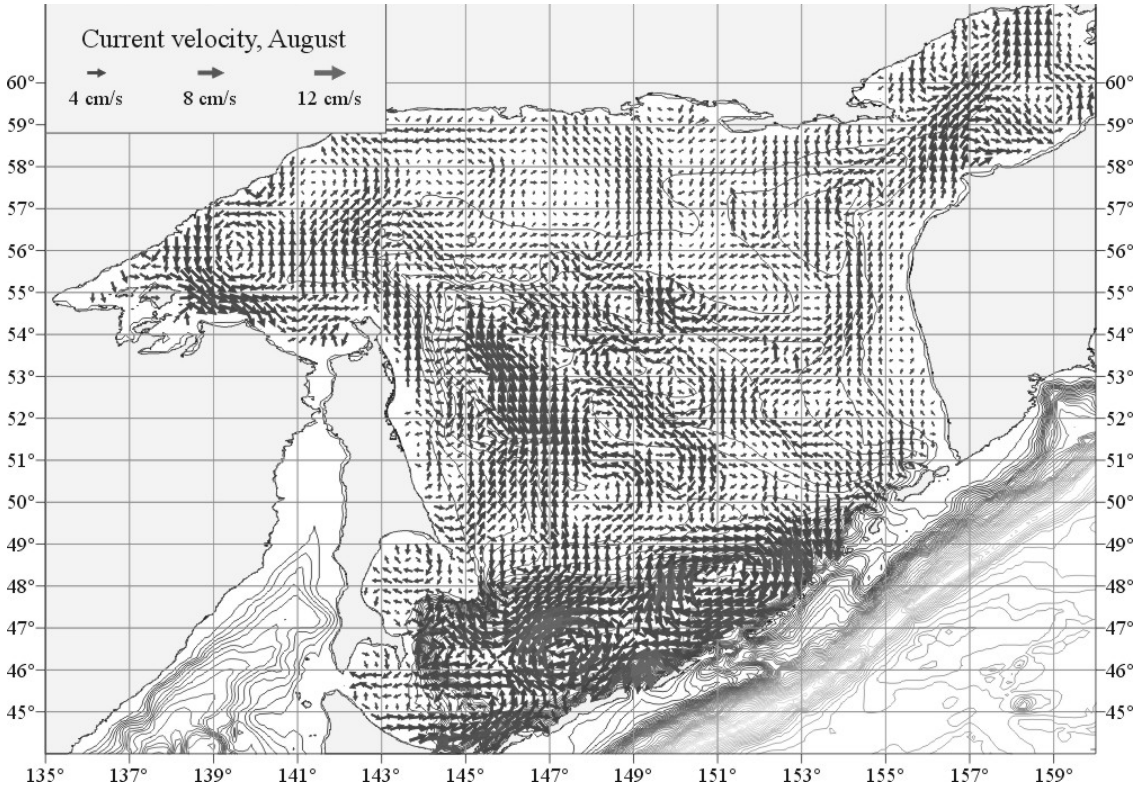

Fig. 2 Currents at 10 m depth in August.

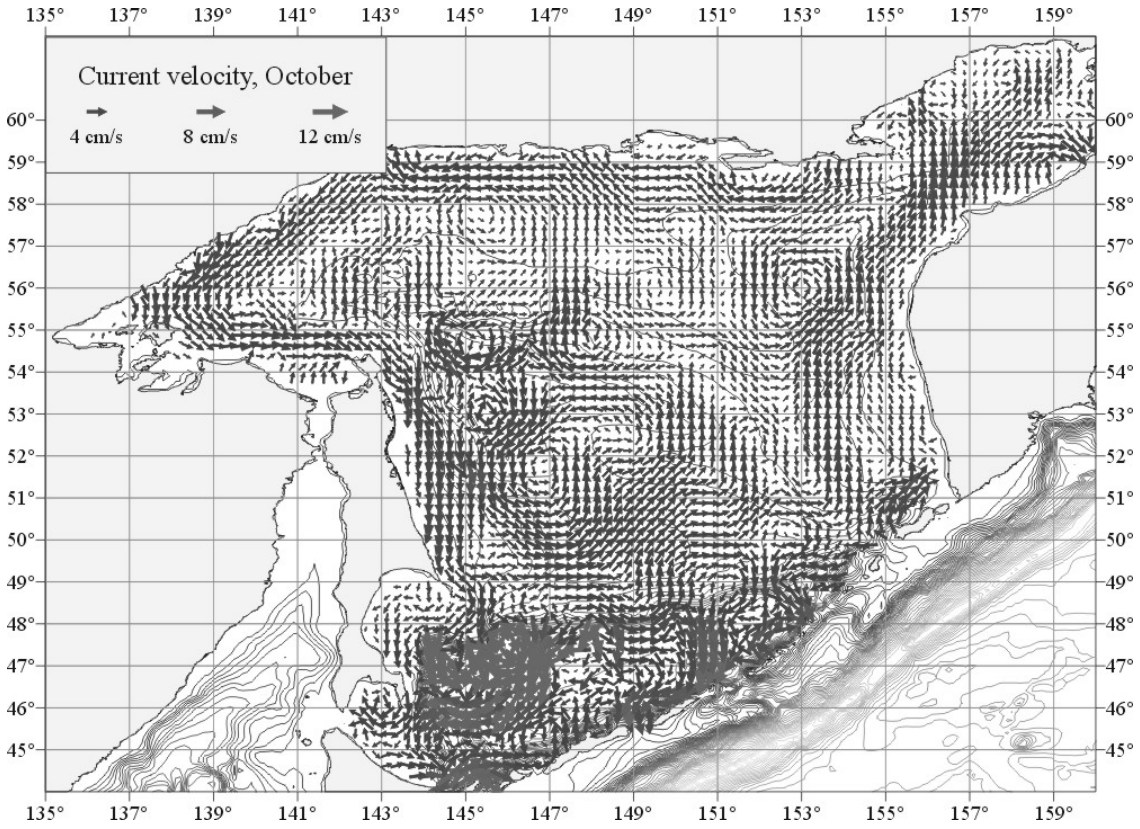

Fig. 3 Currents at 10 m depth in October.

Sakhalin Current turns to the east and joins with Soya Current. The latter can be traced in the southwestern part of the Okhotsk Sea where it reaches Ekaterina Strait and enters the Pacific Ocean. The current structure in the southwestern part of the Okhotsk Sea is characterized by a number of anticyclonic eddies that change their magnitude and location by seasons (Figs. 1-3).

Seasonal variability

The West Kamchatka Current is seen in all three current schemes. It is generated by the Kamchatka Current flowing into the Okhotsk Sea through the Fourth Kuril Strait. The current velocity is 7-10 cm s^{-1}, and it can be traced to a depth of 100 m. The velocity of the northward flow amounts to 10 cm s^{-1} at the surface. The cyclonic ring in Shelikhov Bay occurs only in August; its velocity ranging from 4 to 7 cm s^{-1}. At the same time, the October scheme points to a cyclonic eddy to the west of Kamchatka with its center at 56°N. The Yamskoe Current is also prominent in October with the light flow of 5-6 cm s^{-1}. The North Okhotsk Current can be traced in August and October (when it is well expressed) with the current velocity over a wide area amounting to 10 cm s^{-1}. In June, the North Okhotsk Current is narrow and immediately adjoins the coast. On the contrary, the North Okhotsk reverse flow is readily apparent in June. Both flows form a number of cyclonic eddies in the northeastern part of the Okhotsk Sea (Figs. 1-3).

In June and August, the East Sakhalin Current adjoins the coast and can be seen distinctly near the south of Sakhalin Island only. In October it is very well expressed along the eastern Sakhalin coast, with current velocities amounting to 12 cm s^{-1}. In summer, near Cape Terpeniya, the East Sakhalin Current divides into two flows, the East Sakhalin reverse flow and the Northeastern Current. The current velocity in the first flow amounts to 5 cm s^{-1} in June and 7 cm s^{-1} in August. The current velocity in the second flow amounts to 8 cm s^{-1} in June and 12 cm s^{-1} in August. To the east of Sakhalin Island, the currents form

anticyclonic circulation. The Middle Current, generated by a branch of the West Kamchatka Current, flows into the eddy. The location of the anticyclonic eddy changes by season. In June, its center is located at 53°30'N 146°30'E, while in August it is going to the south to 51°30'N 145°30'E, and in October, to the east to 52°N 147°E (Figs. 1-3).

The Soya Current can be identified in the surface layer in August and October, with current velocity amounting to 15 cm s^{-1}. It flows through Ekaterina Strait and enters the Pacific Ocean.

The current scheme of the southwestern part of the Okhotsk Sea is characterized by anticyclonic eddies with depths up to 1,000 m. Here the surface current velocity amounts to 15-30 cm s^{-1} (Figs. 1-3).

Just as in August, the current structure of the central Okhotsk Sea in October is characterized by two eddies, cyclonic and anticyclonic. The latter is traced to the depth of 1,000 m. The anticyclonic eddy is located to the east of Cape Aniva, current velocity amounting to 10-15 cm s^{-1}.

Conclusion

Water circulation in the southern part of the Okhotsk Sea and small and middle bays is presented as a number of small eddies that change their magnitude and direction by season. The largest eddy occurs above the Deryugin depression, but it shifts to the south by autumn.

References

Anonymous. 1998. Sea hydrometeorology and hydrochemistry. The Okhotsk Sea. Volume 9 (1). Hydrometeorological conditions, pp. 233-256.

Budaeva, V.D. and Makarov, V.G. 1999. A peculiar water regime of sea currents in the area of the eastern Sakhalin shelf. PICES Scientific Report 12: 131-138.

Budaeva, V.D. and Makarov, V.G. 1996a. Seasonal variability of the pycnocline in La Perouse Strait and Aniva Gulf. PICES Scientific Report 6: 13-16.

Budaeva, V.D. and Makarov, V.G. 1996b. Modeling of the typical water circulation in the La Perouse Strait and Aniva Gulf region. PICES Scientific Report 6: 17-20.

Darnitskiy, V.B. and Luchin, V.A. 1997. Specific features of horizontal structure of the climatic currents in the Okhotsk Sea (discreteness by month). Complex investigation of the Okhotsk Sea ecosystem. pp. 19-25.

Figurkin A. L. 2002. Seasonal variability of oceanological conditions in the West-Kamchatka region based on the data of monitoring surveys in 1997 and 2000. Izvestiya TINRO 130: 103-116.

Figurkin, A. L. and Zhigalov, I.A. 1999. Season variability and specificity of the oceanological conditions in the northern Okhotsk Sea in 1997. PICES Scientific Report 12: 55-60.

Gruzevich, A.K., Arzhanova, N.V., and Sapozhnikov, V.V. 1996. Hydrochemical processes in the system of joint mesoscale eddies on the Sakhalin Shelf. Okeanologiya 36(5): 719-726.

Khen, G.V., Vanin N.S. and Figurkin A.L. 2002. Peculiarity of the hydrological conditions in the northern part of the Okhotsk Sea in the second half of 90s. Izvestiya TINRO 130: 24-43.

Luchin, V.A. 1982. Diagnostic calculation of the water circulation in the Okhotsk Sea in summer. Trudy DVNIGMI 96: 69-76.

Luchin, V.A. 1987. Water circulation in the Sea of Okhotsk and peculiarities of its interannual variability by results of diagnostic calculation. Trudy DVNIGMI. 36: 3-13.

Marchuk, G.I. 1989. Computational mathematic methods. M.: Nauka.

Marchuk, G.I. and Sarkisyan, A.S. 1988. Circulation mathematic models". M.: Nauka.

Marchuk, G.I. and Shaydurov, V.V. 1979. Raising the accuracy of the difference schemes decision. M: Nauka.

PICES. 1995. The Okhotsk Sea and Oyashio Region. PICES Scientific Report 2.

Rykov N. 1999. The oceanographic data bases on Sakhalin shelf. PICES Scientific Report 12: 139-144.

Sarkisyan, A.S. 1977. Numerical modeling and forecast of the sea currents. L.: Hydrometeoizdat.

Vasiliev, A.S. and Khrapchenkov, F.F. 1996. Seasonal variability of integral water circulation in the Okhotsk sea. PICES Scientific Report 6: 158-166.

Simulation of the thermohaline dynamics of the Sea of Okhotsk

S.E. Kontorovsky
Institute of Numerical Mathematics, Russian Academy of Sciences, 8 Gubkina Street, Moscow, 119991 Russia.

A primitive equation sea dynamics model with spherical sigma coordinates is presented. The model describes a wide spectrum of sea motion including wind currents, tidal waves, and thermohaline circulation. The numerical algorithm of the model is based on implicit splitting schemes and conservative finite-difference approximations. Combination of the implicit splitting schemes and special grid approximations increases the model's efficacy that allows one to carry out numerical experiments under broad range of input parameters and external conditions. The model is applied for the Sea of Okhotsk with space resolution $10' \times 15'$ with respect to longitude and latitude and 15 vertical levels. Sea motion is generated by wind stress, heat and salt forcing at the sea surface, and tidal oscillations along the Kuril Islands. Numerical results for the tidal wave K_1 and for the marine baroclinic currents are presented. The numerical experiments show that the model adequately reproduces the structure of the hydrological fields of the Sea of Okhotsk.

For the present, there is no appropriate fine resolution three-dimensional hydrodynamic model that describes and forecasts the structure and variability of the hydrographic fields in the Sea of Okhotsk. This is related to the difficulty of the problem and to the fact that the observational data in different years and seasons are frequently contradictory.

The main features of the hydrodynamic conditions in the Sea of Okhotsk are the following:

- large depth differences;
- the presence of a wide northwestern shelf;
- strong variable winds;
- large number of straits and strong currents;
- high tides;
- and others.

All the things mentioned above highlight significant difficulties for modeling and forecasting currents in the Sea of Okhotsk. In relation to this, the problem of developing a full numerical model of the Sea of Okhotsk, which would allow us to take into account all the main factors forming the structure and variability of the hydrographic fields, becomes realized.

This study is devoted to the solution of this problem. We present a mathematical model of the Sea of Okhotsk dynamics based on full (primitive) nonlinear equations of the general circulation written in a spherical coordinate system. We use a reduced vertical σ-coordinate, related to the bottom topography $H(\lambda,\theta)$: $\sigma = \dfrac{z}{H(\lambda,\theta)}$ The advantage of the σ-system is the possibility to describe accurately the vertical structure of the computational fields in the shelf zone and continental slope as well as the fields in the bottom boundary layer. The numerical algorithm is based on the application of implicit schemes for splitting with respect to physical processes and geometrical variables.

The model of marine circulation is developed on the basis of the model of the thermohaline circulation in the ocean. The improvement of the model includes an account for the tidal waves, an important high energetic component of the dynamics in the Sea of Okhotsk.

Several numerical experiments were carried out to simulate tidal, wind, and thermohaline currents in the Sea of Okhotsk. Results show that the tidal currents possess the maximum energy. Near the eastern coast of Sakhalin Island, the velocity of the currents related to the K_1 wave reaches 30-40 cm s^{-1}. The characteristic velocity of the wind currents in the upper layer of the sea near the coast of Sakhalin Island is of the order of 10 cm s^{-1}. The general structure of the K_1 tidal wave is formed by the incident wave from the basin of the Pacific Ocean. The thermohaline and wind effects make

insignificant the contribution of this tidal wave to the dynamics.

The model describes the main currents in the Sea of Okhotsk known from the observations and numerical calculations by different authors such as the West Kamchatka Current, the East Sakhalin Current, the East Sakhalin Countercurrent, the Soya Current, and the cyclonic gyre in Penzhinskaya Bay.

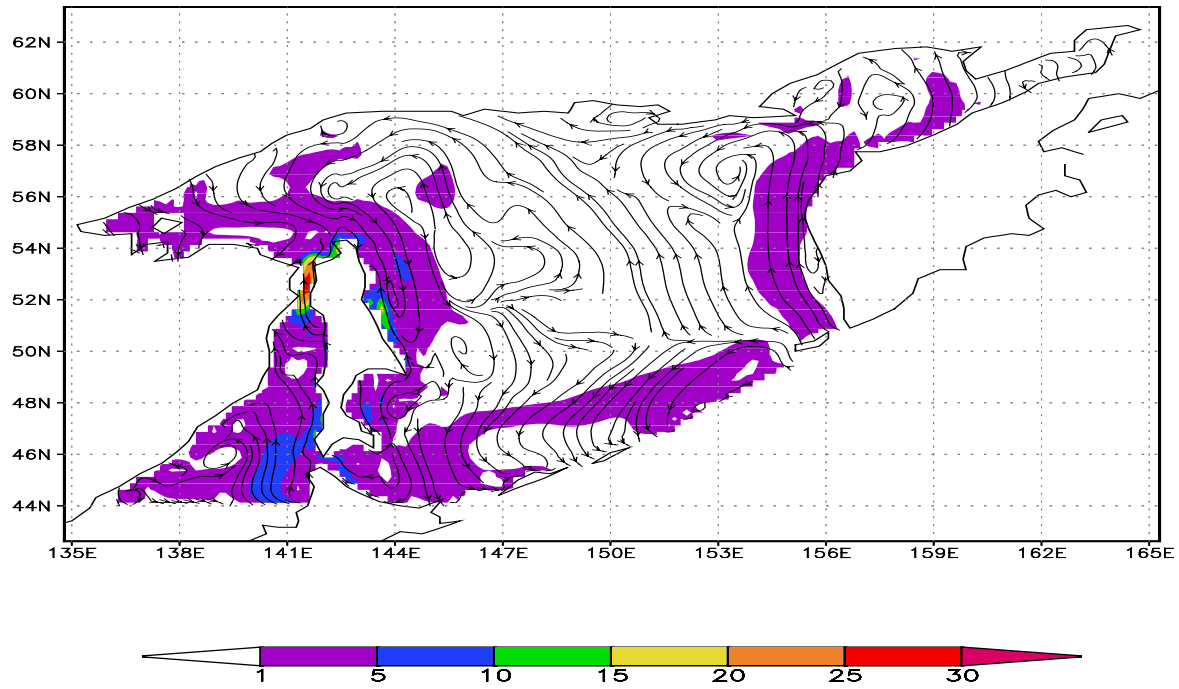

Fig. 1 Scheme of currents at a depth of 6 m, wind and thermohaline circulation.

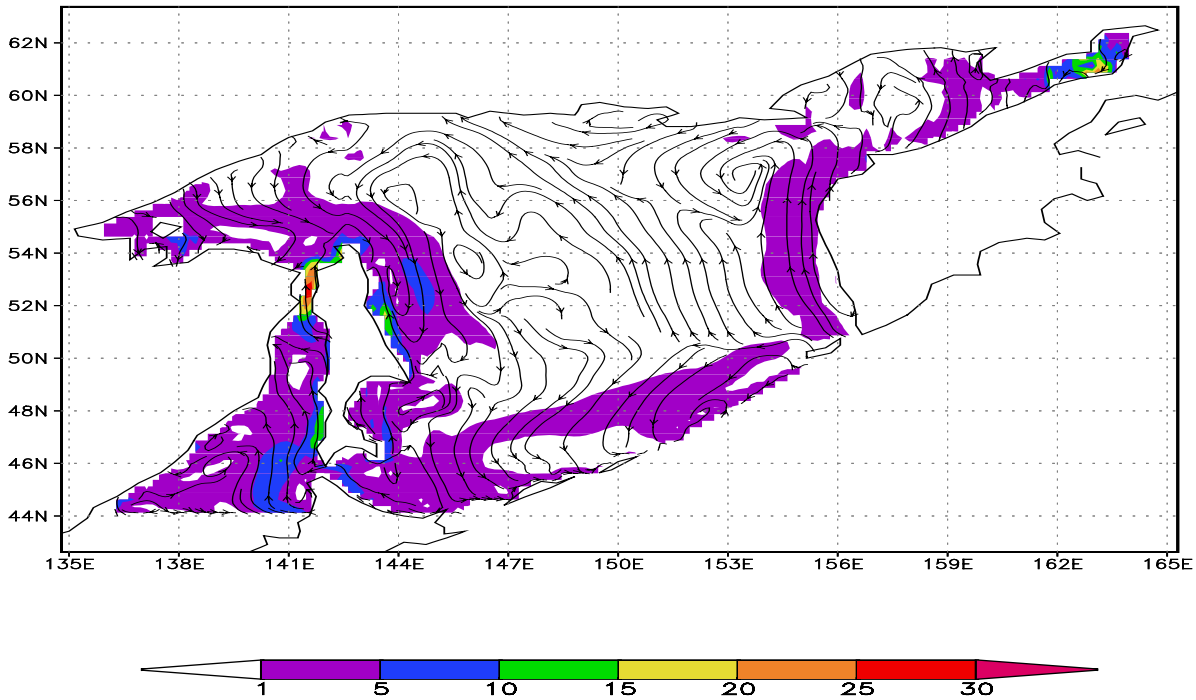

Fig. 2 Scheme of currents at a depth of 6 m, tidal wave K_1, wind and thermohaline circulation.

Calculation of the ULF (Ultra Low Frequency) electro-magnetic field parameters over the typhoon zone

Vladimir I. Korochentsev[1], V.V. Korochentsev[2], V.A. Kochetova[1], S.A. Shevkun[1], E.M. Titov[1] and L.V. Gubko[1]

[1] Far Eastern State Technical University, Department of Hydroacoustics, Aksakovsky Pereulok 3a, Vladivostok, 690950 Russia. e-mail: vkoroch@mail.ru

[2] Far Eastern State University, Oktyabrskaya 27, Vladivostok, 690600 Russia. e-mail: vkorochen@vido.dvgu.ru

A stringent mathematical model is proposed for calculation of the electromagnetic field of ultra low and low frequencies propagating within a typhoon area. The electro-magnetic zone of typhoon is shown to be like imaginable ellipsoidal dielectric lens with severe absorption of the electromagnetic waves.

Long and short axes of ellipsoid vary within a few hundred kilometers of width and up to12-15 km height. The wave equation can be such mathematical model that satisfactorily interprets the process of propagation of electromagnetic waves in typhoon zone. The results of ULF (ultra low frequency) calculation at 8, 20 Hz and 15 kHz are presented.

The work under question considers the theoretical results and compares them with the experimental dimensions acquired from Intercosmos satellites by researchers of IZAMIRAN (Troitsk, Moscow region). The mathematical model is offered for determination of coordinates of electrical discharges (lightnings, thunderstorm) generated by clouds in the zone of typhoons. Dense cloudiness, heavy meteorological conditions in typhoon zone make difficult the research of natural place and coordinates of the thunderstorms formation directly on the Earth surface.

One of the available methods of investigation of thunderstorm formation can be measuring electromagnetic waves from the satellites or aircrafts. The mathematical model offered to determine the coordinates of electrical discharges as integral equations is under consideration. As initial data there is proposed to apply the results of experimental measurements of modul and phase of electric field of electro-magnetic waves on trajectory of moving satellite or aircraft. It is supposed that computation using integral of estimated measured field and Green' s function of wave equation admit to identify approximate coordinates of certain medium.

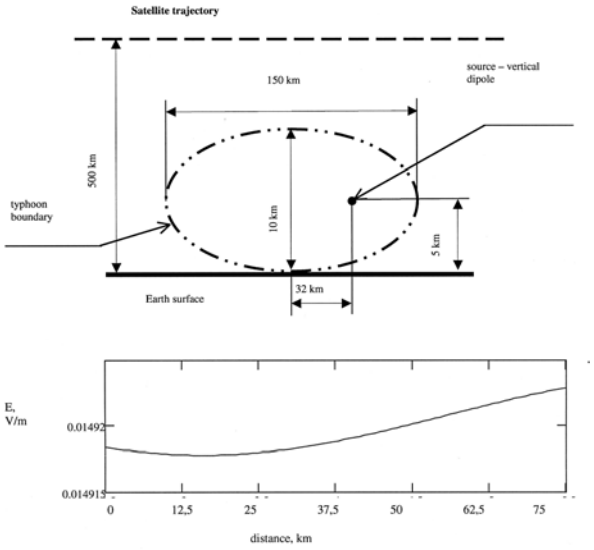

Fig. 1 Voltage of electric field along the satellite trajectory.

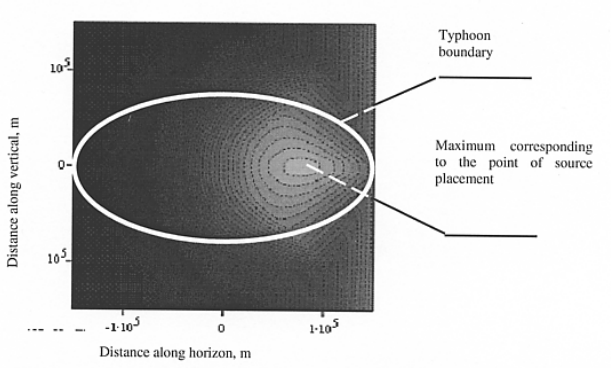

Fig. 2 Function of density of the source amplitude distribution inside typhoon.

Satellite radar sensing of the Okhotsk sea ice cover: from Kosmos-1500 Real Aperture Radar to Envisat Advanced Synthetic Aperture Radar

Leonid M. Mitnik, V.A. Dubina and I.A. Gurvich
V.I. Il'ichev Pacific Oceanological Institute, Far-Eastern Branch of Russian Academy of Sciences, 43 Baltiyskaya Street, Vladivostok, 690041 Russia. e-mail: mitnik@poi.dvo.ru

Monitoring the formation, development, melting, concentration, thickness, movement and other parameters of ice in the Okhotsk Sea is vital importance to physical oceanographers to study regional climate changes, air/sea/ice interaction, and formation of ocean water properties. Information about sea ice is used also in activities associated with transportation, fishing, disaster mitigation and commercial development in the Okhotsk Sea.

In 1983-2000 data on ice cover of the Okhotsk Sea were obtained by Side-Looking Real Aperture Radar (RAR) installed on Kosmos-1500, -1766 and Okean series satellites. RAR operates at the wavelength l = 3.15 cm at vertical polarization. A swath width DL = 450 km at a ground resolution Dl = 1-3 km (Mitnik and Viktorov 1990).

Detailed regional ice mapping can be carried out with the high resolution (10-150 m) satellite Synthetic Aperture Radar (SAR). SARs were installed on ERS-1, ERS-2, JERS, Radarsat and Envisat satellites. A swath width of these SARs varied from several tens to about 400 km with the Dl decreases with the increase of DL. A great body of ERS-1/2 SAR data on ice cover of the southwestern Okhotsk Sea was obtained since 1992. Other areas of the sea are beyond the sight of the ground receiving stations in Hatoyama and Beijing. ERS-1/2 SAR operates at the wavelength l = 5.6 cm at vertical polarization. A swath width DL = 100 km at a ground resolution Dl = 25 m. Now SAR sensing continues from ERS-2. Information on ice cover for the whole Okhotsk Sea can be obtained with the Advanced Synthetic Aperture Radar (ASAR) installed on Envisat. ASAR operates at the wavelength l = 5.6 cm at vertical (V) or horizontal (H) or cross polarization. A swath width DL = 100-405 km at a ground resolution Dl = 25-150 m. The first ASAR images of the Okhotsk Sea ice cover were taken in December-March 2003.

The radar images permit monitoring of the formation and transformation of the ice cover, provide information on the ice type, concentration, roughness, floe size and velocity under the influence of winds and currents. Below the images of the Okhotsk Sea ice cover obtained by Okean-7 RAR, ERS-2 SAR and Envisat ASAR are considered. They are analyzed and interpreted with the usage of supplementary satellite (NOAA AVHRR) and meteorological (weather maps) information. The brightness pattern of a radar image is determined by the variations of the normalized radar cross section (NRCS). It is assumed that the backscatter from the snow/ice cover is dominated by surface scattering which is related to the dielectric constant and temperature of the ice as well as depending on conditions of ice formation. Dielectric characteristics changed with the change of ice age, snow humidity, depth, and salinity, etc. (Carsey 1992). The values of he NRCS depend on the wavelength and polarization of radar signals and on an incidence angle. Sea ice is observed against the background (open sea surface) brightness of which is determined by wind speed and direction. As a result the sea ice can look both brighter and darker relative to the open sea surface. Radar contrasts are enhanced in the marginal ice zone on account of the great difference in the scattering properties of pancake ice and grease ice. The letter possesses by a high viscosity that damps the small-scale surface waves. The areas covered by the grease ice look dark since backscatter decreases sharply from the smooth sea surface. In contrast, the pancake ice is characterized by enhanced backscatter because of abundant roughness. The marginal ice zone is very dynamic. Different regular motions were registered in this zone such as ice bands and jets,

ice edge waves, eddies and chains of eddies, mushroom-like structures with dimensions ranging between several and 100-120 km.

Although the Okhotsk Sea is geographically located at temperate latitudes, it has many characteristics of a polar ocean. The first ice in the Okhotsk Sea appears at the end of October-beginning of November in the western and north-eastern regions of the sea. Cold air from the East Siberia produces sea ice in the Okhotsk Sea and at the same time pushes away the new ice from a coast. Such conditions maintain the coastal polynya and formation of thin ice which are the characteristic features in the northern part of the Okhotsk Sea and along the Sakhalin. After two months the ice on the northern half of sea connects into ice massif and drifts southward filling its central part. Coastal polynyas were frequently observed in the Aniva and Terpenya bays. Eddies along the Sakhalin coast and off Hokkaido were also detected. The maximum ice extent occurs in mid-March and thereafter the ice extent retreats and all ice disappears by the beginning of June.

The Okhotsk Sea ice occurs as fast ice and pack ice. Fast ice lies in the coastal area; the estimated mean maximum annual ice thickness distributes geographically from 0.4 to 1.1 m. The pack ice is of dynamic nature, driven by winds and currents. The drift speed of ice is as much as 35 km/day on average in coastal regions off Sakhalin and Hokkaido.

RAR images

Two Okean-7 RAR images covering the eastern Okhotsk Sea and Kamchatka are depicted in Figure 1. Strong north- and northwestward winds (15-17 m/s) were observed over the Eastern Okhotsk Sea as follows from the weather map for February 5, 2000 at 12 UTC and confirmed by orientation of wind shadows on RAR image (Fig. 1a). This synoptic situation manifests itself as the light area with cyclonic bend where the imprints of convective rolls stretched along wind direction are clearly visible. A narrow band of the sea ice which is adjacent to the Kamchatka coast has a darker tone compare to the wind-roughened open sea surface. It is especially true for an outer part of the band which is characterized by the minimum brightness likely due to the presence of grease ice. Its width is about 6 km. Ice zone broadens west of the southern Kamchatka coast where wind speed weakens. Upwind side of the ice zone has the increased backscatter due to likely the decrease of the of pancake ice size.

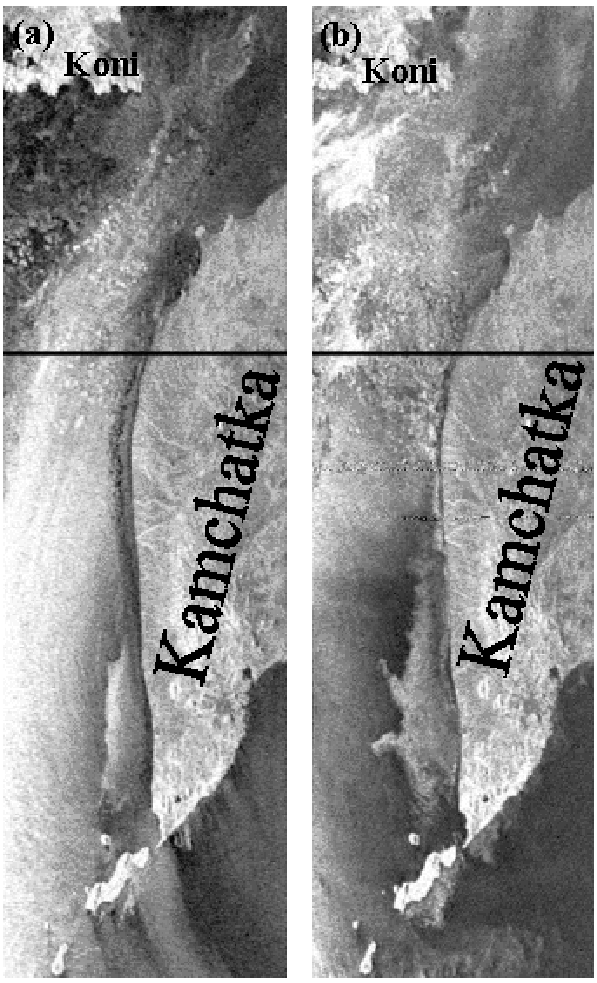

Fig. 1 Okean-7 RAR images for February 5 at 10:47 UTC (a) and February 8 (b) 2000 at 10:47 UTC showing fast growth of the ice cover in the Northern Okhotsk Sea, near Kamchatka coast and south of Paramushir.

In three days cold air advection in the eastern Okhotsk Sea significantly decreased and the zone with strong winds moved to the west (Fig. 1b). Dark tone of the open sea surface points to low wind speed due to the low air pressure gradients. An area of ice cover distinctly increased. At the northern part of the image the ice edge moved far to the south. Formation of ice continues to the south of Koni Peninsula where there are several bright patches which consist very likely of

pancake ice. The sea ice area along the southern Kamchatka coast as well as near Lopatka Cape and to the south of Paramushir also markedly increased. To the south of a dark line in Figure 1, the increase is estimated as 15000 km^2. As follows from the surface analysis and wind and wave analysis maps it was happen for the most part between February 5 and 6 when strong cold air outbreak was observed. Then the location of ice edge changed modestly. The vast and giant ice floes (bright patches) are visible on both RAR images. However it is difficult to identify the same giant floes on two images in three days. Severe weather conditions produced the change not only floe's location but their NRCS as well.

SAR images

Detailed ice mapping of the area between Southern Sakhalin and Hokkaido as well as Sakhalin and Kamchatka coastal zones can be carried out with a SAR installed on ERS-2 and Envisat satellites. The ice conditions in the Aniva Bay are reliably identified on numerous ERS-1/2 SAR images obtained in 1992-2003. Their boundaries are shown in Figure 2.

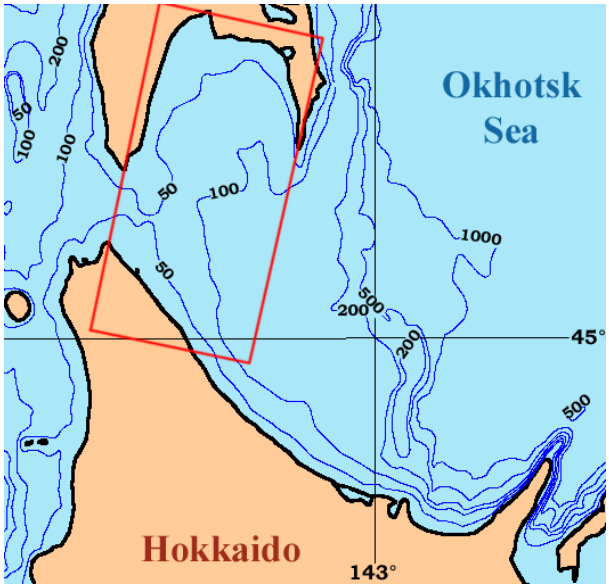

Fig. 2 Bathymetric map off the Hokkaido coast. Solid rectangle marks the location of the ERS-1/2 SAR frames along track 489.

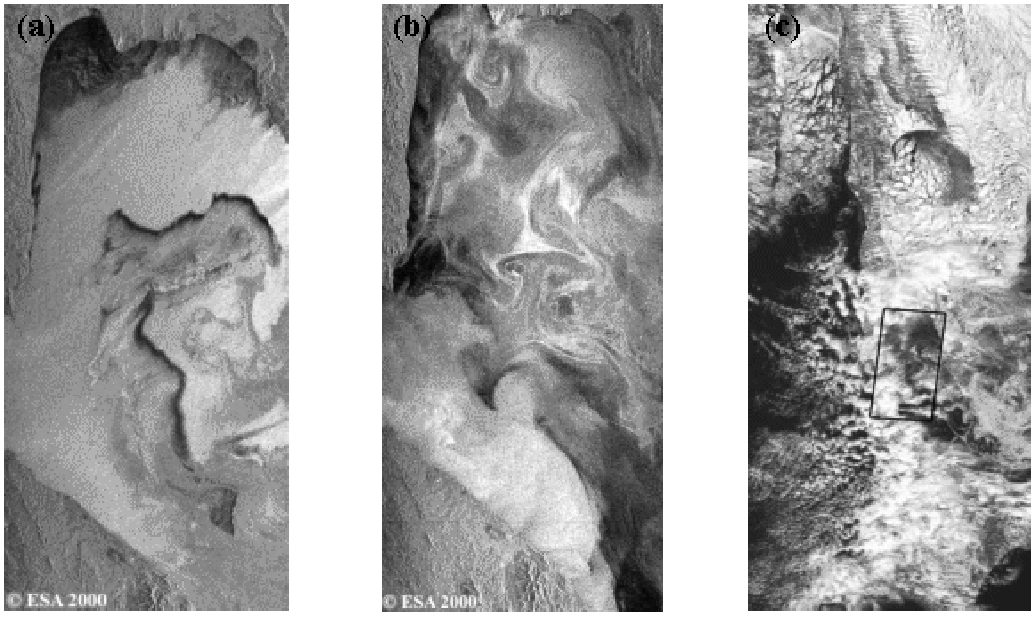

Fig. 3 The features of sea ice distribution in the area between Sakhalin and Hokkaido as revealed by ERS-2 SAR images acquired at 01:17 UTC on January 24, 2000 (a) and March 3, 2002 (b). NOAA AVHRR visible image taken on 3 March (c). Solid dark rectangle marks the boundaries of the SAR images.

Fig. 4 ASAR Envisat image with HH polarization for December 9, 2002, at 12:11 UTC.

ERS-2 SAR images for January 24, 2000 at 01:17 UTC (Fig. 3a) were acquired when strong northwestward winds blew over the Bay. As a result the open sea surface has a light tone on the image. The stretched features show wind direction. Sea ice is observed near the Sakhalin coast, in a central part of the Aniva Bay and near Hokkaido. Dark belts of variable width adjacent to an ice massif in the central part of Aniva Bay are grease ice. They are located upwind and visualize the area of intensive ice formation. The area of the grease ice is estimated as 700 km^2. Other types of sea ice (nilas, young ice, grey ice, gray-white ice) which were formed in the Aniva Bay or somewhere northeast Sakhalin and drifted to the south have a grey tone on the SAR image.

Sea ice serves a tracer of sea surface circulation when strong winds are absent. The ERS-2 SAR image for March 3, 2002 of the area between Sakhalin and Hokkaido (Fig. 3b) shows the eddy-like and mushroom-like structures. It is evident that NOAA AVHRR image acquired at the same day (Fig. 3c) gives only an approximate estimate of sea ice distribution. Dark rectangle marks the boundaries of the SAR image.

Envisat ASAR image for March 9, 2002 at 12:11 UTC (Fig. 4) visualized the areas of new ice formation under strong cold air flow. According to the surface analysis map, air temperature at the coastal stations changed from -24 to -20°C. The stretched bands of the variable brightness crossing the image from the northwest to the southeast are due to the sea surface wind. The differences in the brightness (in the values of the NRCS) are caused by the effect of coastal orography. Ice is generated both near the coast and in the open sea. The ice drifts from the coast and forms bands extended in wind direction. In the open sea the areas of grease ice and pancake ice are estimated as 1600 and 3100 km^2, respectively. Transformation of grease ice in pancake ice is fast enough under the particular weather conditions. These two types of ice development are visible very clearly due to high radar contrast between them. The sea ice is also well distinguished in the Sakhalin Bay (in its western and southern parts), Amursky Liman, along the eastern Sakhalin coast and in Tatarsky Bay.

Acknowledgments
This study was carried out within ESA ERS project AO3-401: "Mesoscale oceanic and atmospheric phenomena in the coastal area of the Japan and Okhotsk seas: Study with ERS SAR

and research vessels" and ESA Envisat project AO-ID-391: "Study of the interaction of oceanic and atmospheric processes in the Japan Sea and the Southern Okhotsk Sea". This work is partially sponsored by a grant for a project: "Investigation of ocean-atmosphere system with passive and active microwave sensing from new generation satellites" from Far Eastern Branch of the Russian Academy of Sciences.

References

Mitnik, L.M. and Viktorov, S.V. (Eds.). 1990. Radar Sensing of the Earth's Surface from Space. Gidrometeoizdat, Leningrad, 200 pp. (in Russian).

Microwave Remote Sensing of Sea Ice. Frank D. Carsey, Editor. 1992. Geophysical monograph 68. 462 pp.

Development of ice cover in the Okhotsk Sea in 2002-2003 as viewed by Aqua AMSR-E and Envisat ASAR

Leonid M. Mitnik, V. A. Dubina, V. K. Fishchenko, M. L. Mitnik and A. V. Golik
V.I. Il'ichev Pacific Oceanological Institute, Far Eastern Branch of Russian Academy of Sciences, 43 Baltiyskaya Street, Vladivostok, 690041 Russia. e-mail: mitnik@poi.dvo.ru

Meteorological and oceanic characteristics of the Okhotsk Sea are close to those of the polar ocean. They include severe winters with low air temperature and enhanced cyclone activity, extended period of ice cover, etc. Gale winds accompanying cyclones and convective atmospheric vortices significantly influence the formation, development of ice cover, and the position and structure of the ice edge. From this follows the need of gaining operational information about ice cover and surface wind characteristics. In turn, this information is essential for solving scientific problems, in particular those involving ice margin processes (water mass formation, oceanic upwelling, eddy formation, etc.), synoptic and mesoscale processes in the atmosphere including instability generation, air-sea-ice interaction.

Only space measurements can provide a pattern of ice distribution over the whole sea practically at a single moment. Continuous monitoring of ice cover is impossible with satellite visible and IR data only. NOAA AVHRR visible and IR images have the spatial resolution of about 1 x 1 km, however, cloudiness limits the possibilities of surveying. Low brightness and thermal contrasts also hinder application of the AVHRR data except for grease ice and dark nilas.

Substantial progress can be made toward solving this problem by using the microwave passive (radiometric) and active (radar) data due to weak influence of weather conditions and the possibilities of estimating both ice and oceanic/atmospheric characteristics. Satellite passive microwave systems provide low resolution information but with good spatial and temporal coverage independently on cloudiness and sun illumination. This information is used for global and regional climate studies. In particular, Nimbus SMMR and DMSP SSM/I data were used to reveal the relationship between SMM/I-derived sea ice extents of the Bering and Okhotsk seas and atmospheric circulation, to relate ice cover with oceanic processes, etc. Ice concentration data were used to estimate the production rates of ice, salt and dense shelf water in polynyas over the Kashevarova Bank and over the northwest continental shelf. Cold air from the East Siberia produces sea ice in the Okhotsk Sea and at the same time pushes away the new ice from a coast. Such conditions maintain the coastal polynyas and formation of thin ice which are the characteristic features in the northern part of the Okhotsk Sea and along the Sakhalin. SSM/I-derived evidence on thin ice area fluctuations is important for estimates of heat flux, sea ice productivity and formation of saline water. Young ice is mapped using Polarization Ratio (PR) or a scatter plot of PR and Gradient Ratio. The daily fluctuations of thin ice area were investigated by making daily ice charts. In the case of advance of ice edge, thin ice zone expands.

The surface resolution of the SSM/I DMSP data is 30×30 km at frequency $\nu = 37.0$ GHz or 15×15 km at $\nu = 85.0$ GHz that determines the possible error in estimation of the ice edge position, the possibilities of studying different scale motions, etc. Aqua and ADEOS-II satellites were launched on polar orbits on May 4 and December 14, 2002, respectively. A most important instrument for sea ice study is microwave imaging radiometer AMSR (Advanced Microwave Scanning Radiometer). AMSR measures outgoing microwave emission of the atmosphere-underlying surface system at frequencies of 6.6, 10.65, 18.7, 23.8, 36.5 and 89.0 GHz with the vertical and horizontal polarization. The AMSR has wider swath width, higher radiometric sensitivity and higher spatial resolution as compared with SSM/I. (For example, the pixel size is 10×10 km at $\nu = 36.5$ GHz and 5×5 km at $\nu =$ of 89 GHz. The

increased resolution and the broader swath (more frequent coverage) serve as the basis of ice drift estimation.

In this report, the main attention is focused on the demonstration of the high potential of Aqua AMSR-E data for the sea ice study in the Okhotsk Sea. Aqua AMSR-E data for January 25-31, 2003 were used in our research. Supplementary information included the NOAA AVHRR images, weather maps as well as the Envisat Advanced Synthetic Aperture Radar (ASAR) images taken in December 2002 - February 2003. The resolution of the wide swath (405 km) ASAR images is 150 x 150 m that allows us to investigate the fine details of sea ice distribution.

On January 25-31 the weather conditions in the Okhotsk Sea were determined by the southern cyclones. On January 25-26 strong northwestern winds were observed almost over the whole sea. Wind speed reached 15-20 m s^{-1} in the Kuril straits area. Cloud streets which are typical for a cold outbreak extended over the most of the sea as follows from AVHRR visible image for January 26 at 02:26 UTC. Clouds hinder to detect the sea ice in the eastern Okhotsk Sea as opposite to the western and centrals parts where cold advection was no so intensive, cloud rolls were rear and the sea surface was distinctly seen. Different types of ice and ice-free space in the area of Kashevarova Bank were well distinguished. In the northern Okhotsk Sea and along eastern Sakhalin coast where winds were weak and clouds were absent, the differences between young (dark) and snow-covered (bright) ice as well as the ice eddies between Sakhalin and Hokkaido were reliably detected. The young ice area in Terpeniya Bay broadened during January 25-26. The features of ice cover in the fields of brightness temperatures measured by AMSR-E on descending and ascending Aqua orbits were in a good agreement with the AVHRR visible image.

On January 27, zone of northwestern winds shifted to the eastern part of the Okhotsk Sea and in the west Okhotsk Sea winds were weak as follows from the surface analysis maps at 00, 06 and 12 UTC. However the western and northern parts of the sea were left under the action of a cold outbreak to the rear of a deep cyclone located to the south of Aleutian Islands according to the surface analysis map for January 27 at 00 UTC. The sea ice near the eastern and southern Sakhalin became poorly distinguished on the AVHRR visible image for January 27 at 5:38 UTC (Fig. 1) due to displacement of the cloudiness associated with the cold front and cyclone. The marginal ice zone and the features of sea ice distribution in the area of Kashevarova Bank were observed very clearly. The AMSR-E data covered only the western Okhotsk Sea. The microwave observations fit the AVHRR visible image reasonably well.

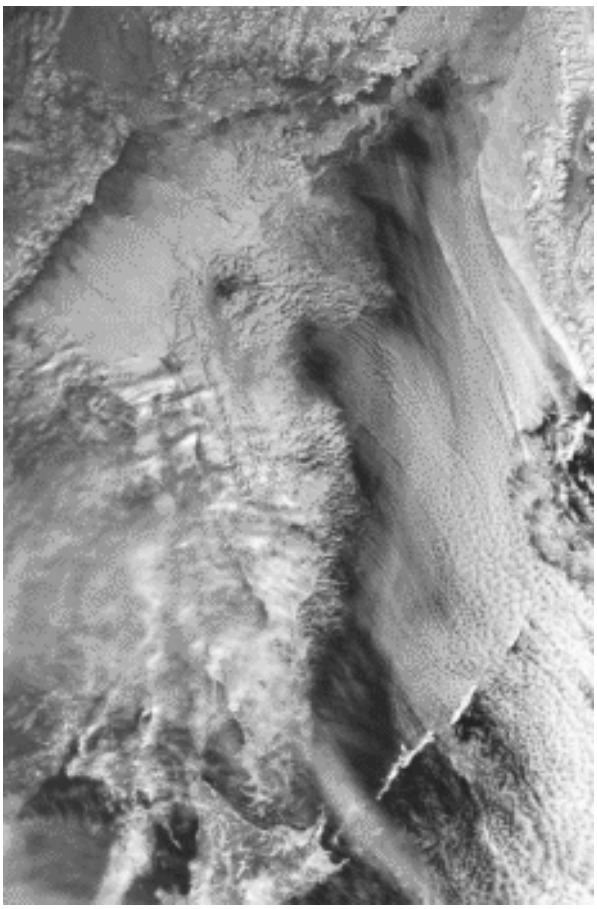

Fig. 1 NOAA AVHRR visible image for January 27, 2003, at 5:38 UTC.

On January 28 and during the first half of January 29 the cyclone moved to the Okhotsk Sea across Sakhalin. The winds were southeastward in the Southern Okhotsk Sea and east- and northeastward in the northern part of the sea. Wind speed reached 15-20 m s^{-1}. Coincidence of cyclonic circulation with the outlines of the coastline was

favorable to the wind speed increase in the northern Okhotsk Sea. The center of the cyclone on the AVHRR visible image for January 29 was in the center of convergence of cloud spirals. Cloud rows extended along the Northern Okhotsk Sea. The heavy clouds impeded the observations of sea ice. Application of microwave measurements is of a special value under cloudiness and gall winds when the ice edge position and polynyas' area changed rapidly. Figure 2 shows the fields of brightness temperatures TB(ν) at ν = 37.0 GHz (a) and 18.7 GHz (b) with the horizontal polarization acquired on January 28 at 17:15 UTC.

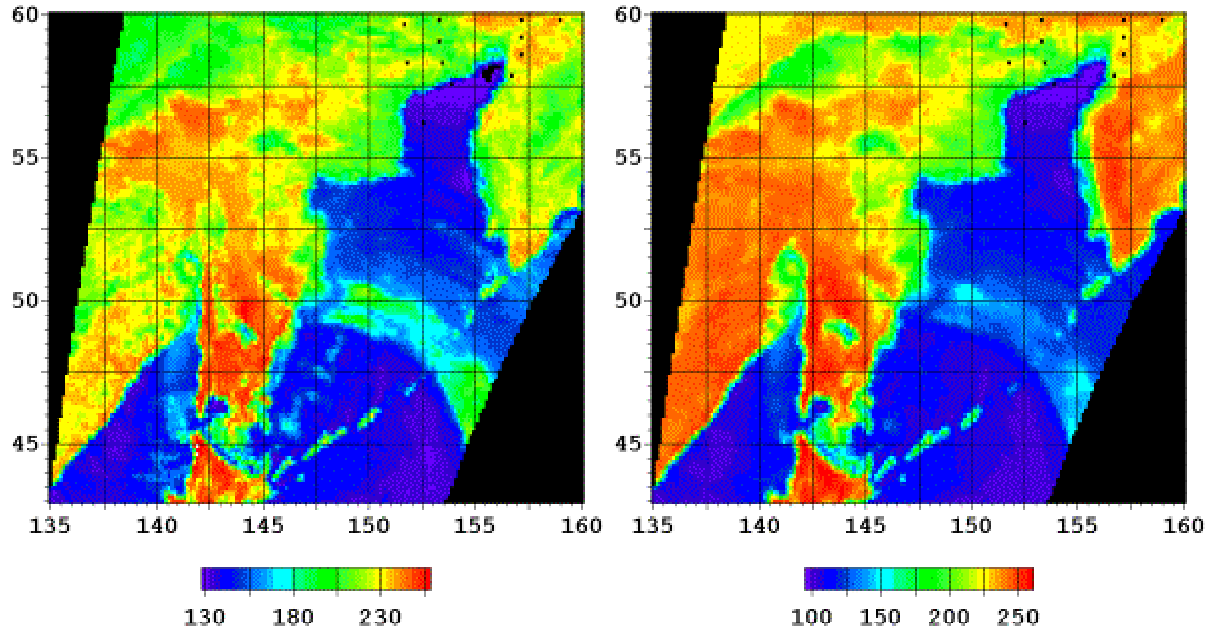

Fig. 2 Brightness temperatures at 36.5 GHz (a) and 18.7 GHz (b) with the horizontal polarization over the Okhotsk Sea obtained by Aqua AMSR-E on January 30 at 02:12 UTC.

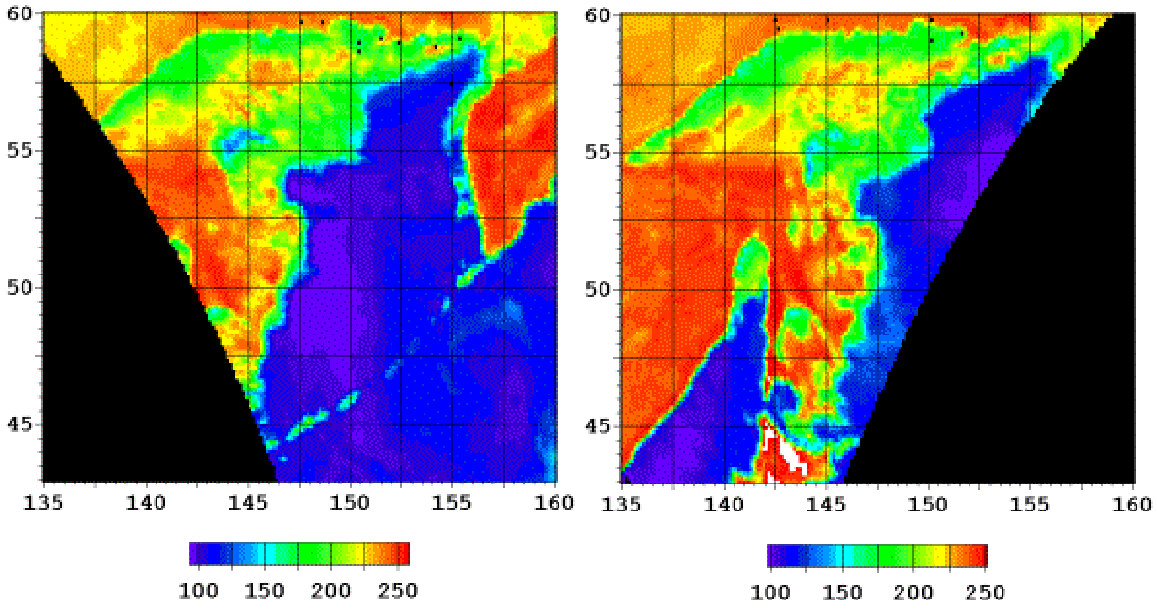

Fig. 3 Brightness temperatures at 18.7 GHz with the horizontal polarization over the Okhotsk Sea obtained by Aqua AMSR-E on (a) January 30 at 02:50 UTC, and on (b) January 31 at 17:20 UTC.

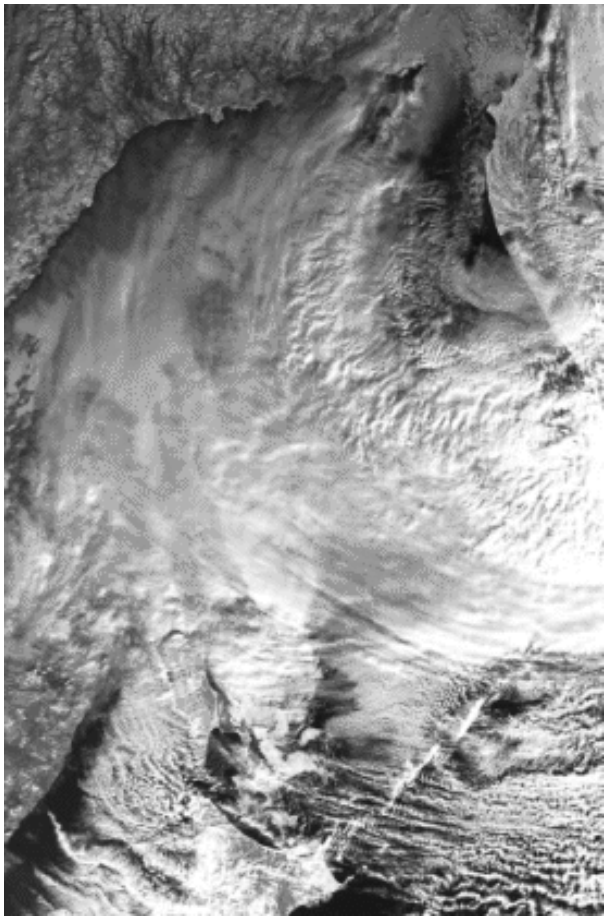

Fig. 4 NOAA AVHRR visible image for January 31, 2003 at 5:51 UTC.

The TBs variations over the sea are due to the differences in the sea ice properties and concentration as well as due to the variations in the total cloud liquid water content Q. In particular, a broad arc-like band over the ice-free waters is the cloud band cyclone. The similar features are reliably detected by using spectral and polarization differences. The corresponding examples are given in the paper.

Comparison of AVHRR visible images taken on January 29 and 30 shows the further development of the synoptic processes. The cyclone to the east of Sakhalin began to occlude as follows from the image for January 30. A cold front which was located over the central Okhotsk Sea shifted fast to the east. Strong southwestward winds associated with the occlusion front continued in the northwestern Okhotsk Sea. At the same time, the gale winds caused by the cold front moved to the southeastern part of the sea. Weak winds were observed over the Sakhalin shelf. On January 29, ice edge was clearly visible to the east of southern Sakhalin. On January 30, in spite of cloudiness, almost all ice was covered by clouds. Aqua AMSR-E measurements gave an estimate of sea ice pattern (Fig. 3a).

On January 31, the whole Okhotsk Sea was in the rear of a deep cyclone which displaced to the northeast in the Bering Sea (Fig. 4). As a result the gale northern and northwestern winds were observed over the whole Okhotsk Sea excepting its northern coast where winds blew from northeast. Gale winds were favorable for to push ice away from Terpeniya Bay as follows from visible images for January 30 and 31 and confirmed by AMSR-E data. The TBS fields over the sea ice were also used to estimate the ice drift by application of multiple cross-correlation technique. Ice cover development in December 2002 and February 2003 was traced by analysis of Envisat ASAR images.

Acknowledgments

This study has been carried out within the cooperation between the National Space Development Agency (Japan) and the V.I. Il'ichev Pacific Oceanological Institute, FEB RAS (Russia) in the ADEOS-II Research activity (project A2ARF006) as well as within ESA Envisat project AO-ID-391: "Study of the interaction of oceanic and atmospheric processes in the Japan Sea and the Southern Okhotsk Sea". This work is partially sponsored by a grant for a project: "Investigation of ocean-atmosphere system with passive and active microwave sensing from new generation satellites" from Far Eastern Branch of the Russian Academy of Sciences.

Okhotsk Sea waters around Cape Krilion: Satellite and mooring station observations

Leonid M. Mitnik[1], G. V. Shevchenko[2], V. A. Dubina[1], and Y. A. Sophienko[1]

[1] V.I. Il'ichev Pacific Oceanological Institute, Far Eastern Branch of Russian Academy of Sciences, 43 Baltiyskaya Street, Vladivostok, 690041 Russia. e-mail: mitnik@poi.dvo.ru

[2] Sakhalin Research Institute of Fisheries and Oceanography (SakhNIRO), 196 Komsomol'skaya Street, Yuzhno-Sakhalinsk, 693023 Russia.

Warm saline waters of the Japan Sea flow into the Japan Sea through the La Perouse (Soya) Strait. These waters control the important features of the oceanographic regime of the whole Sakhalin-Kuril region. In spite of this fact, the dynamic phenomena and processes in the strait, in particular, the exchange of waters between the Japan and Okhotsk Seas have not been adequately studied. A primary consideration is small amount of long-term current measurements in the strait. Recent observations carried out in the La Perouse Strait and to the east of it improved the situation. Analysis of experimental data allows us to determine total flow velocity and its seasonal variations as well as the current variations in the strait caused by tides and winds.

At the same time many other questions remains to be answered. They are in particular associated with comprehensive study of spatial and temporal variability of the water exchange, structure of current field, penetration of the Okhotsk Sea waters into the Japan Sea caused by tidal flows and displacement of low pressure atmospheric systems. The usage of surface analysis maps and NOAA AVHRR images helps to interpret the features of current measurements. The weather maps show the location of cyclones, their trajectories, the values of surface pressure, wind speed and direction. The AVHRR infrared (IR) images or AVHRR-derived fields of SST provide a rough idea of the position of the different water masses and boundaries dividing them. Interference caused by clouds and inadequate spatial resolution of the AVHRR hinder the oceanic phenomena study. Moreover, the phenomena with minor thermal contrast or with the size under several hundred meters cannot be detected by an AVHRR. Application of satellite Synthetic Aperture Radar (SAR) images in combination with other satellite and *in situ* observations allows us to study the submesoscale and fine scale features of the oceanic processes independently on cloudiness since the cloudy atmosphere is practically transparent for C-band radar signals and a ground resolution is 25 × 25 m.

SAR sensing of the La Perouse (Soya) Strait was carried out from ERS-1 and ERS-2 with C-band SAR. The SAR imagery was mainly obtained when the satellites were in 35-day exact repeat orbits, which precludes short-term temporal sampling. The position of two ERS-1/2 images covering the strait on descending track 260 is shown in Figure 1. The size of an image is about 100 × 100 km and a spatial resolution is 25 × 25 m. The first ERS-1 SAR image of the strait was taken on April 15, 1992 and the last one - on April 12, 1996. The first SAR image from ERS-2 was taken on July 12, 1997 and the last one was taken on April 12, 2003. Observations from ERS-2 continue.

Information collected in the European Space Agency (ESA) was screened to estimate the dates and time of the individual SAR images. The results of this screening are given below. More than 150 images were taken from ERS-1 and ERS-2. All images of the La Perouse (Soya) Strait presented on the web sites of ground stations and the ESA were downloaded. They represent the so named quick look (QL) images having the reduced spatial and radiometric resolution and thus we were able to detect only high -contrast cases. The cases with low-level radar signatures were missed. One precision (PRI) high-resolution ERS-2 SAR images was ordered at the ESA to carry out the detailed study of the surface manifestations of the oceanic phenomena.

The SAR images were used to verify hypotheses for tidal nature of the cold waters near the western coast of Cape Krilion. These cold waters are regularly observed on IR images obtained by AVHRR (ground resolution Dl = 1.1 km) from NOAA satellite as well as by IR sensors from Meteor_Priroda (Dl = 250 m) and Landsat (Dl = 120 m) satellites. The cold waters are traced from Cape Krilion. It forms a cold belt parallel to the Soya Warm Current (see Danchenkov et al. 1999 and references cited in it). Figure 2 shows SST pattern in the area under study on MSU-SK and Landsat-5 images. The main features of the SST field are the cold waters 1 to the west of Krilion Cape, Soya Warm Current 2 along the Hokkaido coast and a narrow belt of cold water 3 adjointing to the current. They are considered in detail by Mitnik et al. (2002).

To verify the tidal hypotheses all 75 SAR strips were screened to detect the presence or absence of the oceanic fronts to the west of Krilion Cape. The radar signatures in a form of the light curvilinear bands were detected on 19 strips. No features to the west of Cape Krilion were found on other 56 strips. On these strips, the signatures were absent or observed in other places such as to the east of Cape Krilion and/or near the Hokkaido coast. Fourteen strips were taken at a period when mooring stations measured currents in the strait at a point shown in Figure 1 (Kantakov and Shevchenko, 2001).

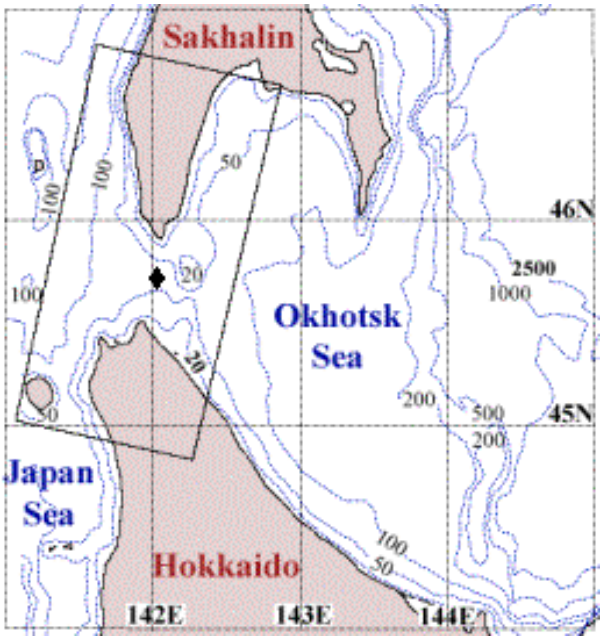

Fig. 1 Bathymetry map of the La Perouse Strait area and the Southwestern Okhotsk Sea. Solid rectangle marks the location of the ERS-1/2 SAR frames taken on 260 track. ♦ shows the location of Clione mooring stations.

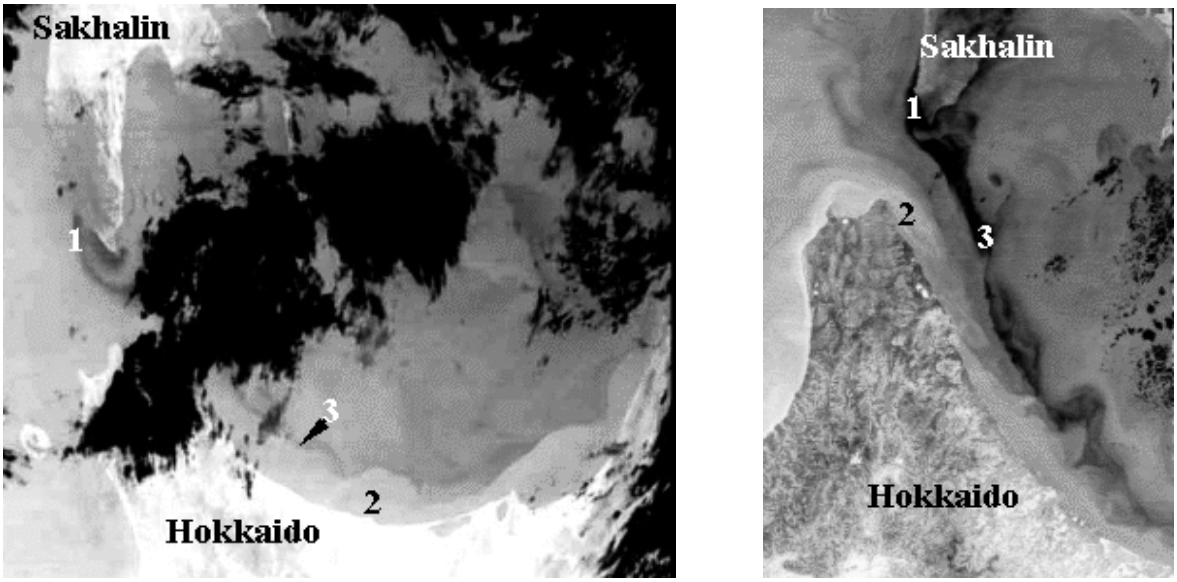

Fig. 2 SST distribution between Sakhalin and Hokkaido as detected by Meteor-Priroda MSU-SK on August 13, 2000 (left) and by Landsat-5 on July 7, 1992 (right). Clouds are depicted by dark tone (left image). Light tone corresponds to the higher values of the sea surface temperature (Soya Warm Current).

Instrumental current measurements were analyzed for several cases both when the frontal zones were detected and when they were not detected on ERS SAR images. It has been established that the presence of the fronts to the west of Cape Krilion corresponds to such tidal phases when tidal flow was directed from the Okhotsk Sea into the Japan Sea. Typical example is shown in Figure 3a. ERS-2 SAR image of the La Perouse (Soya) Strait was acquired on August 5, 2000, under favorable weather conditions: wind speed varied in the range of 3-6 m/s. The cold waters near Cape Krilion and to the southeast of it look darker than the background ones. The frontal boundaries in a form of narrow light bands caused by the increased sea surface roughness separate them from the surrounding warmer waters. These boundaries are detected both to the west of Cape Krilion in the Japan Sea and to the east of the Cape in Aniva Bay. The boundaries coincide with thermal contrasts on NOAA-derived SST field (not shown). The image was taken at 01:20 UTC at the instant a flood phase was almost finished and shows the approximate boundary of cold water penetration in response to tidal flow. East-directed (u) and north-directed (v) current components at the depth of 40 m measured by Clione mooring in the middle of La Perouse (Soya) Strait (Fig. 1) and the predicted tidal currents at the depth of 15 m on August 4-5, 2000, are shown in Figure 3b, c. Dot and dash line corresponds to the moment of ERS-2 SAR sensing.

The similar radar signatures were observed on the SAR images taken at 260 track on October 7, 1992, July 14 and August 18, 1993, August 11 1995, September 20, 1997, October 10, 1998, August 21, 1999, September 9, 2000, August 25, 2001, etc. The SST patterns on the AVHRR IR cloudless images correlated with the SAR features.

When direction of tidal flow coincided with the general flow the frontal zones to the west of Krilion Cape were absent on the SAR images. At the same time they were detected east and south of the cape. Figure 4 illustrates a situation when general flow was directed to the east and tidal flow was weak as follows from Clione measurements. The frontal zone in a form of light curvilinear line is clearly visible on ERS-2 SAR image for June 12, 1999 at 01:20 UTC.

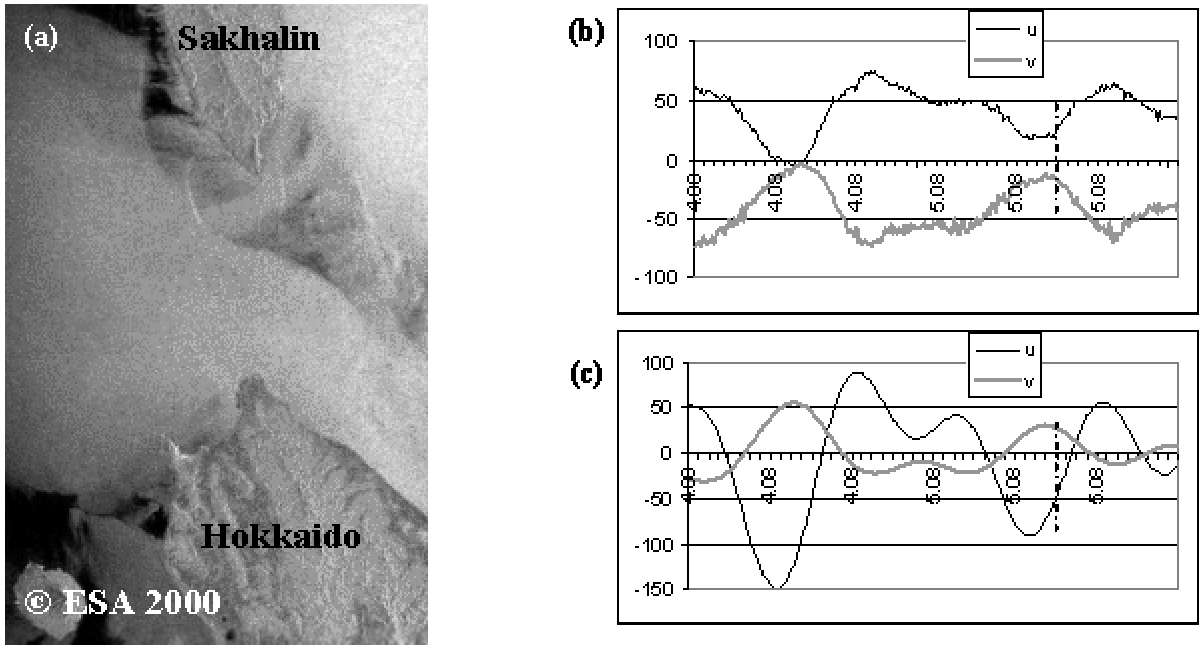

Fig. 3 ERS-2 SAR QL image of the Soya Strait area for August 5, 2000, at 01:20 UTC during strong westward tidal current (a). The east-west (u) and north-south (v) components of currents at the depth of 40 m recorded by Clione mooring station (b) and computed u and v current components at a depth of 15 m (c) on August 4-5, 2000.

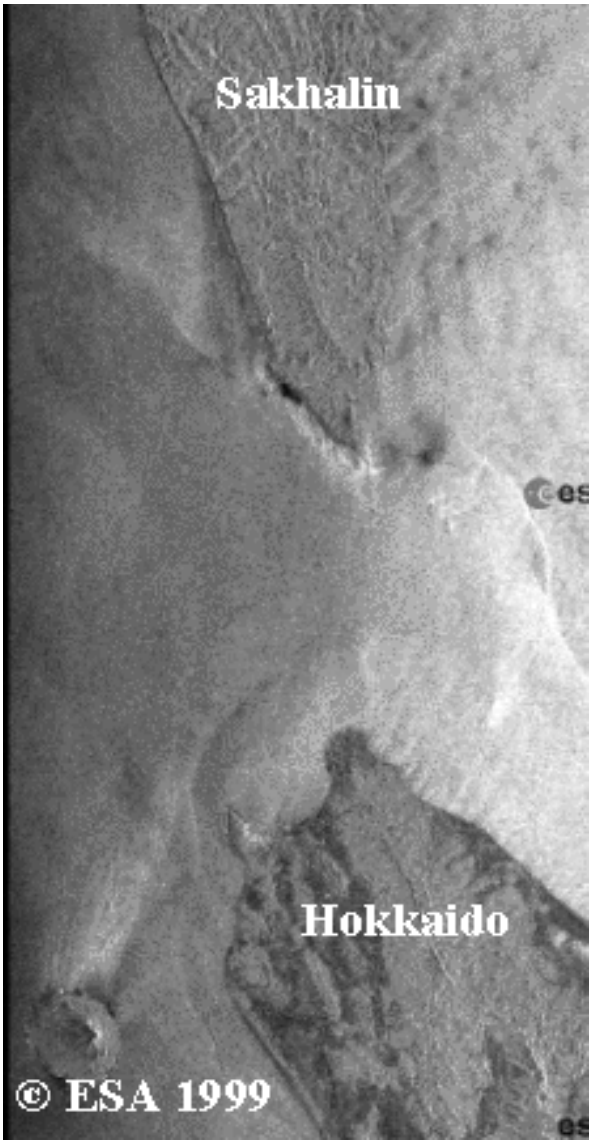

Fig. 4 ERS-2 SAR QL image of the Soya Strait area acquired on June 12, 1999, at 01:22 UTC at eastward general surface current.

Velocity of tidal current in the La Perouse (Soya) Strait is high. Under definite astronomical conditions, surface current velocity at the centre of the strait can reach 3 m s^{-1}. Flood tide can overcome main flow of the SWC. It is especially true for the northern part of the strait where general flow weakens flood tide and the flood tide increases due to the increase of meridional components. According to the computations up to 100 km^3 of water can be transported from the Okhotsk Sea into the Japan Sea and back during a tidal cycle. The volume should be decreased to 40-50 km^3 if take into account the counteraction by the SWC. Cold waters from the Okhotsk Sea enter largely through the northern part of the strait northwestward. These conclusions are in a good agreement with the results of analysis of satellite SAR and IR observations.

Acknowledgments

This study was carried out within ESA ERS project AO3-401: "Mesoscale oceanic and atmospheric phenomena in the coastal area of the Japan and Okhotsk seas: Study with ERS SAR and research vessels" and ESA ENVISAT project AO-ID-391: "Study of the interaction of oceanic and atmospheric processes in the Japan Sea and the Southern Okhotsk Sea". This work is partially sponsored by a grant 03-01-0-07-006 for a project: "Investigation of ocean-atmosphere system with passive and active microwave sensing from new generation satellites" from Far Eastern Branch of the Russian Academy of Sciences.

References

Danchenkov, M.A., Aubrey, D. and Riser, S.C. 1991. Oceanographic features of the La Perouse Strait. In PICES Scientific Report No. 12, 159-171.

Kantakov, G.A. and Shevchenko, G.V. 2001. The analysis of residual currents in the La Perouse (Soya) Strait associated with the sea level variation and wind effect. Dynamic Processes on the Shelf of Sakhalin and the Kuril Islands. G.V. Shevchenko, editor. Institute of Marine Geology & Geophysics. Sakhalin Science Center, FEB RAS. 62-74.

Mitnik, L., Dubina, V. and Sugimori, Y. 2002. ERS SAR observations of dynamic features in the Soya Warm Current. Proc. PORSEC 2002; Bali, Indonesia, 3-6 September 2002, Vol. 1, 182-187.

Intermediate water masses of the Kuril Island zone and the adjacent areas

Valentina V. Moroz
V.I. Il'ichev Pacific Oceanological Institute, Far-Eastern Branch of Russian Academy of Sciences, 43 Baltiyskaya Street, Vladivostok, 690041 Russia. e-mail: moroz@poi.dvo.ru

Multi-year observations (by Japan and the Russian Pacific Oceanological Institute) of intermediate water masses in the Kuril Islands zone and adjacent areas formed the basis of this study. It was found that in the Okhotsk Sea along the Kuril Islands, there is an abrupt "end" of the cold intermediate layer core (minimum <1°C at a distance of 40-60 miles from the islands coast (Fig. 1a). The abrupt "end" of the cold intermediate layer is evidence of the existence of a clear division of intermediate water of the Okhotsk Sea and the transformed waters in the tidally mixed straits. The cold intermediate layer in the Okhotsk Sea is not connected with the same in Oyashio Current and is identified by winter temperature conditions in the region.

The hydrological structure of water in the straits is more complicated than was believed earlier. First, the transformation of water in the straits is exposed differently. Water with intrinsic signs of Kuril-type subarctic structure is observed mainly on the shelf of the Kuril islands where tidal mixing is more evident. In the shallow water zone, tidal transformation results in the formation of a vertically homogenous water column. In the deepwater areas of the straits, highly stratified waters are observed. Secondly, the characteristic presence of variously scaled non-homogeneous structures that are being formed through eddy-formation and frontogenesis as near-Kuril currents touch, on a background of tidal mixing.

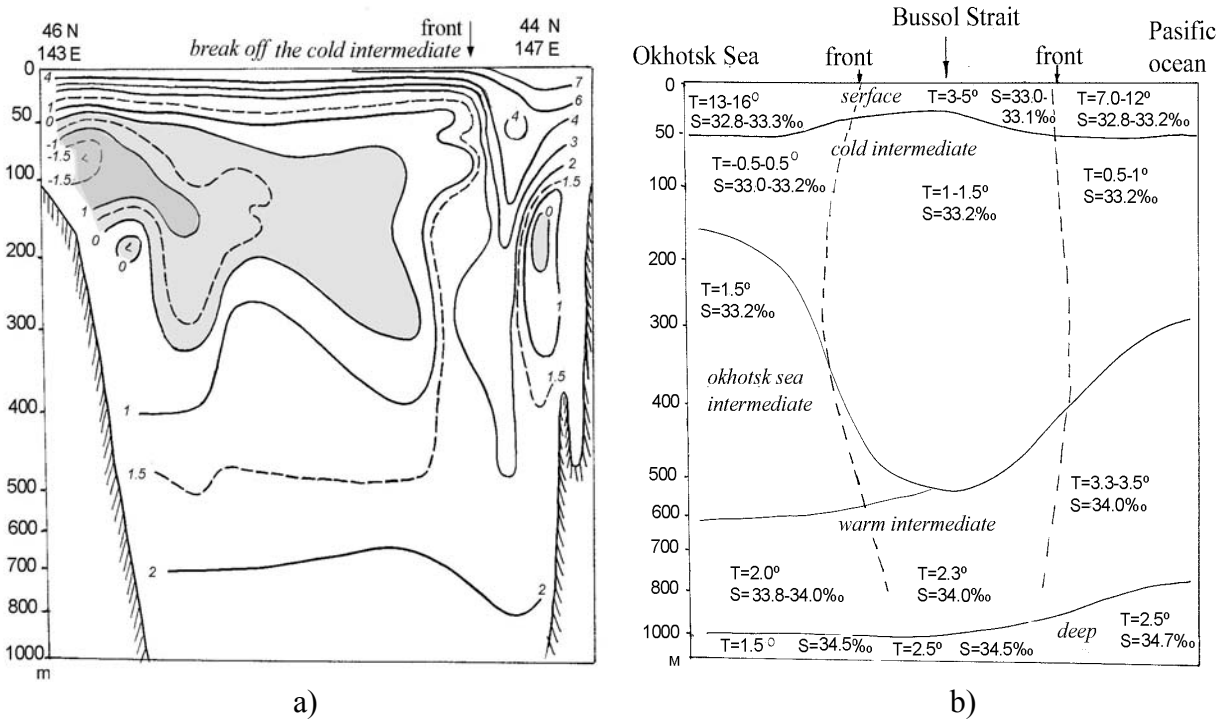

a) b)

Fig. 1 (a) The abrupt "end" of cold intermediate layer, and (b) thermohaline water structure scheme in Bussol Strait.

As well, alteration of the location of intermediate layers boundaries and extremes occurs in the thermohaline structure. In the eddies and also in the currents stream, that carry and preserve their own parameters, are homogeneous cores of minimal temperature in cold intermediate layer. Thirdly, the water structure in the area of the straits is being corrected by the changeability of the water that is exchanged in the straits. In every major Kuril strait, depending on the annual development of any link of current systems in the region, there is possibility of both a dominant outflow of Okhotsk Sea water, a dominant inflow the Pacific Ocean water or bidirectional water circulation. The thermohaline water structure scheme in Bussol Strait is shown in Figure 1b.

In the Pacific Ocean, the water of the Kuril Current (from the Bussol Strait - the Oyashio Current), that is being formed by very cold and relatively fresh waters of the east coast of the Kamchatka Peninsula and Pacific waters in the Kuril Straits zone, mixes with Okhotsk Sea transformed water. This water enters the North Pacific Ocean as a prototype of North Pacific Intermediate Water.

Experimental study of dynamic processes in Aniva Bay, Sea of Okhotsk during fall 2002

George Shevchenko and Valery Chastikov
Sakhalin Research Institute of Fisheries and Oceanography (SakhNIRO), 196 Komsomol'skaya Street, Yuzhno-Sakhalinsk, 693023 Russia. e-mail: shevchenko@sakhniro.ru

Introduction

Investigations of water dynamics in Aniva Bay, Sea of Okhotsk, located on the southern coast of Sakhalin Island have a wide interests ranging from sea urchin larval distribution, to fall storm influences on scallops, to the offshore structures liquefied natural gas (LNG) plant developed near Prigorodnoe. Detailed knowledge of water movements is necessary to understand the characteristics of extreme current speeds and directions in the area. On other hand, the residual current distributions in Aniva Bay help to understand how East Sakhalin Current filaments and West Sakhalin Current jets interact with the nearby La Perouse (Soya) Strait in this semi closed bay. The most intriguing moment was to clarify where and how the currents associated with the clockwise circulation at depth (up to 105 m) in Aniva Bay interact with the anticlockwise circulation around Aniva Bay in the nearshore. This has been unclear based on the references, but recent experimental results with drifters (Oshima et al. 2002) and the appearance of juveniles of subtropical species in the cold Sea of Okhotsk waters inside Aniva Bay and vicinity are providing clues.

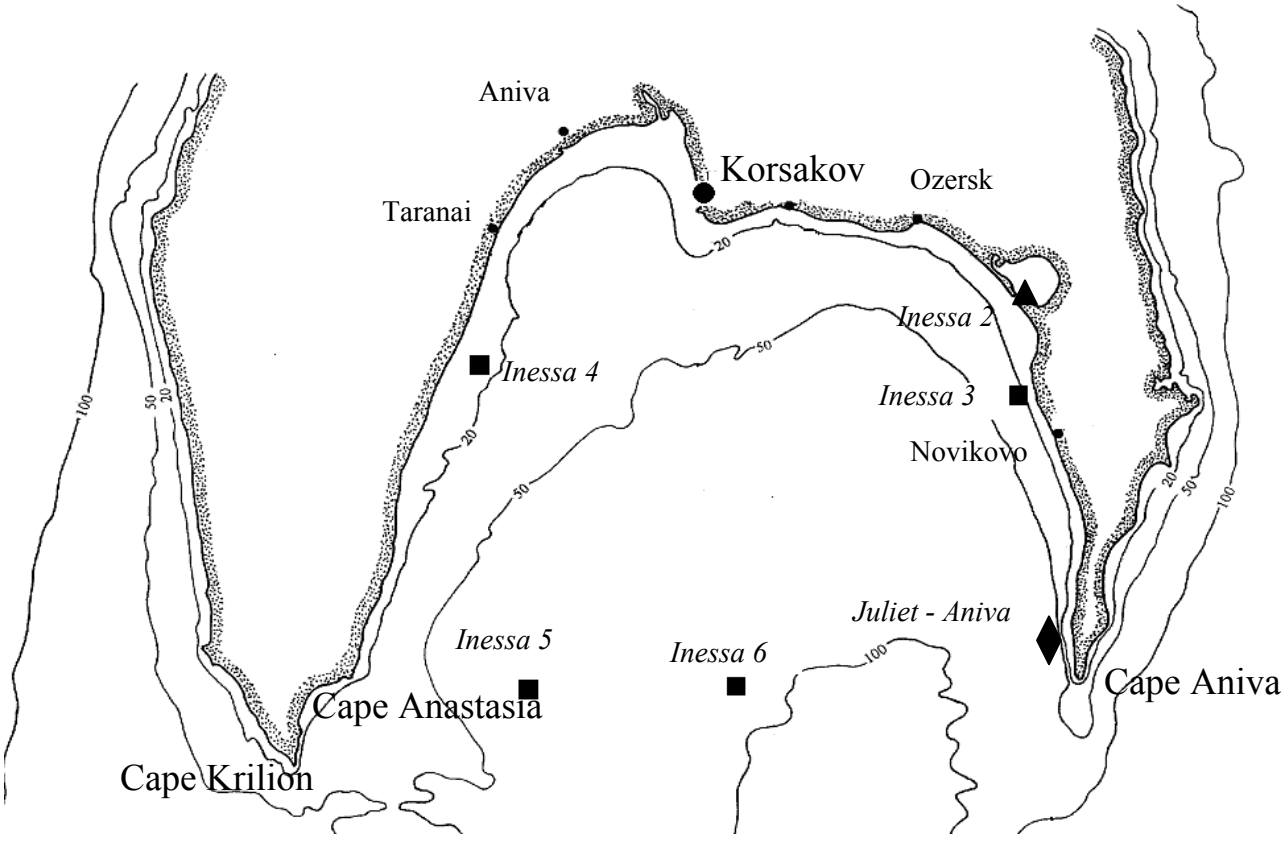

Fig. 1 Scheme of SakhNIRO instrumental measurements of currents in the Aniva Bay in fall season, 2002.

Table 1 Information about SakhNIRO mooring experiment in Aniva Bay in 2002-2003.

Station index	Period of measurement (DD,MM,YYYY)	Coordinates (N,E)	Depth (m)	Horizon (m)	Current meter
Inessa 2	07.09.2002-31.10.2002	46˚ 31' 142˚ 25'	8	4	SonTek Argonaut
Inessa 3	23.09.2002 – 06.11.2002	46˚ 31' 143˚ 18'	20	15	SonTek Argonaut
Inessa 4	21.09.2002 – 02.11.2002	46˚ 29' 142˚ 24'	20	15	SonTek Triton
Inessa 5	19.09.2002 – 02.11.2002	46˚ 01' 142˚ 30'	50	40	SonTek Argonaut
Juliet Aniva	09.11.2002-11.04.2003	46˚ 03' 142˚ 20'	80	profile	SonTek ADP 500 KHz

The knowledge of dynamics processes in Aniva Bay is limited by small quantities and short durations of direct current measurements. The view of currents inside Aniva Bay is based mainly on the results of different numerical models (Budaeva and Markarov 1996; Pishchalnik and Arkhipkin 1999). Thus, the need for direct current observations in Aniva Bay was required.

Data

SakhNIRO deployed 5 moorings (Table 1) in the fall of 2002. Two (Inessa 4, Inessa 3) were installed close to the coast, one inside Busse Lagoon (Inessa 2) and two (Inessa 5, Inessa 6) recorded currents at the open southern border of Aniva Bay (Fig. 1). Most moorings were retrieved in November 2002 (Table 1). In the southeastern part of Aniva Bay, an Acoustic Doppler Profilograf (ADP) was deployed on November 9, 2002. It worked for five winter months, mainly under ice floes. At all stations, water temperature was measured, coastal stations had also gauges of hydrostatic pressure (sea level). Inessa 4 had the ability to measure waves once every 2 hours.

Results and Discussion

The resulting data were analyzed with statistical and spectral analysis techniques. Amplitudes and phases of the main diurnal (Q1, O1, P1, K1) and semidiurnal (N2, M2, S2, K2) harmonics were calculated using a least square method. Tidal currents at all stations had approximately identical intensity. The amplitudes of the basic diurnal waves (K1 and O1) and the main semidiurnal constituent (M2) were about 3-4 cm s^{-1}. Tidal currents increased up to 10-15 cm s^{-1} at the station Inessa 4, located not far from La Perouse (Soya) Strait where tidal currents can reach 5-6 knots (Oshima et al. 2002; Shevchenko and Kantakov 2001). As a whole, the influence of tides on dynamic processes in the Aniva Bay is insignificant except in the southeastern part.

At coastal stations Inessa 3 and Inessa 4, an intensive residual current of variable direction, induced by the wind, was observed. The maximal velocities near the coast reached 30-40 cm s^{-1} when a deep cyclone (minimal value of atmosphere pressure was 983 millibars) crossed over Aniva Bay from October 1-3, 2002. At station Inessa 5, a flow of modified Japan Sea water penetrated Aniva Bay during the initial period of measurements. In the middle of October, the stream changed to the opposite direction.

At station Inessa 6 the quasi-periodic variations of currents were observed caused probably by influence of an anticyclonic ring that usually occurred in this area (Budaeva and Makarov, 1996; Pishchalnik and Arkhipkin 1999). In the first decade of October at ashore stations (Inessa 3,4) were observed intensive inertial currents which amplitude reached 20-25 cm s^{-1} (Fig. 2). The spectral analysis of current velocity obtained

at Inessa 6 and Inessa 5 moorings (Fig. 3) showed a strong well-expressed peak with period about 16.6 hours. This period is very close to the Coriolis period at the latitude of Aniva Bay (f = 12/sinφ = 12/sin46° = 16.68 h). A polarization of current rotation was also found; clockwise motion, that is typical to inertial currents, dominated. In contrast to inertial motions, diurnal currents have counterclockwise rotation in this area. A similar situation with strong clockwise-rotated inertial currents was observed in this area in October 2001 (Shevchenko et al. 2002).

The cause of intensive inertial currents in Aniva Bay is unclear; Aniva Bay seems too small for this type of wave. Probably, they are induced by strongly winds that were connected with deep cyclone from October 1-3. Another source of inertial motions can be the interaction between a low-frequency anticyclonic ring in Aniva Bay and the flow of the East Sakhalin Current.

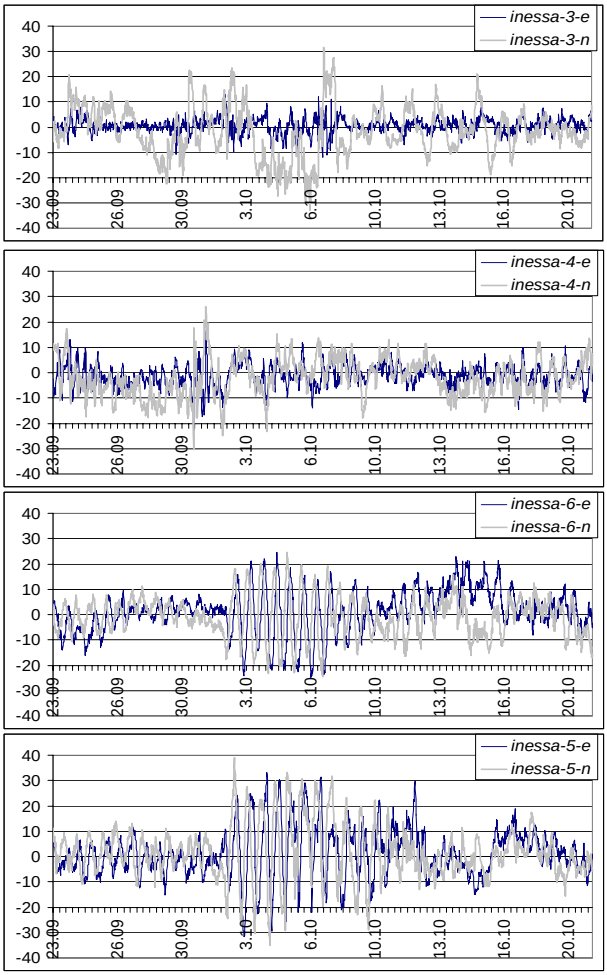

Fig. 2 East-directed (e, cm s^{-1}) and north-directed (n) components of residual current on different stations in Aniva Bay in fall of 2002.

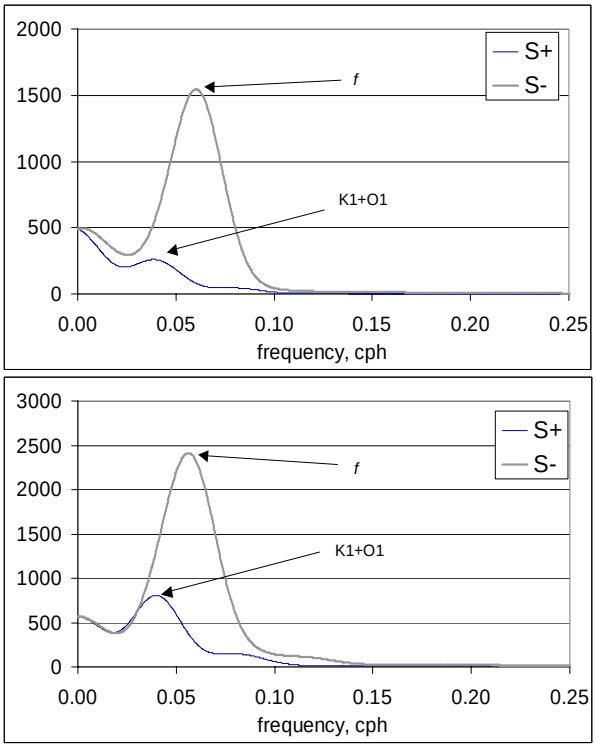

Fig. 3 Rotary spectra of current velocity obtained by Inessa 6 (upper picture) and Inessa 5 moorings. Number of degrees of freedom equals 38. Peaks corresponding to diurnal tides and Coriolis period are marked.

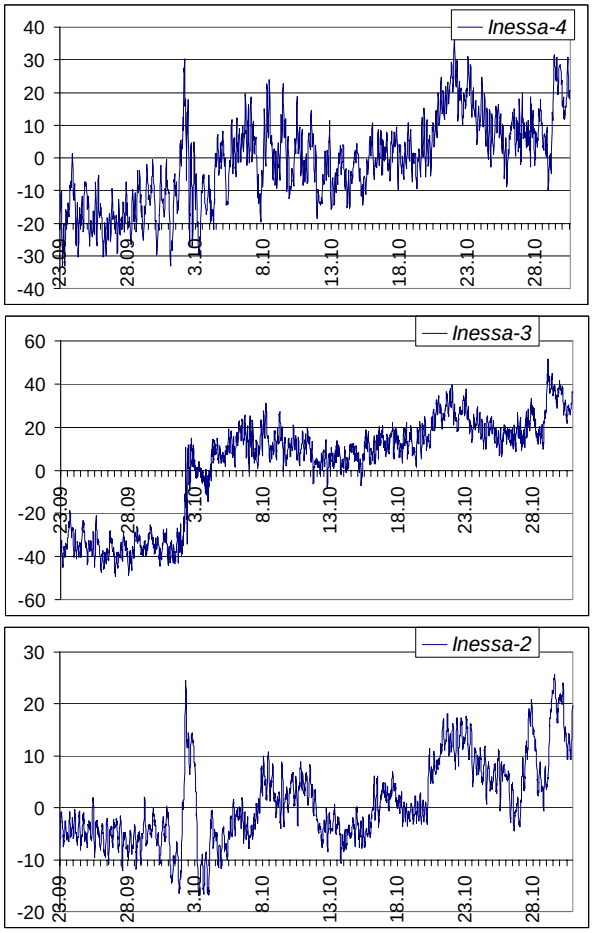

Fig. 4 Bottom hydrostatic pressure (sea level) series obtained in the coastal zone of Aniva Bay in falll season 2002.

Sea level (bottom hydrostatic pressure) changes are shown in Figure 4. There was a storm surge on October 2, mostly manifested in Busse Lagoon at the Inessa 2 mooring, probably influenced by rain. Sea level increased at all stations with the arrival of relatively warm and low salinity water of the East Sakhalin Current in the fall season. An interesting result of this was a sharp increase of sea level inside Busse Lagoon. It means that there is ventilation of lagoons (marine water inflow) of Sakhalin Island in a fall and winter seasons when Okhotsk Sea mean sea level is high (Poezzhalova and Shevchenko 1997).

Water temperature changes are shown in Figure 5. It is obvious that East Sakhalin Current waters reached the Inessa 6 mooring in the middle of

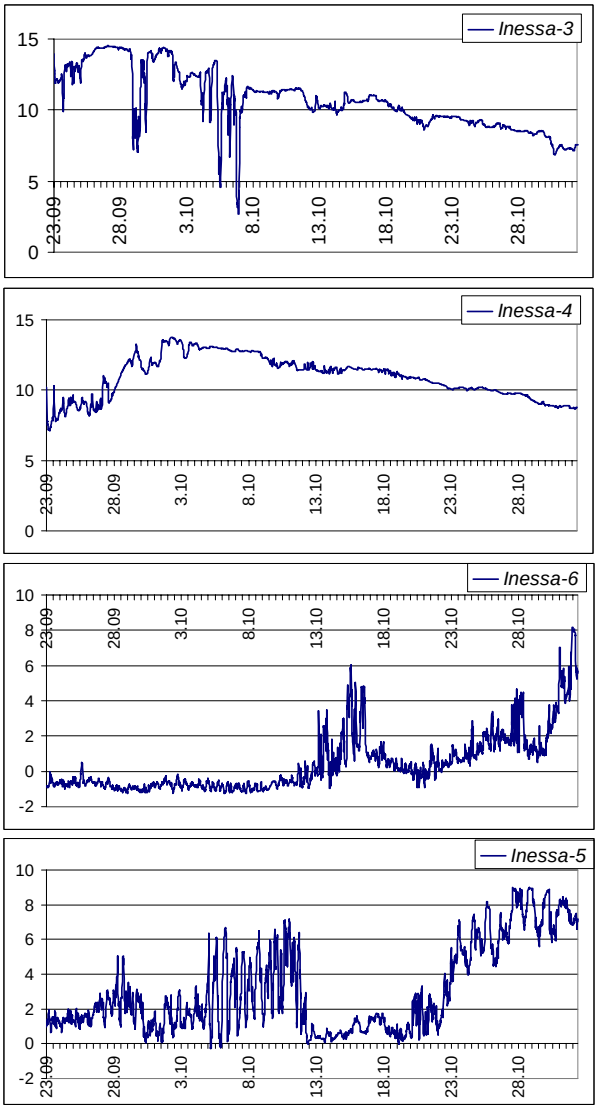

Fig. 5 Water temperature changes at different moorings in Aniva Bay in fall season 2002.

October, and the Inessa 5 mooring one week later. In that time, the cooling of water masses occurred in the coastal zone. A very interesting phenomena is the water temperature changes of 2-3°C at Inessa 5 mooring under influence of the inertial current. Almost no changes occurred during the same period at the Inessa 6 mooring. Perhaps, the cause of this difference is a boundary between cold and warm waters close to Inessa 5 mooring.

Near the southeastern coast of Aniva Bay during the autumn and winter periods an intensive stream directed aside of the deep sea (ADP mooring) was

observed. Probably, it was caused by the influence of a winter monsoon with prevailing northwesterly winds.

References

Budaeva, V.D. and Makarov, V.G. 1996. Modeling of the typical water circulation in the La Perouse Strait and Aniva Bay region. PICES Scientific Report 6: 17-20.

Odamaki M. 1994. Tides and tidal currents along the Okhotsk Coast of Hokkaido. Journal of the Oceanographic Society of Japan 50: 265-279.

Oshima, K.I., Wakatsuchi, M., Fukamachi, Y. and Mizuta, G. 2002. Near-surface circulation and tidal currents of the Okhotsk Sea observed with satellite-traced drifters. Journal of Geophysical Research 107.

Pishchalnik, V.M. and Arkhipkin, V.S. 1999. Seasonal variations of water circulation in the Okhotsk Sea area of Sakhalin Shelf. FERHRI Special Issue 2: 84-95. (in Russian).

Poezzhalova, O.S. and Shevchenko, G.V. 1997. The Okhotsk Sea mean level variations; tsunami and accompanying phenomena. IMGG RAS, Yuzhno-Sakhalinsk: 131-144 (in Russian).

Shevchenko, G.V. and Kantakov, G.A. 2001. Results of direct measurements of the currents in the La Perouse (Soya) Strait. The 16th International Symposium on Okhotsk Sea Ice, 4-8 February 2001, Mombetsu, Hokkaido, Japan: Abstracts: 323-333.

Shevchenko, G., Kantakov, G. and Chastikov, V. 2002. Measurements of currents and water parameters in Aniva Bay, Southern Sakhalin. PICES Eleventh Annual Meeting, Program & Abstracts (October 18-26, 2002, Qingdao, People's Republic of China). p.150.

Diapycnal entrainment of shelf waters into intermediate depths across the Sakhalin continental slope (Sea of Okhotsk)

Valery Sosnin[1], Pavel Tishchenko[1] and N. Biebow[2]

[1] V.I. Il'ichev Pacific Oceanological Institute, Far-Eastern Branch of Russian Academy of Sciences, 43 Baltiyskaya Street, Vladivostok, 690041 Russia. e-mail: pacific@online.marine.su (Sosnin, Tishchenko)

[2] GEOMAR Research Center for Marine Geosciences, Wischhofstrasse 1-3 Kiel, 24148 Germany e-mail: nbiebow@geomar.de

Introduction

Northern shelf of the Sea of Okhotsk is the main source area of dense water for formation of the Sea of Okhotsk Intermediate Water (OSIW). It is generally accepted that shelf waters ventilate sea interior. Oceanographic observations confirm the existence of wide area with low salinity and low temperature waters on the northern and north - western shelf and narrow belt of those east off Sakhalin with southward permanent currents along the continental slope (Itoh et al 2001; Mizuta et al 2001).

The density of shelf waters they have during wintertime varies from year to year but does not exceed 26.7-26.8 σ_t in general. The distribution of isopycnal surface of 26.8 σ_t in the Sea of Okhotsk indicate the average depth of 250-300 meters through out the sea and 350-400 meters near the Kurile Straits (Gladyshev et al 2000). The value of density of shelf waters is lower than that on intermediate depths and is not sufficient for ventilation of deep sea by the isopycnal transport. Numerous attempts to find water as dense as Kitani Water (27.02 σ_t) have failed.

We propose a new approach to the problem supporting the idea of diapycnal entrainment of shelf waters across the continental slope to ventilate deep layers with more high density.

Data

The CTD data have been obtained in five cruises during 1998-2000 within the framework of the joint German–Russian KOMEX project and the subproject "Methane monitoring in the Sea of Okhotsk". The observations were carried out in the same sections for all seasons, even in wintertime from drifting ice.

Results

The maximum density of water was found on the bottom layer on the NE shelf off Sakhalin in winter and spring does not exceed 26.84 σ_t. The most characteristic feature of the seasonal variability of oceanographic conditions along the continental slope is the seasonal manifestation of cold intrusions with negative temperatures. They appear in winter and spring directly on the bottom of the shelf and slope and on intermediate depths as well. The vertical scale of these intrusions is up to 400 m.

During winter, an extraordinary unstable hydrological situation is created in the vicinity of shelf break. It is found that the values of salinity and density of the waters on the shelf are higher than at corresponding depths offshore. On the other side, at the bottom of the slope the water density is lower than at corresponding depths offshore. These features of density and salinity distribution have thoroughly been tested and are neither artifacts nor defects in calculation (Fig. 1).

The situation on the shelf break becomes unstable and favorable for producing of gravitation flow on the sloping plane. Such phenomena are well known in geophysics and hydraulic (Turner 1973). Our data demonstrates that shelf waters with lower than Kitani Water density is sufficient to initiate the sinking of water down to the slope. CTD observations demonstrate that shelf water can sink down to depths where the density of the surrounding waters is higher than 27.1 σ_t. In other words, a diapycnal entrainment of shelf water into intermediate depths takes place across the continental slope.

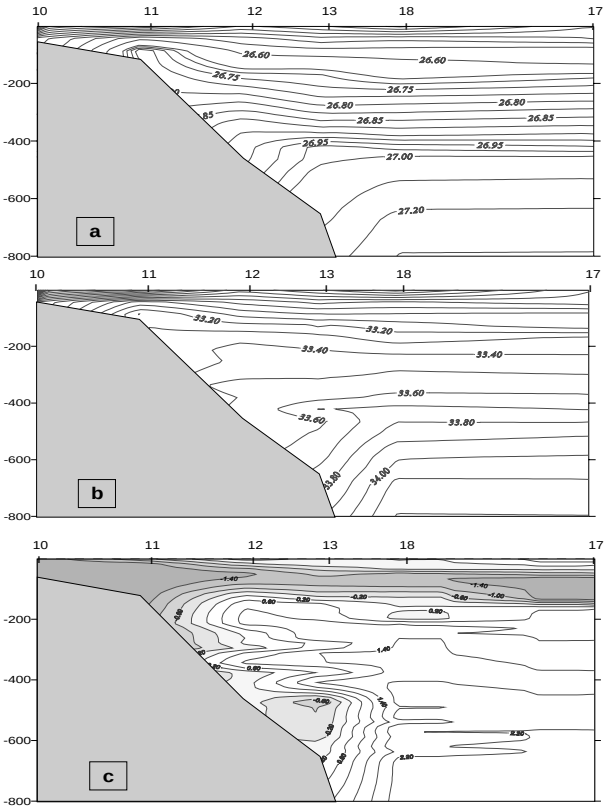

Fig. 1 Sections of density (a), salinity (b) and temperature (c) at 53˚N across the continental slope off Sakhalin in June 1999. Negative temperature values are shaded.

We consider the potential energy shelf waters have during cold periods is the main energy source for this process.

If shelf waters for some reasons (mean flow, tidal currents) start to move into the open sea, they would cause a static instability and start to penetrate the deep sea. The static stability of the offshore water column (for example, St.17) according to shelf water is calculated by the equation (Ivanov-Frantskevich 1956):

$$EH = 0.5 \cdot \frac{g}{\rho} \cdot \left[\frac{\partial \rho}{\partial \theta} \frac{\Delta \theta}{\Delta Z} + \frac{\partial \rho}{\partial S} \frac{\Delta S}{\Delta Z} \right] \qquad (1)$$

Results of calculation demonstrate negative values of EH down to 330 dB show that the potential density of the profile of St.17 at these depths is lower than 26.84 σ_t. This is the reason why the replacement of water parcels from deep layers by upper ones leads to a release of energy (Fig. 2).

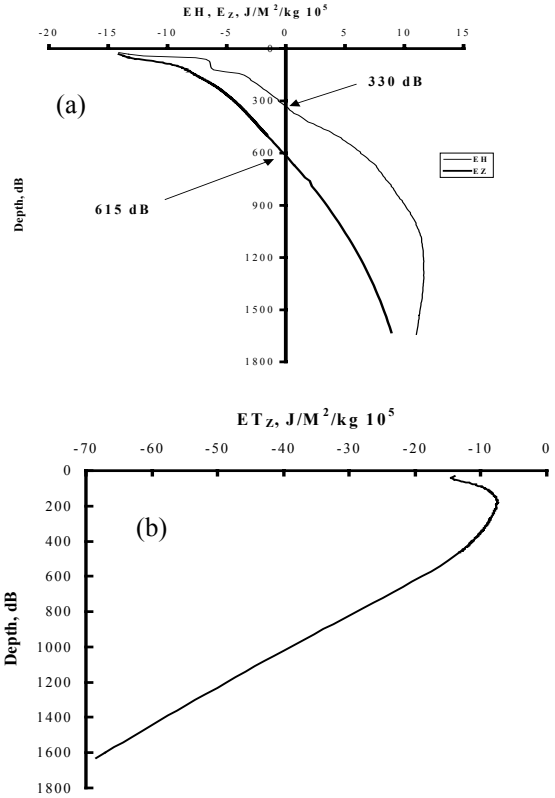

Fig. 2 Specific energy interaction of shelf water with water column with properties of st.17. (a) Static stability (EH) of shelf water relatively temperature and salinity values of st.17. Energy (Ez) release (negative values) under replacement of water on st.17 by shelf water. (b) Energy (Ez) release under replacement of water of st.17 by shelf water with following mixing with surrounding waters in proportion 1:1.

Without a doubt, the shelf water sinking down to 330 dB gets kinetic energy and moves further on its way, pushing upward the already more dense water. To determine the possible penetration depth of shelf waters we calculated the energy necessary for replacement of water column of St.17 by shelf water.

$$EZ = \frac{1}{n} \sum_{i=1}^{n} \frac{1}{z_i} \int_{z_i} EH \cdot dz \qquad (2)$$

Results of calculation demonstrate that shelf waters can penetrate down to 615 dB depth. So, the water column of earlier undisturbed water is filled by shelf water up to these depths.

We calculated the energy, which would be necessary if sinking shelf waters mix with surrounding waters in proportion 1:1. Results of calculations prove that the penetration of shelf waters across the continental slope and mixing with surrounding waters is energetically profitable for the whole water column. The cabbeling effect is considered to be the main reason for this. This effect is an additional source of energy and plays an important role in the diapycnal mixing of shelf waters with surrounding waters across the continental slope.

Conclusions

- CTD data demonstrate the seasonal manifestation of static instability of water column in the vicinity of shelf break. We consider the potential energy of shelf waters during cold period is the main source of energy for sinking of shelf waters across the slope. The process of ventilation of intermediate depths in the Sea of Okhotsk starts with the diapycnal entrainment of shelf waters and mixing with surrounding ones near the continental slope. Okhotsk shelf waters with densities 26.84 σ_t have enough potential energy for penetration up to 600 m depths. Vertical mixing is inevitable process for near slope region during cold season.
- It is supposed that the sinking of shelf waters across the continental slope is seasonally dependent and takes place most intensively at the northern edge of Sakhalin in the vicinity of 53°N – 55°N. Further south lateral advection and dissipation processes predominate.
- The penetration depth of shelf waters depends on its density during winter, as well as on the heating of the offshore waters during spring, i.e. on the density contrast between the shelf and offshore waters.
- The shelf–slope conveyor works until the summer heating eliminates the energetic difference between shelf and offshore waters.

Application of independent gauges of temperature of model “Pirate - 2000” for studying temperature conditions in a benthic layer in northern part of Sea of Okhotsk in 2002

V.B. Tjurnin
Magadan Scientific Research Institute of Fisheries and Oceanography, 36/10 Portovaia St., Magadan, 685500 Russia. e-mail: sofi@magadanniro.ru

The results of using temperature recorders on the benthic layers of the northern Sea of Okhotsk in 2002 are considered. Significant variability of water temperature with wrong diurnal and semidiurnal rhythms reveals isothermal areas (amplitude of fluctuations - 0˚C) are revealed. The most significant amplitudes of temperature fluctuations are recorded near hydrological fronts and in areas with active dynamics of water masses.

The spatial characteristic of variability of temperature conditions at the bottom can be observed in Figure 1. Analysis of the complex data on the spatial distribution of maximal amplitude of temperature fluctuations (the shaded areas in Fig. 1) and depth contours essential distinction of temperature conditions the given area is evidently traced. In the easternmost part within the coordinates (57º28’ - 57º35’N and 153º00’ - 153º10’E), at depths from 460–490 m, was a dynamical area in which the maximal amplitudes of fluctuations ranged from 0.4-0.5ºC. To the east were gradual reductions of daily pulsations of temperature and near 57º33’N - 152º00’E, an isothermal area (amplitude of fluctuations 0ºC) which is more close to a deep-water trench was discovered.

During a research cruise of the vessel *Nagorsk* in June – July, two areas with maximal amplitudes of temperature fluctuations (Fig. 2) were recorded. The first area occurs in the northeastern part of range (the intra-daily changes of temperature were 0.31ºC). The second area is in the southwestern part (maximal amplitude - 0.66ºC). In the second area, it is possible to explain the maximum daily pulsations of temperature as the influence of a hydrological front which usually starts to form at this time year. Therefore, in a zone where Iamskoi mixed water masses and CIL (a cold intermediate layer) appeared at the bottom, sharp daily changes of temperature were observed.

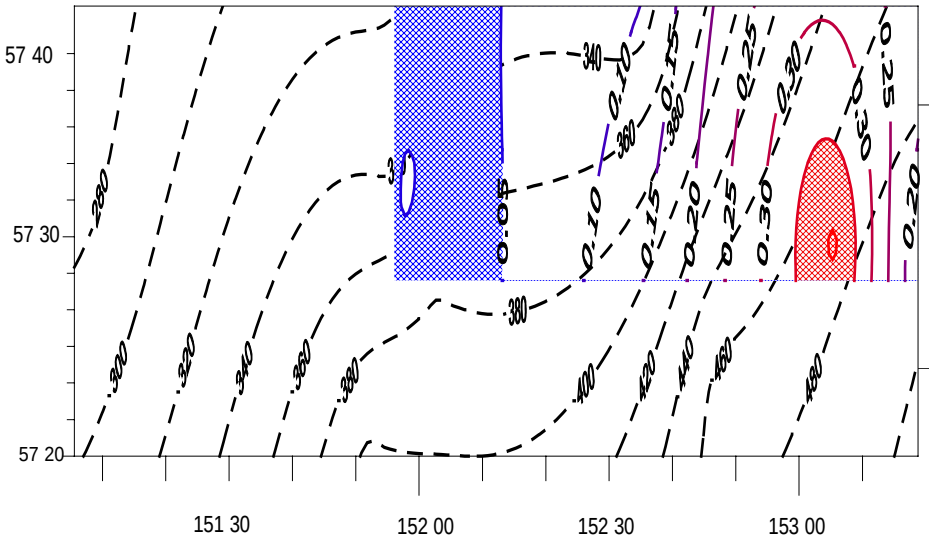

Fig. 1 The maximal amplitudes of fluctuations of temperature in October-November, 2002.

The lowest daily temperature fluctuations at the bottom were observed at two extensive isolated sites. The first is in coordinates 58º11' - 58º28'N and 151º37' - 151º47'E; the second is in coordinates 58º11' - 58º26'N and 152º12' - 152º37'E. It is interesting to note, that at a local site (58º26'N - 151º47'E) at a depth of 129 m, an isothermal area (amplitude of fluctuations 0ºC), similar to the data of supervision "Pivan" was observed. For the most part of the surveyed area, daily temperature fluctuations varied within limits of 0.1-0.2ºC.

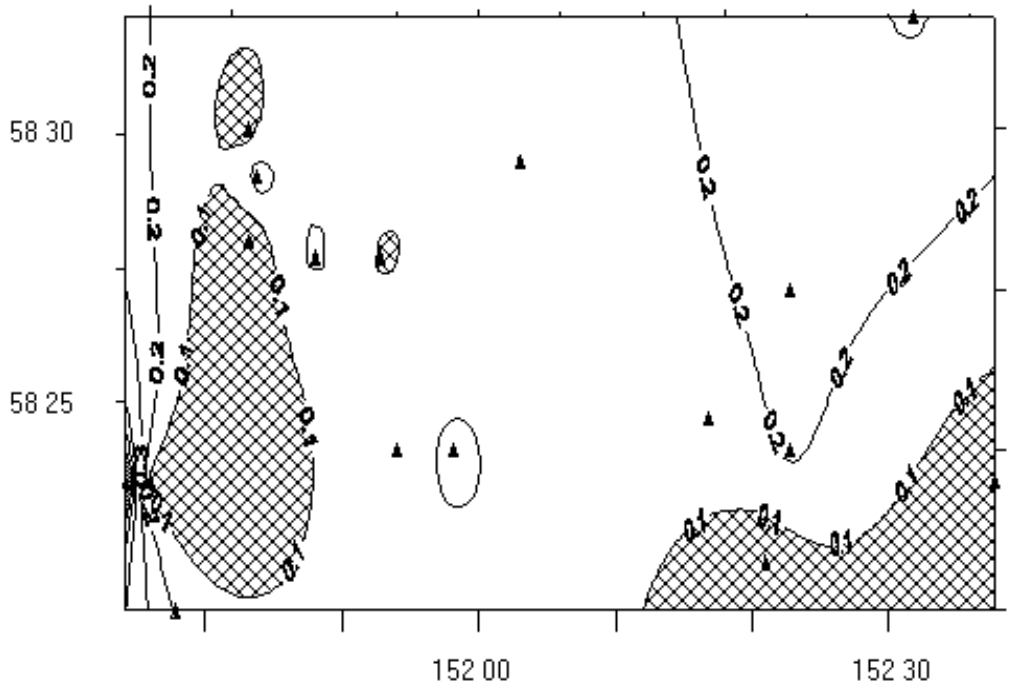

Fig. 2 The maximal amplitudes of fluctuations of temperature in June-July, 2002 from data obtained during the *R/V Nagorsk* cruise.

About the connection of ice processes of the Okhotsk and Bering Seas

Lubov N.Vasilevskaya[1], L.S. Muktepavel[2] and T.M. Tzhuravleva[3]

[1] Far Eastern State University, Institute of Environment, 27 Octyabrskaya Street, Vladivostok, 690950 Russia. e-mail: lubavass@yandex.ru

[2] Pacific Fisheries Research Centre (TINRO-Centre), 4 Shevchenko Alley, Vladivostok, 690950 Russia. e-mail: larisamk@tinro.ru

[3] Far Eastern Hydrometeorological Research Institute, 24 Fontannaya Street, Vladivostok, 690999 Russia. e-mail: tzhurav@hydromet.com

The purposes of this paper are to reveal long-term variations of Okhotsk and Bering Seas ice-cover during 1960-2000, to determine temporary bounds of the periods, and to determine when the ice developed in-phase our out of phase in the two seas, and to research macrosynoptical processes responsible for ice conditions over Far Eastern seas.

The present work is based on temporal series of monthly ice-cover of the Okhotsk Sea and Bering Sea from 1960-2000 and on the state of the midtroposphere thermobaric field, which was characterized by Girs (1974) to occur in one of three forms of atmospheric circulation (3, M1 or M2).

According to climatic atlas based on USSR data, the edge of Okhotsk Sea ice practically coincides with the orientation and location of the -10ºC atmospheric isotherm during December - February. In March and April this edge conforms to the –8° and -6ºC isotherms, respectively. The edge of Bering Sea ice coincides with the -8ºC isotherm in January, -6ºC during February - March, and -2ºC in April.

Vasilevskaya (2001) previously researched the nature of Okhotsk Sea ice-cover. During the period 1960 through 1978, a total of about 19 years, there was a time of abnormally excessive ice-cover in the Bering Sea. During this period, as in the Okhotsk Sea, there was a decade of metastable ice-cover (1966 through 1975). Over the years 1978 through 1997 (about 20 years) the ice-covered areas in the Bering Sea have never reached the average yearly figures.

It has been reported previously that the extents of ice-formation in the Okhotsk and Bering seas are negatively correlated (Yakunin 1966, and others). During years of severe ice-cover formation in the Okhotsk Sea, conditions in the Bering Sea were relatively mild. Nevertheless, a close examination of parallel integral curves of seasonal ice-cover anomalies (Fig. 1) shows that for some years of the specified period, this pattern is not evident.

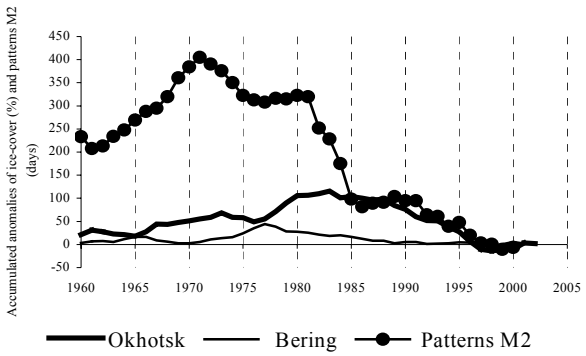

Fig. 1 The integral curves of seasonal ice-cover anomalies of the Okhotsk and Bering Seas (%) and Girs (1974) M2 circulation pattern.

The simultaneous link between the ice-covers of the two seas, over the entire ice season (excluding May), is reciprocal ($r < 0.$). There is a significant lagged (2 months) negative correlation between ice-cover in the Okhotsk Sea in February and in the Bering Sea in April. The milder the ice-cover conditions were in Okhotsk Sea in February, the more intensive they were in April in Bering Sea.

Lagged correlations between ice-cover formation processes in these seas, for the majority of the months examined over the entire period, are

generally negative. Out of 30 correlations, 9 are positive. During periods of generally out of phase ice-formation processes, the number of positive correlations is just 1 or 2. And during the periods of generally coincident patterns, the number of direct non-synchronous links increases significantly up to 17 in 1970-1975, and up to 21 in the most recent period of 1986-2000. The non-synchronous positive correlations are not significant. The temporal displacement of positive links is from 1 to 5 months. In the main, the ice-cover formation processes in the Bering Sea are determined by previous processes in the Okhotsk Sea.

The most widespread pattern of atmospheric circulation over the Pacific-American sector during the ice-season is meridional M2. It is the nature of anomalous behavior of this meridional condition that is responsible for the direction of ice-formation over the examined seas. Thus, when the M2 pattern repeats frequently, ice-formation processes are out of phase (Fig. 1).

On the other hand, when the integral curve of anomalies of this circulation pattern shows decline, the processes are simultaneously directed.

Thus, over the last 15 years there was noticable trend in ice-cover formation dynamics over the Far-eastern seas areas. Probably it could be some kind of indicator of common climate and circulation shifts over the Far-eastern region and North Pacific. The important role in the formation of ice-processes belongs to thermodynamic layer of the middle troposphere over the Pacific American sector.

References

Girs, A.A. 1974. Many-yearly variations of the atmospheric circulation and long-term trends in the change of hydrometeorological condition in the Bering Sea area. In: Oceanography of the Bering Sea, Proc. Int. Symp., Ch. 25. P. 475- 482.

Features of the water circulation in the northwestern Pacific under influence of the atmospheric baric systems

Galina A. Vlasova and S.S. Sugak
V.I.Il'ichev Pacific Oceanological Institute, Far Eastern Branch of Russian Academy of Sciences,
43 Baltiyskaya Street, Vladivostok, 690041 Russia. e-mail: gavlasova@mail.ru, sugak@poi.dvo.ru

Introduction

The northwestern Pacific is characterized by extremely complex hydrological conditions. First of all, there are powerful currents such as the Aleutian, Kuril-Kamchatka, Oyashio, Kuroshio, and North Pacific. As well, the formation of hydrological conditions in the NW Pacific is strongly affected by the transformed waters of the Bering Sea, Okhotsk Sea, Sea of Japan, and the East-China Sea that discharge waters to the Pacific Ocean via straits of the Aleutian and Kuril Island arcs, and also through Tsugaru Strait and Korean Strait. All these conditions make the region to be a powerful zone of the Pacific Ocean, and a unique natural base for investigating a complex of hydrophysical and meteorological processes, the understanding of which is necessary for the solution of many fundamental and applied problems in oceanography.

Initial data

In the present work, and on the basis of a hydrodynamic model (Polyakova and Vlasova 2002), it is possible to estimate the water circulation as integral functions of the flow from the surface to the bottom for the NW Pacific, taking into account the influence of various types of the atmospheric circulation: "North-western", "Okhotsk-Aleutian" and "Cyclones over the Ocean" (Polyakova 1999). The study area is confined to 20° – 50°N, 146°E– 180°. The given model allows us to consider the atmosphere influence, spatial distribution of water density, variable coefficients of the vertical and horizontal turbulent exchange, β-effect, bottom topography and the coastal outline.

The input information for the calculation of the waters circulation are:

- average monthly fields of the atmospheric pressure for the period of 1949-2000, corresponding to the earlier distinguished types of the atmospheric processes (Polyakova 1999);
- the GDEM archive (Generalized Digital Environmental Model) – global monthly averaged climatic data on temperature and salinity on a regular grid 10 x 10;
- the vertical spatial distribution of the water density.

The depth values were taken from the navigational chart (1:5 000 000). To conduct calculations, a regular grid with the space of 10 in latitude and 10 in longitude was used.

All input information was processed by optimal interpolation with the aim of distributing values onto the nodes of a regular calculated grid.

Analysis

The region is characterized by some quasi-stationary features that are independent of the type of atmospheric circulation and season. It is possible to distinguish three areas of strong anticyclonic activity and two of cyclonic activity (Fig. 1). For instance, in the areas bounded by 36-42°N and 145-154°E, 27-33°N and 157-163°E, 40-42°N and 176°E-180, powerful anticyclonic vortices are found. The first is located near the zone of the subarctic front (Bulgakova 1972). The second anticyclonic vortex corresponds to the passing subtropical counter-current; one of the branches of the Kuroshio. The presence of the third heat source is probably related to the influence of the warm North Pacific Current.

In the regions bounded by 33-36°N and 148-156°E, and also 22-27°N and 158-166°E, cyclonic vortices are observed. The first one coincides with the cold Oyashio. The origin of the second cyclonic vortex has not been yet ascertained, by it is probably due to the stationary cyclonic eddy occurring in this area (Muromtsev 1972).

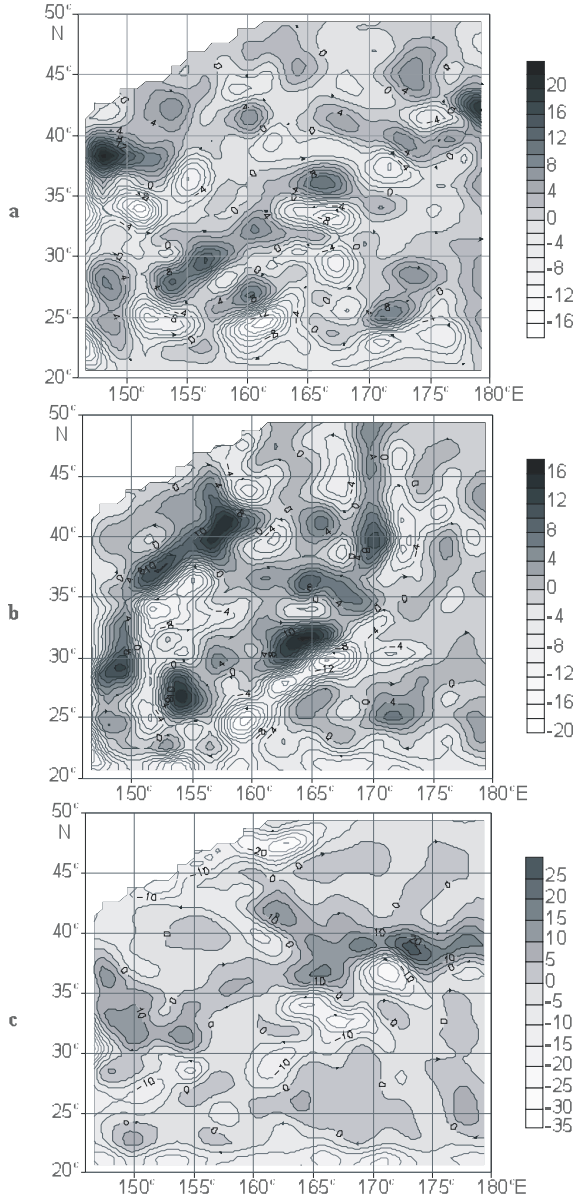

Fig. 1 Integral function of the stream (Sv) for: (a) northwestern type of atmospheric circulation in March, (b) Okhotsk-Aleutian type of circulation in March, and (c) "Cyclones over the Ocean" type of circulation in February.

The inequalities in bottom depth in this area should be also taken into account: along the whole Kuril Ridge, along the underwater rises and troughs where there is a sharp increase in depth. In front of any ridge, a sort of backwater is formed, which is either turning around the ridge, or is concentrated in the general water flow. For instance, the third anticyclonic vortex coincides with the location of the Emperor seamounts, and is partially copying its configuration, while stretching meridionally.

The first and the third anticyclonic vortices are located in the area of the subarctic front, and the second anticyclonic one and both two cyclonic ones are in the subtropical area. Nelepo et al. (1984) show that on the surface of the subarctic front, 83 cold anomalies and 72 warm anomalies can be found, and on average for the whole year, 7-8 anomalies of both signs are found. We should note the influence of seasons on these formations: in winter and autumn they are distinct, while in spring and summer they are somewhat diminished. The region is characterized by specific features with regard to the type of baric formations (Polyakova 2002).

For the "Northwestern" type of atmospheric circulation, the integral function of the flow from the surface to the bottom for all 12 months was calculated. As a whole, for the given type, the predominance of warm waters of anticyclonic origin is typical.

In winter, all hydrodynamic structures are distinctly. In spring, the current pattern starts to diminish: the subtropical counter-current starts to merge with the main branch of the Kuroshio, and an area of demonstrated anticyclonic activity in the area of the North Pacific Current stretches latitudinally, to 160°E, where the Kuroshio Current is passing into the North Pacific Current, and warmer waters start to prevail (Fig. 1a). This is most distinctly exhibited in summer. During this season, only individual cyclonic vortices are exhibited. In autumn, cold cyclonic eddies start to become more active and turn into vortices. As a whole, the autumn pattern of currents is identical to the winter pattern.

For the "Okhotsk-Aleutian" type of atmospheric circulation the function of the flow from the surface to the bottom for 8 months, excluding the winter period was calculated. As a whole, in comparison to the "Northwestern" type, the pattern of currents is retained, but with the predominance of a number of warm anticyclonic vortices (Fig. 1b), which stretch meridionally while corresponding to the geomorphology of the bottom. Probably, just at the given type of the

atmospheric circulation, the effect of bottom topography prevails. In spring, the first anticyclonic vortex is completely retained, owing to the stability of the heat source in this region. The second big anticyclonic eddy breaks up into individual small anticyclonic vortices, while preserving the positive sign of the water area, as a whole. The third one is the most poorly exhibited. Areas with the cyclonic vortices are retained. In summer, the cyclonic vortices are breaking up into individual small vortices, giving the place to the warm waters. And just in autumn, the current pattern is again restored over to the spring one.

For the "Cyclones over the Ocean" type, the function of flow from the surface to the bottom for the winter-autumn months was calculated. As a whole, preserving the general specifics of the current pattern, a dominant cyclonic vortex in the area of 46-50°N and 158-165°E is observed (Fig. 1c). Probably, this is related to the fact that in the area of the Kuril-Kamchatka Current, this type of atmospheric circulation activates the western subarctic gyre.

Conclusions

The influence of atmospheric processes on the hydrodynamic regime in the NW Pacific is shown. Quasi-stationary characteristics of the NW Pacific, regardless of the type of the atmospheric circulation and season, include three anticyclonic and two cyclonic vortices.

Specific features of the region are shown, with regard to the type of baric formations and their spatial-temporal variability: For the "North-western" type, the predominance of warm waters of anticyclonic origin are evident; for the "Okhotsk-Aleutian" type, the largest number of anticyclonic eddies of different scales, and also the apparent influence of the bottom topography are evident. For the "Cyclones over the Ocean", a cold cyclonic eddy in the area of the Kuril-Kamchatka Current appears.

References

Muromtsev, A.M. (ed.) 1972. Kuroshio and the adjacent areas of the Pacific Ocean. Trudy Gos.okeanogr.in-ta. 106, 210 p.

Nelepo, B.A., Bulgakov, N.P., Blatov, A.S., Ivanov, V.A., Kosarev, A.N. and Tuzhilkin, V.S. 1984. Classification and distribution of synoptic eddy formations in the World Ocean. Preprint BYa N 09556, Marine Hydrophysical Institute of the Ukrainian AS, Sebastopol, 40 p.

Polyakova, A.M. 1999. Calendar of atmospheric circulation types with regard to non-stationarity over the Northern Pacific, and their brief characteristics. Vladivostok, DVGU, 116 p.

Polyakova, A.M., Vlasova, G.A. and Vasiliev, A.S. 2002. The Atmosphere effect on the underlaying surface and hydrodynamic processes of the Bering Sea. Vladivostok. Dal'nauka. 203 p.

Bulgakova, N.P. (ed.) 1972. Subarctic front of the NW Pacific. Monograph, Vladivostok, 133 p.

Tidal fronts in the Okhotsk Sea

Igor Zhabin[1], N. Vanin[2] and Y. Zuenko[2]

[1] V.I. Il'ichev Pacific Oceanological Institute, Far-Eastern Branch of Russian Academy of Sciences, 43 Baltiyskaya Street, Vladivostok, 690041 Russia. e-mail: zhabin@poi.dvo.ru

[2] Pacific Fisheries Research Centre (TINRO-Centre), 4 Shevchenko Alley, Vladivostok, 690950 Russia.

The location of regions of strong tidal mixing and tidal fronts, which separated stratified waters and vertically well-mixed waters on the Okhotsk Sea continental shelf during the summer period are investigated on the basis of satellite infrared images, historical bottle and modern CTD measurements. The tidal fronts are located near Shantarskiy Island and Shelikov Bay. The oceanographic conditions over the Kashevarov Bank, Iona Bank and around Saint Iona Island are also determined by tidal mixing. Tidal fronts appear in June-July when the thermocline is formed, and disappear in the fall (September-October) when the stratification is destroyed. The positions of tidal fronts and intensity of the mixing are subjected to changes due to a variety of factors: strength of the tidal currents on the shallow shelves, water depth and river runoff. The regions of of intensive tidal mixing are areas of high biological productivity.

SESSION 3
BIOLOGICAL VARIABILITY: EVIDENCE AND CONSEQUENCES
(Convenor: Elena Dulepova)

Pinniped resources in the Okhotsk Sea

Alexey E. Kuzin, A. S. Perlov and E. P. Shvetsov
Pacific Fisheries Research Centre (TINRO-Centre), 4 Shevchenko Alley, Vladivostok, 690950 Russia. e-mail: smperlov@tinro.ru

In the Okhotsk Sea, there are four species of true, or else ice-form seals (Phocidae): ringed seal (*Pusa hispida*), ribbon seal (*Histriophoca fasciata*), bearded seal (*Erignatus barbatus*), larga (*Phoca largha*). In addition, there are two species of eared seals: northern fur seal (*Callorhinus ursinus*) and Steller sea lion (*Eumetopias jubatus*). The Kuril Islands are inhabited by the isle form of the common seal, also called antour (*Phoca vitulina stejnegeri*).

According to their spatial distributions during the main periods in their life cycle (reproduction, rearing pups, molting), and taking into consideration their gatherings during other life periods in the Okhotsk Sea, Fedoseyev (2000) distinguished three populations of ringed seals:

- East-Sakhalin, numbering up to 130,000 animals;
- Tatarsko-Shantarskaya, or Northeastern (485,000);
- Shelikhovskaya (110,000).

The ribbon seal has two populations in the Okhotsk Sea:

- East-Sakhalin (160,000);
- Northwestern (210,000).

The larga seal has three populations in this region:

- Terpeniya Gulf (55,000);
- Northern (215,000);
- Kuril (3,500).

Bearded seal forms two populations:

- East-Sakhalin (60,000);
- Northern (from Okhotsk to Shelikhov Bay) with 140,000 animals.

The Kuril population of isle seal makes up 2,000-2,500 individuals (Kuzin et al. 1974), but according to census data in 2000, it holds 3,000-3,500 animals (Kornev et al. 2001).

Of the two species of eared seals living in the Okhotsk Sea, the northern fur seal is the most numerous. Its breeding grounds, occupied during summer and autumn, are located at Tyuleniy (Robben) Island and in the middle Kurils. At present, there are more than 80,000 fur seals at the former and about 24,000-26,000 are born every year. The annual take amounts to 1,600-1,800 animals. In the Kuril Islands, the rookeries of this species are known to be at both Srednego Island, where, according to the data of total count in 1988, 7,100 adult fur seals lay and 8,100 were born, and in the Kamenniye Lovushki Islands, where about 9,100 adults and 5,700 pups live (Kuzin et al. 1988). In 2000 (a count was carried out before the reproductive cycle was over although there was no landing at the rookeries at Vysokaya and Chyornaya) 6,508 adults and 4,206 pups were counted on the Srednego Islands, and 6,742 adults and 2,755 pups on the Kamenniye Lovushki.

Steller sea lions in the Okhotsk Sea form several rookeries. There are bachelor haul-out sites and juvenile ones. The most numerous group of Steller sea lions inhabits the Kuril Islands. Here the animals form numerous harem rookeries (islands: Brat Chirpoyev, Srednego, Kamenniye Lovushki, Raykoke, Antsiferova), and juvenile and bachelor haul-out sites (Perlov 1970). The total count of sea lions inhabiting the Kurils made up a little more than 5,000, among them 1,900 pups (Burkanov et al. 2002). A rather numerous

reproductive group of Steller sea lions is situated on the Iony Islands, where 952 pups were born in 2001, and the number of adult individuals exceeded 1,500 (Zadalskiy 2002). At Tyuleniy (Robben) Isl. in 2002, according to our counting data, the number of adult Steller sea lions was close to 1,500, with more than 400 pups. In the Iamskiy Islands in 2001, the number of newborn totaled 360, and the number of adults counted exceeded 900 animals. On the Lisyanskiy Peninsula there lay a little more than 200 adults and two dozens of newborn in 2000. There is one not large bachelor haul-out here too. On Zavyalova Island, there was a juvenile haul-out site with a total of about 100-130 individuals (Zadalskiy 2002). One bachelor haul-out with unsteady numbers (200-500 animals) is located at Opasnostiy Rock (LaPerouse Strait) and another is at Sivuchiy Cape (Western Kamchatka), where the number of animals ranges from a few dozen to 2,500 in winter and in March depending on the season (Burkanov 1988).

On the whole, the numbers of fin-footed seals in the Okhotsk Sea, together with those from the Kurils, make up 1.8 million animals; 90% are true seals (ringed seal, ribbon seal, bearded seal, larga, isle seal/antour) and the rest (10%) are eared seals (northern fur seal and Steller sea lion). Among the former, ringed seal and ribbon seal are the most numerous, amounting to 40% and 20%, respectively, of all seal bioresources in the region. Bearded seals and larga have equal indexes (each 12%).

All the true seals were commercially harvested species in the past. Before 1968, sealing was not regulated (annual catch of 66,000-102,000 animals), that naturally resulted in harsh population decline. Later on, due to some reduction in total sealing (down to 38,000-47,500) and strict limiting of its rates, the stocks were restored. In the following years, sealing was carried on in keeping with scientifically-based recommendations. Since the middle 1980s, the quota has been raised to 72,000-89,000 animals per year, and catches reached 95% of this in the Okhotsk Sea and 70-80% in the Bering Sea (Perlov 2000). However, sealing from ships in Far Eastern seas has been discontinued completely since 1995 as the specialized ships became out of date and too depreciated, and because of well-known changes caused by the politics of the country.

Along with ship sealing, there was land sealing in which coastal kolkhozes and sovkhozes participated. Their share of the sealing quotas was up to 20%, but the realized catch was not more than 60% of this.

Today, ship sealing in Far Eastern seas is not being carried on, though the annually approved sealing forecast for Okhotsk Sea of makes up nearly 60,000 animals. Coast brigades take not more than 30% of 24,800 seals yearly apportioned for hunting.

Taking into consideration the stability of seal abundance in the Okhotsk Sea during the 1990s, and a prolonged absence of sealing, and a positive response to the reduction of hunting, with subsequent numbers increasing, we may suggest the seal stock in the Okhotsk Sea is in a safe state at present. However, when considering sealing for true seals in the future, we should keep in mind that it must not be as large-scale as in the past.

The number of fur seals at Tyuleniy (Robben) Island has been increasing steadily since 1993, and on the Kurils it has apparently remained at the reached level since 1988. The number of Steller sea lions on the Kuril Islands has been in steady state after the depression of 1970-90s, but on the rookeries of other parts of the Sea of Okhotsk, it is increasing each year. The number of true seals in the Kurils has increased a little for late years.

References

(All in Russian)

Burkanov V.N. 1988. Current status of marine mammals in Kamchatka. Sustainable use of bioresources of the Kamchatka Shelf, Petropavlovsk-Kamchatskii, pp. 138-178.

Burkanov V.N. et al. 2002. Cursory results of the survey of rookeries of Steller's sea lions in the Russian Far East in 2001. Marine mammals of the Holarctic. Proceedings of the international conference, Moscow, pp. 56-57.

Perlov. A.S. 1970. Distribution and numbers of Steller's sea lions on the rookeries of the Kuril Islands. TINRO Izv. 70, pp. 96-202.

Perlov. A.S. 2000. The possibility of the renewal of vessel-based sealing in the Far East (economic and biological aspects). Marine mammals of the Holarctic. Proceedings of the international conference, Archangelsk, pp. 309-313

Kuzin A.E., Maminov, M.K., Tikhomirov E.A. 1974. Distribution and numbers of true seals on Kuril Islands. TINRO Izv.92: 158-167.

Kuzin et al. 1988. Interannual dynamics of atmospheric processes as a factor of survival of northern fur seals. Sustainable use of natural resources of the Ocean. The 2nd Pacific Marine Science Symposium. 11-19 August 1988. Vladivostok: FEB AS USSR, pp. 120-121.

Zadal'skii S.B. 2002. The population status and migrations of the Steller's seal lion in the northern part of Okhotsk Sea. Marine mammals of the Holarctic. Proceedings of the international conference, Moscow, pp. 109-110.

Seasonal and annual dynamics of nektonic community in the western Kamchatka region

Alexei Yu. Merzlyakov
Pacific Fisheries Research Centre (TINRO-Centre), 4 Shevchenko Alley, Vladivostok, 690050 Russia. e-mail: interdept@tinro.ru

Western Kamchatka and Shelikhov Bay are among the most highly productive areas within the Okhotsk Sea where high biomasses of bottom and pelagic fish species are found. For a long period of time, the fish communities of these regions experienced permanent pressure from the fishery, which had a considerable impact on the dynamics of species abundance.

TINRO-Centre has conducted annual expeditions to the Okhotsk Sea during spring and autumn/winter for several years. The basic objective of these expeditions was to collect diversified information on the condition of biological resources in the pelagic zone. Collection of baseline data was made under a unified approach, accepted in TINRO-Centre. Research and survey schemes occurred at the same time every year. Baseline data, collected in 1998-2002, provided information on yearly and seasonal dynamics in nektonic abundance.

During the period of research, considerable quantitative changes were observed in the nektonic communities in the western Kamchatka region. A sharp drop in total biomass from 5.1 down to 2.5 million metric tonnes (mmt) in spring, and from 3.5 to 1.8 mmt in autumn was observed in 1999 compared to 1998. In the following year, total biomass increased to 3.6 mmt in spring and continued to grow to 4.35 mmt in 2001, with a subsequent decline to 3.99 mmt in 2002. Biomass dynamics were slightly different in the autumn-winter period. After a sharp drop in 1999, the biomass continued to decline, though with less intensity down to 1.66 mmt in 2000. In the ensuing two years, there was a smooth, continuous growth of biomass, up to 2.2 mmt in 2002.

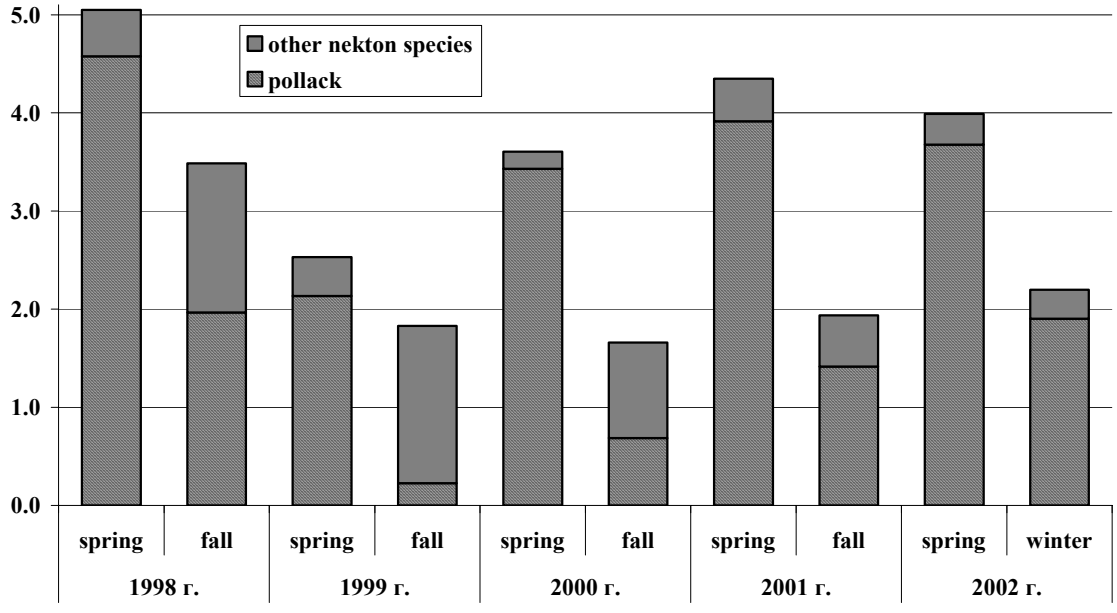

Fig. 1 Dynamics of nekton biomass (million tonnes) and the walleye pollock fraction (% of biomass) in community composition in the West Kamchtaka region and Shelikhov Bay in 1998 – 2002.

The total assessed biomass of the nektonic community fluctuated both annually and seasonally. Spring estimates during 1998-1999 were 1.4 times higher than autumn estimates. In the succeeding two years, this ratio increased up to 2.2, and was 1.8 in 2002. The reasons for such drastic changes in biomass are associated with the structural features of high latitude nektonic communities in general, and of the northern Okhotsk Sea in particular. Only two to three species provide the basis for the observed biomass estimates in the area.

The most abundant species were: walleye pollock (*Theragra chalcogramma*), capelin (*Mallotus villosus*), Pacific herring (*Clupea pallasi*), and northern smoothtongue (*Leuroglossus schmidti*). Along with these species, considerable amounts of Sakhalin flounder (*Limanda sakhalinensis*) have been also found in the region. The share of these five species exceeded 89.9% in the total assessed biomass of nekton during the whole period of research. At the same time, the share of each of these species in the total community biomass varied from year to year.

Walleye pollock biomass varied considerably during the time of research (Fig. 1). Nevertheless, almost without exception, it was the key species within the nektonic community. Pollock was much more abundant in spring, comprising 84.3-92.5% of the total biomass, than in autumn when its share ranged from 12.4-86.5%. During the last two years, the extent of pollock dominance in nektonic community has noticeably increased. The observed seasonal variability in pollock biomass fits within the known scheme of the functional structure of the species range in the eastern Okhotsk Sea. During the period of spawning from March to May, almost all mature pollock are concentrated in the area of the outer shelf and slope. After spawning, most large individuals, that make up the bulk of the species biomass, scatter over vast areas in the epi- and mesopelagic layers. The growth of the pollock share in autumn during recent was evidently due to the fact that individuals larger than 40 cm stayed in the shelf-slope region all year round. That is why, taking into consideration seasonal distribution patterns, spring surveys provide the most reliable estimates of the species biomass.

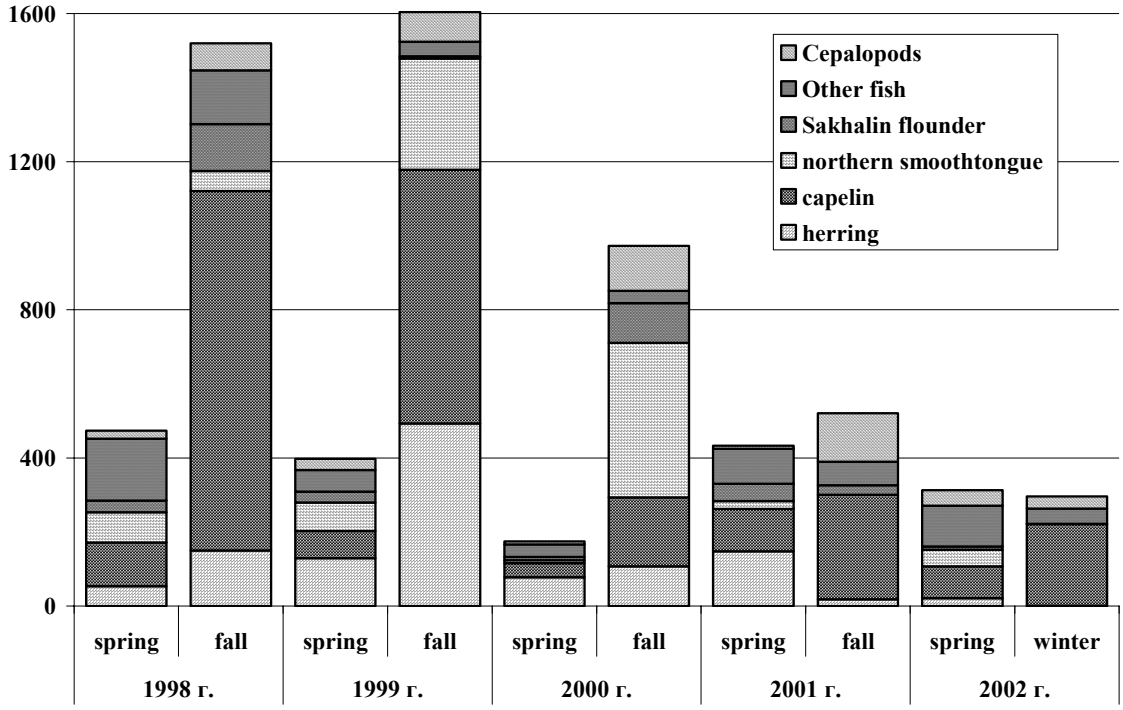

Fig. 2 Dynamics of biomass (thousand tonnes) of species other than pollock in the nekton community in the West Kamchtaka region and Shelikhov Bay in 1998 – 2002.

As for the annual dynamics of pollock biomass, it ded sharply in 1999 and began to recover in 2000. Pollock removals by the fishery could have caused the decline in the species abundance. From 1997, when fishing pressure on the depressed pollock stock increased, until 1999, the exploitation rate was the highest in the last 20 years; much higher than the maximum allowable catch, with as much as 68% withdrawal from the stock in 1998. The increase of stock biomass in 2000 and its further stability were partly due to the average weight gain of fish, and to the immigration of individuals from adjacent areas.

As for the other components of the nektonic community, their seasonal pattern of total biomass variability was opposite to that observed in pollock (Fig. 2). Biomass estimates for those species were higher in autumn than in spring, except for the last two years. Changing distribution might have accounted for such variability in the biomass assessments. In spring, most capelin and herring migrate to coastal spawning areas that are not covered by the surveys. These two species had high biomass (1.5-1.6 mmt) in 1998 and 1999. Sakhalin founder added considerably to the non-pollock nektonic biomass in 1998, as did northern smoothtongue in 1999. Stock abundance of most of these species ded significantly during the next three years, except for northern smoothtongue that had its highest biomass in the autumn of 2000. Dynamics of abundance as well as migration and distribution patterns served as basic reasons for the observed biomass decline. The former cause is characteristic for short-lived species such as capelin, whose distributional range is restricted to the shelf zone. The decline in herring abundance is related to its distribution pattern. Both factors could have influenced observed biomass changes of northern smoothtongue and Sakhalin flounder. Other taxa within the nektonic community are cephalopods, for which the total assessed biomass increased from 73.3 up to 131.2 thousand t by 2001, judging from autumn surveys. In 2002 however, cephalopods abundance ded down to its minimum estimate of 32.4 thousand t.

Interannual variation of Pacific herring stocks in the Okhotsk Sea in connection with last year's cooling

Igor V. Melnikov and S.V. Loboda
Pacific Research Fisheries Centre (TINRO-Centre), 4 Shevchenko Alley, Vladivostok, 690950 Russia.
e-mail: melnikov@tinro.ru; waltz@mail.primorye.ru

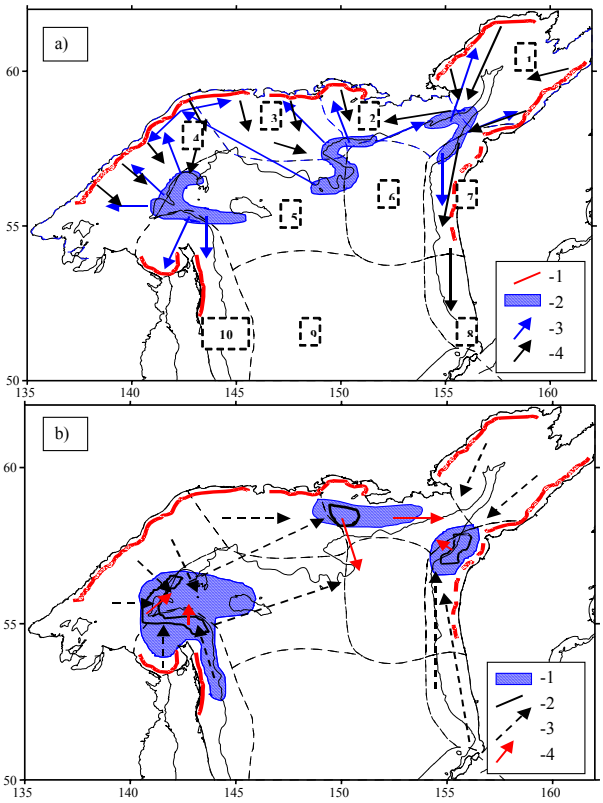

Fig. 1 Consensus scheme of distribution and migrations of mature herring in spring (a) and autumn (b). (a) – spawning part of the range; 2 – wintering regions; 3 – spawning migrations; 4 – feeding migrations; punctuated is boundaries and numbers of standard areas of averaging of the biostatistical information; (b) 1 – regions where autumn aggregations are formed; 2 – boundaries between pre-wintering aggregations; 3 – autumn migrations; 4 – wintering migrations.

Two large populations of Pacific herring are known to exist in the northern Okhotsk Sea: Okhotsk and Gizhiginsk-Kamchatsk (Naumenko 2000). Lately, considerable fluctuations in abundance were observed in these populations, which led to changes in migration timing and routes, as well as in location of feeding and wintering areas (Melnikov and Vorobyov 2001; Melnikov 2002; Radchenko and Melnikov 2001). This seriously affects the fishery for herring during the autumn period. In order to analyze the distribution, migration and stock abundance of herring, we used data from large-scale trawl surveys, conducted by TINRO-Centre in September-October 2001 and November-December 2002. All data on herring were analyzed using standard techniques accepted in TINRO-Centre and published in a number of papers (Radchenko and Melnikov 2001; Melnikov 2002).

In 2001 and 2002 only 68-71% of the recommended quotas for the Okhotsk herring were taken in the fishery. In our opinion, this was largely due to the influence of the cold winter of 2000-2001, and to the existence of intra-population groupings (two in Okhotsk herring and two in Gizhiginsk-Kamchatsk herring), that are thought to have different patterns of dynamics in their abundance.

In September-October 2001, the distribution of herring was very similar to that in July - August 1997, when the main aggregations of herring were observed in the northwestern Okhotsk Sea with features characteristic of feeding aggregations. The shift in time of pre-wintering aggregations by almost a month in autumn 2001 was related to the late approach of herring to most spawning sites in the spring of 2001 due to the cold winter 2000-2001. As a result, the shorter feeding period did not allow mature fish to accumulate enough fat for overwintering by September 2001, and they continued to feed until October-November (this was not observed in immature fish). Slow maturation rates in the 1996 and 1997 cohorts, together with increased natural mortality of older fishes were also observed.

The analysis of data on Pacific herring collected during wide scale trawl surveys in recent years has allowed us to make some suggestions about the herring stock structure. Four relatively isolated groups were observed (two in the Okhotsk and two in Gizhiginsk-Kamchatka herring), that differ in locality during feeding and wintering (Fig. 1), in periods and directions of migrations, growth rates and other features. In the Okhotsk population, the large extent of the spawning area might account for its subdivision into groups, while in Gizhiginsk-Kamchatka herring, it may be due to differences in oceanographic conditions between the Gizhiginsk Bay and northwestern Kamchatka. We shall briefly consider these groupings. First of all, it is necessary to notice that they are apparently not independent populations, for their appearance and numbers depends on a pattern of filling of spawning grounds in various parts of the spawning area. As for the Okhotsk herring, the western group is highly abundant when ice conditions in spring allows spawning fish to get to the central and western parts of the spawning grounds. Later on, this group acquires certain independence and becomes relatively stable. It means that during their lifetime, most fish feed and overwinter separately from individuals of the eastern group, mixing with them only during spawning period.

Western group of the Okhotsk herring

Its spawning grounds are located in the western part of the spawning region (southwest of 58°N). After spawning, yearlings and mature herring migrate in a southeast direction, and actively feed on the shelf in 4, 5 and 10 areas. Fish of age 3 and older start to form pre-wintering aggregations in August above northwestern Deryugin Trench. At low abundance, all of them overwinter in this area, moving to depths over 200 m. At high numbers, some schools migrate into the Taui area (2) at the end of August, while some migrate in October - November right to the wintering area south of the Kashevarov Bank. Mostly old (8 years and older) and immature fish remain in the pre-wintering area. The share of fish migrating to the other areas is smaller during periods of low abundance. Mature herring of this group, especially at high abundance, can spawn beyond its usual spawning sites in case they are closed by ice fields. Under favorable conditions, they occupy the natal spawning regions. Individuals of the western group differ by having a lower growth rate, later maturation and later spawning migrations. At low abundance, this group is not harvested by the fishery its aggregations are located under the ice during winter and therefore, can be taken only occasionally during fishery for pollock at the Kashevarov Bank. At high abundance, this group partly migrates to the Taui area in autumn, where it is taken commercially together with fish from the eastern group.

Eastern group of the Okhotsk herring

The eastern group has been studied best of all. Its spawning grounds are located in the central and eastern parts of the range (from the Okhotsk area up to Taui Bay). Post-spawning fish and yearlings feed on the shelf in areas 2 and 3, and in the northern part of area 4. Pre-wintering aggregations of this herring are found in the Taui area (2), the traditional area of the fishery. It moves southward and descends to 200 m and deeper to over-winter. The spawning migration is usually observed on the shelf off Okhotsk as the fish move to their spawning grounds, as they become ice-free. It is this group of herring that suffers most from the fishery both in spring and in autumn-winter periods.

Gizhiginsk group of the Gizhiginsk-Kamchatka herring

The spawning grounds are located in Gizhiginsk Bay along the northern coast of Shelikhov Gulf. Post-spawning fish and juveniles over 2 years old move away from the gulf area to feed in the central and eastern Taui area. Pre-wintering and overwintering aggregations are distributed together with the Okhotsk herring of the eastern group above the northern continental slope of the TINRO Trench. It is taken in the Taui area together with the Okhotsk herring.

Kamchatka group of the Gizhiginsk-Kamchatka herring

This group is almost uninvestigated. It spawns from Penzhin Bay up to Ust-Chairusovo (possibly further south) in weakly populated areas. Young fish feed in southeastern Shelikhov Gulf and off the western Kamchatka coast. Fish aged 3 and older occur on the shelf of western Kamchatka down to the southernmost part of this area, and are

frequently distributed to near the bottom. Pre-wintering and overwintering aggregations are formed offshore bounded latitudinally by the Southern Cape in north, and Chairusov Cape in the south (57°10'-57°50'N). It spends autumn at depths of 120-170 m, and overwinters at 220-270 m. It is less abundant than the Gizhiginsk group and is practically not harvested by commercial fishery in recent years.

It is easy to notice that all three areas of feeding and overwintering of herring in the northern Okhotsk Sea are highly productive areas connected with periphery of strong upwelling.

The trawl survey carried out in autumn 2001 (September - October) completely confirmed earlier results. The main aggregations of herring were observed in the northwestern part of the sea in September - October. The biomass of the herring stock was estimated at approximately 1.8 mmt. The pre-wintering aggregation in the Taui area was almost totally absent (approximately 50 thousand t of fish were counted here, with only 10 thousand t within the aggregation) and schools migrating into this area were observed very seldom. There was also no pre-wintering aggregation of the Gizhiginsk-Kamchatka herring that usually forms from the end of September till the beginning of October along the northwestern Kamchatka coast. On the whole, patterns of herring distribution and behavior had a marked "feeding" character, and were approximately the same as in the middle of July/August 1997. However, the analysis of distribution by age groups showed that the location of "summer" type aggregations was characteristic only for the mature fish. Immature individuals had already moved away from the coastal zone and were widely distributed on the shelf, as is usual in autumn.

In October, the autumn cooling apparently prevented usual migrations of fish from Kashevarov Bank to the Taui area along the shelf. That is why a number of herring schools migrated into the wintering area via a non-conventional way – to the east south of the Kashevarov Bank, passing by the area where pre-wintering aggregations are usually formed. This led to certain complications for the commercial fishery and as a result, only 78% of the Okhotsk herring quotas were taken.

Interesting results were obtained in November - December 2002. Herring distribution and behavior had characteristic pre-wintering and over-wintering features (Fig. 2). Both mature herring and some immature individuals aggregated near Iona Island and on the central northern Okhotsk Sea shelf. Its biomass was estimated at 424 thousand t for the Iona aggregations alone, while in the main fishing area it was estimated at 563 thousand t. South of Taui Bay migrating schools, mainly immature fish, were rare. There was no pre-wintering aggregation of the Gizhiginsk-Kamchatka herring, which usually forms from the end of September to the beginning of October off the northwestern Kamchatka coast. In the western part of the sea, local aggregations of large herring, identified by a number of features as the Gizhiginsk-Kamchatka population, was registered. As a result of research conducted in 2002, it was shown that herring from the two populations overlaps in their distributions, both during feeding and over-wintering. The existence of pre-wintering and over-wintering aggregations

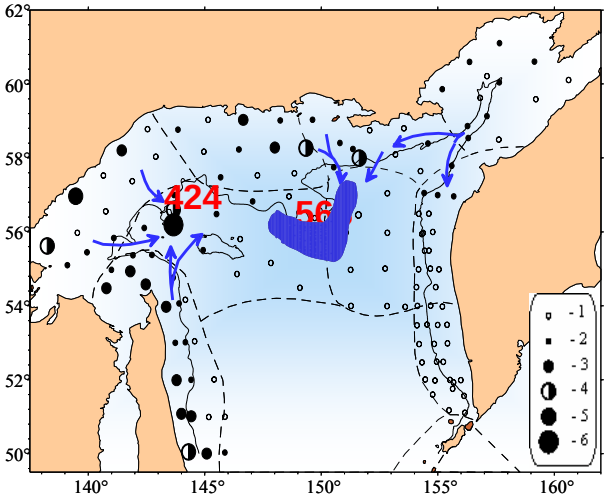

Fig. 2 Distribution of herring biomass (th. t) in the northern Okhotsk Sea in November-December 2002. Designations: 1:0; 2:<0.1; 3:0.1-1.0; 4:1.0-10.0; 5:10.0-100.0; 6:>100 t per km^2. Arrows indicated presumed migration routes to the wintering areas. Shaded areas indicate mixing of Okhotsk and Gizhiginsk-Kamchatka herring.

of the Okhotsk herring in the Iona-Kashevarov area confirms that there is a relatively independent intrapopulation group of the Okhotsk herring in the northwestern Okhotsk Sea (Melnikov and Vorobyov 2001; Melnikov 2002).

The abundance of herring in the autumn - winter of 2002 was much higher than in 2001, due to a high abundance of yearlings, estimated at 44.5 billion individuals, while total biomass decreased by over 1 million t and was estimated at 1.65 million t (Table 1). Fish from the high-yielding 1996 and 1997 generations dominated among recruits, and the very low abundance of the 1999 cohort was confirmed. In 1998 and 2000, cohort strength was average.

The considerable drop in biomass of herring in 2002 was primarily connected with natural and fishery removals of older fishes (age 10+ and higher). The biomass (Table 1) in the autumn of 2001 exceeded 500 thousand t, and in 2002 decreased to 134.4 thousand t. Severe oceanographic conditions during the 2000-2001 winter, and a reduction of the feeding period in the summer - autumn of 2001, apparently resulted in increased natural mortality of all age groups forming commercial stock. Preliminary data show that there was a decrease in growth rate, individual fecundity, life span, and an increase in age at mass maturity in age groups of recruits. The commercial fishery for pre-spawning fish that was permitted beginning from 2001 (formerly, harvest operations on these fish were conducted as a scientific monitoring), also might have played a negative role. By our assessments, along with official catch of 73 thousand t of pre-spawning herring in spring 2001, the real number of harvested fish amounted over 120-150 thousand t. Most males, and female caracasses (after roe is removed) were discarded. To make uncontrollable catch lower, it is necessary to forbid a fishery for pre-spawning fish, and to stop supplying local and foreign markets with herring roe.

Table 1 The number and biomass of herring in different age groups in the northern Okhotsk Sea basing on data from trawling survey in September-October 2001, and November-December 2002.

Age, years	2001		2002	
	Million individuals	Thousand tons	Million individuals	Thousand tons
0+	2766.6	21.3	36342.0	120.7
1-1+	3300.8	99.4	144.8	3.5
2-2+	592.6	67.0	790.0	58.2
3-3+	3048.5	364.1	697.4	84.6
4-4+	3818.1	487.7	1238.5	207.0
5-5+	1937.1	333.5	1953.4	356.3
6-6+	1216.4	240.5	973.1	191.4
7-7+	1247.2	280.7	440.1	95.0
8-8+	808.2	206.6	645.5	163.0
9-9+	926.4	271.3	523.7	141.8
10-10+	1134.5	355.4	334.1	97.6
11-11+	577.4	181.4	210.0	62.8
12-12+	175.2	59.0	150.4	47.6
13-13+	20.6	7.1	49.5	14.7
14-14+	2.1	0.7	24.2	9.3
Total	21571.5	2975.9	44516.8	1653.5

References

Melnikov, I.V. 2002. Results of estimation of herring stock in the northern part of the Okhotsk Sea by the 2000 trawl surveys. *Izv. TINRO*: 130: 1098-1114. (In Russian).

Melnikov, I.V. and Vorobyov, P.V. 2001. Distribution and migration of immature herring in the northern Okhotsk Sea. Problems of Fisheries 2 №3(7): 403-421. (In Russian).

Melnikov I.V. 2002. Effect of the cold winter 2000 - 2001 on allocation and migrations of the Pacific herring in the northern Okhotsk Sea. PICES Abstracts (Qingdao, China, October 18-26, 2002, p. 201.

Naumenko, N.I. 2001. Biology and fishery for marine herrings in the Far East. Petropavlovsk-Kamchatskyi: Kamchatskyi Printing House. 330 p. (In Russian).

Radchenko, V.I. and Melnikov, I.V. 2001. Present State of Okhotsk Herring Population after Large-Scale Fishery Resumption. Herring: Expectations for a new Millennium. Alaska Sea Grant Program. pp. 689-702.

The biological indices of wild and hatchery Pacific salmon fry of Sakhalin Island and Primorskiy region

Yuriy Mitrofanov and O.V. Dogadova
V.I. Il'ichev Pacific Oceanological Institute, Far-Eastern Branch of Russian Academy of Sciences, 43 Baltiyskaya Street, Vladivostok, 690041 Russia. e-mail: pacific@online.marine.su

It is known that the viability of some Pacific salmon bred at fishery hatcheries is considerably lower than that of natural populations. This is illustrated by decreasing returns of the hatchery-reared fish. Methods of dry fertilization used at the hatcheries results in low activity sperm participating in fertilization along with vigorous sperm. This is probably one of the causes of the decrease in quality of salmon offspring at the hatcheries. The paper presents studies of specimens of natural and hatchery populations of chum and pink salmon. The material for study was obtained from the Barabashevskiy Fish Hatchery (Primorskiy Region) and the Sokolovsky Fish Hatchery (Sakhalin Island), as well as from the Rivers Melkaya, Tym' and Belaya (Sakhalin Island) in 1988-1994.

At the hatcheries, eggs were fertilized with the help of trivial dry method of fertilization (control). Besides, we received the posterity using the technique of spermal selection (SS) - selection of the most active fraction of sperm. In this case, before fertilizing the sperms were activated in the absence of eggs in definite conditions, and after that they were mixed with the eggs. Then the less active sperms were loosing their activity and didn't participate in fertilization.

The level of fluctuating asymmetry (FA) was selected as a criterion of stable ontogenesis and significance of heredity during the formation of some characteristic features in the study populations. The features measured included: number of pores of seismosensory channels, gill rakers, rays in pectoral fins and ventral fins, spots along the side line. The indices of viability and sex ratio were studied too. The chum studied in the presented work are characterized by high occurrence of fluctuating asymmetry (FA). Disorder in fry symmetry reflects the state of the population and the level of individual viability. Generally, the FA level was highest in chum fry from the hatchery populations of Sakhalin Island (Sokolovskiy hatchery) and Primorskiy Region (Barabashevskiy hatchery) when dry method of fertilization was applied (Table 1). The fry of natural populations (in the rivers Melkaya and Tym', Sakhalin Island) and those bred using the SS method had reduced levels of FA.

The study populations were distinguished from each other by several features, such as number of spots along side line, number of rays in pectoral fins, number of gill rakers, and number of pores.

We note that the use of the SS method increases the sizes and weights of fry. The power of this method is that the level of individual viability is higher in SS fry (Table 2).

The summarized results indicate that FA level is lower in chum salmon that reproduced in natural conditions than those populations which bred in hatchery. It is possible because those wild specimens that are fittest for survival after natural selection that took place. But better FA indicators were noticed in the experiments with SS that were conducted at Sokolovskiy hatchery. The lowest FA values were observed in number of spots, gill rakers, rays of pectoral fins and pores. Their values were nearer to the FA values of wild fishes from the rivers Melkaya and Tym' (Table 1). FA indicators of fishes from Barabashevskiy hatchery are 1.5–2.0 times greater than fishes from other study regions, according to features such as pores of seismosensoric channels on the preoperculum, rays of pectoral fins, and number of gill rakers. This may be linked with an unfavorable water regimen at the Barabashevskiy hatchery during the period of study. Also, conditions of dry fertilization are an additional unfavorable factor.

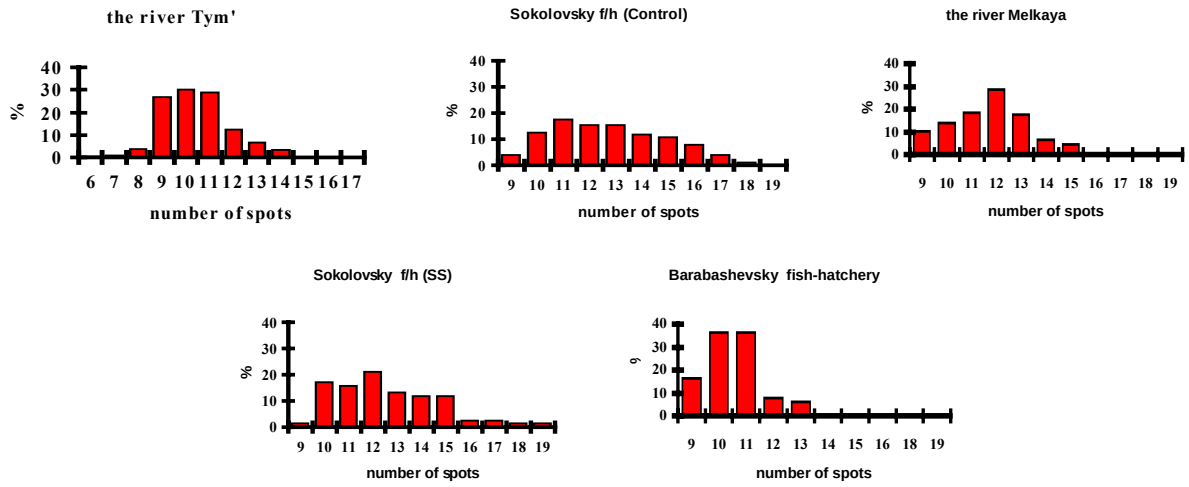

Fig. 1 Variability in numbers of spots.

It should be noted when considering various features that the coincidence of number of spots is not a vital feature and it is unlikely to be evidence for symmetry of body sides. This is perhaps the reason why the greatest variations of values (from 6 to 19 spots) were observed in this feature (Fig. 1). The greatest feature variability was observed at the Sokolovskiy hatchery. In experiments using the SS method, the variability of features was reduced. The same picture was observed in pectoral fins and gill rakers (Figs. 2 and 3). Apparently, sperm selection decreased fish feature diversity.

Considering FA magnitudes among all studied populations, these were certainly distinctive from each other (Table 1). The lowest level of spot FA was characteristic of the experimental (SS) fry of Sokolovskiy hatchery.

The pore feature is conservative. The number of pores is the lowest among other features (Fig. 4). Numbers of pores are rather similar among fishes from different areas. Fishes from the rivers Melkaya and Tym' were distinguished slightly (Table 1). The lowest level of FA in pore numbers

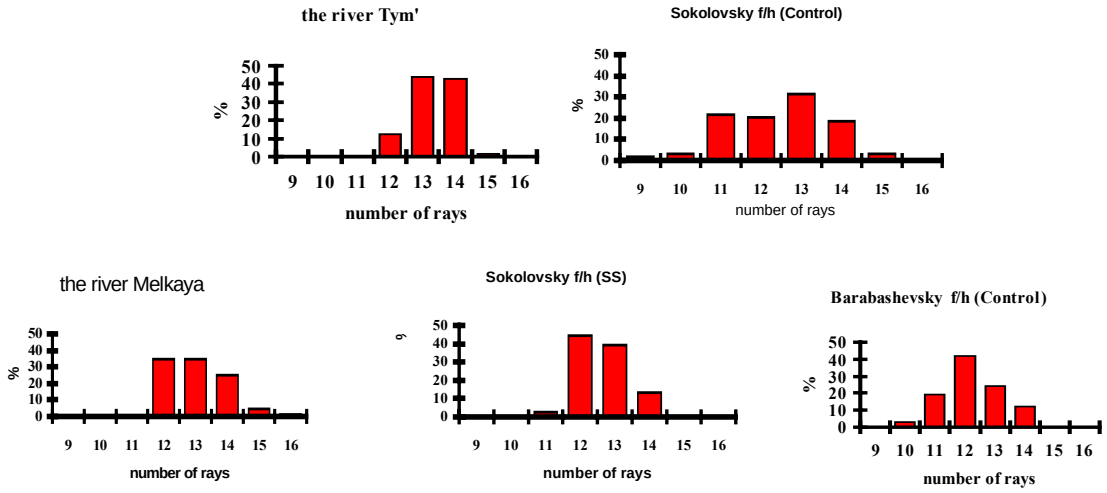

Fig. 2 Variability in numbers of pectoral fin rays.

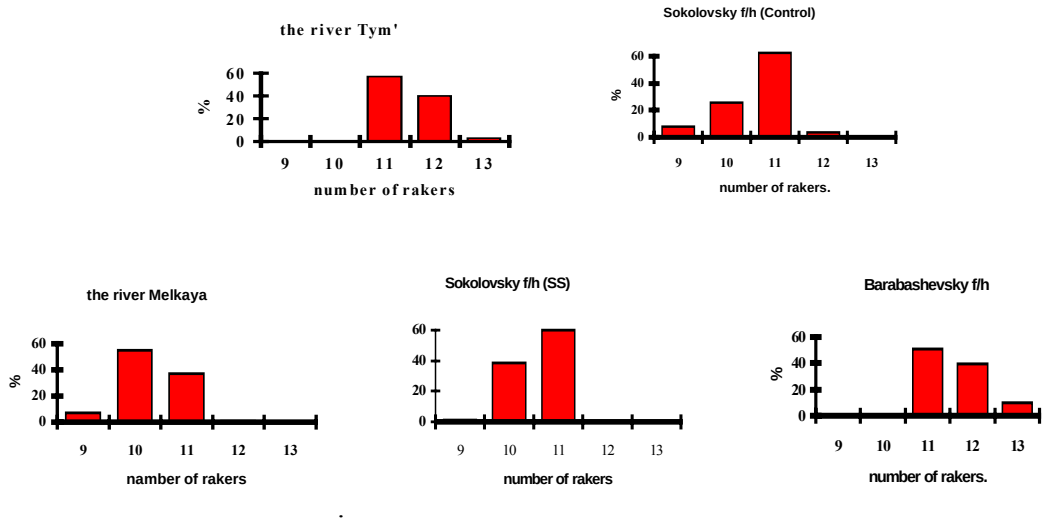

Fig. 3 Variability in number of gill rakers.

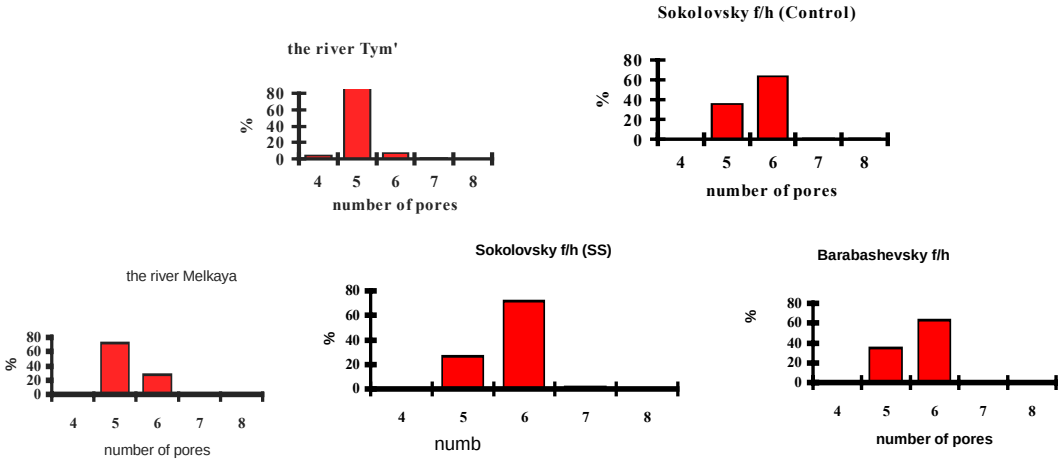

Fig. 4 Variability in number of pores.

was for fry from the rivers Melkaya and Tym', and also for fry bred with the SS method at Sokolovskiy hatchery (0.16, 0.16, and 0.17 respectively, Table 1).

Deviations in numbers of gill rakers indicate asymmetry of gills. Observed values ranged from 9-13 (Fig. 3). Individuals from Barabashevskiy hatchery were distinguished by greater numbers of gill rakers. The Barabashevskiy hatchery population was essentially distinctive from the rest (0.34) in regard of FA magnitude of gill rakers number. We have already pointed to unfavorable water regimen at this hatchery as a possible source of this developmental asymmetry. It should also be pointed out that defective spade-shaped pectoral fins (>70%) occurred in fry from this hatchery. They looked like stumps, half the length compared with usual ones. They were like nibbled round edges that made it difficult to count the number of rays. This phenomenon could be linked with unfavorable water regimen and an aggressive bacterial medium at the hatchery.

FA differences in pectoral fins rays of fishes from hatchery and natural populations proved to be significant (Table 1). Wild fry were frequently similar to the experimental (SS) fry. On the one hand, the similarity resulted from fertilization by dry method at Barabashevskiy and Sokolovskiy hatchery (0.69 and 0.63), and on the other hand they occurred in wild populations from the rivers Melkaya, Tym' and the experimental ones from Sokolovsky hatchery.

Mean FA indicators of numbers of rays were equal to 12-13 (Fig. 2); the range was 9-16. The range was greatest (9-15) in pectoral fins of fishes from Sokolovsky hatchery although the fry was smaller, comparing to other locations. It was considerable at Barabashevskiy hatchery (10-14). Application of SS produced fry that differed less. They were similar to fishes from the river Melkaya, because under natural conditions, there is natural selection of the fittest, including among sperm. The most frequent occurrences of fish with 12-13 rays in pectoral fins are displayed clearly. Fry with 9-11 rays have smaller body parameters.

Considering the number of the ventral fins rays, we found that this feature is conservative indicator of FA. It is mentioned only to report its non-significant variability. Representative distinctions between numbers of indicators in left and right sides of the fishes were not disclosed, to be precise there were not observed the prevailing increase in a feature indication for one side.

Variability in the above features of the studied populations has been described. It is evident that specimens of each studied population were characterized by certain typical indices of these features and FA of the paired features.

Pink salmon fry had of lower values of some indices of FA (Table 1). It had reduced level of FA of pectoral fin rays and gill rakers and had the highest level of FA of for pores in the seismo-sensory channels.

Table 1 Fluctuating asymmetry indicators in chum salmon (*O. keta*) and pink salmon (*O. gorbuscha*).

Number of fish	**Fluctuating asymmetry**			
	Spots	**Pores**	**Pectoral fins rays**	**Gill rakers**
O. keta				
Barabashevskiy hatchery(Control)				
60	0.85	0.37	0.69	0.34
Sokolovskiy hatchery (Control)				
99	0.7	0.19	0.63	0.24
Sokolovskiy hatchery (Sperm selection)				
36	0.58	0.17	0.27	0.19
River Melkaya				
52	0.75	0.16	0.33	0.22
River Tym’				
94	0.92	0.16	0.32	0.27
River Belaya				
66	0.122	0.21	–	0.35
O. gorbuscha				
(Sokolovskiy hatchery)				
42	–	0.38	0.21	0.22

Table 2 Weight and size of chum (*O. keta*) at 5 and 6 months of age.

		5th month	**6 months**
Control	Weight (mg)	324.1±10.50	403.2±13.50
	Length (cm)	3.3±0.02	3.6±0.03
SS	Weight (mg)	383.0±6.20	646.1±20.90
	Length (cm)	3.5±0.02	4.0±0.04

Nekton communities of the upper epipelagic layer of the southern Okhotsk Sea – Current status and tendencies of long-term dynamics

Alexander N. Starovoytov, Olga S. Temnykh, Igor I. Glebov and Vladimir V. Sviridov
Pacific Fisheries Research Centre (TINRO-Centre), 4 Shevchenko Alley, Vladivostok, 690950 Russia.
e-mail: interdept@tinro.ru

Summer surveys in the southern Okhotsk Sea from 1991-2002 have shown that the nekton fish species biomass is dominated by three or four taxa (Table 1). Up to the mid 1990s, the proportion of walleye pollock (*Theragra chalcogramma*) and Pacific sardine (*Sardinops s. melanosticta*) in the overall fish biomass was notable. A short period of high abundance of Pacific sardine (exceeding 1 million t during the 1980s in the southern Okhotsk Sea), ended by the early 1990s. By the late 1990s, no Pacific sardines were noted in the southern Okhotsk Sea. A concurrent decrease of walleye pollock biomass took place as its foraging migrations to the southern deep-water part of the Okhotsk Sea ceased. In particular, the share of walleye pollock equaled 90% of the overall fish species biomass in the deep-water regions of the sea. By the late 1990s, walleye pollock and Pacific sardine ceased to appear in the epipelagic layer of the southern Okhotsk Sea.

During the summer of the late 1990s, the leading role in the upper epipelagic fish community was taken by representatives of southern-boreal and subtropical complexes - Japanese anchovy (*Engraulis japonica*) and arabesque greenling (*Pleurogrammus azonus*). The scale of these species migrations into Okhotsk Sea depends both on their abundance and on hydrological conditions of a particular year. Mass northward migrations of southern species occur during abnormally high sea surface temperatures in the southern part of the Okhotsk Sea, resulting from an increase in Soya Current flow. Besides these species, other subtropical fishes migrated up to the northern continental coast of the Okhotsk Sea in the late 1990s. In 1999 and 2000, several specimens of striped mullet (*Mugil cephalus*) were caught in the Tauisky region. There were no previous reports of this species migrating so far to the north.

Table 1 Composition (%) and average biomass (thousand t) of major taxonomic groups and species of nekton in the southern Okhotsk Sea during summer of 1991-2002 period.

Taxonomic group	Survey period (years, months)					
	1991-1995 June-July		1996-2000 July-August		2001-2002 August	
Pink salmon	119.78	25.0%	43.54	10.0%	38.55	10.3%
Chum salmon	19.60	4.1%	37.80	8.7%	80.45	21.5%
Other salmon species	2.46	0.5%	2.20	0.5%	1.70	0.5%
All salmon species	***141.84***	***29.6%***	***83.54***	***19.1%***	***120.70***	***32.2%***
Pacific herring	16.14	3.4%	0.60	0.1%	–	–
Pacific sardine	61.60	12.8%	–	–	–	–
Northern smoothtongue	162.28	33.8%	83.06	19.0%	81.35	21.7%
Walleye pollock	42.20	8.8%	–	–	–	–
Pacific saury	–	–	9.48	2.2%	–	–
Japanese anchovy	12.76	2.7%	104.56	23.9%	–	–
Arabesque greenling	16.68	3.5%	144.18	33.0%	105.80	28.2%
Salmon shark	6.92	1.4%	3.82	0.9%	6.55	1.7%
Other fish species	19.14	4.0%	7.62	1.7%	60.40	16.1%
All fish species	***479.56***	***100%***	***436.86***	***100%***	***374.80***	***100%***
Squid	***46.86***		***20.30***		***19.35***	

Table 2 Composition (%) and average biomass (thousand tons) of major taxonomic groups and species of nekton in the southern Okhotsk Sea during autumn of 1998-2002 period.

Taxonomic group	Survey period (years, months)			
	1998-2000 September-October		2001-2002 October	
Juvenile pink	180.98	26.1%	189.86	42.2%
Mature pink	0.19	0.03%	0.05	0.01%
Juvenile chum	92.12	13.3%	85.89	19.1%
Mature chum	5.87	0.8%	1.98	0.4%
Immature chum	10.98	1.6%	3.64	0.8%
Juvenile sockeye	1.02	0.1%	5.97	1.3%
Juvenile chinook	0.41	0.1%	3.53	0.8%
Juvenile coho	1.65	0.2%	2.32	0.5%
Juvenile masu	2.27	0.3%	4.46	1.0%
All salmon species	***295.50***	***42.6%***	***297.68***	***66.1%***
Northern smoothtongue	152.07	21.9%	108.86	24.2%
Arabesque greenling	2.66	0.4%	1.91	0.4%
Japanese anchovy	213.95	30.8%	0.16	0.03%
Other fish species	29.77	4.3%	41.41	9.2%
All fish species	***693.94***	***100%***	***450.01***	***100%***
Squid	***74.23***		***57.72***	

The northern smoothtongue (*Leuroglossus schmidti*), a mesopelagic species, is a constant component of both northern boreal and southern boreal fish communities of the upper epipelagic layer in Okhotsk Sea. Large interannual changes of northern smoothtongue abundance depend mostly on the intensity of its vertical migrations from the mesopelagic layer into the upper layers. In the 1980s, it was considered that total northern smoothtongue biomass in the Okhotsk Sea was comparable with that of walleye pollock (Ilyinsky 1998). Due to the decrease of walleye pollock biomass during the 1990s, it is most likely that the total northern smoothtongue biomass is highest among pelagic fish species in the southern deep-water part of the Okhotsk Sea.

Pacific salmon species (*Oncorhynchus* spp.) in the southern Okhotsk Sea are represented mostly by mature pre-anadromous spawners during the summer. Almost every year during the 1990s, the total Russian catch of Pacific salmon was more than 200 thousand t. The major share of catch was of the most abundant species – pink salmon (*O. gorbuscha*). During the last decade its catches exceeded 100 thousand t, reaching 216 thousand t in 1991. During June-July of 1991-1995 period and July-August of 1996-2000 period, pink salmon was the most abundant among salmon species in the southern Okhotsk Sea. In August of 2001-2002, the biomass of this species in this area was lowered significantly. At the same time, growth of chum salmon (*O. keta*) biomass (mean: 80.45 thousand t, Table 1) was observed. These changes were due to the autumn chum salmon migrations into this region, while the part of pink salmon has already departed for the spawning grounds.

The cephalopod biomass was highest in the first half of the 1990s (46.9 thousand t) and declined after the second half of 1990s, as was observed for pink salmon.

It seems that the presence of significant amounts of forage plankton has a major effect on the migrations of the following groups. The first group is subtropical and boreal fishes and squids, which migrate into the southern Okhotsk Sea, and the second is the plankton-consuming mesopelagic fishes and squids, which migrate from the mesopelagic layer into upper epipelagic layer. For

instance, the relative abundance of macrozooplankton in this part of the sea during the summer of 1997-2001 period amounted 65-196 t/km^2. The ratio between planktonic and nektonic biomass during the summers of 1997-2002 in the southern Okhotsk Sea ranged between 29 and 113, which is significantly higher than the northern Okhotsk Sea (7.5– 20.5 for the same time period).

With the start of autumn, significant changes occur in the composition and structure of southern Okhotsk Sea nekton communities. These changes are mostly the result of migrations of salmon spawners into the rivers, the migrations of juvenile salmon to the sea, and partially to the migration of subtropical species towards the south due to the seasonal cooling of surface waters. During 1998-2000 and 2001-2002, the overall biomass of Pacific salmon species in the southern Okhotsk Sea amounted 296-298 thousand t, on average (Table 2). Pink salmon juveniles comprised 26.1-42.2% from this biomass, and 0+ chum salmon comprised 13.3-19.1% during this time period.

Besides Pacific salmon, Japanese anchovy and northern smoothtongue did comprise a substantial share in the overall fish species biomass (21.9 and 31.8%, respectively) in September-October of 1998-2000 (Table 2). During the October of 2001-2002 only northern smoothtongue had a significant biomass (108.86 thousand t) in the upper epipelagic layer. Juvenile arabesque greenling, which is quite abundant in summer, migrates into benthic habitats in shelf zone in the autumn and occurs only incidentally in the epipelagic layer.

In October-November, after the seasonal southward migration of Japanese anchovy, two groups dominate in the upper epipelagic layer of deep-water part of Okhotsk Sea – juvenile Pacific salmon (mostly pink and chum salmon) and northern smoothtongue.

Measurement of bio-optical properties and its application to ocean color remote sensing in the Okhotsk Sea

Sei-ichi Saitoh[1], H. Suzuki[1], K. Sasaoka[2], T. Nakatsuka[3] and M. Wakatsuchi[3]

[1] Laboratory of Marine Environment and Resource Sensing, Graduate School of Fisheries Sciences, 3-1-1, Minato-cho, Hakodate, Hokkaido, 041-8611 Japan. e-mail; ssaitoh@salmon.fish.hokudai.ac.jp

[2] Earth Observation Research Center, National Space Development Agency of Japan, 1-8-10, Harumi, Chuo-ku, Tokyo, 104-6023 Japan.

[3] Institute of Low Tempreature Science, Hokkaido University, Kita-19, Nish-8, Kita-ku, Sapporo, 060-0819 Japan.

Introduction

The Okhotsk Seawater is a source of cold, fresh, and high-oxygen water contributing to the formation of Oyashio water and North Pacific Intermediate Water (NPIW) characterized by a salinity minimum at the density of about 26.8 σ_θ (Talley 1991; Yasuda et al. 2002; Yamamoto et al. 2002). The Okhotsk Sea and its water exchange with the North Pacific play an important role, not only in the local environment, but also in determining the water properties of the North Pacific (Ohshima et al., 2002). Physical and chemical properties in the Okhotsk Sea have been studied but the optical properties of seawater has not been clarified in this region. Understanding the bio-optical characteristics of seawater is essential and important for ocean color remote sensing. Therefore we collected optical data sets during research cruises in the Okhotsk Sea in 2000 (Fig. 1 and Table 1). Our objective was to characterize the spatial variability of chlorophyll *a* and water column optical properties (i.e., in situ reflectance) and apply these data sets to ocean color remote sensing including development of regional bio-optical algorithm for the Okhotsk Sea.

Data and methods

Sampling

Water and particulate samples were collected from the *R/V Mirai* and the *R/V Kromov* in the sampling stations shown in Figure 1. The cruises were carried out from May 15 to June 6, 2000 (*R/V Mirai*) and from June 4 to June 28, 2000 (*R/V Kromov)*. Surface samples were collected by plastic bucket. Water column irradiance and radiance measurements were performed at each station. The data sources we observed are summarized in Table 1. Station M3 is typical clear ocean water region as a reference in comparison with the water in the Okhotsk Sea.

Chlorophyll a analysis

For the determination of phytoplankton chlorophyll *a*, a 200 ml of water sample was filtered onto a Whatman GF/F (25mm) filters. The filter was immediately soaked in N, N-dimethylformamide (DMF) were extracted in the dark (Suzuki and Ishimaru 1990). The concentration of chlorophyll *a* was determined with a fluorometer (10-AU, Turner. Inc.) after extraction (Parsons et al. 1984).

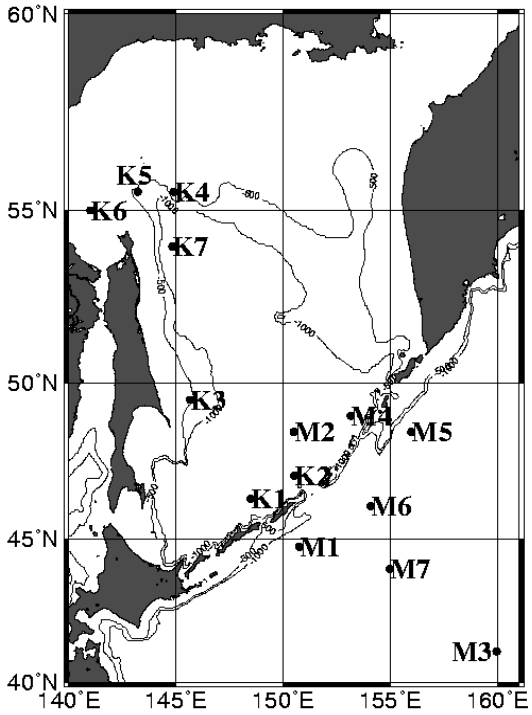

Fig. 1 Location of the sampling stations in this study. K: *R/V Kromov*, M: *R/V Mirai.*

Table 1 List of cruises and data sampling.

Cruise name	Spectroradiometer	Station number	Date
R/V *Mirai*	MER2040/2041	M1	May 15, 2000
		M2	May 17, 2000
		M3	May 27, 2000
		M4	May 31, 2000
		M5	June 2, 2000
		M6	June 4, 2000
		M7	June 6, 2000
R/V *Kromov*	PRR600/610	K1	June 4, 2000
		K2	June 10, 2000
		K3	June 15, 2000
		K4	June 19, 2000
		K5	June 21, 2000
		K6	June 24, 2000
		K7	June 28, 2000

Particulate analysis

Particulate absorption, a_p, spectra were determined using the quantitative filter pad technique (e.g., Mitchell and Kiefer 1990). Seawater volumes of 0.2 to 1 L water vacuum filtered through Whatman GF/F (25mm) filters. The absorption of particles retained on the filter was determined over the spectral range 350 to 750 nm. Triplicate spectra ware averaged and then zeroed using data 750 nm as a baseline. A correction for multiple scattering by the filter (beta correction) was applied using the function derived by Cleveland and Weidemann (1993). The spectral absorption coefficient (per meter) was calculated by accounting for the volume filtered and the effective area of the filter. To examine waveform difference, we normalized data sets at 440 nm or 490 nm.

Remote sensing reflectance

Submersible spectroradiometers (MER2040/2041 and PRR600/610, Biospherical. Inc.) were used to measure upwelling radiance, $L_u(\lambda)$, and downwelling irradiance, $E_d(\lambda)$, simultaneously. The spectra data we observed are summarized in Table 2. Downwelling irradiance and upwelling radiance were averaged every 1 m. Values of $E_d(\lambda)$ and $L_u(\lambda)$ at just below the sea surface, $E_d(\lambda, 0\text{-})$ and $L_u(\lambda,0\text{-})$, were defined as coefficients fitting the data between 0 and 10 m according to the following equations (Gordon et al. 1983):

$$E_d(\lambda, z) = E_d(\lambda, 0\text{-}) \cdot \exp[- K_d(\lambda) \cdot z] \qquad (1)$$

and

$$L_u(\lambda, z) = L_u(\lambda, 0\text{-}) \cdot \exp[- K_u(\lambda) \cdot z] \qquad (2)$$

where λ is wavelength, z is depth, $K_d(\lambda)$ is diffuse attenuation coefficient of downwelling irradiance, and $K_u(\lambda)$ is diffuse attenuation coefficient of upwelling radiance. Water leaving radiance (Austin 1974), $L_w(\lambda)$, was calculated by following equation:

$$L_w(\lambda) = (t/n_w^2) \cdot L_u(\lambda, 0\text{-}) \qquad (3)$$

where t is surface transmittance from sea to air, t and n_w are approximately 0.98 and 1.34, respectively (Austin, 1974). Remote sensing reflectance (apply to the test of SeaWiFS algorithm and reflectance model), $Rrs(\lambda)$, can be written the following equation:

$$Rrs(\lambda) = L_w(\lambda) / E_{ds}(\lambda), \qquad (4)$$

where $E_{ds}(\lambda)$ is downwelling irradiance at just above the sea surface.

Wavelength spectral bands of radiometers used in this study were different from each other (Table 2). The PRR600 do not have channels at 510 nm and 555nm. Therefore we interpolated data sets from 510 nm to 520 nm and from 555 nm to 565 nm using MER2040 data sets, which contain both wavelengths (Hirawake et al. 2000).

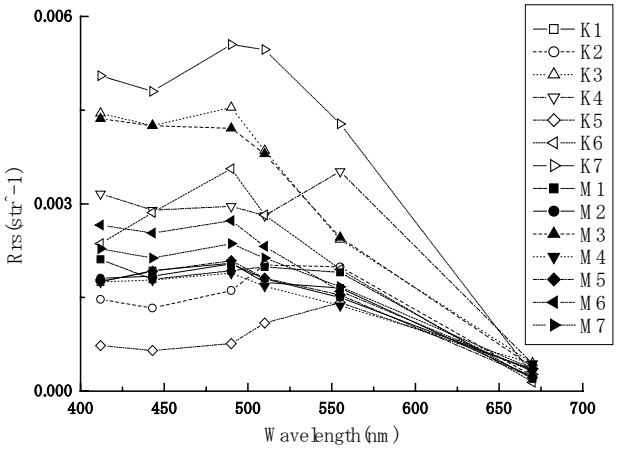

Fig. 2 Remote sensing reflectance.

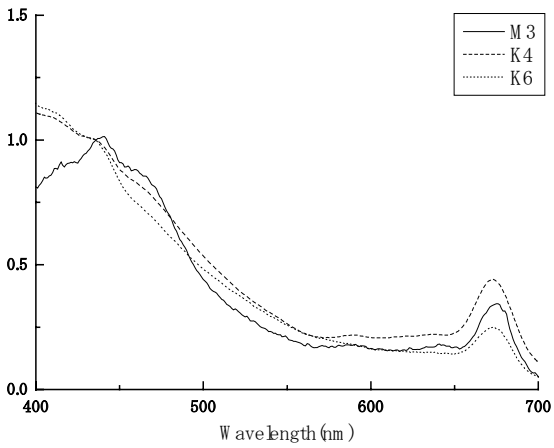

Fig. 4 Normalized particulate absorption at 440 nm.

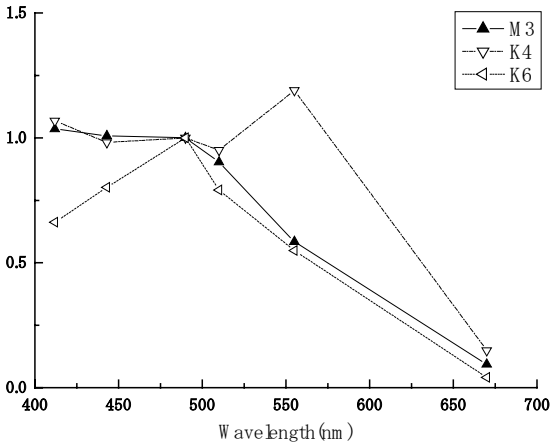

Fig. 3 Normalized remote sensing reflectance at 490 nm.

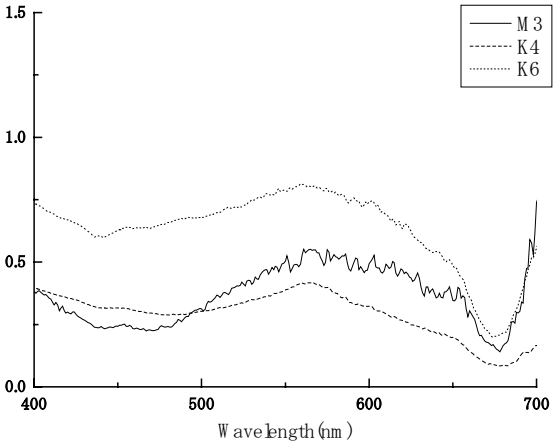

Fig. 5 Ratio between ad and ap.

Table 2 Spectral bands of ocean color sensor SeaWiFS and spectroradiometers.

Satellite Sensor	Spectroradiometers	
SeaWiFS	**MER2040/2041**	**PRR600**
412	412	412
443	443	443
	465	
490	490	490
510	510	
	520	520
555	555	
	565	565
	625	
	665	
670	670	670
765		
865		

Results and discussion

Remote sensing reflectance of each stations and normalized remote sensing reflectance at 490 nm are shown in Figures 2 and 3, respectively. Using Rrs spectral signatures, we could categorize to three groups: M3 type represents clear ocean water as Case I, K4 type represents high chlorophyll *a* concentration water (refer to Table 3) and K6 type represents high particulate materials concentration water.

Normalized particulate absorption at 440 nm and the ratio between suspended materials absorption and total particulate absorption are shown in Figures 4 and 5, respectively. M3 has a typical Case I spectral signature with high absorption at 443 nm and 683 nm. K4 and K6 has similar spectral signature but absorption at 683 nm is different. Magnitude of absorption at 683 nm for K6 is lower than one for K4. The ratio of a_d/a_p of K6 is twice value (Fig. 5). It is clear that K6 is strongly affected by absorption of suspended materials in comparison with the other stations.

In the Okhotsk Sea, Case I type water (M3 type) exists at the station K3 and K7 near Sakhalin Island. On the other hand, in the region with Amur River discharge effect, there are two kinds of water with bio-optical properties, high chlorophyll *a* concentration water (K4 type) and high suspended materials concentration water (K6 type).

We will discuss on application of these results to ocean color remote sensing more detail in the symposium.

References

Austin, R.W. 1974. The remote sensing of spectral radiance form below the ocean surface. pp. 317-344. *In* N.G. Jerlov and E.S. Nielsen (Eds.) Optical Aspects of Oceanography. Academic Press, London.

Cleveland, J.S. and Weidemann, A.D. 1993. Quantifying absorption by aquatic particles: A multiple scattering correction for glass fiber filters. *Limnol. Oceanogr*. 38: 1321-1327.

Gordon, H.R. and Morel, A. .1983. Remote Assessment of Ocean color for interpretation of Satellite Visible Imagery. Springer-Verlag, New York, 114 pp.

Hirawake, T., Satoh, H., Ishimaru, T., Yamaguchi, Y. and Kishino, M. 2000. Bio-optical relationship of Case 1 waters: the difference between the low- and mid-latitude waters and the Southern Ocean. J. Oceanogr. 56: 245-260.

Nakatsuka, T., Yoshizawa, C., Toda, M. and Kawamura, K. 2002. An extremely turbid intermediate water in the Sea of Okhotsk: Implication for the transport of particulate organic matter in a seasonally ice-bound sea. Geophys. Res. Lett. 29 10.1029/2001GL014029

Michell, B.G. and Kiefer, D.A. 1988. Chlorophyll a specific absorption and fluorescence excitation spectra for light-limited phytoplankton. Deep-Sea Research 35: 639-663.

Ohshima, K.I, Wakatsuchi, M., Fukamachi, Y. and Mizuta, G. 2002. Near-surface circulation and tidal currents of the Okhotsk Sea observed with satellite-tracked drifters. J. Geophys. Res., 107, C11, 3195, doi:1029/2001JC001005.

Parsons, T.R., Maita, Y. and Lalli, C.M. 1984. A Manual of Chemical and Biological Methods for Seawater Analysis. Pergamon Press, New York, 173 p.

Suzuki, R. and Ishimaru, T. 1990. An improved method for the determination of phytoplankton chlorophyll using N, N-Dimethylformamide. J. Oceanogr. Soc. Japan, 46: 190-194.

Talley, L.D. .1991. An Okhotsk Sea water anomaly: Implications for ventilation in the North Pacific. Deep Sea Res. 38 Suppl. 1: S171-S190.

Yamamoto, M., Watanabe, S., Tsunogai, S. and Wakatsuchi, M. 2002. Effects of sea ice formation and diapycnal mixing on the Okhotsk Sea intermediate water clarified with oxygen isotopes, Deep-Sea Research Part I, 49: 1165-1174.

Yasuda, I., Kouketsu, S., Katsumata, K. and Ohiwa, M. 2002. J. Geophys. Res. 107, C12, 3237, dol:10.1029/2001JC001037

The accuracy of chlorophyll *a* concentration estimates of SEAWIFS satellite color scanner from the data for the Sea of Okhotsk in the spring-summer time

Elena A. Shtraikhert and S.P. Zakharkov
V.I. Il'ichev Pacific Oceanological Institute, Far-Eastern Branch of Russian Academy of Sciences, 43 Baltiyskaya Street, Vladivostok, 690041 Russia. e-mail: straj@poi.dvo.ru

Introduction

Global information about the chl-*a* concentration at the ocean surface can be obtained by remote sensing of the optical spectrum range. Deploying remote sensing equipment on aircraft or satellites make it possible to conduct such investigations. The existence of a correlation between chl-*a* concentration and the sea brightness spectrum was experimentally considered in Clarke (1970). The possibility of developing a chl-*a* determination method by passive ocean remote sensing was thereby shown.

The first Nimbus-7 satellite with a CZCS scanner on board collected information about ocean color from 1978 to 1986 (Tassan 1994). The next satellites observing the ocean color were as follows: FY-1A/B (1990-1991) with the VHRSR (Very High Resolution Scanning Radiometer); ADEOS (Advanced Earth Observing Satellite, 1996-97) with the OCTS (Ocean Color and Temperature Scanner) (Mitomi et al. 1998). Nowadays information about ocean color is collected by satellites such as ROCSAT (launched in 1998) with OCI (Ocean Color Imager) scanner; OrbView-2 (launched in 1997) with a SeaWiFS scanner (Delu et al. 1998).

The spectra of upwelling radiance from the surface water layer are registered by satellite sensors and translated at the storage and processing center of satellite information (GDAAC - Goddard Distributed Active Archive Center) or at autonomous stations for information reception (HRPT - High Resolution Picture Transmission). Thereupon these data are translated to level 2 data, i.e. to chl-*a* concentration, using bio-optical algorithms. The more common choices are the algorithm of blue-green ratio. It is based on the empirical chl-*a* concentration dependence on the spectral bands ratio of sea brightness in the blue-green spectral region to determine the chl-*a* concentration. However, existing bio-optical algorithms of chl-*a* concentration determination are not accurate and require verification and corrections, determined from comparisons of satellite and *in situ* ship data.

For open sea and ocean waters, classed as Case-1, the discrepancy between chl-a concentrations from satellite versus ship-based estimates is significantly lower than for coastal regions. So, for Case-1 waters, using the blue-green ratio algorithm, the error of chl-*a* concentration determination ranging in values from 0.5 to 50 mg/m^3 (McClain et al. 1992; Hooker et al. 2000) is more than 30%. Discrepancies of the satellite estimates from ship-based ones can reach large values in the coastal regions where the water is more often classed as Case-2. Here, the correlation between phytoplankton, and the content of suspended particles and yellow substances may exhibit large local spatial and temporal variations (Tassan, 1994). For example, the error of chl-*a* concentration determined by the SeaWiFS scanner in the Case-2 waters of the southwestern part of the Barents Sea reaches 2170%, i. e. the satellite data overestimate the ship ones in 22 times (Burrenkov et al. 2001). Satellite data usually overestimate ship-based estimates in the coastal regions. It is related to the predominance of suspended particles of organic origin and the yellow substances taken out by river flow from the sea coast.

Methods

Ship data

Ship-based chl-*a* concentrations were obtained by sampling water during the cruises of the *R/V Professor Gagarinsky* (05.06.00-12.06.00) and the *R/V Utyes* (28.05.99-07.06.99), see Figure 1. Water sampling occurred within the euphotic zone using a Rosette multi-water sampler.

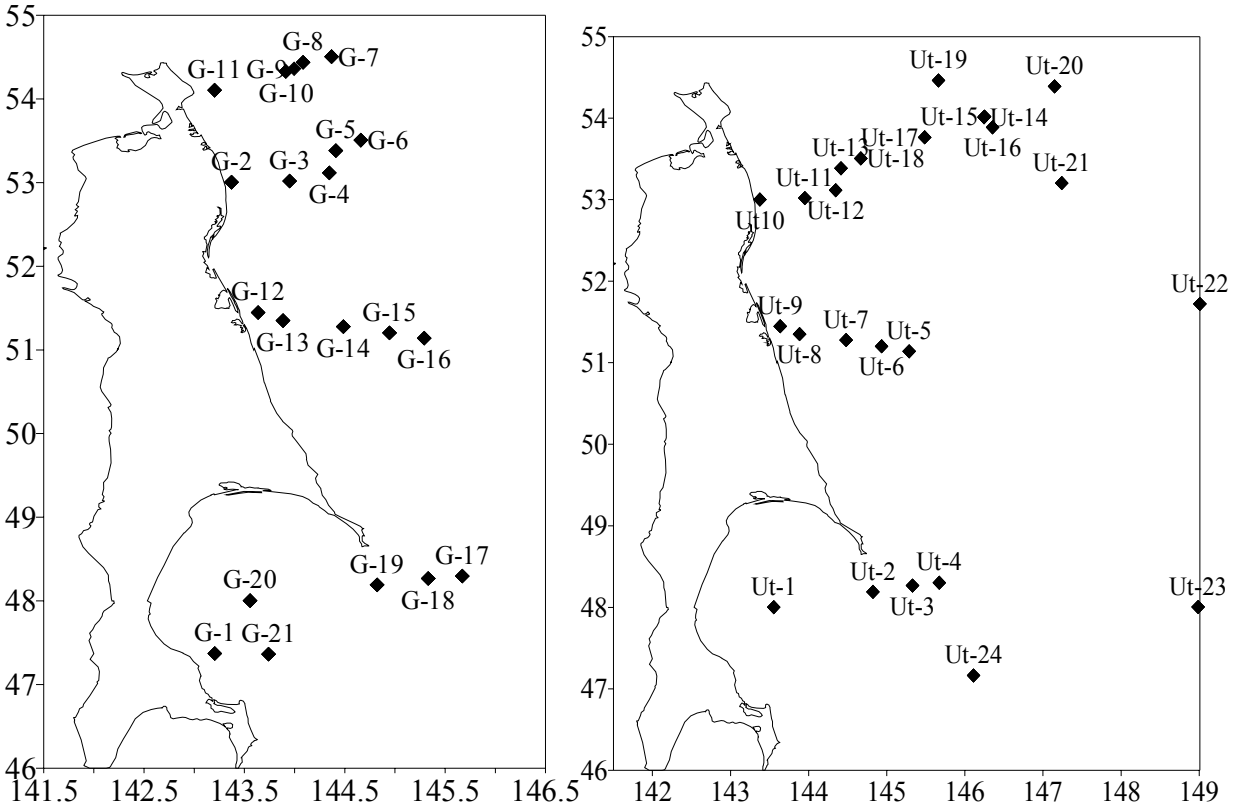

Fig. 1 Location of the sampling stations during the cruises: (left panel) *R/V Professor Gagarinsky* in June 2000 and (right panel) *R/V Utyes* in May-June 1999.

Chl a and pheophytin determination

An integrated sample of the surface layer (at 2-3 geographical coordinates) was taken while on station. This was assumed to provide an area-mean value for a region 1 km × 1 km. Samples of 1 - 1.5 liters in volume were filtered by "SARTORIUS" membrane filters of 35mm diameter with the cell making 0.6 mkm. After filtration, the samples were frozen and preserved at –18ºC. The chl-*a* concentration was measured by standard methods with preliminary extraction and determination of 90% acetone absorption spectra using a "SF-46" spectrophotometer (Anonymous 1990). Hereafter, the designation of chl-*a* concentration is assumed to be the sum of chl-*a* and pheophytin concentrations.

Satellite data

Satellite chl-*a* concentration estimation, level 2 data with GAC (4.48 km) resolution were taken from the storage and processing center of satellite information - GSFS-DAAC (Goddard Space Flight Center Distributed Active Archive Center). JHV 2.3 (Java HDF Viewer) browser was used for processing the satellite data (converting color codes with magnitudes from 0 to 255, to the numerical estimations of chl-*a* concentration related to geographical coordinates). After JHV processing, the satellite data had a spatial resolution equal to about 9 km × 9 km.

For estimating the error, determined by factors 1 and 2, a comparison of the satellite chl-*a* concentrations and the area-mean of 9 km × 9 km and 1 km × 1 km area-mean was performed. To do this, the data with space resolution of 1 km × 1 km were ordered in the GSFC DAAC center and processed with the SeaDAS 4.1 (SeaWiFS Data Analysis System) software.

Verification/correction of satellite data

Difficulties arise in the selection of sets of ship and satellite chl-*a* concentrations that are unique to separate cases of the identical parameters

determining its color (particles of organic and terrestrial origin, yellow substances). Such sets were determined from preliminary analysis of the distribution of chl-*a* concentration obtained by ship method. Distinguishing zones of chl-a concentrations were made according to: 1) the proportionality coefficient of satellite and ship data; 2) chl-*a* content at the ship station; and 3) the geographical location of a station (the distance from the coast).

Least squares was used to determine the equations relating satellite and ship chl-*a* concentration estimates for each zone ("Statistics" programs package in Excel software). Higher correlation coefficients were obtained with a simple quadratic model. Critical values of the correlation coefficients were determined at a significance level of 5% (Table in Jonson et al. 1980).

As the equations were constructed from small sample sizes, the statistical significance of the correlation coefficient in the equation was tested by the method reported in the Afifi et al. (1982). The Student t-test was used:

$$t = \frac{Z}{\sigma_z} \qquad (1)$$

where $Z = \frac{1}{2} * \ln\left(\frac{1 + R}{1 - R}\right)$ is the parameter representing the Fisher transformation, where $\sigma_z = \frac{1}{\sqrt{n-3}}$ is the mean square deviation of Z magnitude, and R is the correlation coefficient.

When t > tcritical at a significance level of 5%, it was agreed that the tested correlation coefficients were significant. The 5% level was chosen because it is optimum when it is necessary to choose between the most width of the confidence interval for chl-*a* concentrations and the lowest level of tcritical. The results of the test on statistical significance for the obtained equations are given in Table 1. The t values for all three equations are larger than t critical, which meets the condition for statistical significance of the correlation coefficients.

The error of equation construction was determined from the formula:

$$\delta = \sqrt{\delta_1^2 + \delta_2^2} \qquad (2)$$

where δ_1 is the absolute deviation for the ship data measured by the extractive spectrometric method, δ_2 is the absolute deviation caused by the inaccuracy of the satellite data. In the determination of chl-*a* concentration by the extractive spectrometric method, the measurement error varies depending on the pigment concentration in the sample. A plot of the relative error against the chl-*a* concentration in the sample is presented in Vedernikov et al. (1973). The accuracy of satellite chl-*a* concentrations are defined by the following factors:

1. satellite chl-*a* concentration estimations are taken with area-averaging over 9 km × 9 km, while the ship ones are 1 km × 1 km;
2. inaccurate relationship between the satellite data to the geographical coordinates;
3. ship chl-*a* concentrations were taken from the surface layer while the upwelling ocean radiance coming on the satellite is integrated by the near-surface layers;
4. Temporal displacement of ship and satellite estimates of chl-*a* concentration because satellite estimates are unavailable due to cloudiness for 2 days.

For estimating the error caused by factors 1 and 2, a comparison of the satellite chl-*a* concentration estimations and the area-mean of 9 km × 9 km and 1 km × 1 km area-mean was performed. To do this, the data with space resolution of 1 km × 1 km were ordered in the GSFC DAAC center and processed by the SeaDAS 4.1 software.

The influence of factor 3 on chl-*a* concentrations was evaluated by comparing chl-*a* concentrations from the ocean surface layer (C) with the parameter of <C>. Parameter of <C> takes into account the fact that the ocean radiance coming to the satellite is integrated by the near-surface water layers. This parameter was calculated by the formula, cited in Gordon (1983):

$$< C >= \int_0^{Z_p} f(z)C(z)dz \Big/ \int_0^{Z_p} f(z)dz \qquad (3)$$

where $f(z) = \exp[-2\int_0^{Z_P} \varepsilon(z)dz]$, C(z) is the chl-*a* concentration at a depth of z, $\varepsilon(z)$ is the attenuation coefficient for the sun radiance in marine water at wavelength of 520nm, Z_P is the depth from which the contribution of the sun light is made to the upwelling ocean radiance integrated by the near-surface layers ($Z_P \approx 22\%$ of the depth of euphotic zone (Z_{euph}); $Z_{euph} \approx 3.3 \times Z_{DS}$ (Sorokin, 1997), where Z_{DS} is the Secchi depth). To calculate <C>, the attenuation coefficient (ε) for sun radiance was expressed over the Secchi depth: $\varepsilon = 8/Z_{DS}$ (Shifrin 1983). To set the function of C(z) an approximation was made for 4-5 points of measurement. At it the dependence of C(z) was expressed over the function of the form $f(x) = ae^{-bx}$ since a higher degree of approximation authenticity was achieved. The expression presented in Platt and Sathyendranath (1988) was used to set C(z) when the deep chl-*a* maximum (DCM) being available:

$$C(z) = C_0 + \frac{X}{\sigma\sqrt{2\times\pi}} \times \exp(-\frac{(H - H_m)^2}{2\times\sigma^2}) \qquad (4)$$

where C(z) is the pigment concentration, B(0) is the "background" of chl-*a* concentration profile or the pigment concentration magnitude from the surface layer, H_m is the depth of the chl-*a* maximum, σ is the breadth of the peak, X is the peak altitude or the pigment concentration maximum.

Results and discussion

There were 14 estimates, averaged over 9 km × 9 km, of satellite-derived chl-*a* concentration that corresponded with ship samples obtained from the same region by the *R/V Professor Gagarinskiy* on cloudless days. As the conditions changed along transects run perpendicular to the coast, the water surface was divided into three zones, designated as sea, intermediate and coastal. There were small and comparable chl-*a* concentrations in the sea and coastal zones. At the same time, they differed by their proportionality coefficient of satellite and ship estimations. In the sea zone, it varied between 0.8 and 2.5, whereas in the coastal zone, between 2.7 and 5.4). The intermediate zone was distinguished from first two zones by its greater chl-*a* concentrations (3.5-6.81 mg/m^3). Variations of values of the satellite (Csattel) and ship (Cship) chl-*a* concentrations and their proportionality coefficient (K) are presented in Table 1.

Verification of the satellite chl-*a* concentration estimations has shown that they are overestimated, moreso in the coastal zones than elsewhere (Table 2). For this reason, the correction of the satellite chl-*a* concentration estimations from ship-based estimates is essential. To do such correction, the equations relating satellite and ship chl-*a* concentrations were obtained. Presented below are the equations subject to factors 1-4, determining the accuracy of them:

$$У = 0.29*x^2 - 0.51*x + 0.93, \qquad (5)$$

$R^2 = 0.93$. N = 5 for the sea zone,

Table 1 Variation in ranges of Csatel, Cship, and K values for waters of the northwestern part of the Okhotsk Sea in June 2000.

	Sea zone	Intermediate zone	Coastal zone
K	0.8-2.5	0.8-1.6	2.7-5.4
Csatel, mg m^{-3}	0.5-3.5	3.6-7.5	2.9-6.1
Cship, mg m^{-3}	0.65 – 2.62	3.5-6.81	0.54-2.06

Table 2 Comparison of chl-*a* concentration determination errors before and after correcting the satellite estimations for the Sea of Okhotsk waters in June 2000 (C1satel, C2satel are the satellite chl-*a* concentration estimations before and after correcting, e1, e2 are the relative errors of chl-*a* concentration determination before and after correcting). (Dates of measurements are indicated in brackets.)

Number of stations	Cship, mg/m^3	C1satel, mg/m^3	C2satel, mg/m^3	ε1, %	ε2, %
a) sea zone					
7	0.87 (09.06.)	2.2 (09.06.)	1.2	153.5	38.5
6	0.65 (09.06.)	0.5 (09.06.)	0.7	-16.8	13.6
14	1.14 (11.06.)	1.5 (11.06.)	0.8	31.2	-29
15	2.62 (11.06.)	3.5 (11.06.)	2.7	32.6	0.9
8	2.38 (09.06.)	3.2 (09.06.)	2.3	34.9	4.8
mean estimations					
	1.53	2.2	1.2	42.6	22.3
b) coastal zone					
2	1.06 (08.06.)	3.5 (08.06.)	1.3	227.6	15.8
3	0.54 (08.06.)	3 (08.06.)	0.4	444.3	-29.3
9	1.75 (09.06.)	5.8 (09.06.)	1.7	230.1	-3.1
12	1.25 (10.06.)	6.1 (10.06.)	1.4	384.3	10.1
11	2.06 (10.06.)	5.5 (10.06.)	1.9	166.5	-7.6
mean estimations					
	1.33	4.8	2.1	256.3	37.5
c) intermediate zone					
4	5.56 (09.06.)	4.6 (09.06.)	6.6	-17.3	19.5
5	3.5 (09.06.)	3.6 (09.06.)	3.1	2.8	-11.2
10	6.81 (09.06.)	5.9 (09.06.)	5.8	-13.3	-14.03
13	4.48 (10.06.)	7.5 (10.06.)	5.5	36.1	23.7
mean estimations					
	5.44	4.9	6.6	-9.9	21.4

$$Y = -0.483 * x^2 + 4.659 * x - 9.105 \quad (6)$$

$R^2 = 0.93$; N = 5 - for the coastal zone;

$$Y = -0.71 * x^2 + 8.15 * x - 16.72 \quad (7)$$

$R^2 = 0.99$; N = 4 for the intermediate zone, where y is the chl-*a* estimate obtained from the ship, x is the chl-*a* estimates obtained from the GSFS-DAAC center, R^2 is the degree of the approximation authenticity or, in other words, the coefficient of determination, and N is the sample size.

Tests of statistical significance of the correlation coefficient in the equations yielded positive results. According to the calculation the parameter of t for all three equations is larger than t critical, which meets the condition for the statistical significance of the correlation coefficients (Table 3).

A comparison of the satellite data area averaged over 9 km × 9 km and 1 km × 1 km was performed to account for the spatial heterogeneity of chl-*a* concentration distribution. To take into account the heterogeneity of chl-a distribution in depth, a comparison of chl-*a* concentration from the surface layer with the parameter <C> was performed.

In summary, the maximum error (18.7%) in chl-*a* concentration estimates, determined by factors 1, 2 occurred at station 13. The maximum error by factor 3 (24%) was observed at station 4 where a sharp decrease of chl-*a* concentration occurred with depth. Both of the above mentioned stations are settled in the intermediate zone. Therefore, the

Table 3 Parameters used for determining the statistical significance of the regional equations for the Okhotsk of Sea in June 2000.

R^2	R	N	Z	σ_z	t	tcritical
1) sea zone						
0.93	0.96	5	2.01	0.707	2.84	2.57
2) coastal zone						
0.93	0.96	5	2.01	0.707	2.846	2.57
3) intermediate zone						
0.99	0.995	4	2.99	1	2.99	2.77

accuracy of calibration equation for the given zone at δ1=18% (Vedernikov 1973), δ2 = 19%+24% is 46.6%. The error for the satellite data that are not calibrated is 9.9%. It is less than the error of the equation construction. That is why the calibration equation for the data of this zone was not used. For the coastal and sea zones the error determined by factors 1 and 2 was not above 9.2% (station 12), whereas maximum deviation of C from <C> (9.8%) occurred at the station 2 which settled in the coastal zone because of the influence DCM. Thus the accuracy of the calibration equation for this zone was 26%. In the sea zone, the difference between C and <C> did not exceed 4.2% at station 6 and the accuracy of the calibration equation equaled 23%. The error of the chl-*a* estimates for the uncalibrated coastal zone data was 256% and for the sea zone – 42.6%. After calibration it decreased to 37.5% and 22.3%, respectively.

The calibration equations were also used to correct the satellite data obtained during the *R/V Utyes* cruise. After correction, the errors were significantly decreased for the stations located in the region for which the equations were constructed. High errors were observed at stations 1, 2, and 9 (Table 4). Stations 1, 2 are located in the region where satellite chl-*a* estimates were absent because of cloudiness. The chl-*a* concentration value at station 9 exceeds the limits of the range of values for which the equation was constructed. This range is from 3 to 6.1 mg/m^3, while at station 9 it equals to 1.2 mg/m^3.

Table 4 Comparison of chl-*a* concentration determination errors before and after correcting the satellite estimations for the Sea of Okhotsk waters in May-June 1999 (Symbols of the parameters are presented in the caption of Table 2).

Number of stations	**Cship, mg/m^3**	**C1satel, mg/m^3**	**C2satel, mg/m^3**	**ε1, %**	**ε2, %**	**Zone**
1	0.33	0.4	0.8	23	-130	Sea
2	3.9	0.8	0.7	81.7	-80.6	Sea
3	9.4	5.5	6.6	-41.1	29.4	Intermediate
4	6.33	4.1	4.6	-36.1	26.7	Intermediate
6	0.77	0.6	0.7	-19.1	5.4	Sea
7	0.55	1.3	0.8	134.5	-37.2	Sea
8	8.3	5.2	6.5	-37	21.9	Intermediate
9	6.9	1.2	-4.2	-82.4	160.3	Coastal

Conclusion

The study area is exposed to the sea coast where particles of organic and inorganic material, together with river flow, influence the optical characteristics of seawater. The correlation between phytoplankton, suspended particles, and yellow substances may exhibit large local spatial and temporal variations. As a consequence of the heterogeneity, the water must be divided into separate zones to estimate chl-*a* concentration estimations from satellite data.

In most cases, the estimates of chl-*a* concentration obtained from satellite data, in waters near the coast, have been overestimated (one error in the coastal zone reached 256%). This is why calibrating satellite chl-*a* estimates from *in situ* sampling is necessary. In the regions with large gradients of chl-*a* concentration, a comparison of ship and satellite chl-*a* concentrations, area-averaged over 9 km × 9 km may give incorrect results. Thus a comparison with the satellite data having a spatial resolution of 1 km × 1 km is necessary in the regions with a heterogeneous pattern of chl-*a* concentration. When correcting satellite chl-*a* concentration estimates, there is also a need to take into account the vertical profiles of chl-*a* concentration. For instance, the difference of the chl-*a* concentration at the water surface from the depth-averaged "translucence" from satellite was 24%. This error appeared because of a sharp decrease of chl-*a* concentration with depth.

The application of the calibration equations constructed from data collected in 2000 to satellite chl-*a* estimates for 1999, for the most part, increased errors. However, there were stations where a decreased error was observed. The reason is that: 1) the chl-*a* concentrations did not fall within the range of values from which the equation was constructed; and 2) the stations are located in the southern part of Sakhalin, whereas the equations were constructed from data obtained from stations at the northern part of the island.

Acknowledgements

The authors thank GSFS-DAAC NASA group and Dr. J. Acker for their help at receiving the satellite data

References

Afifi, A.A. and Azen, S.P. 1982. Statistical Analysis. M.: Mir, pp. 157-158 (in Russian).

Burenkon, V.I., Vedernikov, V.I., Ershova, S.V. and Kopelevich, O.V. 2001. Use of Satellite Ocean Color Data for Assessment of Bio-Optical Characteristics in the Barents Sea. Oceanology 41(4): 485-492 (in Russian).

Clarke, G.L., Ewing, G.C. and Lorenzen, C.J. 1970. Spectra of backscattered light from the sea obtained from aircraft as a measure of chlorophyll concentration. Science 167: 1119-1121.

Delu, P., Li, S.J. and Mao, Z.H. 1998. The activities of ocean color remote sensing. Proceedings of the 4th Pacific Ocean Remote Sensing Conference. Qingdao. China. July 28- 31, 1998, pp.120-122.

Johnson, N. and Leone, F. 1980. Statistics and experimental design in Engineering and the Physical Sciences. Moskva, Mir. 560 p. (in Russian).

Gordon, H.R., Clark, D.K., Brown, J.W., Brown, O.B., Evans, R.H. and Broenkow, W.W. 1983. Phytoplankton pigment concentrations in the middle Atlantic Bight: comparison of ship determinations and CZCS estimates. Applied Optics 22(1): 20-36.

Hooker, S.B. and McClain, C.R. 2000. The calibration and validation of SeaWiFS data. Progress in Oceanography 45(3-4): 427-465.

McClain, C.R., Esaias, W.E., Barnes, W. et al. 1992. Calibration and validation plan for SeaWiFS. S.B. Hooker, E.R.Firestone NASA Technical Memorandum 104566. Greenbelt, Maryland: NASA Goddard Space Flight Center. Vol. 3. p. 41.

Anonymous. 1990. Method of spectrophotometric chlorophyll-a and pheophytin determination. GOST 17.1.04.02-90.

Mitomi, Y., Toratani, M., Simada, M., Oaku, H., Murakami, H., Mukaida, A., Fukusima, H., Ishizaka, J. 1998. Evaluation of OCTS standard ocean color products: comparison between

satellite – derived and ship measured values. Proceedings of the 4th Pacific Ocean Remote Sensing Conference. Qingdao. China. July 28-31, 1998. pp.115-118.

Platt, T. and Sathyendranath, S. 1988. Oceanic primary production: estimation by remote sensing at local and regional scales. Science: 1613-1619.

Sorokin, Yu.I. 1997. Primary production in the Sea of Okhotsk. Combined investigations of the ecosystem in the Sea of Okhotsk. Collection of scientific works. M.: VNIRO: 103-110. (in Russian).

Shifrin K.S. 1983. Introduction to the ocean optics. L.: Gidrometeoizdat: 5-57. (in Russian).

Tassan, S. 1994. Local algorithms using SeaWiFS data for the retrieval of phytoplankton pigments, suspended sediment, and yellow substance in coastal waters. Applied Optics 33 (12): 2369-2377.

Vedernikov, V.I., Konovalov, V.I., Koblenz-Mishke, O.I. 1973. The results of applying spectrometric pheophytin - a determination method in the marine water samples. Tr. IOAN. SSSR. M. 95: 138-146. (in Russian).

Use of multi-sensor remote sensing to detect seasonal and interannual variability in chlorophyll *a* distribution in the Sea of Okhotsk

Chizu Matsumoto[1], S. Saitoh[1], F. Takahashi[2] and M. Wakatsuchi[3]

[1] Laboratory of Marine Environment and Resource Sencing, Graduate School of Fisheries Sciences, 3-1-1, Minato, Hakodate, Hokkaido, 0418611 Japan. e-mail: chizu@salmon.fish.hokudai.ac.jp

[2] Remote Sensing Technology Center of Japan, Harumi Island Triton Square, Office Tower X 21F, 1-8-10 Harumi Chuo-ku, Tokyo, 104-6021 Japan.

[3] Institute of Low Temperature Science, Hokkaido University, Hokkaido University Kita-19, Nishi-8, Kita-ku, Sapporo, 060-0819 Japan.

Introduction

The Sea of Okhotsk experiences not only spring blooms but also fall blooms, a phenomenon that is characteristic of temperate regions. Both types of blooms influence the seasonal variability of chl-*a* concentrations. In the past, however, there were few studies about chl-*a* distribution in the Sea of Okhotsk (e.g. Nezlin et al., 1997, Saitoh et al. 1996). We use multi-sensor remote sensing to analyze the seasonal and interannual variability of chlorophyll *a* (chl-*a*) distributions in the Sea of Okhotsk between 1998 and 2001. Our objectives are: 1) to examine the possibility of ice-edge bloom and open-water bloom and their spatial and interannual characteristics in the Okhotsk Sea after sea ice retreat, and 2) to understand the aerial and year-to-year characteristics of variability of chl-*a*.

Satellite data

The satellite data used are summarized in Table 1. We obtained Sea Wide Field-of-view Scanner (SeaWiFS; v4)-derived chl-*a* concentration data for eight days over the period February 1998 to June 2001, in addition to monthly (January 1998 – December 2001) composite global standard mapped images from NASA Goddard Space Flight Center's Distributed Active Archive Center (DAAC). Chl-*a* data sets have a spatial resolution of about 9 × 9 km. To investigate the seasonal and interannual variability, we used monthly composite chl-*a* data. For the analysis of spring bloom (ice-edge and open-water), we used composite chl-*a* data from eight day periods. We obtained chl-*a* concentration data for each month (eight day) from 1998 to 2001, and generated images of the highest and lowest values to investigate periods of phytoplankton blooms. As a result of cloud cover, some data points were missing from the eight-day chl-*a* concentration data set. To better estimate the highest and lowest chl-*a* concentrations, spatial interpolation was used if more than three normal data points surrounded eight grid points in the eight-day mean chl-*a* image. SeaWiFS-derived eight-day composite photosynthetically active radiation (PAR) data sets (9 × 9 km) were also obtained from DAAC. Advanced Very High Resolution Radiometer (AVHRR)-derived eight-day

Table 1 Relevant information concerning the satellite data used in the present study.

Satellite	Sensor	Parameter	Temporal scale	Spatial scale
Orbview-2	SeaWIFS***	Chlorophyll-a concentration	Monthly mean	9km × 9km
			8 days mean	9km × 9km
	SeaWIFS***	Photosynthetically active radiation (PAR)	8 days mean	9km × 9km
DMSP*	SSM/I****	Sea ice concentration	daily	25km × 25km
NOAA**	AVHRR*****	Sea surface temperature	8 days mean	9km × 9km

*Defense Meteorological Satellite Program
**National Oceanic and Atmospheric Administration
***Sea Wide Field-of view Scanner
****Special Sensor Microwave Imager
*****Advanced Very High Resolution Radiometer

composite sea surface temperature (SST) data obtained from National Oceanic and Atmospheric Administration (NOAA) Special Sensor Microwave Imager (SSM/I)-derived sea ice concentration data obtained from National Snow and Ice Data Center (NSIDC), Distributed Active Archive Center, University of Colorado, Boulder, CO, U.S.A. The data sets that we obtained had had the bootstrap algorithm applied to them (Comiso 1986; Comiso and Sullivan 1986).

Method

To distinguish between bloom types, we used the period from sea ice retreat to spring bloom occurrence. The period of ice retreat was defined as the period when the percent coverage by ice reached zero. The spring bloom was defined as the period of highest chl-*a* concentrations. Both images are 9-km equal-angle grids, so each pixel in the two images has a corresponding counterpart. We defined ice-edge and open-water blooms as phenomena that typically continue for at least one week. Considering the time interval of one period of chl-*a* measurement (8 days), two possible extremes existed for ice-edge blooms: (a) sea ice retreated very early within the eight days, and the bloom occurred within the same interval; or (b) sea ice retreated late during the eight-day interval, and the bloom continued over the next eight days. We defined both cases as ice-edge blooms. Open-water blooms, therefore, were defined as spring blooms that did not occur as either of these cases.

To investigate the seasonal and interannual variability in the distribution of phytoplankton, we used the Binary Decision Tree classifier (BDT) method. We classified seasonal and interannual variability in monthly chl-*a* concentrations into eight classes based on three criteria: (1) the highest monthly chl-*a* concentration associated with phytoplankton bloom (threshold = 3.0 mg·m^{-3}); (2) the lowest monthly chl-*a* concentration associated with nutrient depletion (threshold = 0.3 mg·m^{-3}); and (3) the periods of highest monthly chl-*a* concentration associated with phytoplankton blooms (threshold = before July and after August).

Results and discussion

Throughout the four-year study, ice-edge blooms occurred predominantly on the northeast shelf (ice-edge blooms dominated in 1998 and 1999; open-water blooms dominated in 2000 and 2001) and in the southwest (ice-edge bl0oms dominated in 1999 and 2001; open-water blooms dominated in 1998 and 2000) (Fig. 1). The most important factor required to characterize spatial and temporal variability of spring blooms is the timing of sea ice retreat, while a secondary factor is the adjustment of insolation. Based on this adaptation to light, the mechanics of ice-edge blooms in the Sea of Okhotsk may resemble results observed in the Bering Sea (Niebauer et al., 1990) but different from the result of the Chukchi Sea (Hameedi 1978).

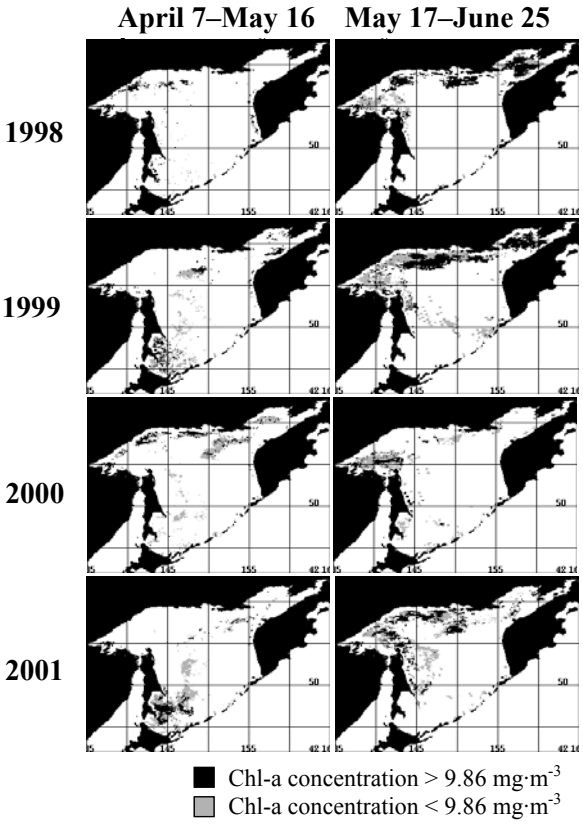

Fig. 1 Temporal and spatial variability of ice edge blooms (left side: from April 7 to May 16, right side: from May 17 to June 25); black indicates the regions where chl-*a* concentrations were higher than that of the four-year mean ice edge bloom (>9.86 mg·m^{-3}) and grey indicates regions where chl-*a* concentration were <9.86mg·m^{-3}.

From the analysis of BDT method, we classified the seasonal distribution of chl-*a* into six provinces. Province A is characterized by high chl-*a* concentrations throughout the year (>1.0 mg·m^{-3}), a peak above 7.0 mg·m^{-3} in May, and

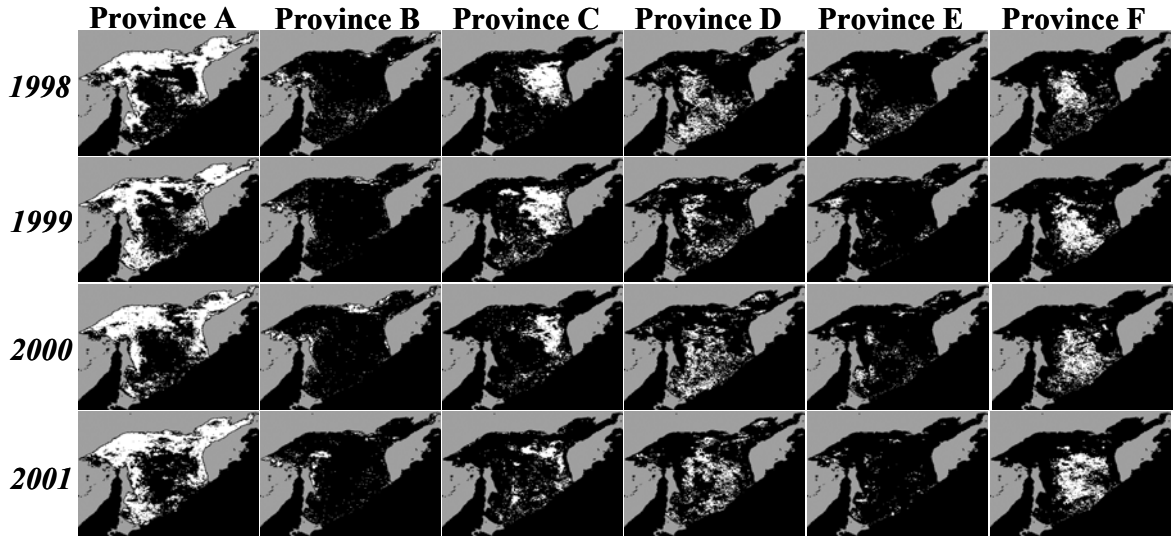

Fig. 2 Spatial distributions of each classified province in 1998 to 2001. White areas in the image show the area of each province as defined by the BDT classification.

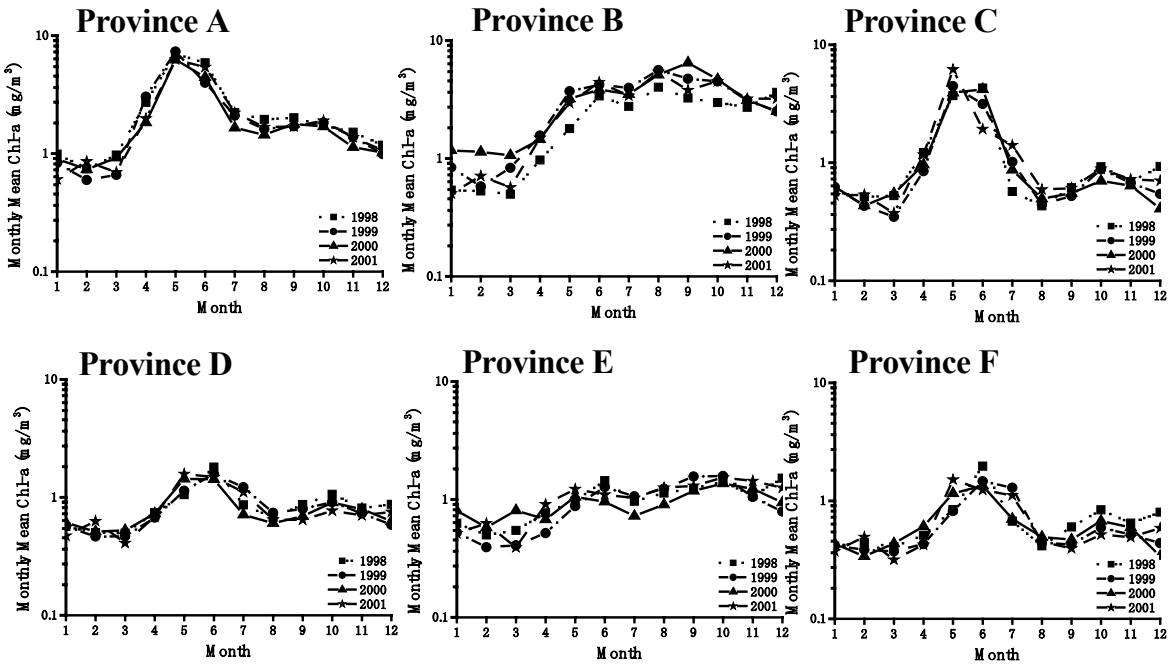

Fig. 3 Seasonal variation in chl-a concentration of each province from 1998 to 2001. Graphs show changes in monthly mean chl-*a* concentrations in each province from 1998 to 2001.

occupying more than 40% of the sea shallower than 200 m. Province B is affected by discharge from the Amur River. Province C occupies areas off the coast of the Kamchatka Peninsula throughout the four study years, and its distribution shows large year-to-year variability, ranging from 10.3-19.5%. Province D and E are characterized, particularly in the southwestern area, by their relation to sea ice distribution and ice-edge blooms. Province F, is located in the central basin, has the lowest monthly minimum chl-*a* concentration (<0.4 $mg \cdot m^{-3}$) of the six

provinces (Figs. 2, 3). Our results suggest that the magnitude of ice-edge blooms affects the extent of primary productivity in the Sea of Okhotsk through atmosphere-ice-ocean coupled influences on biological processes. A more quantitative approach using a physical-biological coupled model is required to better understand energy transfer and the carbon budget in the Sea of Okhotsk.

References

Comiso, J.C. 1986. Characteristics of Arctic winter sea ice from satellite multispectral microwave observations. Journal of Geophysical Research 91 (C1): 975-994

Comiso, J.C. and Sullivan, C.W. 1986. Satellite microwave and in-situ observations of the Weddell Sea ice cover and its marginal ice zone. Journal of Geophysical Research 91 (C8):9663-9681.

Hameedi M.J. 1978. Aspects of water column primary productivity in the Chukchi Sea during summer. Mar. Biol. 48: 37-46.

Nezlin, N.P., Musaeva, E.I. and D'yakonov, V. Yu. 1997. Estimation plankton stocks in the western part of the Bering Sea and the Sea of Okhotsk. Oceanology 37(3): 370-375.

Niebauer H. J., Alexander, V. and Henrichs, S. 1990. Physical and biological oceanographic interaction in the spring bloom at the Bering Sea marginal ice edge zone. Journal of Geophysical Research 95 (C12): 22229-22241.

Saitoh S., Kishino, M., Kiyofuji, H., Taguchi, S. and Takahashi, M. 1996. Seasonal variability of phytoplankton pigment concentration in the Okhotsk Sea. J. Remote Sensing Soc. Japan 16 (2): 86-92.

Determining factors of the spatial distribution of phytoplankton in the Okhotsk Sea: A study by the ecosystem model

Takeshi Okunishi[1] and Michio J. Kishi[2,3]

[1] ECONIXE Co., Ltd., Techno-park 1-2-14, Shimonopporo, Atsubetu-Ku, Sapporo, Hokkaido, 004-0015 Japan. e-mail: t-okunishi@econixe.co.jp

[2] Graduate School of Fisheries Sciences, Hokkaido University, Minato-cho 3-1-1, Hakodate, Hokkaido, 041-8611 Japan.

[3] Frontier Research System for Global Change, 3173-25 Showamachi, Kanazawa-ku, Yokohama, 236-0001 Japan. e-mail: kishi@salmon.fish.hokudai.ac.jp

Introduction

The Okhotsk Sea is one of the most biologically productive regions in the world, and it supports high fisheries production. It has been reported that diatoms are a major component of the phytoplankton in this sea (e.g. Hanzawa et al. 1981). Previous observations revealed maximum diatom cell numbers in spring and minima in autumn. Shiomoto (1997) showed that picoplankton (<2μm) and nanoplankton (2-10μm) (small-sized phytoplankton) generally contributed greatly to Chl-*a* concentration in more than 70% of the southern part of the Okhotsk Sea in late autumn (October) and early winter (November). Previous studies did not discuss thoroughly the factors in determining the spatial distribution of the phytoplankton in autumn and spring bloom periods and the effect of the sea ice on the spring bloom in the Okhotsk Sea.

Using a three-dimensional ecosystem model for the Okhotsk Sea, we attempt to discuss questions such as: What is the most important process to control the autumn and spring bloom? How much does the amount of sea ice effect on the spring bloom?

Model

A three dimensional ecosystem-physical coupled model is applied to the Okhotsk Sea. For the physical model, we use a sigma-coordinate model by developed at Harvard University called Harvard Ocean Prediction System (Lozano et al. 1994; Robinson 1996). Parameterization of Pacanowski and Philander (1981) is adopted to calculate vertical diffusivity and viscosity. For the ecosystem model, we use NEMURO, which is coupled with the physical model. NEMURO is a nitrogen- and silica-based model with eleven compartments. This ecosystem model has eleven compartments including two categories of phytoplankton (diatoms and small phytoplankton other than diatoms) and three categories of zooplankton (small, large and predatory zooplankton).

Results and discussion

Autumn bloom The model was run through October and November in 1996 for 30 days. Small-phytoplankton (PS) contribution to Chl-*a* concentration accounted for more than 65% in this study. The simulated distributions of PS (mg Chl-a/l) agreed with observations. Chl-*a* concentration is high in the east of Sakhalin Island and low in the southern part of the Okhotsk Sea. East of Sakhalin Island, a very shallow mixed layer develops because the salinity of the surface water is reduced by the discharge from the Amur River. Because of a very shallow mixed layer, net primary production is high in the surface layer. On the other hand, in the southern Okhotsk Sea, Chl-*a* concentration is low because the deep mixed layer reduces the growth efficiency of phyto-plankton. However, net primary production is not extremely lower in this area than in other high Chl-*a* areas. Thus, Chl-*a* concentration distri-bution does not necessarily reflect net primary production in the Sea of Okhotsk in autumn.

Spring bloom

An ecosystem-physical coupled model included sea ice effects (light condition under ice, moment and salinity flux between ice and sea). But, nutrient fluxes between ice and sea are not considered. Thickness of the sea ice is estimated from satellite data (Tateyama 2001).

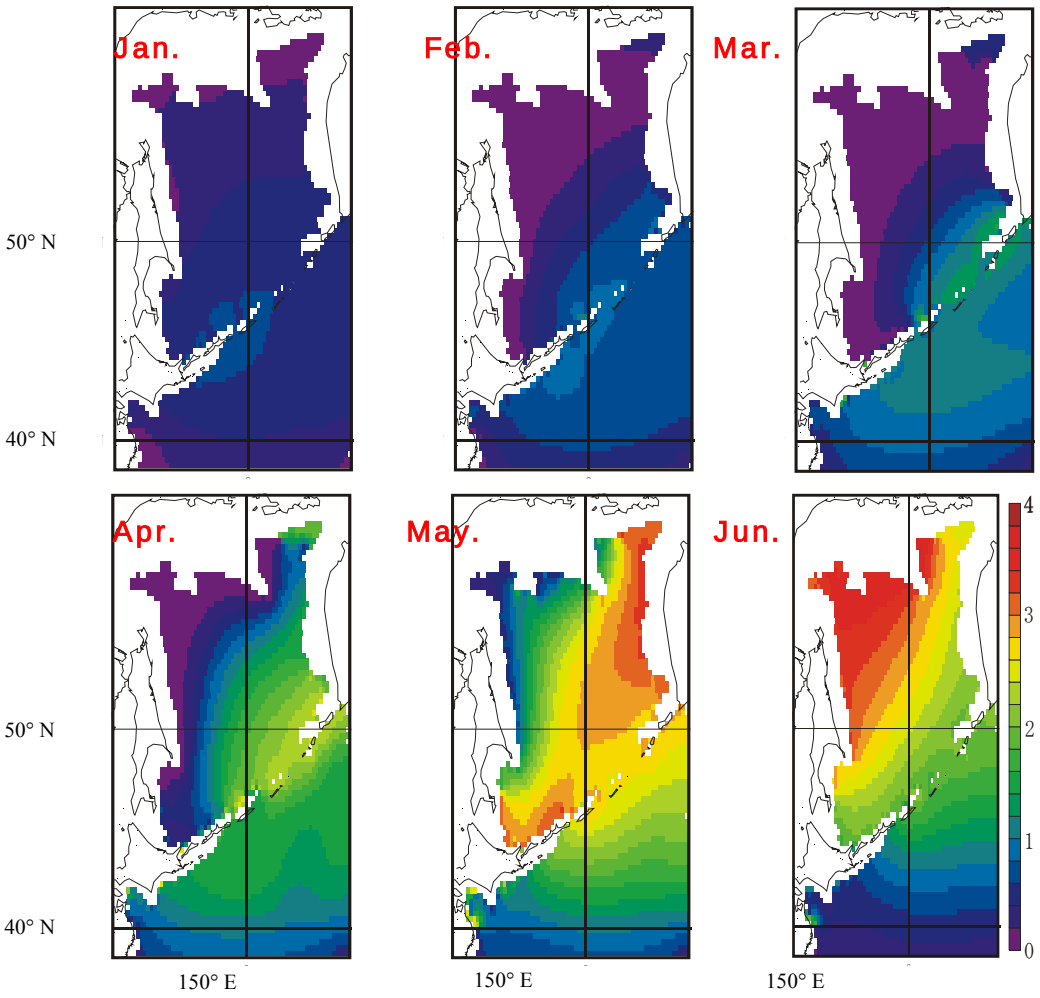

Fig. 1 Time evolution of monthly mean Chl-*a* concentration (mg/m^3) of PS and PL in the surface 3 layers (0-20 m) averages in 2001 as the model results. Conversion from nitrogen to Chl-*a* is done using N:C = 17:133 (mol ratio) and C:Chl-*a* = 50:1 (weight ratio).

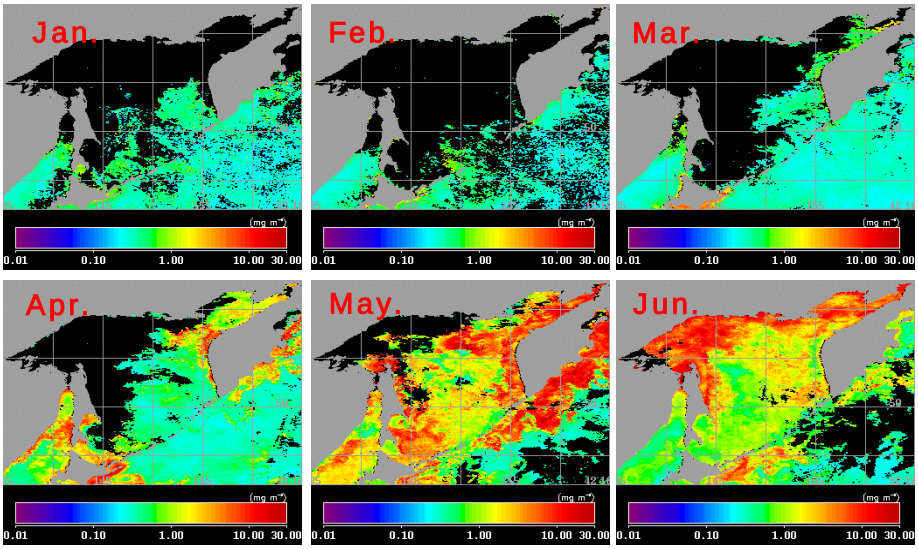

Fig. 2 Time evolution of monthly mean SeaWiF-Chl images during January-June in 2001.

The model was run through winter and spring in 1997 (a year with lesser ice-cover) and in 2001 (a year with large ice-cover). According to the model results, the total stock of $Si(OH)_4$ in the surface layer (0-20 m) in March 2001 is a larger than that in 1997 by about 10%. Vertical mixing of water column develops when the sea ice grows. However, the total stock of $Si(OH)_4$ in the surface was not much different between 1997 and 2001. It suggests that the growth of sea ice may be not important for supplying nutrients to the sea surface. We can reproduce the spatial distribution of phytoplankton at the spring bloom in 1997, 2001 in the Okhotsk Sea by a three dimensional ecosystem-physical coupled model (Figs. 1 and 2 in 2001). From the model, the arrival of the spring bloom in the Okhotsk Sea is a consequence of an increase of photosynthetic rate both in 1997 and 2001. So, the photosynthetic rate of phytoplankton depends on the light environment in the euphotic zone from winter and spring in Okhotsk Sea. The light intensity under the sea ice is too low. The timing of sea ice melting may effect a time-lag of spring bloom, and have an effect on the spatial distribution of phytoplankton in the Okhotsk Sea.

Distribution patterns for the gonatid squid *Gonatus madokai* in the Okhotsk Sea in spring 2002

Oleg N. Katugin, A. Yu. Merzlyakov, N.S. Vanin and A.F. Volkov
Pacific Fisheries Research Centre (TINRO-Centre), 4 Shevchenko Alley, Vladivostok, 690950 Russia. e-mail: okatugin@mail.ru

Squids of the family Gonatidae are of major importance in the North Pacific Ocean, being highly abundant in pelagic communities all over the vast boreal zone (Nesis 1973, 1997; Okutani et al. 1988). At the same time, taxonomy of the gonatid squids remains poorly developed largely due to the fact that there is scarce information on mature stages for most of the species encountered in the family. Taxonomic problems, in turn, produce a lot of uncertainty in evaluation of significance of a particular species in complex pelagic assemblages. Up to 9 species from all three genera of the gonatid family are found in the Okhotsk Sea, namely: *Berryteuthis magister* (one of the most abundant demersal species), *Berryteuthis anonychus* (occasionally observed epipelagic species), *Gonatopsis borealis* (very abundant epi- and mesopelagic species), *Gonatopsis octopedatus* (rarely caught though probably abundant species in the bathypelagic zone), *Gonatopsis japonicus* (rarely though regularly observed bathypelagic species in the deep-water areas), *Gonatus tinro* (rather common mesopelagic species), *Gonatus kamtschaticus* (rarely caught mesopelagic species), *Gonatus onyx* (rarely caught meso- and bathypelagic species), and *Gonatus madokai* (rather common eurybathic species). Information on life history of most of those species is scarce. We have gathered detailed data on occurrence and biology of the squid *G. madokai* in order to reveal whether distribution of different life stages reflects the species life history. Hence, our main objectives were to look at distribution of different ontogenetic stages of this squid, and to relate the observed patterns with physical and biological environmental characters such as currents, temperature, pycnocline, prey availability.

Geographical range of *G. madokai* covers almost the entire subarctic Pacific area, including the Okhotsk Sea where the squid frequently occurs in epi-, meso-, and bathypelagic tows (Kubodera and Okutani 1977; Nesis 1997). An increase of the squid average size with depth has been noticed in the Okhotsk Sea, and both diel vertical migrations and ontogenetic descent were suspected (Nesis 1997). In spite of considerable amount of information collected on the squid occurrence and biology, little is known about its distributional patterns and life cycle. Mostly juveniles and immature adults of *G. madokai* have been caught so far with only occasional occurrence of mature males and gaining maturity females (Kubodera and Okutani 1977; Nesis 1997). No fully mature or spent females have been registered until recently (Katugin and Merzlyakov 2002). Gelatinous degeneration of tissues has been reported only for females, and it starts presumably before the onset of maturation (Nesis 1998; Katugin and Merzlyakov 2002). Herein, we present new data on *G. madokai* different life stages distribution across almost the entire Okhotsk Sea, with particular attention to our findings of degenerated gelatinous spent females, and their occurrence. The material examined was collected by sampling program of TINRO-Centre during annual survey in the Okhotsk Sea from March till early June, 2002, on the research vessel *RV Professor Kaganovskyi* employing midwater trawl 53/360 (40 m horizontal spread at a trawling speed of 3.5 knots on the average) with a 12 mm mesh liner in the cod end. Epi- and mesopelagic layers down to 450 m depth were investigated by trawling hauls.

During the survey, a total of 636 individuals of *G. madokai* were caught, 548 of them immature. The rest 88 specimens were large spent females (Fig. 1). No either fully mature or spent male was registered. Immature squid ranged in size from 25 to 240 mm DML. Exact size of spent females was hard to evaluate due to serious damage of gelatinous and watery bodies in the net (most

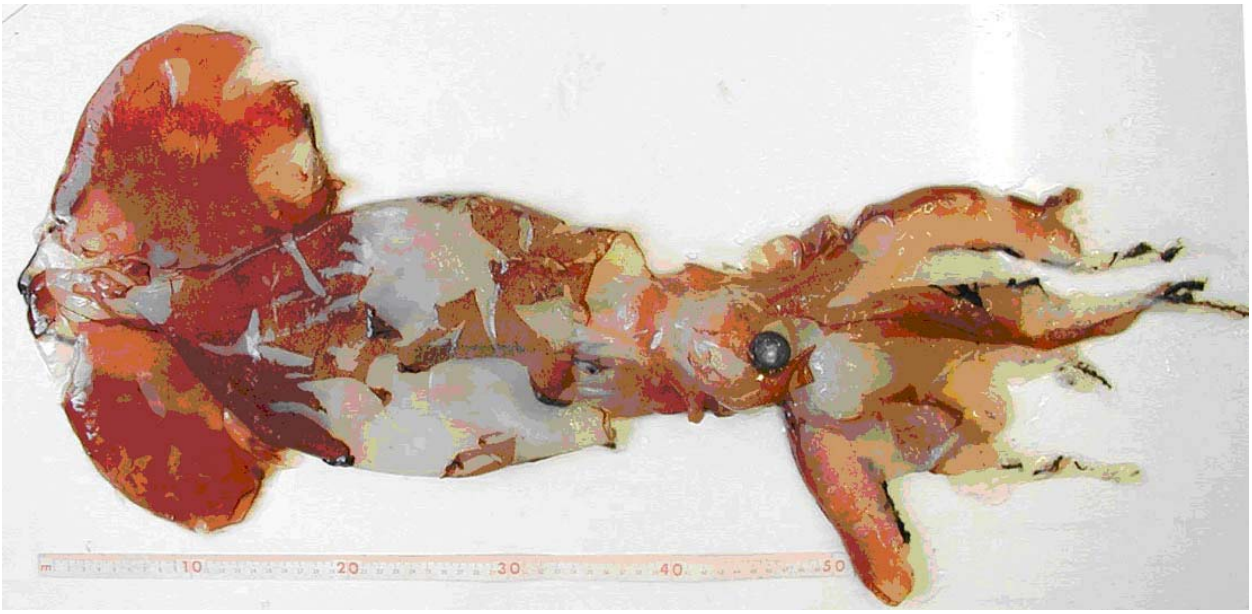

Fig. 1 *Gonatus madokai*: general view of the spent senescent female.

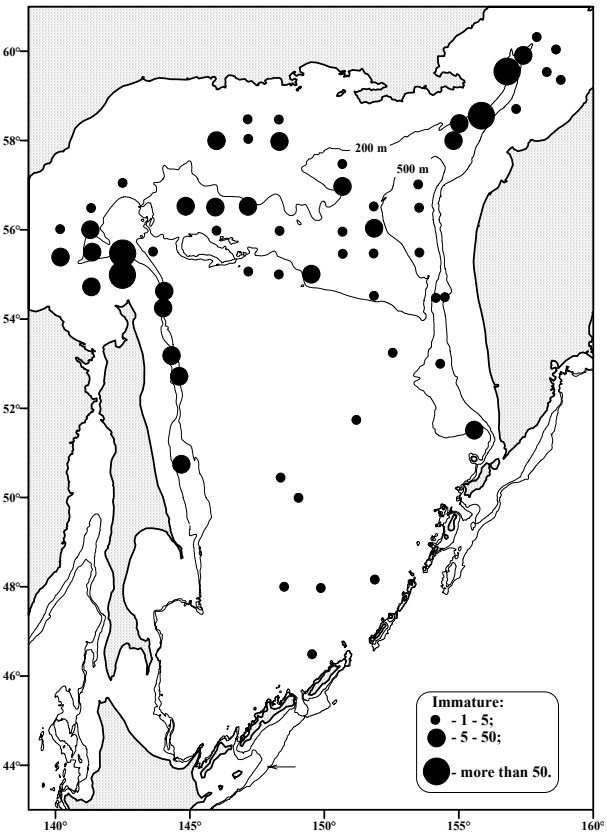

Fig. 2 *Gonatus madokai* distribution of juveniles and immature adults; black circles correspond to ranked occurrence of the squid per hour trawling.

specimens appeared on board the RV with their fins torn off, and mantles broken), and hence gladius length (GL) was measured where possible. GL of 21 spent females with intact gladii ranged from 308 to 385 mm (mean 350.33 mm, mode 340 mm). No individuals with intermediate sizes and with developing reproductive system were present in the trawling hauls. The presence of only immature and spent animals in the epi- and mesopelagic hauls may suggest that at the onset of sexual maturation the squid descend to deeper bathypelagic zone, that was not covered by the trawling operations.

Large senescent females were totally spent with only occasional ripe oocytes (ovoid in shape, and up to 5 mm maximum length) present in the oviducts, and with exhausted dark yellow ovaries. Bodies of spent females were swelled and gelatinous in appearance: mantle wall approximately 10 mm thick, all arms of about 30 mm thick at their bases. No tentacles were present, only their small, approximately 10 mm long remnants were left, suggesting that tentacles were autotomized earlier, presumably at the onset of maturation. Only hooks were left on the arms, and shreds of dark brown to black tissue were associated with the hooks of arms I-III in some animals, which we suppose are remnants of egg-masses that females carry attached to their arms.

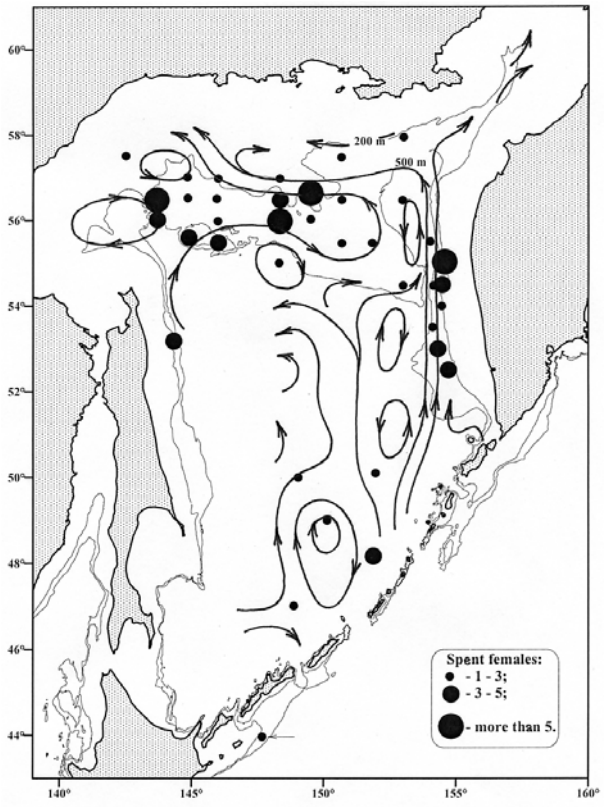

Fig. 3 *Gonatus madokai*: distribution of spent females; black circles correspond to ranked occurrence of the squid per hour trawling; arrows correspond to main geostrophic currents at 100 m depth.

Two strikingly different patterns of *G. madokai* distribution in the Okhotsk Sea were revealed during the spring trawl survey, and were clearly associated with the squid life-cycle stages. First type of distribution was characteristic for juveniles and immature growing up adults. These young and advanced life stages of *G. madokai* did not show differences in their distributional patterns, and occurred unevenly within the entire sea, with incidental catches over great depths in the southern Okhotsk Sea and shelf areas (Fig. 2). Young squid formed comparatively high concentrations in several highly productive areas of the Okhotsk Sea, mostly in its northern part, particularly, in the Shelikhov Bay, north of Kashevarov Bank, in northern Sakhalin frontal zone. Concentrations of juvenile squid were also found off the southwestern Kamchatka over Lebedev Bank, and along the eastern Sakhalin outer shelf. All these regions are areas with complex hydrodynamic systems such as upwellings, counter-currents, frontal zones. We may suggest that young and advanced immature life stages of *G. madokai* gather predominantly in areas with high abundance of food organisms required for the squid rapid growth. Squid in general are known to be active opportunistic carnivores at all stages (Nixon 1987). Few data on stomach contents of *G. madokai* suggest that the species consumes crustaceans, fish and squid, though its food items also include chaetognaths (*Sagitta spp*.), and salps (Nesis 1997). Occurrence of young and immature adult stages of *G. madokai* appeared associated with distribution patterns of the species potential prey, such as dominant zooplankton groups within the Okhotsk Sea: euphausiids (*Thysanoessa raschii* and *T. longipes*), copepods (*Neocalanus plumchrus*) and chaetognaths (*Sagitta elegans*).

Quite different type of distribution was characteristic for spent females of *G. madokai*, and was evidently associated with general circulation pattern and water mass structure. Spent females occurred in constantly low quantities (one to several animals per hour trawling) in the southern Okhotsk Sea, along western Kamchatka area, and all over northern Okhotsk Sea (Fig. 3). In total, 12% of all hauls contained spent *G. madokai*, and of those positive hauls 63% were taken in the northern Okhotsk Sea. On the average, 2.44 animals per positive haul were present, with a mode of 1, and a maximum of 12 animals per haul. No differences in the squid occurrence in epi- and mesopelagic layers were observed suggesting that the animals were possibly caught during taking the net on board the RV from rather narrow upper part of the water column. Most spent individuals were caught over the slope area bounded by 200 and 500 m depth contours, with only few catches on the shelf (northern Okhotsk Sea) and over deep regions (southern Okhotsk Sea). Geographic range of spent females in the Okhotsk Sea generally coincided with the area covered by waters of the Western Kamchatka Current (WKC). This strong current, carrying comparatively warm and high salinity Pacific Ocean water, enters the Okhotsk Sea through the Kruzenshtern Pass, and forms two major streams, with variable strength and position depending on season and year. In the spring 2002, both WKC streams were well developed. Pacific waters penetrated far north into

the northern Okhotsk Sea through the Kashevarov Bank with the western WKC branch, and through the TINRO Basin – with the eastern WKC flow. Northern cyclonic circulation, and southward Compensatory Countercurrent along the Kamchatka coast appeared weakly expressed. Warming up was observed within the pycnocline, and warm water at 100 m depth was distributed as far to the north as 58˚N both in the western and eastern parts of the northern Okhotsk Sea, coinciding with the northern boundary for *G. madokai* spent females range.

Of particular interest is that though confined to the WKC system, spent females of *G. madokai* were found in the regions with comparatively low hydrodynamics, dwelling apart from areas with disturbing physical factors such as strong horizontal flows and upwellings. Spent animals were observed outside the main streams with high velocities, e.g., on the edge of comparatively weak eastern branch of WKC, and at the periphery of eddies, e.g., upon the TINRO Basin, and to the west of Kashevarov Bank.

We may suggest that spent females were confined to relatively warm intermediate (dichothermal) layer, and their distribution pattern generally coincided with positive temperature isotherms at depths of about 100 m. Moreover, several biological considerations, concerning primarily such items as buoyancy, energetics and presumed baby-care burden, suggested that senescent spent females with high water content in muscle tissues aggregated predominantly within a restricted zone of water column that could provide better conditions for them. This should be rather warm layer with comparatively high gradient in water density. Pycnocline with positive temperatures must have provided suitable habitat for spent females to effectively (with a minimum loss of energy) reside during prolonged egg-brooding period, while geostrophic currents provided transportation routes and barriers for water-logged medusa-like females within the vast areas of the Okhotsk Sea thus forming the observed pattern of their spatial distribution.

As a result, our main findings concerning distribution patterns of *G. madokai* in the Okhotsk Sea were as follows: 1) immature and spent individuals were distributed in different manner; 2) immature animals were distributed according to prey availability; 3) spent females carrying egg-masses were distributed in relation to hydrological conditions such as currents, temperature, and pycnocline, thus suggesting that they lead rather passive life, floating within the favorable zone of the water column, presumably within comparatively warm layer of density change.

References

Katugin, O.N., and Merzlyakov, A.Yu. 2002. Spent females of *Gonatus madokai* (Teuthida: Oegopsida) from the Okhotsk Sea. pp. 39-40 in "1st International Workshop of squids, 2nd International Symposium of Pacific Squids", La Paz, Baja California Sur, Mexico.

Kubodera, T., and Okutani, T. 1977. Description of a new species of gonatid squid, *Gonatus madokai* n. sp. from the north-west Pacific, with notes on morphological changes with growth and distribution in immature stages (Cephalopoda: Oegopsida). Venus 36 (3): 123-151.

Nesis, K.N. 1973. Taxonomy, phylogeny and evolution of squids of the family Gonatidae (Cephalopoda). Zoologicheskii Zhurnal (Zoological Journal), 52(11): 1626-1638. (In Russian with English summary).

Nesis, K.N. 1997. Gonatid squids in the subarctic North Pacific: ecology, biogeography, niche diversity and role in the ecosystem. Advances in Marine Biology 32: 243-324.

Nixon, M. 1987. Cephalopod diets. *In* P.R. Boyle (ed.) "Cephalopod Life Cycles. Vol. 2. Comparative Reviews." Academic Press, London. pp. 201-219

Okutani, T., Kubodera, T. and Jefferts, K. 1988. Diversity, distribution and ecology of gonatid squids in the subarctic Pacific: a review. Bulletin of the Ocean Research Institute, University of Tokyo 26 (1): 159-192.

Distribution and biomass of Boreopacific gonate squid (*Gonatopsis borealis*, Sasaki, 1929) in the Okhotsk Sea and Pacific waters off the Kuril Islands during the winter period

Michail A. Zuev
Pacific Research Fisheries Centre (TINRO-Centre), 4 Shevchenko Alley, Vladivostok, 690600 Russia.
e-mail: mokrin@tinro.ru (for Zuev)

The boreopacific gonate squid, or northern gonatopsis, is a robust, muscular, nektonic gregarious squid. *G. borealis* is one of the most common and most widely distributed gonatids (Nesis 1997). This work is based on five complex trawl surveys of the Okhotsk Sea and three in the Pacific waters off the Kuril Islands during winter periods. The purpose of this work was to ascertain the regularities in distribution of the boreopacific gonate squid.

The Okhotsk Sea, especially around the Kuril islands, region is a very complex hydrodynamical region. A current passes from East Kamchatka along the Kuril islands to south the Kuril. Through the northern Kuril straits, the Kuril Current enters the Okhotsk Sea and forms the West Kamchatka Current. From the west, through the La Perouse Strait, the Soya Current penetrates into the southern Okhotsk Sea. The southern part of the Soya Current paaes through Bussol' Strait, meeting the Kuril Current and forming the Oyashio Current. The important influence of the hydrodynamic regime in the Okhotsk Sea waters makes the warm Soya Current and the cool Kuril Current (Istoki Oyashio, 1997).

In the Okhotsk Sea, *G. borealis* occurs mostly south of 58°N, avoiding the shelf zone along the north coast. In different years, abundance of *G. borealis* varied in the epipelagic layer from 13.25 kg km^{-2} during the winter of 1990/91 to 149.5 kg km^{-2} at the end of 1995. In the mesopelagic layer, abundance varied from 55.3 kg km^{-2} along the western part of the Kamchatka Peninsula in 1995, to 132.5 kg km^2 in the southern part of the Okhotsk Sea in 1991. In the northern regions of the Okhotsk Sea, where the surface waters are cool, the northern gonatopsis was observed in the mesopelagic layer. On the whole, especially in the southern part of the Okhotsk Sea, the boreopacific gonate squid is rather uniformly distributed, not forming large shoals (Fig. 1., Table 1).

The Kuril Current influences the density of the northern gonatopsis in the dynamic waters of the Kuril Islands. Frequency occurrence of the boreopacific gonate squid was approximately 78% in tows in the mesopelagic layer and 40% in the epipelagic layer. Nevertheless, density and biomass of *G. borealis* in the epipelagic layer are usually higher than in the mesopelagic layer (Table 1).

In the epipelagic Pacific waters off the Kuril islands, boreopacific gonate squid is capable of forming large shoals. Near the central and the northern Kuril islands, large shoals of the northern gonatopsis squid occurred in epipelagic layer, about 16 t km^{-2} near Lopatka Cape at the end of 1991 (Fig. 1G). Also a large amount of boreopacific gonate squid (> 3 t km^{-2}) was noted in Bussol' Strait at the end of 1995 (Fig. 1F).

In the open Pacific waters of the central Kuril islands during the winter of 1994/95, a large amount of northern gonatopsis was noted, about 8 t km^{-2} (Fig. 1H). Consequently, in the open Pacific waters near the Kuril islands, *G. borealis* is capable of forming large aggregations.

Conclusions

- In the Okhotsk Sea, south of 58°N, *G. borealis* density is distributed evenly, and the thick aggregations are not formed.
- North of 58°N, *G. borealis* is practically absent, avoiding the coastal shelf zone.
- One can frequently encounter *G. borealis* on the Pacific side of the Kuril islands in the mesopelagic layer, but its occurrence in large aggregations are found in the epipelagic layer.

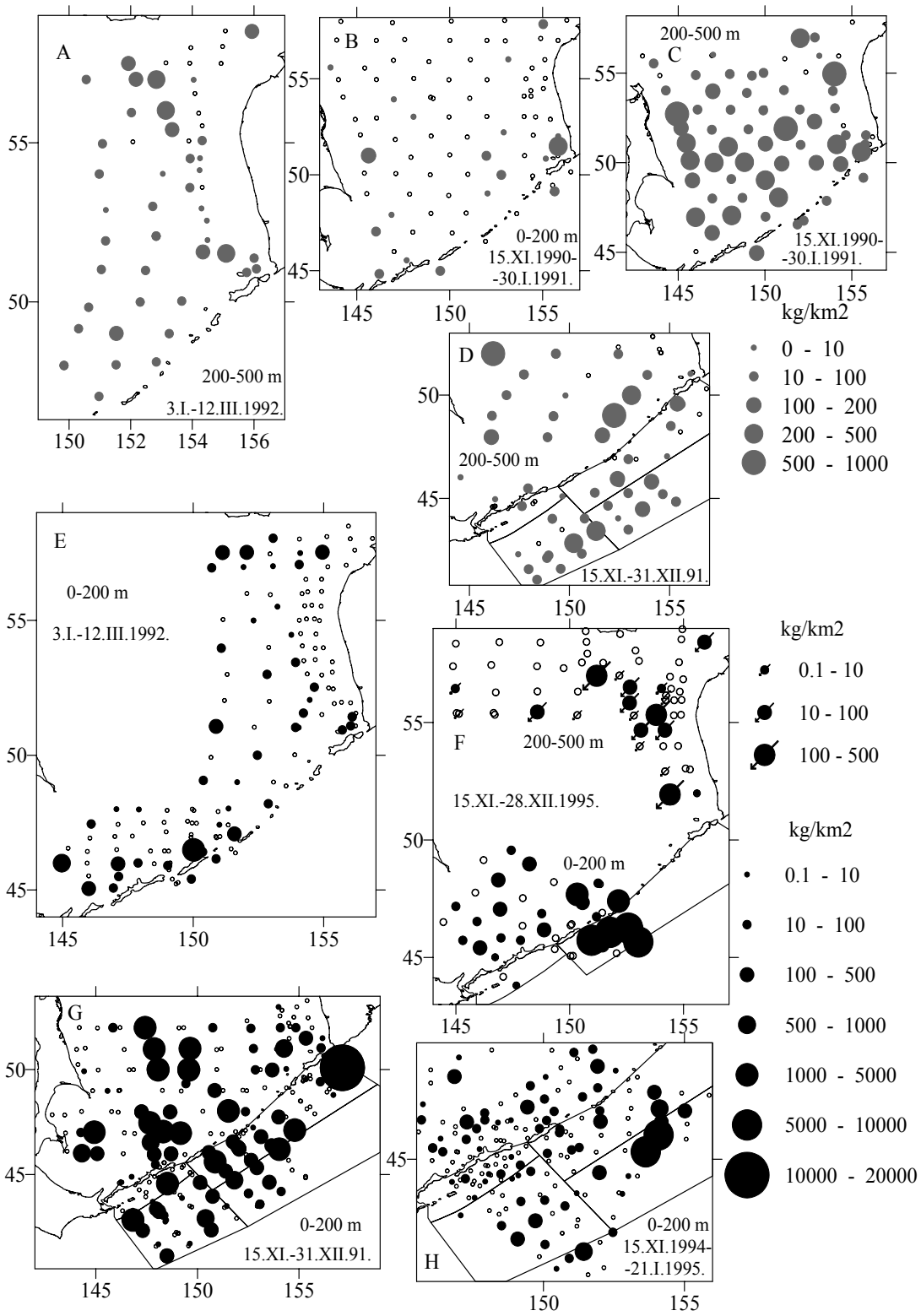

Fig. 1 Abundance of *G. borealis* (kg km^{-2}) in Okhotsk Sea and Pacific waters off the Kuril Islands during the winter period.

Table 1 Period of the investigations, occurrence, abundance and biomass of *G. borealis* in winter period.

Period of investigation	Region of investigation	Layer, m	Freq. of occurrence, %	Abundance, kg/km^2	Area of investigation, thousand km^2	Biomass, thousand t
15.XI.1990-30.I.1991	Pacific waters of central and northern Kuril Islands	0 – 200	33,3	13,8	76,6	1,1
		200 - 500	100,0	67,7		5,2
	Okhotsk Sea	0 – 200	23,5	13,25	1073,4	14,2
		200 – 500	81,3	123,5		132,5
15.XI.-31.XI.1991	Okhotsk Sea	0 – 200	32,7	171,7	655,0	112,5
		200 – 500	50,0	132,5	627,0	83,1
	Pacific waters of central and northern Kuril Islands	0 – 200	42,4	1212,8	153,13	104,0
		200 – 500	64,3	30,1		2,6
	open Pacific waters of central Kuril Islands	0 – 200	35,3	94,3	114,75	0,2
		200 – 500	100,0	82,9		0,17
	Pacific waters of south Kuril Islands	0 – 200	25,0	25,3	39,3	0,3
		200 – 500	33,3	1,0		0,01
	open Pacific waters of south Kuril Islands	0 – 200	44,1	138,7	136,2	2,2
		200 – 500	91,7	81,5		1,3
3.I.-12.III.1992	Okhotsk Sea	0 – 200	35,2	44,7	555,6	24,8
		200 – 500	81,1	54,7	420,5	23,0
15.XI.1994-21.I.1995	Okhotsk Sea	0 – 200	47,5	18,8	215,25	4,0
	Pacific waters of the central Kuril Islands		36,0	53,0	84,2	0,13
	open Pacific waters of central Kuril Islands		53,3	1075,4	114,75	2,2
	Pacific waters of south Kuril Islands		33,3	2,7	39,3	0,04
	open Pacific waters of south Kuril Islands		45,2	52,7	136,2	0,8
15.XI.-28.XII.1995	South part of the Okhotsk sea	0 – 200	63,3	149,5	211,3	36,2
	west Kamchatka region	200 - 500	57,9	55,3	331,0	18,3
	Byssol Strait	0 – 200	55,6	1194,2	–	–

References

Nesis, K.N. 1997. Gonatid squids in the Subarctic North Pacific: Ecology, Biogeography, Niche Diversity and Role in the Ecosystem. Advances in Marine Biology, Vol. 32. Moscow, Russia.

Istoki Oyashio. 1997. Saint-Petersburg State University, Institute of Geography. Saint-Petersburg, Russia.

Migrations of Pacific cod (*Gadus macrocephalus*, Gadidae) in the Okhotsk Sea

A.B. Savin
Pacific Fisheries Research Centre (TINRO-Centre), 4 Shevchenko Alley, Vladivostok, 690950 Russia.
e-mail: savin@tinro.ru

Former research of migration patterns of Pacific cod (*Gadus macrocephalus*) suggested that Pacific cod do not migrate outside the Okhotsk Sea. The data showed that during the summer period, cod stays within the coastal western Kamchatka area at fairly low depths, and by winter, it moves to deeper waters on the outer shelf. At the same time, cod can migrate along the western Kamchatka shelf for up to 230 miles. Later research provided new data and introduced some corrections to the known scheme of migration pattern in that cod can also migrate into the Okhotsk Sea from the eastern Kamchatka coast.

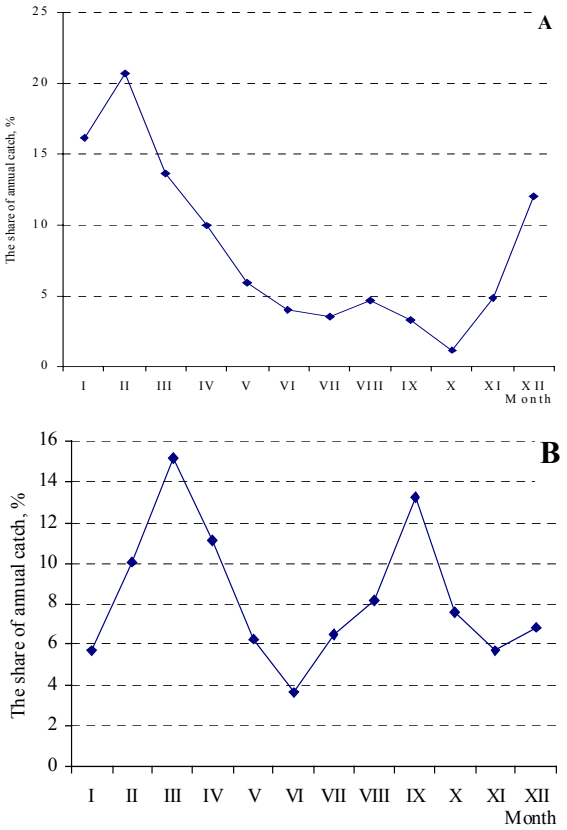

Fig. 1 Average long-standing dynamics of Pacific cod catches by month from 1995-2002: A - off the western Kamchatka coast, B- on the Pacific side of the northern Kuril Islands.

We used daily baseline information on SSD (vessel-days of catch) from the period 1995-2002, comprising a total of 24571 vessel-days. The investigation area covered the Kamchatka coast of the Okhotsk Sea, and the North Kuril islands between 50° and 58°N latitudes and 153° and 157°E longitudes. Data from the Pacific side of the Kuril islands were bounded on the north by 49° and 50°N latitudes.

The catch distribution by month was calculated from catch km^{-2} of the area covered. The total area was split into squares with sides equal to ½° latitudinal/longitudinal. The total catch of cod within each square was related to its area. The resultant catch distribution patterns generally coincide with distribution patterns obtained from trawling surveys, made during the same period.

Monthly dynamics of cod distribution were revealed. Along the western Kamchatka coast, the maximum catch of cod occurred in February, comprising 20.7% of the average annual catch (Fig. 1). The catch declines during the following months, reaching a minimum in October, when it makes up only 1.1% of the average annual catch. After that, the catch increases up to February, when it starts to rise sharply. The fishery for cod off western Kamchatka is distributed correspondingly and has its own cycle (Fig. 2). The largest area is covered by winter fishery. In January and February, the area with catches over 10 kg km^{-2} is the largest, and stretches from the southernmost part of the Kamchatka Peninsula northward to 56° N. During the following months, the area where fishery operates shrinks considerably, and in October the cod fishery remains only on the small area near Paramushir and Shumshu islands, and on the southern tip of Kamchatka. The fishery area starts to expand in November and December.

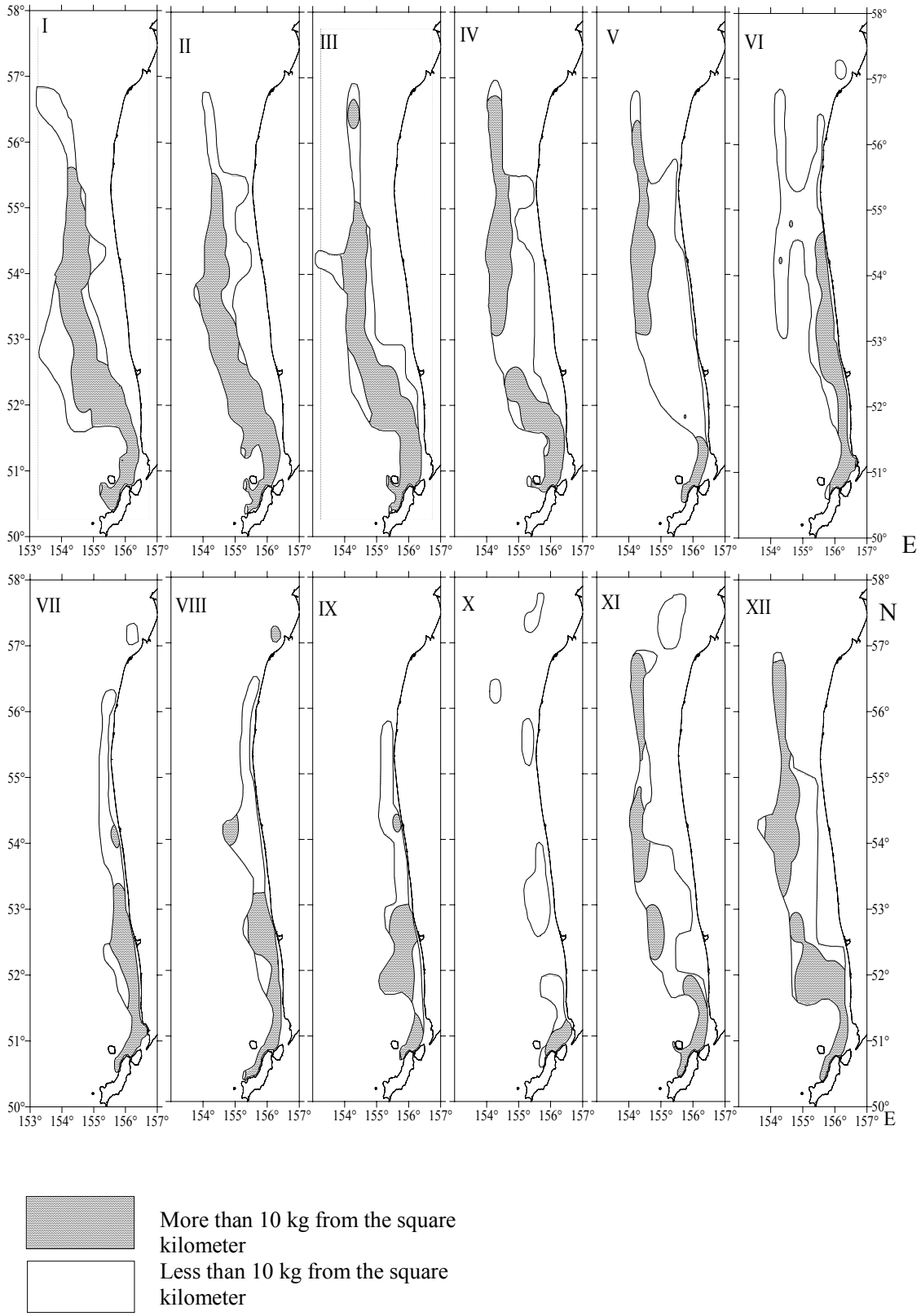

Fig. 2 Average long-term location of cod catches by month of the Kamchatka coast, 1995-2002.

Cod catch dynamics in the Pacific waters of northern Kuril Islands has two peaks during a year. One peak is in March with 15.2%, and the other is in September with 13.3% of the annual catch within this area. The lowest catch is in June and November, with 5.8% and 9.1% of the local annual catch, respectively. These peaks do not coincide with catch peaks along the western Kamchatka coast, and may be attributed to cod migrating through the Kuril straits. The peak in March is produced by cod migrating from the Okhotsk Sea, while that in November, by cod migrating into the Okhotsk Sea. This suggestion is verified by the fact that in the Okhotsk Sea, cod catch drops in the first case, and increases in the second case.

As a result, we think there exists solid evidence that cod inhabiting eastern Kamchatka shelf in summer migrates to winter into the Okhotsk Sea.

Preliminary data on the recent state of macrobenthos on the Okhotsk Sea Shelf of Sakhalin Island

Victor Nadtochy and L. Budnikova
Pacific Fisheries Research Centre (TINRO-Centre), 4 Shevchenko Alley, Vladivostok, 690950 Russia. E-mail: root@tinro.ru

The eastern Sakhalin shelf is a traditional fishing ground for many species of fish and invertebrates, and the feeding grounds of grey whales are located here (Sobolevsky et al. 2000). However, there have been no large-scale investigations of macrobenthos in the area since 1977 (Koblikov 1978, 1983; Averintsev et al. 1982). During this long period, commercial exploitation of oil deposits began in northeastern Sakhalin. For this reason, some small areas of the shelf, located just near the oil drilling, were studied (Belan and Oleinik 2000). In the summer of 2002, a large-scale survey was conducted by TINRO-Center over the whole East Sakhalin shelf with 95 benthic stations ranging in depth from 15-280 m. Station locations were located at the same points as in 1977 (Fig. 1a). Quantitative samples were collected using a bottom probe "Ocean-50" (quadrat size: 0.25 m^2), and qualitative samples were collected using a Sigsbee trawl. The samples were processed by standard methods of benthos sample processing (Neiman 1983).

Within the studied region, total biomass of benthos fluctuated in the range 19 - 4450 g m^{-2} with average 421.50±58.7 g m^{-2} (the range was 9-2170 g m^{-2} with an average of 339.12±42.09 g m^{-2} in 1977). Benthos had the highest abundance - >1 kg m^{-2} in the central part of the shelf between 52-53°N at a depth of 50-150 m in the same area as in 1977 (Fig. 1b). The most usual concentration was 100-500 g m^{-2}. The most common taxonomic groups of macrobenthos in both surveys were sea urchins, bivalves and polychaetas. Sipunculida, Ophiuraidea, and Amphipoda were abundant in 1977, but Cirripedia, Sipunculida, Amphipoda, and Spongia in 2002 (Table 1).

The biomass of sea urchins in 2002 fluctuated from 1 to 2005 g m^{-2}. Their share was slightly lower than in 1977 (Table 1). The distribution of sea urchins was similar in both years, but they were not found south of 51°N and had lower abundance northward from this latitude. The location of their concentrations had not changed (Fig. 1c). Up to 95% of sea urchins biomass was represented by *Echinarachnius parma*.

Bivalves were distributed over the whole region of study with concentrations located as before, with slight increases in biomass. It fluctuated from 0.02 to 666.5 g m^{-2} (Fig. 1d) and was the highest at 51°N at a depth of 50 m, where *Serripes groenlandicus* dominated in silted sand. This species represented 94% of bivalve biomass.

Polychaeta species were observed everywhere with concentrations of 0.06-201.2 g m^{-2} (Fig. 1e). Relative to 1977, areas with Polychaeta biomass >100 g m^{-2} became larger. *Axiatella catenata* dominated in both periods, but some other species were abundant in 2002.

Amphipods were spread over the whole shelf with concentrations of 0.02-645.4 g m^{-2}. Their distribution was distinguished by three areas of heightened abundance (Fig. 1f) and was similar in two years of surveys, in particular in the central part of the shelf at 52°N, where *Ampelisca eschrichti* dominated permanently (>500 g/m^2).

The biomass of Sipunculida fluctuated in the range 0.02-385.1 g m^{-2}. They occurred throughout the whole study region, with predominance of *Golfingia margaritacea*. Both the abundance and the general features of distribution of Sipunculida did not change since 1977 (Fig. 1g).

Cirripedia had several local but wide concentrations, so their abundance had sharp fluctuations from 0.004 to 4180.0 g m^{-2}. In 2002, the location of highest concentrations increased in the northern part of the region and formed three new spots. The highest concentration was in the southernmost of these (Fig. 1h).

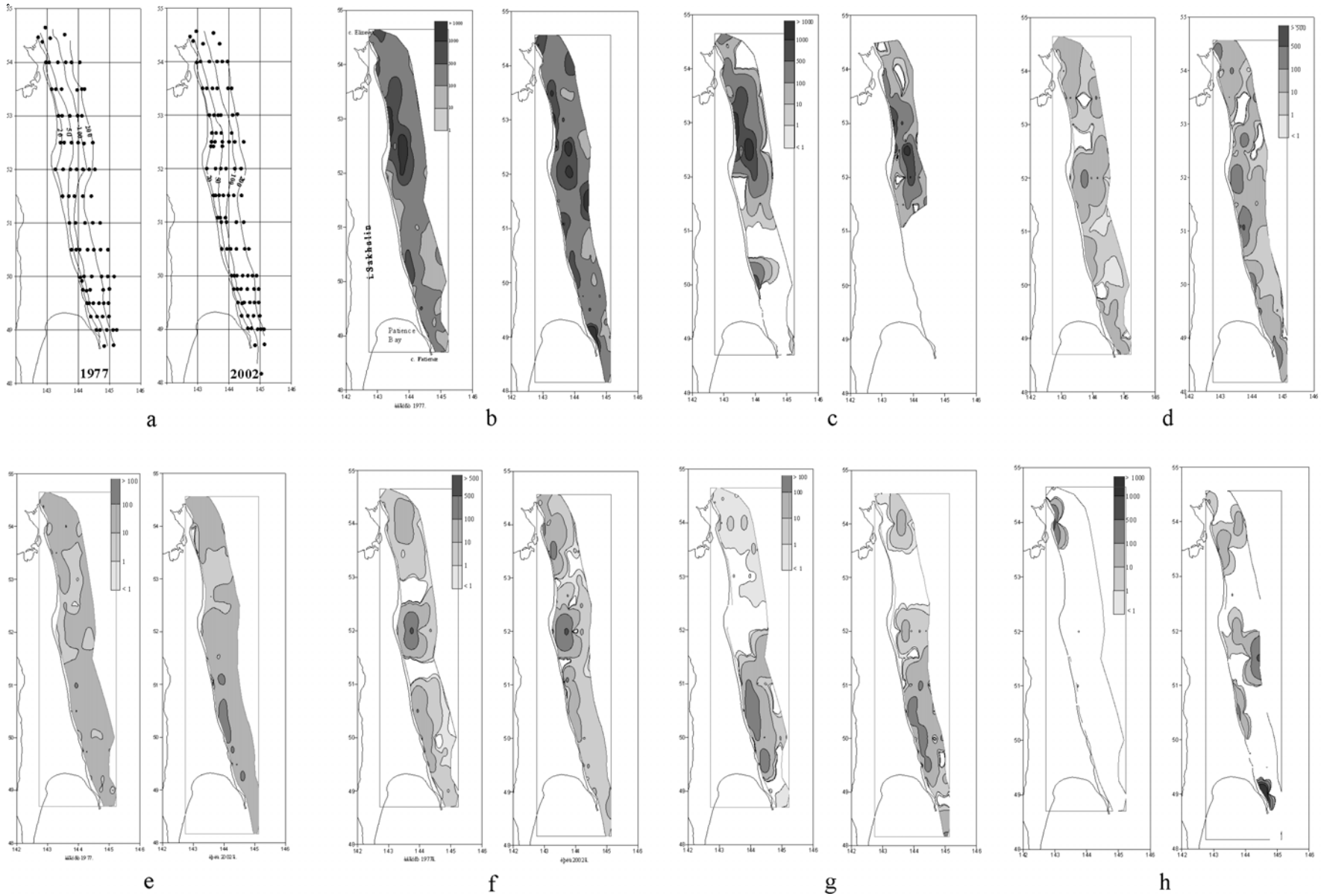

Fig. 1 (a) Station locations, (b) total benthos biomass, and total biomass of (c) Echinoidea, (d) Bivaalvia, (e) Polychaeta, (f) Amphipoda, (g) Sipunculida, and (h) Cirripedia.

Table 1 Mean biomass and composition of macrobenthos on the eastern shelf of Sakhalin Island.

Taxon	1977		2002	
	Biomass (g m^{-2})	Share (%)	Biomass (g m^{-2})	Share (%)
Foraminifera	9.80±4.61	2.89	2.70±0.9	0.64
Spongia	4.15±2.96	1.22	22.44±9.99	5.32
Hydroidea	2.67±0.63	0.79	8.58±3.46	2.04
Pennatularia	0.15±0.11	0.04	0.27±0.19	0.06
Alceonaria	6.09±2.44	1.79	6.13±4.78	1.45
Gorgonaria	0.24±0.1	0.07	5.26±3.56	1.25
Actiniaria	12.01±3.23	3.54	13.12±2.36	3.11
Nemertini	1.35±0.52	0.4	1.25±0.42	0.3
Olygochaeta	+	+	1.25±0.42	0.3
Polychaeta	40.21±7.40	11.86	38.69±4.24	9.18
Echiurida	7.66±2.75	2.26	7.41±2.82	1.76
Sipunculida	20.35±6.60	6	24.63±6.32	5.84
Priapulida	0.14±0.09	0.04	0.09±0.07	0.02
Pantopoda	0.06±0.05	0.02	0.04±0.02	0.01
Cirripedia	9.64±9.49	2.84	55.20±44.85	13.1
Ostracoda	+	+	+	+
Cumacea	2.02±1.11	0.6	8.84±3.49	2.1
Isopoda	0.13±0.04	0.04	0.44±0.15	0.1
Amphipoda	14.91±7.08	4.4	23.24±8.66	5.51
Decapoda	1.81±0.77	0.53	4.64±1.46	1.1
Nudibranchia	+	+	0.31±0.18	0.07
Loricata	0.19±0.16	0.06	0.03±0.02	0.01
Solenogastres	0.1±0.03	0.03	0.03±0.02	0.01
Gastropoda	5.18±1.21	1.53	5.99±1.13	1.42
Scaphopoda	+	+	+	+
Bivalvia	33.82±10.75	9.97	48.32±10.58	11.46
Bryozoa	4.51±1.25	1.33	6.96±2.58	1.65
Brachiopoda	0.18±0.18	0.05	1.37±1.37	0.33
Crinoidea	0.2±0.14	0.06	1.56±1.56	0.37
Asteroidea	6.63±2.18	1.96	2.74±0.96	0.65
Ophiuroidea	19.89±10.49	5.87	9.92±4.31	2.35
Echinoidea	122.78±35.83	36.2	106.29±31.3	25.22
Holothuroidea	4.90±3.44	1.44	8.98±2.08	2.13
Ascidia	6.62±3.13	1.95	4.31±2.28	1.02
Algae	0.01±0.01	+	+	+
Varia	0.73±0.35	0.22	1.72±0.62	0.41
Total	339.12±42.09	100	421.50±58.7	100

Note: + ≤0.01

Sponges also widened their distribution in 2002. Recently they had four areas of high abundance. Two northern ones did not change position since 1977, but maximal biomass of sponges here was in five times higher than in 1977. Two southern ones were not observed in 1977.

The total stock of macrobenthos over the studied region (38,700 km^2) was estimated using the Voronoy method of diagrams (Preparata and Sheymos 1989) as 14.8 million t. The stock of sea urchins was 3.9 million t, bivalves – 1.8 million t, and polychaetas – 1.5 million t.

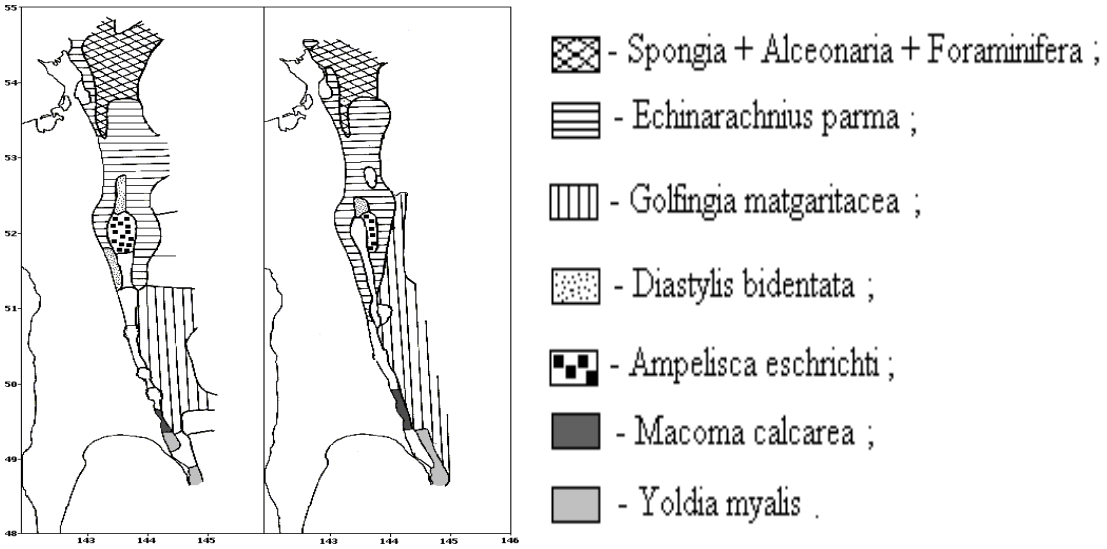

Fig. 2 Communities of macrobenthos.

Within the surveyed depth range of the East Sakhalin shelf, 13 communities of macrobenthos were distinguished by the Vorob'ev (1949) method. Seven of them occupied the major part of the region bottom. These seven communities were common for both surveys (Fig. 2).

The community of flat sea urchin Echinarachnius parma occupied the largest area and had the highest mean biomass. Average biomass of the community was 460.1 g/m^2, the major species had 82%. It was placed on fine silted sand at the depth 20-150 m. This community was one of the most important in 1977, too, when it occupied the same place and depth. However, the flat sea urchin domination was higher in 1977. Minor taxa in 1977 were Bivalva, Bryozoa and Decapoda. In 2002, Cumacea and Gastropoda appeared in this community instead of Bryozoa and Decapoda, moreover, the share of Bivalva increased because of higher abundance of S. *groenlandicus* (Fig. 3).

The other large benthic community, *Golfingia margaritacea*, was located as in 1977, at 81-232 m depth on mixed soils with a significant silt fraction. The average biomass was 241.0 g m^{-2}, with the major species accounting for 31%. This community occupied less area in 1977. Species composition of the community had slight changes till 2002 (Fig. 4). The share of Holothuria and Polychaeta increased, the share of Amphipoda decreased, and Decapoda appeared; other groups did not change their proportion.

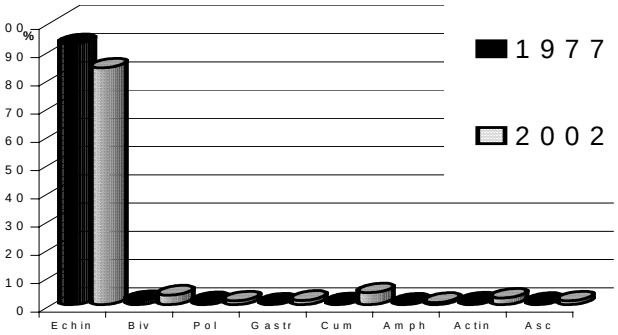

Fig. 3 Composition of the *E. parma* community (Echin: echinoidea; Biv: bivalvia; Pol: polychaeta; Gastr: gastropoda; Cum: cumacea; Amph: amphipoda; Actin: actiniaria; Asc: ascidia).

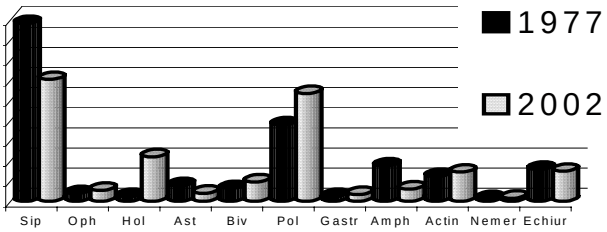

Fig. 4 Composition of *G. margaritacea* community (Sip: sipunculida; Oph: ophiuroidea; Hol: holothuroidea; Ast: asteroidea; Nemer: nemertini; Echiur: echiurida).

Besides the large communities, several local communities with a predominance of one or two species occurred. *Diastylis bidentata* dominated (92% of biomass) in one and was found at 30 m depth on a substrate of small shells, at the same place as in 1977 (Fig. 2). Average biomass of the community was 266.7 g m^{-2}. The composition of this community is shown in Figure 5.

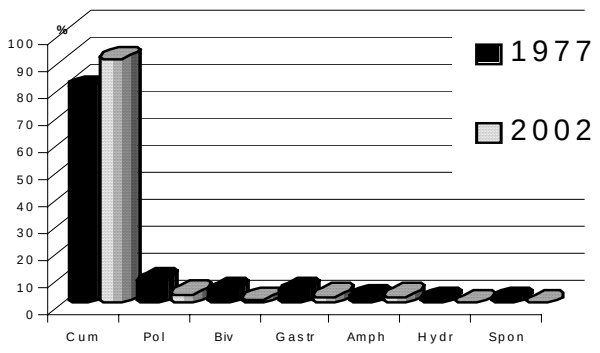

Fig. 5 Composition of *D. bidentata* community (Hydr:hydroidea; Spon: spongia).

By comparing the recent results with the data of 1977, the following conclusions were made:

1. mean total abundance of macrobenthos and its general distribution on the East Sakhalin shelf is largely unchanged from 1977;
2. taxonomic composition of the macrobenthos in 2002 was the same as in 1977;
3. mean abundance of the main taxonomic groups of macrobenthos almost had no change since 1977, except for Cirripedia (5 times greater), Spongia (5 times greater), Ophiuraidea (slight decrease), and sea urchins (slight decrease);
4. two communities, dominate by *E. parma* and *G. margaritacea*, respectively, were the largest both in 1977 and 2002;
5. both in 1977 and 2002, the vast area north of 53°30'N was occupied by epifauna of Spongia, Hydroidea, Bryozoa, Cirripedia, Alcyonaria; and the central part of the studied region was occupied by communities of Cumacea and Amphipoda with stable quantitative parameters;
6. four new communities of macrobenthos were found in 2002, the most important of them was the community dominated by *Serripes groenlandicus*;
7. some widening of the *Golfingia margaritacea* community was noted because of silting of the bottom in the studied region.

So far as species diversity, abundance and concentration of the main taxonomic groups of macrobenthos are still high enough at the East Sakhalin shelf, the recent state of bottom biota in this region is estimated as quite satisfactory, in spite of industrial pressure. Some changes of biomass and ratio of certain macrobenthos groups are possibly reasoned by interannual fluctuations of their abundance, distribution, and aggregation determined by peculiarities of their biology.

References

Averintsev, V.G., Sirenko, B.I., Sheremet'evsky, A.M., Koblikov, V.N., Pavlyuchkov, V.A. and Piskunov, A.I. 1982. Regularities of marine life distribution on the shelves of East Sakhalin, St. Iona Island, and the northwestern Okhotsk Sea. Fauna and hydrobiology of shelf zones of the Pacific Ocean. Vladivostok. pp. 9-14.

Belan, T.A. and Oleinik, E.V. 2000. Composition, distribution, and recent state of the macrobenthos of Piltun-Astokh oil deposits area. Trudy DVNIGMI 3: 166-177.

Koblikov, V.N. 1978. Distribution of bottom fauna at the shelf of Southeast Sakhalin. Regularities of distribution and ecology of coastal bioceonses. Leningrad. pp. 14-15.

Koblikov, V.N. 1983. Composition and quantitative distribution of macrobenthos at the Okhotsk Sea shelf of Sakhalin. *Izvestia TINRO* 106: 90-97.

Neiman, A.A. 1983. Recommendations on studies of benthos on shelves. Moscow: VNIRO. 24 p.

Preparata, F. and Sheynos, M. 1989. Computing geometry: Introduction. Moscow: Mir. 478 p.

Sobolevsky, E.I., Yakovlev, Y.M., Kusakin, O.G. 2000. Some data on macrobenthos composition at feeding grounds of grey whale (*Eschrichtius gibbosus* Enxl., 1977) at the shelf of Northeast Sakhalin. Ecology (2): 144-146.

Vorob'ev, V.P. 1949. Benthos of the Azov Sea. Trudy AzCherNIRO 13:355-358.

The Sea of Okhotsk: A window on the ice age ocean

James D. Hays and Joseph J. Morley
Lamont Doherty Earth Observatory, PO Box 1000, 61 Route 9W, Palisades, NY, 10964-1000 USA
e-mail: jimhays@ldeo.columbia.edu

The modern Sea of Okhotsk and the high-latitude glacial ocean share similar radiolarian faunas suggesting they also share environmental similarities. This sea favors deep- (>200 m) over shallow-living species as evidenced by collections of sediment traps set at 258 m and 1061 m in the central part of the Sea. Of the twelve dominant polycystine radiolarian species, four live above and eight below 258 m. The shallow-living species' productivity maxima coincide with spring and fall phytoplankton blooms while deep-living species' annual production, nearly twice that of the shallow-living species, is concentrated in fall. Summer plankton tows collected higher concentrations of polycystine Radiolaria below than above 200 m with maximum concentration found between 200 and 500 m (Nimmergut and Abelmann, 2002). Okhotsk Sea's zooplankton and fish also have unusual summer biomass maxima between 200 m and 500 m (Gorbatenko 1996). The paucity of Radiolaria and other consumers above 200 m coincides with an upper (0-150 m) cold (-1.5° – 1.5°C), low salinity layer while higher concentrations below 200m occur within warmer saltier water. This unusual biological structure must produce a lower ratio of shallow (<200 m) to deep carbon consumption than elsewhere in the world ocean.

Deep-living radiolarian species, similar to those of the modern Sea of Okhotsk, dominate glacial high-latitude deep-sea sediments. If the water and biological structures that produced these glacial faunas were like those of the modern Sea of Okhotsk then glacial high-latitude oceans would have differed from today's in at least two respects. Surface waters were less saline and more stable enhancing the spread of winter sea ice. This stability, combined with a deepening of nutrient regeneration, reduced surface water nutrients contributing to a reduction of atmospheric carbon dioxide.

Microsporidian infestation of the walleye pollock musculature in the Okhotsk Sea

Nadezhda L. Aseeva, S.V. Mikhailov and Z.I. Motora
Pacific Fisheries Research Centre (TINRO-Centre), 4 Shevchenko Alley, Vladivostok, 690950 Russia. e-mail: shvetsova@tinro.ru

Glugea punctifera is the only species of Microsporidia parasites of the walleye pollock. As with some larvae of helminth worms, the microsporidia could obstruct food utilization of the fish by infection of its muscles. According to previous investigations, the degree of infestation of pollock in the Okhotsk Sea by microsporidia is medium compared with other Far-Eastern seas (Asseyeva and Mikhailov 1991; Mikhailov 2002, and others).

This study was conducted with the aim of revealing a link between walleye pollock abundance and the degree of infestation by spores of microsporidia. For this purpose, 2679 pollock specimens caught in the Okhotsk Sea in 1993, 1995, and 2002-2003, were investigated, taking into account some previous data too.

About 5% of the Okhotsk Sea pollock were infected in 1970-1980, and this level was stable without visible dependence on the stock fluctuations (Aseeva and Mikhailov 1991). All infected fish had a length > 40 cm. The incidence of infestation started to grow in late 1980s – early 1990s and, by 1993, had reached the level of 8.65%. Then it decreased by 2.5 times to 3.74% in 1995. In the winter of 2002-2003, only 3 of 132 specimens investigated in fresh state had microsporidian cysts in their muscles, and the cysts were absolutely absent from 202 frozen specimens. Thus, the microsporidian infestation decreased in the second half of the 1990s, the same as for some other parasites of walleye pollock (Mikhailov, 2002).

The declining incidence is in accord with a change of age-size structure of walleye pollock in the northern Okhotsk Sea. In the 1990s, the stock was composed mainly of several strong generations born in late 1980s, but the mature part of the stock decreased steadily after 1994-1995 (Shuntov et al. 1993; Avdeev et al. 2001). As the microsporidian cysts form in muscles of mature fish only (length > 40 cm), a reduction of the proportion of mature fish led to the decreasing incidence of microsporidias parasites.

Feeding of juvenile *Pleurogrammus azonus* in the southern part of the Sea of Okhotsk and in the Pacific waters of the Kuril Islands in August, 2002

Natal'ya S. Kosenok
Pacific Fisheries Research Centre (TINRO-Centre), 4 Shevchenko Alley, Vladivostok, 690950 Russia.
e-mail: nat-kosenok @yandex.ru

The material on feeding was collected in the southern part of the Sea of Okhotsk (45 - 50°N, 142 - 151°E) and in the Pacific waters of the Kuril Islands (40 - 47°N, 146 - 154°E) in August, 2002. In total, the contents of 275 stomachs were analyzed.

Adult *Pleurogrammus azonus* are predators with mixed type of feeding (Mikulich, 1965). Juveniles are considered to be plankton feeding fishes, as they feed mainly plankton: Euphausiidae, Copepoda, Amphipoda (Kuznetsova 1997).

The dominant food items for juvenile *Pleurogrammus azonus* in the Pacific waters of the Kuril Islands (only daytime trawls) were *Neocalanus cristatus* and *N. plumchrus*, which were present at the alimentary lump equally. In this region, these copepods amounted to 18 and 19%, respectively, from all plankton biomass. Index of stomach fullness was 70.4 0/000.

In the Sea of Okhotsk, the intensity of feeding was higher. In the Bay of Terpenia, the index of stomach fullness was 97.3 0/000. At night, the composition of food was only *Thysanoessa longipes*, whereas in daytime only *N. plumchrus* were consumed, the share of which in plankton was 26%. In Okhotsk Sea waters, the index of stomach fullness was 134.2 0/000. In the dark hours, *Pleurogrammus azonus* consumed only *Th. longipes*, while it was *N. plumchrus* during the day. *Themisto japonica* was found only in very small amounts. *Pleurogrammus azonus* from transformed Pacific waters had a high index of stomach fullness (139.7 0/000). At night, the fishes consumed *Th. longipes*, while during daytime, it consumed *N. plumchrus*.

The entire ration was not distinguished by particularly great variation as it consisted of 4-5 species only. Food composition changed during the day as *Th. longipes* migrates away from the surface at night; in its absence, the fish consumed large numbers of Copepoda.

Researched juvenile of *Pleurogrammus azonus* had two peaks of feeding activity, morning and evening, as was reported earlier (Chuchukalo et al. 1995; Kuznetsova 1997).

Disorder of symmetry in the marine starfishes of Amursky Bay

Yuriy Mitrofanov and O.V. Dogadova
V.I. Il'ichev Pacific Oceanological Institute, Far-Eastern Branch of Russian Academy of Sciences, 43 Baltiyskaya Street, Vladivostok, 690041 Russia. e-mail: pacific@online.marine.su

The presence of symmetry is inherent in various species of animals from Protozoa to Entozoans. Two types of symmetry – bilateral and radial are assumed. Radial symmetry is featured in coelenterates, radiolarians, echinodermata, sponges, ascidia and some others. Bilateral symmetry seems to be more prospective in term of evolution. The animals having it evolved towards segmentation of the body, differentiation of segments, formation of active pedes with different functions. Animals possessing radial symmetry are less intricate in their structure and have a slow moving or sedentary way of life.

Bilateral symmetry is the phenomenon when the formation of a feature on one side of the body is associated with presence of such a feature on the other side. This phenomenon lies at the base of morphological and physiological processes of an organism. It concerns external and internal structure.

At the same time, some organs can be arranged asymmetrically (one-sided location of the heart, gall bladder, and spleen of mammals, etc.). Fundamentals of the asymmetry phenomenon in animals can rise from different processes that affect differently their nature. N.V. Timofeev-Resovsky and V.I. Ivanov (1966) identified a few types of disorder in symmetry and offered a classification. Among animals, there are various possible various types of symmetry disorder. Some types are caused by inheritance-induced adaptive changes (for example, left and right hemisphere functions of the human cerebrum). Such type exposure in different groups of animals seems to be absolutely distinct.

We explored disorder of symmetry in animals with radial symmetry that were not considered in the classification of N. V. Timofeev-Resovsky and V. I. Ivanov.

The marine starfishes possess five-armed radial symmetry but some diversions were depicted. Specimens with four to seven arms are described in the big Indian star *Oreaster reticulates* that normally has five arms. We explored the frequency of occurrence of anomalous marine starfishes of two species from Amursky Bay (regarding number of arms). Samples of *Asterias amurensis* taken in shallow waters near Skrebtsova Island from 0.5-2.5 m depth in 1992 consisted of more than 10,000 specimens and samples of *Patiria pectinifera* included more than 5,000 specimens. The frequency of occurrence of anomalous starfishes was determined according to the number of arms.

Among 11,520 specimens of *Asterias amurensis*, there were found 0.017% (2 specimens) with four arms, 0.113% (13 specimens) with six arms, 0.043% (5 specimens) with seven arms, and 0.009% (1 specimen) with three arms (Table 1). In the case of a decrease in number of arms we counted only such animals that had no signs of secondary loss. Variation of arms number was observed in *Patiria pectinifera* also. This normally five-armed starfish can have from four to seven arms. Specifically, it was noted that diversion from five-armed specimens was often observed as an increase in the number of arms. Most often the 6-armed starfishes were encountered. The 4-armed specimens, as with *Asterias amurensis*, were rarely encountered.

It is necessary to consider the biological significance of five-armed symmetry of starsfishes. This is preserved by hereditary, and as a consequence, has some adaptive value. While attacking bivalve mollusks, starsfishes stand on three of the arms while the other two discloses the shell. 3-, 4-, 6-, 7-armed starfishes are less adaptive therefore they are subjected to selection.

It was noticed that the incidence of asymmetry in number of starfish arms is significantly lower than the FA (fluctuating asymmetry) that occurs in

Pacific salmon (see Mitrofanov and Dogadova, this volume). At the same time, damage during ontogenesis has some common features with FA. The asymmetry of starfishes is observed as either a decrease of the feature or an increase of it. Increases occurred more often. Probably, the high frequency of anomalous starfishes in Amursky Bay was associated with higher levels of contamination by heavy metals and various toxic substances of production and domestic origin that were unique to this bay.

Table 1 Number of specimens with anomalous figures of arms-rays in entire starfish samples of *Asterias amurensis* 11520 specimens.

No.	Number of arms-rays	Number of star-fish with anomalies	Number of star-fish with anomalies, %
1	6	13	0,113
2	7	5	0,043
3	4	2	0,017
4	3	1	0,009

Feeding habits of Pacific halibut *Hippoglossus stenolepis* in the western North Pacific

Ilyas N. Moukhametov [1] and A.M. Orlov[2]

[1] Sakhalin Research Institute of Fisheries and Oceanography (SakhNIRO), 196 Komsomol'skaya Street, Yuzhno-Sakhalinsk, 693023 Russia. e-mail: ilyas@sakhniro.ru

[2] Russian Federal Research Institute of Fisheries and Oceanography (VNIRO), 17 V. Krasnosel'skaya, Moscow, 107140 Russia. e-mail: orlov@vniro.ru

Pacific halibut *Hippoglossus stenolepis* is very important target of the groundfish fishery in the North Pacific Ocean. The feeding habits of Pacific halibut in the western Bering Sea were investigated long ago (Vernidub 1936; Gordeeva 1954; Novikov 1964, 1974). There are several publications dealt with feeding habits of species considered in the Kuril-Kamchatka area (Novikov 1974; Orlov 1997a,b, 1998, 1999a,b, 2000; Moukhametov 2002). However, diet descriptions in most of these papers were based only on frequency of occurrence of dietary components in stomachs.

The stomach contents of Pacific halibut sampled aboard the Japanese trawlers *Kayo Maru No. 28* and *Tomi Maru No. 82* during summer-autumn 1997 were analysed. The study took place in the western Bering Sea (WBS) between 168°E and 178°W (Fig. 1A), in the Pacific waters off the northern Kuril Islands and southeastern Kamchatka (NK) between 48°10'N and 51°30'N (Fig. 1B). Samples for analysis were taken from bottom trawl catches. Fishing was carried out around the clock. The stomach contents were sorted, identified to the lowest possible taxonomic level, and weighed. Prey groups were described in terms of percent total stomach content weight. Fishes showing signs of regurgitation or net-feeding were excluded from analysis.

Stomachs "examined/with food" were as follows: 262/206 in the WBS and 386/270 in the NK. Total number of organisms identified (excluding fishery offal) in stomachs was no less than 25 in the WBS and 32 in the NK. The diet of Pacific halibut in the WBS consisted mostly of fishes (35.12%), fishery offal (31.3%) and cephalopods (26.6%) (Fig. 2A). Walleye pollock *Theragra chalcogramma* was the major fish species consumed (18.7%) followed by Pacific herring *Clupea pallasii* (12.9%). Red squid *Berryteuthis magister* (13.6%) and octopuses (13.0%) were most important cephalopods. In the NK, Pacific halibut fed mainly on fishes (38.9%) and cephalopods (36.8%). The role of fishery offal in the diet of halibut here was significantly lesser than in the previous area (9.3%) (Fig. 2B).

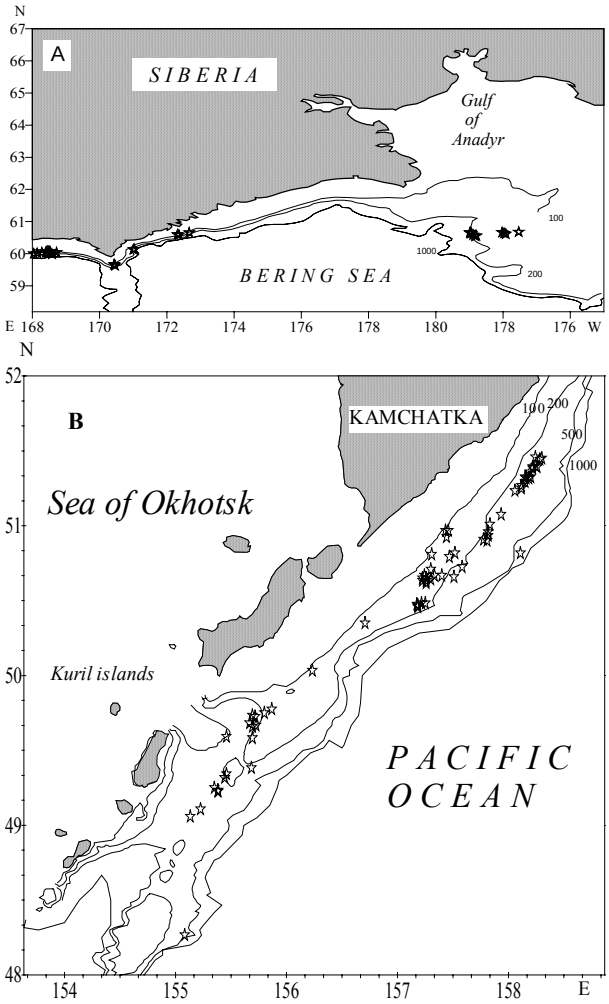

Fig. 1 Study areas.

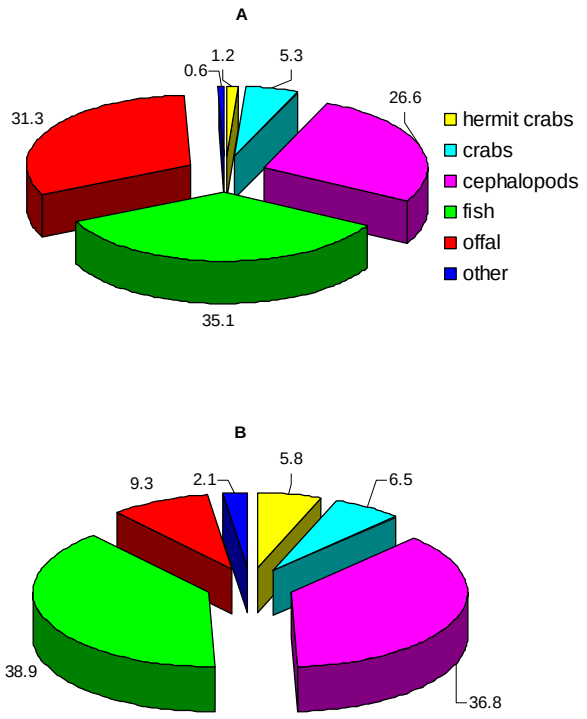

Fig. 2 Diet of Pacific halibut in the western Bering Sea (above) and northern Kuriles/southeastern Kamchatka (below).

Similar to WBS, walleye pollock (21.8%) was most important fish prey though among cephalopods, octopuses were most important (23.5%). Differences in diet composition between areas considered may be explained by regional faunistic distinctions, different levels of fishery activity in both areas, and distinctions of halibut size (mean fork length 73.9 cm vs. 61.4 cm in WBS and NK, respectively).

Changes in diet composition of Pacific halibut with increasing size were observed during previous studies and were detected during our investigations as well. In the WBS, increasing size of Pacific halibut was accompanied by increased fish consumption and decreased feeding on fishery offal. The fraction of cephalopods in the diet was approximately equal for various length classes (Fig. 3A). With increasing predator length, consumption rate of red squid decreased, and that of octopuses increased. In the NK area small size groups of Pacific halibuts (35-45 cm) ate mostly hermit crabs, spider crabs, shrimps and fish. Small crustaceans and fishery offal played some role in the diet of this size group. The proportion of hermit crabs in the halibut diet decreased with increasing of predator length. Spider crabs have significant importance in diet of all analysed length categories. The role of fish in the diet of Pacific halibut gradually increased with increasing of predator length. The proportion of cephalopods and fishery offal increased significantly when halibut attained 80 cm length. Subsequently, with increasing of predator length importance of cephalopods in diet slightly decreased (Fig. 3B). Octopuses and red squid have approximately equal importance in diet of NK Pacific halibut sized 45 to 85 cm. Larger fish eat mostly octopuses.

Considerable differences in diet compositions were detected at various depths. Stomach contents of WBS Pacific halibut at the shallower depths consisted mostly of fishery offal and fish (mainly of walleye pollock). With depth increasing role of fishery offal decreased from 63.8% within 251-300 m to 17.5% in 401-450 m depth range while that of cephalopods contrarily increased from 9.1% to 47.5% respectively. Share of fish in halibut diet increased from 23.5% at 251-300 m to 56.8% at 351-400 m and deeper (451-500 m) it was reduced to 9.4%. In the NK depths increasing was accompanied with decreasing of fish importance in diet and, contrarily, increasing of consumption of cephalopods. Fishery offal constituted 9.5-11.1% of stomach contents within 151-300 m depth range, and hermit crabs played noticeable role (3.7-13.6%) in halibut diet at all investigated depths. Some differences between male and female diets were detected (Fig. 4). Thus, female Pacific halibut in the WBS ate more fishery offal (36.9%), fish (31.2%) and cephalopods (27.1%). In this region male fed mostly on fish (38.0%), fishery offal (27.2%) and cephalopods (26.2%W). Males used a wider spectrum of fish prey. The male list included no less than nine fish species while female stomachs contained remains only of four species. Anyway, the most important prey in halibut diets among fishes were walleye pollock (18.2% and 19.5% for males and females, respectively), and Pacific herring (15.2% and 9.8%, for males and females, respectively). Differences in consumption of red squid and octopuses by males and females were observed. Thus, male diet contained 16.1% red

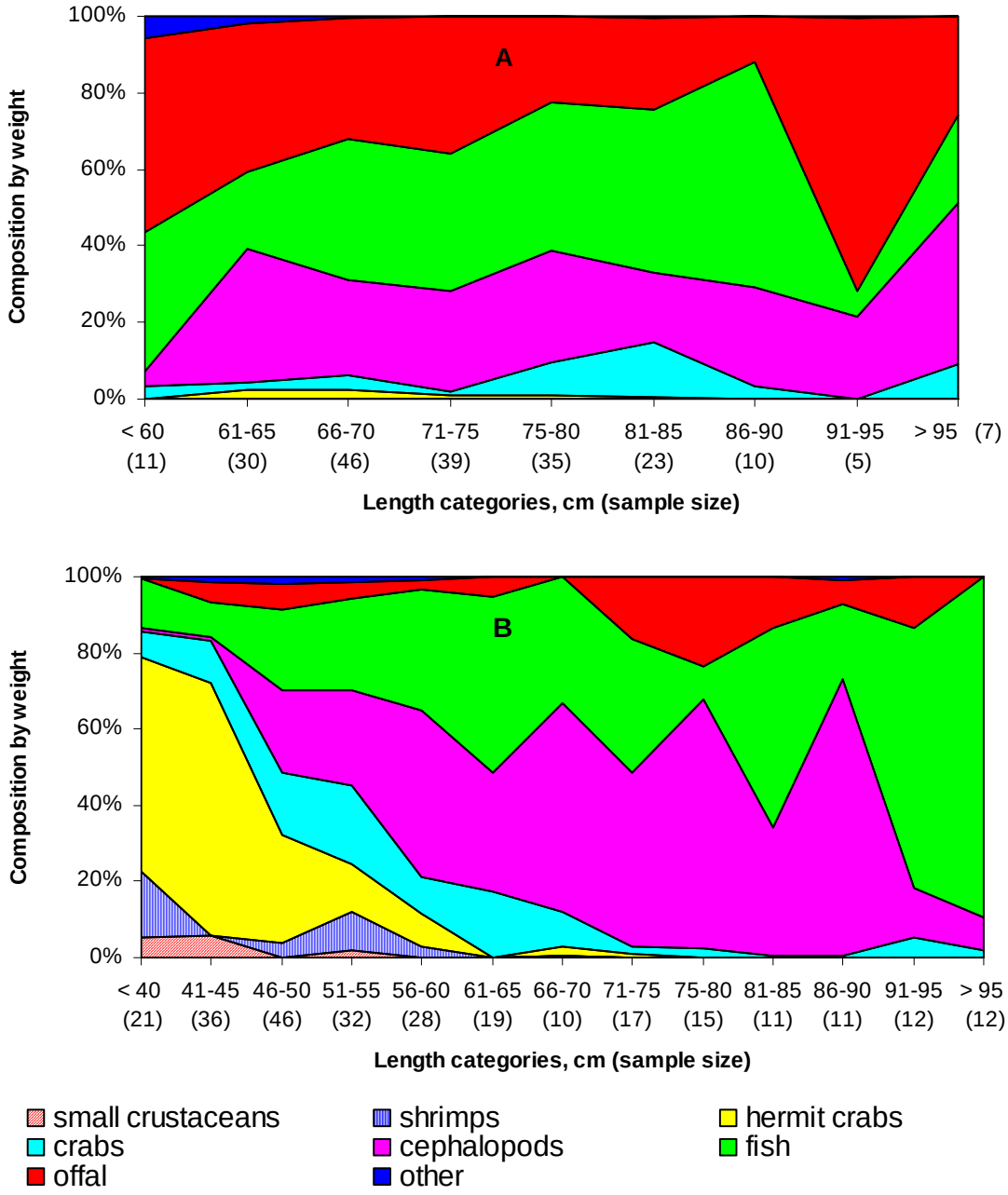

Fig. 3 Diet composition for Pacific halibut by size-class for (a) western Bering Sea and (b) northern Kuriles/southeastern Kamchatka.

squid and 10.1% octopuses while females preferred octopuses (16.8%) and ate red squid in significantly lesser amount (10.2%).

In the NK area Pacific halibut females consumed more cephalopods (42.5%), fish (31.2%) and fishery offal (10.8%) while males ate fish in considerably larger amount (45.1%) and cephalopods were second important dietary component of male halibuts (33.3%). Similar to the WBS region, the spectrum of fish prey of male halibuts was broader, but walleye pollock remained most important prey item of both sexes. There were no significant differences in consumption of red squid and octopuses by male and female, as in the WBS.

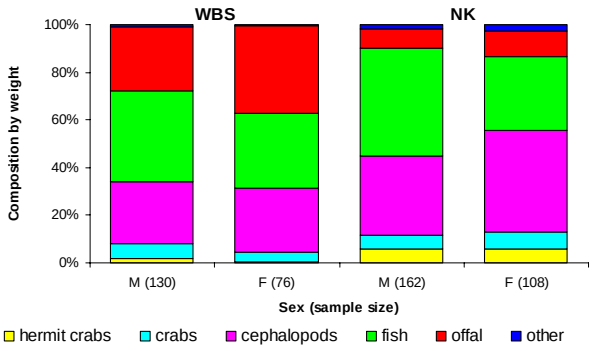

Fig. 4 Diet composition by sex and region.

Differences of male and female diet compositions may be related partly to distinctions in their sizes. In the WBS, the mean length of males was 72.5 cm vs. 75.9 cm for females. In the NK, mean length of Pacific halibut was 59.9 cm vs. 62.3 cm for males and females, respectively. Another reason for the diet differences between males and females is one of mechanisms to decrease intra-specific feeding competition in the areas with limited forage resources such as continental slopes.

Regional differences were observed in the diets of halibut within WBS and NK areas. Thus, fishes (43.9%) and cephalopods (42.9%) were more important in the diet of Pacific halibut caught in the western part of WBS while fishery offal (67.9%) and fishes (23.5%) were the most significant dietary components in the eastern part, where the share of cephalopods was only 5.3%. Orlov and Moukhametov (2002) observed the same situation in respect of Pacific black halibut *Reinhardtius hippoglossoides matsuurae* and Kamchatka flounder *Atheresthes evermanni* in this region. Sufficient differences in halibut consumption of crabs were observed in the western (8.2%) and in the eastern (1.4%) parts of WBS.

The diet of Pacific halibut in the NK area changed from south to north, with the importance of fish increasing in this direction and that of cephalopods decreasing. Thus, in the south part of the study area, the share of fishes was 12.6% and they were third in rank after cephalopods (46.2%) and fishery offal (19.1%). In the middle part, fishes were second in rank (37.2%) and in the north their role reached 41.0% and they became most important dietary component of Pacific halibut. Opposite, importance of cephalopods decreased to 35.9% in the north. Differences in diet compositions between various parts of NK area were considerable in respect of consumption of hermit crabs and fishery offal as well. These differences may be explained by significant distinctions of predator sizes (52.7 vs. 54.9 vs. 65.2 cm in the southern, middle and northern parts, respectively) and also by local faunistic distinctions. Domination of fishery offal in halibut diets in the eastern part of the WBS is probably related to active specialized walleye pollock fishery in this area by numerous fishing vessels.

Distribution of foraminifera in the Sea of Okhotsk

Sergey P. Pletnev and V.K. Annin
V.I. Il'ichev Pacific Oceanological Institute, Far-Eastern Branch of Russian Academy of Sciences, 43 Baltiyskaya Street, Vladivostok, 690041 Russia. e-mail: annin@poi.dvo.ru

Despite the available publications concerning the distribution of bottom foraminifera, these data are very difficult to use for the paleoecological purposes. They are overloaded with detailed elaboration of the selected communities and often are studied without taking into account living foraminifers. Offer model are put in a basis of data basically on live foraminifers, and also behavior of separate kinds in the past.

We selected the following communities: (1) shelf with four subtypes, (2) underwater slope with two subtypes and (3) abyssal. The most indicative forms are presented in Table 1. Symbols of subtypes are: 1A-estuary-lagoon; 1B-inner shelf (0-20 m); 1C-middle shelf (20-50 m); 1D-outer shelf (50-200 m); 2A-top slope (200-600 m); 2B-low slope (600-1300 m) and 3-abyssal (more than 1300 m).

The foraminiferan fauna of the Okhotsk Sea differs essentially from that of the Pacific at the same latitudes. There are no typical deepwater species (genera Plectina, Cyclammina, Bathysiphon), but paleontological findings testify that such abyssal fauna lived in the Okhotsk Sea three times during the last of 40 million years.

Table 1 Foraminifera of the Sea of Okhotsk.

Type	**1 type**				**2 type**		**3 type**
Species	**1A**	**1B**	**1C**	**1D**	**2A**	**2B**	**3**
Miliammina fusca	x						
Iadammina macrescens	x						
Ammotium cassis	x						
Trochammina sp.	x						
Cribroelphidium asterineum	x	x					
Quinqueloculina vulgaris		x					
Q.seminulom		x					
Elphidium excavatum		x					
E.depressulum		x					
Canalifera fax		x					
Buccella depressa		x					
B.frigida		x					
Protelphidium sp.		x					
Elphidiella recens		x	xx				
Buliminella elegantissima			x				
Retroelphidium subgranulosum			x				
Nonionella japonica			x				
Buccella arctica			x				
Cribroelphidium subarcticum			x				
Cassandra limbata			x				
Dentalina baggi			x				
Lagena sp.			x				
Retroelphidium subclavatum			x				
Elphidiella arctica			x				
Islandiella japonica			x				

Type	**1 type**				**2 type**		**3 type**
Species	**1A**	**1B**	**1C**	**1D**	**2A**	**2B**	**3**
Cibicides lobatuls			x				
Alabamina weddelensis			x	x			
Trifarina kokuzuraensis				x			
Epistominella pacifica				x			
Cribroelphidium batiale				x			
Nonionella labradorica				x			
Trochammina inflata				x			
Uvigerina parvocostata				x	xx		
Globobulimina hanzawai					x		
Gyroidinoides soldani					x		
Globulimina auriculata					x		
Melonis pompiloides					x		
Valvulineria ochotica					x		

Nutrients and chlorophyll *a* distribution in Aniva Bay, Sea of Okhotsk during 2001-2002

Louisa N. Propp[1] and L. Yu. Gavrina[2]

[1] Institute of Marine Biology, Far-Eastern Branch of Academy of Sciences, 17 Palchevskii Street, Vladivostok, 690041 Russia. e-mail: inmarbio@mail.prymorye.ru

[2] Sakhalin Research Institute of Fisheries and Oceanography (SakhNIRO), 196 Komsomol'skaya Street, Yuzhno-Sakhalinsk, 693023 Russia. e-mail: lusya@sakhniro.ru

In 2001-2002 in Aniva Bay, Sea of Okhotsk, complex research on the seasonal variability of nutrient and chlorophyll-*a* concentrations was conducted to determine lower trophic kevel productivity. The research was carried out in different seasons: in April, June, August, October, November, January 2001 and 2002 respectively. The purpose was to compare analysis of data collected in in 2001 and 2002.

Aniva Bay belongs to the La Perouse (Soya) Strait area. That area is under the influence of the West Sakhalin Current (Sea of Japan) and partly by the East Sakhalin Current (Sea of Okhotsk). The maximum depth in the bay reaches to 100 m. The hydrochemical research was conducted on four latitudinal sections or 14 stations (Fig. 1).

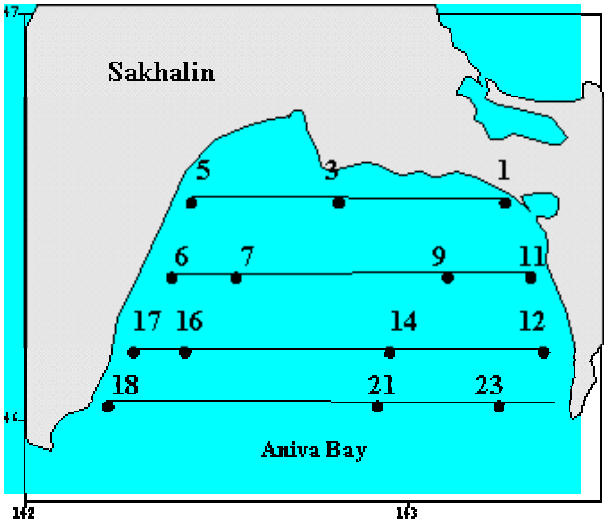

Fig. 1 Scheme of stations. Aniva Bay. 2001-2002.

The water was selected with the help Rossette, supplied by the cartridge from 12 plastic Niskin 1.7 liter bottles on given depth 10, 20, 30, 50, 75 and 90 meters.

Research cruises in Aniva Bay during 2001-2002 have allowed a characterization of the hydrochemical parameters of water features and to determine seasonal peculiarities of their distribution in two different years.

In April 2001, immediately after ice sampling was carried out, the distribution of chlorophyll-"*a*" and nutrients are shown. The phytoplankton bloom develops at the ice edge and at shoals. Active upwelling, enriched by nutrients was marked, favoring the creation of an intensive peak in primary production. The chlorophyll *a* concentration reached 20 mg l^{-1} (Fig. 2). In addition, there was an expressed influence of water masses from Sea of Japan and Sea of Okhotsk.

In June 2001, nutrients were distributed vertically homogenously. The seasonal loss of chlorophyll *a* was determinated up to 4.87 mg l^{-1}. In August 2001, water temperatures varied from –1.230 to plus 20.470°C. Thus a well-expressed intermediate cold layer at a depth 10-15 m was evident, creating very strong stratification (Fig. 3). The stratification prevented the penetration of nutrients from depth and in the upper layer, nutrients were depleted. Chlorophyll *a* in the upper layer was absent and phytoplankton remains (maximum 1.65 mg l^{-1}) were founded at depths with an oxygen maximum (132% saturation) (Fig. 4) in an interval of average temperatures from 7.380°C up to 10.790°C (Fig. 5).

In October 2001 after storms, the layers of water become similar on structure, and the concentration ammonia (20 μM) increased. The distribution chlorophyll *a* becomes spotty and concentrations in thicker waters grew up to 3.74 mg l^{-1}.

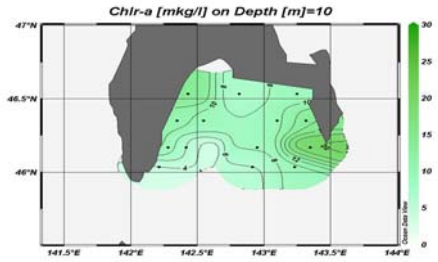

Fig. 2 Chorophyll "a", depth 10 m, April 2001.

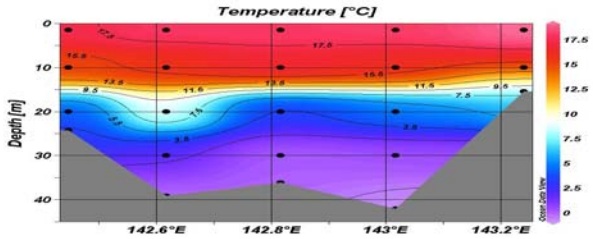

Fig. 3 Intermediate cold layer, section 1, August 2001.

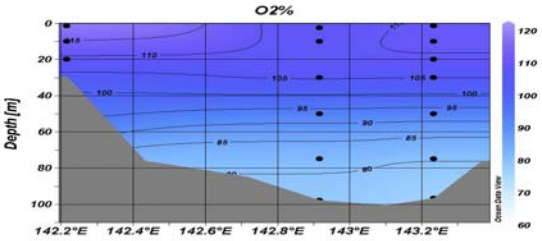

Fig. 4 Distribution of oxygen, section 4, August 2001.

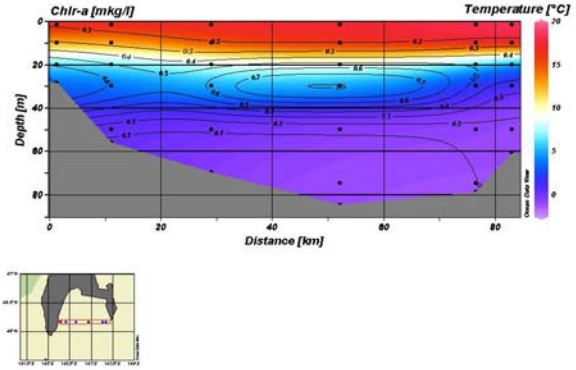

Fig. 5 Distribution of oxygen, chorophyll "a" and temperature, section 3, August 2001.

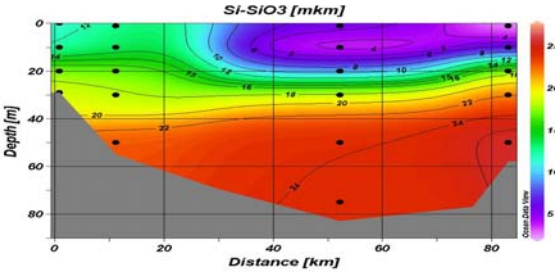

Fig. 6 Distribution of silica, April 2002.

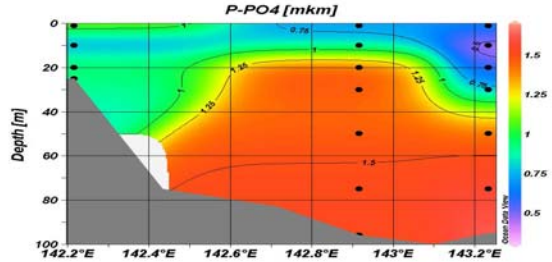

Fig. 7 Distribution of phosphorus, April 2002.

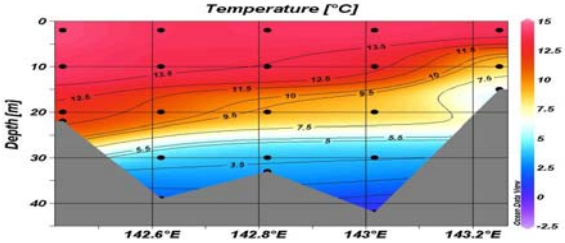

Fig. 8 Intermediate cold layer, section 1, August 2002.

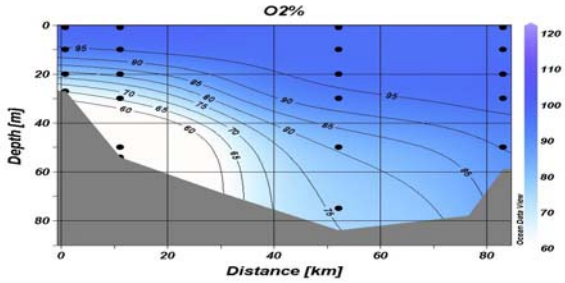

Fig. 9 Distribution of oxygen, section 3, August 2002.

By November, concentrations of inorganic forms of nitrogen, phosphorus and silica had increased. Chlorophyll *a* was obtained from the upper layer, up to the depth 50 m. Despite low chlorophyll *a* concentration (0.22 – 2.85 mg l^{-1}) this phenomenon can possibly be described as a second, fall peak in phytoplankton presence.

In January 2002, the nutrient stock had increased. Chlorophyll *a* was absent in all layers, silica contents were 27.7 μM. Chlorophyll *a* and silica have an opposite dependence, because diatoms, which use the silica to construct their frustules, are the dominant taxa in the phytoplankton community in spring. Oxygen saturation varied from 69 up to 92%. As we expected, a direct connection between chlorophyll *a* and dissolved oxygen exists.

The spring of 2002 arrived early, so in April the ice had already left and the beginning of the vegetative period was not apparent. Nutrients were rather high: phosphorus up to 3 μM, silica up to 33.5 μM (Figs. 6, 7) and chlorophyll *a* concentration reached 2.72 mg $^{-1}$, growing by June up to 7.96 mg l^{-1}. Thus, production processes in spring of 2002 proceeded more slowly in comparison with a similar period in 2001, not creating an appreciable large burst of phytoplankton.

The rainy weather conditions of the cool summer of 2002 supplied large inflows of freshwater with terrestial sediments in the upper layer of Aniva Bay. By August of 2002, compared with the same period in 2001, the cold intermediate layer formed deeper, up to 30-40 m (Fig. 8), complicating the inflow of nutrients from depth. Oxygen saturation varied from 65 up to 105% (Fig. 9), and maximum chlorophyll *a* concentration peaked at 1.98 mg/l^{-1}.

The autumn of 2002 was characterized by low nutrient concentrations in the photic layer. Saturated oxygen reached 62%, only because of storms and active sedimentation in Aniva Bay.

Concerning internal comparison of 2001 and 2002, it is necessary to note the sharp distinction in hydrochemical conditions of Aniva Bay. Climatic peculiarities of an early, cold spring in 2002, heavy rains in the summer prevented active phytoplankton blooming, so the low chlorophyll *a* concentration was obtained. The cold intermediate layer in August 2001 was formed at a depth of about 15 m, but in August 2002, at a depth of about 30 m. That had a strong influence on the hydrochemical parameters of water masses inside Aniva Bay.

The development of malacofauna and reconstruction paleoenvironmental changes in coastal areas of Sakhalin during the Holocene

Vladimir A. Rakov[1] and S.V. Gorbunov[2]

[1] Far East State University, Department of Marine Biology and Aquaculture, Oktjabrskaya 27, Vladivostok, 690600 Russia. e-mail: vokar@mail.primorye.ru

[2] Timovsky Museum, Haritonova 14, Timovo, Sakhalin, 694400 Russia.

The modern malacofauna in the coastal areas of Sakhalin have been rather well investigated. However, over the last thousand years or so, large changes in taxonomic composition have occurred. These are closely connected to changes of climate and environmental conditions. To track such changes it is possible only on the basis of biogeographical analysis of mollusks from various archaeological collections in view of radiocarbon dates of shells.

A total of 60 species of mollusks, including fisheries species were collected from more than hundred archaeological sites (middens) around Sakhalin Island: These included 1 - Loricata, 35 – Gastropoda, and 33 - Bivalvia (Tables 1 and 2). The age of mollusks corresponds to the period from the early Neolithic (5-6 thousand years ago) up to the 1800-1900s. Biogeographical analysis allows tracking changes in structure of the malacofauna and a climate, hydrology for the last thousand years or so at coast of Sakhalin.

The periods of existence of the archaeological collections were determined by radiocarbon dating of the mollusk shells collected. The Neolithic culture developed on Sakhalin since 5-6,000 years ago and ended 2-2,500 years ago. The Susuja culture existed in the southern half of the island from 2,5-1,500 years ago. During the first few centuries of the current era, 100-500, the North-Sakhalin culture was distributed mostly in the in northern part of Sakhalin. In the southern part of Sakhalin, from 500-700, there was a Tovada culture. The greatest distribution in the south of Sakhalin, and also on the north of Hokkaido and Kuriles during the period from 700 to 1300 was the Okhotskaja culture. From 900-1300, in the south of the island, the Minami-Kaizuku culture developed, and from 1200-1400, the Pokrovskaja culture. At last, from 1300 to the 20th century, the Northern Sakhalin culture developed, and in the south, the Ajnu cultures, the Neizi and Nivh.

At the Neolithic site of Aleksandrovsk, the subtropical species *Crassostrea gigas* and *Anadara sp*. are found as part the Northern Sakhalin culture. They testify to climate warming, corresponding period of a climatic optimum in the Holocene. At this time, the subtropical species of mollusks penetrated through Tsugaru Strait to the western coast Hokkaido, and then into the northern part of Tatar Strait where shallow lagoons existed. During the Atlantic period (8,000-4,500 years ago), subtropical species of mollusks existed along the entire coast of Sakhalin. However, about 4,500 years ago they disappeared from this area in connection with the cold Subboreal period (4,500-2,200 years ago). Therefore during the subAtlantic period (2,200 years ago to present), the Pacific oyster (*C. gigas*) existed only in the southern part of Sakhalin (Aniva Bay) where numerous sites (Susuja-1, Solovjevka-1, etc.) occured in the Susuja culture. On the western coast of Sakhalin, only subboreal species of mollusks (*Spisula sachalinensis, Neptunea arthritica, Buccinum sakhalinensis*, etc.) occurred at this time. In the Northern Sakhalin culture, about 2,000-1,500 years ago, objects of a craft served also *Corbicula japonica, Mya arenaria* and *Crypthochiton stelleri*, etc. From sites on rivers located on the coast (Ado-Timovo, Cape Bauri), fresh-water mollusks *Dahurinaia laevis* and *Kunashiria* sp. were extracted.

With the formation of La Perouse Strait during the Early Holocene, many gastropods of the genera *Neptunea* and *Buccinum* penetrated from Sea of Okhotsk to Japan. Some species of mollusks from these sorts were distributed far to the south, to the the Korean Peninsula (*Neptunea arthritica*).

Table 1 Bivalve mollusks from archaeological collections in coastal areas of Sakhalin Island.

	Community[1]								
Species	***1***	***2***	***3***	***4***	***5***	***6***	***7***	***8***	***9***
Anadara sp.	+	-	-	-	-	-	-	-	-
Arca broughtoni	-	+	-	-	-	-	-	-	-
Crassostrea gigas	+	+	+	+	+	?	?	+	+
Crenomytilus grayanus	+	?	-	+	?	?	+	-	+
Ruditapes philippinarum	+	+	+	+	?	?	?	-	+
Corbicula japonica	+	?	+	+	?	?	+	?	+
Mizuhopecten yessoensis	+	?	+	+	?	+	+	+	+
Swiftopecten swifti	+	+	+	+	+	?	+	?	+
Spisula sachalinensis	+	+	+	+	+	+	+	+	+
Peronidia venulosa	+	?	+	+	+	?	?	-	+
Peronidia sp.	+	?	?	+	?	+	?	-	+
Dahurinaia laevis	+	?	+	+	+	?	+	+	+
Mactra chinensis	-	+	-	-	-	-	-	-	-
Peronidia lutea	-	+	+	+	+	?	+	-	+
Keenokardium californiense	-	+	?	+	?	?	+	?	+
Mya arenaria	-	+	+	+	+	?	+	+	+
Mercenaria stimpsoni	-	-	+	?	?	?	+	+	+
Kunashiria sp.	-	-	+	?	-	-	?	-	+
Meretrix lusoria	-	-	-	+	-	-	-	-	-
Nuttalia sp.	-	-	-	+	?	?	?	-	+
Callista brevisiphonata	-	-	-	+	?	+	+	-	+
Protothaca euglypta	-	-	-	+	?	?	+	-	+
Mya priapus	-	-	-	+	?	?	+	?	+
Panomya arctica	-	-	-	+	?	?	+	?	+
Callithaca adamsi	-	-	-	+	+	?	+	?	+
Heteromacoma irus	-	-	-	+	?	?	+	-	+
Chlamys behringianus	-	-	-	+	-	-	-	-	+
Tridonta borealis borealis	-	-	-	+	-	-	-	-	+
Macoma balthica	-	-	-	-	+	?	?	-	+
Siliqua alta	-	-	-	-	-	-	+	-	+
Pododesmus macrochisma	-	-	-	-	-	-	+	-	+
Macoma middendorffi	-	-	-	-	-	-	+	?	+
Macoma orbiculata	-	-	-	-	-	-	+	?	+

[1]Community: 1 – Neolithic; 2 – Susuja; 3 – North-Sakhalin; 4 – Okhotskaja; 5 - Minami-Kaizuku; 6 – Pokrovskaja; 7 – Ainu culture Neizi; 8 – Nivh culture; 9 – modern time; ? – possible.

Table 2 Gastropoda and Loricata (*) mollusks from archaeological collections in coastal areas of Sakhalin.

	Community[1]								
Species	**1**	**2**	**3**	**4**	**5**	**6**	**7**	**8**	**9**
Haliotis cf. discus	+	?	?	+	?	-	?	-	+
Buccinum sp.	+	+	+	+	?	?	?	?	+
Buccinum sakhalinense	-	+	?	?	?	-	?	-	+
Neptunea arthritica	-	+	+	+	+	?	+	-	+
N. arthritica var. typical	-	+	?	+	?	?	?	-	+
N. arthritica var. lurida	-	?	?	+	?	?	?	-	+
Neptunea lyrata	-	+	?	+	?	-	+	-	+
Neptunea constricta	-	+	+	+	?	?	+	-	+
N.constricta var.euliminata	-	?	?	+	?	?	?	-	+
Littorina squalida	-	+	+	+	+	?	+	-	+
Lottia sp.	-	+	+	+	?	-	?	-	+
Acmaea pallida	-	-	+	+	?	?	+	+	+
Rapana sp.	-	-	-	+	-	-	-	-	-
Littorina kurila	-	-	-	+	?	-	?	-	+
Mitrella burchardi	-	-	-	+	?	-	?	-	+
Neptutea bulbacea	-	-	-	+	?	-	+	-	+
N.bulbacea var. laevigata	-	-	-	+	-	-	+	-	+
Neptunea sp.	-	-	-	+	?	?	+	?	+
Buccinum middendorffi	-	-	-	+	?	-	+	-	+
Buccinum vercruzeni	-	-	-	+	?	-	?	-	+
Nucella heyseana	-	-	-	+	?	?	+	?	+
Lunatia pallida	-	-	-	+	?	-	?	-	+
Cryptonatica janthostoma	-	-	-	+	?	?	+	-	+
Cryptonatica hirasei	-	-	-	+	?	-	?	-	+
Criptonatica sp.	-	-	-	-	+	-	+	-	+
Buccinum bayani bayani	-	-	-	-	-	+	?	-	+
Buccinum verrucosum	-	-	-	-	-	+	?	-	+
Buccinum percrassum	-	-	-	-	-	+	?	-	+
Buccinum ohotense	-	-	-	-	-	-	+	-	+
Plicifusus plicatus	-	-	-	-	-	-	+	-	+
Nucella freycinetti	-	-	-	-	-	-	+	?	+
Fusitriton oregonense	-	-	-	-	-	-	+	-	+
Turritella fortilyrata	-	-	-	-	-	-	+	-	+
Lottia cassis	-	-	-	-	-	-	+	-	+
Lottia radiata	-	-	-	-	-	-	+	-	+
*Criptochiton stelleri**	-	-	+	+	+	?	+	?	+

[1]Community: 1 – Neolithic; 2 – Susuja; 3 – North-Sakhalin; 4 – Okhotskaja; 5 - Minami-Kaizuku; 6 – Pokrovskaja; 7 – Ainu culture Neizi; 8 – Nivh culture; 9 – modern time; ? – possible.

The early Middle Ages (700-1100) was a warm period along the coast of Sakhalin. Therefore, during this time, many collections from the early Okhotskaja cultures had shell middens containing *C.gigas*. This abundant species also occurred along the coast of Aniva Bay and Patience Bay where there were sea lagoons. Finds of tropical mollusks *Meretrix lusoria* (Kalinino-1) and *Rapana* sp. (Gardeners - 1) testify to warmer climates in southern Sakhalin. The average annual temperature of water at this time was approximately on 3 - 5°C greater than at present. Except for oysters extracted *S. sachalinensis*, *Mizuhopecten yessoensis*, *Crenomytilus grayanus*, *N.arthritica*, *Acmaea pallida*, etc. From coast of Sea of Okhotsk delivered to settlements and other species Gastropoda, and also some Boreal-Arctic species (*Tridonta borealis borealis*).

From 1000-1300, the sharp decrease in the number of extracted species of mollusks, connected with the beginning of a cold period in the 1200s, is marked. At this time, not only did the tropical species disappear from the malacofauna, but the subtropical ones too. For example, *C. gigas* disappeared from Patience Bay and its shells became rare on the western coast. Only with occurrence of the Ainu cultures in the 1300s, Neizi in the south and Nivh in the north, did the quantity of extracted species of mollusks increase. The basic objects were *S. sachalinensis*, *M. yessoensis*, *C. japonica*, *Mercenaria stimpsoni*. The Nivhy culture also had fisheries for pearl-oyster *D. laevis* (Grotto Puzi), and the Ainu for gastropods of the genera *Neptunea* and *Buccinum*. However because of a cold period from 1600-1900, the number of mollusks fauna was rather small.

Thus, the structure and number of extracted mollusks along the coast of Sakhalin are closely connected to changes in climate during the last several thousand years. During warm periods, the malacofauna appears to be more subtropical and even tropical, that coincides with an increase in the number of human settlements and to occurrence in shell middens of *C.gigas* and other species. During cold periods, the number of species of mollusks decreases. The basic species of mollusks of coastal areas of Sakhalin appeared in the Early Holocene on parts of the southern Kuriles and from Hokkaido. The greatest similarity among malacofauna collections on Sakhalin is with malacofauna coastal areas of northern Hokkaido.

Developing of the regional ocean color chlorophyll *a* algorithms for SeaWiFS for the Okhotsk Sea

Pavel Salyuk[1] and D. Akmaykin[2]

[1] V.I. Il'ichev Pacific Oceanological Institute, Far-Eastern Branch of Russian Academy of Sciences, 43 Baltiyskaya Street, Vladivostok, 690041 Russia. e-mail: mak@dfu.min.dk

[2] G.I. Nevelskoy Maritime State University, 50a Verhneportovaya Street, Vladivostok, 690059 Russia.

The method of laser-induced fluorescence (LIF) of the seawater was used to calibrate satellite measurements of chlorophyll *a* concentrations in coastal water of the Sea of Okhotsk during scientific cruises in 2000-2002. Measurements were made by pumping laser fluorometer installed on the sailboard. The second harmonic of the Nd:YAG laser was used to induce the fluorescence spectra. The scanning monochromator measures the fluorescence intensity from 540 nm to 740 nm during 1.5 minute. Measurements were done from a moving ship; the spatial resolution of chlorophyll *a* concentration determination was about 200 meters. The shipboard measurements were compared with chlorophyll *a* concentrations received by SeaWiFS scanner (level 1a data) at the same time and area by using the global positioning system. The features of the fluorescence spectra were used to determine the seawater areas where the satellite and fluorometer data were very close. Satellite chlorophyll *a* concentrations, calculated by the OC-2 algorithm, describe the large-scale changes correctly in general, though absolute values retrieved from the satellite may be more than two times as large. It is possible to get large volume of necessary measurements for comparative analysis and correction of satellite data with the help of LIF. It is possible to develop regional ocean color chlorophyll *a* algorithms for SeaWiFS using the LIF method.

Distribution of phytoplankton in the coastal waters of Sakhalin Island (Sea of Okhotsk) in summer 2001

Marina S. Selina, T.V. Morozova, I.V. Stonik and T. Yu. Orlova
Institute of Marine Biology, Far-Eastern Branch of Russian Academy of Sciences, 17 Palchevskogo Street,Vladivostok, 690041 Russia.
e-mail: marsel@mail.primorye.ru; bondartsova@mail.primorye.ru; inna@hotbox.ru; tatiana_orlova@mail.primorye.ru

The distribution of phytoplankton in the coastal waters of Sakhalin Island was studied from June-August 2001. Samples were collected using a 1-liter bathometer from the surface layer. The material was fixed with Utermel's solution and concentrated by sedimentation. Cell number was counted in 1 and 0.05 ml Nojott's chambers. Wet algal biomass was estimated by the volumetric method. Species with a density no less than 20% of the total phytoplankton density were considered to be dominant.

We found 147 species and intraspecific taxa of microalgae belonging to 7 taxonomic divisions: dinoflagellates (68 species), diatoms (64), euglenophytes (5), chrysophytes (4), cryptophytes (3), chlorophytes (2) and cyanophytes (1). Among the diatoms, the most diversified genera were *Chaetoceros* (13 species) and *Thalassiosira* (7); among dinoflagellates *Protoperidinium* (17).

During the observation period, the phytoplankton density in the coastal waters of Sakhalin Island varied from 0.03×10^3 to 742.1×10^3 cells l^{-1}; and its biomass from 0.69 to 2407.7 mg m^{-3}. The distribution of phytoplankton density in the coastal waters of Sakhalin Island was not uniform (Table 1).

High average values of phytoplankton density and biomass were found for Aniva Bay. The maximum outbreak of phytoplankton density was recorded in the innermost part of the Bay. The smallest values of phytoplankton densities were found for the seaward areas of the Bay (Fig. 1). The flagellate algae - cryptophytes and dinoflagellates constituted the bulk of the phytocenoce (at average 69% of the total phytoplankton density and 80% of the total biomass). Small flagellates *Plagioselmis prolonga*, *P. punctata*, *Cryptomonas acuta*, *Katodinium rotundata* were dominant in terms of density, dinoflagellates *Alexandrium tamarense*, *Gyrodinium spirale*, *G. lachryma* and diatoms *Thalassiosira anguste-lineata*, *Thalassionema nitschioides* were dominant in biomass. This species composition is characteristic of the summer of phytoplankton.

Table 1 Density and biomass of phytoplankton in the coastal waters of Sakhalin Island. Underlined values indicate the range of variation in phytoplankton density and biomass; below the line are average values during the investigation period.

Area	**Date**	**Phytoplankton density, $\times 10^3$ cells l^{-1}**	**Phytoplankton biomass, mg/m^3**
Aniva Bay	15.06-3.07.01	6.2-742.1 279.3	22.2-1702.4 781.6
Southeastern coastal waters of Sakhalin Is.	20-22.08.01	0.03-87.3 25.3	0.69-685.3 177.8
Northeastern coastal waters of Sakhalin Is.	23-24.08.01	6.8-22 12.7	25-170.5 74.6
Northern coastal waters of Sakhalin Is. and Sakhalinsky Bay	25-26.08.01	2.5-644.7 219.3	20.9-2407.7 817.7

Low densities of phytoplankton were found in southeastern coastal Sakhalin Island (Table 1). Some increases in numbers of microalgae cells occurred north of Cape Terpeniya. Diatoms dominated in the plankton. Among the diatoms, *Leptocylindrus mediterraneus*, *Pseudo-nitschia pungens*, *Skeletonema costatum* make up the greater part of the phytoplankton density. Large dinoflagellates *Ceratium fusus* and *C. longipes* dominated in terms of biomass.

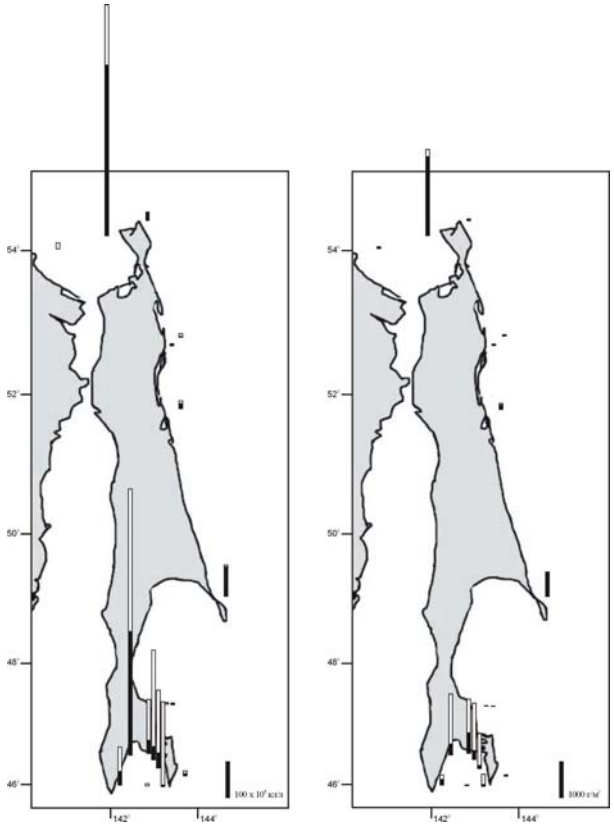

Fig. 1 Distribution of phytoplankton density and biomass in the coastal waters of Sakhalin Island in summer 2001 (black – diatoms, white – flagellates).

Low densities of phytoplankton were found in the northeastern coastal waters of Sakhalin Island (Table 1). Diatoms were the most abundant and constituted 51% of total density and 69% of total biomass of phytoplankton. *Guinardia delicatula*, *Chaetoceros* sp. and small flagellates dominated.

The distribution of phytoplankton in the northernmost area was highly irregular. Diatoms were the most abundant and constituted 73% of total density and 88% of total biomass of phytoplankton. Average values of density and biomass had relatively high development of phytoplankton in the open part of Sakhalin Bay. Small cells *Thalassiosira*, *Skeletonema costatum* and *Ditylum brightwellii* dominated. The peak of biomass (2.4 g m^{-3}) was caused by abundant development of *Ditylum brightwellii* in this area. Low quantitative characteristics were found at the other stations.

Thus, the distribution of phytoplankton density and biomass along the coast of Sakhalin Island (Sea of Okhotsk) shows significant spatial heterogeneity. This is connected with significant spatial and temporal extension of our study. Waters of the study area were classified as mesotrophic according Yamada et al. (1980), a classification based on phytoplankton density and dominant phytoplankton species. Species composition and quantitative characteristics of phytoplankton of the study area are typical for the summer phytoplankton of the coastal waters of Sakhalin Island.

Distribution and age structure of *Metridia okhotensis* in the Okhotsk Sea during the year

Marina A. Shebanova
Pacific Fisheries Research Centre (TINRO-Centre), 4 Shevchenko Alley, Vladivostok, 690950 Russia.
e-mail: dolganova@tinro.ru or napazakov@tinro.ru

Metridia okhotensis is a large grazing copepod occurring in the Okhotsk Sea and is the most predominant component of zooplankton biomass of surface layer during the year. It is known to be prey for various pelagic fishes, whales and sea birds (Nemoto 1963; Odate 1994; Hunt et al. 1998) and is therefore a vital link between primary production and predators in these regions.

Over the last few decades there have been reports of changes in the zooplankton biomass and age structure of *M. okhotensis* in the Okhotsk Sea. Maximal concentrations of this species were observed on the shelf of the northern part of the Okhotsk Sea (200-500 mg m^{-3}) and the southern deep part of the Okhotsk Sea (200-1000 mg m^{-3}) in spring, summer and autumn. The biomass of *M. okhotensis* was uniformly distribution throughout the region, with a mean density of 50 mg m^{-3} in winter. The seasonal pattern seen in the biomass of *M. okhotensis* is parallel to that of total copepods, so that *M. okhotensis* was an important determinant of the seasonal variation pattern of copepod biomass in Okhotsk Sea.

All stages of copepodite are present in the population of *M. okhotensis* in spring and summer. They are predominantly individuals of copepodite stages CIV-VI (IV-47%, V-23%, VI-21%), with a small number CI-III stages (I-18%, II-15%, III - 23%).

In autumn and winter, the population consisted mostly of individuals of copepodite stages CII-VI, CIII - 25%, CIV- 10.4%, CV 15%. Among the copepodites, stage CVI was the most numerous at 48%. Younger copepodites, stages CI-II, of this species were completely absent from the plankton during these seasons.

The present results from field survey suggest that *M. okhotensis* in the Okhotsk Sea has a one year life cycle. The spawning season continues from late May to late August, with maximal intensity in July and a progression from south to north. Early nauplii in late May-June developed to CIV-V by the beginning of August – September and the majority of CV had molted to adult stages in April-May.

These results on the *M. okhotensis* population show that in winter this species was not multiplying in the Okhotsk Sea. The onset of unfavorable conditions slows growth at developmental stages IV-V and the population enters a resting state. This phase lasts until the onset of more favorable conditions for development, reproduction starts again in April-May together with the warm waters.

Peculitiarities of ontogenetic and seasonal migrations of demersal commercial fish in the Okhotsk Sea and adjacent waters of the Northwest Pacific

Vladimir N. Tuponogov
Pacific Fisheries Research Centre (TINRO-Centre), 4 Shevchenko Alley, Vladivostok, 690950 Russia.
e-mail: tuponogov@ tinro.ru

Macrocirculation of the ocean plays an important role in dispersion of fish and in the formation of ichtyofauna. Currents, systems of the currents, and eddys influence the distribution, reproduction, ontogenetic and seasonal migrations of many fish (Marti 1980; Moiseyev 1989; Kodolov, etc. 1991, etc.).

The Okhotsk Sea is not a closed system. Currents connect parts of areas of many species in the Okhotsk Sea with adjoining waters of northwest Pacific through the Kuril straits, in the same way as the Bering Sea is connected through the Aleutian straits (Fig. 1).

Two of the most numerous and widely distributed of demersal fish groups live in the deep ocean only as adults (Kodolov, etc. 1991):

1. Grenadiers and longfin codling have a pelagic or planktonic stage of development and drift passively as larvae with the currents, living a pelagic lifestyle in the open ocean as juveniles;
2. Halibuts, sablefish, flounder, and rockfish have a littoral juvenile stage.

The species considered below, have different distributions. They are most interesting by the extent of their ontogenetic and seasonal migrations in the Okhotsk Sea and adjoining waters, and also the major role of these migrations in associations with systems of currents. The purpose of this publication is to consider the biology, distribution, and life cycle compared with features of ontogenetic and seasonal migrations of these species to understand their differences and the general laws.

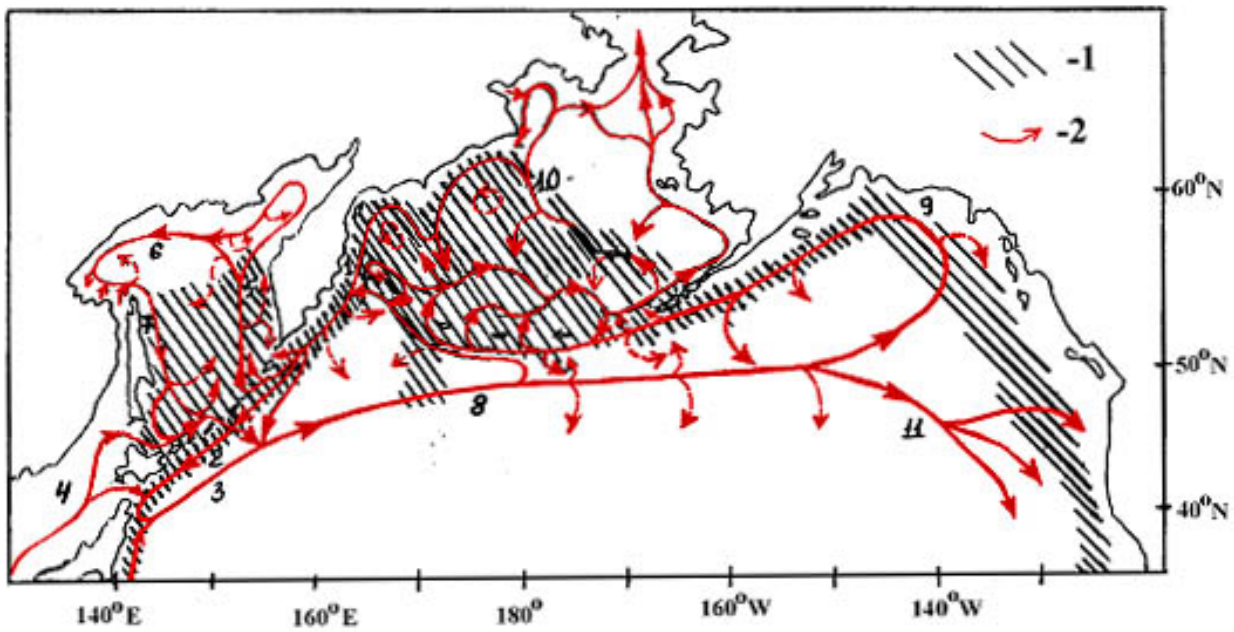

Fig. 1 Area of Giant grenadier (Tuponogov 1991) and currents of northern Pacific Ocean (Favorite et al. 1976).

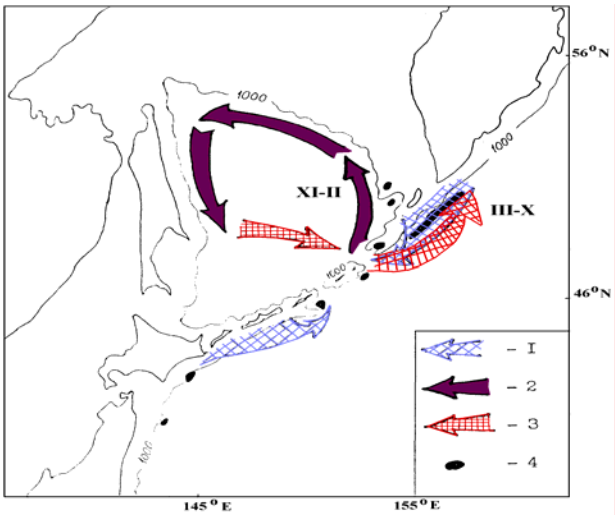

Fig. 2 The scheme of horizontal migrations of the giant grenadier along the Kuril Islands and in the Okhotsk Sea. 1- autumn-winter migrations of adult fish along the slope of Kuril Islands. 2- drifts of fish eggs and larvae. 3- spawning migration of adult fish. 4- concentrations of adult fish.

This publication is based on research conducted by TINRO on demersal fish of the northern Pacific from the beginning of the 1960s up to the end of 1990s. Data are from ichtyoplanktonic, trawling ground and pelagic surveys, and research fishing vessels. The results of tagging, morphometric, genetic-biochemical and parasite analyses, publications and materials are used in this publication.

The features of biology and distribution of demersal fish have been investigated rather insufficiently. Data were collected irregularly in different years and seasons in different areas but it provides an opportunity to develop a hypothetical scheme of seasonal cycles.

Giant grenadier (*Albatrossia pectoralis*)
This species is distributed in the Okhotsk Sea and along the Kuril Islands everywhere from depths of 400-600 m. It is the most numerous species of benthic fish on the continental slope and prevails from 600-700 m (up to 70-90 % of the catch). It is considered "the pollock of the depths" and with an increasing value in recent years, catches have been increasing.

The life cycle scheme of the species was proposed (Tuponogov 1986,1991) based on own data and on literary data (Novikov 1970, 1974; Tuponogov 1986, 1991, 1993, 1997; etc.). Females make up 80-90% of all in benthic layers at the continental slope. A small fraction comes from the bottom at significant distances and meets in thickness of water on depths from 300-500 up to 1300-1500 m (Fig. 2).

The distribution of giant grenadier in the Okhotsk Sea differs from other areas by the absence of significant aggregations. Maximal densities occur at the southwestern part of Kamchatka, and the northern Kuril Islands under the influence of Okhotsk Sea waters through the northern Kuril straits. More dense aggregations are formed on the Pacific side of the Kuriles near Kruzenstern's and Bussol' deep-water straits, at depths of 900-1450 m. Spawning of some individuals probably occurs constant within all year lengthways slope depths within the limits of deep water. The most intensive aggregations are during spawning on the Pacific side off the Kuril Islands during the spring-summer period at depths about 1200 m. A fraction of the stock is not spawning within the year.

Fish eggs of giant grenadier develop in depths more than 500-1000 m. The majority of eggs, larvae and juveniles this species in the Okhotsk Sea are found near to the northern Kuril Islands. Captures of eggs in adjoining waters of the Okhotsk Sea are dated to the Pacific waters, entering through the Fourth Kuril Strait at depths of about 500 meters. The branches of the Kamchatka-Kuril Currents penetrating through the northern Kuril straits, where there is a cyclonic system of currents in the Okhotsk Sea, carry eggs and larvae from the Pacific side of the northern Kuril Islands along the Kuril slope and on all water areas of the sea. Eggs and juveniles live in a layer of water located above the deepwater Kuril Basin and slope in the central part of the Okhotsk Sea.

Benthic aggregations of giant grenadier from the Pacific side of the Kuril islands are formed by mature fish (75-100% of all giant grenadier). The proportion of juveniles in the benthic aggregations in the Okhotsk Sea is significant. The proportion of mature fish here is always much less than in

adjoining areas. The Okhotsk Sea is a feeding area for juvenile giant grenadier from adjoining areas.

The annual migratory cycle of the giant grenadier in the northern Kuril Islands and in the Okhotsk Sea (Tuponogov 1991,1997) reflects a more extended seasonal migration, than was considered earlier (up to several hundreds miles) (Fig. 2). All data distributions and biology of giant grenadier in both areas correspond to this scheme.

Agreement of the morphometric and genetic-biochemical analysis suggests that the summer distributions of this species in the northern Kuril Islands are from two groups - Northern Kuril and Okhotsk Sea. The southern Kuril islands has a complex structure and consists of several groupings. Currents transfer and mix eggs of different groupings. Therefore reproductive isolation is not present, decreasing distinctions between separate groupings (Tuponogov and Malinina 1991).

The proportion of immature females is especially high in the Okhotsk Sea. The proportion of pre-spawning females is small even during spawning. The limited spawning can go here in the summer in separate sites the Okhotsk Sea. The larger fraction of pre-spawning individuals from the Okhotsk Sea moves, during the process of sexual maturation to the area adjacent to the Kuril Islands.

Migration of the giant grenadier for winter begins in the autumn on the Pacific side of the Kuril Islands along the slope to the deep Kuril straits. In the winter-spring here, it is not found in concentrations comparable with summer.

Longfin codling (*Laemonema longipes*)
This species is distributed everywhere in the Okhotsk Sea and adjacent waters of Kuril Islands. It is a deepwater species living on the slope, and in bathyal, meso-, bathypelagic areas. It is numerous in the Japanese and Kuril islands, and only in some years in the Alaid area (northernmost Kurils). The fishing conducted in Alaid area, as for the Japanese Islands, now carries on in the southern Kuril Islands (Pautov 1980; Kodolov, Pautov 1986; Savin 1986, 1991, 1993, 1998).

The scheme of the life cycle was first composed by Kodolov and Pautov (1986) was changed (Fig. 3) by Savin (1993, 1998). The seasonal migration of mature fish is directed toward southwestern Honshu coast for spawning. The pelagic eggs and larvae drift from the spawning areas, and early juveniles are found north in an area of periodic localization of quasi-stationary curls along the east coast about Honshu inside the main jet of the Kuroshio during its meandering processes. The eddy structure and transverse jets in the Kuril and Oyashio currents are favorable for this migration. The performances about the schemes of currents (Burkov 1980) do not explain the further process of moving longfin codling juveniles from Honshu in a northward direction to the Okhotsk Sea. The northeast branch of the Kuroshio consists of a chain of anticyclonic eddies moving in a northward direction (Bulatov 1980). A large anticyclonic eddy can intersect the Subarctic front and reach the central Kuril Islands. The Oyashio and its branches have mainly cyclonic eddies. Between eddy (curls) of the opposite sign and on periphery of chains of one-direction curls, the ink-jet currents can form. Migrations from east Honshu to the southern Kuril Islands occurs due to intrusions of warm waters of a northeastern branch of the Kuroshio on north in case of ink-jet streams, and also in western sectors anticyclonic and in east sectors cyclonic of curls (between cyclones of the first branch Oyashio and anticyclones of a northeast branch Kuroshio).

After transforming to an active lifestyle, the juveniles migrate to the Okhotsk Sea through the northern halves of the deep-water straits in the southern Kuril islands (especially Bussol). The migrations to the Okhotsk Sea last for 1-2 years. The Okhotsk Sea the main area of growth of juveniles from age 1 to age 3-5 years, then the fattening in the Alaid Strait area for one to two years follows. In the sea of the adults it is not enough and 95% of longfin codling makes 1-3 years. Such juveniles outside the Okhotsk Sea are rare. After fattening for two to three years in the Okhotsk Sea juveniles in process of propagation are displaced to the Kuril straits, lengthways along the Kuril Islands. The main migratory route goes along Northern Kuril Islands on to the Okhotsk Sea side up to deep-water straits. Then longfin

codling quits on the ocean side of the Kuril Islands through Krusenstern and farther south.

The fattening on the Kuril slope lasts one year, the fattening on the small Kuril Islands, for no more than one season. Then the migration to Hokkaido and Honshu and addition of trade accumulations of the adults follows. See the scheme of annual migratory cycle (Fig. 3) composed by Savin (1991, 1998).

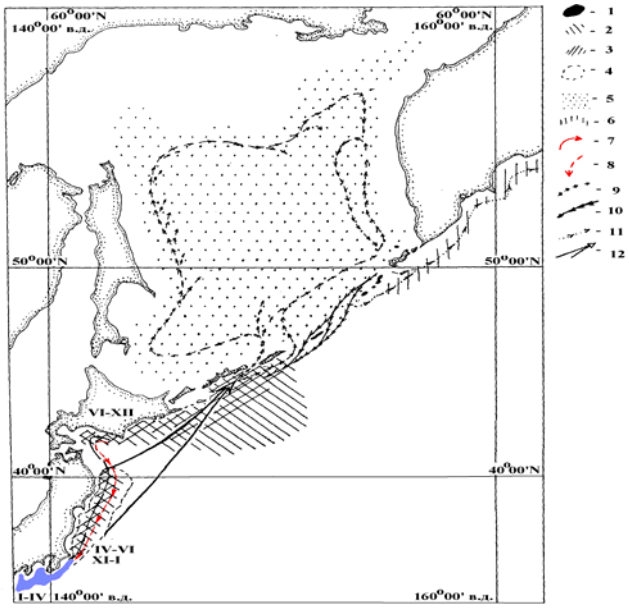

Fig. 3 The general scheme of longfin codling migration (Savin 1991,1998). 1-spawning area of (2) mature females and (3) males; 4-the regional migration initial eggs and larvae drift; 5-early juveniles life zone; 6-zone of eviction migrations; 7-postspawning; 8 - prespawning; 9-juveniles; 10-migration of first matured fish; 11-migration of eviction; 12 - transport of yearling (the Roman numerals designate months when are adults found).

The fattening adult of longfin codling happens on the Hokkadio slope from June till December, and along the small Kuril ridge, from July till December. The fattening on the slope happens mainly for males, females mainly live outside slope in waters in the Oyashio. Part of the adults moves lengthways along the Kurils up to northern Kuril Islands, and Kamchatka in the summer. In Alaid basin and the Fourth Kuril Strait strong cohorts are observed. The start of maturation for Japan starts in August. The beginning of spawning migration to the southern spawning areas occurs in October. It proceeds lengthways along Honshu from November up to middle of winter - till February. The majority of individuals migrate to depths of 600-900 m and go, at least, in two waves. Spawning occurs in January, and the peak occurs in March-April for southeast Honshu. To the north, spawning of longfin codling is not present, but a little pre-spawning and post-spawning fish are seen. The post-spawning migration from Honshu occurs from the middle of April until June.

Shortraker rockfish (*Sebastes borealis*)
Compared to the giant grenadier and longfin codling, this species forms aggregations on both the Asian and American coasts. It is more numerous in the eastern part of Gulf of Alaska, in the southeastern part of the Bering Sea, on Shirshov's Ridge, east Kamchatka, and near the Aleutian and Kuriles Islands (Polutov et al. 1966, Orlov 2002, 2003). It is more valuable than giant grenadier or longfin codling.

The life cycle was constructed by Orlov (2001, 2002, 2003) based on distribution and biology in separate areas of Pacific Ocean (Tokranov and Davidov 1997, 1998; Tokranov 1998; McDermott 1994) considering the dimensional structure and ocean circulation in North Pacific Ocean. Shortraker rockfish is a far migrating species whose basic areas of dwelling are located within the limits of the basic macrocyclonic circulations: Alaska subarctic, Western subarctic and cyclonic circulation of the Bering Sea (Fig. 4).

Females make extended migrations from feeding areas to spawn. Larvae are widely carried by currents on the shelf, settling in bays. They live here in the first years of a life and in process of growth are displaced to areas of dwelling for mature fish.

The basic areas of reproduction within the limits of the western subarctic circulation are, apparently, the slopes of Kronozki, Kamchatka and Awatschao bays of east Kamchatka. One more area of spawning, most likely, is the slope of the central coast of island Paramushir.

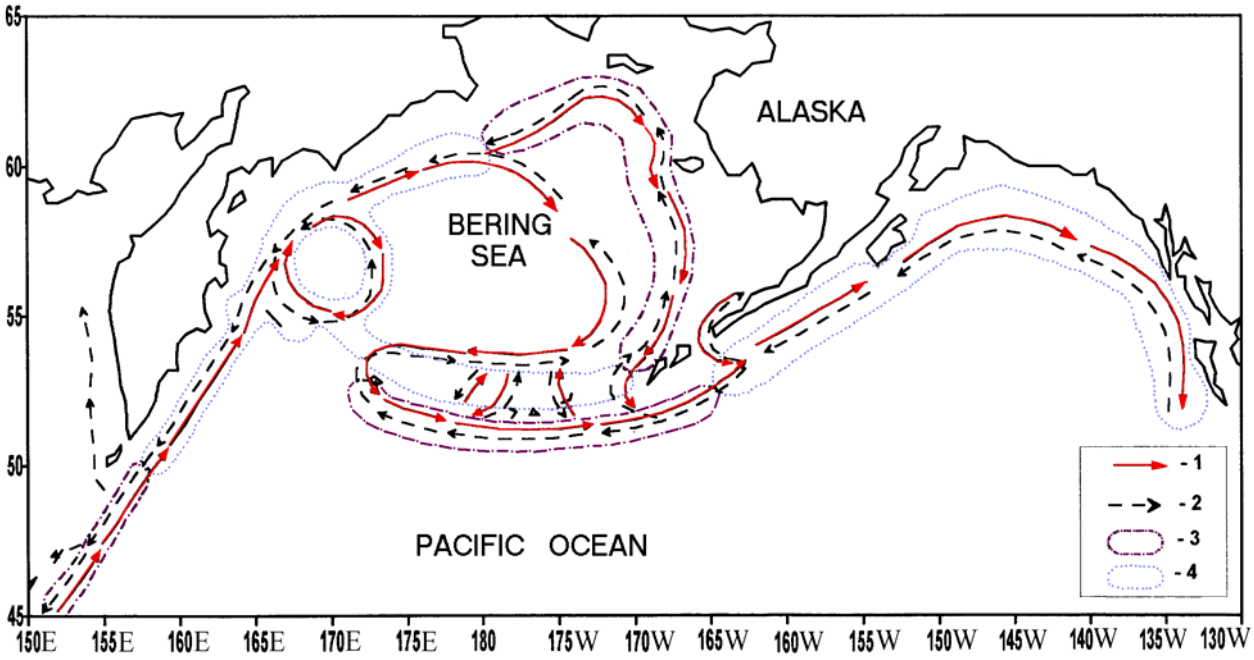

Fig. 4 The hypothetical scheme of horizontal migrations of shortraker rockfish in the northern Pacific Ocean (Orlov 2002, 2003). 1 - the basic directions of active migrations of adult individuals, 2 - the basic directions of passive migrations of larvae and pelagic juveniles, 3 - the basic areas of dwelling of juveniles, 4 - the basic of area of reproduction.

Large mature individuals concentrate here during the aestivo-autumnal period. The average sizes of fish gradually decrease to the south from east Kamchatka to Kuriles.

Larvae in the northeast Pacific Ocean appear in April (Westrheim 1975), and in various areas in the Bering Sea from April till July (Novikov 1974). Larvae occur in benthic layers as with other deep-water sea perches (Moiseyev and Parakezov 1961). Larvae of rockfish *Sebastes* develop in the superficial covered layers (Barsulov 1971, 1981).

Larvae from the east coast of Kamchatka, are transferred by the East-Kamchatka Current to the Kuril Islands. An insignificant portion pass through the North Kuril Strait to the Okhotsk Sea and by currents to the southwestern part. The area along the southeast coast of Sakhalin has none.

The fraction of larvae from the western part of the Bering Sea can be carried by the East-Kamchatka Current through Kamchatka Strait to the east coast of Kamchatka and further to Kuril islands. Larvae from the southern part of the Bering Sea can be carried to the Pacific Ocean through the straits of the central part of the Aleutian archipelago. Larvae of British Columbia and Gulf of Alaska are transferred by currents to the Aleutian islands. They can be carried into parts of the Bering Sea through straits along the Aleutian islands.

During passive migrations, juveniles can be late to join currents, diverted to underwater heights and near to straits creating time-dependent populations in these areas. On a regular basis, they replenish migrating of feeding areas with individuals. Such time-dependent populations, by virtue of oceanographic features, can be characteristic for Pacific waters of the Kuril and Aleutian islands. Stable anticyclonic eddies occur from 90-120 miles from the coasts of Paramushir and southeastern Kamchatka above an underwater height to the southeast from about Onekatan (Lobanov 1983; Stabeno et al. 1994). Here are constantly observed higher catches of mainly immature shortraker rockfish. The pelagic stage of development lasts for a long enough time.

Juvenile shortraker rockfish appear in bottom trawling catches in the northwest part of Pacific Ocean at a length of about 8-10 cm. Juveniles start to pass from a pelagic to a demersal lifestyle in the Pacific waters of northern Kuriles at lengths greater than 10 cm at an age of 2 years. They start appearing in large trawls at lengths over 15 cm at ages of 3-4 years (Leontiev et al. 1998; Orels 2003).

After transition to a demersal lifestyle, after achieving a body length over 30 cm (mainly >40-45 cm) vertical and horizontal migratory behaviour increases. Some individuals start return migrations that can extend for many years. Shortraker rockfish is capable of overcoming opposing ocean currents.

Mature shortraker rockfish in Pacific waters of northern Kuriles and southeast Kamchatka start to occur in the catches at 30-35 cm length; 50% of individuals have mature gonads at 45-50 cm (Orlov 2003).

The annual migration cycle is less well investigated.

Shortraker rockfish is a viviparous species with internal fertilisation. Summer and autumn is the period between the termination of spawning and pairing of the species. In the autumn during pairing and in the spring during larval parturition (Novikov 1974; McDermott 1994; Snitko 1986, 2001) shortraker rockfish remains at certain sites on the slope for a long time. In winter, the males and females remain separate. Juveniles are also distributed in separate aggregations at lesser depths.

Sablefish (*Anoplopoma fimbria*)

Sablefish is a very valuable commercial species whose distribution is centred toward the Northeast Pacific. The biology and distribution have been studied more thoroughly in this area than in the Northwest Pacific (Shubnikov 1963; Kulikov 1965; Kodolov 1976, 1986; Novikov 1974; etc.).

The biological cycle (Fig. 5) was described by Kodolov (1986) and Novikov (1974) with additions. Earlier, it was considered that the reproductive area for sablefish occurred only in the northeastern part, an area including waters of Washington-Oregon area, British Columbia, Gulf Alaska, and probably California. Spawning here occurs in the autumn-winter period from September to February. It was considered that passive drift of the larvae and juveniles occurred in a western direction, determined by the current. Larvae and juveniles in the first years of life remain in the uppermost layers, above the slope. Accumulations of juveniles and of nonmature fish of length <44 cm are known only east of the Aleutian Islands, in the Gulf Alaska and to the south. Juveniles in the Gulf of Alaska make active migrations westward. A significant fraction of the juveniles live in the open ocean, far beyond the reproductive area. In the process of propagation, migrations occur in the opposite direction. Before sexual maturation, juveniles have a bottom-pelagic lifestyle and live in upper layers of water in the pelagic, in deeper waters above the shelf, on the bottom of the shelf and in top of the continental slope. Mature fish are found throughout a large range of depths, from 0 - 2560 m. By results of tagging, sablefish make significant extended migrations from the American to the Asian coast. But the migrations of the basic mass of the species are limited to the eastern part if the northern Pacific.

The views of experts were divided on the status of sablefish in Asian waters and there link with populations on the American coast. A number of researchers (Kodolov 1968, 1976, 1986; Tokranov 1997; Dudnik et al. 1998; Kim Sen Tok 2000) consider the Okhotsk Sea, Kuril Islands, East Kamchatka and western Bering water as the zone of eviction from reproductive areas on the American coast. It is considered that spawning on the Asian coast does not have a stable, regular and large-scale character. Juveniles are seldom found here, and the number depends mainly on immigration from the eastern Pacific. But the sablefish, even in the western part of the Bering Sea, do not have the character of regular mass migrations (constant unit deepwater ichthyofauna, and in separate sites of North Kuril waters - forming a small accumulation, and per 60 years

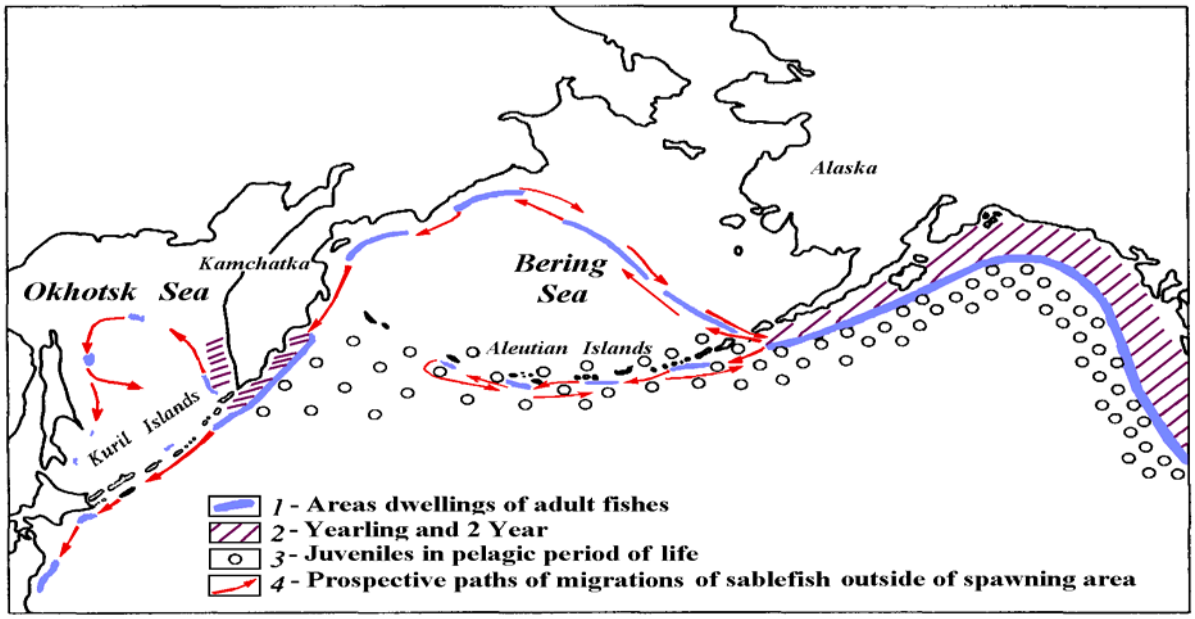

Fig. 5 Distribution and migrations of sablefish (*Anoplopoma fimbria*) in North Pacific Ocean (Kodolov 1968; Novikov 1993; Dudnik et al. 1998 with additions).

even engaging the significant place in catches (Novikov, 1965) in the usual catches of species in the northwestern Pacific. In the Okhotsk Sea from separate captures to regular catches throughout the Okhotsk Sea, and in the North Kuril Islands and Southeast Kamchatka, an increase in number and frequency of occurrence (Novikov 1969,1994; Dudnik, Dolganov 1992; Orlov 1997; Tokranov 1997). It is possible to explain the wide circulation and constant occurrence just by the migrations of the adults and drifts juveniles from the American coast.

The data on distributions of mature and juvenile sablefish (yearling, 1 Year, 2 Year) suggest that, on the whole, there was weak migratory activity, the majority were observed to remain in the area of discharge without migrations of a defined direction. In Asian waters, the greatest aggregations occur deeper than on the American coast. This is connected to the more severe hydrological conditions in the west. Spawning is likely. The problem of existence of classifications up to the extremity is not clarified (Novikov et al. 2003).

For the sablefish, the northwestwern Pacific is most likely, not an area of eviction from the main areas. Here, the populations are common constituents in this area of the North Pacific and their distribution is more poorly connected to the main areas in the eastern part of Pacific than was considered earlier.

Conclusions

1. Giant grenadier, longfin codling, shortraker rockfish and sablefish are endemic to the North Pacific Ocean. Their distributions reach a continuous arch from the Japanese islands to the coast of North America. These species will not penetrate into the Japan Sea because the shallow depth of straits.

All four species prefer sites of the continental slope with the dismembered relief of the bottom, sharp differences of depths and the big biases of the bottom. Food habits are isolated mainly on the interzonalplankton, and in smaller measure on benthic fauna on the continental slope. All of them are long-lived species with low rates of reproduction.

2. Absence of high concentrations of fish eggs and juveniles above aggregations of adult fish and the high occurrence of these fish in open waters testifies to significant horizontal movements due

to ontogeny and the role of ocean currents. All four species have these characteristics:

- seasonal prevalence of distribution in currents of the year, connected to migratory activity;
- ontogenetic migrations;
- interseasonal and interannual differences of features of distribution.

Separation of the places of spawning and feeding, seasonal distribution and ontogenetic migrations reflect the difference of conditions of the environment, forage reserves, density of settling, competitive attitudes in different areas within a year. The cold temperatures in the Okhotsk Sea do not provide most deepwater species the normal conditions for reproduction. Only the black halibut (*Reinhardtius hippoglossoides matsuurae*) has managed to reach high numbers at the expense of adapting to severe conditions of dwelling juveniles.

Giant grenadier, shortraker rockfish and sablefish are Pacific boreal species. Spawning occurs during the spring-summer period in warm Pacific waters at the Northern Kuril Islands and East Kamchatka. Longfin codling, an Asian speces, is more attached to subtropical waters for reproduction. Spawning of the longfin codling occurs during the winter-spring period in southeastern Japan.

Giant grenadier – a bathybenthic species, only the part of adult individuals comes off the bottom on significant distances and meets in the thickness of water. It has benthic spawning - more local and longer duration.

Longfin codling, shortraker rockfish and sablefish – mesobenthic species, forms aggregations at shallower depths and smaller areas adhered to the bottom, therefore their spawning is also more pelagic and consequently more on the area.

Giant grenadier and longfin codling in the Okhotsk Sea and at Kuril Islands have oceanic (pelagic or planktonic) stages of development and are more numerous than sablefish, a flounder, and shortraker rockfish (littoral juveniles). Because of distinctions in thermal conditions between western and eastern parts of the Pacific Ocean, the pelagic period at the Asian coast can be longer, and times of spawning are shifted.

The migratory cycles of the species considered in the Okhotsk Sea and off the Kuril Islands are defined by the nature of drift of eggs and larvae. Eggs and larvae are carried by the currents and are carried large distances as occurs with many pelagic and ground fish. The role of currents is especially great in the development of eggs and the distribution juveniles. The Okhotsk Sea is a place of feeding for giant grenadier and longfin codling.

3. The scheme of migrations for giant grenadier and shortraker rockfish reflect more extended seasonal movements than was considered earlier (up to several hundred miles). The routes are more hypothetical as little is known about the pelagic juveniles of bathyal fish. Migrations routes can be specified by studying the intraspecific structure of morphometric, genetic-biochemical analyses, biology and distribution. For this purpose application of distinctions in seasonal variability of distribution of aggregations of fish, distributions of spawning individuals, occurrences of eggs, larvae and juveniles, intensity of feed, and fatness is possible. Tagging is only possible to apply on sablefish, for the species considered.

Described migration routes have the general character. They can vary appreciablly depending on large-scale oceanolographic changes that influence the intensity of streams of the basic currents in North Pacific and define a level of water exchange between the Pacific Ocean and Bering Sea. Variability in ocean circulation defines various ways of passive migrations of young juveniles and the subsequent numbers of adult fish. The interannual fluctuations in numbers is especially seen in the field of eviction, which in many respects, are caused by variability of oceanographic conditions, particularly the intensity of currents. Change of volume of waters entering the Okhotsk Sea also varies the emigration of early stage juveniles of giant grenadier, shortraker rockfish and sablefish in jets of the East-Kamchatka Current that is reflected further in the number of adult fish.

Localization of spawning areas of *Thysanoessa raschii* in the Sea of Okhotsk in spring

Anatoly Volkov
Pacific Fisheries Research Centre (TINRO-Centre), 4 Shevchenko Alley, Vladivostok, 690950 Russia.
e-mail: vaf413@tinro.ru

Of all species of euphausiids living in the Sea of Okhotsk, by abundance and biomass in the planktonic community, and in consideration of nutrition for nekton, the leading place is occupied by *Thysanoessa raschii.* Features of her biology and ecology require specification (Chuchukalo et al. 1996; Shuntov 2001; Zhuravlyov 1984). The basic habitat of this species in the Okhotsk Sea is the boreal shelf zone. The most dense aggregations occur at depths up to 200-500 m (Volkov 1996; Volkov 2002; Volkov and Efimkin 2001). Data on abundance of eggs and nauplii of *Th. raschii* and season in which observation have been have been carried out from 1998-2002 are recorded in Table 1.

All these years concern the same season, but sampled during years of high but variable extent of ice cover (Figs. 1, 2). The spring of of 1998 was the first year after the abnormally warm winters of 1996 and 1997. The spring of 2001 followed a year with maximal ice cover. The spring of 2002 followed a winter of high, but less than maximal coverage. Although the season of spawning of euphausiids and appearances of the nauplial stages in different years cannot be determined to within a day, nevertheless its beginning and peak can be determined to within a 10 day period.

Table 1 Time of occurrence of eggs and nauplial stages of *Thysanoessa raschii* in the plankton.

1998	5-9 May	13-27 May	12-30 May	16-26 May	29 May - 2 June	2-7 June
Eggs	4	8,5	1,5	71,5	83,5	315
Nauplial	0	0	1,5	0	10,5	90,5
1999	1-9 May	3-9 May	1-16 May	25-31 May	16 May - 5 June	19 May - 3 June
Eggs	0	15	34	68	87	120
Nauplial	0	9	1	2	22	24
2000	1 - 4 May	8-15 May	25 May - 7 June	10-20 May	12-29 May	25 May - 9 June
Eggs	1	0	16	40	227	208
Nauplial	0	0	1	0	15	119
2001	25 May - 4 June	30 April - 9 May	30 May - 5 June	1-19 June	4-12 June	11-18 June
Eggs	0	1	40	16	227	208
Nauplial	0	8	0	1	15	119
2002	28 April-7 May	20 April-16 May	27 April-18 May	18 – 26 May	17-30 May	26 May - 3 June
Eggs	0	0	10	8	11	38
Nauplial	0	0	0	0	0	0,35

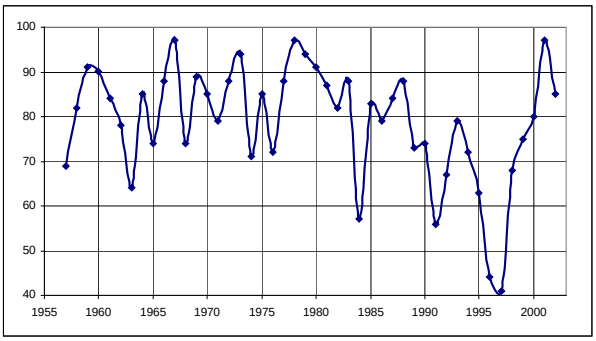

Fig. 1 Sea ice extent (%) in the Okhotsk Sea (1957-2002).

From 1998-2002 in the boreal shelf zone (areas 1-6 in Fig. 3) spawning had not begun anywhere during the first five days of May. In second five-day period, the beginning of spawning was observed only in 2000 and 2001. In third five-day period, the beginning of spawning was observed in all years, but in 2001 separate events of spawning in a mouth a hall were observed only. In Shelikhov Bay and in other areas, spawning was evident only at the end of May. In first ten days of June, spawning everywhere had a mass character. Appearance of the nauplial stages begins normally during the last 10 days of May, but in different years, it may occur 5-10 days earlier (1999) or later (in 2002, the nauplial stages were caught only at one station). The period between the beginning of spawning and the appearance the first nauplial stage normally takes 12-16 days.

This distribution of biomass of *Th. raschii* in spring has the greatest values across the peripheral regions (Fig. 4), that shows and in distribution of different size-classes of animals (Figs. 5-7).

Mass spawning begins only in first ten days of June and lasts through the second 10 day period, and then spawning by those parts of the population that, from any one of a number of causes, may have matured late. Most “in due time” dead-ripe

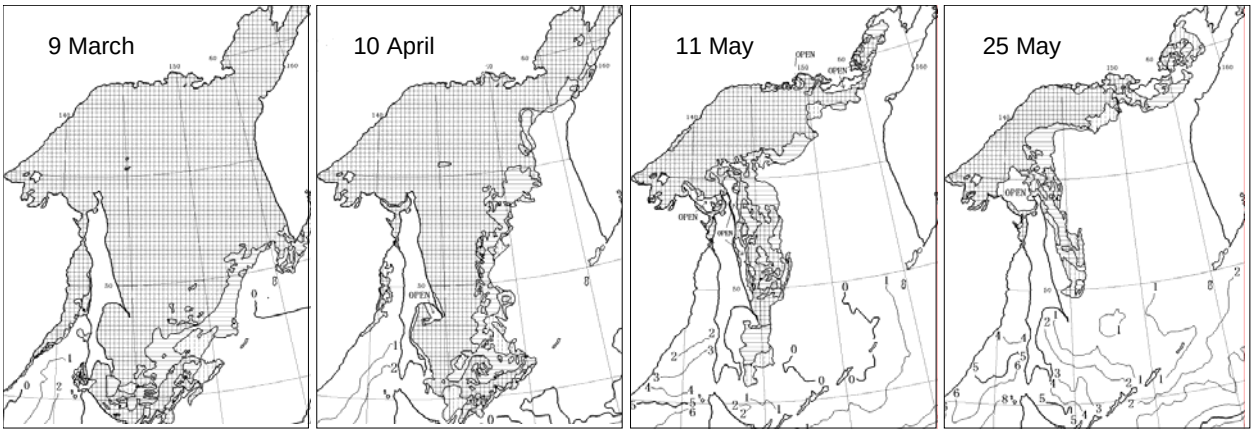

Fig. 2 Thawing of ice in the Sea of Okhotsk in the spring of 2001.

part - jumboes with a length of 20-25 mm. At the beginning of spawning, they are concentrated closer to periphery of the shelf, and are most eurysynusic and numerous young (10-15 mm) which can ripen only by end of summer - to beginning of autumn or even by next spring and middle-sizes (15-20 mm) which part together with large spawning in spring. All others start breeding later.

Thus, eggs and nauplii are the result of spawning by animals in the 20-25 mm size-class (from the previous year) and in part by the 15-20 mm size-class of the same year. Furcilia with lengths less than 10 mm that are the result of late spawning in a year that had to overwinter, therefore their abundance in spring is the lowest among other size-classes.

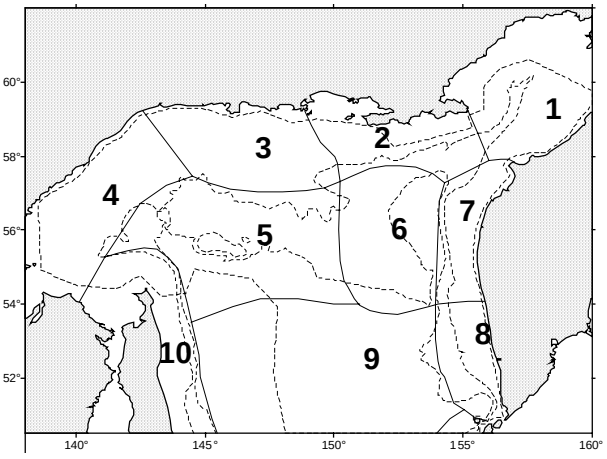

Fig. 3 Borders and numbering of standard biostatistical areas of the Okhotsk Sea. Dotted lines designate isobaths 200 and 500 m, sold lines - borders of areas. Rough terms of planktonic samplers: areas 7-8 - April, 6 - on May, 1-10, 1 - on May, 1-15, 2, 3, 4, 5 - on May, 15 June.

The following spring, the overwintering animals can become the large size-class part of the population. Accordingly, to reveal "locuses" of spawning it is necessary to compare the production of eggs and nauplial stages by adults born in the same year (15-20 and 20-25 mm), and it is possible to judge the dislocation of late spawning on allocation of furcilia of lengths <10 mm.

In March and April spawning does not begin even in the warmest waters of western Kamchatka. Lower abundance nauplii at end of May - beginning of June speaks that spawning began only recently and has not yet reached a maximum.

Thus, the basic areas of breeding *Th. raschii* range in shelf zone from depths of 100-200 m. Clumps of large and middle-dimensional euphausiids (15-20 and 20-25 mm) form adult spawners or pre-spawning individuals.

In these places it is necessary to expect the appearance of plenty of eggs, nauplii, and then calyptopis from the beginning to middle of June and, with each subsequent stage of development, a nucleus of high abundance will be diminished more and more, so in the summer and autumn seasons, such high concentrations of young and

adult *Th. raschii* are not observed. The animals of 10-15 mm will most likely begin spawning late in the year or in early-autumn; furcilia achieve sexual maturity only in late autumn of the next year, but their abundance is insignificant in the spring, and in summer, will be even more reduced, therefore their influence on the population size is insignificant.

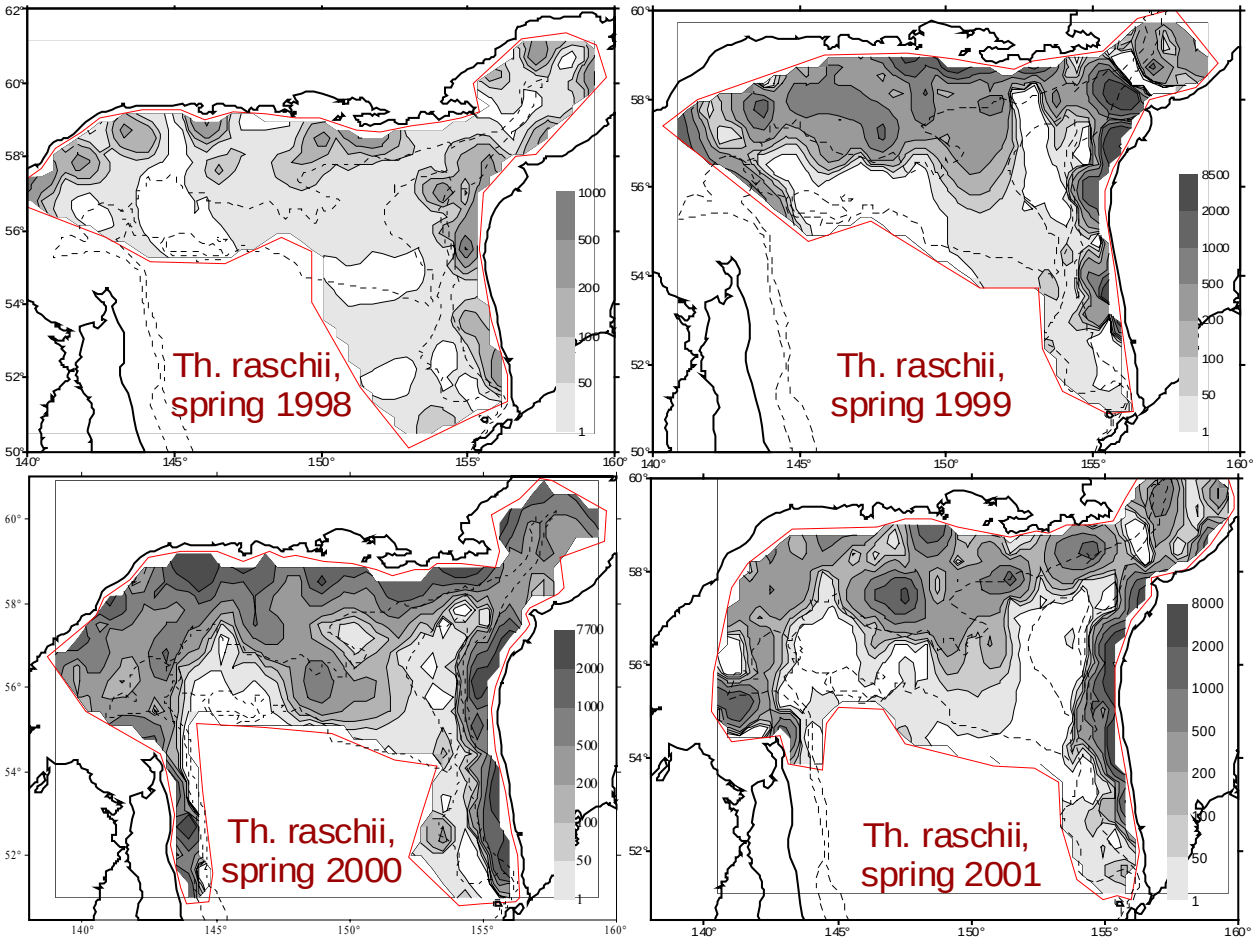

Fig. 4 Distribution of biomass of *Thysanoessa raschii* in the northern part of the Okhotsk Sea, mg m^{-3}.

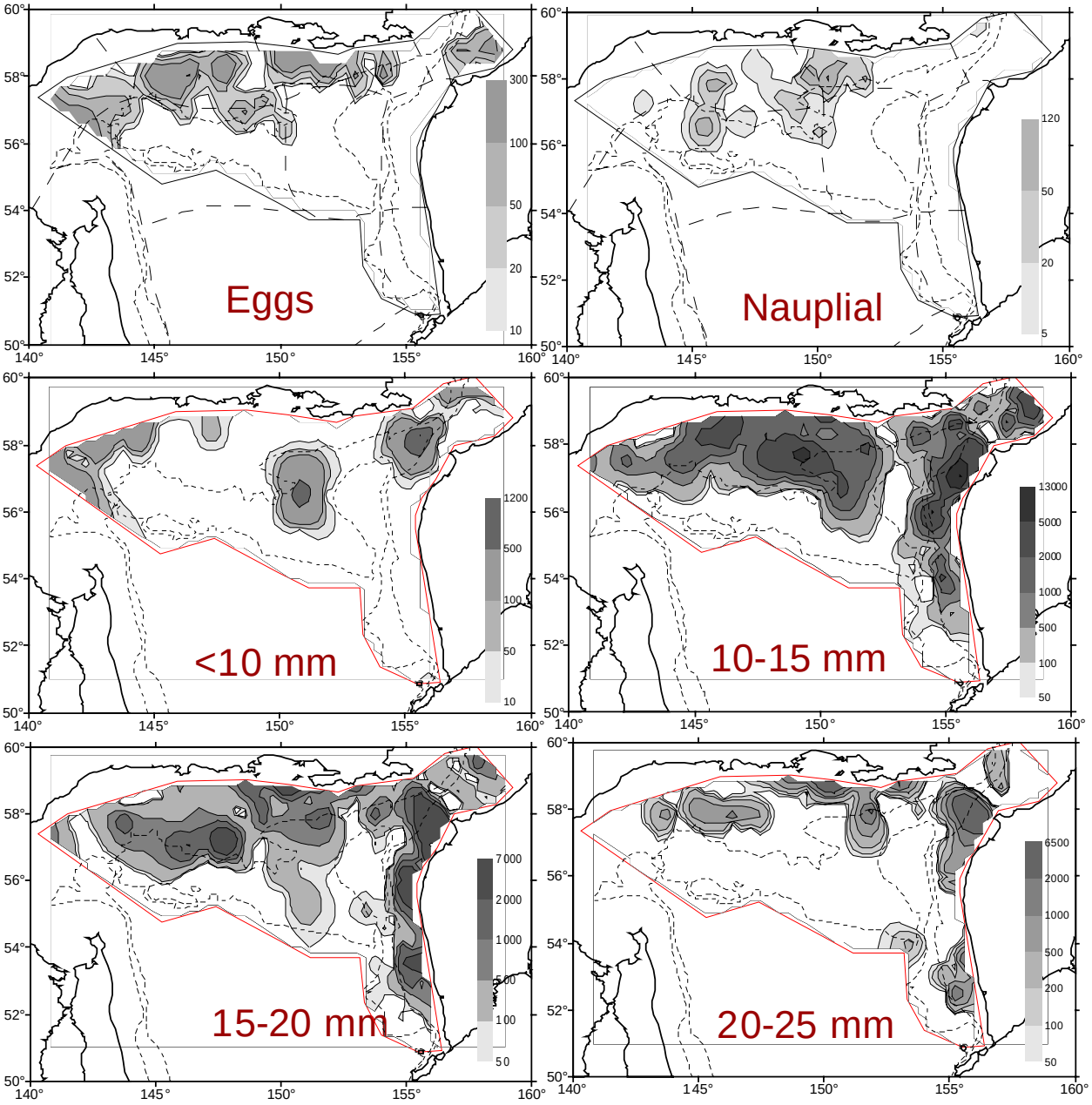

Fig. 5 Distribution of number *Th. raschii* in the northern part of the Okhotsk Sea in the spring of 1999. Eggs and nauplii – ind. m^{-3}, other – anim. m^{-2}.

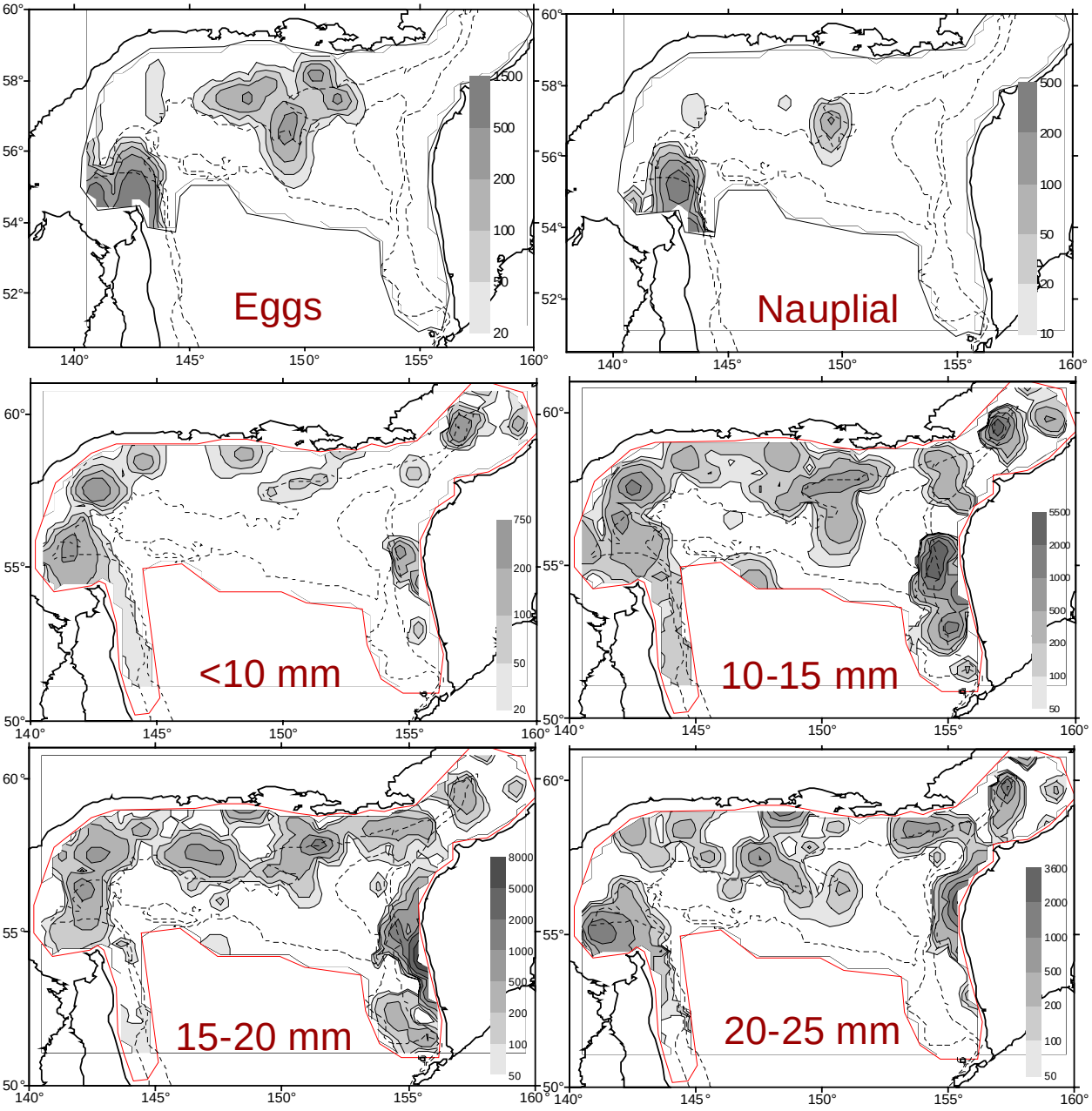

Fig. 6 Distribution of number *Th. raschii* in the northern parts of the Okhotsk Sea in the spring of 2001 (eggs and the nauplii – ind. m^{-3} ; other – anim. m^{-2}).

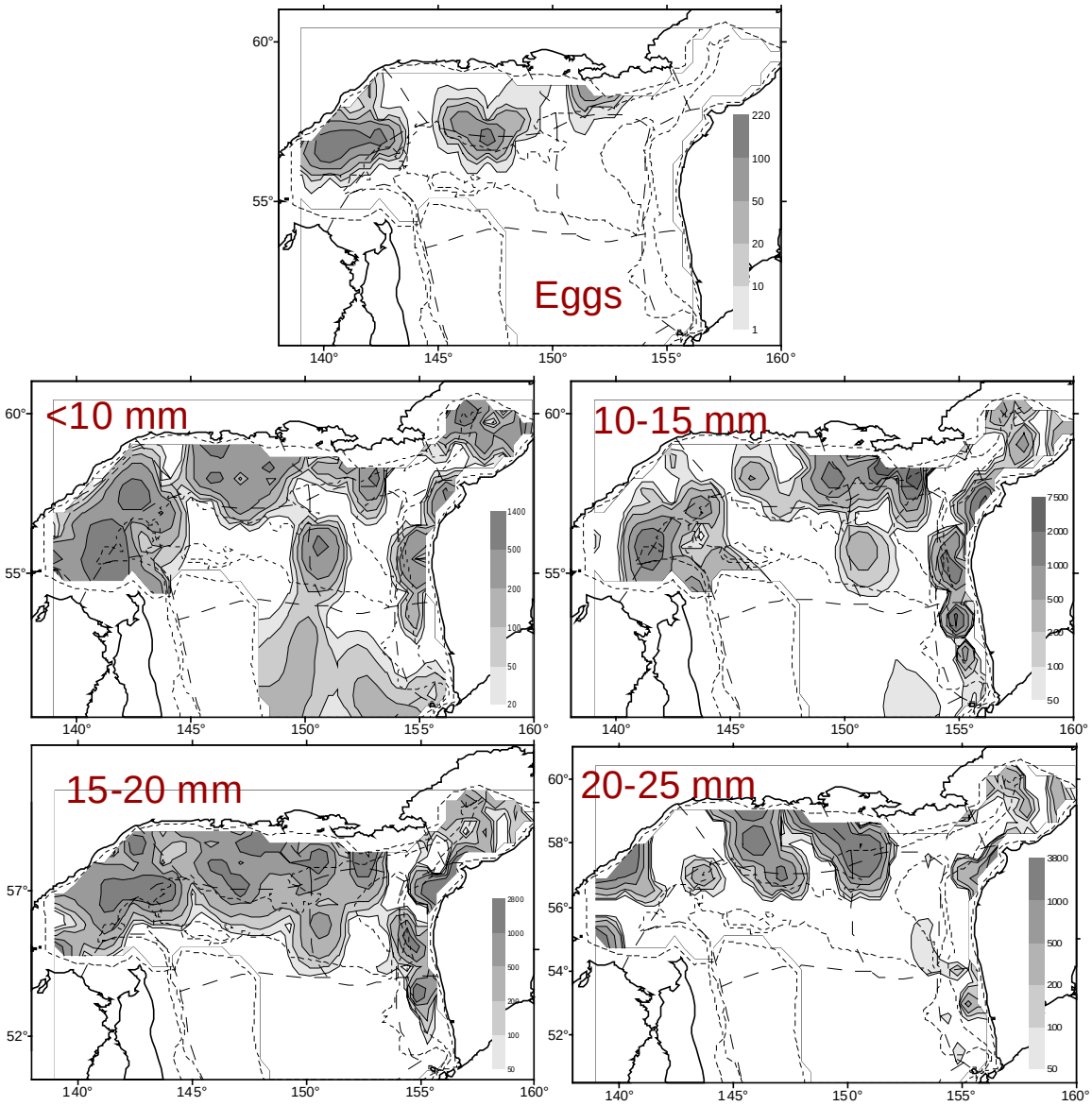

Fig. 7 Distribution of number *Th. raschii* in the northern part of the Okhotsk Sea in the spring of 2002 (eggs - ind. m^{-3}; other – anim. m^{-2}).

References

Chuchukalo, V.I., Kuznetsova, N.A. and Napazakov, V.V. 1996. Seasonal distribution of euphausiids in the Bering and Okhotsk Seas and adjacent waters of Pacific Ocean. Izv. TINRO 119: 256-281.

Shuntov, V.P. 2001. Biology of the Far-eastern Seas of Russia. Part 1. - Vladivostok: the TINRO-CENTER, 580 p.

Zhuravlyov, V.M. 1984. Ecology of euphausiids of the Okhotsk Sea. M.: VNIRO. 74 p.

Volkov A.F. 1996. Epipelagic zooplankton of the far-eastern seas: structure of communities, interannual dynamics, value in a feed of nektonic animals. Doctoral diss. Vladivostok. the TINRO-CENTER. 69 p.

Volkov, A.F. 2002. Biomass, abundance and size structure of euphausiids of the northern Okhotsk Sea in the spring periods of 1998-2001. Izv. TINRO 130: 336-354.

Volkov A.F. and Efimkin, A.Ya. 2002. Current status of planktonic epipelagic community of the Okhotsk Sea. Izv. TINRO 130: 355-407.

The results of investigations of golden king crab, *Lithodes aequispinus*, from eastern coast of Sakhalin Island

Lubov A. Zhivoglyadova
Sakhalin Research Institute of Fisheries and Oceanography (SakhNIRO), 196 Komsomol'skaya Street, Yuzhno-Sakhalinsk, 693023 Russia. e-mail: lubov@sakhniro.ru

The golden king crab (*Lithodes aequispinus*, Benedict) is widely distributed in waters of the North Pacific from the shores of British Columbia to Honshu Island (Rodin 1970, Jewett et al. 1985, Somerton and Otto 1986). In the Okhotsk Sea *L. aequispinus* inhabits the northern part of the sea, near East Sakhalin, western Kamchatka, and along the islands of the Greater Kuril Ridge at depths from 150 to 800 m (Nizyaev 1992, Shuntov 1997, Klitin and Nizyaev 1999). Results to date (Nizyaev 1992, Shuntov 1997) indicate the existence of three populations of golden king crab in the northern part of the Okhotsk Sea: Western-Kamchatka group, North-Okhotsk Sea group and East-Sakhalin group (Shuntov 1997). The East-Sakhalin group is the smallest of them by number.

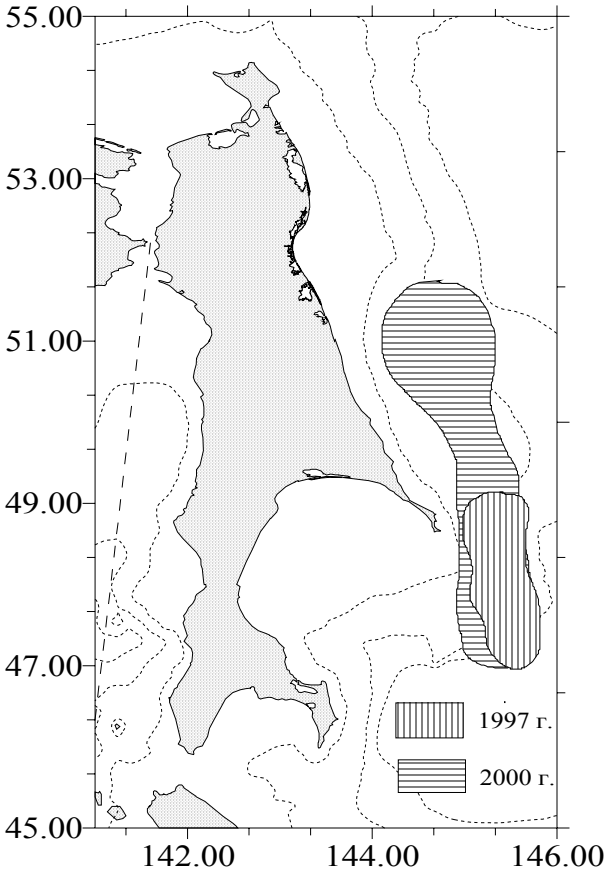

Fig. 1 Geographical localization of region of research.

The analysis of the East-Sakhalin group was carried out according to three aspects: distribution, commercial parameters (catch on a crab pot, mean size of commercial crabs) and some biological features of the group (size-frequency structure, the size at sexual maturity, fecundity).

Studies were carried out from August to November 1997 and 2000 on catcher boats in the area between lat. 47°20'N and 51°40'N at a depth of 205 – 680 m. Crab pots (175 × 175 × 80 cm) were used. The carapace length (CL), carapace width (CW), right chela height (RCH) were measured to the nearest 0.1 mm. Altogether 7391 specimens of golden king crab were taken for analysis.

Near East Sakhalin Island, the golden king crab forms a few small aggregations extended in a chain at depths of 200–600 m. In 1997 commercial crabs were concentrated in the area between lat. 47°30'N and 48°00'N. In 2000, the area of search was expanded (Fig. 1) and two aggregations of commercial males were registered. One of them is located on the same site, as in 1997, and another to the north of Mys Triennia, within lat. 49°00'N. The mature females formed only one aggregation, which was located in the area between lat. 47°50'N and 48°20'N. Commercial crabs mainly accumulate at depths of 350–500 m. The maximum catch (18.3 crabs per pot) was registered at a depth of 300 m. The main part of noncommercial males live at depths of 350–400 m, maximum catch (28 crabs per pot) was found at depths of 400 m. At depths of more than 500 m, the catch of noncommercial males is sharply reduced. The only group whose abundance is not reduced by a depth of 600-650 m, are mature

Table 1 Mean and maximum catch per a crab pot of golden king crab in 1997 and 2000.

Catch per pot	Commercial crabs >130 mm CW	Noncommercial crabs <130 mm CW	Mature females	Immature females
1997				
maximum	17.47	25.04	3.3	8.35
mean	4.89	1.71	0.24	0.51
2000				
maximum	18.5	28.6	10.5	2.8
mean	4.17	1.70	1.14	0.15

females. The maximum number (10.5 crabs per pot) was registered at a depth of 550 m. The immature females were seen mainly at a depth of 300–450 m. Commercial characteristic *L. aequispinus* of East Sakhalin is submitted in Table 1.

Near the island of Shiashkotan in 1997- 2000, the average catch of commercial crabs per pot was 35.7 specimens. Near the island of Iturup, there were 25.4 commercial crabs per pot, 6-8 times the catch near East Sakhalin. The mean carapace width (CW) size of commercial crabs from East Sakhalin is 150.50 mm. Near the Kurils Islands the mean size of commercial crabs is much more; the mean CW of crabs on the island of Shiashkotan was 178.2 mm. Crabs of the island of Iturup average 161.5 mm (average data from 1997 – 2000).

The size-frequency distribution of golden king crab is shown in Figure 2. A modal class of males is 140-155 mm, and for females at 115 – 125 mm.

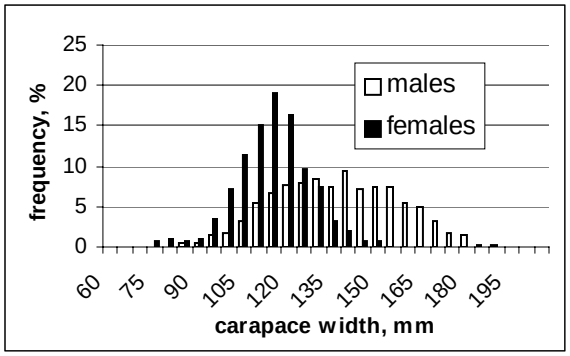

Fig. 2 Size-frequency histograms for males and females of golden king crab from eastern coast of Sakhalin Island.

The maximum size of males is 200.8 mm, and 160.9 mm for females. According to Klitin and Nizyaev (1999), a modal class of males is 205 – 210 mm and the maximum size is 284 mm CW for crabs near the northern Kuriles. The mean size of males from East Sakhalin was 143.5 ± 0.3 mm (n = 2986), and for males from the island of Shiashkotan, 164.1 ± 1.1 mm (n = 1091), and for males from the island of Iturup, 157.2 ± 0.7 mm (n = 686). A pairwise t-test indicated that the mean size of males from all comparable groups differed significantly (t = 5.1 – 18.4, $t_{0.95}$ = 1.96).

The size at maturity for males (SM) was determined by the beginning of the changes in the growth allometry of the right chela (RCH) (Jewett et al. 1985; Somerton and Otto 1986). For males from East Sakhalin SM = 113.2 mm CL. Coefficients of equation of chela growth (RCH = a + bCL) for immature males: a = 3.32 ± 2.74, b = 0.17 ± 0.03 (n = 18), for mature males: a = -29.47 ± 1.67, b = 0.46 ± 0.01 (n =1438).

The size at which 50% of females were mature (SF_{50}) was estimated by fitting a logistic equation to the percentage mature by size (Jewett et al. 1985). For females from East Sakhalin SF_{50} = 107.5 mm CW. Coefficients of the logistic equation (Lakin 1976) were: a = 16.07 ± 3.8, b = 0.14 ± 0.00014. According to Nizyaev (2002), for females from the island of Iturup, SF_{50} = 115.3 mm CW, and for females from Shiashkotan Island SF_{50}= 113.6 mm CW. According to t-test results, the differences between coefficients b of logistic equation among all compared groups was significant (t = 2.51 – 3.94,$t_{0.95}$ = 2.00 – 2.02). For the coefficients, differences were significant only

between Shiashkotan and East Sakhalin ($t = 2.23$, $t_{0.95} = 2.02$).

Individual absolute fecundity (IAF) for golden king crab from East Sakhalin, calculated according to Ivankov (1974), was 7.81 ± 0.68 thousand eggs (n=53, CW 97 – 150 mm). According to Nizyaev (2002), IAF for females from Iturup is 7.98 ± 0.45 thousand eggs, and for Shiashkotan group, 10.96 ± 0.8 thousand eggs. Pairwise t-test indicated that IAF of crab from East Sakhalin and Shiashkotan differed significantly ($t = 2.95$, $t_{0.95} = 1.98$) and IAF of crab from East Sakhalin and Iturup did not differ ($t = 0.22$, $t_{0.95} = 1.98$).

Thus, the first data have already shown the existence of some differences between groups of golden king crab from East Sakhalin and the Kuril Islands. That testifies to the benefit of assuming that these groups should be considered separate populations. However these results should be considered preliminary, further studying of the peculiarities of these groups will determine its rank more precisely and allow recommendations for commercial exploration of resources (to identify the areas of accumulation, total volume of fishing).

Model and main indexes of primary production of the North Sakhalin coastal waters

Vladimir I. Zvalinsky
V.I. Il'ichev Pacific Oceanological Institute, Far-Eastern Branch of Russian Academy of Sciences, 43 Baltiyskaya Street, Vladivostok, 690041 Russia. e-mail: viz@poi.dvo.ru

The Northwest coastal waters near the Piltun-Astokh Oil Field, (52°30' – 53°10'N, 143°20' – 144°10'E; hereafter, Polygon No. 1) and waters of Sakhalin Bay (53°40' – 54°24'N, 140°20' – 142°20'E; hereafter, Polygon No 2) were investigated from 3 – 11 October 1988 on R/V *Akademik M.A. Lavrentyev*. Several indices of primary production (PP) were measured:

1. water transparency and photic layer thickness by using of underwater photometer and Secchi disk;
2. chlorophyll *a* concentration by standard method after extraction of pigment by 90% acetone from filters;
3. volume PP rate at light saturation by the method with using of label carbon (C14).

The probes of marine water for analysis were sampling from standart horizons of photic layer (0, 5, 10, 25 m).

The data were used to estimate daily PP rate of the whole photic layer. For this purpose, our simplest model of gross photosynthesis-light relationship in form of nonrectangular hyperbola was used (Zvalinsky and Litvin 1986, 1988):

Eq. 1

$$I = \frac{V}{1-V} * (1 - \gamma_I * V) \text{ or } \quad V = \frac{1+I}{2*\gamma_I} * \{1 - \sqrt{1 - \frac{4*\gamma_I * I}{(1+I)^2}}\}.$$

where $V = P/P^m$ – a relative PP rate, P and P^m – rate and light-saturation rate, $I = [I]/I_k$ – relative light intensity, *[I]* – light intensity, I_k – "substrate constant" for light of investigated phytoplankton (the intensity at which extrapolation of the initial slope of the *P-I* curve intersects the maximum rate (Talling 1957), γ_I – index of nonrectangular hyperbola (for marine alga $\gamma_I \approx 0.95$). We believed that index I_k corresponds to about 5% of the surface irradiance.

After integration of Eq. (1) in the limits of whole photic layer we obtain the expression for calculation of daily production P:

Eq. 2

$$P = 0.825 * An * C_{Chl} * Z_{ph} * T_L \ (mgC * m^{-2} * d^{-1}).$$

where 0.825 is a factor, taking into account nonlinear photosynthesis dependence on light intensity, *An* – mean assimilation number or photosynthesis normalized to chlorophyll ($mgC * mgChl^{-1} * h^{-1}$), C_{Chl} – mean chlorophyll concentration of photic layer column ($mgChl * m^{-3}$), Z_{ph} – photic layer thickness in *m*, T_L – effective duration of a light day in *h* (in our case $T_L \approx 8$ *h* for total duration of light day about 10.5 *h*).

The main indices of primary production for Polygons No. 1 and No. 2 are presented in Tables 1 and 2, respectively.

Table 1 Indexes of primary production for Polygon No. 1.

Chl a mg*m^{-3}		***PP mgC*m^{-3}*h^{-1}***		***An mgC*mgChl^{-1}*h^{-1}***		***PP gC*m^{-2}*day^{-1}***	
Z_{ph} = 9 m	Z_{ph} = 13 m	Z_{ph} = 9 m		Z_{ph} = 9 m		Z_{ph} = 9 m	
3.16±1.64	2.55±0.75	42±20	21.4±9	13.8±3.6	8.8±3.9	2.6±0.5	1.9±0.5

Table 2 Indexes of primary production for Polygon No. 2.

Chl a $mg*m^{-3}$		*PP* $mgC*m^{-3}*h^{-1}$		*An* $mgC*mgChl^{-1}*h^{-1}$		*PP* $gC*m^{-2}*day^{-1}$	
Z_{ph} = 6 m	Z_{ph} = 12 m	Z_{ph} = 6 m	Z_{ph} = 12 m	Z_{ph} = 6 m	Z_{ph} = 12 m	Z_{ph} = 6 m	Z_{ph} = 12 m
4.6±2.9	1.8±1.2	39±21	20.6±14	9.1±2.8	9.8±2.8	1.7±0.5	1.4±0.4

Photic layer thickness, Z_{ph}

The photic layer thickness Z_{ph} (the depth where penetrates 1% of surface light intensity) increased from 8 m on stations that are about 10 km from the shore to 15 m at stations that are about 30-60 km from shore on Polygon 1. Such transparency is typical for coastal waters. On Polygon No. 2 the same values changed from 6 to 15 meters. The most turbid waters were near the estuary of the Amur River (Z_{ph} were about 5-7 meters).

Chlorophyll *a* concentration, C_{Ch}

On Polygon 1 C_{Chl} in the photic layer changed from 0.5 to 5.6 mg/m^3. Maximal concentrations were near the shore (depth up to 30 m). The remote offshore waters had not more then 3 mg Chl m^{-3} (Table 1). At Polygon No. 2, there are two places with higher chlorophyll content. The first one was in the southeastern part of polygon, near the Amur estuary where salinity was low, up to 15psu with mean C_{Chl} = 4.6 $mg*m^{-3}$. The second one was in the northwestern part of the polygon where salinity was high, not less then 31psu (Table 2).

Volume of primary production

On both Polygons, the stations near the shore had about twice the volume of *PP* compared with the offshore stations (Tables 1 and 2).

The index of activity of phytoplankton chlorophyll (assimilation number)

An had high value for both Polygons (*An* = 9-14 $mgC*mgChl^{-1}*h^{-1}$; Tables 1 and 2). On Polygon No. 1, stations nearest to shore had *An* values about 1.5 higher compared with offshore stations. *An* values were similar for all waters of Polygon No. 2.

The estimated values of daily primary production

The values were relatively high for waters of both Polygons (Tables 1 and 2). On Polygon No. 1, the daily PP of nearshore stations had values of about 3.4 $gC*m^{-2}*day^{-1}$. In Polygon No. 2, the maximal daily PP was seen near the Amur estuary (about 2.2 $gC*m^{-2}*day^{-1}$).

All of the measured and calculated data show that investigated waters were highly productive in the first half of October 1988.

SESSION 4
ANTHROPOGENIC IMPACTS ON THE OKHOTSK SEA ECOSYSTEM(S)
(Convenors: Tatyana Belan, Keiichi Mito and Vladimir Radchenko)

Killer whales and Greenland turbot fishery in the Sea of Okhotsk

Konstantin A. Karyakin
Pacific Fisheries Research Centre (TINRO-Centre), 4 Shevchenko Alley, Vladivostok, 690950 Russia.
e-mail: tinro@tinro.ru

As an active predator, killer whales (*Orcinus orca*) have broad spectrum of potential prey including fishes, cephalopods, sea mammals and even sea birds. With the development of longline fisheries for bottom fishes, the spectrum of the killer whale's prey expanded to include the Greenland turbot (*Reinhardtius hippoglossoides*), Pacific halibut (*Hippoglossus stenolepis*), arrowtooth flounder (*Atherestes stomias*), sablefish (*Anoplopoma fimbria*) from the southeastern part of the Bering Sea (Yano and Dahlheim, 1995a). Aggressive killer whale behaviour has been observed near the vessels longlining for Patagonian toothfish (*Dissostichus eleginoides*) in waters off the Falkland Islands (Nolan et al. 2000). Although these kinds of fishes are not normally accessible to killer whales due to depth, the killer whales have learned to remove fish from fishing gear (longline, bottom nets) during hauling operations.

In the Russian Far East seas, longline and bottom net fisheries began to develop in the 1990s, but until recently, fishermen had not seen aggressive killer whale behaviour. Often these animals were observed near fishing vessels and their reactions to vessel could be characterized as indifferent. However, since 1999, killer whales attacks on fishing gear began in the western Bering Sea and since the autumn of 2000, in the Okhotsk Sea.

Studies of killer whales were conducted in Okhotsk Sea from June to September 2001 (Fig. 1) on the longliner *Vostok 1*. Data from other fishing vessels were also used. Longlining for Greenland turbot was conducted at depths from 400 - 750 m, basically in the range of 500-700 m. A bottom longline was 9 - 12.5 km long and consisted of 50-70 cartridges. Each cartridge contained 145 hooks fixed at 1.2 m intervals. *Eagleclaw #6* hooks were baited with herring. A cartridge was 175-180 m in length, requiring an average hauling time of about 3.5 minutes. Usually four sets were made daily.

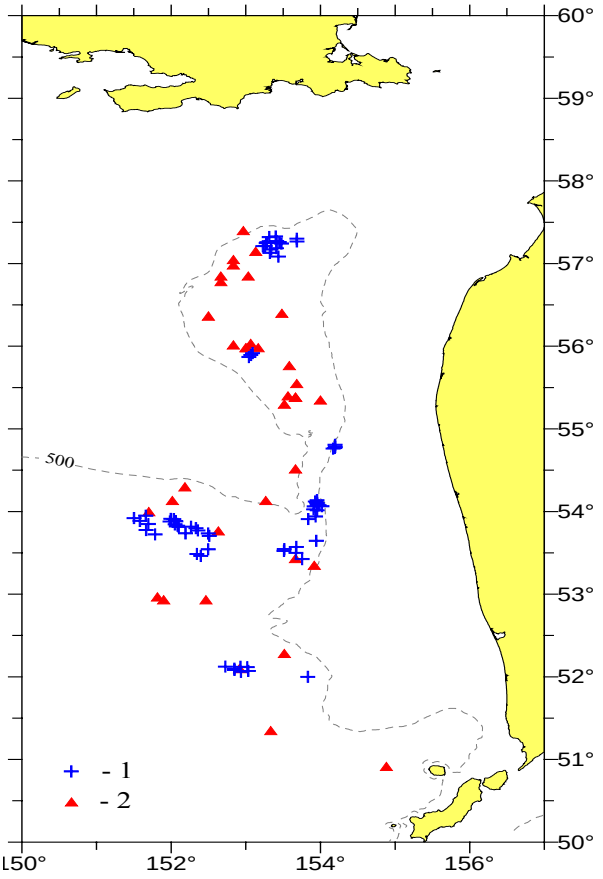

Fig. 1 Locations of killer whales attacks on catches of fishing vessels in the Sea of Okhotsk in 2001. 1 - data from long-liner *Vostok 1*, 2 – data from other fishing vessels.

Table 1 Losses to orcas of catch of Greenland turbot on longliner *Vostok 1* in January - October 2001.

Month	Fishing operations	Depredated fishing operations	Rate of depredated fishing operations, %	Catch, m.t.	Predation, m.t.	Total withdrawal, m.t.
January	67	–	–	143.5	–	143.5
February	60	8	13.3	61.7	6.6	68.3
April	94	2	2.1	276.2	5.4	281.6
May	93	–	–	91.6	–	91.6
June	92	4	4.3	71.3	8.8	80.1
July	114	20	17.5	183.0	24.4	207.4
August	96	23	24.0	173.8	31.8	205.6
September	93	16	17.2	165.4	15.6	181.0
October	100	–	–	152.3	–	152.3
Total (average)	809	73	9.0	1318.8	92.6	1411.4

The effect of killer whale predation was estimated by comparing turbot catches on the part of the haul when the animals were not present, with the catches obtained when the animals were present. If all of the turbot catch was removed, the predation effect was determined by comparing with average catches of the nearest fishing operations.

Behaviour of killer whales

After the start of hauling operations, killer whales would first appear within 30 minutes or less, and after 20 additional minutes, they would reach a vessel. During this period, the catch of Greenland turbot was saved from 15-20 cartridges, and orcas then consumed the turbot from all hooks completely. Sometimes animals appeared at the end of a hauling operation. If killer whales were observed before the beginning of fishing, the fishing did not start, and the vessel moved to another area.

The predation on fishing gear was mostly due to the behaviour of 5-6 individuals, including 1-2 adult males and 3-4 animals of indefinite sex. There were cases when about 20 individuals were observed near a fishing vessel, but as a rule, orcas kept in separate groups. In one group, there were three individuals with completely white colouring without black spots. One albino was an adult male, one was an adult female, and one an immature male. Albinos were sighted in July (two events) and in August (1 event).

Killer whales were active usually in the daytime, both in calm and stormy weather. However, cases of fishing gear predation were observed at night. The killer whales' behavior varied from June till September. In June and July, orcas took fishes in immediate proximity to a vessel, a distance of 10-15 m from it. When fishermen used guns or various sound bombs, the orcas departed to a distance of 100-150 m from the vessel and rested, returning but diving to take the fish. In August – September, the killer whales did not approach within 200-400 m due to the use of various guns, alarm rockets, self-made explosives.

The usual diving time ranged from 5-6 minutes, and on the color echosounder monitor, killer whales appeared as red curves, like a parabola, to a depth of 200 m. According to Yano and Dahlheim (1995), diving time varies from 2 to about 10 minutes. They assumed that orcas start to take fish from depths of more than 200 m.

Killer whales removed only Greenland turbot and did not eat other species. Bycatch included skates, eelpouts and grenadiers. There is a customary pattern of behaviour. For example, on August 10-

11, 2001, three longliners were fishing within visibility. Orcas removed the catch from only one vessel. After hauling operation ceased they departed to another vessel and returned to the original vessel when hauling operation continued. The same feature was marked on bottom net vessels in October - November.

From January till October, 2001, 809 fishing operations were made by the longliner *Vostok 1,* with killer whales affecting 73 of them (9%) (Table 1). Losses of Greenland turbot for 9 months were estimated to be 92.6 t or 7.0% of the catch. Naturally, these losses were not taken into account in total catch by the vessel.

We suppose that other fishing vessels also were affected by killer whales in the same way. And if total annual catch of Greenland turbot is known we can determine the turbot withdrawal for all vessels. The total annual catch of turbot by longliners and bottom nets vessels was 15,600 t, therefore the total turbot loss to killer whales will be about 1,100 t. Thus, the general turbot removals for the northeastern Sea of Okhotsk was 17,362 t including annual turbot catch by all gears (16,262 t) and predation (1,100 t). General turbot removals did not exceed Total Available Catch (TAC) for 2001 for this area (18,000 t).

In summary we shall note, that during 2001 the abundance of killer whales and the frequency of their attacks on catches of fishing vessels had an increasing tendency.

References

Yano, K. and Dahlheim, M.E. 1995. Killer whale, *Orcinus orca*, depredation on longline catches of bottomfish in the southeastern Bering Sea and adjacent waters. Fishery Bulletin 93: 355-372.

Nolan, C.P., Liddle, G.M. and Elliot, J. 2000. Interaction between killer whales (*Orcinus orca*) and sperm whales (*Physeter macrocephalus*) with a longline fishing vessels. Marine Mammal Science 16: 658-664.

Yano K. and Dahlheim M.E. 1995. Behavior of killer whales *Orcinus orca* during longline fishery interactions in the southeastern Bering Sea and adjacent waters. Fisheries Science 61: 584-589.

Food supply for the sea urchin, *Strongylocentrotus droebachiensis,* in the coastal part of the Sea of Okhotsk

Tatiana Krupnova and B.A. Pavlyuchkov
Pacific Fisheries Research Centre (TINRO-Centre), 4 Shevchenko Alley, Vladivostok, 690950 Russia.
e-mail: tinro@tinro.ru

The food supply of sea urchins regulates their abundance, defines their fecundity and determines stocks, and affects their commercial properties. As no data had been collected on urchins inhabiting the Sea of Okhotsk, the food supply of green urchins *Strongylocentrotus droebachiensis* from the coastal North Okhotsk Sea was studied.

It was made a bonitational estimation of the Tauj Inlet and Babushkin Bay in points from 0 to 111 on the basis of simultaneous definitions of gonadosomatic indices (GSI), indices of fullness of digestive tract (IF) and composition of consumed food. Along with this it was conducted daily (24 hours) station to determine daily food rations (DFR).

The western part of Odan Bay is estimated as the zero point, according to the scale developed. It is characterized by a total absence of algal food, a low value of GSI (1-2%) and IF (300°/ooo). The coast of the Umara Island has bad feeding conditions (1-11 points) where GSI values do not exceed 3-7%, and IF is equal to 300-400°/ooo. Kortical algae, *Bossiella* or detritus prevailed in sea urchins' digestive tracts. Gertnera Bay has relatively good feeding conditions (11-111 points) where GSI values increased to 10-12% and IF –up to 710°/ooo. Besides kortical algae, *Bossiella*, sponges, and Polychaeta there were a great number of brown algae, mainly *Laminaria appressirhia* in sea urchin digestive tracts. Babushkin Bay and the continental side of Nedorazumenia Island have favorable feeding conditions, where GSI values increased to 18-23% (for some specimens, 25-30%), and IF values up to 940°/ooo, with brown algae, mainly *Laminaria appressirhiza*, *L. gurjanova* and *Alaria marginata* prevailing in sea urchin digestive tracts (Fig. 1). Thus, the inclusion of brown algae to *Strongylocentrotus droebachiensis* ration considerably increases the gonadosomatic index.

Fig. 1 *Strongylocentrotus droebachiensis* sampling sites in the northern Okhotsk Sea.

Daily sampling in Gertner's Bay in June showed that the DFR for *S. droebachiensis* was 3.9% of body mass, which is comparable with the DFR indices for the grey urchin, *S. intermedius*, at that time inhabiting closed plots along the coast of Primorye in June. It allows model calculations of algal food requirements, developed for *S. intermedius*, to be used for *S. droebachiensis* as well (Fig. 2). The model is based on calculations of conformity of *Laminaria* growth indices and daily rations of grey urchin during yearly cycle. When the actual quantitative data on biomass of *Laminaria* and sea urchins are entered in column "Initial data", the information of food supply sufficiency in the given plot appears in the right side of mode.

Conducted investigations make it possible to develop the recommendations on improvement of food supply for *S. droebachiensis* in the coastal Okhotsk Sea. For example, algae bottom plantations may be created in the western part of the Odan Bay by spore seeding the artificial substrates or systematically delivering them from the eastern part of the Bay to accommodate them at the bottom of urchin habitat.

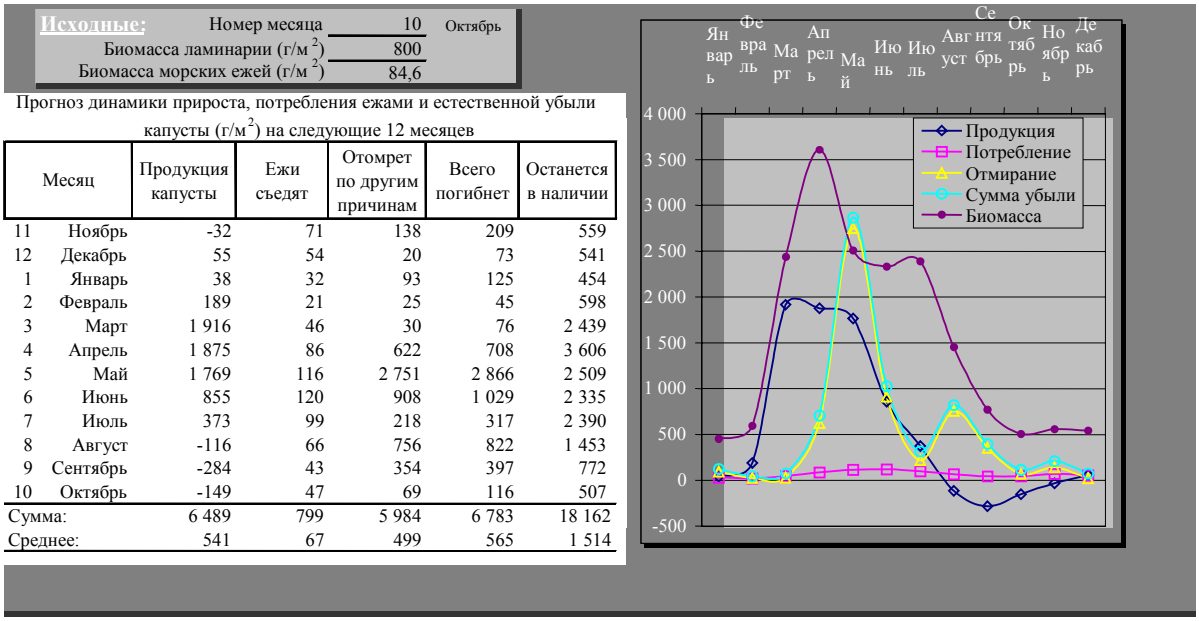

Исходные:			
	Номер месяца	10	Октябрь
	Биомасса ламинарии (г/м^2)	800	
	Биомасса морских ежей (г/м^2)	84,6	

Прогноз динамики прироста, потребления ежами и естественной убыли капусты (г/м^2) на следующие 12 месяцев

Месяц		Продукция капусты	Ежи съедят	Отомрет по другим причинам	Всего погибнет	Останется в наличии
11	Ноябрь	-32	71	138	209	559
12	Декабрь	55	54	20	73	541
1	Январь	38	32	93	125	454
2	Февраль	189	21	25	45	598
3	Март	1 916	46	30	76	2 439
4	Апрель	1 875	86	622	708	3 606
5	Май	1 769	116	2 751	2 866	2 509
6	Июнь	855	120	908	1 029	2 335
7	Июль	373	99	218	317	2 390
8	Август	-116	66	756	822	1 453
9	Сентябрь	-284	43	354	397	772
10	Октябрь	-149	47	69	116	507
Сумма:		6 489	799	5 984	6 783	18 162
Среднее:		541	67	499	565	1 514

Fig. 2 Model of calculation of food supply sufficiency.

Table 1 Indices of habitat suitability based on feeding conditions for *Strongylocentrotus droebachiensis*. (Food types: kork: cortical algae; Boss: *Bossiella*; detr: detritus; Lam: brown algae)

Points	Location	Food type (%)	GSI
0	Odan	kork-50	1-2
		Boss-30	
		detr-20	
1–11	Umara	kork-40	3-7
		Boss-40	
		detr-20	
11–111	Gertnera	Lam.-70	10-12
		Kork-20	
		Boss-5	
		spongia –3	
		Polychaet-2	
111	Babushkina	Lam.-90	18-23
		Kork-10	
111	Nedorasumenia	Lam-90	18-23
		kork-10	

Estimation of some parameters of habitat of marine ecosystems in areas of gas and oil deposits development

Galina V. Moyseychenko and Y.G. Blinov
Pacific Research Fisheries Centre (TINRO-Centre), 4 Shevchenko Alley, Vladivostok, 690950 Russia. e-mail: moyseychenko@tinro.ru

The object of research that took place in the summer of 2002 during a research cruise of the *R/V Buhoro* was to study the ways of natural structure and regular functioning of ecosystem preservation in the face of bottom sediment pollution in the area of the Sakhalin offshore oil and gas fields. Bottom sediments are one of basic components marine ecosystem. They are very important for the normal functioning of ecosystems on the whole because it provdes habitat for benthos and is a food source for many aquatic animals. It is also the environment where pollutants accumulate. During the research cruise in the summer of 2002, the levels of anthropogenic influence on the offshore biocenosis was studied.

In contrast to water that reflects seasonal changes and quite frequently accidental effects, the bottom sediments accumulate longstanding tendencies of biogeochemical processes, and also the magnitude of anthropogenic hydrocarbons. Consequently, it reflects the real ecological state of the sea much better.

In the research cruise, *in situ* pollutant sources of both natural and anthropogenic origins were identified in areas where oil and gas deposits have been developed. For that purpose, the following research was conducted: bottom sediment granulometric composition; analyses of the qualitative and quantitative composition of phenols, organic carbon and detergents; water and bottom sediments biotesting.

The analyses of complex chemical hydrocarbons included: research of anthropogenic and biogenic polycyclic aromatic hydrocarbons, the quantity and contamination of alkanes, and unsubstituted arenas. The gametes, embryos and larvae of sea urchins were used as test objects for biotesting. Alterations of larval size is an easy and informative method of early diagnosis of disruption in sea urchin reproduction.

The biotesting indicated that in some particular areas, the habitat is hazardous for biota. Bottom sedimentat samples have concentrations of organic hydrocarbons (Corg 0.03-1.89%; aliphatic hydrocarbons- 2.5-89.9 mkg g^{-1}; polycyclic aromatic hydrocarbons- 3.1- 58.7 ng g^{-1}; detergents - 0.3-1.2 mkg g^{-1}) more than in 1994.

The influence of drilling in northeast Sakhalin offshore gas-oil deposits area on the radioactive contamination of sea environment

Galina S. Borisenko and G.V.Moiseychenko
Pacific Fisheries Reasearch Centre (TINRO-Centre), 4 Shevchenko Alley, Vladivostok, 690950 Russia.
e-mail: moyseychenko@tinro.ru

Natural radionuclides such as uranium – thorium and K-40 are concentrated in gas-oil deposit zones so the development and industrial use of these deposits can lead, inevitably, to contamination of technological equipment, industrial wastes, and an environment with natural radionuclides (NRN). In this connection, radiocontrol is necessary to maintain safety while mining gas-oil materials. Monitoring of γ-phone, α-β-γ-activities of the sea environment components must be planned.

The object of our investigation in 2002 was to determine the concentrations of NRN in the bottom sediments taken from Piltoon-Astok and Loonskiy oil fields in Northeast Sakhalin offshore area.

Measurements of specific activities of NRN were conducting with scintillating-spectrometer "Progress" using an NaY(Tl) detector in geometry "Marinelly"1L. The duration of exposure was 2-4 h depending on the activity of samples. The preparation of bottom sediments for measurements assumed removing of traces, drying and careful homogenizing of sample.

The spectrometric result showed that the concentration of NRN in the bottom sediments from Piltoon-Astok gas-oil field, after 2 years of developing these deposits, did not differ from a an analysis carried out in 1977, before drilling. Thus oil mining, at this stage, did not change the radiation of this area.

At the same time, the concentration of Ra-226 and Th-232 in the bottom sediments within range of the Loonsky field increased twice as much, although oil mining here did not commence after drilling. Probably the increase is connected with changing of granular bottom sediments composition owing to mud inclusions, which actively adsorb the radionuclides.

The impact of coastal oil-extraction on contamination of the northeast Sakhalin shelf with oil products

N.V. Stenina
F.S.I. Sakhalinrybvod, 43-a Emelyanova Street, Yuzhno-Sakhalinsk, 693006 Russia. e-mail: ecology@sakhrybvod.ru

The issue of anthropogenic contamination of the littoral waters by oil hydrocarbons is of particular importance, both for the estimation and forecast of conditions of highly productive shelf ecosystems, and for studying the pathways of hydrocarbons in the ecosystem of the Sea of Okhotsk. The objective was to study the pathways of migration, transformation, accumulation, and the extent to which the offshore zone of the Sea of Okhotsk is affected by oil hydrocarbons from the coastal oil extraction sites in the northeast of Sakhalin. At present, the major sources of hydrocarbon pollution in the offshore zone of northeast Sakhalin are the enterprises of oil extracting and oil storage located on the northeastern coast of the island. Oil extraction is carried out in 24 oil-fields containing 2387 oil wells, of which 2301 are operating.

Oil hydrocarbons from oil extraction have increased increased several times (in a number of cases by an order of magnitude) in the lower reaches of rivers. The high level of oil hydrocarbon pollution in the rivers of the northeast of Sakhalin is persistent. Thus, the influence of oil extraction on surface water objects results in significant oil hydrocarbon pollution. Recently the oil-extracting enterprises have undertaken a number of activities to rehabilitate the disturbed territories of oil production, and application of non-polluting technologies.

The migration of terriestrial oil hydrocarbons in the offshore shelf zone of northeastern Sakhalin is represented mostly in some lagoon-type bays. The lagoons of northeastern Sakhalin provide a natural buffer reservoir for terrristrial discharge and, at the same time, are the feeding areas of commercially valuable fish species.

Results of the investigations, carried out in July - October 2000, have shown that the average contents of oil products in the water of the bays exceeds by many times, the level of pollution in the open part of the sea.

The second prominent feature of oil product distribution in the bays was their significant spatial variability. Zones with high contents of oil products alternate with the zones where concentration of oil products is close to values of the natural background. These sites are adjacent to sandy spits as a rule, where the influence of river flow is insignificant. The concentrations and peculiarities of the spatial distribution of oil hydrocarbons in the bays are determined by the isolation of the lagoon and the extent of its water exchange with the sea, the volume and the contamination of the river outflow, as well as by the arrangement river mouth sections.

The maximum average concentrations of oil hydrocarbons were recorded in closed lagoons and bays having little water exchange with the sea. The contents of hydrocarbons in the gulfs Kolendu and Ekhabi, with active hydrodynamic processes, did not exceed the norm.

Considering the dynamics of concentrations of oil hydrocarbons in the bays of northeastern Sakhalin during the last decade, it is possible to note that there is a tendency of decrease in the level of pollution as a whole.

Decomposition of oil hydrocarbons begins as early as on the surface of the ground on the technical platforms of oil extraction. High molecular homologues that get in the rivers are partly decomposed due to the biodegradation as well as the influence of the UV-radiation. So, for example, the concentration of oil hydrocarbons in the Ombo River is 0.76 mg/l below the oil extraction site (Kolendo) is reduced towards the mouth of the river to 0.024 mg/l. Further, the

transformation of oil hydrocarbons proceeds in the lagoons of the northeastern coast.

The available data indicate a change in some biological characteristics in those bays suffering from persistent oil pressure. According to N.V. Pecheneva, the extent of oil hydrocarbon pollution of bottom sediments of the lagoons of northeastern Sakhalin influences the value of Shannon's diversity index in benthos communities. The lowest diversity index of macrobenthos was recorded for the littoral of the southwestern section of the Urkt Bay. The lagoon of Piltun had the greatest value of the index, corresponding with the lowest levels of oil hydrocarbons.

In 1996, SakhSIFO carried out an analysis of the contents of heavy metals in the livers of bottom fishes in the Nyisky Bay. The results have shown that the contents of heavy metals in the inhabitants of the bays was higher than in the same species in the shelf zone, but it did not exceed permissible levels.

Shelf of the open sea

Long-term observations of the northeastern Sakhalin shelf have shown that in general, the contents of oil hydrocarbons in the surface water layer is stable enough and low, that the transport of non-transformed oil hydrocarbons of terrestrial origin to the open sea is insignificant.

In general, studies carried out in the area in 1990-1994 have shown that the concentration of soluble aliphatic hydrocarbons and PAHs in surface waters varied within rather narrow limits of 10-40 mkg / l and 5-12 ng/l, respectively.

The influence of the hydrocarbons of terrestrial origin and their pathways is more clearly traced in the northern part of east Sakhalin shelf from an analysis of quantitative and qualitative composition of hydrocarbons in the top layer of bottom sediments.

Thus, the major processes of oil hydrocarbon biodegradation of the products of coastal oil extraction sites occur in the lagoons of northeastern Sakhalin. However, the influence of hardly decomposed high-molecular and transformed hydrocarbon compounds can be traced to bottom deposits of the open sea as well.

According to the studies carried out in 2000 in the eastern part of the Sakhalin shelf, seawater was generally characterized by the low contents of oil hydrocarbons. Increased amounts of oil hydrocarbons were observed in the surface layer in the water area adjacent to the Gulf of Nabil. But the correspondence of these zones of increased hydrocarbon concentrations with some biogenic elements in the surface layer suggests the existence of a cyclic seasonal eddy in this area.

At the same time, when analyzing the distribution of oil hydrocarbons in the bottom deposits in the eastern Sakhalin, a local zone of high hydrocarbon concentration was clearly pronounced; the center of the concentration reached 200 mkg/g.

Conclusions

The pathway of oil hydrocarbon migration from the coastal oil extraction sites can be traced along the rivers to the bays of northeastern Sakhalin. The increased concentration of oil hydrocarbons in the open part of the shelf zone had an endogenous origin.

The major processes of transformation and biodegradation of terrigenous hydrocarbons take place in the lagoon-type bays, representing natural buffer systems. The part of multinuclear volatile compounds and cyclic alkanes, hardly liable to microbic decomposition, is taken out into the open sea, and affects the composition of the bottom deposits in the shelf zone.

The major loads of oil hydrocarbon pollution from coastal oil extraction sites are carried by the rivers in the zone of their influence. Cumulative effects of oil hydrocarbon accumulation in the bays of northeastern Sakhalin require the further investigations.

The measures taken and the decrease of the extent of pollution by oil hydrocarbons of the rivers and the bays during recent years provide hope for improvement in the ecological situation in this area.

Increasing of methane fluxes in the Sea of Okhotsk in 2002

Anatoly Obzhirov, A. Salyuk and A. Salomatin
V.I. Il'ichev Pacific Oceanological Institute, Far-Eastern Branch of Russian Academy of Sciences, 43 Baltiyskaya Street, Vladivostok, 690041 Russia. e-mail: obzhirov@poi.dvo.ru

Methane fluxes have been studied in the shelf, slope and deep parts of the Sea of Okhotsk from 1984 (Obzhirov et.al., 1989, Obzhirov, 1993). More intensively, they were investigated by the Russian-German project KOMEX from 1988 to 2002. After 1988, methane fluxes (hydro-acoustic anomalies) increased in the water column of the shelf and slope Sakhalin area of the Okhotsk Sea. The number of methane flares before 1995 (Neftegorsk earthquake time) grew from 0 to about 30 in North-East Sakhalin Slope. After earthquake it was stable. In 2002, number of flares in this area sharply increased up to more then 100.

As the result the following were found:

1. Increasing methane concentrations in the water column from 1988 to 1995 occurred before the Neftegorsk earthquake (May 1995). After this, methane concentration decreased very little and now it has the same high level in water column.
2. Increasing number of methane fluxes (flares) in the eastern Sakhalin shelf and slope. Bubbles of methane migrate from the sediment to the water via a fault zone. The bubbles form a sound-scattering body, like a flare. They come from the bottom to about 300-500 m and can be distributed to the surface and in intermediate water layers in a semi-horizontal direction.
3. Sources of methane are oil-gas deposits and destabilized gas hydrates.
4. Destabilized gas hydrates create morphologically low structures in the surface sediments and a mineral assemblage with carbonate concretions.
5. Methane concentrations inside the flares are more than 20000 nl/l and near flare about 1000-3000 nl/l. The sediments in the flare areas contain methane concentration of 5-10 ml/l.
6. Methane monitoring shows that the surface water in shallow areas is anomalously oversaturated with methane (>1000 nl/l) in autumn and spring seasons. In these seasons, methane is more intensively emanating from the surface water to the atmosphere.

Increasing numbers of methane flares and methane concentrations from 1988 are connected with increasing siesmo-tectonic activity of faults in the area of the Okhotsk Sea. This idea is supported by data from mud volcanoes in the East Sakhalin area. Mud volcano activity connected with growth of seismo-tectonic oscillations that lead to opening of fault zones and gas-fluid migration. Moreover, new mud volcanoes are formed.

Experimental study of oil degradation in the Sea of Okhotsk

Vasiliy Mishukov
V.I. Il'ichev Pacific Oceanological Institute, Far-Eastern Branch of Russian Academy of Sciences, 43 Baltiyskaya Street, Vladivostok, 690041 Russia. e-mail: pacific@online.marine.su

Introduction

At present, the Government of Russia has sanctionned industrial development of several marine deposits on Sakhalin shelf to a number of international industrial corporations. As shows from international experience, the development of marine deposits for petroleum and gas production does not avoid occurrences of emergencies that result in petroleum pollution.

The reality of petroleum pollution necessitates the study of mechanisms and rates of petroleum degradation in the conditions of the northerneastern Sakhalin shelf. The analysis of degradation rates of petroleum, determined in various works (e.g. Mishukov and Sokolov 1988) has shown that evaporation influences had the greatest effect on the composition of petroleum. The rates of bacterial and photochemical oxidation are close and much more than rates of thermal oxidation, especially at low seawater temperatures.

The purpose of the present work was study of oil degradation laws by natural condition such as wind, intensity of sunlight, thickness of a film, temperature and main salt composition of a water etc.

Experimental research

To study photochemical oxidation, two installations were developed (Mishukov and Sokolov 1988; Sokolov et al. 1984). Xenon lamps were chosen as the light source because its light is more close to that of sun light, after filtering out the ultraviolet region (λ <290 nm) and the infrared region (λ >2 μm). Reactors were thermal at appropriate temperatures with an accuracy of ±0.10°C. The intensity of light was measured by a photodiode and could be varied in the range (0.02-1.00) Cal/cm^2*min, which is characteristic of northern regions.

The photooxidation rate of petroleum hydrocarbons was measured by the change of concentration of organic and inorganic peroxides by an iodine method (Abramova, Zelenina, Mansurov, and Mishukov 1989) and on the rate of absorption of oxygen at constant volume of cell.

The object of research was oil from a marine deposit at Odoptu, which is classed as slightly resin, slight serum content, and slight paraffin oil. The physico-chemical properties of oil, circuit of the group analysis of petroleum, used by us in this work are indicated in our work (Anikiev, Mishukov, Moiseevsky, and Tkalin 1988). Photooxidation of oil films and oil emulsions was conducted on distilled water, on artificial marine water, on clean natural marine water from the northerneastern Sakhalin shelf, on a water selected from Amursky Bay (Sea of Japan) which is polluted by wastewaters from the city of Vladivostok.

Results of laboratory experiments

Mechanism of initiation of photochemical reactions in petroleum

To study of the mechanisms of initiation of petroleum photooxidation at an initial oxidation stage in an oil film or a water-in-oil emulsion, we added α-tokopherol athetate, or adamantilidenadamantan (Ad = Ad). It is known, that Ad = Ad actively reacts with a singlet oxygen at a constant of rate of 4.6×10^5 l/mole*s, and its addition to petroleum at a concentration of 1.27×10^{-5} mole/l caused a sharp increase of oxidation rate measured by absorption of oxygen. Addition of α-tokopherol in other case completely suppressed photooxidation of petroleum as indicated by absorption of oxygen, and production of peroxide. It is known, that α-tokopherol is a quencher of excited levels of molecules and active acceptor of free radicals. Thus, formation of singlet oxygen and its participation in oil photooxidation on a water surface was established

that is agreed data of work (Larson and Hunt 1978).

Influence of temperature on oil photooxidation

A study of the influence of temperature on oil photooxidation was conducted on a surface of artificial marine water at a thickness of a film of 0.29 mm, at a light intensity of 65 mCal/cm^2 *min. The curves of peroxide accumulation have an S-like image. On tangency of a corner of a inclination to initial sites of experimental curve the significance of initial photooxidation rates (Win) are calculated. The account in coordinates ln Win - f (1/T) has given significance of energy of activation (Ea) at photooxidation equal 46.6 kJ/mole.

Influence of film thickness on oil photooxidation

The study was conducted on an artificial marine water surface at a light intensity of 65 mCal/cm^2 *min and water temperature of 278°K and oil film thicknesses (h) of 0.19, 0.29, 0.59, 0.79 mm. Curves of peroxide accumulation, from which the initial rates of photooxidation (W_{in}) were calculated and the dependence W_{in} on film thickness also, have an S-like image. In coordinates ln (W_{in}) - ln (h) a kind of dependence has been defined $W_{in} = h^{1,1}$.

It appears that the decline of the initial photooxidation rate with the reduction of thickness of a film is connected with suppression of singlet states of molecules and deactivation of radicals on surfaces of a film, though the specific absorbed energy per unit of volume of a film grows. Indirect confirmation of the influence of surface thickness on photooxidation rate is related to peroxide output from the composition of the underlying water. The photooxidation rate and peroxide output had maximal significance on distilled water. On marine water from clean regions, the peroxide output grows, and on marine water from polluted regions, after about an hour illumination, it reaches maximum significance, and then decreases.

Influence of light intensity on oil photooxidation

Study of the influence of light intensity (I_{il}) on initial photooxidation rate of petroleum (W_{in}) was conducted on a surface of distilled water and marine water. The data processing in coordinate ln (W_{in}) - ln (I_{il}) has shown that the dependence has the kind $W_{in} \propto I_{il}^2$. Such kind of dependence testifies to a two-quantum mechanism of photooxidation at an initial stage.

Influence of temperature on photooxidation of "oil in a marine water" emulsion

The oil-in-water emulsion was prepared from artificial marine water using a magnetic mixer, adding drops of oil up to concentration of 1% by weight. The intensity of light was 50 mCal/cm^2*min. The peroxide concentration was calculated by volume of petroleum. On kinetic curves, the initial photooxidation rate (W_{in}) was calculated. The dependence of peroxide concentration (ROOH) on time at temperatures 10-20°C - linear, at 30°C at 120 minutes of illumination, it reaches a maximum, and then is reduced. Initial rates of accumulation of ROOH on marine water were 10-40% below that on distilled water. Account in coordinates ln(W_{in}) - f (1/T) has shown that the energy of activation is equal to (39.6 + 4.3) kJ/mole.

Natural experiments

Natural experiments were conducted on the Northeast coast of Sakhalin Island. In the first series of experiments, at temperature of water 5°C, it was shown that immediately after placing oil on a surface of marine water, a change of physico-chemical structure occurs. Saturated hydrocarbons with numbers of carbon atoms up to 12 quickly evaporated. The absorption of light caused the formation of peroxides, which are accompanied by increasing resins and asphaltenes in oil.

In a second longer series of experiments, formalin was added to half of the reactors with marine water (final concentration - 5%) to suppress biological processes. One half of the reactors with formalin and without formalin were placed in a completely open area, and the other half were placed under a screen (height of 0.5 m). The influence of biological processes to change of the concentration of analyzed hydrocarbons was not marked.

The decline of aromatic hydrocarbons (PhH) in reactors placed under the screen was slower than those located in the completely open area and was

influenced only by evaporation of these hydrocarbons.

Oil photochemical oxidation appeared as an increase of peroxide concentrations and a fall of aromatic hydrocarbon concentrations and in the growth of concentrations of asphaltenes (Asph) in the oil. The resin contents changes only slightly.

In the third series of experiments, the transformation of oil on a surface of natural ice on the Northeast coast of Sakhalin was studied. Reduction in concentrations of saturated hydrocarbons in oil films by evaporation was considerably slower than in the autumn experiments. Growth of peroxide concentrations and concentrations of asphaltenes was observed as was a reduction of the content of resins.

Conclusions

1. Fast transformations of the chemical composition of oil were observed after spilling it on surfaces of water and ice, under the weathering processes at northeast coast of the Sakhalin.
2. Evaporation and photochemical oxidation of oil hydrocarbons were the most intensive processes, which change the oil composition.

References

Mishukov, V.F. and Sokolov, E.A. 1988. Secondary pollution of marine environment by organic peroxides. Okeanologia 33(4): 577-582 (in Russian).

Sokolov, E.A., Mishukov, V.F., Ilyichev, V.I. et al. 1985. Influence of photochemical and bacterial oxidations on physical and chemical properties of hydrocarbon films on water surface and water evaporation rate. Dokludy Akademii Nauk 281 (4):.948-951 (in Russian).

Sokolov, E.A., Mishukov, V.F. and Anikiev V.V. 1984. Organic peroxide distribution in surface water of some World Ocean regions. Dokludy Akademii Nauk 276(6): 1474-1476 (in Russian).

Abramova, O.V., Zelenina, L.G., Mansurov, M.N. and Mishukov, V.F. 1989. Study of oil degradation in seminatural experiments in Sakhalin coastal zone. Dep.in VINITI 06.02.89 N 752-B89 (in Russian).

Anikiev, V.V., Mishukov, V.F., Moiseevsky, G.N. and Tkalin, A.V. 1988. The effect of oil films on water evaporation and oxygen content in seawater. GeoJournal 16.1: 19-24.

Larson, R.A. and Hunt, L.L. 1978. Photooxidation of refined petroleum oil: inhibition by carotene and role of singlet oxygen. Photobiol. 28 (4/5): 553-555.

Fisheries in the eastern Sea of Okhotsk

Pavel A. Balykin and D.A. Terentyev
Kamchatka Research Insitute of Fisheries and Oceanography (KamchatNIRO), 18 Naberezhnaya Street, Petropavlovsk-Kamchatsky, 683000 Russia. e-mail: kamniro@mail.kamchatka.ru

The current state of fisheries (aside from the Pacific salmon fishery) in the eastern Sea of Okhotsk has been analyzed in this work. The area studied was bounded by 153°30'E longitude from the west and by 50°N latitude from the south (Fig. 1). The contribution of this area was more than 20% of total Russian harvest in the Pacific Ocean. The principal object of fishery, providing almost three-quarters of the total harvest, was walleye pollock. Flatfishes were next in the contribution; Pacific cod and saffron cod took the position after the flatfishes. The role of halibuts and sculpins has been important. The volume of the other species in the harvest (Pacific herring, rays, grenadiers, smelts) was insufficient, also it might be higher.

Different species have been harvested in different seasons. The walleye pollock fishery has been carried out from January to April (95% of the annual harvest, in the average for 1999-2001, Fig. 2). It has been accomplished during prespawning period at the motherland slope and shelf by mid-water trawls. For an example the Figure 1 demonstrates the disposition of walleye pollock fishery trawlers in March 2003. In the other months this species has been harvested as by catch. Pacific cod has been harvested mostly in the period from December to April (92% in average for 1999-2001, Fig. 3). By late summer the harvest of Pacific Cod has been insufficient. The Pacific cod fishery has been carried out with long-lines at the motherland slope and with Danish seines at the shelf. Pacific cod distribution in summer 2001 is demonstrated in the Figure 4. Danish seines are used for the fishery of saffron cod mostly. The fishery area has been situated at the less depth being compared to that in the fishery area of walleye pollock and Pacific cod. This conclusion has been illustrated by the Figure 5, where saffron cod distribution in summer 2001 has been demonstrated. Saffron cod have been exploited differently within the southern (southward from 54° N) and northern parts of the area studied. In the first part mentioned intense fishery has been observed in winter-spring period (52% for January-May); in the area northward up to 90% of saffron cod have been harvested from May to September inclusive. These peculiarities perhaps might occur due to the extensive square of the ice cover in the North-East Sea of Okhotsk from January to April. In average from 1999 to 2001 annual dynamics of Saffron Cod harvests in the area studied was more stable being compared to that of Pacific cod and walleye pollock (Fig. 6).

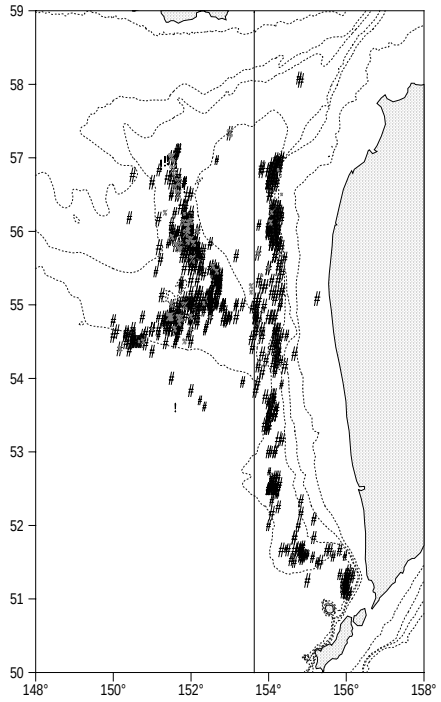

Fig. 1 Walleye pollock fishery area in March 2003.

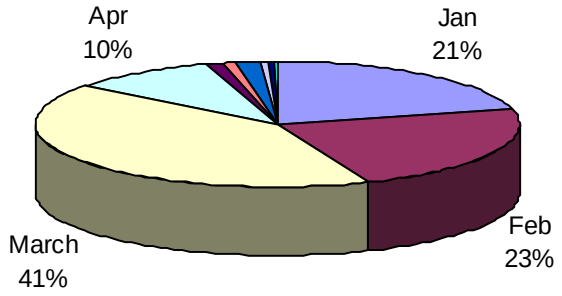

Fig. 2 The contribution of walleye pollock by months averaged from 1999 to 2001(%).

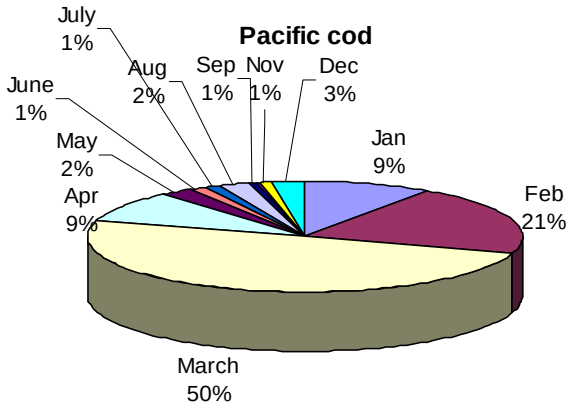

Fig. 3 The contribution of Pacific cod by months averaged from 1999 to 2001(%).

Flatfish have been harvested with Danish seines at the shelf mostly from April to September (77% in average from 1999 to 2001, Fig. 7). Principal part of the harvest consisted of yellow-finned sole. Distribution of this species in summer 2001 has been demonstrated in Figure 8.

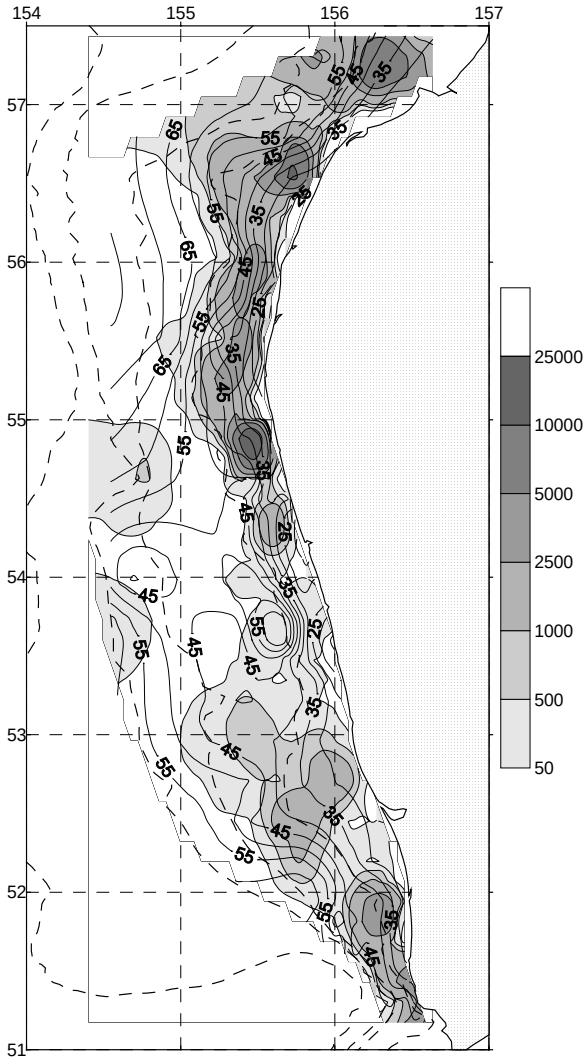

Fig. 4 Distribution of the Pacific cod biomass (kg/km^2, shaded) and average size (cm, continuous lines) from July to August 2001.

During the last two years total harvest in the area studied has been reduced by more than 200 × 103 tons or almost by 40% in the other words what indicates of the necessity to enhance today fishery regulation. That requires us to know the composition of species in the catches by the types of fisheries. Several different types of fishery have been used currently in the eastern Sea of Okhotsk including walleye pPollock trawl fishery, halibut trawl fishery, flatfish bottom-seining (Danish seine) fishery, Pacific cod long-line fishery, halibut long-line fishery, grenadier long-line fishery. The composition of species in the harvest has been described just for several types of fishery (Table 2).

The data collected provide the conclusion that majority of fishery types is multi-special. This circumstance should be taken into account for regulation of fishery what has been reckoned as monospecial till now. Total commercial harvest has been assessed for every species and has been quoted

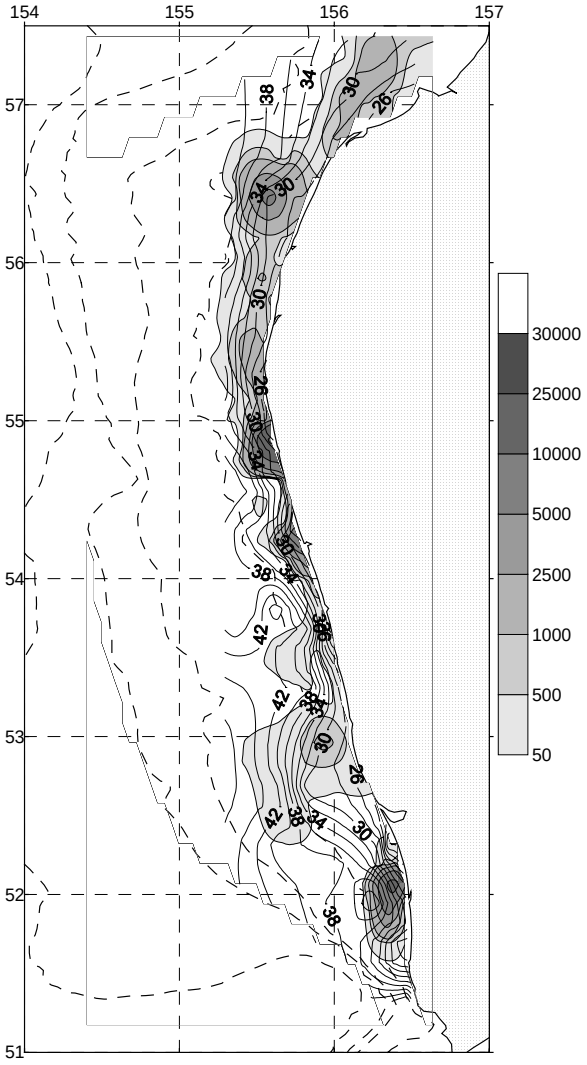

Fig. 5 Distribution of the saffron cod biomass (kg/km^2, shaded) and average size (cm, continuous lines) from July to August 2001.

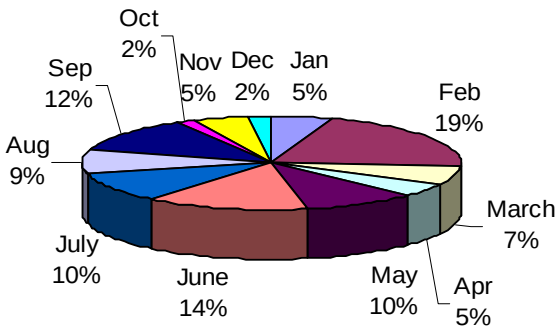

Fig. 6 The contribution of saffron cod by months averaged from 1999 to 2001(%).

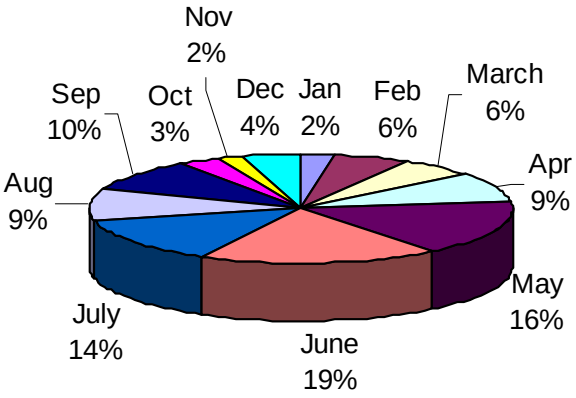

Fig. 7 The contribution of flatfishes by months averaged from 1999 to 2001(%).

among the fishery enterprises without a by catch taken into account. As a result significant volume of by catch has not been included into the fishery statistics what, in its turn, causes mistaken estimation of fishery intensity and stock abundance. In our view, total harvest of all species mentioned above should be recommended by species for every certain area of fishery and with the type of fishery and its type-specific composition taken into account.

Table 1 Object of fishery in the eastern Sea of Okhotsk.

Species, or species group	Harvest, %			Harvest, %
	1999	2000	2001	1999–2001
Walleye pollock	77.61	72.17	70.47	74.05
Pacific herring	0.57	1.98	0.52	0.99
Pacific cod	5.11	4.64	3.98	4.67
Sculpins	1.95	3.18	4.45	2.99
Flatfishes	8.96	13.02	13.87	11.51
Rockfishes	+	0.01	+	+
Halibuts	0.84	2.05	2.12	1.55
Greenlings	0.01	0.01	0.03	0.02
Saffron dod	4.88	2.67	4.24	4.04
Grenadiers	+	0.01	0.16	0.04
Smelts	0.02	0.07	0.11	0.06
Eelpouts		0.01	0.01	+
Capelin	+	0.02		0.01
Rays	0.04	0.16	0.03	0.07
Harvest, thousand t	666.8	474.9	412.7	

Table 2 Species composition in the harvests (%) expressed in weight.

Species or species group	Type of fishery				
	Walleye Pollock trawl fishery	Flatfish bottom seining fishery	Halibut trawl fishery	Pacific cod long-line fishery	Halibut long-line fishery
Walleye pollock	97.68	35.3	10.75	5.46	0.24
Pacific dod	0.07	3.1		80.20	1.87
Saffron cod	0.15	5.0		0.05	
Pacific herring	0.85	4.4	0.01		
Flatfishes	1.13	36.2	5.63	1.61	
Pacific halibut		0.5	0.12	1.91	
Greenland halibut		1.4	67.12		87.24
Sculpins	0.11	6.1		3.80	
Rockfishes		0.3	3.55	0.03	6.14
Rays		1.5	0.56	5.30	3.90
Eelpouts		1.9	4.94	0.63	0.27
Grenadiers			1.18		0.34
Others	0.01	4.3	6.14	1.01	
In total	100	100	100	100	100

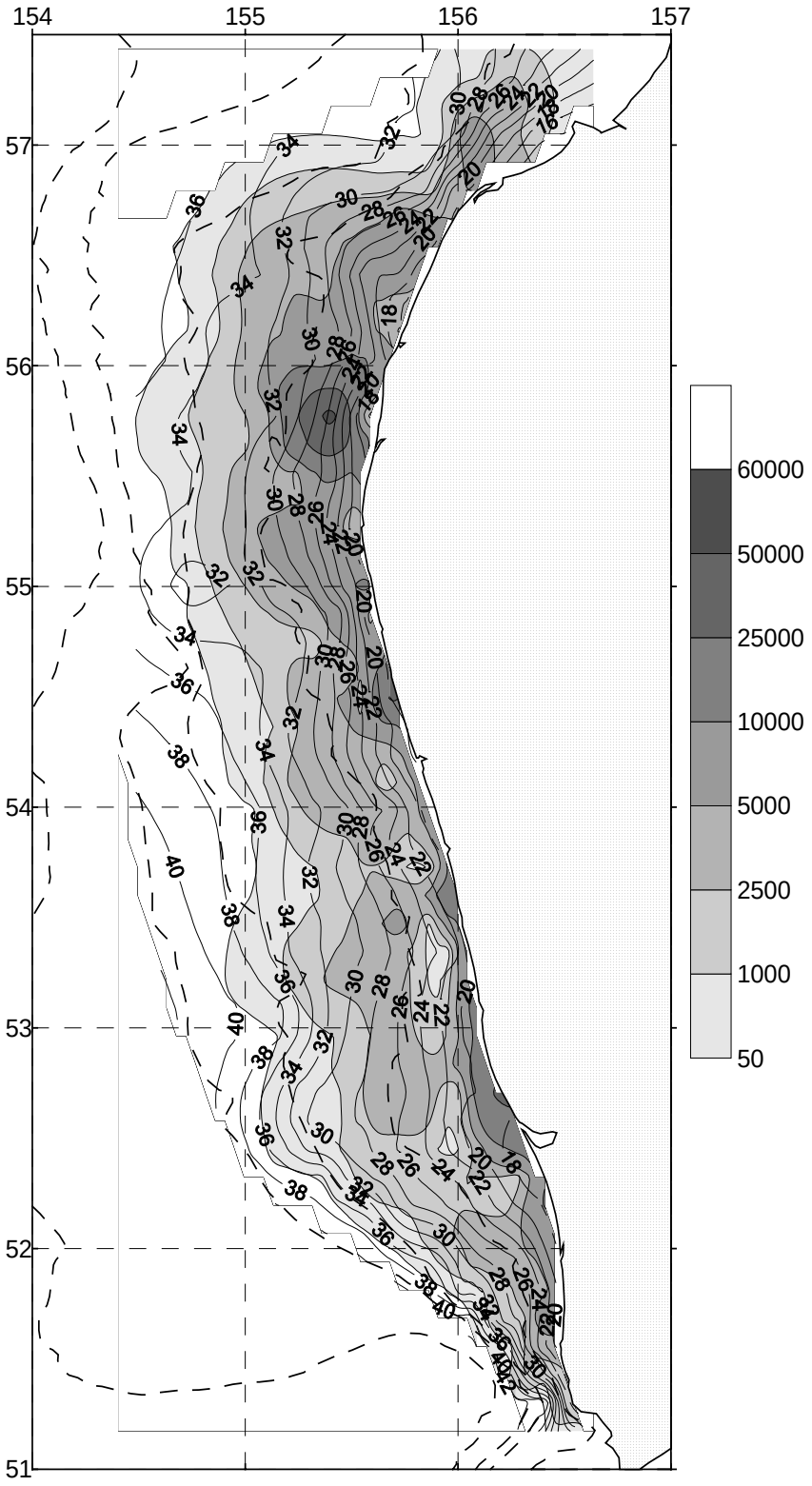

Fig. 8 Distribution of the yellow-finned sole biomass (kg/km^2, shaded) and average size (cm, continuous lines) from July to August 2001.

Characteristics of benthic communities at the northeast Sakhalin Island shelf

Tatyana A. Belan[1,2], E.V. Oleynik[1] and L.S. Belan[3]

[1] Far Eastern Regional Hydrometeorological Research Institute, 24 Fontannaya Street, Vladivostok, 690600 Russia. e-mail: tbelan@hydromet.com

[2] Institute of Marine Biology, Far-Eastern Branch of Russian Academy of Sciences, 17 Palchevskogo Street, Vladivostok, 690041 Russia.

[3] Far Eastern State University, 8 Sukhanova Street, Vladivostok, 690600 Russia.

The Sea of Okhotsk is the primary fishery region in the Russian Far East: it provides about 65-70% of total Russian catch. Pollock, herring, Pacific salmon, cod, flatfish and crab are the main commercially important species. Pacific salmon (pink, chum, coho, sockeye, chinook and cherry) spend some time inside the Okhotsk Sea, and they spawn in freshwater rivers. Recent assessments suggest that there are about 230 million t (mt) of benthic biota in the Okhotsk Sea, 35 mt of fishes, 3.5 mt of squids and 0.5 mt of marine mammals (Lapko and Radchenko 2000).

The most productive zones of the Okhotsk Sea are shelves of the North-East Sakhalin Island and the west side of the Kamchatka Peninsula due to very intensive water dynamics and high content of nutrients. Thus, average concentrations of chlorophyll *a* in the 0-50 m layer can reach 4-5 mg m^{-3} (Mordasova and Metreveli 1997). These areas are characterized by high biomass of phyto-, zooplankton and benthos. For example, average biomass of phyto- and zooplankton at the NE Sakhalin Island shelf in 0-100 m layer often exceeds 1000 and 2000 mg m^{-3}, respectively. Average benthos biomass varies from a few grams to a few kilograms per square meter (Smirnova 1959; Volkov and Chuchukalo 1985; Tkalin and Belan 1993; Belan and Oleynik 1997; Shuntov 2001). The highest density of bottom fishes is observed on the western Kamchatka Peninsula shelf. This area is the place of reproduction and migration of Kamchatka crab and Pacific salmon. The NE Sakhalin Island shelf traditionally is the fishery area of bottom and pelagic fishes and many other species (Borets 1990). On the other hand, huge deposits of oil and gas are found in these shelf areas of the Okhotsk Sea. Two major offshore oil fields at the NE Sakhalin Island shelf – Arkutun-Dagi and Piltun-Astokh fields – contain 73.5% of total recoverable reserves of the Sakhalin shelf oil. Commercial oil extraction has already started in the Piltun-Astokh field; the Kamchatka shelf is considered as a prospective area.

Ecological monitoring of the marine environment was carried out by specialists of FERHRI in the 1990s. According to the data obtained at the end of 1990s, benthos biomass and abundance had considerable fluctuations. The highest biomass was recorded in the northern part of the NE Sakhalin Island shelf (Piltun-Astokh, Arkutun-Dagi) where the sea urchin *Echinarachnius parma* dominated. Average benthos biomass of study areas considered to be more than 1000 g m^{-2}. The highest density was detected in the southern areas of the NE shelf (Lunskoye field). Polychaetes, amphipods and bivalves prevailed in terms of number of species. Actiniaria, Polychaeta, Bivalvia, Amphipoda, Cumacea, Echinoidea and Gastropoda were characterized by the highest occurrence, abundance and biomass.

Distribution of benthic communities had a mosaic pattern, and it was depended on the sediment types (and on near-bottom hydrodynamics activity). Monodominant communities (*E. parma* and *D. bidentata*) characterized by maximum biomass and lowest species diversity, were recorded on the fine sands. The most rich and diverse polydominant communities in which few species prevail (*E. parma*, polychaetes *Nephtys caeca*, *Ampharete lindstromi*, and sea anemones *Halcampa vegae*, *Epiactis* sp.) were found on the coarse sand and gravel. These communities were characterized by low biomass (Belan and Oleynik 2000).

Suspended-feeders (*E. parma*, *D. bidentata*, bivalve *Peronidia lutea*) and sessile animals (sea anemones, sponges, hydroids, some polychaetes) dominated on the trophic structure of benthic assemblages in Piltun-Astokh field. Communities of deposit-feeders (polychaete *A. proboscidea*, bivalves *Y. seminuda*, *Y. myalis*) and suspended-feeders (amphipods *Ampelisca eschrihti* and *A. macrocephala*) were common on the soft silts in Lunskoye field (Belan et al., 1996).

Data obtained in 1990s have shown background pollutant concentrations in seawater and bottom sediments and healthy status of pelagic and bottom communities at the NE Sakhalin Island shelf. Coastal ecosystems were characterized by high richness, diversity and productivity as they were in 1970s and 1980s. Changes in bottom communities near movable drilling rigs were not detected yet (Tkalin and Belan 1993; Belan and Oleynik 1997, 2000). However, increasing commercial oil extraction may cause negative affects on coastal ecosystems of the NE Sakhalin Island shelf.

References

Belan, T.A., Oleynik, E.V., Tkalin, A.V. and Lishavskaya, T.S. 1996. Characteristics of pelagic and benthic communities on the North Sakhalin Island Shelf. *PICES Scientific Report* 6: 227-229.

Belan, T. and Oleynik, E. 2000. Faunal composition, distribution and present status of benthos in the Piltun-Astokh oil and gas field. FERHRI Special Issue No. 3. Vladivostok: Dalnauka, 166-177.

Belan, T.A. and Oleynik, E.V. 1997. Background benthos study at North Sakhalin Island shelf in 1994. Ocean Research 19: 121-126.

Borets, L.A. 1990. Present status of resources of bottom fishes in the shelf of Far-Eastern Seas. Biological Resources of the shelf and marginal Seas. Moscow: Nauka publishing house, 181-196. (In Russian).

Lapko, V.V. and Radchenko, V.I. 2000. Sea of Okhotsk. Marine Pollution Bulletin 41: 179-187.

Mordasova, N.V. and Metreveli, M.P. 1997. Phytopigments in the Sea of Okhotsk. Complex Studies of Ecosystem of the Sea of Okhotsk. Moscow: VNIRO Publishing, 199-205. (In Russian).

Smirnova, L.I. 1959. Phytoplankton of Okhotsk Sea and Kuril Nearshore area. Proceedings of IOAN. Vol. 30: 3-51. (In Russian).

Shuntov, V.P. 2001. Biology of Far-Eastern Seas. Vladivostok: TINRO-Center. 579 p.

Tkalin, A.V. and Belan, T.A. 1993. Background ecological conditions of the NE Sakhalin Island shelf. Ocean Research 15: 169-176.

Volkov, A.F. and Chuchukalo, V.I. 1985. Composition and distribution of mezoplankton in Okhotsk Sea. Proceedings of TINRO 110:125-128. (In Russian).

The status of endangered western gray whales (*Eschrichtius robustus*) off the northeast coast of Sakhalin and the discovery of a new major gray whale feeding area in 2001, based on aerial survey data

Sergei A. Blokhin[1] and Sergei B. Yazvenko[2]

[1] Pacific Fisheries Research Centre (TINRO-Centre), 4 Shevchenko Alley, Vladivostok, 690950 Russia. e-mail: blokhin@mail.primorye.ru

[2] LGL Limited, Environmental Research Associates, 9768 Second Street, Sidney, BC, V8L 3Y8 Canada.

From August 2 to September 9, 2001, seismic surveys for oil and gas off northeast coast of Sakhalin were conducted on behalf of ExxonMobil in the Odoptu polygon, in the vicinity of the only known feeding area of the critically endangered western gray whale (WGW) *Eschrichtius robustus*. Only about 100 individuals are known to survive to date. From August 2 to August 14, calibration experiments aimed at determining the acoustic transmission properties in this area were conducted. Active seismic acquisition occurred from August 17 to September 9. Marine mammal aerial surveys were carried out in this area between July 19 – November 19, 2001, using an Mi-8 helicopter and an An-28 airplane. The objectives of the aerial surveys were to monitor the status of all marine mammals in the area and help mitigate potential effects of seismic activities on them, particularly on feeding WGWs. During the study period, a total of 131 aerial surveys were conducted. In total, 1404 groups including 1792 WGWs were seen by all observers on all transects (excluding the feeding plumes with no associated WGWs). This number includes multiple resightings of the same animals.

The most significant result of the 2001 aerial surveys was the detailed study of a new major WGW summering and feeding area, the "Offshore area", 25-40 km offshore between Nyysky and Chayvo Bays (Fig. 1). This area was discovered on September 9 by our colleagues Mikhail Maminov (TINRO) and Yuri Yakovlev (IBM); in the next two months, 22 intensive aerial surveys were flown over it. The largest number of WGWs that was recorded on transect on a single aerial survey in the Offshore area (An-28) was 43 (53 gray whales were recorded on- and off-transect). In the Piltun Bay area, the largest number of WGWs recorded on and off-transect on a single survey was 39 (Mi-8). This discovery changed our views on the current status of WGWs. During the previous 18 years of studies, only one feeding area of WGWs (the Piltun Bay area) was known. By November, the observed number of WGWs in both feeding areas off northeast coast Sakhalin decreased appreciably; the likely reason was the departure of many WGWs in the direction of their (still unknown) wintering grounds. Aerial surveys of WGWs in the Piltun Bay area carried out during seismic exploration did not show a change in their numbers during this time. A certain redistribution of WGWs within the Piltun Bay area was observed. During active seismic acquisition, some whales moved to the southern half of the Piltun Bay feeding area, away from where the seismic survey was being carried out. Even though the distribution of WGWs in the Piltun Bay area fluctuated over the July – November period, that particular shift indicates that the seismic exploration had some effect on the distribution of WGWs. There are no data showing that this effect was significant: the observed numbers of WGWs did not change, so the whales did not seem to have left the Piltun Bay feeding area. Aerial surveys showed that the whales continued to feed throughout the seismic activity. There was no difference in the intensity of feeding throughout the feeding season (before, during and after seismic acquisition), except at the very end of it in November the feeding intensity decreased. The discovery of a new major WGW summering and feeding area in the Sea of Okhotsk indicates that WGWs are more widespread in their distribution and more flexible in their feeding behavior than previously reported.

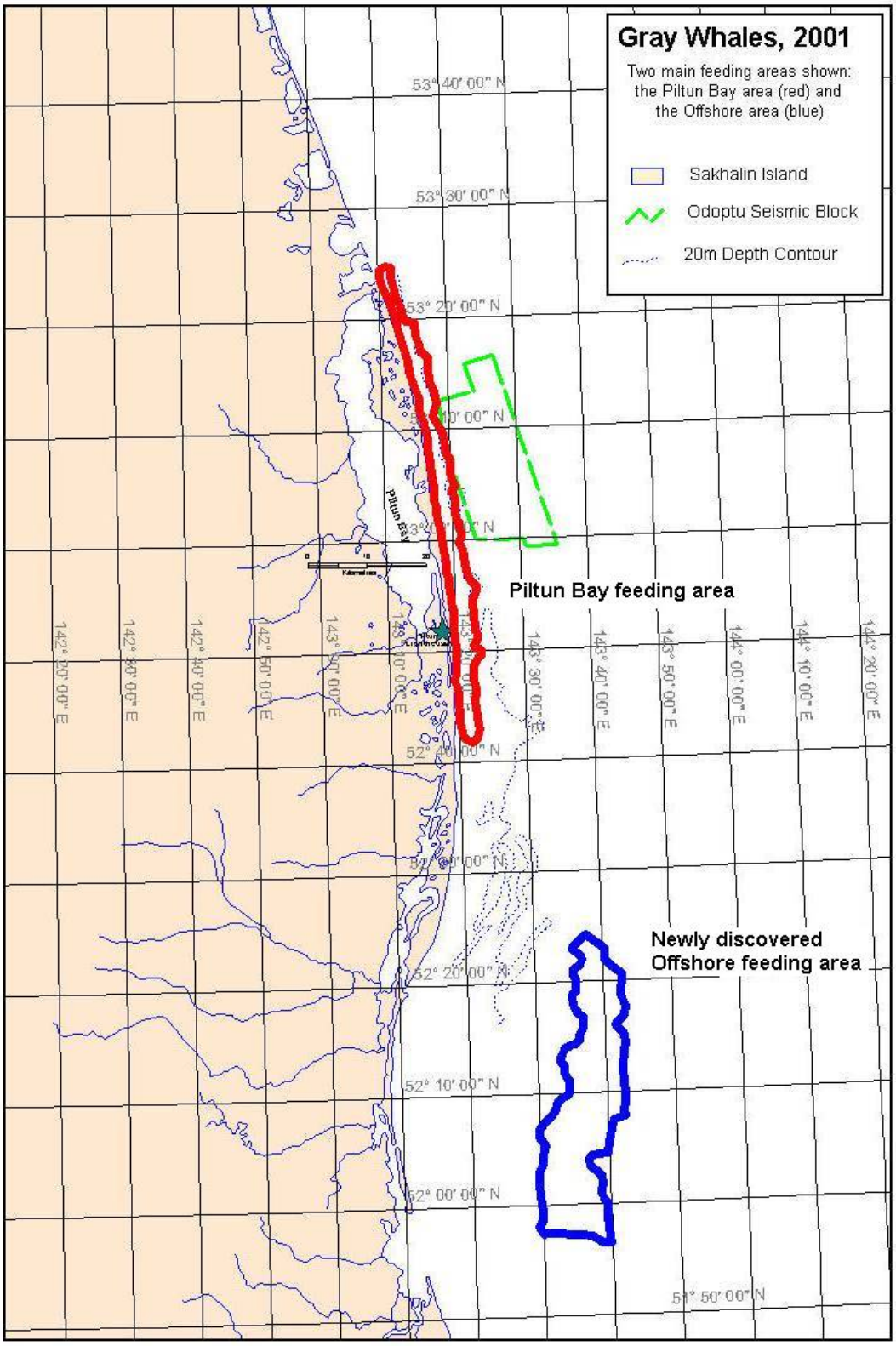

Fig. 1 Two main feeding area of the endangered western gray whales (*Eschrichtius robustus*) based on the aerial survey data in 2001: previously known Piltun Bay feeding area (red) and offhore feeding area discovered in 2001 (blue).

Marine Mammal Mitigation and Monitoring Program for the 2001 Odoptu 3-D Seismic Survey, Sea of Okhotsk, Sakhalin Island: A possible future industry standard

Stephen R. Johnson and Sergei B. Yazvenko
LGL Limited, Environmental Research Associates, 9768 Second Street, Sidney, BC, V8L 3Y8 Canada.
e-mail: srj@LGL.com

The Odoptu Marine Mammal Mitigation and Monitoring Program was based on the findings that the key environmental issue for the planned seismic program was protection of the western gray whales (WGWs, *Eschrichtius robustus*) that spend most of the ice-free season feeding off the northeast Sakhalin coast. WGWs are listed as endangered in the Russian Red Book and critically endangered by the International Union for the Conservation of Nature (IUCN). In addition, over the past few years some individual whales have been reported as emaciated due to unknown reasons. Given these considerations, the primary goal for the mitigation and monitoring programs was to minimize potential impacts of the seismic program on the feeding activity of WGWs.

Earlier studies (1983-2000) showed that feeding WGWs mainly stayed in the area near the mouth of Piltun Bay and northward along the northeast Sakhalin coast (hereafter referred to as the "Piltun Bay feeding area"); >95% of all WGW observations in this area were located shoreward of the 20 m isobath. The key concept in the mitigation strategy was to establish a buffer distance between feeding WGWs and the seismic vessel that would allow the whales to continue to feed without being displaced from the Piltun feeding area. The monitoring program was to ensure that the seismic vessel would stay at or beyond the buffer distance from feeding WGWs.

The Odoptu seismic block was divided into two sub-areas (Areas A and B). Area A was the area within the seismic block extending 4 km seaward from the 20 m isobath. The buffer distance of 4 km was based on seismic experiments conducted near feeding eastern gray whales in the Bering Sea (Malme et al. 1986, 1988). These studies indicated that 10% of the gray whales showed major modifications to behavior (ceased feeding and moved rapidly away from the vessel) when the received sound levels generated by a seismic ship were greater than 163 dB re 1 µPa rms. It was found that the sound attenuated to the 163 dB re 1 µPa rms level over a distance of 4 to 5 km from the seismic vessel. In 2001 in the Odoptu area, calibration experiments with active seismic ship were conducted prior to the start of the actual seismic survey to establish the buffer distance at which the sound was attenuated to the 163 dB re 1 µPa rms.

Seismic acquisition in Area A was restricted to periods with good visibility and daylight so that the location of whales could be determined. With the help of aerial over-flights and vessel-based surveys, shooting seismic lines in Area A was carefully planned to maintain the established primary buffer distance from all observed gray whales. While shooting in Area A, continuous observations were made by vessel-based marine mammal observers (MMO's) onboard the seismic acquisition vessel *M/V Nordic Explorer* and two support vessels, *M/V Rubin* and *M/V Atlas*. Systematic observations were also made by the MMO's while shooting in Area B. Observers aboard the *M/V Rubin* provided additional intensive MMO coverage along the landward edge of the 4-5 km buffer distance from the seismic ship while shooting occurred in Area A.

Area B was the area within the Odoptu seismic block boundary that was at least 4-5 km seaward of the 20 m isobath. Seismic acquisition in Area B adhered to the same buffer distances implemented in Area A. However, because very few gray have ever been documented in Area B, surveys in Area B were not restricted to daylight hours or periods of good visibility.

The gray whale mitigation and monitoring program designed and carried out before, during and after the 2001 Odoptu seismic survey was the most stringent and comprehensive program of this type ever conducted in the world for a marine mammal. As such, it may serve as a prototype of a future world-wide industry standard of mitigation/monitoring programs in relation to offshore seismic surveys. The program included four components: round-the-clock vessel-based observations, (near) daily aerial surveys, behavioral studies of WGWs and acoustic monitoring of the WGW feeding area.

The overall conclusions of the four main mitigation/monitoring/research programs are summarized below.

Vessel-based studies

- No flight behavior by gray whales was observed by any of the vessel-based marine mammal observers during the study period, nor were any unusual gray whale activity patterns observed.
- A previously unknown WGW feeding area was discovered offshore from Chayvo Bay (south-east of the Piltun Bay feeding area) in waters 30-45 m deep. This discovery indicates that WGWs are more widespread in their distribution and more flexible in their feeding behavior than previously reported.

Aerial surveys

- Overall, 131 systematic aerial surveys were conducted in the Piltun Bay area and other adjacent areas on the northeast Sakhalin shelf in 2001. The WGW feeding, distribution and abundance data were analyzed using several statistical methods, including BACI analysis and quasi-likelihood multiple regression, to determine if an effect on WGW feeding activity, distribution, or abundance occurred during the Odoptu seismic survey.
- None of the statistical analyses showed a statistically significant relations between seismic activity and WGW feeding activity. Whales continued to be present and to feed in the same feeding areas as in 1999 and 2000.
- A southward shift in the distribution of some (average ~ 3-4) of WGWs from west of the Odoptu block was statistically correlated ($P<0.05$) with the period of seismic operations. Such movements did not exceed the range of shifts of WGWs in the Piltun area during the feeding season. In other feeding areas, shifts in eastern gray whale distribution have been linked to changes in prey distribution and availability (Bass 2000, Dunham and Duffus 2001, 2002). The distribution and availability of WGW prey in the Piltun area was studied in 2002, and the results are pending.

Behaviour studies

- WGWs remained present near the Odoptu seismic block and continued to feed west of the Odoptu block throughout the seismic survey period. No trends in WGW abundance were correlated with seismic activity.
- All 11 gray whale behavior variables measured were statistically correlated ($P<0.05$) with environmental variables. This result highlights the necessity of considering environmental variables when evaluating potential industry effects on gray whale behavior.
- Average values of most behavioral parameters studied during the Odoptu 2001 study were similar to those recorded in previous behavior studies in the Piltun area. Parameters that differed were either not correlated with seismic activity or the differences could not be explained by the effects of seismic, i.e., expected seismic influences would have changed the parameters in a direction opposite to that expected from a seismic-related influence (i.e., blow interval).
- Multiple regression analyses indicated that five of 11 behavioral parameters studied in 2001 were statistically correlated ($P<0.05$) with Odoptu seismic activity. Behavioral parameters that were correlated with seismic activity showed effects of limited duration (highly transient) and generally within the range of variation attributable to environmental effects.
- Multiple regression analyses indicated that six of 11 behavioral parameters studied in

2001 were not statistically correlated ($P<0.05$) with Odoptu seismic operations.

- These results suggest that the stringent mitigation measures employed to limit exposure of WGWs to high sound levels mitigated potential impacts on the behavior of these whales to very low levels.

Acoustic monitoring

- The 4-5 km buffer zone was effective in limiting sound exposure levels for WGWs.
- Acoustic monitoring at the 20 m contour, which generally defines the outer edge of the WGW Piltun feeding area, showed that received sound levels during the seismic survey were consistently below the target 163 dB re 1 µ Pa rms threshold in Area B of the seismic survey area.
- Acoustic monitoring provided crucial information used to estimate seismic sound exposure levels for WGWs, which were used to investigate the effects of seismic activity on feeding activity, distribution, abundance, and behavior of WGWs in the Odoptu area.

Results of potential oil spill modeling in Aniva Bay and La Perouse Strait

Alexander Bogdanovsky[1], I.E. Kochergin[1], I.A. Arshinov[1], V.D. Budaeva[1], V.G. Makarov[1,2], V.F. Mishukov[3], S.I. Rybalko[1] and V.P. Tunegolovets[1]

[1] Far Eastern Regional Hydrometeorological Research Institute, 24 Fontannaya Street, Vladivostok, 690600 Russia. e-mail: abogdanovsky@hydromet.com

[2] National Politechnic Institute, La Paz, Mexico.

[3] V.I. Il'ichev Pacific Oceanological Institute, Far-Eastern Branch of Russian Academy of Sciences, 43 Baltiyskaya Street, Vladivostok, 690041 Russia.

In 2002-2003, oil spill modeling was carried out for four potential oil spill scenarios in the Aniva Bay and La Perouse Strait areas (Table 1). Oil spills near Prigorodnoe village are regarded as a potential result of increasing emergency probability under Sakhalin-2 project development with the planned construction of an oil-refining plant and marine terminal. La Perouse Strait is an area of on-going and projected tanker operations with a higher risk to navigation due to intensive hydrodynamics and strong winds. Korsakov is the largest Russian port in Aniva Bay and here the risk of emergencies is also high. The areas specified are included in the Regional oil spill response plan and regarded as the highly dangerous sites.

Typical hydrometeorological scenarios were constructed using a method that had already been successfully applied for oil spill statistical modeling on the eastern Sakhalin shelf (Kochergin et al. 2000a). The method incorporates typification of wind situations at the coastal hydromet stations, reconstruction of wind fields with the help of re-analysis data, calculation of non-tidal currents by a linear baroclinic model, calculation of tidal currents by instrumental data and the final composition of hydromet conditions for the trajectory oil spill modeling.

The typical wind fields were constructed from 15-year data from five coastal hydromet stations (Krilion Cape, Novikovo, Salmon Bay, Korsakov and Kirilovo) and surface winds from the retrospective analysis (NCEP NOAA).

Table 1 Potential oil spill scenarios in the region of Aniva Bay and La Perouse Strait.

##	Spill source	Spill volume (t/ ths. barrel)	Spill duration (hour)	Oil type	Spill location	Hydrometeo conditions	Quantity of calculated variants
1	tanker accident	5500/41	0.083 (instantaneous)	oil typical for Piltun-Astokh oil&gas field	nearby vil. Prigorodnoye	November climatic conditions and light north wind situation	4 3-day trajectories for different tide phases, 1 ten-day trajectory for light wind situation
2	– // –	– // –	– // –	– // –	region of La Perouse Strait	November climatic conditions	4 3-day trajectories for different tide phases
3	ship accident	300/2.2	1	mazut, diesel	water area of Korsakov harbour	summer, autumn and winter typical conditions	14 6-day trajectories for typical wind situations, 1 trajectory for extremely strong winds
4	tanker accident	3000/22	6	oil typical for Chayvo oil&gas field	region of La Perouse Strait	summer, autumn and winter typical conditions	16 6-day trajectories for typical wind situations, 1 trajectory for extremely strong winds

Table 2 Example of wind probability table (%) with the wind situations selected for modeling.

Gradations	Winter								Summer								Autumn							
	N	NE	E	SE	S	SW	W	NW	N	NE	E	SE	S	SW	W	NW	N	NE	E	SE	S	SW	W	NW
Calm	7								10(1)								6							
1-4 m/s	43(1)		8(3)	0.5	1.2	0.4	10(4)	(1)	24(2)			4	19(4)	15(6)		1.6	31(5)			1.4	16(1)	14(2)		
5-9 m/s	24(2)			0.2	1.1	0.8		(2)	12(3)			0.8	11(5)			0.3				1.2		3.8	18(3)	2.3
10-14 m/s			0.4		0.1	0.1	1.8		0.2	0.2	0.5		0.3		0.2		0.6	0.5	1.0	0.4	0.9	1.2		0.3
15-19 m/s	0.3	0.3	0.2				0.2				0.1							0.1				0.1		0.1
20-24 m/s	0.1	0.1	0.1								0.1												0.4(4)	
25-29 m/s																								

Notes:

wind situations selected for modeling are marked with gray background;

wind situation #4 for autumn period is not typical and is selected to assess oil spill fate in extremely strong wind conditions;

the wind situations codes are presented in parentheses, names of situations are:

Winter		Summer		Autumn	
(1)	light NW-N-NE winds	(1)	calm	(1)	light and moderate S winds
(2)	moderate and strong NW-N-NE winds	(2)	light N-NE-E winds	(2)	light SW-W-NW winds
(3)	light and moderate E winds	(3)	moderate N-NE-E winds	(3)	moderate and strong W winds
(4)	light and moderate W winds	(4)	light S winds	(4)	extreme strong W winds
		(5)	moderate S winds	(5)	light and moderate N-NE-E winds
		(6)	light and moderate SW-S winds		

Typical wind situations were chosen from a frequency table constructed for the hydromet station closest to the oil release point. Typification is based on the combined wind direction and velocity gradations, taking into account the regional climatic features, influence of surface winds on surface current formation, frequency of a given situation, oil transport specificity and expert assessments (Table 2). In addition, situations with extremely strong wind velocity and rare occurrences were defined. Every wind situation is supported with average vectors calculated at the points with synchronous measurement series and subsequent interpolation of those vectors in the regular grid for the investigated area.

Hydrodynamic calculations using an Ekman-type linear baroclinic model (Budaeva and Makarov 1999) resulted in the construction of diagnostic current schemes for each selected wind situation. Water density fields were constructed by the historical oceanographic data sets (RODC FERHRI, 1948-1992) and data of the hydrological surveys in Aniva Bay conducted by SakhNIRO in 2002.

Tidal current fields were calculated by extracting harmonic constants out of the series of instrumental current observations and interpolating them into the regular grid with account of spatial variability of the amplitude and phase of the six main harmonics.

The fate of oil in the sea was modeled by the VOS 3 Model developed in FERHRI (Kochergin et al. 2000b). Output results include oil transport trajectories with oil locations specified in time (Fig. 1) and other characteristics. The model results allow estimating the most probable oil transport trajectories under the summer, autumn and winter (no ice case only) conditions. Oil weathering processes (evaporation, dispersion, emulsification, etc.) were assessed using POI FEB RAS model (Michoukov and Abramova 1997) and ADIOS II model developed in NOAA and MMS.

The following conclusions were made from the modeling results for statistically reliable situations. In the case where oil was spilled in the northern part of Aniva Bay in summer, the oil will be transported southward to the open sea (over 60% probability), although oil reaching the beaches due to southern winds is also likely (about 30% probability). In autumn the oil will be transported either to the east of the bay under the western winds (over 30% probability) or to the south under the northern winds (about 30% probability). Oiled beaches in the north of the bay are also probable (about 15% probability) under the southern winds.

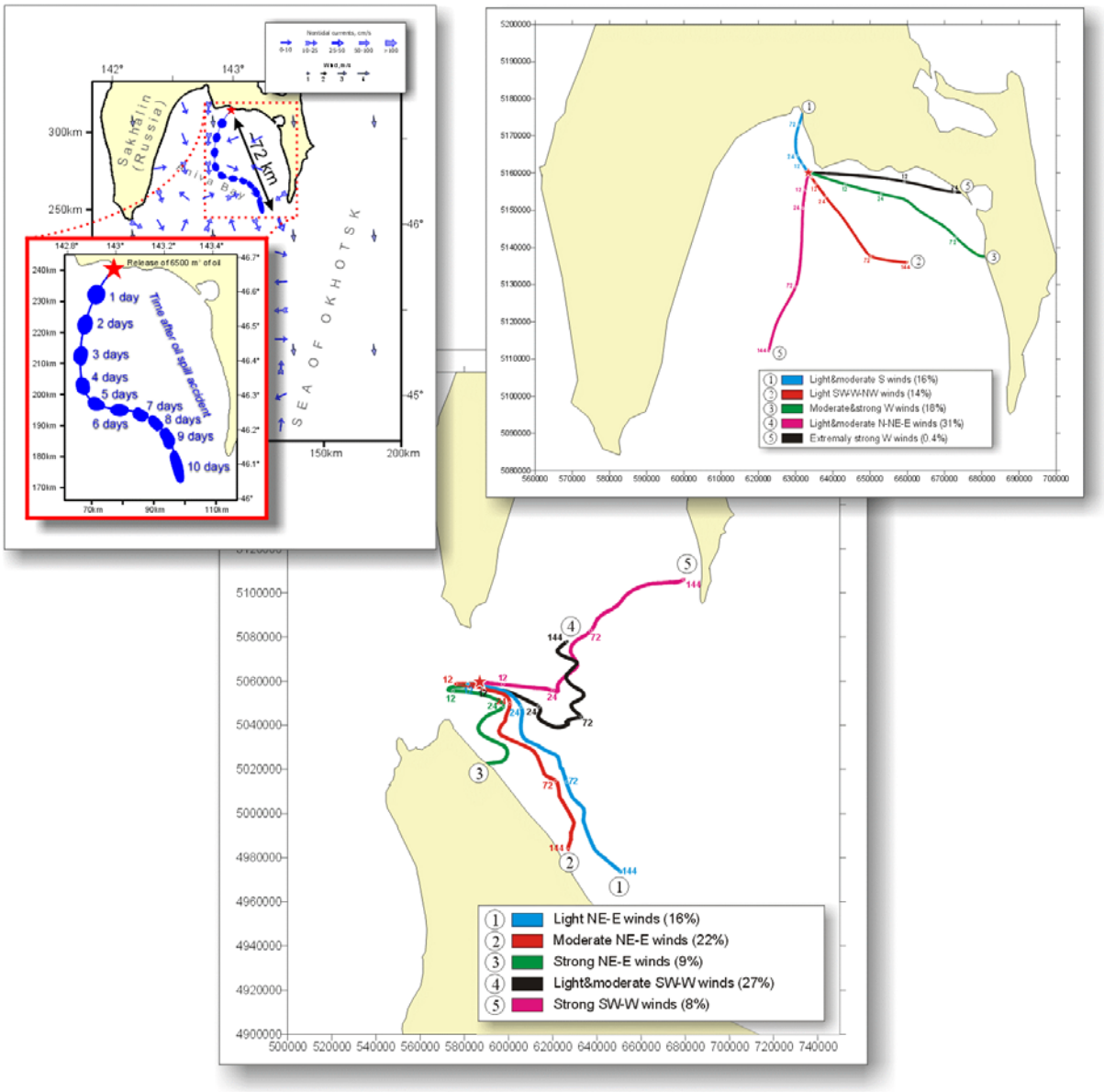

Fig. 1 Examples of potential oil spill trajectory modeling results: (a) spill nearby vil. Prigorodnoe (light north winds situation), (b) spill in the water area of Korsakov harbour (autumn typical and extremely strong winds situations) and (c) tanker accident in the La Perouse Strait (summer typical winds).

In winter, the oil will be transported to the south (75%) and the south-east (10%). The current tidal phase is not significant for the oil spills in the north of Aniva Bay as the tidal current velocity is low.

Modeling of the potential oil spills in La Perouse Strait shows that in summer the oil will be transported towards the Sea of Okhotsk along Hokkaido Island or oiling beaches on it (50%) or be transported to the south of Aniva Bay (35%). In autumn the oil may be transported towards the Sea of Japan (30%) or to the east (60%), but unlike the summer results, oil is not transported to the coastal zone of Hokkaido Island within 6 days. Oil transport to Aniva Bay is only 9% probable. In the rest of the cases, oil is transported to the east. In winter, oil is transported to the Sea of Japan

(about 35% probability), but in rest of the cases the oil is transported southeastward, parallel to the coast of Hokkaido Island. It should be noted that the current tidal phase is of great significance here as the tidal current velocity may amount to 2 m s^{-1} (both in the eastern and western direction). This is especially critical for oil spill response plan development.

Acknowledgements
Authors express their high gratitude to SakhNIRO (G.V. Shevchenko) and Environmental Company of Sakhalin, Ltd. (V.F. Putov) for oceanographic data provided and Sakhalin Energy Investment Company (SEIC) and Central Marine Research and Design Institute (CNIIMF) for the finance granted.

Results of this work are also published as information report in *Pacific Oceanography* (2003) Vol. 1, No. 1.

References

Budaeva V.D. and Makarov, V.G. 1999. Peculiar water regime of currents in the area of Eastern Sakhalin shelf. Proceedings of the Second PICES Workshop on the Okhotsk Sea and Adjacent Areas. PICES Scientific Report 12: 131–138.

Kochergin, I.E., Bogdanovsky, A.A., Budaeva, V.D., Varlamov, S.M., Dashko, N.A., Makarov, V.G., Putov, V.F., and Rybalko, S.I. 2000a. Construction of hydrometeorological scenarios for environmental impact assessments. FERHRI Special Issue 3. Vladivostok: Dalnauka. pp. 223–240.

Kochergin, I.E., Bogdanovsky, A.A., Mishukov, V.F. and Putov, V.F. 2000b. Oil spill scenario modeling for Sakhalin shelf. Proceedings of WITpress "Oil and Hydrocarbon Spills II". pp. 39-50.

Michoukov, V. and Abramova, O. 1997. Experimental Study of Oil Degradation in the Sea of Okhotsk. Proceedings of International Marine Science Symposium on "Biogeochemical Processes in the North Pacific", Mutsu, Japan, November 12-14, 1996, Published by Japan Marine Science Foundation, Tokyo, March, 1997, pp.376-391.

Pacific herring (*Clupea pallasii* Val.) distribution grounds on northeastern Sakhalin Shelf (Okhotsk Sea)

Elsa R. Ivshina and O.Yu. Nemchinov
Sakhalin Research Institute of Fisheries and Oceanography (SakhNIRO), 196 Komsomol'skaya Street, Yuzhno-Sakhalinsk, 693023 Russia. e-mail: elsa@sakhniro.ru, nemetz@sakhniro.ru

Pacific herring spawn in numerous shallow-water bays off northeastern Sakhalin from late May through mid-July. After spawning, local herring migrate for foraging to shelf waters off northeastern Sakhalin (Frolov 1950; 1968; Andreyev 1963).

Bottom trawl surveys performed in August-October 1989 from 6 to 30 m deep and in 1991-1992, 1997-2002 from 20 to 500 m deep made it possible to determine the distribution of Pacific herring during foraging on the northeastern Sakhalin shelf.

Bottom trawl catches show that the frequency of herring occurrence ranges between 20-30%, on average. During the summer season, juvenile fish swim up to 20-30 m deep and separately from mature fish, rarely forming mixed aggregations. Major aggregations of juvenile fish 5-14 cm long are attached to bay areas. Small numbers of fish travel up to 50°N latitude.

Mature herring swim throughout the coastline. Major aggregations, nearly 70%, are concentrated nearly 100 m deep and rarely at 200 m deep. There are three areas of herring localization within the shelf: the area north 52°N, the area of Lunsky and Nabilsky bays, and a small portion south 51°N where fish swim no deeper than 50 meters (Fig. 1). Noteworthy, bigger fish that reach 29 to 32 cm migrate north of 52°N, 17 to 23 cm long fish predominates in the southern and central portions of the shelf. Scientists also detect the Okhotsk population of herring in the northern areas of the shelf (Shuntov 1998; Melnikov and Kuznetsova 2002).

Most probably, major aggregations of Pacific herring are attached to the areas of thickest zooplankton concentrations on northeastern Sakhalin shelf (Bragina 1999). Examinations of herring stomachs found zooplankton of neritic and oceanic groups that are typical of shelf waters off northeastern Sakhalin. Herring diets are based on euphausiids, calanoid copepods, and cumaceans. Most herring slow foraging and reach high fat in August and September.

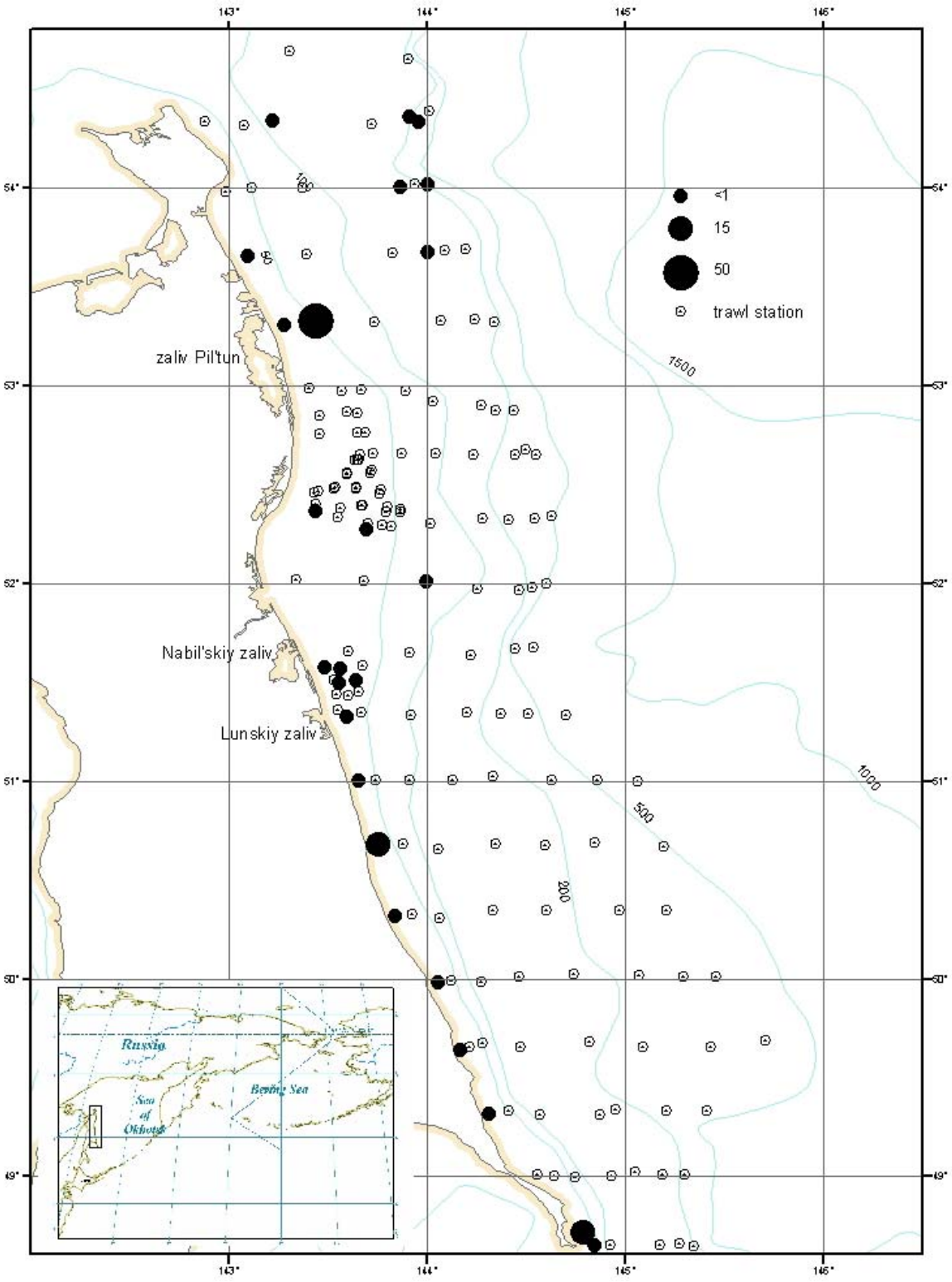

Fig. 1 The scheme of herring distribution typical sites on northeastern shelf of Sakhalin, by results of bottom trawl survey performed in August and September 2000, t mile^{-2}.

Comparative modeling of marine environment impact produced by dredging works planned within the first stage of Sakhalin-1 Project

Igor E. Kochergin[1], A.A. Bogdanovsky[1], S.I. Rybalko[1], M.V. Mischenko[1], B.V. Arkhipov[2], V.V. Solbakov[2] and V.N. Koterov[2]

[1] Far Eastern Regional Hydrometeorological Research Institute, 24 Fontannaya Street, Vladivostok, 690600 Russia. e-mail: ikochergin@hydromet.com

[2] Dorodnicyn Computing Centre of the Russian Academy of Sciences (CC RAS), 40 Vavilov Street, Moscow, 119991 Russia. e-mail: arhip@ccas.ru

Modeling results of the impact of dredging on the marine environment within the first stage of the Sakhalin-1 project are compared. Comparative modeling covered two activities: (1) site leveling including dredging and soil dumping (5,000 m^3) and (2) the construction of an underwater pipeline including trenching, temporary soil storage on the sea bottom and trench backfilling (over 800,000 m^3). The area modelled is on the northeastern Sakhalin shelf, off Chayvo Bay.

The impact was modeled using the models that were previously approved for application in Sakhalin oil and gas fields development projects: VOSTOK model developed in FERHRI (Kochergin and Bogdanovsky 2003) based on a Lagrangian approach and the AKS-ECO model, developed in CC RAS and Environmental Centre IFPA (Arkhipov et al. 2000) based on an Eulerian approach. Both models were tested with *in situ* experiments and justify their applicability. Unified input data used in both models included technical parameters of the impact sources (rate, time of operation, location, soil granulometric composition, etc.) and general requirements for hydrometerological scenarios.

For comparitive purposes, the output results were made the same in kind (the same gradations and units). The following output results were compared: the curves of the maximum extent of suspended solid concentration depending on the distance from the source, the average volumes of contaminated water by the concentration gradations, the lifetime of waters contaminated with a given concentration of suspended solids, and the size of formed bottom sediments by height gradations.

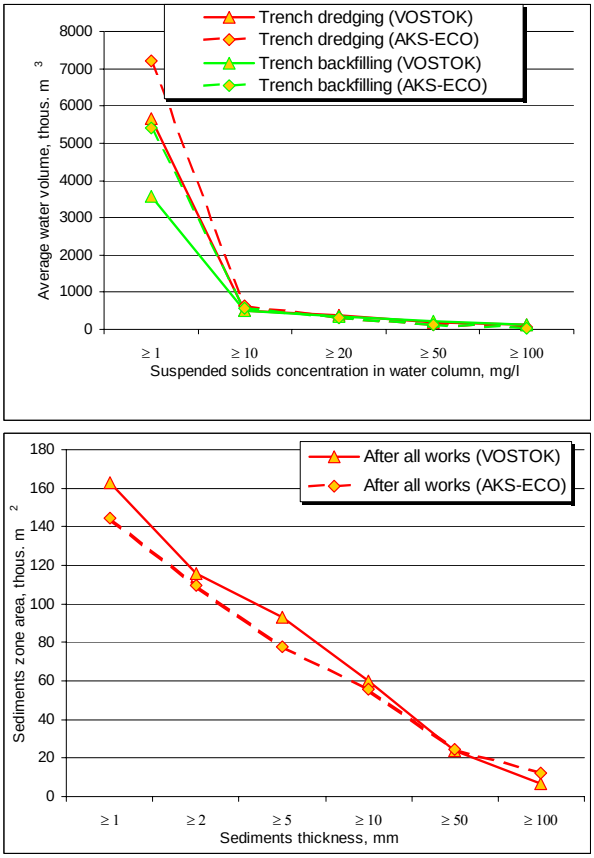

Fig. 1 Example of comparative diagrams on modeling results: (a) average contaminated water volumes during trenching and backfilling (total works volume – 800,000 m^3), (b) area of sediments formed on the sea bottom during site leveling (total works volume – 5,000 m^3).

The comparison of modeling results shows their relatively good convergence. The highest convergence is achieved when calculating the sedimented area on the sea bottom (relative difference within 0-35% for different gradations).

This testifies to the use of approximately the same calculation parameters of solid particles sedimentation velocities. Comparison of calculated water column contamination parameters shows that both models produce almost the same results for the suspended solid concentration in the plume of more than 10 mg/l (10-30%), while results may be considerably different (up to 70%) if the concentration is low. Differences in the modeling results are analyzed and possible reasons are given. Comparative diagrams constructed over calculation results of both models are shown in Figure 1.

Thus, despite the difference in approaches used in modeling, two different models give comparable results. The models can be used to calculate the complex impact on marine environment especially produced by dredging operations and pollutant discharges.

Acknowledgements
The authors express their high gratitude to AMEC and ExxonMobil companies for financing granted.

References

Kochergin, I.E. and Bogdanovsky, A.A. 2003. New Version of Contaminant Transport Model in Sea. *Pacific Oceanography* 1 (1): 53-60.

Arkhipov, B.V., Koterov, V.N. and Solbakov V.V. 2000. AKS model for forecasting distribution of production discharges from marine drilling platforms. Rep. on applied mathematics. Moscow: CC RAS. pp. 68-70.

Assessment of the environmental quality of the shelf and the slope top horizons of eastern Sakhalin in relation with the heavy metals content in bottom sediments

Lydia T. Kovekovdova
Pacific Fisheries Reasearch Centre (TINRO-Centre), 4 Shevchenko Alley, Vladivostok, 690950 Russia.
e-mail: kovekovdova@mail.ru

The east coast of Sakhalin and especially its northern part is a sparsely populated area with underdeveloped industry and agriculture. But in the northern and northeastern parts of the island, open and working oilfields and gas-fields are concentrated. Each year, the effect on the rich natural complex of this area grows in connection with the development of new oilfields. A combination of fishing, on the one hand, and various economic activities on the other hand, and concern for environmental features causes the need to estimate the chemico-ecological conditions of marine ecosystems to maintain their normal functioning. Documenting the environmental quality in these areas is especially significant as it will serve as background estimation before large-scale development of petroleum hydrocarbon resources, adjoining to the Sakhalin shelf, occurs. As a result of increasing pollution, chemical substances including toxic heavy metals fall into the sea environment. It is known, that increasing of the metal content in the environment negatively influences to existence of marine organisms.

Heavy metals in bottom sediments of sea water are due to a number of factors: geomorphological features of water areas, terrestial drainage, output of underground waters, and wind phenomena and climatic conditions. Accumulation and distribution of metals are influenced by hydrodynamic mode of the seas, physical and chemical processes and processes of biogenic sedimentation.

The migration of metals in the seas is connected to their transition in the "water – bottom sediment" system. Values of this factor and the scale of its negative influence on reservoirs increases considerably with growing anthropogenic influence. At the first stage, increases of metal concentrations in water causes their accumulation in bottom sediments. With a change in the dynamic balance, and as a result of physical, chemical, and microbiological processes, heavy metals that accumulated earlier can migrate from bottom sediments to the water, thereby influencing the quality of environment and creating, under certain conditions, a secondary pollution danger in the embayments. Therefore the level of metal concentrations in bottom sediments is one of the indicators of embayment pollution. Pollution of marine sediments is connected directly with the development of human economic activities. Proceeding from this, the content of heavy metals in bottom sediments can be considered as an integrated parameter of marine environmental pollution. The level of pollution is determined by the comparison of metal concentrations in sediments (conditionally background) in water areas that are subjected to, and not subjected to anthropogenic influences.

The purpose of the present work was to assess the marine environmental quality of the shelf and the slope top horizons of east Sakhalin in relation to the content of heavy metals: copper, zinc, nickel, chromium, lead, cadmium, mercury and arsenic in bottom sediments. Bottom sediments for the analysis were collected in June - July 2002 on the shelf and the slope top horizons of Sakhalin.

Measurements of iron, zinc, chromium, nickel, copper concentrations were carried out by an atomic-absorption spectrophotometer "Nippon Jarrell Ash" model AA-855. Determination of barium was carried out in flame N_2O - acetylene.

Concentrations of cadmium, lead and arsenic were determined by atomic-absorption spectrophotometer "Hitachi" 170-70. Concentration of mercury was determined by

flameless atomic-absorption spectrophotometer on the microanalyzer "Hiranuma" Hg - 1.

Maximum concentrations of copper were determined in bottom sediments of Terpenia Gulf. There was 8-12 mg kg^{-1} dry weight. The lowest concentration was characteristic for northeastern part of the investigated area where the range of copper concentration was 0.5-4.5 mg kg^{-1} dry weight.

Maximum concentrations of zinc were found in Terpenia Gulf - 50 mg kg^{-1}, 32 mg kg^{-1}, 27.5 mg kg^{-1}. They are adjusted to the places experiencing significant anthropogenous loading from coastal sources and depth of bottom sediment.

Maximum concentrations of nickel – 79 mg kg^{-1} and chromium - 15 mg kg^{-1} were found in the bottom sediments of coastal water area near Okha. Taking into account that nickel is an indicator of marine pollution by petroleum, it is possible to assume that its increased concentration in the sediments of this area is caused by pollution by mineral oil.

Spatial distribution of lead, cadmium, mercury and arsenic in bottom sediments of the shelf and the slope top horizons of eastern Sakhalin was rather smooth. Some increased concentrations of these elements were found near Terpenia Gulf: lead – 11.2 mg kg^{-1}, cadmium – 0.093 mg kg^{-1}, mercury – 0.046 mg kg^{-1}, arsenic - 4 mg kg^{-1}. It is known that the content of lead in bottom sediments of polluted waters can reach up to 640 mg kg^{-1}, cadmium up to 4 mg kg^{-1}, mercury up to 10 mg kg^{-1}.

In bottom sediments of the shelf and the upper slope eastern Sakhalin, acid-leachable forms of iron, barium and aluminium were found. At present, the concentrations of these metals corresponds with the natural background of this area.

Thus, it is possible to conclude that concentrations of acid-leachable forms of copper, zinc, nickel, chromium, lead, mercury, cadmium and arsenic in bottom sediments of the shelf and the upper slope of eastern Sakhalin currently corresponds with the natural geochemical background of the area investigated. Individual stations with increased concentrations of metals are revealed. The present research confirms the necessity of monitoring toxic element contents in bottom sediments in connection with expansion of the economic activities, including oil recovery on the shelf of Sakhalin.

The fisheries and current state of walleye pollock (*Theragra chalcogramma*) stock abundance in the eastern Sea of Okhotsk

Alexander I. Varkentin and N.P. Sergeeva
Kamchatka Research Insitute of Fisheries and Oceanography (KamchatNIRO) 18 Naberezhnaya Street, Petropavlovsk-Kamchatsky, 683000 Russia. email: alex@kamniro.kamchatka.ru

The walleye pollock fishery in the Sea of Okhotsk has a rather long history. In 1950s, walleye pollock were harvested by Japanese fishermen. Pollock were also bycatch in the Pacific cod and flatfish seine fisheries. Walleye pollock was harvested by Soviet fleet. A specialized Russian fishery for walleye pollock in the Sea of Okhotsk started in 1963. The annual harvest was 15×10^3 t, approximately (Fig. 1). From 1966, a Korean fleet started harvesting walleye pollock. The fishery developing rapidly until 200 vessels were active by 1969; removals increased much more. The fishery has been carried out generally in the eastern Sea of Okhotsk, where the principal spawning grounds are situated (Fig. 2); economically the most effective fishery occurred when the fish were aggregated for reproduction.

In 1974, the maximum removasl for the whole period (1340×10^3 t) was observed. The contribution by the Japanese fleet was 501×10^3 t approximately, and 100×10^3 t by the Korean fleet. From 1975 until 1981, the harvest was declining in relation to the declining stock abundance (Fig. 1). Growth of biomass afterwards provided harvests of 1265×10^3 t in 1984. For 1985-94 the harvest was about 700×10^3 t, on average. From 1995-97, catches in the eastern Sea of Okhotsk increased significantly up to $1035\text{-}1153 \times 10^3$ t; it was not related to an increase in biomass. From 1998, pollock harvesting in the eastern Sea of Okhotsk coincided with OCP recommendations, however, it decreased steadily to no more than 300×10^3 t in recent years (Fig. 1).

In the 1960-80s, the walleye pollock fishery in the eastern Sea of Okhotsk occurred from January to July. This period is the most favorable due to the fact that the fishes create dense aggregations within a limited area during the spawning and prespawning period. In particular years (1971, 1975, 1977-79, 1981) the fishery was carried out in November-December, however, that was not reckoned as a profitable endeavour because of poor catches and unfavorable weather. As the state of walleye pollock stock abundance in the eastern Sea of Okhotsk has been unfavorable, the fishery is allowed only after January 15 until the mass spawning starts, and not later than April 1 and out of the boundaries of the spawning grounds.

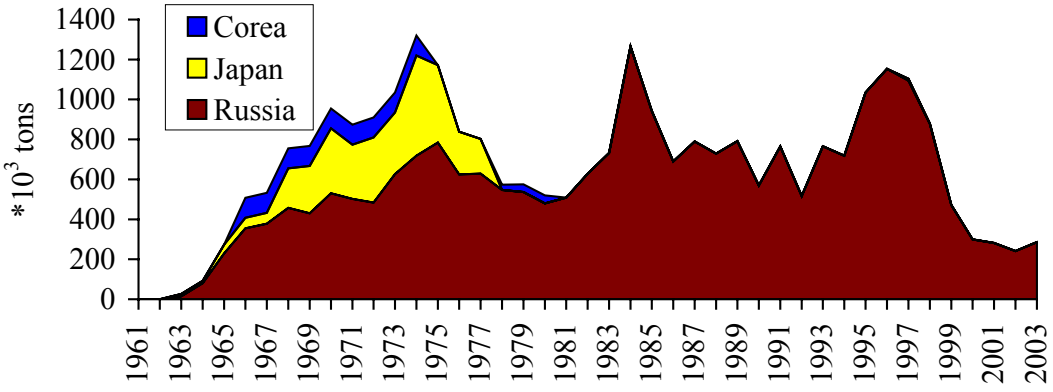

Fig. 1 The dynamics of walleye pollock harvesting in the eastern Sea of Okhotsk.

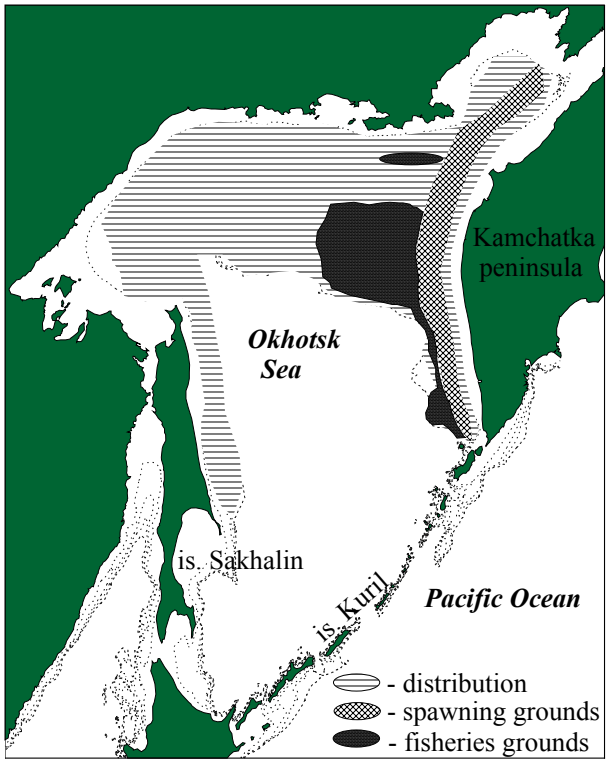

Fig. 2 Schematic distribution of principal of spawning grounds and fishery areas of walleye pollock in the eastern Sea of Okhotsk for recent years.

Until 1977, walleye pollock harvests in the Sea of Okhotsk were not limited. A forecast of the harvests used to be made according to the fishery abilities of the fleet. The forecasts of Okhotsk Sea walleye pollock stock abundance and the prospects based on aspects of the biology for nearest two years began from 1976 (in 1974), but OCP has been forecasted since 1980, made possible due to the methods of OCP and stock abundance forecasting. Since 1972, the biomass of adults in the eastern Sea of Okhotsk has been estimated from egg survey data. In the 1980s, virtual population analysis models of stock abundance have been used.

Walleye pollock biomass in the eastern Sea of Okhotsk varies annually due to the abundance of different cohorts, which is related mostly to global climate change influencing the effectiveness of reproduction and survival. From 1972 to 2002, spawning stock biomass (SSB), assessed from the ichthyoplankton surveys, produced estimates that varied from 1009 – 4175 × 10^3 t, 2172 × 10^3 t on average (Fig. 3). Similar estimates were obtained from an extended analysis of survival model, XSA).

From 1997, SSB in West Kamchatka declined to be, in 2001, similar to that in 1979, i.e. 1059 × 10^3 t. However, the further biomass increases did not follow afterwards. According to the forecast in 2003, the biomass should increase up to 2000 × 10^3 t, approximately at the expense of the 1997 recruitment, but in 2004 it has to be reduced again (Fig. 3). The principal cause is the absence of abundant recruitment.

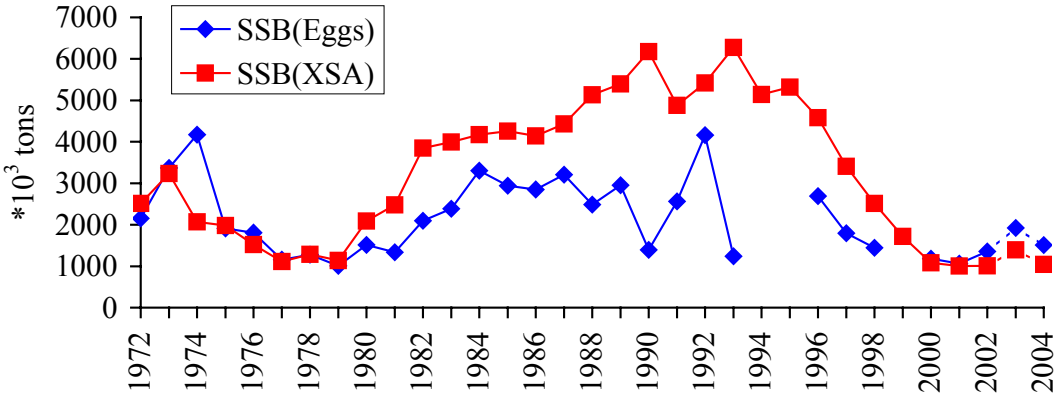

Fig. 3 Dynamics of walleye pollack reproduction stock abundance in the eastern Sea of Okhotsk.

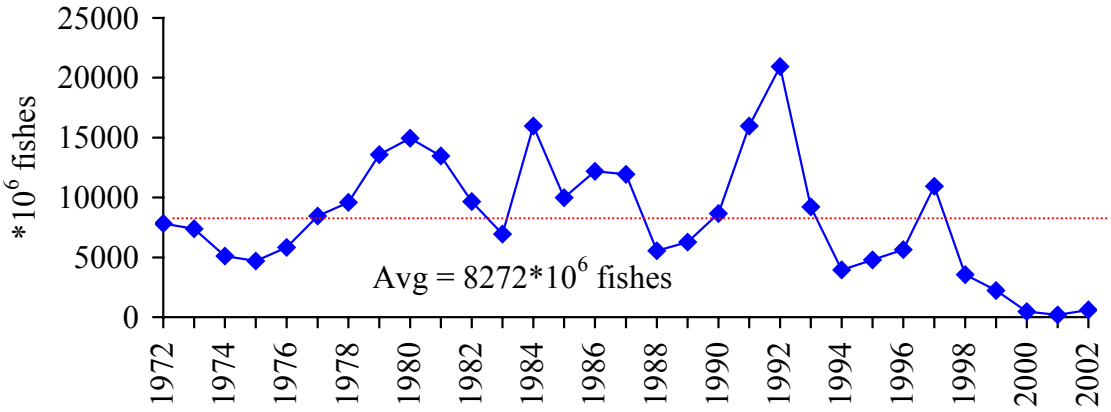

Fig. 4 Estimated abundance of 2 year old walleye pollock in the eastern Sea of Okhotsk, by year of sampling.

From the results of the XSA model, the estimates of average recruitment for the recent five years was equal to 1406.5 × 10^6, about six times lower than the longterm average (Fig. 4). The abundance of a weak 1998 cohort (observed in 2000), of 470.8 × 10^6 individuals was followed by an even weaker 1999 cohort; at 185.5x10^6, it was an historical minimum for this stock. The 2000 cohort is considered as more abundant and promising so the stock abundance enhancement before should be estimated as medium abundance generation.

The fishery decreases the potential abundance of walleye pollock generation significantly. Representatives of many generations have been observed in the catches from the age of 1-2-years. According to the long-term observations, all walleye pollock of <32 cm length have not been processed, but thrown overboard. That, for example, explains the fact that abundant generation 1995, that could have provided the growth of stock abundance since 1999, has been too poor to the age of 6 years.

Biological parameters of snow crab, *Chionoecetes opilio*, and walleye pollock, *Theragra chalcogramma*, in the southwestern area of the Okhotsk Sea in summer

Takashi Yanagimoto and Keiichi Mito
Hokkaido National Fisheries Research Institute, Subarctic Fisheries Resources Division, 116 Katsurakoi, Kushiro, Hokkaido, 085-0802 Japan. E-mail: yanagimoto@fra.affrc.go.jp

Bottom trawl surveys were conducted to collect information on the distribution and biological parameters of the snow crab *Chionoecetes opilio* and walleye pollock *Theragra chalcogramma* in the southwestern area of the Okhotsk Sea in summer, 1997-2001. Water temperatures at each station were measured by XBT (Tsurumi Seiki Co.) and Memory STD (ALEC ELECTRONICS CO.).

For each haul, the fish captured were sorted into species, counted and weighed. Captured snow crabs were measured for carapace width (CW), chela height (CH) and body weight. Male maturity was determined by analyzing the CW-CH relationship to determine the morphometric maturity. Female maturity was determined by examining for the presence or absence of eggs attached to the abdomen. Snow crabs with blat mat syndrome (BMS) were counted. Captured walleye pollock were measured for fork length, body weight, and gonad weight. Daily otolith rings from pollock in 1999 were counted and hatching dates estimated.

Almost all snow crabs were collected from depths of 100 - 300 m, and especially high densities occurred in the depth range of 150 - 200 m. Only a few occurred at depths greater than 300 m (Fig. 1). The size distribution of collected crabs was significantly larger by depth for both male and female (data not shown). The range of bottom temperatures at the stations where the snow crabs were collected was between –0.96°C and 7.05°C, and temperature of stations where more than 500 individuals · km^{-2} were collected ranged between -0.96°C and 5.77°C (Fig. 2). The CW at which 50% individuals had finished the terminal molt was estimated at 106.0 mm and 63.4 mm for males and females, respectively (Fig. 3). Annual changes of snow crab biomass estimated from the survey did not agree with those of catch by fisheries trawler (Fig. 4). The period of the survey (August) was different to the main fishing season (May). There were only a few individuals infected with BMS among the collected snow crabs during the survey period. However, there were a lot of snow crabs with BMS in May. Judging from these results, it was suggested that snow crabs might migrate from the Japanese EEZ to outside during the period June through July.

The biomass of walleye pollock was stable at a low level through the survey period with no clear strong year-class observed in recent years. However, it was considered that the 1999 year-class was dominant based on pollock size distributions during 1997-2001 (Fig. 5). In 1999, the observed modal length was 95-105 mm (Age 0), in 2000 it had increased to 225-245 mm (Age 1), and in 2001 to 320-340 mm (Age 2). Age 0 fishes were mainly distributed in the depth range of 100 – 300 m, and age 1 fishes were distributed over all depths surveyed, and age 2 fishes were mainly sampled at the depth range of 150-200 m and over 300 m. It seems that pollock distributions, with increasing age and size, move from shallow to deeper areas. It was considered that the 1999 year-class hatched in late February, based on daily rings of otoliths. From the estimated hatch date of the 1999 year class and the pollock spawning period around Hokkaido, it indicates the possibility that the spawning ground of the 1999 year-class was not the Okhotsk Sea but the Japan Sea.

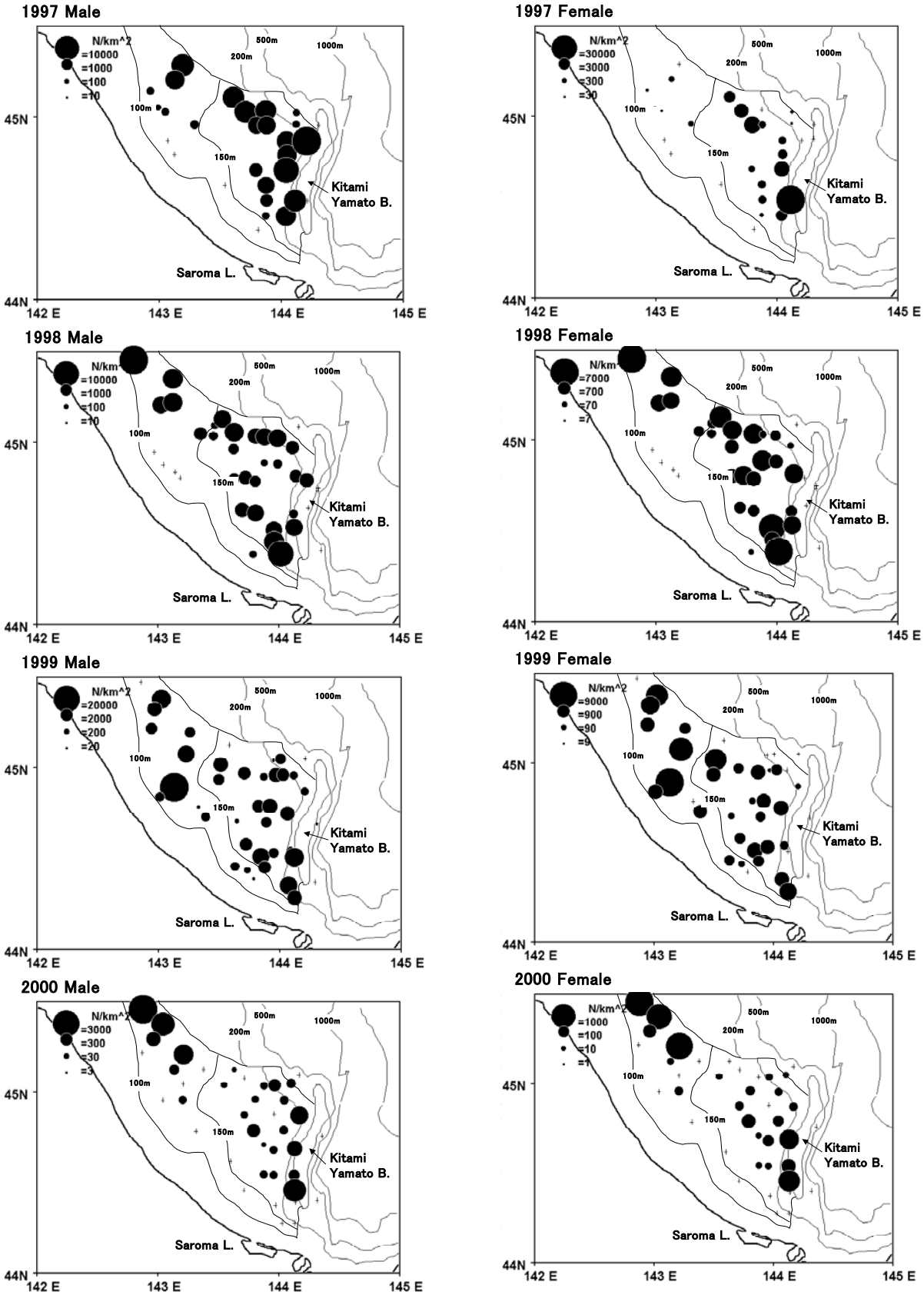

Fig. 1 Density of male (left) and female (right) snow crabs in summer during 1997-2000.

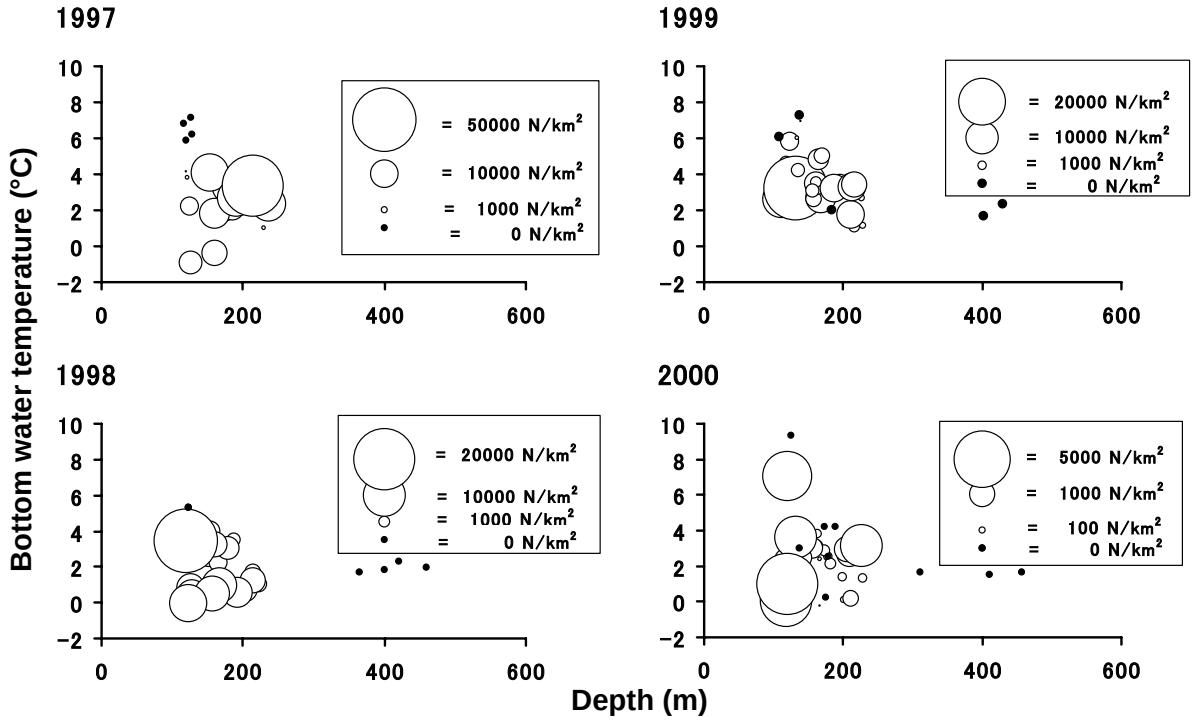

Fig. 2 Relationships among depth, bottom water temperature, and density (No. km^{-2}) of snow crab in summer.

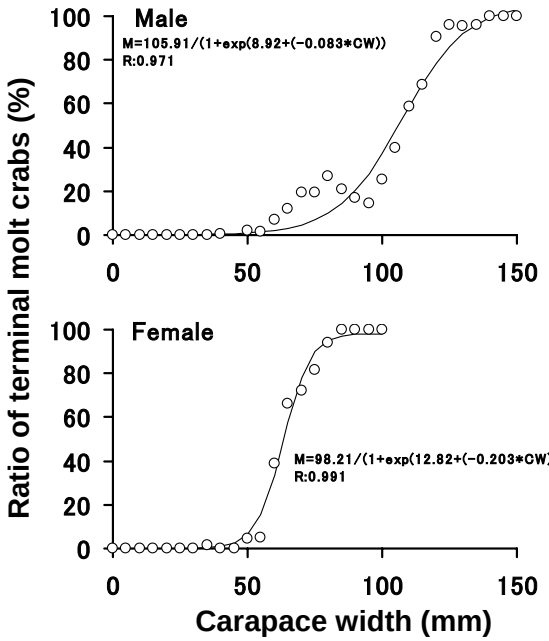

Fig. 3 The ratio of snow crabs that had finished the terminal molt at each carapace width size class: male (upper). Solid lines indicate the regression curves of carapace width to the ratio of terminal molt crabs.

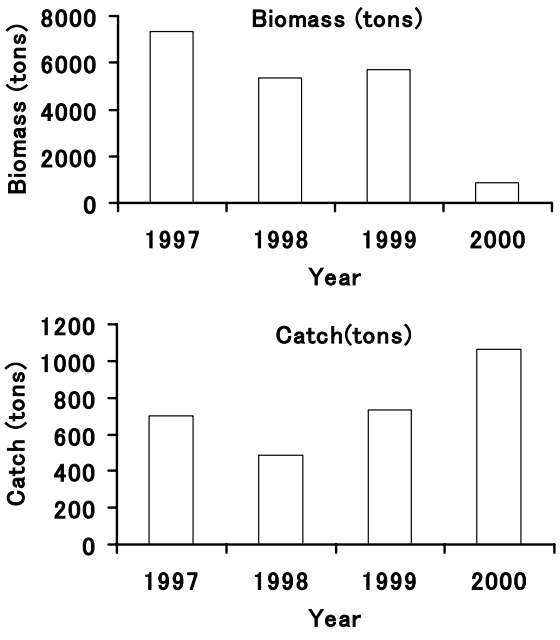

Fig. 4 Annual changes of the estimated biomass and catch of snow crab.

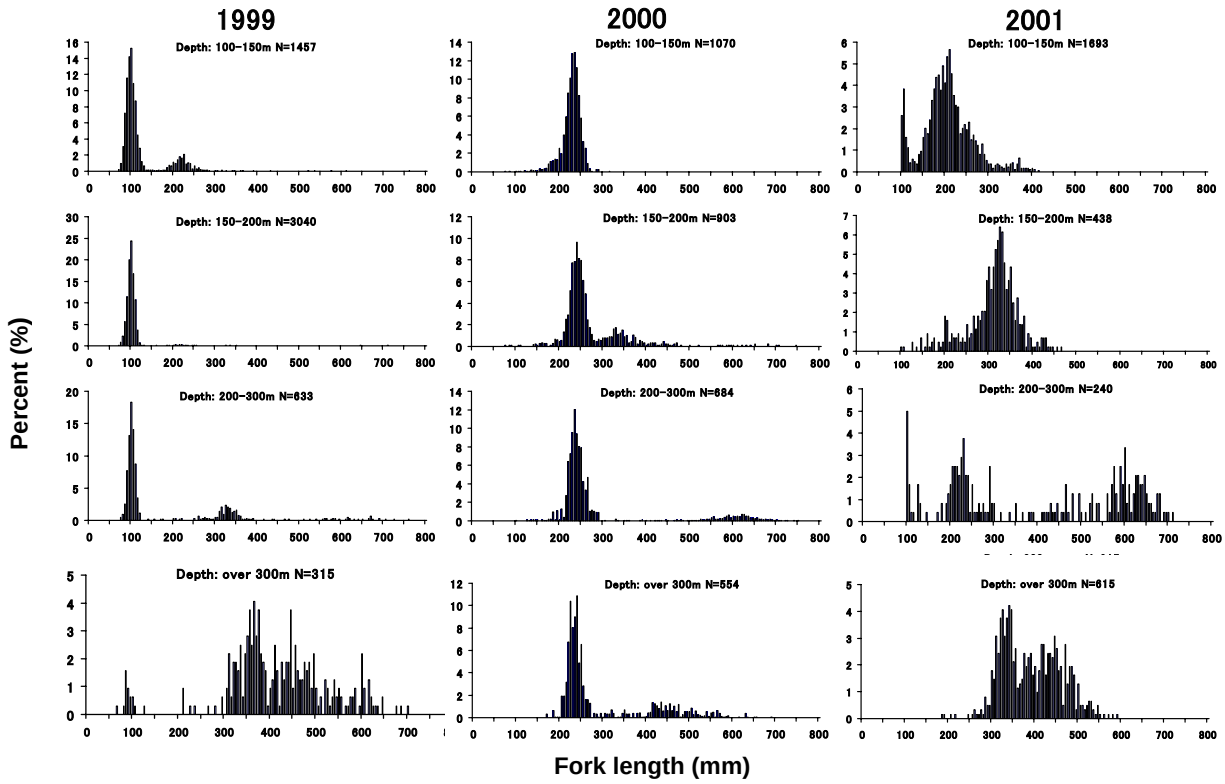

Fig. 5 Size distributions of walleye pollock in each depth range (100-150, 150-200, 200-300, >300 m) for 1999, 2000, 2001.